Symposium 18: The Alternating Access Mechanism in the Era of Transporter Structures

2786-Symp
Alternatives in Alternating Access
Christopher Miller.
Brandeis University, Waltham, MA, USA.

2787-Symp
The old Man and the Membrane
H. Ronald Kaback.
Univ of CA, Los Angeles, Los Angeles, CA, USA.
Lactose permease of Escherichia coli (LacY) is highly dynamic, and sugar binding causes closing of a large inward-facing cavity with opening of a wide outward-facing hydrophilic cavity. Therefore, lactose/H+ symport via LacY very likely involves a global conformational change that
allows alternating access of single sugar- and H+-binding sites to either side of the membrane. This presentation will review in camera the various biochemical/biophysical approaches that provide experimental evidence for the alternating access mechanism.

2788-Symp
Structure of Multidrug Resistance Transporters
Geoffrey Chang, Andrew Ward, Rupali Aggarwal, Alexandra Caya.
The Scripps Research Institute, La Jolla, CA, USA.
P-glycoprotein (Pgp) detoxifies cells by exporting hundreds of chemically unrelated toxins but has been implicated in multidrug resistance in the treatment of cancers. Substrate promiscuity is a hallmark of Pgp activity, thus a structural description of polyspecific drug-binding is important for the rational design of anticancer drugs and MDR inhibitors. The x-ray structure of apo-Pgp at 3.8 Å reveals an internal cavity of ~6,000 Å3 with a 30 Å separation of the two nucleotide binding domains (NBD). Two additional Pgp structures with cyclic peptide inhibitors demonstrate distinct drug binding sites in the internal cavity capable of stereo-selectivity that is based on hydrophobic and aromatic interactions. Apo- and drug-bound Pgp structures have portals open to the cytoplasm and the inner leaflet of the lipid bilayer for drug entry. The inward-facing conformation represents an initial stage of the transport cycle that is competent for drug binding. We will present our latest findings on P-glycoprotein and present strategy on obtaining other conformations, extending the diffraction resolution, and new co-crystal structures with inhibitors/drugs.

Symposium 19: Molecular Motors and the Cytoskeleton: Moving to the Boundaries

2790-Symp
To Cut or not to Cut?: Physically Regulating Microtubule Severing Enzymes
Jennifer Ross.
University of Massachusetts, Amherst, MA, USA.
Microtubule-severing enzymes are AAA (ATPases associated with cellular activities) proteins that remove tubulin dimers from the microtubule lattice. Severing proteins are known to remodel the cytoskeleton during interphase and mitosis, and are required in proper axon morphology and mammalian bone and cartilage development. We have performed the first single molecule imaging to determine where and how severing enzymes act to cut microtubules. We have focused on the original member of the group, katanin, and the newest member, fidgetin to compare their biophysical activities in vitro. We find that, at lower concentrations, both katanin and fidgetin can depolymerize microtubules by removing terminal dimers. Katanin preferentially removes dimers from the plus-end, while fidgetin removes from the minus-end. This activity reflects their cellular localization and activity, where katanin is localized to the cell cortex and fidgetin at the microtubule-organizing center. At higher concentrations, both katanin and fidgetin can sever microtubules, but katanin cuts cleanly through, while fidgetin appear to remove long strips of protofilaments, without a clean break. Further, we find that katanin and fidgetin prefer different types of tubulin to bind and sever. These studies reveal the physical regulation schemes to control severing activity in cells, and ultimately regulate cytoskeletal architecture.

2791-Symp
Invited Speaker
Michael Welte.
Brandeis University, Waltham, MA, USA.

2792-Symp
Active Patterning and Contractile Dynamics in Actin Networks Driven by Myosin Motors
Gijsje H. Koenderink[1], Marina Soarese Silva[1], Martin Depken[2], Bjorn Stuhrmann[1], Fred C. MacKintosh[2].
[1]FOM Institute AMOLF, Amsterdam, Netherlands, [2]Free University Amsterdam, Amsterdam, Netherlands.
Self-organized contractile arrays of actin filaments and myosin motors drive cell division, migration, and tissue morphogenesis. Biophysical studies have provided many insights into the mechanisms of force production by individual motor molecule. However, a mechanistic explanation of collective self-assembly into force-generating arrays is still lacking. We studied how the collective activity of myosin motors organizes actin filaments into contractile structures in a simplified model system devoid of biochemical regulation. We showed that myosin organizes actin into contractile arrays by a 3-stage process. First, the actin filaments mediate the formation of dense foci by active motor transport and motor coalescence. The myosin foci then accumulate actin filaments in a disordered cloud around them, and these actomyosin condensates finally merge into superaggregates by contractile coalescence. We propose that the origin of this multistage aggregation is the highly nonlinear load response of actin filaments, which can support large tensions but buckle already under picoNewton-compressive loads. Since the motor generated forces well exceed this buckling threshold, buckling is induced by the elastic resistance of connected actin networks to filament sliding. We furthermore mapped the spatiotemporal characteristics of the motor-induced contractility by tracking embedded particles, and found that myosin induces long-range, but localized, contractile fluctuations. The contractile dynamics and actomyosin superaggregates closely mimic observations *in vivo*. However, the localization and turnover of actomyosin arrays and directed cortical flows likely require an interplay of collective self-organization and biochemical regulation.

2793-Symp
Myosin Molecular Motors: Transporting Cargo in All Directions
David Warshaw.
University of Vermont College of Medicine, Burlington, VT, USA.

Platform AW: Cell and Bacterial Mechanics & Motility II

2794-Plat
Mechanical Load Induces a 100-Fold Increase in the Rate of Collagen Proteolysis by MMP-1
Arjun S. Adhikari, Jack Chai, **Alexander R. Dunn**.
Stanford University, Stanford, CA, USA.
Both mechanotransduction and extracellular matrix (ECM) proteolytic remodeling are critical during embryonic development and in disease progression. Although mechanical stress is known to profoundly influence ECM remodeling, its effect on ECM degradation by matrix metalloproteinases (MMPs) is largely unexplored. We used a single-molecule magnetic tweezers assay to study the effect of force on collagen proteolysis by MMP-1. We show that the application of ~10 pN in extensional force (far less than cell traction forces) causes a ~100-fold increase in proteolysis rates. Our results support a mechanistic model in which the collagen triple helix unwinds prior to proteolysis. The data and resulting model predict that cell-generated traction forces may dramatically increase localized collagen proteolysis, suggesting that cells may use mechanical force to regulate proteolytic ECM remodeling.

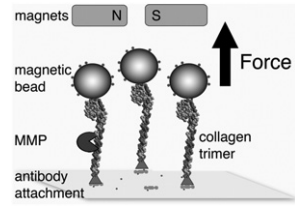

2795-Plat
Cell Shape Dynamics: from Waves to Motion
Wolfgang Losert[1], Meghan Driscoll[1], Colin McCann[1], John Fourkas[1], Carole Parent[2].
[1]University of Maryland, College Park, MD, USA, [2]National Cancer Institute, Bethesda, MD, USA.
We investigate the dynamic changes in cell shapes during cell motility. Using active contour algorithms, we demonstrate the existence of wave-like dynamic shape changes during the migration of Dictyostelium discoideum, a model system for the study of chemotaxis. Cell shapes have regions of high boundary curvature that propagate from the leading edge toward the back along usually alternating sides of the cell. To study the relationship between these curvature

waves and surface contacts, we have used fluorescence and internal reflection microscopy to simultaneously image the cell and the cell-surface contact region. We find that while some curvature waves are retracted before they reach the side of the cell, those that do reach the side couple to the surface and, hence, remain stationary relative to the surface. Regions of high curvature usually start at the front of the cell and are associated with protrusive motion. The protrusion location shifts rapidly in a ballistic manner at speeds nearly double that of cell migration. To examine protrusive motion and curvature waves in the absence of a surface contact, we fabricated micro-cliffs. The curvature wave speed of cells extending over the cliff was double the wave speed of cells migrating to the cliff, which is consistent with the higher wave speeds observed near the non-adherent leading edge of cells. We connect the waves we observe in protrusive activity to wave-like dynamics of intracellular signaling molecules. We also use persistent waves to explain the zig-zag-like appearance of cell tracks and the directional persistence of cell motion during chemotaxis.

2796-Plat

Separate Locations of the Active and Passive Microtubule Interfaces in Kinetochores Inferred from Direction-Dependent Structural Changes

Sophie Dumont[1], Edward D. Salmon[2], Timothy J. Mitchison[1].
[1]Harvard Medical School, Boston, MA, USA, [2]University of North Carolina at Chapel Hill, Chapel Hill, NC, USA.

Chromosomes must be evenly segregated between daughter cells for cell viability, and the kinetochore, a protein complex linking chromosomes to microtubules, is crucial to this process. Despite a long list of kinetochore molecules, our understanding of kinetochore mechanics, and higher-level structural organization, is still poor. Here, we use live imaging of a two-color sensor with sub-pixel resolution to measure structural dynamics of individual kinetochores under both natural force fluctuations provided by metaphase chromosome oscillations in Ptk2, and external mechanical perturbations. The distance between our probes (CenpC and Cdc20) decreased by ~ 16% in poleward-moving (P) compared to away-from-poleward-moving (AP) kinetochores. Informed by extensive analysis of sister kinetochore dynamics, we interpret this change as due to compression within P kinetochores, where microtubules are depolymerizing, compared to AP where they depolymerizing. The data point to two mechanically relevant microtubule interaction interfaces: an active, force-generating interface located between the CenpC and Cdc20 probes, and a passive, frictional interface located at least 8 nm outward from the active interface. P kinetochores are compressed by movement of the active interface outward towards the passive interface, while in AP kinetochores the force at the passive interface is exerted in the opposite direction, leading to increased distance between the probes. Our assay relates kinetochore structure and dynamics at 10 nm and 10 s scales to mechanical behavior, and should be useful for generating a spatial map of all the interactions between kinetochore subunits and microtubules that participate in chromosome movement.

2797-Plat

Imposing Local Magnetic Fields to Control Magnetotactic Bacteria Through Combining Microfabrication and Magnetism

Lina M. Gonzalez[1], Warren C. Ruder[2], SiYen Chou[1], Eli Zenkov[1], William Messner[1], Philip R. LeDuc[1].
[1]Carnegie Mellon University, Pittsburgh, PA, USA, [2]Boston University, Boston, MA, USA.

The ability to impose localized magnetic fields on magnetic bacteria has a variety of applications including in biophysics, nature inspired materials, and non-destructive sensors. Herein we demonstrate our ability to locally direct swimming magnetotactic bacteria, *Magnetospirillum magneticum* strain AMB-1, through microfabricated magnetic field concentrators. To accomplish this, a pair of Helmholtz coils was built to magnetize microfabricated permalloy structures of shapes including circles, squares, and triangles, which may affect the local magnetic fields near the structures. The permalloy structures were fabricated through photolithography and depositing a thin film of NiFe on a master mold. The substrate was a #1 glass coverslip that permitted us to observe the interactions of the magnetotactic bacteria with the permalloy structures. These microfabricated structures were positioned at the center and along the axes of the Helmholtz coils. The response of the bacteria around the structure was quantified through analyzing the images of the bacteria in terms of orientation and velocity. The results indicate that the AMB-1 appeared to cross or stop at the regions on the structures possessing higher magnetic field intensity relative to the surroundings. Furthermore, the bacteria appeared to alter their orientation as they approached sharp corners of the structures. We also developed a model using Finite Element Method Magnetics (FEMM) to investigate the regions of local magnetic field gradients, which indicated higher magnetic fields at the protrusions and the sharp points of the magnetic structures. This work supports the idea of using these magnetotactic bacteria as an aqueous non-destructive sensor and also has implications in fields including physics, biology, material science, and engineering.

2798-Plat

Mechanisms for Maintaining Cell-Shape in Rod-Shaped Gram-Negative Bacteria

Leon Furchtgott[1], Ned S. Wingreen[2], Kerwyn Casey Huang[3].
[1]Harvard University, Cambridge, MA, USA, [2]Princeton University, Princeton, NJ, USA, [3]Stanford University, Stanford, CA, USA.

For the rod-shaped Gram-negative bacterium *Escherichia coli*, changes in cell shape have critical consequences for motility, evasion of the host immune system, proliferation, and adhesion. For most bacteria, the peptidoglycan cell wall is both necessary and sufficient to determine cell shape. Yet, despite decades of biochemical, genetic, and cytological studies of cell-wall synthesis, an understanding of how the synthesis machinery assembles a peptidoglycan network with a robustly maintained micron-scale shape and size has remained elusive. To explore shape maintenance across rod-shaped Gram-negative bacteria, we have quantified the robustness of cell shape in *E. coli* and two other Gram-negative bacteria in different nutrient environments, genetic backgrounds, and in the presence of an antibiotic that inhibits cell division. Previous biophysical modeling of the static relationship between cell-wall organization and cell shape has proven successful in predicting the mechanism of shape determination in vancomycin-treated *E. coli* cells and in the spiral bacterium *Helicobacter pylori*, suggesting that mechanical forces play a prominent role in shape regulation. In this work, we introduce a biophysical model for the growth dynamics of rod-shaped cells that we employ to investigate the roles of spatial regulation of peptidoglycan synthesis, biochemical properties of glycan strands, and mechanical stretching during insertion. Our studies reveal that rod-shape maintenance requires insertion to be insensitive to fluctuations in cell-wall density and stress, and that a helical pattern of insertion is sufficient for over six-fold elongation in a fixed direction without significant loss in shape. In addition, we demonstrate that both the length and prestretching of newly inserted strands regulate cell width. In sum, we show that simple physical rules can allow Gram-negative bacteria to achieve robust, shape-preserving cell-wall growth.

2799-Plat

Non Invasive Inference of Chemotaxis Responses from Bacterial Trajectories

jean-baptiste masson, Guillaume Voisinne, Jerome Wong-NG, Antonio Celani, Massimo Vergassola.
Institut Pasteur, CNRS URA 2171, Paris, France.

Bacteria perform chemotaxis by regulation of their tumbling frequency. Quantitatively, the frequency of tumbling is regulated by the convolution of the history of the attractant detections with the impulse response function (kernel), which measures the response of the bacterium to an impulse stimulus. At the molecular level, the response is shaped by the molecular processes of (de)phosphorylation and (de)methylation. Experiments to measure the chemotactic response function are currently realized using the classical tethering technique (Silverman and Simon, 1974) where flagella are tethered to a glass slide via a flagellin antibody . Flagella cannot rotate, whilst counter-rotation of the bacterium is visible at the microscope. This occurs when only a single flagellum is tethered and E. coli is pre-treated to reduce it to a mono-flagellated state. The statistics of rotations clock-wise or anti-clockwise (corresponding to runs and tumbles) are thus measured in response to different stimuli.
We have developed a novel inference method to measure the chemotactic response function [1]. Bacteria are introduced in a 300-μm deep channel where a static and homogeneous gradient of a chemical is established. The inference is performed on the recorded trajectories of bacteria swimming in chemoattractant (or repellent) and is thus non-intrusive. Only the concentration of chemoattractant (repellent) and the times of tumble are necessary to extract the response function. Using this method we have characterized the chemotactic response of E. coli for numerous attractants and repellents. We studied the modification of the chemotactic response with the concentration of attractant and repellent, with the magnitude of the gradients and with gene deletions. Finally, we analyzed the modification of the response function due to the loss of adaptation to one attractant induced by a second attractant.
[1] Voisinne et al, submitted to Cell

2800-Plat

Measuring Peptidoglycan Elasticity and Stress-Stiffening of Live Bacterial Cells

Yi Deng, Mingzhai Sun, Joshua W. Shaevitz.
Princeton University, Princeton, NJ, USA.

The mechanical properties of gram-negative bacteria are governed by a rigid peptidoglycan (PG) cell wall and the turgor pressure generated by the large concentration of solutes in the cytoplasm. The elasticity of the PG has been measured in bulk and in isolated sacculi and shown to be very compliant compared to the overall stiffness of the cell itself. However, the stiffness of the cell wall in live cells has not been accurately measured. In particular, the effects that pressure-induced stress might have on the stiffness of the meshlike PG network have not been addressed even though polymeric materials often exhibit large

amounts of stress-stiffening. In this study, we use two experimental systems to probe the effects of pressure on the wall stiffness. First, we study blebbing E. coli cells using atomic force microscopy to separate the contributions of the cell wall and turgor pressure to the overall cell stiffness. Second, we study the relationship between cell stiffness and external osmotic pressure which allows us to probe higher turgor pressures. Combining these two types of measurements, we find strong evidence of a power-law stress-stiffening in the E. coli cell wall such that the wall is significantly stiffer in live cells (E~5 MPa) than the relatively compliant sacculus stiffness (E~34 MPa).

2801-Plat
Ballistic Motion of Spirochete Membrane Proteins
Holger Kress[1,2], Rostislav Boltyanskiy[2], Alexia A. Belperron[3], Cecile O. Mejean[2], Charles W. Wolgemuth[4], Linda K. Bockenstedt[3], Eric R. Dufresne[2].
[1]Eindhoven University of Technology, Eindhoven, Netherlands, [2]Yale University, New Haven, CT, USA, [3]Yale University School of Medicine, New Haven, CT, USA, [4]University of Connecticut Health Center, Farmington, CT, USA.
Borrelia burgdorferi spirochetes are pathogenic bacteria which can cause Lyme disease. *B. burgdorferi* use membrane proteins to anchor themselves inside ticks which act as intermediate hosts. Human immune cells that fight bacterial infections bind to bacteria to internalize them. This binding can be mediated by antibodies against bacterial membrane proteins. Therefore these proteins and their mechanical behavior in the membrane play a key role for the disease transmission and the immune response.
The mechanical behavior of proteins in bacterial membranes is still poorly understood. We investigated membrane protein dynamics in *B. burgdorferi* with microparticles coated with monoclonal antibodies against the spirochete outer surface protein A (OspA). We used holographic optical tweezers to attach the microparticles to membranes of live *B. burgdorferi* and we tracked the subsequent particle motion.
Surprisingly the particles were transported ballistically to one end of the bacteria. The average speed of this transport was 3.1 $\pm$ 0.2 um/s. To determine if the microparticle motion is driven by the proteins, we are using speckle microscopy with fluorescently labeled OspA. In addition, we measured the stall force of the transport and found that a few piconewtons were sufficient to inhibit the motion. Although *B. burgdorferi* have a symmetric morphology, the protein motion showed a preferred direction of transport towards one end in individual bacteria. The origin of this symmetry breaking still needs to be unraveled. Mutant *B. burgdorferi* which lack the flagella that are found in wild-type bacteria did not show directed transport of membrane proteins, but only diffusive motion. Therefore we hypothesize that the protein transport is enabled by the bacterial motility machinery. We will discuss the proposition that this transport of membrane proteins could be a novel type of bacterial defense mechanism against immune cells.
[HK and RB contributed equally]

Platform AX: Protein Folding & Stability II

2802-Plat
Protein Protein Interactions - the Effects of Cosolvents, Crowding and Pressure
Roland Winter.
TU Dortmund University, Dortmund, Germany.
The effects of various kosmotropic and chaotropic cosolvents and salts on the intermolecular interaction potential of proteins (e.g., lysozyme, SNase) was evaluated at low to high protein concentrations by using synchrotron small-angle X-ray scattering in combination with liquid state theoretical approaches. The experimentally derived static structure factors $S(Q)$ obtained without and with added cosolvents and salts were analyzed with a statistical mechanical model based on the DLVO potential which accounts for repulsive and attractive interactions between the protein molecules. Different cosolvents and salts influence the interactions between protein molecules differently as a result of changes in the hydration level or solvation, in charge screening, specific adsorption of the additives at the protein surface, or increased hydrophobic interactions. Experimentally derived static structure factors were also obtained for the aggregation-prone protein insulin. The data reveal that the protein self-assembles into equilibrium clusters already at low concentrations. Striking differences regarding interaction forces between aggregation-prone proteins such as insulin in the pre-aggregated regime and natively stable globular proteins are found. Finally, the effects of crowding and pressure on the solvational properties and intermolecular interaction of the proteins were studied, and a tentative temperature-concentration-pressure phase diagram has been obtained.

2803-Plat
Markov State Models of Millisecond Folder ACBP Reveals New Views of the Folding Reaction
Vincent A. Voelz[1], Marcus Jäger[2], Li Zhu[3], Shuhuai Yao[4], Olgica Bakajin[5], Shimon Weiss[2], Lisa J. Lapidus[3], Vijay S. Pande[1].
[1]Stanford University, Stanford, CA, USA, [2]University of California, Los Angeles, Los Angeles, CA, USA, [3]Michigan State University, Lansing, MI, USA, [4]Hong Kong University of Science and Technology, Hong Kong, Hong Kong, [5]Lawrence Livermore National Laboratory, Livermore, CA, USA.
A combination of large-scale distributed computing efforts and Markov State Model (MSM) approaches have recently been used to simulate the folding of proteins on the millisecond timescale. These models predict new views of the folding reaction–a complex set of metastable intermediates, multiple pathways, a hub-like network structure, and compact unfolded states with residual structuring–yet, experimental observables often report simple two-state kinetics. To study the events that precede folding, we used MSM approaches to model the folding reaction of ACBP (acyl-CoA binding protein), an 86-residue helix-bundle protein that folds on the ~10 ms timescale, with an ~80 μs collapse phase that can be probed both by simulation and experiment. Our combined results suggest that the fast kinetic phase is not due to barrier-limited formation of a well-defined intermediate, but rather the surprisingly slow acquisition of unfolded-state structure.

2804-Plat
Is the Serpin Folding Mechanism Conserved? The Folding Pathways of Human Alpha-1 Antitrypsin and Neuroserpin
Anindya Sarkar, Crystal Zhou, Patrick L. Wintrode.
Case Western Reserve University, Cleveland, OH, USA.
Inhibitory serpins are unusual because they fold to a kinetically trapped metastable state. In their lowest energy conformation serpins have a large 6 stranded central beta-sheet (sheet A), while in the metastable state this sheet is 5 stranded, and strand 4 is a flexible solvent exposed loop. How serpins avoid folding to their lowest energy conformation is an open question. We have used pulse labeling hydrogen/deuterium exchange coupled with mass spectrometry to probe the folding pathways of two serpins: alpha-1 antitrypsin (A1AT) and neuroserpin. Both proteins fold surprisingly slowly. Upon dilution from 6 M GuHCl, A1AT folds to completion in approximately 50 minutes, while nearly 90 minutes are required for neuroserpin. In A1AT the ''B-C barrel'' region, comprising much of the hydrophobic core and securing the C terminus of strand 4, folds first while beta-sheet A is among the last regions to fold. Most strikingly, beta strand 5 at the center of sheet A shows a lag phase of nearly 350 seconds before any protection from H/D exchange is seen. Strand 5A forms part of the insertion site for strand 4, and we propose that the separation of folding timescales in different regions of A1AT plays a role in guiding it to its metastable structure. Surprisingly, neuroserpin folds via a different pathway in which the center of beta-sheet A, including strand 5, is the first region to fold, securing the N terminus of strand 4, while the ''B-C barrel'' folds later. Our results indicate that multiple folding routes can lead serpins to be trapped in their metastable conformation. Apparently, securing either end of strand 4A (also called the reactive center loop) early in the folding process is a requirement for folding to the metastable state.

2805-Plat
Engineered Allosteric Activation of Kinases in Living Cells
Andrei Karginov, Feng Ding, **Pradeep Kota**, Nikolay Dokholyan, Klaus Hahn.
University of North Carolina, Chapel Hill, Chapel Hill, NC, USA.
Studies of cellular and tissue dynamics benefit greatly from tools that can control protein activity with specificity and precise timing in living systems. Here, we describe a new approach to confer allosteric regulation specifically on the catalytic activity of kinases. A highly conserved portion of the kinase catalytic domain is modified with a small protein insert that inactivates the catalytic activity of the kinase, but does not affect other protein interactions. Catalytic activity is restored upon addition of rapamycin or its non-immunosuppressive analogs. We demonstrate the approach by specifically activating focal adhesion kinase (FAK) within minutes in living cells, thereby demonstrating a novel role for FAK in regulation of membrane dynamics. Molecular modeling and mutagenesis indicate that the protein insert reduces activity by increasing the flexibility of the catalytic domain. Drug binding restores activity by increasing rigidity of a specific region in the kinase that is critical for function. We further demonstrate the wide applicability of our approach by successful regulation of Src and p38 kinases in living cells.

2806-Plat
Molecular Simulations of Mutually Exclusive Folding in a Two-Domain Protein Switch
Lillian T. Chong.
University of Pittsburgh, Pittsburgh, PA, USA.
A major challenge with testing designs of protein conformational switches is the need for experimental probes that enable the individual domains to be independently monitored. One way to circumvent this issue is to use a molecular simulation approach in which each domain can be directly observed. Here we report the first molecular simulations of mutually exclusive folding in an engineered two-domain protein switch, providing a detailed view of how folding of one protein drives unfolding of the other in a barnase-ubiquitin fusion protein. These simulations successfully capture the experimental effects of interdomain linker length and ligand binding on the extent of unfolding in the less stable domain. In addition, the effect of linker length on the potential for oligomerization, which eliminates switch activity, is in qualitative agreement with experiment. We also perform the first simulations exploring the ease of unfolding a protein via localized compression. Finally, we report the effect of linker length on rates of unfolding and refolding of each domain, providing novel kinetic insights on mutually exclusive folding. Our results demonstrate that molecular simulations can be useful virtual assays of switch activity that can aid the rational design of bi-functional switches.

2807-Plat
Exploring the Trafficking, Ligand-Binding Activity, and Unfolding of a Model GPCR
Andrea N. Naranjo[1], Michelle A. O'Malley[2], Amy N. Chavalier[1], Anne S. Robinson[1].
[1]University of Delaware, Newark, DE, USA, [2]Massachusetts Institute of Technology, Cambridge, MA, USA.
G protein-coupled receptors (GPCRs) are integral membrane proteins vital for cellular signaling and constitute one of the major drug targets. Despite their importance, relatively little information regarding their structure, folding, and stability has been published.
This work describes the impact of disulfide bonds on the expression and structural stability of the human adenosine receptor, A_{2A} ($hA_{2A}R$). The crystal structure of this receptor revealed four disulfide bonds present in extracellular loops that could contribute to expression, stability, or ligand binding or to a combination of these.
To test the role of these residues, cysteine to alanine mutants of $hA_{2A}R$ were created; expression and ligand-binding activity of the constructs were tested in mammalian (HEK293) and yeast (*Saccharomyces cerevisiae*) cells. Once purified from yeast, unfolding of the $hA_{2A}R$ through thermal and chemical means was monitored via intrinsic tryptophan fluorescence and circular dichroism. The effect of ligand addition and reduction of disulfide bonds was also investigated.
Thermal and chemical denaturation were not reversible, yet clear differences in the unfolding behavior were observed upon ligand binding via circular dichroism and fluorescence spectrometry. We found that the stability of $hA_{2A}R$ was increased upon incubation with the agonist N6-cyclohexyladenosine or the antagonist theophylline. When extracellular disulfide bonds were reduced with a chemical reducing agent, the ligand binding activity decreased by ~40%, but reduction of these bonds did not compromise the unfolding transition observed via urea denaturation. Overall, these approaches offer a general strategy for characterizing the effect of disulfide bonds and ligand effects on the stability of GPCRs.

2808-Plat
Determinants of Cooperativity in Repeat Protein Folding
Tural Aksel, Ananya Majumdar, Doug Barrick.
Johns Hopkins University, Baltimore, MD, USA.
Repeat proteins have been popular model systems in protein folding research due to their modular architecture. Although each repeat has the same fold, because of sequence variation, the folding energy is not distributed evenly among the repeats. Therefore, it is challenging to quantify the repeat-repeat interactions and the intrinsic folding energies of every repeat. To overcome this difficulty, we designed a consensus ankyrin repeat(CANK), which is brought together to make arrays of identical repeats. By solution NMR, we solved the structure of our three repeat CANK, NRC, and verify that NRC adopts the canonical Ankyrin repeat protein fold. Our SAXS measurements show that CANKs in different length arrays also adopt the same fold. By fitting unfolding transitions of a limited number of constructs to Ising model, we found that the individual repeats have low intrinsic stability, but the interfacial interactions are highly stabilizing. We also extended our Ising formalism to include the temperature dependence of unfolding free energy and we quantified the enthalpic and entropic contribution to intrinsic and interfacial stabilities, as well as, the uneven distribution of heat capacity of unfolding into the intrinsic and interfacial components. Our results suggest that intrinsic folding resembles secondary structure formation(loss of conformational entropy) and interfacial folding involves hydrophobic desolvation(entropy increase and negative heat capacity change upon folding). To separate out the contribution of long range electrostatics to intrinsic and interfacial stability, we measured the salt dependence of CANK stabilities. Our results show that NaCl stabilizes the interfaces and has marginal destabilizing effect on intrinsic stability. Currently we are trying to identify the charge-charge interactions responsible for the high salt dependence of interfacial stability by NMR techniques and single point substitutions.

2809-Plat
Outer Membrane Secretion Efficiency of Autotransporter Virulence Proteins Correlates with Passenger Domain Folding Properties
Jonathan P. Renn, Mirco Junker, **Patricia L. Clark**.
University of Notre Dame, Notre Dame, IN, USA.
Autotransporters (ATs) are the largest class of extracellular virulence proteins secreted from Gram-negative bacteria. Each AT is synthesized as a tripartite pre-protein containing an N-terminal signal sequence that directs secretion across the inner membrane, a central ''passenger'' domain that becomes the mature extracellular virulence protein, and a C-terminal outer membrane (OM) porin domain that is essential for OM transport. AT passenger domains have highly diverse sequences, lengths, and functions, but almost all are predicted to contain β-helical structure. It was originally proposed that an AT protein autonomously catalyzes transport of its own passenger domain across the OM, but recent results have cast doubt on this model. Moreover, in the absence of a significant quantity of ATP or proton gradient across the OM, the driving force for efficient OM secretion remains unclear. Here we demonstrate a direct correlation between localized regions of AT passenger domain stability ($\Delta G_{unfolding}$) and OM secretion efficiency. Destabilizing the C-terminus of a passenger domain β-helix significantly reduced OM secretion efficiency. In contrast, destabilizing more N-terminal portions of the passenger domain produced a linearly correlated increase in OM secretion efficiency. Thus, C-terminal passenger domain stability facilitates OM secretion, whereas N-terminal stability hinders it. The contributions of regional passenger stability to OM secretion efficiency demonstrate a crucial role for the passenger domain itself in directing its secretion across the OM. These results indicate that the folding properties of distinct regions of the passenger domain provide a directed molecular driving force, for use as a generalized transporter device. The regionalized distribution of AT passenger domain stability provides a unique solution for the directed transport of macromolecules across biological membranes, defining a new category of ATP-independent Brownian motor.

Platform AY: Calcium Signaling Pathways

2810-Plat
Phospholipase C-Epsilon Couples cAMP Production and Epac2 Activation to the Facilitation of Calcium-Induced Calcium Release (CICR) in Pancreatic Beta Cells
George G. Holz[1], Igor Dzhura[1], Oleg Chepurny[1], Colin A. Leech[1], Elvira Dzhura[1], Parisa Afshari[1], Grant G. Kelley[1], Michael W. Roe[1], Michael J. Rindler[2], Xin Xu[3], Youming Lu[3], Sundeep Malik[4], Alan V. Smrcka[4].
[1]State University of New York Upstate Medical University, Syracuse, NY, USA, [2]New York University School of Medicine, New York, NY, USA, [3]Louisiana State University School of Medicine, New Orleans, LA, USA, [4]University of Rochester School of Medicine, Rochester, NY, USA.
We provide the first report that a novel phosphoinositide-specific phospholipase C-epsilon (PLC-epsilon) is expressed in the islets of Langerhans, and that the knockout (KO) of PLC-epsilon gene expression in mice disrupts the action of GLP-1 receptor agonist Exendin-4 to facilitate CICR in the beta cells of these mice. Thus, in the present study in which wild-type (WT) C57BL/6 mouse beta cells were loaded with the photolabile Ca2+ chelator NP-EGTA, the UV flash photolysis-catalyzed uncaging of Ca2+ generated CICR in only 9% of the beta cells tested, whereas CICR was generated in 82% of the beta cells pretreated with Exendin-4. This action of Exendin-4 to facilitate CICR was reproduced by cAMP analogs that activate PKA (6-Bnz-cAMP-AM) or Epac2 (8-pCPT-2'-O-Me-cAMP-AM) selectively. However, in beta cells of PLC-epsilon KO mice, and also Epac2 KO mice, these test substances exhibited differential efficacies in the CICR assay such that Exendin-4 was partially effective, 6-Bnz-cAMP-AM was fully effective, and 8-pCPT-2'-O-Me-cAMP-AM was without significant effect. Importantly, transduction of PLC-epsilon KO beta cells with recombinant PLC-epsilon rescued the action of 8-pCPT-2'-O-Me-cAMP-AM to facilitate CICR, whereas a K2150E

PLC-epsilon with a mutated Ras Association (RA) domain, or a H1640L PLC-epsilon that is catalytically dead, were both ineffective. Since 8-pCPT-2'-O-Me-cAMP-AM failed to facilitate CICR in WT beta cells transduced with a GTPase activating protein (RapGAP) that down-regulates Rap activity, the available evidence indicates that a signal transduction ''module'' comprised of Epac2, Rap, and PLC-epsilon exists in beta cells, and that the activities of Epac2 and PLC-epsilon are key determinants of CICR in this cell type.

2811-Plat

PKA is a Control Node in a Calcium-Dependent Oscillatory Circuit in Pancreatic Beta Cells

Ambhighainath Ganesan, Qiang Ni, Nwe-Nwe Aye-Han, Xinxin Gao, Michael D. Allen, Andre Levchenko, Jin Zhang.
Johns Hopkins University School of Medicine, Baltimore, MD, USA.

Protein Kinases are often critical nodes in signaling cascades that encode diverse inputs and effect appropriate outcomes requiring complex spatiotemporal regulation of kinase activities. We show here using FRET-based biosensors that calcium, cAMP and PKA activity oscillate synchronously in insulin secreting MIN6 pancreatic beta cells, suggesting the presence of a tightly regulated oscillatory circuit involving PKA mediated feedback onto calcium signaling. We observed that PKA is essential for this circuit as well as capable of initiating oscillations. Further, mathematical modeling in conjunction with experimentsindicates that PKA activity could modulate the frequency of oscillations resulting in diverse spatiotemporal outcomes (simulations shown in figure).

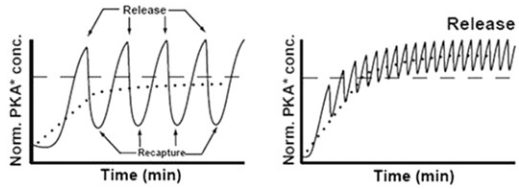

Catalytic subunits of PKA could be periodically released and recaptured for ''local'' target phosphorylation at low frequency conditions (left panel). However, at high frequency conditions (right panel), the mean PKA activity (dotted line) may cross an arbitrary threshold (dashed line) leading to continued release of catalytic subunits resulting in phosphorylation of ''global'' targets. Our findings therefore suggest that temporal regulation of PKA activity could be used to control complex cellular functions and thus influence the functionality of the pancreatic beta cell.

2812-Plat

Basal Phospholipase C (PLC) Activation is Obligatory for Cardiac Pacemaker Activity

Tatiana M. Vinogradova, Edward G. Lakatta.
NIA, NIH, Baltimore, MD, USA.

Spontaneous firing of sinoatrial node cells (SANC) is controlled by sarcoplasmic reticulum (SR) generated local subsarcolemmal Ca^{2+} releases (LCRs) which appear during diastolic depolarization and activate an inward Na^{+}-Ca^{2+}exchange current, regulating diastolic depolarization rate and SANC beating rate. Whether the ubiquitous enzyme, PLC that plays a key role in Ca^{2+} signaling of numerous cell types, controls spontaneous SANC firing is unknown. Here we show that PLC inhibitor U-73122 (6μmol/L, n=7), but not its inactive analog U-73343 (n=4), stops spontaneous firing (perforated patch-clamp recordings) of freshly isolated rabbit SANC, indicating important role of basal PLC activity for cardiac pacemaking. To determine whether signaling via the cAMP-sensor Epac elevates PLC activity in SANC and stimulates PLC-mediated IP_3-dependent Ca^{2+} release, we employed Epac activator cpTOME or IP_3 receptor inhibitor 2-APB, respectively. Neither cpTOME (10 μmol/L, n=3), nor 2-APB (2 μmol/L, n=4) altered the spontaneous SANC beating rate. PLC inhibition by U-73122, in a time-dependent manner, suppressed LCRs (confocal microscopy, Ca^{2+}indicator Fluo-3), i.e. decreased LCR's size, amplitude and prolonged the LCR period (the interval between AP-induced Ca^{2+} transient and subsequent LCR); afterwards eliminated LCRs and stopped SANC firing. The time-dependent increase in the LCR period predicted the concomitant increase in the spontaneous cycle length, suggesting that Ca^{2+} cycling could be a major target of PLC-dependent control of SANC firing. LCRs are critically dependent upon amount of Ca^{2+} in SR, supplied by L-type Ca^{2+}current ($I_{Ca,L}$). U-73122, but not U-73343, markedly suppressed $I_{Ca,L}$ amplitude (from -11.8 ± 4.8 to -5.9 ± 2.4 pA/pF, n=6, $P<0.001$). We conclude that PLC-dependent control of spontaneous SANC firing, independent of either Epac signaling or IP_3-dependent Ca^{2+} release, regulates Ca^{2+} influx through L-type Ca^{2+} channels and, thus, SR Ca^{2+} cycling and via these mechanisms, in part at least, is obligatory for SANC normal automaticity.

2813-Plat

Altered Nuclear Calcium Signaling in Tachycardia-Induced Remodeling in Rabbit Atria: A Mechanism of Altered Excitation-Transcription Coupling in Atrial Fibrillation?

Benoit-Gilles Kerfant, Marion Kuiper, Arne Van Hunnik, Maura Greiser, Sander Verheule, Ulrich Schotten.
CARIM, Maastricht, Netherlands.

Nuclear calcium (Ca2+) signalling play a major role in cardiac excitation-transcription coupling. The origin of nuclear Ca2+ transient is still controversial. It has been suggested that Ca2+ diffusion from the cytosol through the nuclear pores or perinuclear and intranuclear Ca2+ release mechanisms, mostly via the inositol-3-phosphate receptors (IP3R), participate to nuclear Ca2+ transient. In rabbits subjected to rapid atrial pacing (RAP, 600bp, 5 days), a model for atrial fibrillation (AF), we recently observed that central-cellular, but not subsarcolemmal Ca2+ transient, was largely reduced. Since nuclei are often at the center of atrial myocytes, we hypothesized that nuclear Ca2+ transient is also decreased in RAP cells. Using confocal microscopy we recorded transverse line-scan images in field-stimulated sham and RAP atrial cells. Nuclear Ca2+ transient amplitude in relation to subsarcolemmal Ca2+ transient was decreased in RAP compared to sham cells (at 1Hz, DFnuclear/DFsubsarcolemmal was $0,38 \pm 0,03$ in 17 RAP cells, compared to $0,81 \pm 0,06$ in 16 sham cells, $p<0,01$). Isoproterenol restored central-cellular as well as nuclear Ca2+ transient amplitude in RAP cells. Interestingly, at 2,5Hz, in 9 out of 16 sham cells and in 4 out of 16 RAP cells, a nuclear Ca2+ transient did not follow the cytoplasmic Ca2+ transient suggesting that cytosolic Ca2+ diffusion is not the only mechanism eliciting atrial nuclear Ca2+ transient. Indeed, we observed that, in RAP, L-phenylephrine enhanced both nuclear Ca2+ transient and perinuclear Ca2+ release, via the IP3R, while it had no effect in sham cells. Taken together, our data indicate that both cytoplasmic Ca2+ transient and perinuclear Ca2+ release determine atrial nuclear Ca2+ transient. Furthermore, nuclear Ca2+ transient is reduced while IP3-mediated nuclear Ca2+ signalling is enhanced in RAP, possibly affecting Ca2+-mediated transcription pathways.

2814-Plat

Alterations of Membrane Currents, Contractility and Calcium Signaling in Gq/G11 Single and Double Ko Mice

Qinghai Tian, Sara Pahlavan, Sandra Ruppenthal, Anke Scholz, Kathrina Wiesen, Martin Oberhofer, Lars Kaestner, **Peter Lipp**.
Saarland University, Homburg/Saar, Germany.

In contrast to its role in pathophysiology very little is known about the role of the Gq/G11 signaling cassette in the physiology of cardiac myocytes. We have generated transgenic mice combining a G11-KO approach with the Cre-recombinase tool to knock-down (KD) Gq in a tissue-specific inducible manner. Western-blot analysis depict the rapid loss of Gq protein in less than 2 weeks while the use of a reporter mouse substantiated tissue specificity. We analyzed the effects of (i) Cre expression, (ii) vehicle/Tamoxifen injection, (iii) G11-KO and (iv) Gq-KD on resting potential and capacitance, action potentials (AP) and I(to) by patch-clamping ventricular myocytes. Calcium homeostasis was investigated by Fura2 video-imaging and contraction behavior by measuring sarcomere length. While basic cellular parameters were largely unchanged (cell capacitance, resting membrane potential) in all genotypes and treatments, AP, calcium handling and contractile behavior were altered by vehicle/Tamoxifen injection, G11-KO and Gq-KD. Vehicle injection alone caused upregulation of I(to) and shortening of APs similar to G11-KO. In contrast additional Gq-KD, restorated'' AP properties and I(to). Vehicle injection itself into wt mice caused increases in basal calcium that were absent after Tamoxifen injection, Cre expression had mild effects on calcium handling. Tamoxifen injection and Gq/G11-KO caused major changes in calcium handling and contractile behavior. In conclusion, despite the broad application of the Cre-recombinase system, care has to be taken for possible effects of Cre expression and vehicle/Tamoxifen injection. The Gq/G11 signaling system plays an important role in the physiological modulation of proteins involved in electrophysiology and calcium homeostasis most likely regulated by basal levels of neurohormonal stimulation.

This work was supported by the DFG (KFO196) and the Medical Faculty (HOMFOR).

2815-Plat

Nuclear Inositol 1,4,5-Triphosphate is an Absolut Requirement for Cardiomyocyte Hypertrophy

Lilian M. Arantes[1], Carla J. Aguiar[1,2], M. Jimena Amaya[3], S. Guatimosim[1], M. Fátima Leite[1,4].
[1]UFMG, Belo Horizonte, Brazil, [2]Izabela Hendrix Institute, Belo Horizonte, Brazil, [3]Yale School of Medicine, New Haven, CT, USA, [4]Howard Hughes Medical Institute, Chevy Chase, MD, USA.

Ca^{2+} mediates a wide range of cellular responses and the release of this ion from inositol 1,4,5-triphosphate receptor ($InsP_3R$) is known to play a critical

role in transcription of genes involved in cardiac hypertrophy. The goal of this work is to investigate the relative role of nuclear $InsP_3$ in hypertrophy response induced by endothelin-1 (ET-1). For that, we used an adenovirus construct that has the ability to act as selective $InsP_3$ buffer in the nucleus ($InsP_3$-sponge-NLS), inducing local changes in Ca^{2+} levels. We used a primary culture of neonatal cardiomyocytes, and cells were examined by confocal microscopy and immunofluorescence. We found that ET-1 increased cell surface area by 54.3 ± 6.87% compared to control ($p<0.05$), and that $InsP_3$-sponge-NLS prevented hypertrophy induced by ET-1. We also found that ANP expression levels remained at control levels when ET-1 treated cardiomyocytes had $InsP_3$ buffered in the nucleus. Then, we investigated whether buffering nuclear $InsP_3$ would affect the signaling pathway as calcineurin (Cn)/ nuclear factor of activated T cells (NFAT) and histone deacetilase 5 (HDAC-5) preventing the activation of hypertrophic genes. We observed that buffering nuclear $InsP_3$ decreased translocation of Cn, and NFAT (1.22 ± 0.13 and 0.46 ± 0.16 pixel/nuclear area for control and buffered cells, respectively, $p<0.001$) upon ET-1 stimulation. On the other hand, the HDAC-5 exportation to citosol was prevented by $InsP_3$-sponge-NLS (2.965 ± 0.13 and 5.548 ± 0.25 pixel/nuclear area for ET-1 treated cells and $InsP_3$-sponge-NLS infected plus ET-1 cardiomyocytes, respectively, $p<0.001$).Together, these results show that nuclear $InsP_3$ plays a central role in the hypertrophic effect induced by ET-1. Suport:HHMI/CNPq/Fapemig/CAPES.

2816-Plat

Ca2+ Binding and Transport: A Novel Function for Coenzyme Q

Ivan Bogeski[1], Rubin Gulaboski[1], Valentin Mirceski[2], Reinhard Kappl[1], Markus Hoth[1].
[1]Saarland University, Homburg, Germany, [2]Ss. Cyril and Methodius University, Skopje, Macedonia, Germany.

Coenzyme Q10 (CoQ10) is one of the essential components of the mitochondrial electron-transport chain (ETC) with a primary function to transfer electrons along and protons across the inner mitochondrial membrane (IMM). The concomitant proton gradient across the IMM is essential for the process of oxidative phosphorylation and consequently ATP production.

We report that CoQ10 and its analog CoQ1 have an as-of-yet unknown potential in Ca2+ binding and transport. Using voltammetry, UV-VIS spectrometry, electron paramagnetic resonance (EPR) and nuclear magnetic resonance (NMR) we show that the native form of both CoQ10 and its analog CoQ1 neither bind nor transport Ca2+ ions. However, when exposed to alkaline media or monoxygenase enzymes such as cytochrome P450, both CoQs undergo structural changes through a complex reaction pathway and form quinone structures with distinct properties. In a time dependent manner, one or both methoxy groups at position 2 and 3 on the quinone ring are replaced by a hydroxyl group. Contrary to the native form, the new hydroxylated products (of CoQ1 or CoQ10), depending on its redox transformation, are effectively chelating and transporting Ca2+ across artificial biomimetic membranes.

Our results open new perspectives about the physiological importance of CoQ10, not only as electron and proton transporter, but also as a potential regulator of mitochondrial Ca2+ homeostasis.

2817-Plat

Calcium Signalling in Red Blood Cells

Lars Kaestner[1], Patrick Steffen[2], Jue Wang[1], Asya Makhro[3], Achim Jung[2], Duc Bach Nguyen[2], Ingolf Bernhardt[2], Anna Bogdanova[3], Peter Lipp[1], Christian Wagner[2].
[1]Saarland University, Homburg/Saar, Germany, [2]Saarland University, Saarbrücken, Germany, [3]University of Zürich, Zürich, Switzerland.

Thrombus formation is believed to be the major cause of stroke and infarction. Current understanding imposes mechanisms based on leucocyte and platelet activity. However, red blood cells make up a significant part of the clot. An active participation of red blood cells was hypothesised.

Cell based methods, namely the patch-clamp technique and observing as well as manipulating optical methods (video-imaging and holographic laser tweezers, respectively) were used to characterise human red blood cells to explore cellular signalling and cellular interactions.

Extracellular signalling molecules such as lysophosphatidic acid, prostaglandin E2 or homocyseine can activate cation channels in the red blood cell membrane. The consecutive calcium influx and accumulation shows a distinct cell to cell variation throughout the red cell population. The calcium signal results in several cellular responses: (i) cell shrinkage due to the Gardos-channel activity, (ii) lipid asymmetry breakdown and phosphatidyl serin exposure to the outer membrane leaflet due to scramblase activity and (iii) irreversible cellular adhesion within individual red blood cells. The adhesion mechanism can just be speculated about. Using atomic force spectroscopy we measured an adhesion force of appoximately 100 pN.

We provide further evidence derived from single cell experiments for the active participation of red blood cells in thrombotic events. In light of an increasing number of clinical indications, especially under pathophysiologica conditions, such as sickle cell disease, thalassemia or dialysis patients, red blood cells may slowly move into the focus of comprehensive pharmacological strategies for preventing such thrombosis related events such as stroke and cardiac infarction.

Platform AZ: Member-organized Session: Disordered and Self-aggregated Peptides and Proteins

2818-Plat

The Evolution of the Natively Disordered Region in P53 Family Proteins

Buyong Ma, Ruth Nussinov.
SAIC-Frederick, NCI-Frederick, NIH, Frederick, MD, USA.

Protein disorder in N- and C-terminal regions is among the major structural factors that coupled to the amino acid evolution in p53. Using three independent predictors of protein disorder (Foldunfold, IUPred, and Foldindex), we found that the percentage of disordered fragments in p53 steadily increases with evolution, which is not the case for p63/p73. The increase in natively disordered segments may help p53 interact with many partners while making it less sensitive to mutational perturbations.

2819-Plat

Conformational Discrepancies Between Molecular Dynamics Force Fields and Vibrational Spectroscopy in Short Alanine-Based Peptides

Daniel Verbaro[1], Indrajit Gosh[2], Werner Nau[2], Reinhard Schweitzer-Stenner[1].
[1]Drexel University, Philadelphia, PA, USA, [2]Jacobs University, Bremen, Germany.

Structural preferences in the unfolded state of peptides determined by molecular dynamics still contradict experimental data. A remedy in this regard has been suggested by MD simulations with an optimized Amber force field ff03* (R. Best and G. Hummer, J. Phys. Chem. B 113, 9004-9015). The simulations yielded a statistical coil distribution for alanine, which is at variance with recent experimental results. To check the validity of this distribution, we investigated the peptide H-A5W-OH, which with the exception of the additional terminal tryptophan is analogous to the peptide used to optimize the force field. Electronic circular dichroism, vibrational circular dichroism, infrared spectroscopy as well as J-coupling constants obtained from NMR experiments were used to derive the peptide's conformational ensemble. Qualitatively, the experimental 3J(HN,Cα), VCD, and ECD indicated a preference of alanine for polyproline II-like conformations. Additionally, Förster-resonance-energy transfer between the terminal fluorophores of another analogous peptide Dbo-A5W-OH was used to determine its average length. In order to check whether the above statistical coil distribution quantitatively accounts for experimental data, we employed an excitonic model to calculate the amide I' profiles of the IR and VCD spectrum of H-A5W-OH as well as the distance between the two terminal peptide carbonyls by using the distribution obtained from ff03*. This led to an underestimated negative VCD couplet and an overestimated distance between terminal carbonyl groups. A better representation of experimental data was desired so we changed the distribution parameters in line with results recently obtained for alanine in GAG. This distribution model satisfactorily reproduced the amide I' profiles, the J-coupling constant and the end-to-end distance of H-A5W-OH, which reinforces alanine's high structural preference for polyproline II.

2820-Plat

The Role of Dynamic Protein Complexes in the Ubiquitin-Proteasome Pathway

Tanja Mittag[1], Stephen Orlicky[2], Xiaojing Tang[2], Frank Sicheri[2], Mike Tyers[3], Julie D. Forman-Kay[4].
[1]St. Jude Children's Research Hospital, Memphis, TN, USA, [2]Samuel Lunenfeld Research Institute, Toronto, ON, Canada, [3]Wellcome Trust Centre for Cell Biology, Edinburgh, United Kingdom, [4]The Hospital for Sick Children, Toronto, ON, Canada.

Intrinsically disordered proteins (IDPs) have been implicated in the regulation of many important cellular processes, such as regulation of cell cycle progression, of transcription and of translation. IDPs are thought to function primarily in the mediation of protein-protein interactions, but detailed analysis of the molecular mechanisms that render disorder beneficial in protein interactions is required. According to a common view, IDPs are usually thought to undergo disorder-to-order transitions upon interaction with their binding partners. It is becoming increasingly clear that predominantly disordered protein complexes

are functionally relevant. We have shown previously that the intrinsically disordered cyclin dependent kinase (CDK) inhibitor Sic1 interacts with the substrate adapter, Cdc4, of its ubiquitin ligase via multiple phosphorylated binding motifs in a dynamic complex. Cdc4 is the substrate recognition subunit of a culin ubiquitin ligase and targets Sic1 for degradation at the G1/S phase transition of the yeast cell cycle. Individual binding motifs in Sic1 are ordered transiently without a global disorder-to-order transition upon binding Cdc4. The dynamic complex allows for engagement of several phosphorylation sites in a dynamic interface resulting in an affinity that depends on the number of phosphorylation sites in an ultrasensitive manner. The dynamic nature of the complex allows for 'counting' of phosphorylation sites via largely electrostatic interactions. The Sic1-Cdc4 interaction therefore acts as a sensor of the concentration of active kinase and the cell cycle status. We continue to use NMR spectroscopy and other biophysical methods to study dynamic interactions in the ubiquitin proteasome pathway with the objective of unraveling nature's repertoire of disorder in protein function. The combination of disorder with multisite phosphorylation may serve as a general means to set thresholds in regulated protein-protein interactions.

2821-Plat
Intrinsic Disorder in the Basic Regions of bZIP Transcription Factors: What it Means to Be Disordered and Why it Might Matter!
Rahul K. Das, Scott L. Crick, **Rohit V. Pappu**.
Washington University, St. Louis, MO, USA.
Intrinsically disordered proteins constitute roughly 30% of the eukaryotic preteome and these include a majority of transcription factors. Our recent work has identified certain organizing principles that have yielded predictive phase diagrams of IDPs. We put these predictions to the test through quantitative studies of disorder in bZIP transcription factors. The results suggest important and novel insights on the evolution of disorder and its implications for DNA binding.

2822-Plat
Intrinsically Disordered Proteins Evolve Differently from Ordered (Structured) Proteins
Celeste J. Brown[1], Gary W. Daughdrill[2], A. Keith Dunker[3].
[1]University of Idaho, Moscow, ID, USA, [2]University of South Florida, Tampa, FL, USA, [3]Indiana University School of Medicine, Indianapolis, IN, USA.
There are important differences between the evolution of disordered and ordered proteins. These differences include the types of acceptable amino acid substitutions and the rates at which those substitutions occur. In general, substitutions for most amino acid types occur more rapidly in disordered versus ordered proteins, and this behavior is attributed to relaxed purifying and positive selection. The lack of sequence conservation in disordered regions does not mean that these sequences are functionally unimportant as evidenced by the frequent conservation of characterized or predicted disorder in various functional domains. Additionally, the pattern of amino acid substitutions observed for disordered proteins provides important functional clues. In particular, the least frequent amino acid types in disordered proteins are the most conserved and this conservation is correlated with burial at the interfaces with interaction partners. There are also distinct compositional and structural differences between disordered and ordered proteins. These differences were observed in the initial investigations of disordered proteins, but refining developments are leading to a deeper understanding of the structure and dynamics of disordered proteins. These recent studies show that disordered proteins have sequence-dependent conformational features ranging from extended random coil to collapsed random coil to molten globule, lending support to the concept of a structural continuum connecting disordered and ordered proteins.

2823-Plat
Negative Design in Protein Coils
Lauren L. Perskie, George D. Rose.
Johns Hopkins, Baltimore, MD, USA.
The classic folding paradigm, established by Anfinsen and others, has been interpreted to mean that under folding conditions, the native fold is selected from an astronomical number of conceivable alternatives by the constellation of favorable interactions among its amino acid sidechains. This plausible idea is entirely consistent with the characteristic close-packing seen in protein crystal structures, where it is apparent that residues distant in sequence are brought together in space, presumably providing both topological specificity and structural stability. Accordingly, organizing interactions are believed to persist into the native state. This supposition is the basis for knowledge-based potentials, Go models, and the like. Contrary to this view, we present evidence from simulations coupled with an analysis of the protein coil library (http://www.roselab.jhu.edu/coil/) that the overall fold is established prior to eventual sidechain close-packing. In this process, chain organization depends not only on selecting favorable interactions but also on rejecting unfavorable ones. Eliminating those interactions that result in steric clashes or unsatisfied hydrogen bonds winnows fold space substantially. Accordingly, such interactions play a crucial role in determining the native state, but given their mode of action, they are not visible in solved structures (like the dog that didn't bark in the night*).
**Gregory (Scotland Yard detective): "Is there any other point to which you would wish to draw my attention?"*
Holmes: "To the curious incident of the dog in the night-time."
Gregory: "The dog did nothing in the night-time."
Holmes: "That was the curious incident."

2824-Plat
Evolution of Structure and Dynamics for a Family of Disordered Proteins
Wade M. Borcherds, Hongwei Wu, Anne T. Pine, Katie M. Mishall, Gary W. Daughdrill.
University of South Florida, Tampa, FL, USA.
Intrinsically Disordered Proteins (IDPs) are frequently found in vital cellular pathways including transcriptional activation and signal transduction. There is however a dearth of atomic models available for IDPs, hampering insight into how the structural ensemble is specified by the amino acid sequence. Nuclear Overhauser Effect (NOE) data was collected from the intrinsically disordered transactivation domain of a series of p53 (p53TAD) orthologues to investigate the conservation of dynamic behavior. The data suggest the presence of recurring but variable structural elements among the orthologues in the region aligning with the ubiquitin ligase MDM2 binding domain of human p53TAD, and to a lesser extent in the region correlating to the RPA binding domain of human p53TAD. The data also show significant variation in the backbone dynamics at these regions. The recurrence of these structural features across evolutionary time as suggested by the NOE data gives some credence to the idea that transient secondary structures within IDPs are constrained, though with possibly varying degrees of dynamic behavior. Future atomic modeling of the structural ensembles of these homologues should allow for a better understanding of the effect of residue similarity on the final structural ensemble in IDPs.

2825-Plat
Transient Protein-Protein Interactions in the IDP Alpha-Synuclein Detected by NMR: Implications for Protein Aggregation
Kuen-Phon Wu, Jean Baum.
Rutgers University, Piscataway, NJ, USA.
BioMaPS Institute for Quantitative Biology and Department of Chemistry and Chemical Biology, Rutgers University, Piscataway, NJ, 08854.
NMR paramagnetic relaxation enhancement experiments (PREs) have been applied to the intrinsically disordered protein alpha-synuclein, the primary protein in Parkinson's disease, to directly characterize transient intermolecular complexes at neutral and low pH as well as ionic strength-dependent solutions at pH 6.0. At neutral pH, we observed weak N- to C-terminal inter-chain contacts that are driven by electrostatic interactions while at low pH, C- to C-terminal inter-chain interactions are significantly stronger and driven by hydrophobic contacts. In addition to the pH-dependent transient self-associated alpha-synuclein complex, we also detected the changes of transient protein-protein interactions of alpha-synyclein in solution at varied [NaCl] (0-500 mM). By using titration-based PRE experiments, we have calculated approximate 6% and 2% transient head-to-tail complexes of alpha-synuclein in solution without and with the addition of 100 mM NaCl, respectively. The results presented here show that ^{1}H NMR paramagnetic relaxation experiments are a powerful tool for visualizing transient low-populated initial encounter complexes in intrinsically disordered proteins. Characterization of these first inter-chain interactions correlated to the aggregation kinetics will provide fundamental insight into the mechanism of amyloid formation.

Platform BA: TRP Channels

2826-Plat
Activation Mechanisms and Molecular Properties of Cyclopiazonic Acid (CPA)-Evoked TRPC Channels in Vascular Myocytes from TRPC1-/- Mice
Anthony P. Albert, Jian Shi, Min Ju, Lutz Birnbaumer, William A. Large.
St. George's, University of London, London, United Kingdom.
Phosphatidyinositol-4,5-bisphosphate (PIP2) has an obligatory role in activating heteromeric TRPC1 subunit-containing channels in vascular myocytes, which also requires protein kinase C (PKC)-mediated phosphorylation of TRPC1 proteins. The aim of the present work was to further investigate these proposed activation mechanisms in freshly isolated mesenteric artery myocytes from TRPC1-/- mice.

In wild-type mice, bath application of cyclopiazonic acid (CPA) and the Ca2+ chelator BAPTA-AM activated cation channel currents with a single unitary conductance of about 2 pS in cell-attached patches, which were inhibited by the PKC inhibitor chelerythrine. In addition, PIP2 and the PKC activator PDBu evoked the same 2 pS cation channels. Using anti-TRPC antibodies as blocking agents, these 2 pS cation channels were identified as heteromeric TRPC1/C5 structures.
In contrast, BAPTA-AM, PIP2 and PDBu did not activate cation channel activity in TRPC1-/- mice. However, CPA did activate cation channel activity in cell-attached patches from TRPC-/- mice, but unlike the channels in wild-type mice these CPA-evoked channel currents had sub-conductance states between 11-55 pS. Furthermore, activities of CPA-induced 11-55 pS channels were potentiated by chelerythrine, and inhibited by both PIP2 and PDBu. Bath application of Ca2+ to the cytosolic surface of quiescent inside-out patches from TRPC1-/- mice also activated 11-55 pS channels. CPA- and Ca2+-activated 11-55 pS channels were identified as being homomeric TRPC5 structures.
These studies provide strong evidence that PIP2 and PKC have key roles in activating TRPC1-containing channels and also indicate that vascular myocytes from TRPC1-/- mice express homomeric TRPC5 channels which are activated by Ca2+-dependent mechanisms.

2827-Plat
Engineering of the TRPC3 Selectivity Filter Identifies a Unique, Dual Signaling Function of TRPC3 in the Heart
Michaela Lichtenegger[1], Michael Poteser[1], Thomas Stockner[2], Hannes Schleifer[1], Christoph Romanin[3], Klaus Groschner[1].
[1]Institute of Pharmaceutical Sciences, Pharmacology and Toxicology, Graz University, Graz, Austria, [2]Institute of Pharmacology, Medical University of Vienna, Vienna, Austria, [3]Institute of Biophysics, University of Linz, Linz, Austria.
Cardiac TRPC3 has been suggested as a crucial upstream component of Ca^{2+}/calcineurin/nuclear factor of activated T cells (NFAT) signaling. The linkage between TRPC-activity and NFAT nuclear translocation may involve either Ca^{2+} entry directly through the TRPC pore or promotion of voltage-dependent Ca^{2+} entry. Here we show that a point mutation in the TRPC3 selectivity filter (E630Q), which disrupts Ca^{2+} permeability but preserves monovalent permeation, abrogates agonist-induced NFAT translocation in HEK293 cells as well as in murine HL-1 atrial myocytes. The E630Q mutation fully retains the ability to translate activation of phospholipase C-linked stimuli into L-type ($Ca_V1.2$) channel-mediated Ca^{2+} entry, which is effectively isolated from the NFAT pathway. We demonstrate a dichotomy of TRPC-mediated Ca^{2+} signaling in the heart involving two distinct pathways that are differentially linked to downstream effectors and gene transcription. Coupling of TRPC3 signaling to NFAT activation is mainly initiated by Ca^{2+} permeation through the TRPC3 pore and recruitment of calcineurin into a TRPC3 signaling microdomain.
supported by FWF, P21925-B19.

2828-Plat
Effects of Extracellular Ca^{2+} on TRPM2 Channel Gating
Balázs Tóth, László Csanády.
Semmelweis University, Budapest, Hungary.
TRPM2 is a non-selective cation channel, which is activated by intracellular ADPR and Ca^{2+}. ADPR binds to the C-terminal NUDT9-H domain of the channel, while the binding sites for Ca^{2+} remain unidentified. In a previous study (*J. Gen. Physiol.*, 133(2):189-203), we demonstrated that extracellular Ca^{2+} has no effect on steady-state channel gating, however, it can slow channel closure in response to sudden removal of intracellular Ca^{2+}. Based on this result, we hypothethized that the Ca^{2+} binding sites are intracellular, but lie near the channel gate, so that upon rapid removal of Ca^{2+} from the cytosolic side Ca^{2+} influx can keep the binding sites saturated, thereby delaying channel closure.
In our present work, we investigated this process in more detail. We used two approaches. First, we attempted to create pore mutants impermeable to Ca^{2+}. We made several aminoacid replacements in the presumed selectivity filter, based on the homologous sequences of two Ca^{2+} impermeable TRPM channels - TRPM4 and TRPM5. Although these mutations affected the Ca^{2+} permeability of the channel only slightly, we found that introduction of negative charges increases channel conductance by about 50%, and considerably reduces the run-down effect observed for wild type channels. Second, we tested whether the effect of extracellular Ca^{2+} on channel closure can be competed by raising extracellular [Na^+]. We indeed found that the ability of 1 mM extracellular Ca^{2+} to slow channel closure upon rapid removal of intracellular Ca^{2+} was largely abolished by the presence of 1 M extracellular Na^+. These results provide new insight into the coupling of Ca^{2+} permeation and gating in TRPM2.

2829-Plat
TRPAI is a Co2 Sensor in Nociceptors
Yuanyuan Wang, Rui B. Chang, Emily R. Liman.
University of Southern California, Los Angeles, CA, USA.
In humans, high concentrations of CO2, as found in carbonated beverages, evoke a mixture of sensations that include a stinging or pungent quality. The stinging sensation is thought to originate with the activation of nociceptors, which innervate the respiratory, nasal, and oral epithelia. The molecular basis for this sensation is unknown. Here we show that CO2 specifically activates a subpopulation of trigeminal neurons that express TRPA1, a mustard oil- and cinnamaldehyde-sensitive channel, and that these responses are dependent on a functional TRPA1 gene. TRPA1 is sufficient to mediate responses to CO2 as TRPA1 channels expressed in HEK-293 cells, but not TRPV1 channels, were activated by bath-applied CO2. CO2 can diffuse into cells and produce intracellular acidification, which could gate TRPA1 channels. Consistent with this mechanism, TRPA1 channels in excised patches were activated in a dose-dependent manner by intracellular protons. We conclude that TRPA1, by sensing intracellular acidification, constitutes an important component of the nociceptive response to CO2.

2830-Plat
Molecular Basis of Thermal Sensitivity of Heat-Activated Vanilloid Receptor ion Channels
Beiying Liu, Jing Yao, **Feng Qin**.
SUNY-Buffalo, Buffalo, NY, USA.
In contrast to a hailstorm of information about voltage- or ligand-dependent gating, our knowledge of temperature-driven gating of ion channels is scarce. Temperature-gated channels, as epitomized by thermally active transient receptor potential (TRP) channels, are necessary for thermal sensation, an ability that is vital to survival and conform-seeking of all living organism. Residing at nerve endings underneath skins, these channels figure a role as biological thermometers for perception of ambient temperature. Here we are concerned with the molecular foundations of thermal sensitivity in heat-sensitive vanilloid receptors. We show that, when exposed to rapid temperature jumps, these homologous channels display markedly different activation kinetics and temperature dependence. We construct chimeric channels at strategic positions to delineate contributions of distinct molecular regions of the channels. We identified a cytoplasmic domain to be essential to temperature gating. Alterations of the region were able to fundamentally change the kinetics and temperature dependence of functional wild-types while rescue the heat response of normally temperature-insensitive isoforms. Other regions of the channels, on the other hand, exhibit negligible chimeric effects on the large energetics of thermal gating, suggesting that the gating by temperature in these channels involves localized structural domains for interaction with ambient temperature.

2831-Plat
The Pore Turret of ThermoTRP Channels is a Portable Domain Contributing to Temperature Sensing
Cui Yuanyuan[1,2], Xu Cao[1,2], Fan Yang[1], KeWei Wang[2], Jie Zheng[1].
[1]UC Davis, Davis, CA, USA, [2]Peking University, HSC, Beijing, China.
ThermoTRP channels sense ambient temperature and function as thermosensor, however, the mechanism for sensitive temperature-dependent activation remains unknown. Recent studies point to the outer pore region as an important gating structure. Our previous study shows pore turret moves substantially during temperature-driven activation, which isn't seen during capsaicin-driven activation. Present research focuses on contribution of pore turret to heat-induced activation using a structural perturbation approach. Partial deletions and sequence replacements are performed with TRPV1 turret. Additionally, the turret is swamped between TRPV1 and TRPV2/TRPV3. All mutant channels exhibit similar capsaicin sensitivity to wildtype TRPV1 with a less than 10-fold shift in EC_{50}, which is consistent with the notion that temperature and ligand activate TRPV1 through different pathways. In contrast, deletion and replacement mutants exhibit activation at a very different temperature, show rapid inactivation during heating, or lose temperature response. Interestingly, TRPV1 chimera containing TRPV3 turret V1/3S behaves like wildtype TRPV3 and activates at a much lower temperature, while TRPV1 chimera containing TRPV2 turret V1/2S activates at a much higher temperature like wildtype TRPV2. These results reveal that pore turret is a portable domain contributing to temperature sensing.

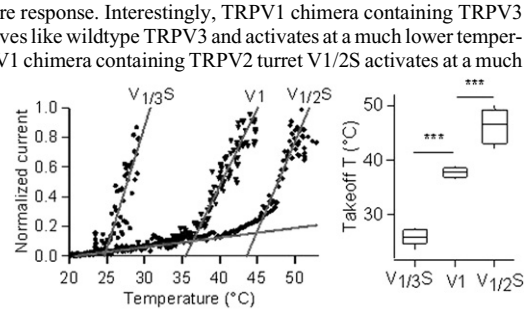

2832-Plat
Identification of a Tetrameric Assembly Domain in the C-Terminus of Heat-Activated TRPV Channels
Feng Zhang[1], Shuang Liu[1], Fan Yang[2], Jie Zheng[2], **KeWei Wang**[1].
[1]Department of Neurobiology & Neuroscience Research Institute, Peking University, Beijing, China, [2]Department of Physiology and Membrane Biology, University of California, Davis, Davis, CA, USA.
Transient receptor potential channels (TRPs) as cellular sensors are thought to function as tetramers. Yet, the molecular determinants governing homotetramerization of heat-activated TRPV1-4 remain largely elusive. In this study, we identified a segment comprising 20 amino acids after the known TRP-like domain in the channel C-terminus that functions as a tetrameric assembly domain (TAD). Purified recombinant C-terminal proteins of TRPV1-4, but not the N-terminus, mediated the protein-protein interaction in *in vitro* pull-down assay. Western blot analysis combined with confocal calcium imaging further demonstrated that the TAD exerted robust dominant-negative effect on wild-type TRPV1. When fused with membrane-tethered peptide Gap43, the TAD blocked the formation of stable homomultimers, and removal of the TAD from the full length TRPV1 resulted in nonfunctional channels. Calcium imaging and current recording showed that deletion of the TAD in a poreless TRPV1 mutant subunit suppressed its dominant-negative phenotype, confirming the involvement of the TAD in assembly of functional channels. Our findings suggest that the C-terminal TAD in heat-activated TRPV1-4 channels functions as a conserved domain that mediates a direct subunit-subunit interaction for tetrameric assembly.

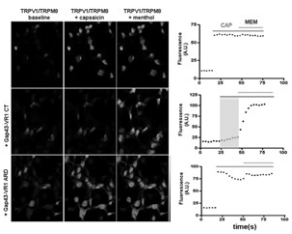

2833-Plat
Complex Regulation of TRPV1 by Phosphoinositides
Viktor Lukacs, Baskaran Thyagarajan, Tibor Rohacs.
UMDNJ, Newark, NJ, USA.
TRPV1 is a nonselective calcium permeable cation channel present in polymodal nociceptors that plays a crucial role in the development of inflammatory pain and thermal hypersensitivity. Plasmamembrane phosphoinositides are recognized as important regulators of TRPV1; the precise nature of their effect is, however, controversial. Recent studies indicate that phosphatidyl inositol (4,5) bisphosphate [$PI(4,5)P_2$] and other phosphoinositides activate TRPV1 in excised patches. In concert with previous studies, we have shown that calcium influx-mediated activation of PLC results in a robust depletion of both phosphatidyl inositol (4) phosphate [PI(4)P] and $PI(4,5)P_2$ and is one of the mechanisms of TRPV1 desensitization. It is difficult however to reconcile these observations with preceding data indicating that $PI(4,5)P_2$ inhibits TRPV1, and relief from this inhibition by GPCR activation-induced PLC activity may contribute to TRPV1 potentiation during inflammation. In the present work we utilize several independent approaches to demonstrate that under specific circumstances TRPV1 currents are inhibited by $PI(4,5)P_2$. We show that selective dephosphorylation of $PI(4,5)P_2$ in the plasma membrane activates, while an increase in $PI(4,5)P_2$ levels inhibits TRPV1 currents elicited by low to moderate, but not high agonist concentrations. We also show that potentiation of whole-cell TRPV1 currents by bradykinin is partially impaired by dialyzing diC8-$PI(4,5)P_2$ as well as the PKC pseudosubstrate inhibitory peptide (19-31) through the pipette. Our data indicate that in addition to the well documented role of PKC-mediated phosphorylation in TRPV1 channel sensitization, $PI(4,5)P_2$ may also be involved in this phenomenon, implying a TRPV1 agonist concentration-dependent dual regulatory effect of $PI(4,5)P_2$. Such dual effects of $PI(4,5)P_2$ have previously been described for voltage-gated calcium channels as well as other TRP channels. Our findings support distinct roles for both activation and inhibition of TRPV1 by $PI(4,5)P_2$ and raise important questions as to the molecular background of the differential effects.

Platform BB: Micro and Nanotechnology; Nanopores

2834-Plat
DNA Translocation Through Graphene Nanopores
Chris Merchant.
University of Pennsylvania, Philadelphia, PA, USA.
We report on DNA translocations through nanopores created in graphene membranes. Devices consist of nanometer-thick graphene membranes with electron-beam sculpted nanopores. Due to the thin nature of the graphene membranes, we observe larger blocked currents than for traditional solid-state nanopores. Unlike traditional solid-state nanopore materials that are insulating, graphene is an excellent electrical conductor. Use of graphene as a membrane material opens the door to a new class of nanopore devices in which electronic sensing and control are performed directly at the pore.

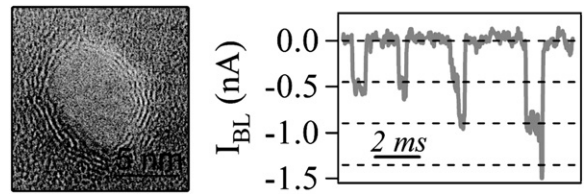

2835-Plat
Using Measurements of the ion Current Through a Synthetic Nanopore to Discriminate Nucleotides in a Single *DNA* Molecule
Deqiang Wang[1], JiWook Shim[1], Winston G. Timp[2], Anthony Ho[3], Aleksei Aksimentiev[3], Gregory Timp[1].
[1]University of Notre Dame, Notre Dame, IN, USA, [2]School of Medicine, Johns Hopkins University, Baltimore, MD, USA, [3]University of Illinois, Urbana, IL, USA.
Sequencing DNA with a nanopore relies on a distinctive electrical signal associated with each nucleobase that develops when a single DNA molecule, immersed in electrolyte, translocates across a membrane through the pore. We show that it is possible to discriminate nucleobases in DNA through measurements of the electrolytic current through a synthetic nanopore. We use a pore smaller in diameter than the double helix, in a silicon nitride membrane 15 nm thick. When an electric field is applied, biotinylated DNA homopolymers bound to streptavidin are impelled into and through the pore, but prevented from full translocation by the large streptavidin molecule at one end. Subsequent long time measurements of the blockade current through the pore reveal distinctive electrical signatures for poly (dA), poly (dC), and poly (dT) on a scale >100pA at high voltage (>100mV); differences much larger than the ~pA-level currents used to discriminate nucleotides in proteinaceous pores like α-hemolysin.

2836-Plat
In Vitro Measurements of Single-Molecule Transport Across an Individual Biomimetic Nuclear Pore Complex
Cees Dekker[1], Stefan Kowalczyk[1], Larissa Kapinos[2], Roderick Y.M. Lim[2].
[1]Delft University of Technology, Delft, Netherlands, [2]University of Basel, Basel, Switzerland.
Nuclear pore complexes (NPCs) regulate the exchange of RNA and proteins between the nucleus and the cytoplasm in eukaryotic cells. We present a new method to investigate NPC transport at the single molecule level. We construct a biomimetic NPC by covalently bonding natively unfolded Phe-Gly rich (FG) domains of human nucleoporins (Nups) to a solid-state nanopore. Trans-pore ionic current measurements provide a probe to monitor single molecules traversing the pore. Importantly, we find that translocation events are indeed observed for transport receptors (Impβ) whereas the passage of non-specific proteins (BSA) is inhibited. A single type of Nups is thus sufficient to form a transport barrier that exhibits the selectivity found in NPCs. We find a translocation time for transporter molecule Impβ of 3 ms for both Nup153 and Nup98, which is 20-fold slower than the passage time through a bare pore, but comparable to in vivo measurements on NPCs. By reproducing key features of the NPC, our biomimetic approach opens the way to study a wide variety of nucleocytoplasmic transport processes at the single-molecule level in vitro.*
*Kowalczyk et al, Nature Nanotechnology, under review

2837-Plat
Integrated Microfluidic Platform for Studies on Membrane Proteins and Drug Screening Assays
Verena Stimberg.
MESA+ Institute for Nanotechnology, Enschede, Netherlands.
The combination of microfluidics with BLM (bilayer lipid membrane) experimentation provides a promising route towards high-throughput screening platforms for studies and drug screening on membrane proteins. The microfluidic format is ideal for multiplexed and automated assays, the miniaturization of the device goes together with enhanced electrical capabilities and more stable bilayers, and dual optical and electrical measurements are possible with a horizontal configuration of the membrane.
In that context, we have developed a sandwich device consisting of two glass substrates separated by a Teflon membrane. The glass substrates contain two independent and orthogonal microfluidic channels being the two fluidic

reservoirs for BLM experimentation; the Teflon film presents a micrometer-size aperture, located at the intersection of the microchannels, and across which BLMs are made. Leakage-free assembly of the three layers is demonstrated using an optical adhesive.

The closed configuration of the device prompted us to develop a novel methodology for BLM preparation. Lipid solution and buffer are successively flushed in both channels, so that the lipid plug deposited in the aperture spontaneously thins into a bilayer. BLM formation is monitored electrically (patch-amplifier) and optically ((fluorescence) microscopy). This lipid-plug-thinning technique gives highly stable BLMs (> 7 hrs lifetime) with an almost 100% success yield. The resulting membranes exhibit reproducible characteristics in terms of sealing quality (14 ± 4 giga-ohm) and surface area (~80% aperture coverage, measured optically and electrically (10 ± 3.4 pF capacitance)). Insertion of alpha-hemolysin (in the BLM) confirms the formation of a bilayer structure and demonstrates the potential of the platform for single protein measurements.

We will present the detailed fabrication of the microfluidic platform, BLM formation and characterization in the closed environment, and on-chip single proteins studies using optical and electrical techniques.

2838-Plat

Interfacial Tension Controlled Fusion of Individual Femtoliter Droplets and Triggering of Confined Chemical Reactions on Demand

Charles P. Collier, Scott T. Retterer, Seung-Yong Jung.
Oak Ridge National Laboratory, Oak Ridge, TN, USA.

Droplet-based microfluidic platforms offer many opportunities to confine chemical and biochemical reactants in discrete ultrasmall reaction volumes, and investigate the effects of increased confinement on reaction dynamics. Current state-of-the-art microfluidic sampling strategies for creating ultrasmall reaction volumes are predominately steady-state approaches, which result in difficulty in trapping reacting species with a well-defined time-zero for initiation of biochemical reactions in the confined space. This talk describes stepwise, on-demand generation and fusion of femtoliter aqueous droplets based on interfacial tension. Sub-millisecond reaction times from droplet fusion were demonstrated, as well as a reversible chemical toggle switch based on alternating fusion of droplets containing acidic or basic solution, monitored with the pH-dependent emission of fluorescein.

2839-Plat

Elucidation and Control of the Hybridization Chain Reaction

Victor A. Beck, Justin S. Bois, Robert M. Dirks, Niles A. Pierce.
Caltech, Pasadena, CA, USA.

We previously introduced hybridization chain reactions (HCR), in which metastable DNA hairpins undergo conditional self-assembly to form long nicked double-stranded 'polymers' in the presence of a DNA initiator molecule (RM Dirks and NA Pierce, PNAS 2004, 10, 15275). HCR systems have been engineered to function as orthogonal in situ amplifiers for multiplexed bioimaging (HMT Choi et al., Nat Biotech, in press) and as programmable mechanical transducers for selectively killing cultured human cancer cells (S Venkataraman et al., PNAS 2010, 107, 16777). Here, we model the equilibrium and kinetic properties of HCR, revealing sources of non-ideal behavior and methods for controlling system performance. Our results demonstrate that HCR is accurately modeled as a living alternating copolymerization.

2840-Plat

Precise Transfection Control of Cell Reprogramming Factors via a High Throughput Electroporation System

Ebrahim Ghafar-Zadeh, Erh-Chia Yeh, Chi-cheng Fu, Luke P. Lee.
University of California, Berkeley, Berkeley, CA, USA.

There is great interest in reprogramming of human fibroblasts to induced pluripotent stem (iPS) cells as an autologous cell source for therapeutic applications, but the utility of iPS Cells is hampered by the use of viral delivery systems. We demonstrate the ability to reprogram the cells by transducing the transcription factors including Oct4 via electroporation method (EPM). A major drawback of conventional EPMs is high cell mortality and low efficiency. To overcome these limitations, we are using a novel hybrid microfluidic/thin film transistor system (μF-TFTS) to precisely control the electroporation potential for each individual cell. Here, we present the recent works on the characterization of μF-TFTS for electro-transfecion of cell reprogramming factors. We search for optimum electrical with accuracy of 0.003% over dynamic range to transfect a certain cell programming factor into single cells using μF-TFTS. We perform the electroporation on 60,000 sample five different factors (PI, DAPI, Oct4) in a few second. This technologically integrated approach offers new prospects for understanding the biophysical complexity of cell reprogramming as well as cell behaviors in a precisely controllable electrical field using a high throughput and rapid EMP system.

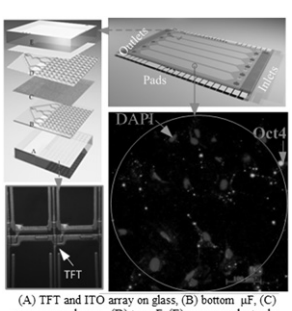

(A) TFT and ITO array on glass, (B) bottom μF, (C) porous membrane, (D) top μF, (E) common electrode.

2841-Plat

A pore-Cavity-Pore Device to Trap and Investigate Single Nano-Scale Objects in Femto-Liter Compartments: Confined Diffusion and Narrow Escape

Martin Langecker, Daniel Pedone, Robin D. Nagel, Friedrich Simmel, Ulrich Rant.
Technische Universität München, Garching, Germany.

Spatial confinement from the nano- to the micro-scale is ubiquitous in nature. Striving to emulate biological compartmentalization and to understand the fundamental physical behavior of molecules in confined domains, micro- and nano-structuring techniques have been used extensively to create artificial devices comprising liquid-filled compartments and channels. In addition, the development of robust solid-state structures, which allow for the observation and manipulation of single nano-scale objects is key for the realization of future lab-on-chip devices with improved functionality.

Here we introduce an electrically addressable nano-fluidic silicon device that consists of two stacked nanopores forming the in/outlets to a pyramidal cavity of micrometer dimensions, i.e. femto-liter volume. The electrical properties of the PCP structure are investigated by impedance spectroscopy. Furthermore, we present a FEM simulation of the electric field inside the device. We then demonstrate how individual fluorescent nano-particles and DNA can be actively (by electrical means) and passively (entropically driven) loaded into, trapped inside, and unloaded from the 'pore-cavity-pore' (PCP) device.

A fundamentally important problem in biology is the escape of nano-objects from a micro-domain through a small opening (narrow escape problem). Using the PCP device it is possible for the first time to obtain data on the narrow escape time under well-defined geometrical and experimental conditions. Single particle tracking and residence time data are presented and quantitatively compared to random walk simulations and analytical theories on confined diffusion and the narrow escape problem. Furthermore, we extend the escape studies towards polymeric analytes like DNA.

Symposium 20: Single Molecule Biophysics of the Central Dogma

2842-Symp

Single Molecule Probing of Helicase Dynamics

Sua Myong.
Univ of Illinois, Urbana - Champaign, Urbana, IL, USA.

Helicase is an important genome caretaker protein which plays a central role in biological processes including replication, transcription, recombination and repair of DNA. Helicase, by definition is an enzyme which unwinds a duplex nucleic acid into its single strand components. However, many helicases found in biological systems are not processive unwindases. We have employed single molecule fluorescence detection techniques to unveil detailed mechanism of noncanonical helicases which perform unique translocation activities.

Using single molecule FRET, we discovered an unexpected shuttling motion of an e. coli protein, Rep. The ATP-driven repetitive translocation of Rep on single stranded DNA was visualized as a sawtooth pattern of FRET change. Furthermore, we showed that the repetitive motion may play a functional role of maintaining single strand DNA free of unwanted protein such as recombination protein, RecA (1).

We have developed a newly developed single molecule fluorescence method, termed "protein induced fluorescence enhancement" (PIFE) to probe a translocation activity of an antiviral receptor protein, RIG-I. The translocation was inhibited by its own N-terminal CARD domain whereas the inhibition was completely lifted by a viral mimic RNA which contained unique pathogenic signatures. Our result demonstrates how RIG-I exhibits an exquisite mechanism to self-regulate its activity by sensing the pathogenic moiety (2).

Reference

1. S. Myong, I. Rasnik, C. Joo, T. M. Lohman, T. Ha, Nature 437, 1321 (Oct 27, 2005).
2. S. Myong et al., Science 323, 1070 (Feb 20, 2009).

2843-Symp
Forward and Backward Motion of Replicative Polymerases and Their Coupling with the Helicase
Vincent Croquette[1], Maria Manosas[1], Fangyuan Ding[1], Michelle Spiering[2], Stephen Benkovic[2].
[1]CNRS, Paris, France, [2]Penn State, University Park, PA, USA.
While quantitative data has been obtained on helicases and polymerase working in primer extension, a detailed analysis of these polymerases in the strand displacement configuration is missing. We investigate polymerases and their helicase coupling in single molecule assays using a DNA hairpin in an unzipping configuration. In this simple fork model we assist these enzymes by an external force which provides a control parameter. If we apply 15 pN force on both strands of the DNA hairpin, it opens mechanically. Modulating the force between 0 and 15pN is a mean to assist a molecular motor opening the fork and thus to replace a partner in the collaborative work. Using this assay with different polymerases, we find that their exonuclease activity is responsible for the generally accepted statement that they do not work in strand displacement. We show that strand displacement polymerization is possible with if assisted.
This finding leads to a Cyclic Polymerase Assay where a polymerase is periodically switched from olymerization to strand degradation by force modulating. Such an assay allows us to characterize the different polymerase phases (synthesis and exonuclease phases) as a function of force and propose a minimal model for T4 and T7 polymerases. Moreover, this assay can be used for a single molecule version of the Sanger sequencing.
The same assay can also be carried out to study the coupling between helicase and polymerase. We find that the coupled system is very efficient and advances at maximum rate without showing any pauses or fork regression, in stark contrast to the case of the isolated polymerase. We explain these results by a collaborative model where both the helicase and the polymerase are described by the Betterton-Julicher helicase model.

2844-Symp
The Price of Being Right: Transcript Elongation, Backtracking, and Post-Incorporation Proofreading
Stephan W. Grill.
Max Planck Institute for the Physics of Complex Systems, Dresden, Germany.
RNA polymerases have evolved a proofreading mechanism by which they are able to remove copy errors already incorporated into the transcript. Though the theoretical basis for calculating the fidelity gain was established over 30 years ago, little is known of the effects of this mechanism on overall transcriptional performance. To address this we integrate kinetic proofreading with RNA chain elongation, and show that the fact that the polymerase removes already inserted bases during proofreading puts strict bounds on the achievable fidelity. Through stochastic modeling we elucidate the precise interplay between transcriptional fidelity, velocity, and energy consumption. We highlight how specific design choices are essential for reaching the experimentally measured fidelity. Our work offers a functional interpretation of the broad distribution of pauses times observed for transcribing polymerases in terms of the direct consequence of an efficient transcription process.

Symposium 21: Mechanotransduction at the Cellular Level: Detection and Response

2846-Symp
TRP Channels and Cell Mechanosensitivity
Ching Kung.
University of Wisconsin, Madison, WI, USA.
All cells respond to osmotic and mechanical forces. The rapid responses are attributed to certain ion channels. The prokaryotic MscL and MscS open by bilayer stretch force to release solutes, relieving osmotic stress in rain. In eukaryotes, some members of the transient-receptor-potential channel superfamily such as the TRPV4 of animals and TRPY1 of the budding yeast are mechanosensitive. Rat TRPV4s in patches, excised from expressing Xenopus oocytes, open instantly upon membrane stretch. This observation makes it unnecessary to invoke a mechanosensitive enzyme that produces a ligand to open TRPV4. Bone constantly gauges its weight load. Unloading osteoporosis develops in bed-ridden patients or astronauts in microgravity. Mice deleted of TRPV4 do not show unloading osteoporosis. Constitutive TRPV4 activities due to "gain-of-function" mutations cause severe bone-development and other problems in human. Recent findings on TRPV4 mutations will be reviewed. Whether the lipid bilayer or the cytoskeleton opens animal channels is an interesting question. I will also review evidence, the bulk of which points to a protective role of the cytoskeleton that prevents instead of causes channel opening.

2847-Symp
Sensory Mechanisms in Mammalian Touch Receptor Cells
Ellen A. Lumpkin.
Columbia University, New York, NY, USA.
The sense of touch is critical for hand dexterity that allows mammals to recognize and grasp objects. Different qualities of touch are encoded by sensory neurons with distinct properties. Shapes and curvature are encoded by Merkel cell-neurite complexes, which mediate slowly adapting type I (SAI) responses. Merkel cells, which cluster in fingertips and other highly touch-sensitive skin areas, are enigmatic epidermal cells first described in 1875. The role that these cells play in SAI responses has been debated for 40 years.
Based on morphology, Merkel cells are proposed to be mechanosensory cells. If so, Merkel cells should 1) transduce force into membrane-potential changes that gate voltage-activated ion channels and 2) signal afferent neurons through synaptic transmission. Functional studies testing these predictions in intact skin have produced conflicting results. To tackle these questions, my laboratory uses a combination of mouse genetics, in vitro systems and intact electrophysiological recordings. Our in vitro studies have demonstrated that Merkel cells are intrinsically force-sensitive and that voltage-activated channels open downstream of mechanical stimuli. Moreover, Merkel cells express numerous ion channels and presynaptic proteins. Collectively, these results suggest that Merkel cells are capable of serving as touch receptor cells and pave the way to discover transduction mechanisms.
To determine whether Merkel cells are necessary for touch responses, we used Cre-loxP technology to generate mice that completely lack Merkel cells in the body skin. We then used an ex vivo skin-nerve preparation to survey the classes of touch-sensitive afferents in the saphenous nerve. Although we found no significant differences in nociceptive sensory fibers, we observed a complete loss of SAI responses among light-touch receptors in mice lacking Merkel cells compared with wild-type mice. These results demonstrate that Merkel cells are required for appropriate sensory coding of light touch.

2848-Symp
Mechanotransduction and Developmental Control
Donald Ingber.
Harvard University, Boston, MA, USA.
This lecture will focus on the molecular basis of cellular mechanotransduction, how mechanical forces contribute to embryogenesis, and how physical forces influence tissue physiology. In addition, I will describe recent development of novel human organ-on-a-chip microdevices that can be used to study cellular mechanotransduction in a more physiologically relevant context.

Minisymposium 4: Non-Equilibrium Statistical Mechanics: Theory & Experiment

2850-MiniSymp
Thermodynamic Efficiency Out of Equilibrium
David Sivak, Gavin Crooks.
Lawrence Berkeley National Laboratory, Berkeley, CA, USA.
Much research effort focuses on understanding the thermodynamics, and in particular the efficiency, of molecular-scale machines such as the linear motor kinesin or the rotary F0F1-ATPase. Notably, molecular machines typically operate far from thermodynamic equilibrium, limiting the applicability of equilibrium statistical mechanics. Thermodynamic length analysis, a nonequilibrium framework based on the differential geometry of macroscopic thermodynamics, relates a non-equilibrium property (dissipation) to equilibrium properties (equilibrium fluctuations and their relaxation time). It thus promises a computationally and experimentally tractable method to understand non-equilibrium thermodynamic efficiency. Herein we demonstrate that the thermodynamic length framework follows directly from the assumptions of linear response theory. Uniting these two frameworks promises the dual advantages of providing thermodynamic length analysis a firmer statistical mechanical grounding, and equipping linear response theory with a metric structure to facilitate the prediction and discovery of optimal (minimum dissipation) paths in complicated free energy landscapes. To explore the applicability of this theoretical framework, we examine its accuracy for simple bistable systems, parametrized to model single-molecule force-extension experiments. Through analytic derivation of the equilibrium fluctuations

and numerical calculation of the dissipation and relaxation time, we verify that thermodynamic length analysis (though derived in a near-equilibrium limit) provides a strikingly good approximation even far from equilibrium, and thus provides a useful framework for further study of biomolecular motor efficiency.

2851-MiniSymp

Adaptive Steered Molecular Dynamics: Unfolding of Neuropeptide Y and Decaalanine Stretching

Gungor Ozer[1], Stephen Quirk[2], **Rigoberto Hernandez**[1].
[1]Georgia Institute of Technology, Atlanta, GA, USA, [2]Kimberly-Clark Corporation, Atlanta, GA, USA.

The energetics of an unfolding event can be obtained using steered molecular dynamics (SMD) and Jarzynski's inequality with the cost of the calculation increasing dramatically with the length of the path. An adaptive algorithm has been introduced* that allows for the path to be nonlinear and staged while reducing the computational cost. The potential of mean force (PMF) obtained for neuropeptide Y (NPY) in water along an unfolding path confirmed that the monomeric form of NPY adopts the pancreatic-polypeptide (PP) fold. Adaptive SMD can also be used to reconstruct the PMF obtained earlier for stretching decaalanine in vacuum[#] at lower computational cost. The PMF for stretching decaalanine in water solvent (using the TIP3P water potential) at 300K has now been obtained using adaptive SMD. Not surprisingly, the stabilization from the water solvent reduces the overall work required to unfold it. However, the PMF remains structured suggesting that some regions of the energy landscape act partially as doorways.

*G. Ozer, E. Valeev, S. Quirk and R. Hernandez, *J. Chem. Theory Comput.* (2010), doi:10.1021/ct100320g.
[#]S. Park and K. Schulten, *J. Chem. Phys.***120**, 5946 (2004).

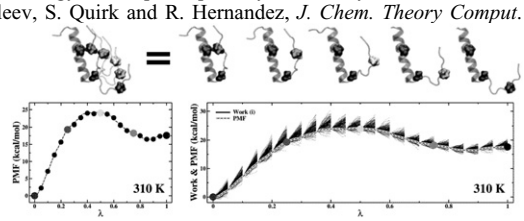

2852-MiniSymp

Non-Equilibrium Work Dissipation in Mechanical Unfolding of Large RNAS

Pan T.X. Li.
University at Albnay, SUNY, Albany, NY, USA.

Non-equilibrium thermodynamics is indispensible in studying mechanical unfolding of single RNA molecules. In a typical experiment, single RNA molecules are pulled and relaxed at fast loading/unloading rate that structure transitions occur under non-equilibrium. Work dissipation is reflected by hysteresis between forward and reverse trajectories in force-extension curve. Ligand and protein binding can stabilize a specific domain within a large RNA, which further complicates work dissipation in mechanical unfolding. Using experiment and simulation, we examined mechanical unfolding of large RNAs containing secondary and tertiary folding. The RNAs follow hierarchical folding pathways. Secondary structure forms before tertiary contacts, and tertiary interaction is disrupted before unfolding of secondary structure. Factors that selectively bind and stabilize tertiary structure lead to increased work dissipation by protecting secondary structure from unfolding. Furthermore, work dissipation is quantified as a function of pulling rate and factor binding.

2853-MiniSymp

Atomistic Simulations of the Force-Induced Dissociation of Retroviral RNA Kissing-Loops

Alan A. Chen, Angel E. Garcia.
Rensselaer Polytechnic Institute, Troy, NY, USA.

Retroviruses require two copies of their ssRNA genomes in order to form infectious virus particles. This is accomplished via a Dimerization Initiation Site (DIS), which forms a rivet-like ''kissing-loop'' that binds the two genomes together. Retroviral DIS kissing-loops have been shown to be unusually resistant to heat denaturation or mechanical pulling, given the small number (2-6) of Watson-Crick base-pairs involved. High mechanical stability is apparently required for retroviral fitness, as mutations that destabilize the DIS loop in-vitro also result in greatly reduced virus infectivity rates in-vivo. DIS kissing-loops are therefore attractive targets for antiretroviral therapeutic design; however, we must first understand the physical determinants that give rise to enhanced DIS kissing-loop stability.

The Moloney Murine Leukemia Virus (MMLV) serves as a particularly tractable model system due to its simplicity, as it composed of two GACG tetraloops held together by just two intermolecular base-pairs. Single-molecule pulling experiments (by Pan Li at SUNY Albany) have shown that it requires as much force to break these two loop-loop base pairs as is required to unfold an entire 11-bp hairpin. Using a combination of equilibrium and non-equilibrium all-atom molecular dynamics simulations, we have developed a detailed model for the kinetic intermediates of the force-induced dissociation of the MMLV DIS kissing-loop. We find that the transition state geometry allows for an equal distribution of the applied force among all of the intermolecular hydrogen-bonds, which is intrinsically more stable that the sequential h-bond breaking exhibited by simple RNA hairpins. In addition, we observe that stacking interactions with adjacent, unpaired loop adenines are able to further stabilize the complex, and that the breaking of these stacking interactions are the rate-limiting step for force-induced dissociation of the MMLV DIS complex.

2854-MiniSymp

An Intrusive Entropic Barrier Induced by Force

Ronen Berkovich[1], Sergi Garcia-Manyes[1], Joseph Klafter[2], Michael Urbakh[2], Julio M. Fernandez[1].
[1]Columbia University, New-York, NY, USA, [2]Tel Aviv University, Tel Aviv, Israel.

Single-molecule force spectroscopy has opened up new approaches to the study of protein dynamics. For example, an extended protein folding after an abrupt quench in the pulling force was shown to follow variable collapse trajectories marked by well-defined stages that departed from the expected two-state folding behavior that is commonly observed in bulk. Here, we explain these observations by developing a simple approach that models the free energy of a mechanically extended protein as a combination of an entropic elasticity term and a short-range potential representing enthalpic hydrophobic interactions. The resulting free energy of the molecule shows a force-dependent energy barrier of magnitude, $\Delta E = \epsilon(F - Fc)^{3/2}$, separating the collapsed state of the molecule from a force-driven extended conformation, that vanishes at a critical force Fc. By solving the Langevin equation under force quench conditions, we generate folding trajectories corresponding to the diffusional collapse of an extended polypeptide that mimics those observed experimentally. Further we apply this model to force extension conditions in order to investigate the role played by the force-induced energy barrier on the two-state hopping phenomena that has been observed in single protein molecules placed under a stretching force. Langevin dynamics across such force induced barrier readily demonstrates the hopping behavior observed for a variety of single molecules placed under force. Our model interprets AFM force-clamp data and accounts as well for force-extension and hopping observed in optical tweezers, thus unifying the field of protein force spectroscopy. Moreover, given that this barrier does not exist at zero force, extrapolating hopping trajectories to zero force could not be compared to bulk measurements.

2855-MiniSymp

Building Stochastic Feedback Models from Limited Data; A Maximum Entropy-Based Solution

Steve Presse.
University of California, San Francisco, South San Francisco, CA, USA.

We present a general, maximum entropy-based method for modeling stochastic feedback dynamics of small chemical and biochemical systems. Our method, Maximum Caliber, uses experimental data in the form of dynamical averages and correlations to construct ensembles of system trajectories. These theoretical ensembles are used to infer long-time dynamics from short-time trajectories. In particular, the method does not have to invoke complex reaction schemes to predict dynamical features such as multistability. On the other hand, traditional stochastic modeling methods often require knowledge of rates and reaction networks. Such parameters are rarely validated independently of the experimental curve-fitting. Maximum Caliber requires both fewer assumptions regarding the reaction network and fewer parameters to capture the effects of feedback. We demonstrate the principle on the genetic toggle switch and the circadian clock.

Platform BC: Interfacial Protein-Lipid Interactions

2856-Plat

Lung Surfactant Peptide-Mimic KL4 Improves Reversibility of Synthetic Model Lung Surfactant Collapse Behavior

Niels Holten-Andersen[1], Phillip W. Miller[1], Alan J. Waring[2], Frans J. Walther[3], **Ka Yee C. Lee**[1].
[1]The University of Chicago, Chicago, IL, USA, [2]UCLA and UC Irvine, Los Angeles and Irvine, CA, USA, [3]LA Biomedical Research Institute, Harbor-UCLA, Torrance, CA, USA.

We have investigated the origin of the effect of the peptide KL4 on lung surfactant lipid monolayers containing DPPC and POPG. Using surface balance techniques, fluorescence microscopy and atomic force microscopy we

have observed that KL4 containing monolayers demonstrate an increased tolerance to repeated compression and expansion due to a softening in folding collapse behavior caused by direct interactions with POPG. This change in folding dynamics leads to increased monolayer reversibility due to almost complete reincorporation of folds upon expansion. We will discuss the potential role of KL4 in lowering the resistance to in-plane shear in POPG containing monolayers in the context of the overall importance of collapse mode in establishing robust and reversible synthetic model lung surfactant.

2857-Plat

Exploring Supramolecular Aspects of the Effect of Sphingomyelinase D On Sphingomyelin-Containing Membranes

Kerstin Wagner[1], Blanca Ramos-Cerrillo[2], Roberto P. Stock[2], Luis A. Bagatolli[1].
[1]University of Southern Denmark, Odense M, Denmark, [2]National Autonomous University of Mexico, Cuernavaca, Mexico.

Lipid-modifying enzymes play a vital role in the regulation of lipids as mediators of cell function. At the same time, the activity of these enzymes is highly affected by the lipid membrane structure. These processes at lipid membranes can be observed in situ through the application of different biophysical techniques. Thus, we are investigating a spider venom enzyme termed sphingomyelinase D (SMD). SMD hydrolyses sphingomyelin (SM) into ceramide-1-phosphate (Cer-1-P). While SM is an integral constituent of many cell membranes, Cer-1-P occurs in very low concentrations and is suggested to be a novel lipid second messenger. At present, the physiologically relevant mechanism following Cer-1-P formation by SMD is incompletely understood, but possibly related to the modulation of membrane properties.

Our results show a strong dependency of SMD activity on the phase state of the substrate. SMD is two orders of magnitude more active towards fluid- than gel-phase liposomes. The presence of cholesterol evens out this difference in activity at an intermediate level. The effect of SMD on fluid-phase giant unilamellar vesicles (GUVs) is observed by confocal fluorescence microscopy. GUVs composed of lauroyl-SM show a macroscopic domain formation and/or shrinking and buckling accompanied by the multiple formation of membrane tubes. GUVs composed of egg-SM display a beveling of the membrane and the formation of caps (outside curvature) approx. three days after the addition of SMD. Which membrane morphology evolves is likely a question of enzyme kinetics vs. the dynamics of lipid reorganization.

GUVs of raft-like mixtures exhibit a single homogenous phase after the addition of SMD. The consequences of SMD activity and Cer-1-P formation on cellular systems are currently being examined. This will indorse the correlation between enzymatic activity and membrane structure influencing the regulation of physiological processes.

2858-Plat

Protein-Lipid Interactions Shaping the Electrostatic Membrane Search of a Pleckstrin Homology Domain

Anna R. Chase[1], Jefferson D. Knight[1,2], Joseph J. Falke[1].
[1]University of Colorado-Boulder, Boulder, CO, CO, USA, [2]University of Colorado-Denver, Denver, CO, USA.

The membrane-targeting domains of peripheral proteins play an important role in mediating cell signaling events originating at the plasma membrane. The pleckstrin homology (PH) domain is the most common membrane targeting domain, and many PH domains specifically recognize membrane-bound PIP lipids. Recently, the representative PH domain of the General Receptor for Phosphoinositides (GRP1 PH) has been found to use an electrostatic search mechanism requiring anionic background lipids of the plasma membrane to more rapidly and tightly bind the rare phosphatidylinositol-3,4,5-phosphate (PIP_3) lipid second messenger. The contributions of the seven basic residues on the GRP1 PH membrane-proximal face to the protein-lipid interactions that occur during electrostatic searching were investigated. Point and double mutants of the isolated Grp1 PH domain were purified with alanine replacing each of the seven basic residues. For each mutant domain, the relative affinities for phosphatidylinositol-(3,4,5)-trisphosphate (PIP_3) were determined in the presence and absence of anionic background lipids. While the wild-type PH domain displays a ~10-fold enhanced affinity for PIP_3 in the presence of anionic background lipids, this enhancement is significantly decreased in the point and double mutant PH domains possessing the R322A and K279A mutations. Thus far, the results suggest that while most basic residues interact with the membrane at a detectable level, the protein-lipid interactions between basic residues R322 and K279 and the membrane are most crucial to electrostatic searching. Additional experiments are in progress to determine the specificity of these protein-lipid interactions, and the effect of mutations on membrane binding kinetics.

2859-Plat

Binding Affinities of WT and H93R PTEN to Lipid Membranes Containing PS and PI(4,5)P_2

Siddharth Shenoy[1], Arne Gericke[2], Alonzo Ross[3], Mathias Lösche[1,4].
[1]Carnegie Mellon University, Pittsburgh, PA, USA, [2]Kent State University, Kent, OH, USA, [3]University of Massachusetts Medical School, Worcester, MA, USA, [4]NIST Center for Neutron Research, National Institute of Standards and Technology, Gaithersburg, MD, USA.

PTEN is a phosphatidylinositolphosphate (PIP) phosphatase frequently mutated in human cancer [1]. By lowering PI(3,4,5)P_3 levels in the plasma membrane, it functions as an antagonist to PI3-kinase in the regulatory circuit that controls cell proliferation and survival. wt PTEN has only weak affinity to zwitterionic phosphatidylcholine (PC) membranes but a strong interaction with anionic lipids. Its C2 domain was shown to bind in a Ca^{2+} independent manner to phosphatidylserine (PS) and phosphatidylglycerol (PG), whereas a short N-terminal domain binds specifically to PI(4,5)P_2 [2,3]. H93R PTEN is an autism related mutant which has decreased phosphatase activity [4].

Using Surface Plasmon Resonance (SPR), we characterized the affinity of wt and H93R PTEN to tethered bilayer lipid membranes (tBLMs) that contain PC and PS, PC and PI(4,5)P_2, and PC, PS and PI(4,5)P_2. As compared with wt PTEN, we find that the H93R mutation is sufficient to cause significant changes in the protein's association with lipid membranes. H93R PTEN has a stronger affinity to membranes containing PS than wt PTEN. PI(4,5)P_2 enhances the apparent binding constant for both proteins and leads to intriguing binding kinetics of the protein to the membrane. The binding of either protein to membranes containing both PS and PI(4,5)P_2 shows a biphasic behavior, suggesting two independent binding sites. This supports the hypothesis of non-competitive binding of the protein to PS and PI(4,5)P_2 [5]. We estimate and compare the amount and the thickness of the adsorbed protein layers which is further investigated in neutron reflectivity experiments.

1) Shaw et al., Nature (2006) 441, 424-430
2) Lee et al., Cell (1999) 99, 323-334
3) Das et al., PNAS (2003) 100, 7491-7496
4) Redfern et al., Protein Science (2010) 19, 1948-1956
5) Redfern et al., Biochemistry (2008) 47(7), 2162-2171

2860-Plat

A Proline Kink in GWALP23

Roger E. Koeppe II.,[1], Johanna M. Froyd-Rankenberg[1], Vitaly V. Vostrikov[1], Christopher D. DuVall[1], Denise V. Greathouse[1], Christopher V. Grant[2], Stanley J. Opella[2].
[1]University of Arkansas, Fayetteville, AR, USA, [2]University of California, San Diego, La Jolla, CA, USA.

GWALP23 (acetyl-GGALW^{5}LALALALALALW^{19}LAGA-ethanolamide) is a proven model membrane-spanning peptide (see JACS 130, 12584) that moves "beyond" WALP family peptides by employing, for the purpose of interfacial anchoring, only one tryptophan residue on either end of a central alpha-helical core sequence. Because of its systematic behavior in lipid bilayer membranes of differing thickness (see JBC 285, 31723), we utilize GWALP23 as a framework for introducing guest residues within the transmembrane sequence. For example, we have incorporated a central proline residue to give acetyl-GGALW^{5}LALALAP^{12}ALALALW^{19}LAGA-ethanolamide. We have synthesized the resulting GWALP23-P12 with selected ^{2}H and ^{15}N labels for solid-state NMR spectroscopy, to enable analysis of the peptide orientation and segmental tilt in oriented lipid bilayer membranes using combined (^{2}H)-GALA and (^{15}N/^{1}H)-PISEMA methods. In DMPC bilayer membranes, the peptide segments N-terminal and C-terminal to proline are tilted substantially with respect to the bilayer normal, by about 34°-40° and 27°-29° (± 6°), respectively, with a proline-induced kink angle of 20°-23°. The proline places restrictions on the dynamics of both segments. As has been described previously for GWALP23, the C-terminal helix ends before Ala-21.

2861-Plat

Rhodopsin - Rhodopsin Oligomerization in Model Lipid Bilayers - Functional Implications

Olivier Soubias, Walter E. Teague, Kirk G. Hines, Klaus Gawrisch.
NIH, Rockville, MD, USA.

We studied rhodopsin oligomerization as a function of rhodopsin concentration and lipid composition and related oligomerization to shifts in rhodopsin function. In the rod outer segment disks of the retina, rhodopsin is densely packed in phospholipid bilayers with a high content of polyunsaturated acyl chains. In model membranes, increasing rhodopsin packing density was linked to a shift in the metarhodopsin-I (MI)/metarhodopsin-II (MII) equilibrium towards MI as well as to lower rates of MII formation. We reconstituted rhodopsin into various phosphatidylcholine bilayers at rhodopsin/lipid ratios ranging from 1:1,000 to 1:70 and followed rhodopsin oligomerization by cross linking of rhodopsin

and changes in lipid-rhodopsin interactions by ^{2}H NMR. The amount of MII formed after photoactivation was determined by UV/vis spectroscopy and the rate of transducin activation studied with a GTPγS-assay. At low rhodopsin concentrations (1/300 and lower) rhodopsin appears to be predominantly monomeric. At rhodopsin/lipid ratios higher than 1/300, the level of oligomerization increases in a highly cooperative fashion with concentration such that at physiological concentrations rhodopsin is mostly oligomeric. Protein function correlated tightly with rhodopsin oligomerization. Data on the influence of bilayer properties on the monomer - oligomer transition of rhodopsin and the rate of transducin activation will be presented.

2862-Plat
Effects of Membrane Geometry on Voltage-Gated ion Channel Distribution Studied with a Model System
Sophie Aimon, Gilman Toombes, Domanov Yegor, Patricia Bassereau.
Institut Curie, paris, France.
Voltage-gated ion channels are inhomogeneously distributed between the highly curved axons and distal dendrites and the relatively flat soma and proximal dendrites. To investigate the effects of membrane geometry on channel distribution and diffusion, we developed a model system based on membrane nano-tubes connected to cell-sized Giant Unilamellar Vesicles (GUVs). KvAP, a bacterial analog of eukaryotic Kv channels [1], was purified, fluorescently labeled and reconstituted into GUVs. Channel density and homogeneity in GUVs were quantified via confocal microscopy while patch-clamp was used to measure the activity of the reconstituted channels. To study the effect of membrane curvature, we pulled a membrane nano-tube from a GUV and could set the tube radius between 10 nm and 200 nm by varying the tension of the GUV membrane. The concentrations of channels in the tube and GUV were measured via confocal microscopy while diffusion was measured by tracking individual channels labeled with quantum dots. As the tube radius decreased, the channel concentration increased while the diffusion coefficient decreased. Results obtained with this model system should give insight into the diffusion of membrane proteins into and out of synaptic boutons.
[1] Ruta et al., Nature 2003, 422 : 180-185.

2863-Plat
The Role of Cardiolipin Domains in Protein Localization in Bacterial Cells
Lars D. Renner, Douglas B. Weibel.
University of Wisconsin Madison, Madison, WI, USA.
A central question in cell biology is how the spatial organization of machinery within the cell is established, maintained, and replicated in response to external stimuli. In Eubacteria, our understanding of the spatial and temporal organization of proteins is beginning to take shape. Many proteins localize to regions of rod-shaped bacterial cells that are characterized by a high intrinsic curvature (e.g. the poles). Recent data suggested that there are geometric cues for the localization of proteins and lipids in bacteria. We present data testing the hypothesis that membrane anisotropy at highly curved regions of the cell wall leads to protein localization. This research takes a top-down approach that focuses on a combination of in vivo and in vitro experiments with Escherichia coli cells. To study the response of lipids to the geometry of the cell wall in vitro, we have developed a technique for controlling the curvature of bacterial cells using microstructured polymers and quantitatively measuring the spatial localization of lipids in the resulting membranes. This approach allows to engineer an 'artificial' pole with a user-defined curvature into the E. coli inner membrane and to measure the spontaneous localization of lipids and polar proteins to this region of the cell. Using this approach we have determined that a critical radius of curvature of ~1.3μm-1 is required to drive the formation of cardiolipin-rich domains in the membrane. We have observed that the bacterial division protein MinD localizes to regions of high curvature and co-localizes with cardiolipin domains. Our data provide support for the curvature hypothesis as a general mechanism for regulating spatial organization in bacterial membranes. This research is expanding our understanding of Eubacteria and provides insights into the spatial and temporal dynamics of membranes relevant to cell biology.

Platform BD: Protein-Ligand Interactions

2864-Plat
Protein Affinity Pattern Calculations using Protein-Fragment Site Identification by Ligand Competitive Saturation (SILCS)
E. Prabhu Raman, Wenbo Yu, Alexander D. MacKerell Jr.
University of Maryland, Baltimore, MD, USA.
We demonstrate the applicability of a computational method, Site Identification by Ligand Competitive Saturation (SILCS) to identify regions on a protein surface with which different classes of functional groups interact. The method involves MD simulations of a protein in an aqueous solution of chemically diverse small molecules. In the present application, SILCS simulations are performed with an aqueous solution of 1 M benzene and propane to map the affinity pattern of the protein for aromatic and aliphatic functional groups. In addition, water hydrogens and oxygen serve as probes for hydrogen bond donor and acceptor functionality, respectively. The method is tested using a set of proteins for which crystal structures of complexes with several high affinity inhibitors are known. SILCS simulations are performed for these proteins and the affinity pattern is obtained as 3D probability distributions of fragment atom types on a 3D-grid surrounding the protein called ''FragMaps''. Good agreement is obtained between FragMaps of each type and the positions of chemically similar functional group in inhibitors as observed in the Xray crystallographic structures. For proteins for which inhibitor decoy sets are available, we demonstrate the statistical significance of the SILCS predictions by showing a significantly higher degree of overlap of the ligand atoms in the experimental conformation with the FragMaps. For a few test cases, we correlate the extent of overlap of the ligand functional groups with FragMaps to the experimental binding affinities. SILCS is also shown to capture the subtle differences in protein affinity across homologs, information which may be of utility towards specificity-guided drug design. Taken together, our results suggest that SILCS can recapitulate the location of functional groups of bound inhibitors, suggesting that the method may be of utility for rational drug design.

2865-Plat
CHARMM Additive All-Atom Force Field for O-Glycan and N-Glycan Linkages in Carbohydrate-Protein Modeling
Sairam S. Mallajosyula[1], Olgun Guvench[2], Alexander D. MacKerell Jr.[1]
[1]University of Maryland School of Pharmacy, Baltimore, MD, USA,
[2]University of New England College of Pharmacy, Portland, ME, USA.
The O-glycosidic and N-glycosidic linkages are important protein modifications in which oligosaccharides are linked to Ser/Thr and Asn residues, respectively. These linkages involve the anomeric carbon of the carbohydrates and the alcoholic side groups of Ser/Thr or the amide group of the Asn side chain. The O- and N-glycosidic linkages are ubiquitous in biological systems including glycoproteins like mucin, epidermal growth factor (EGF), domains of different serum proteins and Notch receptors, among many others, where the presence of the carbohydrate moiety is important for the biological functions of the proteins.
In an ongoing effort to develop the CHARMM all-atom additive carbohydrate force field we present and validate parameters that will enable the modeling of the O- and N-glycosidic linkages. The parameters represent an extension of the existing CHARMM carbohydrate and protein force fields.1-2 The target data for the optimization process included quantum mechanical (QM) potential energy scans of the torsions involved in the glycosidic linkages. Force field validations included comparison of the intermolecular geometries for the QM and crystal studies, comparison of the crystalline unit-cell properties and experimental NMR J-coupling constants. The optimized parameters were then used to rationalize the differences between the Ser and Thr O-glycan linkages using a Hamiltonian Replica Exchange protocol (HREX). We found that the solvent structure closely governs the linkage geometry due to the involvement of bridged waters between the carbohydrate and protein regions.
(1) Guvench, O.; Hatcher, E. R.; Venable, R. M.; Pastor, R. W.; Mackerell, A. D. J. Chem. Theory Comput 2009, 5, 2353-2370.
(2) Guvench, O.; Greene, S. N.; Kamath, G.; Brady, J. W.; Venable, R. M.; Pastor, R. W.; Mackerell, A. D. J. Comput. Chem. 2008, 29, 2543-64.

2866-Plat
Kinetic Properties of the Two-State Model for Cooperativity
Sargis Simonyan, **Nadja Hellmann**.
Institute for Molecular Biophysics, Mainz, Germany.
Cooperativity is a regulation mechanism of protein function which is defined by equilibrium binding properties, namely the shape of the oxygen binding curve. This sigmoid shape is the consequence of the existence of different conformations which differ in ligand and effector binding affinity.
Positive cooperativity also leads to characteristic behavior in the kinetics of ligand binding and dissociation. Oxygen dissociation from hemocyanins is typically ''auto-catalytic'' since the off-rate for oxygen is slower for the initial high affinity state than for the final low affinity state. The relative change of the off-rate at the beginning of the reaction compared to the final phase might serve as a measure for kinetic cooperativity. We compared the oxygen dissociation kinetics of 6 different arthropod hemocyanins. The modulation of the kinetics by allosteric effectors in most cases is what might be expected, leading to an increased rate for negative effectors and an decreased rate for positive effectors. A rather unexpected finding was the mostly linear change in apparent rate of dissociation with decreasing saturation degree. Simulations based on the MWC-model showed that the observed relationship between off-rate and saturation degree is typical for relatively slow conformational transitions and not-too-large allosteric equlibrium constants. It can be shown that under the conditions employed here (high cooperativity) the maximal increase in the off-rate is

limited by the size of the allosteric unit and not by the off-rate from the T-state. Thus, one driving force for the development of large allosteric units might be an increased plasticity in terms of modulation of ligand dissociation rates.
This work was supported by DFG (N.H.)

2867-Plat
Multiscale Simulation of Intra-Protein Communication
Jordi Silvestre-Ryan, **Jhih-Wei Chu**.
University of California, Berkeley, Berkeley, CA, USA.
We develop a new computational framework to model intra-protein communication. The configurations sampled in atomic molecular dynamics trajectories are used to compute bond lengths and force constants in an elastic network approximation of the distribution of protein structures. To go beyond the harmonic approximation, a key novelty is to compute model parameters in consecutive time windows with a user-specified size to follow the time evolution of the mechanical coupling network of protein conformation. In analogy to spectrogram of sound waves, sequential elastic network models calculated from atomic trajectories are termed the fluctuogram of protein dynamics. By analyzing and comparing the fluctuograms of Ca2+-bound and apo subtilisin, we illustrate that intermittent conformational changes and mechanical coupling variation are important mechanisms of intra-protein communication. We also show that the fluctuogram can be used to predict residues with high tendency to co-evolve by comparing with the results of statistical coupling analysis of a multiple sequence alignment. In addition to the strength of mechanical coupling, we found that the fluctuation of inter-residue force constants is also an important descriptor for co-evolution. Together, the results of this work (a) reveal the intermittent nature of conformational changes and the mechanical coupling variation, (b) show that intra-protein communication can proceed without a drastic change of protein structure and the pathways of which can be identified by the fluctuogram, and (c) support the theory that mechanically coupled residues tend to co-evolve.

2868-Plat
Enhancing Allosteric Response in Thermus Thermophilus Phosphofructokinase
Maria Shubina-McGresham, Gregory D. Reinhart.
Texas A&M Univ, College Station, TX, USA.
Phosphofructokinase (PFK) from an extreme thermophile, Thermus thermophilus (TtPFK), exhibits 17-fold stronger binding to its inhibitor, PEP, and 34-fold weaker coupling between the binding of PEP and substrate, Fructose-6-phosphate (F6P), when compared at 250C to the PFK from another thermophile, Bacillus stearothermophilus (BsPFK). BsPFK is 57% identical in sequence. Since no 3-dimensional structural information is available for TtPFK, we turned to the crystal structures of BsPFK in search for the possible explanation. There is a network of residues, D59, T158, and H215, that leads from the allosteric site to the nearest active site, and that undergoes a significant rearrangement when PEP binds to free enzyme. In the apo form of BsPFK, H215 forms a hydrogen bond with T158. In the inhibitor-bound form, T158 is further removed from the allosteric binding site, and D59 forms a hydrogen bond with H215. In TtPFK these interactions are not possible due to nature of residues at these positions: N59, A158, and S215. We hypothesized that recreating this network of residues would strengthen the coupling between the PEP and F6P binding in TtPFK. Single amino acid substitutions at each of these positions resulted in some increase in binding free energy. The three combinations of double mutations produced a more significant increase in coupling free energy, which appeared in each case to be roughly the sum of the changes in coupling free energy produced by the individual mutants. Interestingly, the level of coupling attained by introducing all three mutations is similar to that seen in BsPFK, and the binding affinity of PEP was weakened to the level exhibited by BsPFK ($\Delta Gay = 3.98 \pm 0.03$ kcal/mol, $\Delta Gy = -5.61 \pm 0.01$ kcal/mol). Supported by NIH grant GM33216 and Welch Foundation grant A1548.

2869-Plat
Structural and Thermodynamic Origins of Ligand Specificity in Homologous PDZ Domains from the Tiam-Family of Guanine Exchange Factors
Ernesto J. Fuentes, Tyson R. Shepherd.
University of Iowa, Iowa City, IA, USA.
PSD-95/DlgA/ZO-1 (PDZ) domains are among the most abundant protein-protein interaction domains in the human proteome and typically bind the 4-10 most C-terminal residues of its interaction partner with exquisite specificity. To investigate the origin of this specificity, we used two homologous PDZ domains from the Tiam-family of GEFs that have distinct but overlapping specificity for ligands. The Tiam1 PDZ domain binds 8-residue long C-terminal peptides derived from the proteins Syndecan1 and Caspr4 with micromolar affinity but does not bind Neurexin1. In contrast, the Tiam2 PDZ domain binds to peptides derived from Caspr4 and Neurexin1 with low micromolar affinity but not Syndecan1. Analysis of the X-ray crystal structure of the Tiam1 PDZ domain bound to a ''model'' peptide shows two specificity pockets created by four residues in the Tiam1 PDZ domain. Moreover, comparison of nuclear magnetic resonance (NMR) titrations of the Tiam1 PDZ domain with the Syndecan1 and Caspr4 peptides showed substantial differences in the changes in chemical shift in these residues. Sequence comparison of Tiam-family PDZ domains revealed that these residues are not conserved, further suggesting that they play a role in establishing ligand specificity. Double mutant cycle analysis of residues in these two pockets revealed ligand-dependent cooperativity, supporting their role in specificity is ligand specific. Remarkably, substitution of all four residues in the Tiam1 PDZ domain with the amino acids found in the Tiam2 PDZ domain switched the specificity to that of Tiam2. Collectively, our data suggest that Tiam-family proteins have highly evolved PDZ-ligand interfaces with distinct specificities, and that they have disparate PDZ-dependent biological functions.

2870-Plat
The Binding Energetics of a T-Cell Receptor Show a Bias Toward the Conserved Antigen Presentation Molecule, HLA
Kurt H. Piepenbrink, Brian M. Baker.
The University of Notre Dame, Notre Dame, IN, USA.
T-cell receptors (TCRs) are heterodimeric receptors on the surface of T-cells with Complementarity Determining Region (CDR) loops similar to immunoglobulins. Their ligands are peptides presented by Major-Histocompatiblity Complexes (MHCs) on the surface of most nucleated cells. The TCR binds to an MHC presenting an antigenic peptide with a dramatically stronger affinity than MHCs presenting ''self'' peptides despite the fact that the majority of the interface is conserved between the two. To assess the energetic contributions of different portions of the TCR-pMHC interface, we quantify the contributions to binding of the side-chain contacts between the residues at the interface through alanine double-mutant cycles. The interaction energy between those residues is defined as native free energy change minus the free energy changes of the two single mutants, plus the free energy change of the double-mutant; ddGoint = dGo(Xwt-Ywt) - dGo(Xz->a-Ywt) - dGo(Xwt-Yz->a) + dGo(Xz->a-Yz->a). Our results for the A6 TCR and the tax9 peptide show that contrary to expectations, the contacts between the central CDR3 loops and the peptide do not have a unique energetic importance, but CDR3α has a ''hot-spot'' ~3 kcal/mol interaction with the MHC, HLA-A2. This interaction motif between a positively charged residue in the α1 helix of the MHC and a negatively charged residue in the CDR3α loop appears to be commonly utilized based on a comparison of TCR-pMHC x-ray crystal structures. Additionally, CDR1α and β both make significant hydrogen bonds to the peptide. These data show that the energetic basis for T-cell recognition is not parsed into recognition of the peptide by CDR3 and the MHC by CDR 1 and 2 but rather that TCRs bind a composite interface.

2871-Plat
Structural Basis of Ligand Recognition by the Tollip C2 and CUE Domains
Sharmistha Mitra, Gayatri Ankem, Urmila Maitra, Iriscilla Ayala,
Anna C. Moreno, Derrick Zhang, Hugo F. Azurmendi, Carla V. Finkielstein,
Liwu Li, **Daniel G. Capelluto**.
Virginia Tech, Blacksburg, VA, USA.
Toll-like receptors (TLRs) provide a mechanism of host defense responses by activating the innate and adaptative immune responses. Subsequent downstream events result in the recruitment of one or more adaptor proteins, a process mediated by the cytosolic tail of TLRs. These protein-protein interactions promote the activation of the interleukin-1 receptor-associated kinases (IRAKs) 1, 2, M, and 4 that act upon their transcription factor targets to influence the expression of genes involved in the innate immune response. The Toll-interacting protein (Tollip) controls IRAK function in the TLR signaling pathway. Tollip presents an N-terminal Tom1-binding domain, a central C2 domain, and a C-terminal coupling of ubiquitin to endoplasmic reticulum degradation (CUE) domain. We found that the Tollip C2 domain preferentially interacts with phosphoinositides including phosphatidylinositol 3-phosphate (PI3P) and phosphatidylinositol 4,5-bisphosphate ($PI(4,5)P_2$) in a calcium-independent manner. NMR and lipid-protein overlay analyses suggest that PI3P and $PI(4,5)P_2$ share the same binding site in the protein. Kinetic analysis reveals that the Tollip C2 domain reversibly binds PI3P and $PI(4,5)P_2$ with affinities in the low micromolar range. Mutational analysis identifies key phosphoinositide-binding basic residues in the Tollip C2 domain located in a flexible region nearby the beta-groove. The CUE domain binds ubiquitin, although the biological consequences of the association as well the molecular basis of the interaction are unknown. Using NMR spectroscopy, we have identified the Tollip CUE domain residues that recognize ubiquitin as well as the ubiquitin residues that bind to the Tollip CUE domain. Structural and kinetical analyses suggest that a dimeric Tollip CUE domain forms a complex with ubiquitin in conserved binding pockets with nanomolar affinity. Overall, our findings will provide the basis to understand how Tollip is intracellularly partitioned in a ligand-dependent manner and how these interactions modulate TLR signaling.

Platform BE: Voltage-gated Ca Channels

2872-Plat

A Spider Toxin and its Recombinant Isoform Block T-Type and N-Type Calcium Channels with High Affinity

Xiao Zhang, Li Dai, Michael E. Adams.
University of California, Riverside, Riverside, CA, USA.

T-type calcium channels are widely distributed in diverse tissues and dysfunctions of these channels contribute to a variety of disorders and diseases. Notably, few specific ligands are available for physiological identification of T-type calcium channels. Here we identify ω-agatoxin IIA (ω-Aga-IIA), a polypeptide toxin purified from venom of American Funnel Web spider, *Agelenopsis aperta,* as a high affinity low voltage-activated (T-type) calcium channel antagonist. In whole cell recordings of the human α_{1I} channel stably expressed in HEK cells, ω-Aga-IIA partially inhibited T-type current with an EC_{50} of 1.05 ± 0.62 nM. ω-Aga-IIA also partially blocked α_{1B} calcium channels with a higher efficacy than its effect on α_{1I} channel, with a comparable EC_{50} of 0.17 ± 0.056 nM. ω-Aga-IIA partially inhibited T-type and N-type calcium current at saturating concentrations without shifting the *I-V* curve. We also developed a heterologous expression system (*E. coli*) and a modified on-column protein refolding method for production of a ω-Aga-IIA isoform, ω-Agatoxin IIC (ω-Aga-IIC). Recombinant ω-Aga-IIC exhibited similar RP-HPLC elution profiles as ω-Aga-IIA and blocked α_{1I}/α_{1B} channels with high potency (EC_{50} of 1.01 ± 0.38 and 0.16 ± 0.049, respectively). The high affinities of ω-Aga-IIA and ω-Aga-IIC for α_{1I} and α_{1B} calcium channels indicates the presence of an evolutionarily conserved binding site on high- and low voltage-activated calcium channels. With the successfully production and refolding of recombinant ω-Aga-IIC, a valuable tool has become available for further studies of calcium channel pharmacology and function.

2873-Plat

Caveolin-3 Inhibits $Ca_v3.2$ (α1H) Currents and Regulates Hypertrophic Signaling in Ventricular Myocytes

Yogananda S. Markandeya, Jonathan M. Fahey, **Ravi C. Balijepalli**.
University of Wisconsin, Madison, Madison, WI, USA.

Voltage gated T-type Ca^{2+} channel $Ca_v3.2$ subunit, responsible for T-type Ca^{2+} current (I_{Ca_vT}) is expressed in different tissues including the heart and participates in Ca^{2+} influx, hormonal secretion, pacemaker activity and arrhythmia. The $Ca_v3.2$ channels are reported to be up regulated and contribute to the altered Ca^{2+} signaling and pathogenesis of cardiac hypertrophy via the activation of calcineurin/nuclear factor of activated T cells (NFAT) pathway. Caveolae containing scaffolding protein caveolin-3 (Cav-3) localize many ion channels and signaling proteins, and provide temporal and spatial regulation of intracellular Ca^{2+} in cardiomyocytes. However, the mechanism of altered Ca^{2+} signaling in cardiac hypertrophy is not clearly defined. We investigated the role of caveolae and $Ca_v3.2$ channels in the regulation of Ca^{2+} signaling during angiotensin-II induced cardiac hypertrophy in ventricular myocytes. Immunogold labeling and electron microscopy analysis demonstrated the co-localization of $Ca_v3.2$ channel and Cav-3 relative to caveolae in the ventricular myocytes. GST pull-down analysis confirmed that the N-terminus region of Cav-3 interacts with $Ca_v3.2$ channels. Impact of Cav-3 association with $Ca_V3.2$ was analyzed by whole cell patch clamp technique. Co-expression of Cav-3 specifically inhibited $I_{Cav3.2}$ in heterologously expressed HEK293 cells. In the neonatal ventricular myocytes, overexpression of Cav-3 inhibited $I_{Ca,T}$ and specifically inhibited the adenovirus ($AdCa_v3.2$) mediated peak $Ca_v3.2$ currents. In addition, overexpression of Cav-3 prevented the angiotensin-II induced hypertrophic responses in neonatal mouse cardiomyocytes. Over expression of Cav-3 prevented the angiotensin-II induced translocation of NFAT4 to the nucleus and also inhibited the phosphorylation of extracellular signal-regulated kinase, ERK. Overall our results demonstrate that over expression of Cav-3 suppresses pathological hypertrophic responses in cardiomyocytes via the inhibition of the $I_{Cav3.2}$. We conclude that Cav-3 may play a crucial role in protective signaling mechanisms in the ventricular myocytes during hypertrophic cardiomyopathy.

2874-Plat

Molecular Mechanism of Calcium Channel Regulation in the Fight-Or-Flight Response

Matthew D. Fuller, Michelle A. Emrick, Martin Sadilek, Todd Scheuer, William A. Catterall.
University of Washington, Seattle, WA, USA.

During the fight-or-flight response, the sympathetic nervous system stimulates L-type calcium currents in the heart conducted by Cav1.2 channels through activation of β-adrenergic receptors, adenylyl cyclase, and phosphorylation by cAMP-dependent protein kinase (PKA), thereby increasing cardiac contractility and beat rate. The channel α_1 subunit C-terminus contains binding sites for multiple regulatory proteins including the PKA/A kinase anchoring protein 15 (AKAP15) complex. The C-terminus is proteolytically cleaved but remains associated non-covalently with the truncated channel and acts as a potent autoinhibitor of channel activity. Relief of this autoinhibition provides an attractive mechanism for cellular regulatory signals to produce the large increases in calcium current observed physiologically. We reconstituted regulation of Cav1.2 channels in non-muscle tsA-201 cells by forming an autoregulatory signaling complex composed of the Cav1.2Δ1800 channel, the noncovalently-associated distal C-terminal domain, the auxiliary $\alpha_2\delta_1$ and β_{2b} subunits, and AKAP15. During whole-cell recordings of channel activity we observed a 3.6-fold range of Cav1.2 activity from a minimum in the presence of protein kinase inhibitors to a maximum with activation of adenylyl cyclase with forskolin. Equivalent modulation was not observed for the full-length (untruncated) channel or the truncated channel without the distal C-terminus. Basal channel activity in unstimulated cells was regulated by phosphorylation of two novel sites at Ser1700 in a PKA consensus sequence and Thr1704 in a casein kinase 2 consensus sequence, both strategically located at the interface between the distal and proximal C-terminal regulatory domains. Further stimulation of channel activity via PKA signaling required only phosphorylation of Ser1700. Phosphorylation at Ser1928 did not significantly alter channel activity. These results define the signaling complex required for Cav1.2 channel regulation and elucidate the sites of phosphorylation that regulate channel activity.

Supported by NIH grants R01 HL085372, T32 HL007312-31 and AHA fellowship 09POST2080270

2875-Plat

The Calcium Channel Single Channel Conductance Heirarchy is N>L>T at Physiological External Calcium: Implications for Presynaptic Transmitter Release Site Gating

Elise F. Stanley[1], Fiona K. Wong[1], Alex M. Weber[1], Adele R. Tufford[1], Lyanne C. Schlichter[1], Victor Matveev[2].
[1]TWRI, UHN, Toronto, ON, Canada, [2]New Jersey Institute of Technology, Newark, NJ, USA.

A number of studies support the conclusion that single Ca_V channels Ca^{2+} nanodomains gate molecular signaling pathways. Thus, at presynaptic terminals single $Ca_V2.2$ channels trigger fusion of synaptic vesicle (SVs) by saturating a nearby calcium sensor.[2] It is generally accepted that Ca_V1, Ca_V2, and Ca_V3 families (L, N and T, respectively) exhibit a decreasing order of single channel conductance.[1] Since nanodomain dimensions are proportional to single channel current amplitude (*i*), high-conductance L type channels would be expected to be favored over the intermediate conductance N-type. Since the L>N>T hierarchy was determined with high $Ba^{2+}{}_{EXT}$, we tested the idea that this sequence may differ at physiological $Ca^{2+}{}_{EXT}$.

We recorded *i* values for all three Ca_V families across a broad range of $Ca^{2+}{}_{EXT}$, spanning the physiological range. We focused on i_{-65mV} to avoid non-linear current-to-voltage relationship complications and for direct relevance to the gating of synaptic transmission.[3] A $Ca_V2.2>Ca_V1>Ca_V3.2$ hierarchy was determined for i_{-65mV} at 1-2 mM $Ca^{2+}{}_{EXT}$. Mathematical modeling predicts that the $Ca_V2.2$ Ca^{2+} nanodomain is ~25% more extensive than that generated by Ca_V1. We also calculated single channel 'SV fusion' domains, defined as the radii where the channel would saturate ≥50% of 5-binding site calcium sensors. With a sensor binding affinity of 10μM a single $Ca_V2.2$ can activate a calcium-fusion sensor located on the proximal face of the synaptic vesicle.[4] These findings may explain why Ca_V2 family channels are preferred for transmitter release site gating.

1. Fox AP, Nowycky MC & Tsien RW JP 394:173(1987).
2. Stanley EF Neuron 11:1007(1993).
3. Llinas RR, Sugimori M & Simon SM PNAS 79:2415(1982).
4. Weber AM,* Wong FK*, Tufford AR, Schlichter LC, Matveev V & Stanley EF Nature Neurosci *in press* (2010).

2876-Plat

Mechanism of Auxiliary Beta-Subunit-Mediated Membrane Targeting of $Ca_v1.2$ Channels

Kun Fang, Henry M. Colecraft.
Department of Physiology and Cellular Biophysics, Columbia University, New York, NY, USA.

Ca^{2+} influx via Ca_V1 and 2 channels drives essential physiological processes ranging from synaptic transmission to muscle contraction. Membrane-targeting of Ca_V1 and 2 channels is requisite for their physiological function. Association of a pore-forming α_1 with a cytosolic β is necessary for trafficking Ca_V1 and 2 channels to the cell surface, but the mechanisms underlying this phenomenon are poorly understood. One prevalent idea is that β binds to the intracellular I-II loop of α_1 and masks an endoplasmic reticulum (ER) retention signal, while other work suggests a critical, but undefined role for the α_1 C-terminus. We hypothesized that major determinants of $Ca_V1.2$ channel ER retention and β-dependent export reside within the five intracellular loops and termini of the pore-forming α_{1C} subunit. We generated 31 chimeric

channels featuring a systematic swap of all possible permutations of intracellular loops/termini of α_{1C} into analogous positions in the β-independent, low-voltage-activated $Ca_V3.1$ channel α_{1G} subunit, and studied functional reconstitution of β-dependence using electrophysiological recordings in HEK 293 cells. Surprisingly, functional analyses of chimeras yielded a pattern consistent with α_{1C} I-II loop possessing a net ER export capability that was opposed by discrete ER retention signals in the other cytoplasmic domains. Alanine scanning mutagenesis identified a cluster of acidic residues responsible for the ER export function of the α_{1C} I-II loop. Reconstitution of β-dependent increase in current required at least four α_{1C} intracellular domains, with both the I-II loop and C-terminus being essential. The results support a new model of $Ca_V1.2$ trafficking where β binding to α_{1C} I-II loop causes a C-terminus-dependent rearrangement of intracellular domains that shifts the balance of power between export signals on the I-II loop and retention signals elsewhere on the protein.

2877-Plat

Molecular Determinants of Voltage-Gated Calcium Channel Inhibition by Gem

Zafir Buraei, Rose Levenson-Palmer, Jian Yang.
Columbia University, New York, NY, USA.

High voltage-activated (HVA) Ca^{2+} channels, including L-, N- and P/Q-type channels, are potently inhibited by the Rem, Rem2, Rad, and Gem/Kir (RGK) family of small GTP-binding proteins. This inhibition was widely thought to depend on the direct association between RGK proteins and the β subunit ($Ca_v\beta$) of HVA Ca^{2+} channels, but we recently found that P/Q channel inhibition by Gem protein in inside-out membrane patches required $Ca_v\beta$ but not the Gem-$Ca_v\beta$ interaction, and that Gem coimmunoprecipitated with the P/Q channel α_1 subunit in a $Ca_v\beta$-independent manner. Thus, we proposed that direct interactions between Gem and the α_1 subunit ($Ca_v\alpha_1$) of HVA Ca^{2+} channels are critical for Gem inhibition. In this study, we investigate the molecular determinants on $Ca_v\alpha_1$ that are important for Gem inhibition. We construct chimeras between the α_1 subunit of P/Q channels and the Gem-insensitive low voltage-activated T-type channels, which do not bind or require $Ca_v\beta$. We find that grafting the α-interaction domain (AID), the high-affinity $Ca_v\beta$ binding site on $Ca_v\alpha_1$, or grafting the entire AID-containing I-II loop from P/Q channel into T-channels ($T_{PQ\ I\text{-}II\ loop}$), is sufficient for $Ca_v\beta$ binding and gating regulation but does not bestow RGK inhibition. However, adding the first two transmembrane segments (IIS1-IIS2) of the second homology repeat onto the $T_{PQ\ I\text{-}II\ loop}$ construct, produced a Gem-sensitive T-channel. This inhibition persists with non-interacting Gem and $Ca_v\beta$ mutants, indicating that the $Ca_v\beta$-Gem interaction is not necessary, just as in the case of Gem inhibition of P/Q channels. In complementary experiments, substituting only IIS1-IIS2 of P/Q channel α_1 with that of T-channel's severely attenuates RGK inhibition. This supports a paradigm in which Gem directly binds and inhibits $Ca_v\beta$-primed $Ca_v\alpha_1$ on the plasma membrane. We are currently investigating the role of other $Ca_v\alpha_1$ regions in Gem inhibition.

2878-Plat

Calmodulin Interferes with $Ca_v1.2$ C-Terminal Regulation of L-Type Channel Current

Shawn M. Crump, Elizabeth A. Schroder, Gail A. Sievert,
Douglas A. Andres, Jonathan Satin.
University of Kentucky, lexington, KY, USA.

The L-type Ca channel (CaV1.2) distal carboxyl-terminus (CCt) has multiple functions. CCt inhibits L-type channel current, and is a mobile element that translocates to the nucleus where it regulates CaV1.2 transcription. CCt interacts with CaV1.2 in a similar domain as calmodulin (CaM). The purpose of this study is test the hypothesis that CaM and CCt compete for functional interaction with CaV1.2. CaV1.2 calcium current (ICa,L) and barium current (IBa,L) were recorded from HEK 293 cells transfected with CaV1.2 + CaVbeta2a. This background was compared to cells additionally transfected with CaM and/or CCt. The CaV1.2 expressed was deleted at position 1733 or 1801 (numbering based on rabbit sequence), and CCt corresponded to amino acids 1821-2171. CCt co-expression significantly reduced IBa,L, but not ICa,L. CCt inhibition of ICa,L is reversed by exogenous CaM co-expression, but not by calcium binding deficient apo-CaM. Examination of the peak I(V) curves suggests that midpoint of activation was not affected. Mouse ventricular cardiomyocytes transfected with CCt also showed a reduction in Cav1.2 IBa,L, but no reduction in ICa,L. Exogenous CaM co-expression also relieved CCt auto-inhibiton in mouse ventricular cardiomyocytes. We conclude that CCt attenuation of current occurs only with Ba, and is consistent with a Ca alleviation of CCt block. Thus, CaM and Ca functionally compete to limit CCt auto-inhibition of CaV1.2 current.

2879-Plat

Molecular Events Beyond apoCAM Preassociation in the CAM Regulation of Cav1.3 Channels

Manu B. Johny, Philemon S. Yang, David T. Yue.
Johns Hopkins University, Baltimore, MD, USA.

Ca_V channel regulation by calmodulin (CaM) is a central prototype for ion-channel modulation. Despite long study, relatively little is known mechanistically, beyond the initial preassociation of Ca^{2+}-free CaM (apoCaM) with an IQ domain on the carboxy-terminus of channels. Most studies have focused on the IQ domain and immediate upstream 'preIQ' regions, despite hints that further upstream elements in the carboxy-terminus could be important. Accordingly, we here undertake alanine scanning mutagenesis of the entire carboxy-terminus upstream of the IQ domain (the proximal CI-region, PCI). For analysis, we chose $Ca_V1.3$ channels (highly homologous to classic $Ca_V1.2$), because they exhibit robust CaM-mediated inactivation (CDI), with particularly well-resolved profiles for both N- and C-lobe forms of inactivation. Several unexpected results were obtained. First, mutations throughout the preIQ domain left CDI essentially unchanged, at odds with functional hotspots in the homologous region of $Ca_V1.2$. Second, newly identified segments, situated upstream of the preIQ region, proved selectively critical for the C-lobe form of CDI. Specifically, we argue that the PCI region is the Ca^{2+}/CaM effector site for C-lobe CDI, as revealed by quantitative comparison of the effect of PCI mutations on CDI, to their effect on PCI binding with Ca^{2+}/CaM ('Ψ-analysis'). Third, we further exploit Ψ-analysis to extend and confirm that the Ca^{2+}/CaM effector site for the N-lobe form of CDI is structurally distinct, residing in the *NSCaTE* element of the channel amino terminus (*Nature* **451:**830). Finally, while the IQ-domain is a primary site for apoCaM preassociation, our scan surprisingly reveals that PCI harbors additional preassociation sites, especially important for the N-lobe of apoCaM. Overall, this alanine scan of the $Ca_V1.3$, together with that of the IQ domain (companion abstract), outlines the long-sought molecular events beyond the initial apoCaM preassociation with the channel.

Platform BF: Microtubular Motors

2880-Plat

Detailed Analysis of the Dynein Stepping Mechanism using Multicolor Tracking

Mark A. DeWitt[1], Peter Combs[1], Bruce Cohen[2], Ahmet Yildiz[1].
[1]University of California, Berkeley, Berkeley, CA, USA, [2]Lawrence Berkeley National Laboratory, Berkeley, CA, USA.

Cytoplasmic dynein is a motor protein that moves processively towards the microtubule minus end. To characterize dynein's step size at both limiting (5 μM) and saturating (1 mM) ATP concentrations, we have improved the temporal resolution of FIONA to 2 milliseconds and tracked the movement of single yeast cytoplasmic dynein motors, each labeled with one quantum dot. In contrast to kinesin, dynein's step size is highly variable, and backwards and sideways steps are frequently observed. As the tail domain takes ~8 nm steps, the heads advance by taking both short (~8 nm) and long (~16 nm) steps. These data indicate that the heads do not move in a strictly alternating manner, as is the case with kinesin and myosin. To further characterize how the dynein heads move relative to each other, we have tracked the movement of both heads simultaneously. To precisely measure the head-head separation vector, we have developed novel small quantum dots (10 nm diameter) that specifically attach to each dynein head. The fluorescent signals of the differently-colored quantum dots attached to dynein are then registered with 2 nm precision. Using this technique, we find the heads to be widely separated, mostly in the off-axis, indicating that the two heads walk along separate filaments. Our two-color stepping data also show that the dynein heads advance mostly by taking alternating steps, as is the case with kinesin. However, the heads may also move independently of each other, and one head may take multiple steps before its partner moves forward. Both the leading head and the trailing head may initiate a step. Taken together, these unprecedented behaviors indicate that cytoplasmic dynein achieves processive movement via a mechanism unique among the molecular motors.

2881-Plat

Two Motor Domains of Cytoplasmic Dynein Directly Interact Each Other

Tomohiro Shima[1], Kohji Ito[2], Takahide Kon[3], Motoshi Kaya[1],
Hideo Higuchi[1], Kazuo Sutoh[1].
[1]University of Tokyo, Tokyo, Japan, [2]Chiba University, Chiba, Japan, [3]Osaka University, Osaka, Japan.

Cytoplasmic dynein is a two-headed molecular motor, which can take hundreds steps processively along a microtubule (MT) without dissociation. This processive movement requires coordination of the two heads, because at least one head must remain bound to a MT. In other two-headed processive motor proteins, it has been reported that intramolecular tension through mechanical elements connecting two motor domains (eg., kinesin's neck linker) plays an

important role in such coordination. Therefore, we examined the effect of intramolecular tension on dynein movement by linking two dynein motor domains with Gly-rich flexible linkers instead of the dynein tail domain. Unlike the other two-headed motors, the dimeric dynein with the flexible linkers moved processively in a similar manner as the dimer without the flexible linker. Since this result suggests that the tension through the tail domain is not necessary for dynein's processive movement, the two dynein motor domains may directly interact and communicate each other. To test whether the two motor domains experience intramolecular tension through this direct interaction instead of the tail domain, we expressed a heterodimer with an inactive motor domain. Although the inactive head completely lost its motile activity and needed external force to detach from a MT, this heterodimer with the flexible linkers showed processive movement. The results suggest that direct interaction of two motor domains is physically strong enough to allow the active head to pull the inactive head off from MT.

2882-Plat

Structures of the Motor Subunits from a Novel Asymmetric Kinesin Provide Insight Into its Motile Mechanism

John Allingham, Da Duan, Darlene Davis.
Queen's University, Kingston, ON, Canada.

The spatial arrangement of a cell's contents, and its ability to redistribute them, is fundamental to its survival. In all animal and plant cells, kinesins fill a large part of this need, hauling chromosomes and vital cargo-containing sacks to their required destinations. Many kinesins operate as a homodimer in which the two subunits coordinate their movement along microtubules and perform a single cellular function. However, a few kinesins in certain species mix-and-match different molecules in ways that allow the motor to perform multiple functions. Certain types of pathogenic fungi harbor an unusual group of kinesins that form heterodimeric complexes with one or more non-catalytic kinesin-like proteins that regulate the function and cellular localization of their catalytic partner. A challenge in the motor protein field is to provide a mechanistic view of how these asymmetric motors move using this unconventional form of motor subunit arrangement. Our recent determination of the X-ray crystal structures of the motor domain region of both the catalytic and non-catalytic subunits of a heterodimeric kinesin from Candida glabrata revealed that certain regions of the latter subunit are highly dynamic. Specifically, our crystals of CgVik1 (the non-catalytic subunit) exhibit three very different conformations of an alpha-helical segment that is analogous to the force-producing 'neck' element of kinesins. The intramolecular interactions of the CgVik1 neck and its motor core differ in each conformation and are accompanied by movements in elements that are analogous to the nucleotide binding 'P-loop' and part of the microtubule binding surface of catalytic kinesins. This suggests a functional link between CgVik1 neck orientation and microtubule interactions and motility of the motor complex, and sheds light on how this kinesin works at the atomic level as an asymmetric motor complex.

2883-Plat

Mechanistic Analysis of Human Mitotic Kinesin CENP-E

Harjinder S. Sardar, Susan P. Gilbert.
Department of Biology and Center for Biotechnology and Interdisciplinary Studies, Rensselaer Polytechnic Institute, Troy, NY, USA.

Centromere protein CENP-E is a dimeric kinesin (Kinesin-7 family) with critical roles in mitosis including establishment of microtubule (MT)-chromosome linkage and processive movement of monooriented chromosomes on MTs for proper alignment at metaphase. A single molecule of CENP-E has two motor head domains containing an ATP and a microtubule binding site. The motor heads are dimerized through an extended α-helical coiled-coil stalk (~200 nm in length) followed by C-terminal globular domains involved in cargo or kinetochore binding. Mechanistic studies were peformed using a dimeric CENP-E-6His motor. Presteady-state and steady-state kinetics were performed to determine the rate constants of the individual steps of ATP binding, ATP hydrolysis, phosphate release, CENP-E dissociation from the MT, and its reassociation to the MT with ADP release. Preliminary studies with pulse chase experiments reveal that MgATP binding to MT•CENP-E follows a two-step process, formation of a collision complex and a fast (47.5 s-1) nucleotide isomerization step. Acid quench studies indicate that the ATP hydrolysis occurs at 24.6 s-1. MT dissociation studies show that the motor detachment from MT is slow at 1.35 s-1. The steady state kcat determined was 0.9 s-1, K1/2,MT = 1.5 μM, and Km,ATP = 18.3 μM. These studies are directed to define the distinctive mechanochemistry for CENP-E processive movement associated with chromosome congression and MT plus-end elongation. Supported by NIH GM54141 to Susan P. Gilbert.

2884-Plat

Loop L5 Acts as a Conformational Latch in the Mitotic Kinesin Eg5

William M. Behnke-Parks[1], Jeremie Vendome[1], Zoltan Maliga[2], Carolyn Moores[3], **Steven Rosenfeld**[1].
[1]Columbia University, New York, NY, USA, [2]Max Planck Institute, Dresden, Germany, [3]University of London, London, United Kingdom.

All members of the kinesin superfamily of molecular motors contain an unusual structural motif consisting of an alpha helix that is interrupted by a flexible loop, referred to as L5. The function of L5 remains unclear, although its length varies considerably among different kinesins with different physiologies. We have examined this issue in the mitotic kinesin Eg5 by combining site directed mutagenesis of L5 with transient state kinetics and molecular dynamics simulations. We find that mutation of a highly conserved proline within this loop profoundly slows nucleotide induced structural changes both at the catalytic site as well as at the microtubule binding domain and the neck linker. Molecular dynamics simulations reveal that this mutation affects the flexibility not only of L5 itself, but also of the switch I structural elements that sense ATP binding to the catalytic site. Separate fluorescence lifetime measurements of L5 also demonstrate that this loop can assume two different conformations, whose equilibrium is affected by nucleotide. Taken together, our results lead us to propose a model in which L5 regulates the rate of conformational change in key elements of the nucleotide binding site through its interactions with α3, and in so doing, controls the speed of movement and force generation in kinesin motors.

2885-Plat

Mitotic Functions and Motile Properties of the S. cerevisiae Kinesin-5 motors

Vladimir Fridman[1], Adina Gerson-Gurwitz[1], Christina Thiede[2], Maria Podolskaya[1], Movshovich Natalia[1], Stefan Lakamper[2], **Christoph F. Schmidt**[2], Larisa Gheber[1].
[1]Ben-Gurion University of the Negev, Beer-Sheva, Israel, [2]Georg-August-Universitaet, Goettingen, Germany.

Mitotic chromosome segregation is mediated by mitotic spindle, a highly dynamic microtubule-based structure, which undergoes a distinct set of morphological changes in each mitotic cycle. Major factors that contribute to spindle morphogenesis are microtubule (MT) plus-end dynamics and function of molecular motors from the Kinesin-5 family. Kinesin-5 family members are conserved, homotetrameric motors with two catalytic domains located on opposite sides of the active complex. This special architecture enables these motors to crosslink and slide anti-parallel MTs originating from opposite spindle poles and thereby perform their essential functions in mitotic spindle morphogenesis. It was recently shown that Kinesin-5 motors affect anaphase spindle symmetry and midzone organization (1). S. cerevisiae cells express two Kinesin-5 homologues, Cin8p and Kip1p that overlap in function during spindle assembly, metaphase and anaphase B and at least one of them need to be expressed for viability. So far, the extent of redundancy between these two Kinesin-5 proteins and their motile properties in vitro have not been thoroughly investigated.

In the present study, we use high temporal and spatial resolution imaging and FRAP to characterize interpolar MT (iMT) plus-end dynamics during spindle morphogenesis in S. cerevisiae cells expressing tubulin-GFP(2). This approach allowed us to study the role of the major midzone organizing protein Ase1(2) in controlling iMT plus-end dynamics and to compare between the effects of Cin8 and Kip1 on these dynamics during anaphase. In addition, in order to understand in vivo functions of the Kinesin-5 Kip1, we characterized its motile properties in single-molecule fluorescence motility assay. Results from this assay will be presented.

(1) Movshovich N, et al. J Cell Sci. 2008; 121:2529.
(2) Fridman V, et al. EMBO Rep. 2009; 10:387.

* Supported by the Lower-Saxony collaboration grant between BGU and GAUG

2886-Plat

Kinetics of Microtubule Assembly

Melissa K. Gardner[1], Blake D. Charlebois[2], Imre M. Jánosi[3], Jonathon Howard[4], **Alan J. Hunt**[2], David J. Odde[1].
[1]University of Minnesota, Minneapolis, MN, USA, [2]University of Michigan, Ann Arbor, MI, USA, [3]Loránd Eötvös University, Budapest, Hungary, [4]2Max Planck Institute of Molecular Cell Biology and Genetics, Dresden, Germany.

Understanding how microtubules (MTs) assemble and disassemble is vital to understanding fundamental cellular processes, such as mitosis and polarization, and their regulation via proteins and therapeutic drugs. Our current understanding of assembly kinetics is based on the classic one-dimensional (1D) assembly model of Oosawa, which assumes that the multiprotofilament MT can be modeled as if it were a single protofilament. In the classic 1D model the subunit off-rate is independent of free subunit concentration, an assumption that has yet to

be confirmed experimentally. Using TIRF-microscopy and laser tweezers assays to measure microtubule self-assembly from GMPCPP-tubulin in vitro with nanoscale accuracy, we find that the off-rate is not constant but rather increases with increasing free subunit concentration. Consistent with this observation, we find that a simple two-dimensional (2D) model predicts the increasing off-rate with subunit concentration due to a shift in tip structure from relatively blunt at low concentrations to relatively tapered at high concentrations, which we confirmed experimentally by TIRF-microscopy. Because both the on-rate and off-rate increase with free tubulin concentration, the 2D model requires an association rate constant that is an order-of-magnitude larger than the 1D model. We tested this prediction by measuring the variability in assembly rate, and found that the on- and off-rates are consistent with the 2D model predictions and are an order-of-magnitude higher than predicted by the 1D model. In summary, we find that the kinetic rates of microtubule self-assembly have been severely underestimated in the literature, by at least an order-of-magnitude. Because net growth results from a small difference between large on-rates and off-rates, the net rate can be significantly altered by weak microtubule associated protein and therapeutic drug interactions with the microtubule.

2887-Plat
Tension Directly Stabilizes Reconstituted Kinetochore-Microtubule Attachments
Charles L. Asbury[1], Bungo Akiyoshi[2], Krishna K. Sarangapani[1], Andrew F. Powers[1], Christian R. Nelson[2], Steve L. Reichow[1], Tamir Gonen[1], Jeffrey A. Ranish[3], Sue Biggins[1].
[1]University of Washington, Seattle, WA, USA, [2]Fred Hutchinson Cancer Research Institute, Seattle, WA, USA, [3]Institute for Systems Biology, Seattle, WA, USA.
Kinetochores are macromolecular machines that couple chromosomes to dynamic microtubule tips during cell division, thereby generating force to segregate the chromosomes. Accurate segregation depends on selective stabilization of correct 'bi-oriented' kinetochore-microtubule attachments, which come under tension due to opposing forces exerted by microtubules. Tension is thought to stabilize these bi-oriented attachments indirectly, by suppressing the destabilizing activity of a kinase, Aurora B. However, a complete mechanistic understanding of the role of tension requires reconstitution of kinetochore-microtubule attachments for biochemical and biophysical analyses *in vitro*. Here we show that native kinetochore particles retaining the majority of kinetochore proteins can be purified from budding yeast and used to reconstitute dynamic microtubule attachments. Individual kinetochore particles maintain load-bearing associations with assembling and disassembling ends of single microtubules for >30 min, providing a close match to the persistent coupling seen *in vivo* between budding yeast kinetochores and single microtubules. Moreover, tension increases the lifetimes of the reconstituted attachments directly, via a catch bond-like mechanismthat does not require Aurora B. Based on these findings, we propose that tension selectively stabilizes proper kinetochore-microtubule attachments *in vivo* through a combination of direct mechanical stabilization and tension-dependent phosphoregulation.

Platform BG: Protein Aggregates

2888-Plat
Alzheimer Aβ Amyloid Annular Fibrils: Insight Into Polymorphism
Yifat Miller[1], Buyong Ma[2], Ruth Nussinov[2].
[1]NCI, NIH, Frederick, MD, USA, [2]SAIC-Frederick, Inc., NCI-NIH, Frederick, MD, USA.
Elucidating the structure of $A\beta_{40}/A\beta_{42}$ fibrils is of interest in Alzheimer's disease research because it is required for designing therapeutics that target fibril formation at an early stage of the disease. Based on the cryoEM measurements and on ssNMR data, we probe various amyloid fibril organizations. Our study demonstrates that the two-fold symmetry tubular $A\beta_{42}$ fibril model with the C-termini facing the external surface of the fibril has a cavity, while model with the C-termini facing the internal surface of the fibril shrinks the tubular cavity. Experimentally, data for the three-fold symmetry structure of the $A\beta_{9\text{-}40}$ fibril suggest formation of tight hydrophobic core through M35 interactions across the fibril axis and strong I31-V39 interactions between different cross-β units. Herein, based on ssNMR data, we probe various models with three-fold symmetry of the full-length $A\beta_{40}$. We revealed that the unique $A\beta_{40}$ triangular structure has a large cavity along the fibril axis. Finally, the N-termini in $A\beta_{40}/A\beta_{42}$ fibrils can assist in the stabilization of the fibrilby interacting with the U-turn domains or with the C-termini domains. Our findings point to the relevance of the cavity in oligomers which should be considered, when targeting oligomer toxicity. This project has been funded in whole or in part with Federal funds from the NCI, NIH, under contract number HHSN261200800001E.

2889-Plat
A solid-State NMR Study of Abeta Protofibrils
Holger A. Scheidt[1], Isabel Morgado[2], Sven Rothemund[3], Marcus Fändrich[4], Daniel Huster[1].
[1]University Leipzig, Leipzig, Germany, [2]Martin Luther University Halle-Wittenberg, Halle/S, Germany, [3]Interdisciplinary Center for Clinical Research, Leipzig, Germany, [4]Max-Planck Research Unit for Enzymology of Protein Folding, Halle/S., Germany.
Aβ(1-40) is the major fibril-forming peptide from Alzheimer's disease, which adopts a highly ordered β-sheet conformation upon aggregation into amyloid fibrils. Several techniques have provided a wealth of structural information on mature Aβ(1-40) fibrils. Yet, the complex formation process of mature fibrils is, from a structural point of view, not well understood. Here we use ssNMR spectroscopy to elucidate the structure of Aβ protofibrils. This analysis is possible since the binding of the antibody B10AP prevents the conversion of these metastable intermediates into mature fibrils. With a set of eight peptides with varying isotope labeling schemes, 30 residues distributed over the entire peptide sequence were covered. ^{13}C CPMAS spectra and 2D correlation experiments were recorded for unambiguous assignment of all carbons. From the conformation dependent chemical shifts we could identify peptide segments of stable secondary structure and evaluated the backbone structure using TALOS. Based on this data, Aβ protofibrils encompass residues 16-22 and 30-36 in β-sheet conformation. Further, three structural regions of the protofibrils present random coil-like chemical shifts, one (residues 23-26) as intermediate segment between the β-strands and two others at the peptide N- and C- terminus. Obviously the structural elements of mature Aβ(1-40) fibrils are already present in protofibrils, but the β-sheet regions apparently elongate during the fibrils conversion. Further information about the dynamics of these regions is provided by measurement of the strength of dipolar couplings, which are converted into an order parameter. Protofibrils show high order parameters (>0.8) within the β-strand regions, while the measured *S* values are below 0.8 at the termini. We never observed *S* values below 0.4 that would have indicated very high mobility. Thus, significant structural order exists also within those sequence segments that have chemical shift values corresponding to a random coil.

2890-Plat
Kinetics of Amyloid-Beta Monomer to Oligomer Exchange by NMR Relaxation
Nicolas L. Fawzi, Jinfa Ying, Dennis A. Torchia, G. Marius Clore.
NIDDK, NIH, Bethesda, MD, USA.
Non-fibrillar oligomers of the amyloid-beta peptide may be the primary toxic species in Alzheimer's disease but detailed structural and kinetic characterization of these states has been difficult. Using NMR relaxation measurements, we observe the kinetics of exchange between monomeric and large, polymorphic oligomeric species of amyloid-beta. 15N and 1HN R2 data at multiple magnetic fields were recorded for several peptide concentrations subsequent to the establishment of a stable pseudo-equilibrium between monomeric and NMR-invisible soluble oligomeric species. The increase in 15N and 1HN R2 rates as a function of protein concentration is independent of nucleus and magnetic field and shows only a small degree of variation along the peptide chain. This phenomenon is due to broadening arising from the conversion of monomer to the NMR-invisible oligomeric species (''dark'' state). At a total amyloid-beta concentration of 300 micromolar, the apparent first-order rate constant for this process is 3 ŝ-1. Fitting the McConnell equations for two dipolar-coupled spins in two-site exchange to transfer-of-saturation profiles at two radiofrequency field strengths gives an estimate for koff of 73 ŝ-1 and transiently bound monomer 1HN R2 rates of up to 42 000 ŝ-1 in the tightly bound central hydrophobic region and ~300 ŝ-1 in the disordered regions, such as the first nine residues. The fraction of peptide within the ''dark'' oligomeric state undergoing exchange with free monomer is calculated to be ~3%.

2891-Plat
Investigating Protein Aggregation using Segmental Isotope Labeling and 2D IR Spectroscopy
Sean D. Moran[1], Eli Bixby[2], Sean M. Decatur[2], Martin T. Zanni[1].
[1]University of Wisconsin-Madison, Madison, WI, USA, [2]Oberlin College, Oberlin, OH, USA.
Protein misfolding and aggregation are important processes in numerous human diseases, but the detailed structural changes that occur therein evade traditional crystallographic and NMR-based techniques. Rapid-scan 2D IR spectroscopy, combined with heavy isotope labeling, provides information on local secondary structure and coupling between IR chromophores, which can be used to study systems that aggregate *in vitro* on a timescale of

minutes to hours. Recently, we have utilized single-position 1-^{13}C=^{18}O labels to develop a detailed kinetic model of the aggregation of synthetic hIAPP, a 37 AA peptide implicated in type II diabetes mellitus. Here we demonstrate a segmental, ^{13}C labeling approach to the study the much larger human gammaD-crystallin, a 173 AA eye lens protein that aggregates via an unknown mechanism during cataract formation. Using bacterial expression and native chemical ligation, we have generated a gammaD-crystallin variant in which the highly similar N- and C-terminal domains are uniformly enriched in ^{12}C and ^{13}C, respectively. This results two well-resolved diagonal peaks in the 2D IR spectrum of the natively folded protein, with a separation of ~40 cm^{-1}. Aggregation under acidic conditions results in spectral changes consistent with amyloid fiber formation in the C-terminal domain and unfolding of the N-terminal domain, with evidence of interaction between the two based on the presence of cross-peaks. The structural model we propose, currently resolved at the level of individual domains, is nonetheless the most detailed available for a gammaD-crystallin aggregate to date. We anticipate that the method described will be broadly applicable to difficult systems including many aggregating, natively unstructured, or membrane-associated proteins.

2892-Plat

Structural Variations in the Aggregation Pathways of Normal and Pathological Huntingtin-Like Peptides

Tatiana Perevozchikova[1,2], Christopher Stanley[3], Helen P. McWilliams-Koeppen[4], Valerie Berthelier[4].
[1]Genome Science and Technology, University of Tennessee, Knoxville, TN, USA, [2]Graduate School of Medicine, University of Tennessee Medical Center, Knoxville, TN, USA, [3]Neutron Scattering Science Division, Oak Ridge National Laboratory, Oak Ridge, TN, USA, [4]Graduate School of Medicine, University of Tennessee Medical Center, Knoxville, TN, Knoxville, TN, USA.

The current challenge in the amyloid field is to obtain structural information on the progression of associated aggregation pathways, relate them to the cause of disease, and specifically point to the species truly responsible for neurotoxicity. Huntington's disease (HD) is linked to the aggregation of mutant huntingtin (htt) peptide, which contains an abnormally long polyglutamine (polyGln) repeat that leads to the formation of fibrils with stable, β-sheet rich structures. Analogous to other neurodegenerative diseases like Alzheimer's, mature htt fibrils are thought to be overall protective while the earlier smaller intermediates are proposed to be toxic to neuronal cells. We performed time-resolved small-angle neutron scattering (SANS) experiments to monitor the structural kinetics for htt peptides having polyGln repeats in the normal (22 Glns) and pathological (42 Glns) range. In addition to observing the expected faster aggregation rate for longer polyGln repeats, we find distinct conformational differences between normal and pathological htt. We also present, for the first time, three-dimensional structures of intermediates formed at the earliest stages of htt aggregation as detected by SANS and obtained using *ab initio* shape reconstruction methods. Finally, we are able to investigate the internal structure of the mature fibrils, where the mass-per-length of pathological htt fibrils is considerably less than normal htt fibrils. These findings provide the first steps toward characterizing the oligomers formed by htt peptides and illustrate the utility of SANS for identifying different aggregate intermediates formed in the development of neurodegenerative diseases.

2893-Plat

Time-Resolved Small-Angle X-Ray Scattering Study of the Early Formation of Amyloid Protofibrils on a Apomyoglobin Mutant

Maria Grazia Ortore[1], Francesco Spinozzi[1], Silvia Vilasi[2], Ivana Sirangelo[2], Gaetano Irace[2], Anuji Shukla[3], Theyencheri Narayanan[3], Raffaele Sinibaldi[1], Paolo Mariani[1].
[1]Università Politecnica delle Marche, Ancona, Italy, [2]Seconda Università di Napoli, Napoli, Italy, [3]ESRF, Grenoble, France.

Early prefibrillar intermediates are a key issue in amyloid researches, as they show the highest cytotoxicity with respect to mature fibrils, which are less toxic or even harmless. However, the early aggregation process is largely unknown, since nucleation events are rare, and elongation and reorganization processes are very fast. Time-resolved synchrotron Small Angle X-ray Scattering (SAXS), coupled to extended model fitting analysis, has been used to provide in a millisecond temporal range the structural and aggregational properties of the early and soluble protofibrils formed by a model protein after a pH jump. The amyloidogenic apomyoglobin mutant W7FW14F has been investigated as fibril former: this mutant, which is in a monomeric, partly folded state at acidic pH, undergoes at neutral pH a nucleation-dependent polymerization reaction, resulting in the formation of cytotoxic amyloid fibrils similar to those detected for proteins involved in amyloid diseases. SAXS evidenced that oligomerization of W7FW14F in solution happens in less than 100 ms after the pH jump from 4.0 to 7.0., while the resulting pattern of protein prefibrillation reveals the simultaneous presence of worm-like species and of cylindrically-shaped aggregates, whose structural features mainly change after 20 ms from the solution pH jump. Model fitting analysis gives the composition of the different oligomers and their relative concentration as a function of time, suggesting that protofibril formation occurs through the presence of aggregation and rearrangement competing processes and through the contribution of multiple coexisting elongated and worm-like protein species. The possibility to use SAXS in monitoring the effects of cosolvents and/or pharmaceutical agents in modifying or preventing the early amyloid aggregation patterns is then demonstrated.

2894-Plat

AFM Imaging and Single-Molecule Force Spectroscopy of Transthyretin Amyloid Intermediates

Ricardo H. Pires[1,2], Maria J. Saraiva[2], Ana M. Damas[2], Miklós S.Z. Kellermayer[1].
[1]Dept. of Biophysics and Radiation Biology, Semmelweis University, Budapest, Hungary, [2]Institute for Molecular and Cell Biology, Porto, Portugal.

Aggregation of Transthyretin (TTR) in the form of amyloid fibrils is associated with systemic and neurological disorders. As part of the amyloid fibrilogenesis process, several oligomeric and protofibrillar intermediate structures have been identified and found to possess greater cytotoxicity than the mature amyloid fibrils. The structural dynamics and the molecular mechanisms behind the cytotoxicity of these intermediates are largely unknown.

In the present work we explored the structure, dynamics and mechanics of TTR amyloid intermediates with a combination of AFM imaging and single-molecule force spectroscopy. We show that annular oligomers display a tendency of association into a linear array. AFM imaging and force measurements indicated that annular oligomers are constituted by 8 TTR dimers that are largely unfolded when compared with native TTR. Associated annular oligomers undergo a collapsing structural transition before the appearance of amyloid protofibrils. The emerging TTR protofibrils display morphological features predicted by the double-helical model of the amyloid protofilament. Upon evoking their disassembly, protofibrils dissociated into annular oligomers. Thus, annual oligomeric species represent an important structural intermediate along both the assembly and disassembly pathways.

In this study we have dissected several structural transitions associated with the formation of TTR amyloid protofibrils. Because amyloidogenic aggregation is a potentially universal feature of proteins, the transitions reported here might be also relevant for other amyloidogenic disorders as well.

2895-Plat

Characterization and Single Molecule Conformational Studies of Soluble Alpha-Synuclein Oligomers

Adam Trexler, Elizabeth Rhoades.
Yale University, New Haven, CT, USA.

Alpha-Synuclein (αS) is a natively unstructured protein central to the pathology of Parkinson's disease. A growing body of evidence suggests that soluble oligomeric αS species are responsible for cell death which perpetuates Parkinson's. A variety of protocols have been described which populate oligomers *in vitro* for biophysical characterization, yet it remains unclear if these disparate protocols yield similar species and if these species are relevant to disease states. Furthermore, detailed structural analysis of these oligomers, which could be exceptionally useful towards elucidating mechanism of toxicity and avenues for disease treatment, remains difficult given their low abundance and apparent heterogeneity. In order to compare their bulk structural characteristics, we have prepared αS oligomers from a variety of protocols and characterized them using anti-oligomer antibody A11, cytotoxicity assays and colocalization studies with SH-SY5Y neuroblastoma cells, and ThT fluorescence to probe their ability to seed amyloid fibrillation. Our studies have identified a subset of oligomers which are on the order of 50 αS monomers in size, are A11-reactive, linking them to disease states *in vivo*, and are toxic to and readily taken up by cells in culture. We use single molecule Förster resonance energy transfer to measure the conformational states of individual αS monomers incorporated into oligomers. We have found in multiple regions of αS the protein apparently adopts a highly heterogeneous ensemble of conformations within oligomers, which emphasizes the suitability of single molecule techniques for their study. Through understanding the conformational states of αS before and after aggregation to toxic oligomeric species, we will provide insight into the mechanism of oligomer formation and toxicity.

Protein Dynamics - Simulations

2896-Pos Board B1

Identifying Binding Cooperativity in Protein Kinase a through Community Analysis

Mikolai Fajer, J. Andrew McCammon.

The binding of ATP and PKI to the catalytic sub-unit of protein kinase A is highly cooperative. A point mutation distal from both binding sites abolishes the cooperativity, and appears to be part of an allosteric network. To further investigate the allosteric network the apo, bound and mutated forms of the protein are simulated with replica exchange accelerated molecular dynamics (REXAMD). The REXAMD ensembles are validated by comparing computed NMR chemical shift perturbations against those derived from experiment.

Network models of the residue level correlation are constructed and separated into coarse grained communities that capture the allosteric network. The generality of these network models is tested by comparing mutations made directly to the network models against the mutated simulation. A broader mutational analysis of the network models is then performed in order to map out the allosteric network and identify key residues including the catalytic and regulatory spines.

2897-Pos Board B2

Molecular Dynamics Investigation on Conformational Dynamics of G Proteins

Jackson Chief Elk, J.B. Alexander Ross, Stephen R. Sprang.

We have carried out Principle Component Analysis (PCA) on a set of Molecular Dynamics (MD) trajectories computed from a set of G Protein X-ray crystal structures. G Proteins are comprised of three subunits and are important signal amplifying molecules that initiate secondary messenger cascades. Messenger cascades are responsible for initiating many biological processes and cataloging the behavior of the individual steps provides important data on cellular signaling that has potential pharmaceutical applications. In our studies the α subunit was studied exclusively because it contains the binding pocket for GDP/GTP and is the first in a series of molecules activated in signaling cascades. The specific regions Switch I-III, and P-loop on these proteins compose the binding pocket for GDP/GTP, and Switch III serves as an antenna for effector recognition. The Cα atoms on the polypeptide backbone were used in the PCA to examine the dynamics of the protein's conformation. These conformational dynamics are proposed to play an integral role in the enzyme's natural ability to shift from the resting to the active state where further rearrangements promote catalysis.

2898-Pos Board B3

Microscopic Picture of the Mechanism of Energy Transmission in F1-ATPase as Revealed by Molecular Dynamics Simulations

Jacek Czub, Helmut Grubmueller.

FoF1-ATPase is a rotary motor protein that synthesize ATP using the proton gradient across a membrane as a free energy source. The proton flow through the membrane-embedded Fo generates the rotary torque that drives the rotation of the F1 asymmetric shaft. Mechanical energy of the rotating shaft is used by the catalytic subunit of F1 to synthesize ATP against thermodynamic potential gradient. Here, we used fully atomistic molecular dynamics simulation to study the distribution of torsional elasticity in the F1 motor. Structural analysis of the rotational fluctuations revealed that the elasticity of the F1 shaft, as sensed by Fo or observed experimentally, arises from two distinct contributions: its intrinsic elasticity and an effective potential imposed by the catalytic subunit. We proposed also a simple model of the F1 energetics along the rotary degrees of freedom in the proximity of the resting state observed in the crystal structures. As opposed to the usually employed models where the motor mechanical progression is described by a single angular variable our multidimensional treatment emphasizes the spatially non-homogeneous nature of the central shaft and its interactions with the stator. We used it to predict the distribution of elastic energy stored within F1 when it is driven away from the resting state by the Fo power stroke. To directly investigate the mechanism of energy transmission between the rotor and stator subunits of F1 we employed a non-equilibrium MD approach where the central shaft is driven to rotate by externally applied torque. These simulations allowed for the elucidation of the mechanism by which the rotating shaft induces a sequence of conformational changes at the active sites.

2899-Pos Board B4

Class a Beta-Lactamase Dynamics from Molecular Dynamics Simulations

Olivier Fisette, Patrick Lagüe, Stéphane Gagné.

Two model class A beta-lactamases were studied using molecular dynamics. TEM-1, responsible for ampicillin resistance in E. coli, is the canonical beta-lactam-hydrolying enzyme. PSE-4 confers carbenicillin resistance to P. aeruginosa, an opportunistic pathogen. A total simulation time of 1.0 us for each enzyme in the free form allowed a precise determination of protein dynamics on the ~ 100 ns timescale. Comparison with NMR relaxation experiments and their model-free analysis shows quantative agreement between the two techniques. We also demonstrate how simulations can be used to interpret relaxation results and identify instances of over- and under-fitting in model-free analysis. Benzylpenicillin and carbenicillin were parameterised within the context of CGenFF, and an additional 1.0 us simulation time was acquired for both the TEM-1-BZP and PSE-4-CBC enzyme-substrate pairs. The dynamics of these complexes will be discussed, along with the effects of substrate binding and the role of the omega-loop.

2900-Pos Board B5

"DFG-flip" in the Insulin Receptor Kinase is Facilitated by a Helical Intermediate State of the Activation Loop

Harish Vashisth, Cameron F. Abrams.

The insulin receptor (IR) is a ligand-activated tyrosine kinase, whose ligand-stimulated catalytic activity and biological function depends upon trans-autophosphorylation of three activation loop (A-loop) tyrosines located in each of its cytoplasmic kinase domain (IRKD). Excised crystal structures of the inactive and active IRKD reveal that the A-loop is displaced by ~20A on activation. The highly conserved residues Asp1150, Phe1151, and Gly1152 at the N-terminus of the A-loop (the "DFG" motif) collectively "flip" to bury the Phe1151 underneath alpha-C-helix, and simultaneously present Asp1150 for ATP binding. However, the exact mechanism of the DFG-flip in the IRKD remains elusive, chiefly due to the unavailability of structural data on intermediate conformations of the A-loop. In this work, we have studied the inactive to active structural transition of the A-loop using temperature accelerated molecular dynamics (TAMD). Starting with the inactive A-loop conformation, a 50-ns of TAMD generated a target A-loop conformation within ~8A (RMSD) of the known active A-loop conformation. A further 20-ns MD-equilibration of this structure in the presence of ATP and phosphotyrosines stabilizes the A-loop conformation to an RMSD of ~4A with respect to its active state. Significantly, we also capture the DFG-flip during TAMD, and observe that this flip is facilitated by a transient three-turn helical conformation of the A-loop, the folding of which draws the placement of the side-chains of Phe1151 and Asp1152. Such transient helical conformations of the A-loop can potentially be exploited for the design of novel inhibitors that target a specific DFG conformation.

2901-Pos Board B6

Heirarchical Constrained Molecular Dynamics Simulations for Proteins

Nagarajan Vaidehi, Gouthaman Balaraman, In-Hee Park, Jeff Wagner, Abhinandan Jain.

Here we report a constrained molecular dynamics method that allows molecular models ranging from all-torsion to freezing parts of the protein as rigid body connected by flexible hinges, and studying the dynamics of proteins. This method is known as GNEIMO (Generalized Newton-Euler inverse mass operator method). We have derived new algorithms to assign initial velocities in the torsional space that obey the Boltzmann distribution. The effect of assigning initial velocities in the dihedral space (as opposed to transforming the Cartesian velocities to dihedral velocities), on the time taken for equilibrating the molecular system is analyzed.

We have demonstrated the capability of the GNEIMO method in handling a range of constrained dynamics simulations - from all torsion dynamics to freezing secondary structures as rigid bodies while modeling the rest of the protein connecting the rigid bodies with torsional degrees of freedom. The simulations where secondary structures are kept rigid, allowing torsions connecting these rigid bodies, are termed here as ''hierarchical'' simulations. We have applied the the hierarchical constrained dynamics for folding of small proteins, and refinement of low resolution protein models to high resolution structures. We find that the conformational sampling in hierarchical simulations is not only wider in range, but samples ''native like'' conformations more often than all-torsion or all-atom molecular dynamics simulations. We demonstrate the application of GNEIMO method for protein structure refinement.

2902-Pos Board B7
Unbiased Simulation of the Back and Forth Apo to Holo Conformations for the Calmodulin N-Terminal Nodule: A Sequence of Specific Events
Dupuis Lilianne, Normand Mousseau.
The 76-residues N-terminal nodule of the Calmodulin protein undergoes strong structural rearrangement as two calcium atoms bind or unbind from their EF-hand sites. Calmodulin is widely used in all kind of cells for a variety of tasks activated by the calcium ion. Calcium arrival allows 2 Helix-loop-Helix motives (EF-hands) to open cooperatively their hydrophobic core, allowing binding to protein targets. Numerous simulations have been made, with biased potential, to understand the folding pathway from either the apo to holo structures or vice versa. We present the results of an unbiased simulation using a detailed atomistic model extending the coarse-grained OPEP potential coupled with a multiscale saddle-point method for sampling configurations, identifying the two folding pathways and crucial interactions.

2903-Pos Board B8
Molecular Recognition Mechanism of Calmodulin Examined by Perturbation-Response Scanning
Canan Atilgan, A. Ozlem Aykut, Ali Rana Atilgan.
Calmodulin (CaM) has a pivotal role as an intracellular Ca2+ receptor that is involved in calcium signaling pathways in eukaryotic cells [1,2]. Binding of Ca2+ and proteins or small organic molecules to CaM induces large conformational changes that are distinct to each interacting partner [1,3,4]. To design drugs that inhibit Ca2+-CaM formation, the molecular binding mechanism must be thoroughly understood.
In this study, we use a new tool called perturbation-response scanning that is based on systematically exerting directed forces on the residues of the protein [5] and recording the changes in fluctuation profiles as the response. Different conformations of CaM are investigated to locate domains or key residues controlling ligand binding and release. We perform 200 ns long MD simulations on the apo form of CaM. The simulation is divided into chunks which resemble different conformations of the apo form. Using the cross-correlation matrices obtained from these chunks as the kernel in linear response, we determine the residues whose perturbation yields the experimentally determined displacement profiles of the apo and holo forms. We find that it is possible to induce the different conformational changes relevant to the binding of five different ligands, by perturbing varying ligand binding residues, and/or residues on the distant helices in the single apo-form. The findings thus give information on how the flexible linker region acts as a transducer of binding information to distant parts of the protein. This new tool enables us to reveal the essence of ligand recognition mechanisms by which CaM controls a wide variety of Ca2+ signaling processes.
1. Ikura M. et.al., PNAS 103:1159-1164.
2. Fallon J.L., et.al Structure 11:1303-1307.
3. Vandonselaar M.,et.al., Struct.Biol. 1:795-801.
4. Shepherd C.M., Vogel H.J., Biophys.J. 87:780-791.
5. Atilgan C., Atilgan A.R., PloS Comput.Biol. 5:e1000544.

2904-Pos Board B9
Modeling the Unbinding Mechanism of the Neutral and Anionic Semi-Quinone from the QA Site of Bacterial Reaction Centers Using Steered Molecular Dynamics Simulations
Jennifer Madeo, Maja Mihajlovic, Themis Lazaridis, M.R. Gunner.
Bacterial photosynthetic reactions centers are large integral membrane proteins that carry out a series of light initiated electron transfer reactions between bound co-factors. In the QA binding site ubiquinone is singly reduced to the anionic semi-quinone. Previous experimental studies using hydroxyl quinones at a pH above the pKa, showed that neutral and anionic quinone species have similar affinity for the QA site (Madeo et. al Biochemistry, 2005, 44 10994-11004). Despite this, anionic quinones dissociate from the QA site $10 \perp 3$ times more slowly than neutral quinones. This suggests that there are large kinetic barriers created by the protein for the dissociation of anionic quinones that are not present in the neutral state. The present study further investigates these barriers by applying constant-velocity steered molecular dynamics (SMD) to compare the unbinding of the neutral native ubiquinone and its anionic semiquinone. The same starting structure (1aij.pdb) is used in ubiquinone and semiquinone simulations, with partial charges adjusted to represent the equilibrated residue charge states. All simulations were performed with the GROMACS package with the OPLS-AA force field. A structural analysis of the trajectories generated during the unbinding of quinones identifies residues of the protein making stronger interactions with semiquinone than with ubiquinone and thus possibly contributing to the kinetic barriers. The magnitude of the energetic barrier is compared to the measured dissociation rate of anionic hydroxyl quinones.
Supported by NSF-MCB-1022208.

2905-Pos Board B10
Hierarchical Elastic Network Modeling of cryo-EM Data
Virginia Burger, Ivet Bahar, Chakra Chennubhotla.
Cryo-EM images of molecules are increasing in resolution, extending their uses from rigid-body docking to generation of atomistic density maps independent of prior structural information. Single molecule cryo-EM provides images of a molecule from many viewpoints, which are averaged and compiled to form a 3D reconstruction. This reconstruction determines the smallest possible hull enclosing the molecule, but sacrifices information about dynamic properties of the molecule intrinsically contained in the varied image set.
We suggest projecting the images into 3D space, without averaging out inconsistent densities, to form a probability map for the reconstruction. This map contains flexibility information neglected by earlier analyses of dynamics from density maps. To highlight different levels of molecular flexibility found in this map, we use a hierarchical elastic network model (hENM). The hENM uses the Markov transition probabilities between the voxels in the density map to segment the map into sets of multi-resolution nodes. Each voxel is initially taken as a node in the network, after-which the network is iteratively reduced to increasingly coarser sets of important nodes, forming a hierarchy. This method provides a unifying framework in allowing the derivation of dynamics concurrently with the study of information propagation through the network, with segmentation of the protein into structural sub-regions as an additional benefit. As these nodes highlight the core structural regions of the protein, they can also be used as anchor points for fitting high-resolution structures into EM maps. Preliminary results show excellent overlap between the dynamics computed using a Gaussian Network Model of the C-alpha atoms of proteins and those computed from our hENM nodes, validating the role of hENM in predicting intrinsic protein motions. With the greater goal of inferring function from dynamics, we work here to predict dynamics directly from cryo-EM images.

2906-Pos Board B11
Vectorial Network Model (VNM) for Protein Dynamics: An Analytical Tool for Protein Fluctuations
Yun Xu, Larisa Adamian, Jie Liang.
Dynamics play important roles in how proteins function. Coarse grained network model such as Gaussian Network Model (GNM) and Anisotropic Network Model (ANM) are widely used for studying dynamic changes of proteins. It provides an analytical treatment of different eigen modes of protein fluctuations based on the Gaussian assumption. However, GNM and ANM have limitations. For example, detailed mode analysis needed in these models often requires additional ad hoc knowledge for model selection. ANM can only describe mode specific relative movement between residues. It is difficult to combine different modes with proper weighting to describe the overall dynamic properties of a protein. Here we describe a new theoretical model that overcome these limitations. With a model where both potential energy and kinetic energy are accounted for, we can compute the magnitude and direction of fluctuation of each residue as well as their vectorial correlation analytically, without the aid of eigen mode analysis and with all modes accounted for properly. We describe how this approach can be used to identify the hinge region and model the hinge bending motion of calmodulin originally detected in NMR study.

2907-Pos Board B12
Towards Finding a Better Reaction Coordinate: NtrC and DIMS
Juan R. Perilla, Thomas B. Woolf.
All atom molecular dynamics is appealing due to the detailed insights towards protein function. But, all-atom molecular dynamics is limited due to the small amount of time spent in the transitions between stable states. Dynamic importance sampling (DIMS) enhances this sampling problem by biasing, with correction, to encourage sampling away from the stable states and to thus improve estimates of barrier crossing times. Nevertheless, DIMS has limitations based on the choice of order parameters that define intermediate states. To improve the representation, in DIMS, of order parameters, we have performed simulations of NtrC and have analyzed the transition populations. Our analysis, using techniques of nonlinear time series analysis and nonlinear dimensionality reduction, has enabled us to determine a new numerical method for finding reduced parameter descriptions of transitions in complex biomolecular systems. The results should enable an iterative approach to finding the best order parameter and at the same time improve convergence for estimates of reaction pathways, kinetics and relative free energy differences.

2908-Pos Board B13

The Short-Time Dynamics of Proteins Near Native State Conditions Signal to Robust Mechanisms Accessible at Long Times

Lin Liu, Angela M. Gronenborn, Ivet Bahar.

A number of recent computational studies have indicated that a robust pattern of motions is encoded by the particular architecture of a protein. These patterns have been shown to be of relevance to functional motions that occur on the much slower time scale of microseconds or longer. In addition, experimental data derived from NMR relaxation and other motion-containing NMR parameters as well as computational data from MD simulations indicate that the relative movements of residues at short times exhibit discernable correlations with those observed at long times. This intriguing issue was explored in the present work by conducting systematic molecular dynamics simulations of various durations, varying in the range 1 ns $\leq t_{tot} \leq$ 0.4 μs. While the observed amplitudes of motions are generally confined to 1 Å in short simulations with a general increase to 2-3 Å in the long ones, strikingly, the residue displacement distributions (away from equilibrium positions) exhibit comparable patterns. Careful examination of the relationship between the size of observed motion and the duration of simulations revealed a stretched exponential dependence of the the form y μ $x^{0.26}$, with x as representing the ratio of simulation lengths and y the ratio of the motional amplitudes, consistent with the observations made by Scheraga and coworkers.[1]

1. Senet P, Maisuradze GG, Foulie C, Delarue P, Scheraga HA. How main-chains of proteins explore the free-energy landscape in native states. *Proc. Natl. Acad. Sci. U. S. A* (2008) 105: 19708-19713.

2909-Pos Board B14

Allosterism in Muts Proteins: How DNA Mismatch Recognition Signals Repair

Susan N. Pieniazek, Manju M. Hingorani, David L. Beveridge.

Allosteric communication in multi-domain protein architectures is crucial in complex biological processes such as DNA mismatch repair (MMR). MutS proteins initiate MMR through recognition of mismatch DNA and signaling downstream repair. Mismatch recognition by MutS is followed by a marked decrease in the rate of ATP hydrolysis and DNA binding affinity. However, the nature of the coupling between the ATPase sites and DNA-binding site ~70 Å away remains a mystery, mainly because MutS is a relatively large dimeric protein.

Vast networks of interactions serve as support for protein structure. In MutS proteins, organized networks couple DNA mismatch affinity and ATP hydrolysis. We have performed all-atom molecular dynamics simulations (150 ns) on ATP-bound and ATP-free MutS complexes with mismatch DNA to understand the effect of ATP binding on structural networks connecting the ATPase sites and DNA-binding site. In particular, the eigenvectors of the correlation matrix reveal networks of mutually correlated residues, which are related to the paths of allosteric communication in MutS. Overall, several specific MutS structural components thought to be involved in allosteric coupling between DNA-binding and ATPase domains are present in the four largest eigenvalues: A) the involvement of domain II, which resides at the connection between domains V and III, appears in most of the correlations, especially in eigenvector 1; B) From eigenvector 1, MutS rigid domains III and V move together as a unit supporting their key role in the transmission of the signal from the, more flexible, DNA binding region to the ATPase site; C) the salient networks of correlated residues from eigenvector 4 (MutS-ATP-DNA) and eigenvector 3 (MutS-DNA) predominantly involve highly conserved long α-helical levers (IIIb and IV).

2910-Pos Board B15

Dynamics Encode Dynamically Committed and Uncommitted States in Protein Kinase A

Larry R. Masterson, Gianluigi Veglia.

The catalytic subunit of protein kinase A (PKA-C) is a promiscuous enzyme which phosphorylates a number of proteins in the cell. Our current view of the atomic details of substrate recognition has been derived from crystal structures with standard, largely non-physiologically relevant substrates. Herein, we present the full amide backbone dynamics of PKA-C bound to a physiologically relevant substrate (phospholamban peptide, PLN_{1-20}) and an inhibitor (protein kinase inhibitor, PKI_{5-24}). We found a direct correlation of decreasing dynamics in conserved residues of PKA-C as catalytic efficiency decreased. Strikingly, this decreased dynamics was also accompanied by increased thermal stability and unfavorable binding entropy. The dynamic character of the enzyme in the presence of a substrate or inhibitor is highlighted by residues that line the active site at the conserved glycine-rich, activation, and peptide positioning loops. These residues seem to display similar dynamics as the enzyme recognizes phosphorylatable substrates. The dynamics are severely attenuated when the enzyme binds PKI_{5-24}, particularly under high Mg^{2+} when inhibition is increased 100-fold. The necessity for concerted motions between the loops that line the active site opens the possibility for an evolutionary conserved role of dynamics which are encoded at spatially distinct regions of PKA-C. Molecular dynamics simulations support the observation that the conformational sampling of the enzyme is restricted by inhibition and that its energy landscape becomes well defined. We propose that ligand binding can induce either dynamically committed states in the enzyme that are driven by favorable conformational entropy, or dynamically uncommitted states that are driven by favorable enthalpy. The influence of dynamics on substrate recognition and the slow-step of catalysis will also be discussed.

2911-Pos Board B16

Molecular and Structural Insight for the Role of Key Residues of Thrombospondin-1 and Calreticulin in Thrombospondin-1- Calreticulin Binding

Qi Yan, Joanne E. Murphy-Ullrich, **Yuhua Song**.

Thrombospondin-1 (TSP1) binding to calreticulin (CRT) on cell surface signals focal adhesion disassembly. Residues of Lys 24 and 32 in TSP1 and amino acids 24-26 and 32-34 in CRT are critical for TSP1-CRT binding (Faseb J, 22:3968, 2008; J Biol Chem, 268:26784, 1993). This study investigated molecular and structural basis for the effect of these key residues in TSP1 and CRT on TSP1-CRT binding. Based on a validated TSP1-CRT complex structure (Biochemistry, 47:3685, 2010), we adopted steered molecular dynamics simulations to determine the effect of the mutations of these key residues on TSP1-CRT binding and validated the simulation results with experimental observation. We further performed 30 ns molecular dynamics simulations for wild type TSP1, CRT, TSP1 K24A&K32A mutant and mutant CRT (residues 24-26 & 32-34 mutated to Ala) and studied the conformational and structural changes of TSP1 and CRT by the mutations of the critical residues. Results showed that mutations of residues 24 and 32 to Ala in TSP1 and of amino acids 24-26 and 32-34 in CRT to Ala result in a shortened β strand in the binding site, decreased hydrogen bond occupancy for β strand pairs that are located within or near the binding site, increased conformational flexibility of the binding site, a changed degree of dynamic correlated motion between the residues in the binding site and the other residues in protein, and a changed degree of overall correlated motions between the residues in protein. These changes could directly contribute to the loss or reduced binding of TSP1-CRT complex and further affect TSP1-CRT binding induced cellular activities. Results from this study provide molecular and structural insight for the role of the critical residues in TSP1 and CRT in TSP1-CRT binding.

2912-Pos Board B17

Structural and Dynamic Effects Due to Glycation on Cholinesterases

César Millán-Pacheco, Benjamín Pérez-Aguilar, Noé Salinas-Arreortua, Eduardo Jardón-Valadez, José Luís Gómez-Olivares.

Diabetes mellitus is one of the most common diseases in the world. Currently around 3% of the global population suffers from diabetes and this is expected to double by 2030. During hyperglycemic episodes, protein glycation may occur on lysine residues. Decrease of biological activity as a direct effect of glycation has been shown on calmodulin, superoxide dismutase and calcium ATPase on human erythrocytes. In this work, we evaluated the structural and dynamical effects due to lysine glycation on human acetylcholinesterase and butyrylcholinesterase. Four probable sites were tested and analyzed for each cholinesterase by molecular dynamics simulations, using the CHARMM27 forcefield in NAMD at 298K, for 25ns on each model. The cumulative effect of each site was studied comparing it to the native, unglycated protein structure. The structural and dynamic consequences due to lysine glycation on the conformation of the choline binding site are reported.

Funding: Macroproyecto de Tecnologías de la Información y la Computación (UNAM), Centro Nacional de Supercomputo (IPICYT), Supercomputadora Aitzaloa (UAM). Postdoctoral Funding (CONACYT).

2913-Pos Board B18

Dynamics of Conformational Heterogeneity Within the Michaelis Complex of Lactate Dehydrogenase

Ruel Z. Desamero, Beining Nie, Nick Zhadin, Hua Deng, Robert Callender.

An enzymatic reaction involves the diffusion-controlled formation of an encounter complex between the protein and its substrate followed by the appropriate structural and dynamical arrangements producing Michaelis complex capable of product formation. In forming the Michaelis complex, the binding pocket is substantially rearranged: protein flaps or loops often close over the bound ligand, the binding pocket is desolvated, and catalytically important residues are brought into contact with the substrate. We probed the transient events associated with the binding of oxamate, a substrate mimic, to lactate dehydrogenase isolated from Bacillus stearothermophilus (bsLDH) using temperature jump (T-jump) relaxation techniques. T-jump relaxation monitors the

re-equilibration of a chemical system following an instantaneous increase in temperature induced by a laser pulse tuned to an infrared water band. The re-equilibration results in changes in the concentration of the species involved, and the transient changes are characterized using spectroscopic probes. To investigate the conformational changes associated with the binding of oxamate we studied the LDH from wild type cells as well as those from various single tryptophan mutants. These mutants were created by first replacing all tryptophans with tyrosine in wild type bsLDH to create a tryptophan-less template, followed by reintroduction of a single tryptophan at strategic sites in the protein. We probed the fluorescence emission of NADH in wild type and mutant bsLDH to report on the time evolution of the changes within the NADH environment over 100μs to 3ms time scale. Transients collected were then correlated to those resulting from a probe of tryptophan emissions. The results were then analyzed based on a plausible kinetic model. A comprehensive picture of the dynamics of ligand binding and Michaelis complex formation in bsLDH is obtained from the various structural reporters.

2914-Pos Board B19

Sequence, Structure and Dynamics Analysis of Thermostability in Endoglucanases

Ragothaman M. Yennamalli, Jeffrey D. Wolt, Andrew J. Rader, Taner Z. Sen.

Endoglucanases are crucial enzymes used in the production of biofuels from cellulosic biomass, a process which requires thermostability at high processing temperatures. Despite the economic importance of these industrial proteins, we currently lack a basic understanding of how some endoglucanases can efficiently function at elevated processing temperatures, while others with the same fold have substantial reduction in activity.

Here we explore the origins of thermostability in endoglucanases from sequence, structure, and dynamics perspectives using thermostable and mesostable protein sets. We performed a comparative sequence and structure analysis for thermophilic and mesophilic endoglucanases in $(\alpha/\beta)_8$, β-jelly roll, and $(\alpha/\alpha)_6$ folds, followed by a dynamics analysis of the $(\alpha/\beta)_8$ fold using elastic network models. We observed that thermophilic endoglucanases and their mesophilic counterparts differ significantly in their amino acid compositions. Interestingly, these compositional differences are specific to protein folds and enzyme families and lead to modification in hydrophobic, aromatic, and ionic interactions in a fold-dependent fashion.

We then focused specifically on a pair of thermostable and mesostable endoglucanases for a detailed dynamics analysis. It is often the case that thermophiles have shorter loops than their mesophilic counterparts, which was suggested to impart thermostability. In our case, however, the thermophile surprisingly possessed three insertions in the mesophilic loop regions and therefore has longer loops. The comparative structural dynamics analysis using elastic network models of $(\alpha/\beta)_8$ fold indicate that these three loops may contribute to the thermostability by modulating the direction of correlated motions between the catalytic residues (acid/base donor and nucleophile). We also observed that the thermostable protein showed larger dynamic domains than its mesostable counterpart, which suggests that cooperative dynamics is a critical contributing factor to thermostability.

2915-Pos Board B20

The Role of Dynamics in Protein Evolution

Tyler Glembo.

Protein evolution has most commonly been studied either theoretically, by analyzing the sequence of the protein, or experimentally, by resurrecting ancestral proteins in the lab and performing ligand binding studies to determine function. Thus far, structural and dynamic evolution have largely been left out of molecular evolution studies. Here we incorporate both structure and dynamics to elucidate the molecular principles behind the divergence in the evolutionary path of the gluccocorticoid and mineralocorticoid steroid receptor proteins. We begin by determining the likely structure of three evolutionary diverged, ancestral steroid receptor proteins using the Zipping and Assembly Method with FRODA (ZAMF). Our predictions are within 1.9Å RMSD of the crystal structure of ancestral corticoid steroid receptor. Beyond comparing static structure prediction, the main advantage of ZAMF is that it allows us to observe protein dynamics. Therefore we can investigate differences in the diverged proteins' available dynamic space by performing Principle Component Analysis (PCA) on the last .5ns of the converged MD trajectories obtained from ZAMF. We then analyze fluctuation profiles and cross-correlation maps from the slowest modes. This analysis enables us to identify critical mutations that most affect dynamics, therefore it shows the critical mutations leading to a divergence in function. We observe evolutionary diverged proteins do not share the same dynamic subspace. As this affects phenotype, we then compare binding specificities of these predicted structures to experimentally determined values by docking different ligands using ROSETTALIGAND and DrugScore online server.

2916-Pos Board B21

Conditional Mg^{2+}-Assisted Catalysis: A Master Switching Motif Responsible for Differential Stability Suggests a General Transducing Mechanism

Charles W. Carter, Violetta Weinreb, Li Li, Brian Kuhlman.

B. stearothermophilus Tryptophanyl-tRNA synthetase (TrpRS) uses different conformational states to catalyze tryptophan activation. A single Mg^{2+} ion increases transition state stabilization by −6.5 kcal/mol for optimal catalysis. Catalytic assist occurs if, and only if, the Mg^{2+} interacts with the protein. We are trying to identify the metal-protein interactions that produce this catalytic effect. Physical interactions between Mg^{2+} and TrpRS are mediated indirectly via active-site lysines K111, K192 and K195. Mutations of these lysines showed that they all stabilize the transition state. However, their interactions with the Mg^{2+} significantly reduce their catalytic effects. Catalytically productive interactions between TrpRS and the Mg^{2+} ion must therefore arise from outside the active site. We identified a core set of residues we call the D1 switch because they move during the catalytic conformational transition. The D1 switch lies at the corner of the N-terminal ß-α-ß crossover distal to the active site. It is highly conserved in Rossmannoid proteins. The Rosetta Design program suggested that mutations of D1 residues could ''hyperstabilize'' the activated state observed just prior to catalysis. Multimutant thermodynamic cycles together with substitution of Mn^{2+} for Mg^{2+} and [ATP]-dependent Michaelis-Menten kinetics demonstrate significant long-range *synergistic* coupling between the D1 switch and the Mg^{2+} ion. Thus, long-range interactions to the metal likely drive catalysis indirectly, by changing an inactive Mg^{2+} coordination into one that can stabilize the transition state. In this way transition-state stabilization by Mg^{2+} occurs if, and only if, conformational changes reposition it. We suggest that other NTPase enzymes may use similar conditional activation of Mg^{2+} to couple catalyzed hydrolysis of their purine triphosphate substrates to conformational changes, thereby transducing chemical free energy for cellular work and signaling. Supported by NIGMS 78227, 90406.

2917-Pos Board B22

Evolutionarily Conserved Linkage Between Enzyme Fold, Flexibility, and Catalysis

Pratul K. Agarwal.

Proteins are not static but rather are intrinsically flexible molecules. The role of internal protein motions in designated function, such as enzyme catalysis, is widely debated. The role of protein structure in enzyme catalysis is well established; and conservation of structural features provides vital clues to their role in function. Recently, it has been proposed that the protein function may involve multiple conformations: the observed deviations are not just inconsequential random thermodynamic fluctuations; rather, flexibility may be closely linked to protein function, including the catalytic efficiency of enzymes. We hypothesize that the argument of conservation of important structural features can also be extended to identification of protein flexibility in interconnection with enzyme function. Results from three classes of enzymes (prolyl-peptidyl isomerase, oxidoreductase and nuclease) catalyzing diverse chemical reactions will be presented. The identification and characterization of the internal proteins in multiple species show identical enzyme conformational fluctuations. In addition to the active-site residues, motions of protein surface loop regions are observed to be identical across species, and networks of conserved interactions/residues connect these highly flexible surface regions to the active-site residues that make direct contact with substrates. More interestingly, examination of reaction-coupled motions in non-homologous enzyme systems (with no structural or sequence similarity) that catalyze the same biochemical reaction show motions inducing remarkably similar changes in the enzyme-substrate interactions during catalysis. Examination of conformational sub-states along the reaction pathways also provides vital insights into role of enzyme flexibility in enabling the attainment of transition states. The results indicate that the reaction-coupled flexibility (along with structural features) is a conserved aspect of the enzyme molecular architecture. Protein motions in distal areas of homologous and non-homologous enzyme systems mediate similar changes in the active-site enzyme-substrate interactions, thereby impacting the mechanism of catalyzed chemistry.

2918-Pos Board B23

Probing the Kinetic Network of Folding-Unfolding Transitions in Proteins

Ronan D. Murphy, **Nicolae-Viorel Buchete**.

The formation of secondary and tertiary structure elements in protein folding are intrinsically complex processes, notoriously difficult to study in a systematic manner. We construct coarse master equations for helix formation processes based on data from atomistic molecular dynamics simulations of helix-rich proteins. By carefully controlling the effects of fast, non-Markovian transitions, on one hand, and the typically limited sampling of slow relaxation processes on the other hand, we probe the underlying network of folding-unfolding transitions between the various configuration states of a protein. This systematic analysis reveals the transition states and the

associated folding pathways at multiple levels, from atomistic to coarse-grained representations. We validate our approach in folding studies of short helix-forming polyalanine peptides, as well as of a larger, helix-turn-helix subdomain of a viral scaffolding protein. Our analysis of local, site-specific formation of intra- and inter-chain interactions is a first step towards understanding the elementary stages of secondary and tertiary structure formation in the folding of large proteins, and it allows a direct comparison to data from recent infrared vibrational spectroscopy studies.

2919-Pos Board B24

Flow-Induced Beta-Hairpin Folding of the Glycoprotein Ib-alpha Beta-Switch

Xueqing Zou.

Flow-induced shear has been identified as a regulatory driving force in blood clotting. Shear induces beta-hairpin folding of the glycoprotein Ib-alpha (GPIb-alpha) beta-switch which increases affinity for binding to the von Willebrand factor, a key step in blood clot formation and wound healing. To explore the mechanism underlying the flow-induced conformational transition, we conducted altogether 2.1 microsecond molecular dynamics simulations of flow acting on the beta-switch of GPIb-alpha. Simulations sampling different flow velocities reveal that under flow, beta-hairpin folding is initiated by hydrophobic collapse, followed by interstrand hydrogen bond formation and turn formation. Adaptive biasing force simulations are employed to determine the free energy required for extending the unfolded beta-switch from a loop to an elongated state. Lattice and freely-jointed chain models illustrate how the folding rate depends on the entropic and enthalpic energy, the latter controlled by flow. The results reveal that the free energy landscape of the beta-switch has two stable conformations, loop and hairpin, imprinted on it. Normal flow prefers the disordered state; high shear flow prefers the ordered state, inducing thereby a transition between the two.

2920-Pos Board B25

Protein Flexibility Partitions the Effects of Energy Landscape Roughness Between Activation Energy and Internal Friction

Anna A. Rauscher, Zoltan Simon, Gergely J. Szollosi, Laszlo Graf,
Imre Derenyi, Andras Malnasi-Csizmadia.

The rate of protein conformational changes are usually not only limited by external but also internal friction, however, the origin and significance of this latter phenomenon is poorly understood. By investigating the internal friction during the activation of two trypsin mutants at various temperatures and external viscosities we have discovered that the temperature dependence of the internal friction shows an Arrhenius-like behavior. The characteristic energy of the Arrhenius formula, however, can change dramatically upon the replacement of a single amino acid at a hinge position (thereby affecting the flexibility of the protein), or by crossing a critical temperature. At the same time, the activation energy of the conformational transition also changes with a similar magnitude, but in the opposite direction. These observations shed light on the intricate interplay between the apparent internal friction and activation energy. Moreover, we have found that the more flexible a protein is the greater proportion of its activation energy is partitioned into internal friction. All these results have allowed us to come to the general conclusion that the different hierarchical levels of the roughness of the energy landscape along a conformational transition can be observed as either activation energy or internal friction depending on the degree of flexibility of the protein.

2921-Pos Board B26

Relationship Between Internal Friction and the Roughness of the Energy Landscape of Protein Conformational Changes

Anna Á. Rauscher, Zoltán Simon, Gergely J. Szöllősi, László Gráf,
Imre Derényi, Andras Malnasi-Csizmadia.

We constructed a quantitative model based on experimental data that describes the relationship between the roughness of the energy landscape, activation energy and internal friction of enzyme conformational changes. We investigated an interdomain conformational rearrangement, trypsinogen 4 activation using transient kinetic methods. The temperature and viscosity dependence of the rate constant of the conformational change was measured in order to determine the temperature dependence of its internal friction. To test the effect of flexibility on internal friction, glycine and alanine mutations at a single position of the hinge of the interdomain region were introduced. Internal friction showed an Arrhenius-like temperature dependence, the characteristic energy of which increased with the flexibility of the hinge.

We found that the activation energy, i.e. the height of the energy landscape, is partially converted into internal friction to an extent depending on the flexibility of the protein. We interpret this phenomenon using a model that assumes different hierarchical levels of roughness of the energy landscape.

2922-Pos Board B27

Predicting Sequence of Events upon Ligand Binding Using PMT Model: A Case Study of Adenylate Kinase

Gamze Gursoy, Hsiao-Mei Lu, Jie Liang.

Conformational transitions play a crucial role during the reaction cycle of many enzymes. In the case of adenylate kinase (AK), binding of ATP and AMP induces a conformational change where the closing of the LID and NMP domains over the core domain is followed by the phosphate transfer from ATP to ADP. This conformational change is rate-limiting for the enzymatic reaction, and AK is thought to be in equilibrium between open and close states. In this work, we studied the sequence of events along the conformational transition pathway. Using the Perturbation-based Markovian Transmission (PMT) model [Lu and Liang, PLOS Computational Biology, 2009], we study each of the 45 intermediate conformations available in PDB. We apply an initial perturbation on the binding domains of the enzyme, whose transmission is modeled as a Markovian Process. The dynamics of the probability flow is then computed by solving the Master Equation using a Krylov subspace method. From the landscape of time-evolving probability flow of all residues upon initial perturbation, we calculated the information entropy and related parameter for each residue. By analyzing time-dependent changes in entropy of residues located within or are in-contact with the LID/NMP domains, we predicted contacts that would break first for each conformation. Using the initial open state conformation only we are able to identify the next conformation along the conformation transition pathway with an average accuracy of 85% in predicted bond breakage We also predicted a set of critical residues with distinct dynamic behavior that are important in ligand binding.

2923-Pos Board B28

A Comprehensive Examination of the Contributions to Binding and Activation Entropies

Jie Cao, Arieh Warshel.

The elucidation of the role of entropic effects in enzyme catalysis and binding free energy is a problem of practical and fundamental interest. In order to address this problem it is essential to develop simulation methods capable of evaluating the entropic contribution to the overall free energy. Such an evaluation is useful for assessing temperature effects and exploring specialized options in enzyme design. In fact, the general ability to evaluate activation entropies of chemical reactions in solution has long been a challenge to computational chemists. Here we present what is probably the first microscopic evaluation of all of the relevant components to the relevant entropy, namely, configurational, polar solvation and hydrophobic entropies. All of these contributions are evaluated by the restraint release (RR) approach. In the case of binding entropies we found out major compensation effects in both the solvation and hydrophobic effect, and despite some overestimate, can provide very useful insight. Furthermore, exciting current use of our approach lead to the elucidation of the origin of the puzzling strong temperature dependence of the activation entropy in ADH. It is found that this effect does not reflect any dynamical factor, but rather the change in the polarization of the protein polar groups (plus water molecules) upon moving from the ground state to the transition state. This helps to resolve the long-standing question about the origin of the observed non linear Arrhenius plot.

2924-Pos Board B29

Structural Instability of the Active Site of T1 Lipase where Na^+-π Interaction is Replaced with Water-π Complex

Yohsuke Hagiwara, **Jiyoung Kang**, Masaru Tateno.

The cation-π interaction is one of the strongest noncovalent forces. However, its biological role has been unknown, since few structures containing cation-π interaction have been determined in biological systems. Matsumura, et al. determined the crystal strcture of T1 lipase and found interactions between Na^+ and the aromatic ring of Phe16 in the active site. However, this Na^+-π interaction remained to be discussed whether it really exists or not. To investigate structural stability of Na^+-Phe interactions, we performed molecular dynamics (MD) simulations of T1 lipase.It is well known that the current conventional force fields cannot estimate the cation-π interaction correctly, whereas *ab initio* calculations require huge computational costs for the MD simulations. Accordingly, we developed a novel scheme to calculate the interaction energy with a high accuracy compared with the CCSD(T) level, and with a low calculation cost compared with the force field calculations. The result of our calculations definitely showed that the large enthalpy gain of the Na^+-π interaction was required to preserve the catalytic core structure. Since experimental approaches could not dismiss the possible presence of water instead of Na^+ in the active site of T1 lipase, we also examined the effects of water by performing MD simulations. Our analyses revealed that the water-π complex was unstable and led to the collapse of the coordinated structure of the active site. Thus, we

concluded that the possible presence of water may be excluded. Our novel scheme is currently the only way to perform long-time MD simulations involving cation-π interactions with reasonable computational cost and with high accuracy. Based on this analysis, we propose a novel structural and functional element indentified in the active site of T1 lipase.

2925-Pos Board B30
Protein Degradation Kinetics and Biochemical Oscillations
Lida Xu, Zhilin Qu.
Protein ubiquitination and degradation are very important posttranscriptional regulatory processes which are required for biological systems. It is well known that for biochemical oscillations to occur, besides other posttranscriptional regulation, such as phosphorylation and dephosphorylation, the rates of protein synthesis and degradation have to be properly matched. However, the properties of protein degradation kinetics and how they affect biochemical oscillations are not well understood. In this study, we first developed a biochemical reaction model of protein ubiquitination and degradation based on the up-to-date experimental information and calculated the degradation rate against the concentration of the free substrate. The model was tuned to a recent experimental dataset of protein ubiquitination. We show that when the substrate concentration (or synthesis rate) is low the degradation rate linearly increases with the substrate concentration, but as the substrate concentration increases further it becomes nonlinear and eventually saturates. We then studied analytically how linear and nonlinear degradation kinetics affect the instabilities that leads to oscillations using three generic biochemical oscillation models: pure negative feedback induced oscillations (the Goodwin model); pure positive feedback induced oscillations; and combined positive and negative feedback induced oscillations. In all three cases, nonlinear degradation kinetics promotes oscillations and results in much larger oscillation amplitude than the linear kinetics does. On the other hand, the time delay due to protein ubiquitination and deubiquitination generally suppresses oscillations. We finally used computer simulations of cell cycle and circadian rhythm models combined with the detailed protein ubiquitination and degradation model to demonstrate our theoretical predictions from the simplified models.

Protein Aggregates II

2926-Pos Board B31
Halting the Amyloid March: How a Novel Ca_{2+}-Binding Protein, NUCB1, Prevents the Formation of Amyloid Fibrils
Ruchi Gupta, Neeraj Kapoor, Daniel P. Raleigh, Thomas P. Sakmar.
The aggregation of hydrophobic peptides into amyloid fibrils is a characteristic pathological feature observed in Type 2 diabetes, Alzheimer's disease (AD), Parkinson's disease (PD) and Huntington's disease. Both amyloid fibrils and their pre-fibrillar aggregates exhibit toxicity and it is generally believed that prevention of aggregation of pathogenic amyloid peptides would prevent disease progression. In our recent studies, we have discovered a unique anti-amyloidogenic function of the soluble form of human Ca2+-binding protein, NUCB1, namely sNUCB1. We show that sNUCB1 can inhibit amyloid fibril formation of both Amylin and Aβ42 at sub-stoichiometry concentrations. Amylin and Aβ42 are amyloidogenic peptides implicated in the pathophysiology of adult-onset diabetes mellitus and Alzheimer's disease, respectively. sNUCB1 can inhibit amyloidogenesis even after nucleation and protofibrillar stages and the process is reversed at high concentrations of Ca2+. Once fibrils are formed, sNUCB1 can also disaggregate them in a concentration dependent manner but only in the absence of Ca2+. The mechanistic investigation shows that sNUCB1 stabilizes an oligomeric state of hIAPP aggregate. Ca2+-free sNUCB1 binds to and stabilizes a prefibrillar species of hIAPP by ''capping'' the ends. We further demonstrate that Ca2+-free sNUCB1 bound prefibrillar species are dead-end products incapable of seeding the aggregation reaction of hIAPP. Furthermore, sNUCB1 stabilized prefibrillar species of Aβ42 show no toxicity in cell viability assays.

2927-Pos Board B32
Decrease in Size of Hen Egg white Lysozyme Aggregates with Decrease in Monomer Concentration from Micro to Nanomolar in Alkaline pH
Vijay K. Ravi, Kapil D. Singh, Aditya Iyer, C.N. Reddy,
Rajaram Swaminathan.
Earlier work from our laboratory has demonstrated that hen egg white lysozyme (HEWL) is an excellent model protein for investigating protein aggregation at an alkaline pH of 12.2. Exposure of HEWL to this pH at monomer concentrations from 0.3 to 120 uM, yielded amyloid fibrils as shown previously. Here we present the following concentration dependent changes observed with HEWL aggregates subsequent to incubation at pH 12.2 at room temperature from 0 to 24 hours. A) a two-fold increase in exposure of trp residues in HEWL to water at 0.3 uM compared to 120 uM as revealed by fluorescence quenching experiments with iodide B) a several fold increase in ANS fluorescence intensity accompanied by significantly blue-shifted emission on binding to HEWL moving from 0.3 to 120 uM. C) a marginal increase in dansyl probe fluorescence intensity accompanied by significant blue-shifted dansyl emission in dansyl conjugated HEWL moving from 0.3 to 120 uM. D) a gradual increase in steady state fluorescence anisotropy of dansyl probe in dansyl conjugated HEWL moving from 3 to 120 uM, although the dansyl mean fluorescence lifetime remained concentration independent between 3 and 120 uM. E) presence of all cys in -SH form with absence of any change in free [-SH] between 20 & 120 uM, as revealed by DTNP assays. In addition, FCS measurements with rhodamine conjugated HEWL demonstrated facile aggregation of HEWL in the concentration range 25 nM to 120 uM. The above results imply that, the size of HEWL aggregates, are clearly dependent on the initial monomer concentration, with lower concentrations like 300 nM favoring small aggregates that possess solvent exposed trp, diminished binding towards ANS and shorter mean fluorescence lifetime for dansyl probe.

2928-Pos Board B33
Does Thioflavin-T Detect Oligomers Formed During Amyloid Fibril Assembly
Christopher Persichilli, Shannon E. Hill, Jason Mast, **Martin Muschol**.
Deposits of insoluble protein fibrils with cross β-sheet structure are the hallmark of numerous human disorders, including Alzheimer's disease and type II diabetes.Recent results have indicated that oligomeric intermediates, emerging during amyloid fibril assembly, represent the main molecular species responsible for toxicity to cells and tissues. Hence, detection of oligomers is critical for studying amyloid toxicity, for discerning the details of amyloid fibril self-assembly, and for developing inhibitors of oligomer formation. Thioflavin-T (ThT) is among the most commonly used indicator dye for the detection of mature amyloid fibrils *in vitro*. However, it is not clear which of the various intermediates of fibril growth (oligomers, protofibrils and protofilaments) are detected by ThT fluorescence.
To investigate this question, we used ThT for monitoring amyloid fibril formation of hen egg white lysozyme under partially denaturing conditions. We correlated changes of ThT fluorescence with dynamic light scattering (DLS) and atomic force microscopy (AFM) on the same samples. We have previously shown that the combination of DLS and AFM reliably detects all intermediates formed during amyloid fibril growth [1]. Furthermore, we could study the ability of ThT to discern among two distinct pathways of lysozyme fibril formation: oligomer-free assembly *vs.* an oligomeric assembly pathway.
We found that ThT fluorescence did not detect oligomer growth or the nucleation of oligomeric filaments (protofibrils) during lysozyme fibril growth. However, ThT fluorescence increases did coincide with the formation of monomeric filaments (protofilaments) in the oligomer-free assembly pathway. These observations imply that ThT fluorescence is not a generally suitable tool for the detection of oligomeric intermediates during amyloid fibril growth. The selectivity of ThT for protofilaments over oligomers also suggests that the internal structure of oligomeric *vs.* monomeric filaments is distinctly different.
[1] Hill et al., Biophys. J. (2009), 96:3781-3790.

2929-Pos Board B34
Photo-Induced Fibrillar Formation of Chicken Egg White Lysozyme Under Native Conditions
Jin-Bing Xie, Meng Qin, Zhi-Qiang Yan, Yi Cao, **Wei Wang**.
Proteins are generally quite stable under native condition. However, recent findings showed that many proteins can form amyloid-like fibrils under native conditions by introducing destabilizing mutations or inserting amyloidogenic sequences to proteins at the gene level. Can posttranslational modifications at protein level also induce the fibrillar formation? Here we show that alternation of disulfide bonds, as one kind of such modifications, can initialize fibril formation under native conditions. We used UV-illumination to control the breakage and formation of disulfide bonds in chicken egg white lysozyme (CEWL). Through a cassette of tryptophan based photochemistry, the two terminal disulfide bonds in CEWL can be selectively ruptured. Such alternation mildly disrupts the local structure and results in structural flexibility of the C-terminal fragment, which allows the C-terminal fragment hooping between ''open'' and ''close'' states by thermal fluctuation. The ''open'' state can serve as the precursor for fibrillar aggregation. We found that in these fibrils the CEWL molecules are still native-like and connected through intermolecular disulfide bonds, different from those in amyloid-like fibrils with beta-sheet structures. Based on our experimental evidences and all-atom molecular dynamics simulation, we proposed an ''runaway domain-swapping'' model for the structure of CEWL fibrils, in which each CEWL molecule swaps its C-terminal fragment into the complementary position of the adjacent molecule along the fibrils via intermolecular disulfide bonds. Furthermore, we also found that the fibrils

can mature into fibrillar bundles due to hydrophobic interactions between the fibrils. Besides genetic modifications, our study stands for the first example of formation of protein fibrils under native conditions through posttranslational modification. Our finding suggests that long time exposure of organisms to UV radiation may cause damage of protein functions.

2930-Pos Board B35

A 2DCOS Infrared Study of Fibril Formation

Igor de la Arada, Nerea Andraka, **Jose Luis**, R. Arrondo.

Amyloid fibrils are proteinaceous aggregates that can be formed in the process of degenerative diseases. Insulin is a model of fibril formation that has produced a wealth of biochemical and structural data. The time-course of fibril formation can be followed by infrared spectroscopy looking at the appearance of a characteristic band in the lower region of extended structure. The kinetics is triggered by temperature at 70 °C and pH 2.3.The infrared spectrum shows, that after a lag time (concentration-dependent), the α-helical band decreases and the random coil component increases subsequently. Random coil increases up to a percentage and later a band at 1626 cm-1, associated with extended chains, replaces the random coil component. Infrared 2D-COS has been applied to different stages of the process. Maps have been formed at different incubation times: before random coil formation and at different stages in the random coil-fibril change. Synchronous two-dimensional IR map shows that the process occurs in a two step mode. At pH 7.0, heating of insulin for long periods does not produce the random coil structure and subsequently no fibrils are formed. Human insulin, with a different aminoacid in the N-terminal segment, forms a fibril formation in a lower time than bovine or porcine. The bandshape corresponding to the fibril is different if bovine insulin is compared with human and porcine; what can be associated with a difference in aminoacids 8 and 10 that are located in the intrachain disulfide bond loop. The results show that small changes in protein sequence makes the kinetics different. Lipids have been proposed as one factor influencing fibril formation. The effect of different lipid composition, including anionic lipids, sphingomyelin and cholesterol has also been studied to see changes in kinetics looking at the lipid charge.

2931-Pos Board B36

General *In-Vitro* Catalysis of Amyloid Formation by the Bacterial Curli Protein

Kevin Hartman, Jeffery Brender, Nataliya Popovych, Matthew R. Chapman, Ayyalusamy Ramamoorthy.

Proteins misfolded into insoluble, fibrillar aggregates known as amyloid are a pathological feature of many common and devastating diseases. Amyloid formation is typically a slow process that can be strongly affected by extrinsic factors, among the most critical being the presence of a small amount of preformed seeds that serves to nucleate aggregation. Amyloid nucleation is often considered a highly specific process dependent on a high degree of similarity in both peptide sequence and fiber morphology. However, we show here that amyloid fibers known as curli that are produced in E. coli and related bacteria catalyze amyloid formation of a variety of dissimilar amyloidogenic peptides and proteins, including PAP248-286 (SEVI), insulin, and calcitonin. The preformed curli fibers appear to act as a nucleation site for amyloidogenic proteins and as such, can decrease the induction time, sometimes drastically, and induce the formation of fibers. In particular, cross-seeding of SEVI amyloid formation by curli was more effective than seeding the reaction with SEVI amyloid fibers obtained under a different reaction condition. The elongation rate of fiber formation is also increased for some (but not all) of the proteins tested, indicating curli can also increase in some circumstances the rate of addition of proteins to the ends of amyloid fibers. Curli and curli-like amyloid fibers are ubiquitous in mammalian hosts, in fact, the innate immune response common to almost all amyloids has been proposed to have evolved as a response to curli amyloid formation by E. Coli. Given that certain bacteria that express a curli-like protein colocalize with amyloid deposits in Alzheimer?s patients, the induction of amyloid formation by curli may be a factor of high clinical importance.

2932-Pos Board B37

Structure, Dynamics and Surface Hydrophobicity of the Cataract-Associated Mutant, Pro23Thr of Human Gamma D-crystallin: Molecular Basis of Cataract Formation

Priya R. Banerjee, Swamy Puttamadappa, Ajay Pande,
Alexander Shekhtman, Jayanti Pande.

The cataract-associated Pro23Thr (P23T) mutation in human gammaD-crystallin (HGD) is geographically widespread - thus there is considerable interest in determining the molecular basis of opacity. In an earlier study (1), we found that the mutant showed markedly lowered, retrograde solubility compared to wild-type HGD, leading to the conclusion that the aggregation of P23T was mediated by hydrophobic protein-protein interactions. Subsequently, using NMR (2) and a binding assay with the fluorescent dye Bis-ANS (3), we showed that, in fact, hydrophobic patches were generated on the surface of the mutant protein. Those studies (3) also suggested that the binding site for Bis-ANS on P23T may coincide with the self-association site of the mutant and result in its lowered, retrograde solubility. Here we present new NMR-evidence to identify the Bis-ANS binding sites, and using independent NMR dynamics studies, also show that there is a measurable reduction in the flexibility of the peptide backbone near the hydrophobic patches. These two factors, namely the creation of hydrophobic patches and the lowered peptide backbone flexibility, taken together make a compelling argument that the hydrophobic patches may indeed facilitate the nucleation of aggregates of P23T which are held together by net hydrophobic interactions. Such aggregation would explain the retrograde solubility as well as the lens opacity *in vivo*.

1. Pande et al (2005) *Biochemistry*, **44**, 2491-2500.
2. Pande et al (2009) *Biochem. Biophys. Res. Commun.,* **382**, 196-199.
3. Pande et al (2010) *Biochemistry,***49,** 6122-6129.

Supported by NIH grants GM085006 to AS and EY010535 to JP.

2933-Pos Board B38

Polymorphism of Amyloid Fibrils Formed by a Short Peptide from Yeast Prion Protein Sup35: AFM and Tip Enhanced Raman Scattering Study

Alexey V. Krasnoslobodtsev, Alexander M. Portillo, Tanja Deckert-Gaudig, Volker Deckert, Yuri L. Lyubchenko.

Misfolding of prion protein and its subsequent aggregation is the cause of various prion related diseases. Prions are composed of aggregates of a misfolded prion protein. Although primary structure of prion protein is the same, its infectious form, amyloid fibrils, exist as multiple strains. The ability of prions to generate multiple strains poses an immediate health threat, which renders studies of this phenomenon very important. The strains are thought to represent structurally different prion protein molecules packed into amyloid fibrils. The biophysical properties of the fibrils, such as fragility, represent a major mechanism of prion amplification. Here, we demonstrate that variations in environmental conditions such as pH, salt concentration, temperature and mechanical stress (stirring) produces a variety of fibrillar polymorphs for a short peptide CGNNQQNY from yeast prion protein Sup35. The fibrils differ by their length and diameter as well as their ability to bundle together. We have used Tip-Enhanced Raman Scattering (TERS) in combination with AFM to study underlying conformational peculiarities of peptides within individual aggregates. Two types of fibrils were investigated, one formed in water and another one at pH 5.6. These conditions produce morphologically distinct fibrils in terms of their length and diameter. They also exhibited different kinetics of aggregation. The Raman spectra obtained with TERS also revealed the peptide conformational differences between these two types of fibrils. The observed differences are mostly manifested in the positions of the characteristic amide bands (I and III), suggesting that peptides in these two types of fibrils have different conformational states. This study demonstrates potentials of such a combined method as TERS/AFM for structural analysis of individual protein aggregates.

2934-Pos Board B39

Amyloid Aggregates Alter the Membrane Mobility of GM1 Gangliosides

Martino Calamai, Francesco S. Pavone.

Neuronal dysfunction in neurodegenerative pathologies such as Alzheimer's disease is currently attributed to the interaction of amyloid aggregates with the plasmamembrane. Amongst the variety of toxic mechanisms proposed, one involves the binding of amyloid species to GM1 gangliosides. GM1 takes part into the formation of membrane rafts, specialized microdomains responsible for the compartmentalization of cellular processes such as signalling and protein trafficking. GM1 has antineurotoxic, neuroprotective, and neurorestorative effects on various central neurotransmitter systems. In this study, we investigated the effect of amyloid-like aggregates formed by the yeast prion Sup35 on the membrane mobility of GM1. Although Sup35 is not associated to any disease, it contains a highly amyloidogenic structural motif (Sup35NM) and has been used extensively as a model peptide for studying amyloid aggregation. Preformed Sup35 and Sup35NM aggregates were incubated with neuroblastoma cells and GM1 molecules were subsequently labeled with biotinylated CTX-B and streptavidin quantum dots (QDs). Single QDs bound to GM1 were then tracked. The trajectories of QDs labeled GM1 molecules were used to calculate their mean square displacement (MSD) and extrapolate their diffusion coefficients (D). The diffusion behavior of GM1 in the absence or in the presence of full length Sup35 aggregates was found to be substantially identical. By contrast, the mobility of GM1 decreased dramatically in the presence of Sup35NM aggregates. In this case, the median D of GM1 was found to be approximately one order of magnitude lower. Furthermore, the motion of GM1 appeared to change from mostly Brownian in the absence of the Sup35NM aggregates to mainly confined in their presence. The considerable interference of amyloid-like aggregates with the lateral diffusion of GM1 might imply a consequent loss of function of GM1, thus contributing to explain the toxic mechanism ascribed to this particular interaction.

2935-Pos Board B40

Modulation of Tau Fibril Growth in Vitro by Hsp27 vs FKBP51 and their Mutants

Shannon Elizabeth Hill, Tatiana Miti, Jeffery Jones, Zachary Davey, Jose F. Abisambra, Chad Dickey, Martin Muschol.

Self-assembly of proteins into neurotoxic aggregates and filaments is an event shared by multiple geriatric neurodegenerative diseases. Accumulation of the microtubule associated protein tau, in particular, is associated with a collection of central nervous system neuropathies, including Alzheimer's disease. The role of molecular chaperones in regulating the degradation of disease-associated proteins has received increasing attention. As shown in our group [1], age-related changes of the molecular chaperones Hsp27 and FKBP51 are involved during abnormal tau buildup. Using dynamic light scattering (DLS), atomic force microscopy (AFM) and molecular spectroscopy [2], we investigated the effects of Hsp27 and FKBP51 on the kinetics of tau fibril growth at 37 °C.

We found that both Hsp27 and FKBP51 significantly alter the rates of tau fibrils formation, and do so at surprisingly low stochiometric ratios of 50:1 (tau: chaperone). However, while Hsp27 inhibited tau fibril growth, FKBP51 augmented it. A perpetually pseudo-phosphorylated Hsp27 mutant (3xS/D) was noticeably less efficient in suppressing tau fibril growth. In contrast, the enzymatically inactive FBKP51 mutant F130A completely inhibited tau fibril formation for the duration of our assay (5 days). Either chaperone had to be present at the outset of the incubation period in order to mediate its effect. This indicates that either chaperone exerts its effects during an early stage of the assembly process. We found no indication for the formation of large, permanent chaperone/tau complexes to explain the specific modulatory role of either chaperone. We propose, instead, that the presence of either chaperone causes tau monomers to restructure in different ways, thereby generating the observed modulatory action on fibril growth.

[1] Jinwal et al., J. Neurosci. (2010), 30:591; Asimbra et al., J. Neurosci. (2010), in press.

[2] Hill et al., Biophys. J. (2009), 96:3781-3790.

2936-Pos Board B41

Biophysical Characterization of an Elastin-Like-Polypeptide

Daniel Lyons, Gene L. Bidwell, Wolfgang H. Kramer, Drazen Raucher, John J. Correia.

Perhaps the largest impediment in cancer therapies has been the inability to effectively target systemically delivered therapeutics to cancerous cells. A recent and novel approach to this problem has been to chemically conjugate the therapeutic to an Elastin-Like-Polypeptide (ELP). ELP is a naturally occurring biomolecule which undergoes structural transitions and aggregates in response to temperatures above its transition temperature (T_t). This allows for the specific targeting of a systemically delivered ELP-drug conjugate to an artificially heated tumor. Turbidity experiments on a specific ELP construct, ELP1 (ELP[$V_5G_3A_2$-150]), show a gradual increase in turbidity as early as 28°C that progressively increases until approximately 37°C, above which there is a cooperative, concentration dependent increase in turbidity corresponding to aggregation of ELP1. This aggregation is reversible and exhibits hysteresis in response to lower temperatures. Sedimentation Velocity (SV) and Circular Dichroism (CD) experiments show that at 20°C ELP1 adopts a random coil configuration with a $S_{20,W}$ of 1.92 and a f/f_0 of 2.57 at c=0. As the temperature is raised to 35°C ELP1 shows small amounts of association and sediments with a $S_{20,W}$ of 2.13 and a f/f_0 of 2.32 at c=0. At temperatures greater than the T_t a Critical Concentration (Cc) is observed; at $c \geq Cc$ ELP1 structurally transitions to a β-spiral and aggregates, and at $c < Cc$ ELP1 sediments at a monomeric $S_{20,W}$. The Cc is temperature dependent and decreases as the temperature is raised (38°C - 3.55mg/ml, 39°C - 2.22mg/ml & 40°C - 1.89mg/ml, respectively). This data suggests that at low temperatures ELP1 adopts a random coil conformation and that as the T_t is approached ELP1 association and β-spiral conformation become thermodynamically favorable. Future work is planned examining how drug conjugation affects the system and the behavior of ELP1 in plasma using fluorescence equipped AUC.

2937-Pos Board B42

Fiber Formation of a Synthetic Peptide Derived from Spider Dragline of *Nephila Clavata*

Ko-ichi Kontani, Mitsuhiro Miyazawa, Yuji Hidaka.

Spider dragline is a high performance biopolymer with exceptional mechanical properties. It is 5 times stronger than stainless wire, and high tensile strength and elasticity. The dragline is formed in the major ampullate gland of *Nephila clavata* and is composed of two major silk proteins, spidroin I and II. Our previous study suggested that the synthetic peptide derived from *Nephila clavata* forms large-sized fibers. However, the mechanism associated with spinning and the structure of the dragline silk protein remains to be studied in detail.

To further investigate the relationship between structure and fiber formation, the fiber forming regions of spidroin were predicted, based on the hydrophobicity of individual amino acid residues. The candidate peptides were chemically synthesized by a solid-phase method, purified by reversed-phase HPLC, and the structures confirmed by MALD-TOF/MS analysis.

The conditions for fiber formation for the candidate peptides were screened in a series of aqueous and organic solvents. Large-sized fibers were obtained when an organic solvent was used, under acidic conditions. However, the peptide was not able to form fibers under basic conditions.

To obtain structural information on fiber formation, Circular Dichroism measurements of the synthetic spider peptides were performed. The results suggested that the formation of a β-sheet structure is required for fiber formation of the spider peptide.

To characterize the peptide fibers, Dynamic laser light-scattering measurements were carried out under several conditions. The results indicated that the synthetic peptide formed a homogeneous oligomer at the initial time and moved to a large-sized oligomer at the later time.

In conclusion, the fiber formation of the synthetic spider peptide occurs in organic solvents under acidic conditions and the synthetic peptide forms a homogeneous large-sized oligomer. The results will be discussed in this paper.

2938-Pos Board B43

The Repeat Domain of Pmel17 Orthologs Form Amyloid Fibrils at the Acidic Melanosomal pH

Ryan P. McGlinchey, Candace M. Pfefferkorn, Reed B. Wickner, Jennifer C. Lee.

Most amyloids are pathological. Pmel17 is a functional amyloid, promoting melanin deposition and possibly protecting cells from adverse effects of the reactive groups that comprise this important pigment. Here, we show that at the mildly acidic pH (4 - 5.5) typical of melanosomes, organelles where melanin is synthesized, the repeat domain (RPT) of human Pmel17 can form amyloid *in vitro*. Combined with the known presence of RPT in the melanosomal filaments and the requirement of this domain for fibril formation, we propose that RPT may constitute the amyloid core *in vivo*. While most of the amino acid sequence of Pmel17 is highly conserved across a broad range of vertebrates, the RPT domain length and sequence varies. To address RPT aggregation propensities, we have investigated mouse and zebrafish sequences as well as a smaller truncated variant of human Pmel17. Although there is no sequence conservation amongst RPT domains, amyloid formation at acidic pH is preserved.

2939-Pos Board B44

Studying the Alpha-Synuclein Membrane Interface with Photons and Neutrons

Candace M. Pfefferkorn, Frank Heinrich, Jennifer C. Lee.

Elucidating mechanisms that induce alpha-synuclein (alpha-syn) conformational change is of utmost importance because the transition of alpha-syn from unstructured monomer to beta-sheet containing fibrils is associated with Parkinson's disease. The role of phospholipids is of particular interest because membranes are ubiquitous and synthetic vesicles have been shown to modulate alpha-syn aggregation in vitro. While alpha-syn-membrane interactions have been the focus of substantial research efforts, additional molecular level characterization is required to understand how membranes can promote amyloid formation. To address this issue, we have performed neutron reflectometry measurements as a dual probe of alpha-syn membrane associated conformation and bilayer structure. Moreover, we have extended our prior single tryptophan mutant studies (1) to evaluate the participation of the N-terminal region by comparing W4 fluorescence of the full length protein to that of synthetic peptides (1-4, 1- 6, 1-10, and 1-15) in the presence of small unilamaller vesicles. We find that at least the first six residues are required for membrane interaction. Interestingly, W4 spectral properties for the 1-15 peptide are highly reminiscent of the full length protein and comparable binding affinities were measured.

(1) Pfefferkorn, C. M.; Lee, J. C. J. Phys. Chem. B, 2010, 114, 4615.

2940-Pos Board B45

Molecular Basis of the Interaction Between Zinc and the Amyloidogenic Islet Amyloid Polypeptide

Samer Salamekh, Jeffrey R. Brender, Ravi P.R. Nanga, Sukjoon Hyung, Kevin Hartman, Brandon T. Ruotolo, Ayyalusamy Ramamoorthy.

Human islet amyloid polypeptide, hIAPP, is an amyloidogenic peptide hormone secreted primarily by pancreatic beta-cells in the islet of Langerhans. Human IAPP is cosecreted with insulin, and under normal the two proteins work to maintain glycemice control. The formation of hIAPP amyloid plaques near islet cells has been linked to the death of insulin-secreting beta-cells in humans and the progression of type II diabetes. One of the interesting questions surrounding this peptide is how the toxic and aggregation prone hIAPP peptide can be maintained in a safe state at the high concentrations that are found in the secretory

granule where it is stored. Our studies have shown zinc, which is found at millimolar concentrations in the secretory granule, significantly inhibits hIAPP amyloid fibrillogenesis at concentrations similar to those found in the extracellular environment. We show here by ITC and PICUP cross-linking that zinc binds to a complex of several hIAPP peptides at micromolar concentrations similar to those found in the extracellular environment, and in the process, promotes the formation of small IAPP oligomers. Interestingly, this observed interaction is unique to the hIAPP as membrane disrupting peptides with similar sequences exhibit minimal interaction with zinc. By contrast, the fibrillar amyloid form of hIAPP has only low affinity for zinc. High-resolution NMR structures of hIAPP bound to zinc reveal changes in along residues that would be located along one face of the hIAPP alpha-helix proposed as an intermediate for amyloid formation. These changes occur on the hydrophilic side of the amphipathic alpha-helix, away from the proposed interface for amyloid nucleation on the hydrophobic side. Combined, these results suggest zinc promotes the formation of off-pathway oligomers while creating a thermodynamic barrier for the formation of amyloid fibers.

2941-Pos Board B46

Lipid Composition and Raft Domain Formation on the IAPP-Membrane Interaction: The Role of Cholesterol on the Inhibition of IAPP (Amylin) Fibrilization and the Reduction of Membrane Disruption in Model Liposomes and Mouse Pancreatic Islets

Austin J. McHenry, Jeffrey R. Brender, Kevin Hartman, Ayyalusamy Ramamoorthy.

The misfolding and aggregation of islet amyloid polypeptide (IAPP) is known to exhibit an important role in the etiology of type-two diabetes mellitus. While it has been believed that the peptide becomes toxic in its large fibrous form, recent studies suggest that pre-fibril oligomers are in fact the predominantly toxic species. Permiabilization of IAPP on membranes is thus biphasic in nature. The latter phase is correlated with fiber formation and reaches maximal leakage. The degree of leakage, and hence membrane disruption, of the initial phase is dependent on the peptide to lipid ratio and percent anionic lipid in the membrane. Studies of IAPP toxicity have focused on POPC/POPS(G) vesicle systems. The homogeneity and anionic nature of the membranes have been shown to increase aggregation and toxicity. However, cellular membranes are vastly more complex. In this study, we investigate the in vitro interaction between IAPP and non-homogenous, cholesterol-containing model membranes; extend previous observations of the role of anionic phospholipids in membrane-catalyzed IAPP fibrilogenesis; and show that the presence of cholesterol dramatically inhibits IAPP fribrilogenesis and decreases membrane disruption in large unilamellar vesicles. Additionally, we demonstrate that human IAPP strongly permiablilizes raft type membranes. Fluorescence microscopy of islet cells shows increased IAPP toxicity after the removal of cholesterol from the membrane. These findings demonstrate that the mode of IAPP membrane binding and permiablization is highly dependent on the fluidity and phase of the membrane. The differences in this behavior may have significant implications in the development of type-two diabetes, as the change in membrane composition is dependent on a number of factors also related to the disease.

2942-Pos Board B47

Nucleation of Hybrid Polymers in Sickle Cell Disease

Donna Yosmanovich, Alexey Aprelev, Maria Rotter, Frank Ferrone.

Upon deoxygenation, sickle hemoglobin (HbS) can polymerize into complex, 14 stranded polymers via a double nucleation process. While sickle cell hemoglobin nucleation has been well described, the description has focused on nucleation of a single species, deoxyHbS, with perhaps the presence of a crowding non-polymerizing species. However, there are three important cases of polymerization where hybrid polymers are created, and thus the nucleation process in such situations needs to be characterized and tested. First in vivo, polymerization always occurs in the presence of ligands. Second, polymerization is also possible in the presence of normal hemoglobin (HbA, eg. in sickle trait). Finally, antisickling drugs may not bind to all molecules and thus create a heterogeneous population with the opportunity for hybrid polymerization. Thus we have studied polymerization in the presence of HbA, as well as under cases of partial ligation (with CO, NO and O2). Homogeneous nucleation rates have been measured by laser photolysis of the CO-derivative and analysis of the stochastic fluctuations of onset-times. Heterogeneous nucleation is determined by following the exponential growth of light scattering. Existing models for nucleation have been successfully modified to account for the copolymerization probability of hybrid species, and revised models will also be presented. Incorporation of ligands is particularly challenging since it appears necessary to account for tertiary as well as quaternary effects, and these appear to differ depending on the ligands.

2943-Pos Board B48

Single Sickle Cell Occlusion and Manipulation in Microchannels

Alexey Aprelev, William Stephenson, Hongseok (Moses) Noh, Maureen Meier, Frank A. Ferrone.

Sickle cell disease arises because a point mutation permits the hemoglobin in erythrocytes to form stiff polymers and obstruct the microcirculation. We have developed a microfluidic system to model vaso-occlusion in the smallest vessels to fill a critical gap in understanding the pathophysiology of sickle cell disease. Microfluidic methods heretofore have only studied far larger vessels, and could not observe events of speed comparable to physiologic transit times. We use microchannels of approximately rectangular cross section (3 μm x 1.5 μm). Because the cells fill the channel top-to-bottom, absorbance can determine intracellular concentration. Cells can be flowed, viewed statically, or stopped and restarted. By laser photolysis of COHbS, any desaturation of the cells can be created in milliseconds. Channels are constructed of PDMS, and cells are driven by hydrostatic pressure which can be controlled to stop the cell within the channel. The cell can then be photolyzed, and studied rheologically. Polymerized cells stick in the channels, but can be pushed through, with pressure that rises with the mass of the polymers formed. Cells sickled at the entry into such channels (see Figure) are found to maintain occlusion against much higher pressures.

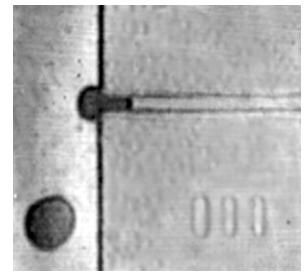

2944-Pos Board B49

Elastic Light Scattering Measurements of Hemoglobin Oligomers

Yihua Wang, Alexey Aprelev, Frank A. Ferrone.

Protein solutions scatter light dominantly by the density fluctuations of the solute. However, the formation of small oligomers can create light scattering that will exceed this background. We are using such light scattering to probe the initial stages of sickle hemoglobin assembly. We employ a novel micro-method for measuring light scattering in which a small rectangular cell (0.2 x 4.0 x 30 mm) is filled with 24 μL of Hb solution. An optical fiber is sealed into the cell in contact with the solution, and scattering from a 785 nm, 1.5 mW laser diode is measured at 90°. Light is colllected by a microscope objective, detected via PMT. Temperature is controlled by a thermoelectric stage. We have measured scattering from deoxygenated sickle hemoglobin, which forms polymers above a readily accessible solubility (and have measured scattering below and above solubility). We have also measured light scattering from COHbS, COHbA, and deoxyHbA which do not form such polymers and differ from deoxyHbS by either a single amino acid (HbA) or by quaternary differences (COHbS). Fluctuation scattering is used to calibrate the relevant scattering volume, allowing for more precise calculation of the concentrations of oligomeric scatterers. As temperature is increased, we observe a relatively constant intensity, which then increases beyond some particular temperature. We interpret this as the appearance of oligomers of sufficient numbers to exceed the density fluctuation background. Whereas deoxyHbS creates more oligiomers at the same concentration and temperature as other derivatives, all derivatives can create equally large oligomeric concentrations with varied temperature and monomer concentration. Thus oligomer concentration is not diagnostic for polymerization. Analysis of this data will address two important questions: is there evidence for off-pathway aggregation in sickle hemoglobin, and must aggregates have the same structure as the polymers?

2945-Pos Board B50

Comparing the Folding and Misfolding Energy Landscapes of Phosphoglycerate Kinase

Gergely Agócs, Bence T. Szabó, Gottfried Köhler, Szabolcs Osváth.

Understanding the sequence specific partitioning of polypeptides between protein folding and amyloid formation is of outstanding physiological and pathological importance. Using yeast phosphoglycerate kinase as model, here we identify the features of the energy landscape that decide the fate of the protein: folding or amyloidogenesis. Structure formation was initiated from the acid-unfolded state by stopped-flow or manual mixing, and monitored by tryptophan and thioflavin T fluorescence from 1 ms to 10 days. Solvent conditions were gradually shifted between folding and amyloidogenesis and the properties of the energy landscape governing structure formation were reconstructed. A continuous transition of the energy landscape between folding and amyloid formation was observed. In the early steps of both folding and misfolding, the protein searches through a hierarchically structured energy landscape to form a molten globule on the seconds timescale. From this intermediate structure, folding to the native structure happens in a cross-barrier step in a few minutes, while

amyloidogenesis progresses much slower, on the days and weeks timescale. As conditions are changed from folding to misfolding, formation of the native structure slows down indicating the increase of the barrier separating the molten globule and native states. In the meantime, the native state becomes more unstable as well. Amyloid formation is only observed among solvent conditions where folding is absent.

2946-Pos Board B51

Probing Aggrecan Interactions by Atomic Force Microscopy

Preethi L. Chandran, Emilios K. Dimitriadis, Peter J. Basser, Ferenc Horkay.

Aggrecan, the major extracellular matrix proteoglycan in cartilage, is a highly charged bottlebrush shaped macromolecule. It consists of negatively charged glycosaminoglycan (GAG) chains attached to a protein backbone. The bottlebrush structure enables aggrecan to maintain an extended conformation responsible for the high osmotic pressure sustaining compressive loads in cartilage. Alterations in aggrecan bottlebrush structure with age and disease lead to bone deformities, dwarfism, arthritis, and other pathological conditions. In solution, aggrecan bottlebrushes show distinct osmotic pressure versus concentration regimes. They self-assemble and form large clusters. Using Atomic Force Microscopy aggrecan molecules adsorbed on controlled mica surfaces were imaged. On positively charged APS mica, the average extension and height of the bottlebrush side chains were practically unaffected by the presence of calcium ions. With increasing aggrecan concentration transition takes place from dispersed, non-interacting bottlebrushes to clusters of conforming chains. At higher concentrations aggrecan molecules form a continuous monolayer. These surface observations are consistent with aggrecan properties in solution. On negatively charged mica, aggrecan shows interesting network patterns at higher concentrations. Understanding aggrecan adsorption onto charged surfaces provides insight into its interactions with bone and implants in the biological milieu.

2947-Pos Board B52

Electrostatic Analysis of the Aggregation of TrV Viral Particles

Marcelo D. Costabel, María J. Amundarain, Fernando Zamarreño, Rubén Sánchez-Eugenia, Jon Agirre, **Diego M.A. Guérin**.

Triatoma virus (TrV) is a member of the insect virus family Dicistroviridae, a family similar to the vertebrate picornaviruses. TrV virions consist of a non-enveloped capsid that encloses the viral genome, a molecule of linear positive sense single-stranded RNA of about 9000 bases. The atomic structure of the capsid is an icosahedron (T=1, pseudo-equivalence p=3) of about 30 nm in diameter that encloses 60 repeats of three structural proteins VP1, VP2, and VP3 (MWs of about 39 kDa, 37 kDa, and 33 kDa; RCSB PDB code 3NAP). TrV particles stand very acidic conditions (pHs lower than 3.0) and at high concentration undergo a reversible aggregation. In this work we calculate the electrostatic energy for the interaction between two TrV particles at different solvent conditions, and we compare these results with the corresponding experimentally measured Static Light Scattering Second Virial Coefficient. The interaction mechanism does not appear to be dominated by an electrostatic effect of the charge at the capsid surface, and a dependence on the solvent ionic strength is observed.

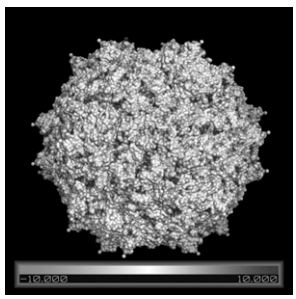

Keywords: Dicistroviridae; Triatoma virus; electrostatic energy; virus aggregation; Second Viral Coefficient.

Figure: TrV surface charge at pH 4.0.

Protein Folding & Stability III

2948-Pos Board B53

High Pressure FTIR Studies on Model α-Helical Peptides

Teraya Donaldson, Alice Smith-Gicklhorn, Sean M. Decatur.

High-pressure conditions force water into internal cavities of proteins; the presence of water in a hydrophobic interior can destabilize the tertiary structure resulting in protein unfolding. This effect has been predicted in molecular dynamics simulations for model alpha-helical peptides at high pressures, where water is forced into closer contact with backbone carbonyls (as measured by an increased in backbone hydration). According to simulations, this increase hydration depends on local sequence and the impact that specific side chains have on backbone conformation. We have investigated the effects of pressure on a series of 20-residue peptides. Model peptides based on the alanine and lysine repeats form water soluble, stable alpha helices (1). The sequence (AAAAK)3-AAAAY is a well-characterized, synthetic polypeptide, ideal for the study of helix properties(2). Using the model peptides, we experimentally confirm that the helical content is conserved under pressure. Perturbations were monitored using a probe of secondary structure, the amide I' band, with infrared (IR) spectroscopy and a diamond anvil cell. Amide I' mode shifts to a lower frequency with the increase of pressure. Local information is obtained by measuring amide I'bands in 13C labeled peptides, where 13C alanines are placed at different positions relative to the lysines within the peptide. We examined the shielding effects of lysine at the various positions and confirm that shielding of backbone carbonyls occurs.

1. Starzyk, A., Barber-Armstrong, W., Sridharan, M., and Decatur, S. M. (2005) Spectroscopic evidence for backbone desolvation of helical peptides by 2,2,2-trifluoroethanol: an isotope-edited FTIR study, Biochemistry 44, 369-376.

2. Paschek, D., Gnanakaran, S., and Garcia, A. E. (2005) Simulations of the pressure and temperature unfolding of an alpha-helical peptide, Proc Natl Acad Sci U S A 102, 6765-6770.

2949-Pos Board B54

SAXS Study of Cytochrome-C Cold Denaturation

Margaret Elmer, Christopher Asta, Katherine Butler, Apratim Dhar, Martin Gruebele, Liang Guo, Thomas Irving, Joseph Marcus, Sarah Rice, **Eric Landahl**.

We present a study of the cold denaturation of proteins using Small Angle X-Ray Scattering. The size and shape of equine cytochrome-c is determined at varying salt and pH conditions from −25 to 60° C and compared to the two-state Ideal Thermal Protein model of Ghosh and Dill (PNAS 2009). The incorporation of a temperature-dependent pH and solvent dielectric constant is critical to model electrostatic interactions over this broad temperature range and properly predict the observed protein stability from sequence. Under suitable conditions, the protein can be made to increase in size by nearly 9 Angstroms (over 60% of its native radius of gyration) when dropped in temperature from 0 to −25 C. Cold denaturation under these conditions is also verified by monitoring fluorescence from the native tryptophan in this protein. This allows us to compare denaturation monitored at one location inside the protein with global structural changes observed by SAXS.

2950-Pos Board B55

Apolipoprotein B Reconstruction at Single Molecular Level

Hsueh-Liang Chu, Tsai-Mu Cheng, Yu-Chuan Chang, Hung-Wei Chen, Wei-Hsien Chung, Chia-Ching Chang.

Low density lipoprotein-cholesterol (LDL-C) is a clinical significant marker of cardiovascular disease risk. Each particle of LDL contains only one protein, apolipoprotein B (apoB). In human, the liver secretes full-length apoB (apoB-100) which also serves as a ligand for receptor-mediated uptake of LDL by a variety of cell types, such as monocyte and A549. Many diseases' progression may cause by the deficiency of the LDL assembly. Therefore, it is desired to reveal the folding/assembly process of apoB. However, it is challenge to refold the apoB, because of its high insolubility in solution. In this study, the native apoB had been purified from LDL by ice cheer method, and truncated mutants of various lengths of apoB were recombinant expressed from *E. coli* system. The apoB-100 and its truncated proteins then were dissolved in the denature buffer which contained additional detergents and were refolded via an over-critical refolding process. The folding intermediates of apoB-100 and its truncated mutants could be observed by immunofluorescence microscopy at the single molecular level and the lipidation processes and secondary structures of apoBs can be also analyzed by SRCD. Moreover, the confocal microscopy showed that the refolded and native LDL could be absorbed by THP-1 and A549 cell. According to our observation the LDL assembly process can be proposed. This is the first study to refold the structural and function of apoB *in vitro*. Meanwhile, this refolded lipoprotein can be used as carrier for hydrophobic particles delivery.

2951-Pos Board B56

Folding Studies of Beta-Strand-Containing Repeat Proteins Through Naturally-Occurring and Consensus-Designed Sequences

Thuy P. Dao, Ananya Majumdar, Doug Barrick.

Repeat proteins, devoid of sequence-distant contacts observed in globular proteins, are ideal candidates for the dissection of local stability, nearest-neighbor contact parameters, cooperativity, and determination of folding energy landscapes. Recent studies on HEAT, TPR, Ankyrin, and Armadillo have contributed to the understanding of the folding of helical repeat proteins. Moreover, constructs composed of simplified ''consensus'' sequence

representations of helical repeat proteins have been found to be well-behaved and highly stable, and facilitate energy dissection using simple nearest-neighbor models.
In contrast, little progress has been made towards understanding the folding of β-sheet containing repeat. To determine the folding stability and cooperativity of these proteins, and to better understand the sequence determinants of structure and stability within these ubiquitous families, we have initiated studies on a series of LRR proteins of both naturally occurring and consensus-designed sequences. We find the LRR proteins PP32 and LC1 to be well-behaved, and to fold in a highly cooperative transition that is consistent with a two-state mechanism. NMR $H/^2H$ exchange shows the repeating β-strands on the concave surface of both proteins to be more protected than the rest of the molecules, and can be regarded as an exchange-resistant core, whereas the terminal caps and convex structural elements are more labile. However, truncations and sequence substitution demonstrate that the caps significantly influence stability and kinetics.
To further simplify our analysis of β-sheet containing repeat protein folding, we designed consensus LRR sequences. On their own, these constructs are unfolded and/or aggregated. By fusing these consensus sequences with naturally occurring LRR protein YopM, we have obtained solublized, folded arrays that exhibit increased stability and drastically decreased unfolding and refolding rates with repeat number. Further studies are needed to dissect the complex folding pathways taken by these constructs.

2952-Pos Board B57
The Structural and Functional Role Fo the Sole Tryptophan Residue in the Human Acidic Fibroblast Growth Factor
Hannah M. Henson, Anna E. Daily, Suresh Kumar.
Department of Chemistry & Biochemistry, University of Arkansas, Fayetteville, AR.
Abstract:
Fibroblast Growth Factor-1 (FGF-1) is a 16kDa heparin binding protein, which has been associated with a variety of important functions including angiogenesis and wound repair. In order for FGF-1 to enter the cell it must interact with the FGF-1 receptor on the cell surface. One vital residue involved in the binding of FGF-1 to the receptor is tryptophan 121 (W121). This study aims to examine the role of W121 on the conformation and functionality of FGF-1. Site-directed mutagenesis will be used to incorporate mutations at position 121. The effect of these mutations will be characterized using various biophysical techniques including fluorescence, CD, ITC, and mutli-dimesional NMR spectroscopy. As FGFs are involved in many crucial cellular processes, the gain from this study is expected to provide useful information on the regulation of the FGF signaling process.

2953-Pos Board B58
Folding Mechanism Revealing of PGB1 by FRET and Molecular Simulation
Chung Wei-Hsien, Yi-Chen Yeh, Nan-Yow Cheng, Chung-Yu Mou, Chia-Ching Chang.
1. Department of Biological Science and Technology, National Chiou Tung University, Hsinchu, Taiwan.
2. Institute of Physics, Academia Sinica, Taipei Taiwan.
3. Department of Physics, National Tsing Hua University, Hsinchu, Taiwan.
Immunoglobulin-binding B1 domain of streptococcal protein G (PGB1) is a small (56 residues) protein with an α-helix (from Ala23 to Asp 36) lying on top of two pairs of anti-parallel β-sheets, β-hairpin 1 (from Met1 to Ala20) and β-hairpin 2 (from Glu42 to Glu56), covering the hydrophobic core. PGB1 contains no disulfide bonds in its structure and makes it an excellent model protein for folding study. Our simulation results showed that the α-helix and β-hairpin 2 had interacted prior than β-hairpin 1 in early folding stage. Similar experimental results can be observed by monitoring the folding intermediates of PGB1, which are performed by an over-critical refolding process, by using fluorescence resonance energy transfer (FRET) technique, the technique is a precisely optical technique which can reveal the distance difference within angstrom scale. The FRET analysis of PGB1 also indicated that the distance between α-helix and β-hairpin 2 remained approximately unchanged in all folding intermediates. However, the distance between β-hairpin1 and β-hairpin 2 decreased during the folding process. Therefore both simulation and FRET analysis were in consistence. The molecular dynamics of PGB1 during its folding process can be demonstrated.

Membrane Protein Functions

2954-Pos Board B59
Probing Mechanism for the Enhancement of Uptake of Fatty Acid into Cells by the Membrane Protein CD36
Su Xu, Michael Kirber, Nasi Huang, Kellen Brunaldi, James A. Hamilton.
CD36 is a membrane protein found in various cell types including adipocytes and endothelial cells. Physiological studies have suggested that CD36 is associated with insulin-resistant diabetes, however, the mechanism remains poorly understood. It is well recognized as a receptor for multiple ligands such as collagen and thrombospondin 1, and possibly acts as a catalyst to enhance the rate of transmembrane movement of fatty acid. To separate the two independent events transport across the plasma membrane and the subsequent intracellular metabolism, we have applied biophysical approaches and metabolic analyses to cells in vitro. Our results using cultured cells (HEK293 cells overexpressing CD36 and 3T3-L1 adipocyte cells) as well as mice adipocyte cells isolated from a CD36 null mouse showed that fatty acids diffuse through the plasma membrane rapidly with or without CD36. In HEK 298 cells, which normally synthesize triglycerides very slowly and to a limited extent, expression of CD36 enhanced the rate and extent of synthesis. Even in the presence of CD36, incorporation into triglycerides is a much slower process (min) relative to the transmembrane movement (sec), indicating that the rate-limiting step of the regulation of fatty acid uptake by CD36 is intracellular metabolism. Lastly, by PCR array analysis of 84 proteins, we have identified several enzymes involved in human fatty acid metabolism with gene expression levels altered by overexpression of CD36. Taken together, our results showed that CD36 increases fatty acid uptake by enhancing triglycerides synthesis rather than acting as a membrane transporter, but as yet by unidentified molecular mechanisms.

2955-Pos Board B60
Membrane Transport of CO_2 and H_2S: No Facilitator Required
Florian Zocher, John C. Mathai, Andreas Missner, Mark L. Zeidel, **Peter Pohl**.
The observation that some membranes and epithelia have no demonstrable gas permeability suggested that membrane channels may be involved in CO_2 transport. Both aquaporins and Rhesus proteins were reported to serve as pathways for CO_2 and H_2S. In contrast, we show here that membrane lipid has such high CO_2 and H_2S permeabilities that the presence of a protein channel does not enhance the flux. Therefore we reconstituted aquaporins into lipid bilayers and used scanning microelectrodes to monitor pH in the immediate vicinity of planar lipid bilayers. The lower limits of lipid bilayer permeabilities to CO_2 and to H_2S were equal to 3.2 ± 1.6 cm/s[1] and 0.5 ± 0.4 cm/s[2], respectively. We also observed that the CO_2 flux through the lipid bilayer decreases several fold when the rate of CO_2 formation from HCO_3^- was not augmented by carbonic anhydrase (CA). Experiments with epithelial cell monolayers grown on permeable support revealed the same result. Inhibition of CA transformed these otherwise highly CO_2 permeable cell monolayers into CO_2 barriers. Finally we tested the CO_2 permeability of the epithelium of the mammalian bladder. It was impermeable to CO_2 even after uroplakin knock-out. We found that the lack of intrinsic intracellular CA activity of these epithelial cells hampers the CO_2 exchange between blood and urine.
[1] A. Missner, P. Kugler, S. M. Saparov, K. Sommer, J. C. Matthai, M. L. Zeidel, P. Pohl, J.Biol.Chem. 2008, 283 25340-25347.
[2.] J. C. Mathai, A. Missner, P. Kügler, S. M. Saparov, M. L. Zeidel, J. K. Lee, P. Pohl, Proc.Natl.Acad.Sci.U.S.A. 2009, 106 16633-16638.

2956-Pos Board B61
F65S Mutation in RhAG is Associated with Decreased Ammonia Flux Through Overhydrated Stomatocytic Erythrocytes
Sandrine Genetet, Pierre Ripoche, Julien Picot, Sylvain Bigot, Jean Delaunay, Corinne Amari-Alla, Yves Colin, **Isabelle Mouro-Chanteloup**.
The Overhydrated Stomatocytic (OHSt) erythrocytes of four patients, characterized by the F65S mutation (Bruce et al, Blood 2009) located in the pore of the ammonia channel Rh Associated Glycoprotein (RhAG), were studied. We have previously demonstrated that the equivalent substitution (F74L) in the non-erythroid analogue RhCG resulted in a reduction of the ammonia influx of 50% in transfected HEK293 cells.
Ghosts prepared by hypotonic lysis of OHSt and control (Ctl) erythrocytes, resealed in the presence of a pH-sensitive probe (pyranine), exhibited echinocytic morphology. Images of 1667 (Ctl) and 1998 (OHSt) echinocytes, visualized by light microscopy, allowed the determination of average ghost diameters: 5.81 ± 0.2 μm (Ctl) and 5.83 ± 0.06 μm (OHSt). RhAG densities, as determined by flow cytometry, were similar for Ctl and OHSt (78 000 to 80 000 copies/cell).

Ammonium permeability (P'_{NH3}) was measured by following the internal compartment alkalinisation, after submitting ghosts to inward ammonium gradients. Alkalinisation rate constants (k) were deduced from stopped-flow analysis of pH variations at 15°C, allowing the determination of P'_{NH3} by using the simplified equation P'_{NH3}=k.r/3 (r: radius of spheric ghosts). The P'_{NH3} values were significantly different between Ctl and OHSt samples (1.7 ± 0.11 vs 0.71 ± 0.004 $\mu m.s^{-1}$). Additionally, water permeability was measured in the same OHSt resealed ghosts but containing 8mM 6-carboxyfluorescein (6-CF), after submitting them to an osmotic gradient (150mosm/kg/H_2O mannitol). The osmotic water permeability (Pf) values deduced from the fluorescence quenching at 15°C were similar between Ctl and OHSt samples (0.035 ± 0.005 vs 0.035 ± 0.04 $cm.s^{-1}$).
In conclusion, the F65S mutation of RhAG induces a reduction of ammonia flux resulting in an alteration of pHi regulation. The decrease of ammonia conductance through the mutated RhAG can result from loss of hydrophobicity and/or from structural modifications inside the pore of the channel.

2957-Pos Board B62
Molecular Modeling of the ATP-Synthase Motor F0 Subunit of Escherichia Coli and Proton Translocation
Megan Scoppa, Margaret Cheung.
An all-atom model based on the ac_{10} subunit of *Escherichia coli* Adenosine-Triphosphate (ATP) synthase complex was created using steered molecular dynamics along with parallel computer programming designed for the ability to view larger biomolecular systems. The salt bridge which is required for proton translocation and thus, proton motive force (PMF), was formed during initial minimization and equilibration simulations. Using physiological parameters and experimental data allows for a unique chance to view this nanoscale motor's rotational mechanism and will also supply more information about the elusive a-c subunit interface.

2958-Pos Board B63
All-Atom Molecular Dynamics Simulation of Multidrug Efflux Transporter AcrB
Tsutomu Yamane, Mitsunori Ikeguchi.
In E. coli, it is known that the tripartite multidrug efflux system (AcrB/ AcrA/ TolC) exists, and AcrB resides in the inner membrane region and take part in substrate recognition and energy transduction for drug export through proton transfer. Recently, x-ray structures provided that AcrB forms trimeric protein where each subunit is different conformation, ''binding state'', ''extrusion state'' and ''access state''. Especially, only extrusion state subunit has different side chain conformation of residues (Asp407, Asp408 and Lys940), which are essential for proton translocation (protonation site). These results suggest that drugs are exported by a three-step structural change involved in proton motive force which is inferred to be caused by change of protonation states of the protonation site residues. However, the structural change process which involved in proton motive force is still unclear. In the present study, we performed 100 ns all-atom molecular dynamics (MD) simulations of three types of AcrB-membrane-water systems which are different from protonation state of Asp407 and/or Asp408 in extrusion state protomer. During all of the 100 ns MD simulations, the global structures of each subunit were conserved. However, in extrusion state protomer, the conformation of the protonation site residues were changed to those of other state protomers only when Asp 407 and 408 residues were deprotonated. In this presentation, we will discuss the structural change and proton transfer mechanism.

2959-Pos Board B64
Pathways to Exit a Receptor: Agonists and Delta-Oppioid Studied via Computer Simulations
Francesca Collu, Matteo Ceccarelli, **Paolo Ruggerone**.
The importance of delta-opioid receptors as target of a large number of drugs is well recognized, but the molecular details of interaction and action of the compounds are largely unknown. In an effort to shade some light on this important issue we performed an extensive computational study on the interaction of two compounds, clozapine and desmetilclozapine, with a delta-opioid receptor. According to experiments, the lacking of a single methyl group in desmetilclozapine with respect of clozapine makes the former more active than the latter, providing a system well suited for a comparative study. We investigated the escape route of the two drugs from the receptor using molecular dynamics simulations and metadynamics. Our results point out that prolonged interactions of the compounds with specific residues of the receptor do not correlate directly with their activity, having clozapine the longest interactions if compared with desmetilclozapine but being also less active. The action of the compound is related to the spatial distribution of the affinity sites it visits during its permanency. Additionally, the role of long-resident water molecules is discussed. Such information might be useful to provide hints and insights that can be exploited in more structure-and-dynamics-oriented drug design.

2960-Pos Board B65
Computational Studies of Translocon-Assisted Processes of Membrane Protein Insertion and Translocation
Anna Rychkova, Arieh Warshel.
Membrane proteins make up about 30% of all the proteins in the body and represent more than 50% of drug targets. The protein-conducting channel, called translocon, is responsible for protein-membrane integration and the understanding of the mechanism of translocon-associated membrane protein folding has a significant biological and pharmaceutical interest.
The translocon is a very large multidomain protein complex and the structural information about the protein-translocon complex is very tentative. Thus brute force all atom MD computer simulations are not expected to be very useful at this stage. In order to advance this challenging direction we introduce a unique coarse grain (CG) method with extended electrostatic treatment. This model allowed us to explore the energetics of the insertion of transmembrane helixes into lipid bilayer trough the translocon and to study the controversial question of the charged residue location in the membrane. More recently we stated to use the CG model in exploring the effect of key mutations that allow the secretion of proteins with defective or absent signal sequences. The preliminary insight provided by this study will also be described.

2961-Pos Board B66
An Atomistic Gating Mechanism of the AMPA-Subtype Glutamate Receptor
Hao Dong, Huan-Xiang Zhou.
Glutamate receptors mediate fast excitatory synaptic transmission in the central nervous system. Agonist binding to an ionotropic glutamate receptor (iGluR) triggers the opening of an ion channel, allowing the flow of cations across the membrane. Although the structures of the isolated extracellular ligand binding domain (LBD) in different states have been determined, it remains unclear how agonist binding is transmitted to open the channel. Here, based on targeted molecular dynamics simulations, we propose an atomistic mechanism for how the closure of the clamshell-like LDB upon agonist binding leads to channel activation. Simulations of an AMPA-subtype iGluR, including both the LBD and the transmembrane domain (TMD) in explicit water and membrane, started with the LBD in the antagonist-bound form. The LBD was then targeted to move toward the agonist-bound form, mimicking agonist binding. The resulting LBD closure was propagated to the TMD, and the pore formed by the M3 helices widened, signifying channel opening. The link peptides between the S2 half lobes of the LBD and the M3 helices of TMD were critical for the communication between the two domains. The M3 helices were rigid, and pore-widening resulted from an increase in tilt angle. At the same time, the whole M3 helix bundle translated upward. The detailed mechanism of coupling and communication between the extracellular and membrane-spanning domains elucidated here may serve to guide new experiments on the glutamate receptor and motivate the use of our methodology for the study of other neurotransmitter receptors in the central nervous system.

2962-Pos Board B67
Modeling KCNQ1 Channel and KCNE1 Interactions
Xuanyu Meng, Yu Xu, Hongxing Zhang, Gea-Ny Tseng, **Meng Cui**.
KCNQ1 is the pore-forming component of the slow delayed rectifier (Iks) channel in human heart. Although KCNQ1 can function as a voltage-gated (Kv) channel on its own, it requires KCNE1 to modulate its functions. To understand the mechanism of how KCNE1 modulate KCNQ1, molecular simulations are employed to model the interactions between KCNQ1 and KCNE1. A homology model of KCNQ1 was constructed based on the crystal structure of Kv1.2-Kv2.1 paddle chimera channel (PDB entry: 2R9R) template. For KCNE1, we used a NMR structure as an initial conformation, and manually adjusted the orientations of its N- and C-terminal domains to avoid their folding into membrane. Then 100ns molecular dynamics (MD) simulations were conducted to sample possible conformations of KCNE1 in POPC lipid bilayers. The cluster analysis was conducted on KCNE1 tansmembrane domain (KCNE1-TMD) from 40ns to 100ns simulation period. Five representative structures of KCNE1-TMD were selected, and used for docking simulations to KCNQ1. We performed 2 dimensional Brownian Dynamics (2D-BD) protein-docking simulations on each representative structure of KCNE1-TMD and KCNQ1 homology model. After selecting compact complexes by using a distance-based filter to remove loose contact complexes, a series of experimental restraints were applied to select one final KCNQ1/KCNE1-TMD complex structure. The N- and C- terminal domains of KCNE1 were reconstructed to generate the whole complex of KCNQ1/KCNE1, and followed by 100ns MD simulations in explicit membrane environment. For comparison, we also conducted 100ns MD simulations on KCNQ1 alone. Based on the two simulation studies, we analyzed the dynamics of the KCNQ1 channel with and without KCNE1 present through a systematic examination of hydrogen bond network patterns and ion permeation pathway of the channel. The results could provide us helpful insights of the molecular mechanism of how KCNE1 modulating KCNQ1 channel.

2963-Pos Board B68
Simulated Substrate Binding to the Inner Membrane Translocase AcrB
Lars Lüdicke.
Functioning as the engine of the AcrAB-TolC efflux pump, AcrB plays a key role in multidrug resistance in Escherichia coli. AcrB occurs as a trimer, where each monomer has a different conformation: loose (L), tight (T) or open (O) - representing different consecutive states in the reaction cycle.
Here we report molecular dynamics simulations of the asymmetric 2GIF AcrB x-ray structure embedded in a phospholipid bilayer / 150 mM NaCl environment. To study the interaction with one of AcrB's simplest substrates, 25 hexane molecules were added to the system, with three hexanes placed directly in front of each monomer's porter domain. Using GroMACS 4.0.3 and the GROMOS96 53a6 force field we performed 5 independent MD runs, each 50ns long. Three runs were further extended by 150 ns.
During one simulation, we observe a hexane entering the presumed drug transport channel of the (L) monomer. Binding occurs in a stepwise process during which the hexane moves towards the hydrophobic binding pocket inside the protein before reaching a final position after 25ns, 9.7 Å away from Phe-628. For the (T) monomer we observe hexane binding in a single step, reaching its final position 9.2 Å away from Phe-628. In none of the runs substrate binding takes place in the (O) monomer. However, an accumulation of hexane molecules in front of the closed porter domain could be observed here.
In a second approach, we repeated the simulations now providing the antibiotic chloramphenicol as transport substrate instead.

2964-Pos Board B69
Utilization of Thermodynamic Linkage Relationships to Test for Interactions between the C2 Domains of Synaptotagmin 1
Sarah C. Kempka, Katie Miller, Jacob W. Gauer, R Bryan Sutton, Greg Gillispie, Anne Hinderliter.
Synaptotagmin I is a calcium ion sensor involved in neurotransmitter release. When a neuron is stimulated by an action potential, an influx of calcium ion occurs causing the synaptic vesicle to fuse with the membrane, releasing the neurotransmitter into the synaptic cleft. This causes a new action potential to propagate to the next neuron, thereby transmitting information from cell to cell by electrochemical signaling. Synaptotagmin I is characterized by a transmembrane region embedded in the synaptic vesicle at its N-terminus which is connected to two C2 domains (C2A and C2B) that are located in the cytoplasm of the neuron. Both C2 domains bind calcium ions, negatively charged phospholipids, and associate with other proteins that are also involved with neurotransmitter release. Whether or not this process is mediated by a protein-protein interaction between the C2 domains is unknown. Since these proteins are tethered together, the very high effective concentration of one in relation to the other means the interaction energies must be very small; otherwise, the proteins would always be associated. Transient interactions represent a means to communicate binding information. Testing this is extremely challenging due to weak interactions. Here, we have utilized a thermal denaturation approach dependent on determination of free energies of stability to test this hypothesis.

2965-Pos Board B70
Mechanistic and Thermodynamic Insights into the Transport Cycle of Lactose Permease
Pushkar Pendse, Jeffery B. Klauda.
The Major Facilitator Superfamily (MFS) is an important class of membrane transporters whose members are found in almost all types of organisms and are very diverse in terms of substrate transport. Lactose permease of *E. coli* (LacY), which transports various sugar molecules across the plasma membrane, is studied as a model for the MFS proteins. LacY undergoes widespread conformational changes between a periplasmic-open and a cytoplasmic-open state during the transport cycle. The focus of this work is to determine the periplasmic-open structure starting with the known cytoplasmic-open crystal structure with an emphasis on the underlying mechanism. A two-step hybrid simulation approach that involves self-guided Langevin dynamics (SGLD) simulations to enhance conformational sampling is used. Our model for the periplasmic-open structure agrees well with various experimental findings. The protonation of Glu269 and binding of a disaccharide to LacY is found to trigger the conformational transition to the periplasmic-open state. The residues and interhelical interactions that are important during the conformational transition are determined. This two-step simulation approach can be extended to determine the conformational changes in other membrane proteins. In addition, sugar binding during structural changes follows the well-established 'alternating access model'. A more extensive study on sugar binding is carried out to understand the 'anomeric binding phenomenon' of LacY (different binding affinities for different anomers of a disaccharide). The alchemical free energy perturbation (FEP) method is used to quantify binding affinities. The calculated binding free energy of α-D-galactopyranoside (NPG) to LacY agrees well with the experimental value (Nie et al., *JBC*, 2006). The FEP calculations for αβ-(Gal*p*)$_2$ and ββ-(Gal*p*)$_2$ reveal a detailed description of LacY's anomeric binding phenomenon. This method is extended to different anomers of other disaccharides to elucidate anomeric binding.

2966-Pos Board B71
Purification of G-Protein Coupled Receptors Using Nanodiscs
Nivedita Mitra, Elsa C.Y. Yan.
G-Protein Coupled Receptors (GPCRs) are seven-transmembrane (7-TM) proteins and belong to the largest gene family in the human genome. They mediate intracellular signaling in response to extracellular stimuli such as light, small molecules, peptides, etc.
GPCRs are expressed in a wide variety of cell types and modulate cellular and physiological responses to the stimuli, which make them ideal drug targets. Despite their importance, GPCRs are not well understood at the molecular level in terms of their activation mechanism because they are notoriously difficulty to purify for quantitative biophysical studies. Due to their 7-TM hydrophobic domain, they need to be purified in detergents, which are often incompatible with their stability. Currently, GPCRs are purified using detergent conditions determined individually for each GPCR using an empirical approach. Thus, only a handful of GPCRs have been purified, which is an impediment to obtaining a molecular understanding of GPCRs. Here, we have developed a method for purifying GPCRs using nanodiscs, which are nanometer sized, disc-shaped, and self-contained lipid bilayer particles. In our method, we incorporate GPCRs straight from the cell membrane of a mammalian expression system into nanodiscs to minimize the amount of time the protein is in contact with detergent. Using this approach, we have successfully purified a family B GPCR, parathyroid hormone 1 receptor (PTH1R). We have investigated the binding of purified PTH1R to its native ligand PTH1 (1-34) using fluorescence anisotropy and obtained a dissociation constant of ~29 nM, in agreement with previous reports. We propose that our method could be a general approach to purify GPCRs that will enable quantitative biophysical studies to yield a better molecular understanding of their activation mechanisms and interactions with downstream signaling proteins.

2967-Pos Board B72
Monitoring Protein Association with a Membrane Bilayer Using Ultraviolet Resonance Raman (UVRR) Spectroscopy
Rauta A. Yakubu.
Ultraviolet Resonance Raman (UVRR) as a means of studying proteins' three states: in solution (state I), embedded on the membrane surface(state II), or inserted within the lipid bilayer (state III). pHLIP (pH low insertion peptide) is the model used for membrane proteins since it can change states based on pH going above or below 8. An artificial lipid membrane made of DMPC is made. After calculating an efficient peptide to lipid membrane ratio for insertion to use and making a suitable solution for an adequate UVRR spectrum, we have seen that when pHLIP is in state II it is partially in the membrane and gaining a helical structure. Using UVRR to study transmembrane proteins in relation to pH gives researchers insight on the functionality of many diseases.
Previous studies have shown that the C helix of bateriorhodopsin, commonly referred to as pH low insertion peptide (pHLIP), is disordered in aqueous solutions and in the presence of membrane bilayers at neutral pH. At low pH, in the presence of membrane bilayers, the peptide spontaneously folds in to an alpha-helix and inserts into the membrane bilayer. Ultraviolet Resonance Raman (UVRR) has been employed to study the three states of pHLIP: in solution (State I), embedded on the membrane surface (State II), or inserted within the lipid bilayer (State III). Ideal peptide-to-lipid membrane ratios were determined using tryptophan fluorescence and ultracentrifugation was used to concentrate liposomes for UVRR measurement. UVRR studies reveal that each state is spectroscopically distinct. The amide S mode, a marker for non-helical structure disappears upon going from neutral to low pH.

2968-Pos Board B73
Thermal Stability of Rhodopsin and Implications for Retinitis Pigmentosa
Monica Yun Liu, Jian Liu, Elsa Yan.
Over 100 mutations in the dim-light photoreceptor rhodopsin are associated with retinitis pigmentosa (RP), a visual disorder characterized by progressive symptoms of night blindness, tunnel vision, and sometimes blindness. We studied the thermal stability of two mutations, S186W and D190N. We hypothesize that these mutations perturb an electrostatic interaction and hydrogen bonds in the active site and destabilize rhodopsin, which undermines the sensitivity to light and causes RP. We compared the rates of thermal decay,

thermal isomerization, and Schiff base hydrolysis of WT, S186W, and D190N rhodopsin. Using UV-visible spectroscopy, we observed that the D190N mutant and WT rhodopsin do not decay over 24 hours at 37°C, whereas the S186W mutant decays with a half-life of 36 ± 4 min. We also measured the half-lives at 55°C, which are 70 ± 2 min for WT, 2.4 ± 0.2 for D190N, and 0.43 ± 0.03 min for S186W. Using HPLC and the acid denaturation assay, we measured the rates of thermal isomerization of 11-*cis* retinal and hydrolysis of the Schiff base linkage between retinal and opsin. We found that the mutations also increase these rates by 1-2 orders of magnitude. Because thermal isomerization of rhodopsin generates the same physiological response as photoisomerization, we suggest that the higher thermal isomerization rate in the mutants increases the level of dark noise, which desensitizes rhodopsin and causes the early symptom of night blindness. Because the drastic destabilizing effect of the mutations is likely correlated with the progressive deformation of the outer segment and subsequent loss of rod cells in RP, we propose that a future systematic study of the thermal stability of the RP-causing mutations can potentially provide more accurate predictions of the pace of vision loss in patients and guide strategies for treatment.

2969-Pos Board B74

Assembly and Function of the Transmembrane Domain of the Two-Component System PhoQ from E.coli

Matteo Dal Peraro, Thomas Lemmin.

In bacteria, two-component systems (TCS) detect the environmental changes via a sensor kinase at the periplasmic level, which triggers a phosphorelay cascade mediating specific gene transcriptions. PhoP/PhoQ is a TCS, which detects and responds to divalent cations and antimicrobial peptides, initiating a resistant response for the reshaping of the bacterial membrane. The PhoQ sensor kinase assembly is characterized by a homo-dimeric structure, which spans the bacterial inner membrane. The multidomain structure of PhoQ from E.coli is largely unresolved, and consequently the mechanism by which the chemical signal is transferred across the membrane remains unclear. We used all-atom molecular dynamics (MD) techniques to assemble the PhoQ transmembrane (TM) domain, which is still structurally unexplored, but appears to be crucial for signal transmission. We observed that the conserved polar amino acids at the TM domain are important for the stability of the tetramer, and are directly involved in rotation of the helical bundle upon solvation. Thus, our computational results, which are consistent with experimental cross-linking data, support a rotating four-helix TM region and give a rationale for the mechanistic transmission of the signal through the bacterial membrane.

2970-Pos Board B75

Dissecting the Oligomeric Behavior of Caveolin-1 using the Analytical Ultracentrifuge

Monica D. Rieth.

The cell membrane is involved in a variety of cellular functions such as signal transduction, membrane trafficking, calcium signaling, and lipid recycling. One unique feature of the cell membrane is small invaginations called caveolae. Caveolae are comprised primarily of an integral membrane protein called caveolin-1, and it is the oligomerization of this protein that is thought to play a role in the formation of the caveolae structure in cell membranes. The caveolin-1 protein has four distinct domains: a soluble N-terminal domain, a short amino acid stretch called the scaffolding domain, a transmembrane domain that is hypothesized to form a putative hairpin-like loop in the bilayer of the plasma membrane, and a C-terminal domain that is believed to closely associate with the surface of the cell membrane. Understanding the oligomerization process of caveolin-1 is critical to understanding the biological role of this protein. We are investigating the self-association of each of the four domains of the caveolin-1 protein to determine the contribution of each domain to the oligomerization process. By performing sedimentation equilibrium experiments in the analytical ultracentrifuge and employing a technique called density matching, it is possible to determine which domains in the caveolin-1 protein are responsible for the oligomerization of the protein in a detergent micelle solution. Using a wide range of concentrations, we can determine which domain contributes most significantly to the oligomerization process by closely monitoring changes in the molecular weight of each domain as a function of increasing peptide concentration. With this comprehensive data we can begin to understand how caveolin-1 behaves in the cell membrane and therefore learn more about its biological role.

2971-Pos Board B76

Synthetic Adhesion and Migration Models of Living Cells

Christian Kreidler, Michael Bärmann, Joachim P. Spatz.

Cells are indivisible units of life. Therefore, mimicking single functions of cells has attracted major interest within the so-called synthetic biology field. In particular, cell adhesion, spreading and migration are fundamental functions for cells, which are worthwhile goals to aim for from a synthetic point of view. In addition, such biomimetic model systems allow for the quantitative description of cellular functions and hence contribute to the physical understanding of living cells.

In our approach, the adhesion protein integrin $\alpha_{IIb}\beta_3$ is reconstituted in giant unilamellar vesicles (GUVs) containing G-actin in buffer solution. For the imitation of the cell's cytoskeleton, actin can be polymerized by the addition of Mg^{2+} ions which can cross the membrane by means of an incorporated ionophore. To mimic the glycocalyx of a cell and to prevent unspecific binding, PEG-functionalized lipids are also included in the membrane.

This bottom-up artificial system could be further developed by adding more proteins successively, for example motor proteins or focal adhesion proteins and is aiming to the synthetic reconstruction of the adhesion and migration apparatus of living cells.

2972-Pos Board B77

Effect of FGFR3 Juxtamembrane Domain on FGFR3 Dimerization

Sarvenaz Sarabipour, Edwin Li, Kalina Hristova.

Receptor Tyrosine Kinases have four distinct domains: extracellular (EC), transmembrane (TM), juxtamembrane (JM), and catalytic (CAT). Receptor Tyrosine Kinase (RTK) dimerization is critical for RTK function, and disregulation of ligand-independent dimerization of RTKs is known to be the underlying cause for a number of human pathologies. Yet, the exact mechanism of RTK dimerization, and the roles of the four RTK domains in the dimerization process are unknown.

To investigate the role of the juxtamembrane domain in ligand-independent homodimerization of RTKs, we are comparing the dimerization of two truncated FGFR3 constructs which both lack the catalytic domain, EC+TM+JM and EC+TM. We assess dimerization in single membrane-derived vesicles using the quantitative imaging FRET (QI-FRET) method [Li et al., 2008, Chen et al., 2010]. The results show that the juxtamembrane domain of FGFR3 increases the measured FRET efficiency and hence contributes to the energetics of lateral dimerization of the FGFR3 receptor.

Li E,Placone J,Merzlyakov M, Hristova K (2008) Quantitative measurements of protein interactions in a crowded cellular environment.Anal Chem 80:5976-5985.

Chen L, Novicky L, Merzlyakov M, Hristov T, Hristova K (2010) Measuring the energetics of membrane protein dimerization in mammalian membranes. J Am Chem Soc 17;132(10):3628-35.

2973-Pos Board B78

Unraveling Two Distinct Binding Interfaces for E Cadherin Dimerization: A Structural Study Using Single-Molecule Super-Resolved Fluorescence Imaging

Yunxiang Zhang, Alexandros Pertsinidis, W. James Nelson, Steven Chu.

Cadherins are homophilic adhesion molecules mediating Ca++ dependent cell-cell adhesion. It is not very clear how exactly cadherins interact and promote cell adhesion at the molecular level. We have previously characterized cadherin interactions with single molecule FRET and single molecule AFM and found cadherins interact mostly through outermost EC1 domains (Zhang & Sivasankar et al 2009). We then developed super-resolution localization microscopy that achieved sub-nanometer precision and accuracy and applied it to measurements of the end-to-end distances of E-cadherin dimers (Pertsinidis & Zhang et al 2010). The majority of the wild type cadherin dimers exhibits an extended EC5-EC5 distance of 32nm matching a strand-swapped trans-dimer model. A smaller population of the wild type dimers shows shorter distances of around 25nm suggesting an alternative binding configuration. We extended this work further by characterizing mutations in E-cadherin that prevent formation of the the strand-swapping interface. Interestingly, we observed that W2A dimers exist in a more compact conformation, similar to the minor population in the wild type dimers. The compact conformation is consistent with a so-called X-dimer interface discovered in recent crystal structures (Ciatto et al 2010, Harrison et al 2010). These new data refine our previous induced-fit dimerization pathway (Sivasankar & Zhang et al 2009) and are consistent with the X-dimer being the initial encounter complex. Furthermore, these results provide evidence that, at near-physiological Ca++ concentrations, E-cadherins can utilize two distinct binding interfaces to facilitate cell adhesion.

2974-Pos Board B79

The Characterization of the Binding of Opacity-Associated Proteins to Human Host Cell Receptors

Jacqueline C. Hodges, Alison H. Dewald, Linda Columbus.

Opacity-associated (Opa) proteins are eight-stranded β-barreled monomeric outer membrane proteins found in the bacterial pathogens *Neisseria meningitides* and *N. gonorrhoeae*. *In vivo*, these proteins interact with specific human host cell receptors to induce phagocytosis of the bacterium, allowing *Neisseria* to breach the plasma membrane and gain entry to targeted human cells. There are at least 26 characterized Opa proteins, nearly identical in sequence except for three extracellular loops. Host-receptor specificity is determined by the variable extracellular loops; however, the specific molecular determinants of the interaction have not been identified. Opa proteins are classified into two families based on their host receptor selectivity, the larger class, Opa_{CEA}, bind to carcinoembryonic antigen-like cellular adhesion molecules (CEACAMs) and the smaller class, Opa_{HS}, bind to heparansulfate proteoglycan receptors (HSPGs) or to integrin receptors via an HSPG-mediated interaction with fibronectin or vitronectin. Though the Opa-host receptor interaction is directly related to the invasion efficiency of *Neisseria*, the thermodynamics (e. g. affinities) of Opa proteins interactions with host receptors is not known. We present a study investigating the binding of two Opa protein variants, OpaI (an Opa_{CEA}) and OpaA (an Opa_{HS}) with their cognate host receptors. A centrifugal ''pull-down'' assay is used with fluorescence spectroscopy to determine the specificity and affinity of the Opa - receptor interactions. Although attempts have been made to study Opa specificity *in vivo*, this study demonstrates Opa protein selective binding to the respective receptors *in vitro*, thereby facilitating investigations of protein determinants relating both to binding specificity and affinity.

2975-Pos Board B80

Tyrosine Replacement Diminishes Association of PSGL-1 with P- and L-Selectins on the Cell Membrane

Botao Xiao, Xiaoling Jia, Rui Guo, ChunFang Tong, Shouqin Lü, Yan Zhang, Rodger P. McEver, Cheng Zhu, Mian Long.

Binding of selectins to P-selectin glycoprotein ligand-1 (PSGL-1) mediates tethering and rolling of leukocytes on endothelium during inflammation. While mutations of three tyrosines at the PSGL-1 N-terminus has been shown to increase the reverse rates and their sensitivity to force of bonds with P- and L-selectins [(1)], the roles of the mutations on the binding affinities and forward rates had not been studied well yet. Here we quantified these effects using an adhesion frequency assay for measuring two-dimensional (2D) affinity and kinetic rates at zero force [(2)]. Comparing to wild-type PSGL-1, binding affinities for P- and L-selectin was 7-164-fold lower for PSGL-1 mutants with two of three tyrosines substituted by phenylalanines and 89-284-fold lower for PSGL-1 mutant with all three tyrosines replaced. These differences were attributed to enhancements in forward rates without major changes in reverse rates, suggesting that these tyrosines regulate the accessibility of PSGL-1 to selectins and that at least one of the three tyrosines is required for selectin-PSGL-1 binding. Our results provided an insight into understanding the receptor-ligand binding at a single residue level.

1. V. Ramachandran *et al.*, *Proc.Natl.Acad.Sci.USA* (1999).
2. J. Huang *et al.*, *Nature* (2010).

2976-Pos Board B81

The Hydrophobic Proteins of Pulmonary Surfactant Reduce Bilayer Elasticity

Leonard E. Schulwitz Jr., Mariya Chavarha, Shankar B. Rananavare, Stephen B. Hall.

Pulmonary surfactant is a complex mixture of phospholipids and proteins that lowers surface tension at the alveolar air-water interface. The hydrophobic proteins SP-B and SP-C drive adsorption of surfactant vesicles to form the interfacial film. To investigate the structural basis underlying the function of the proteins, we used small angle x-ray scattering (SAXS) and 31P NMR to correlate a reduction in membrane elasticity and the formation of highly curved structures, with elevated rates of adsorption. Multilamellar vesicles were prepared using dioleoyl phosphatidylcholine (DOPC) with varying concentrations of the two proteins in their physiological ratios. SAXS patterns exhibited peak-broadening as well as linear increases in the interlamellar d-spacing with greater protein concentrations. In the absence of protein, global analysis of the patterns yielded a relatively low Caillé parameter ($\eta \sim 0.1$), indicating minor bilayer undulations. Incorporating protein into the vesicles induced large increases in the Caillé parameter from 0-4% (w:w), suggesting significant decreases in membrane elasticity as a function of protein concentration. 31P NMR spectra for the same samples showed the presence of an isotropic phase at concentrations as low as 0.25%, which grew in a dose-dependent manner with increasing concentrations of protein. Measured adsorption rates also exhibited dose-dependence in parallel with the SAXS and NMR data. The induced decrease in membrane bending rigidity, indicated by an increased Caillé parameter, and the formation of an accompanying isotropic phase, shown by the NMR spectra, suggests that these structural developments are directly related to the function of the surfactant proteins.

SAXS data was collected at the Stanford Synchrotron Radiation Lightsource.

2977-Pos Board B82

Probing Skeletal Dysplasias Caused by Mutations of FGFR3 Using Qi-FRET

Jesse Placone, Kalina Hristova.

Fibroblast growth factor receptor 3 (FGFR3) is a member of the receptor tyrosine kinase (RTK) family. FGFR3 is a single pass transmembrane protein and is involved in cell signaling, regulation, and proliferation. Signals are mediated via the lateral dimerization of the transmembrane spanning proteins and their interactions with extracellular ligands. It is important for these signaling pathways to be tightly regulated. Several mutations in FGFR3 are known to result in unregulated activation and/or disruption of proper cellular functions leading to pathogenesis. For example, single point mutations in FGFR3 are implicated in diseases such as achondroplasia, a form of dwarfism, and thanatophoric dysplasia, which is a lethal form of skeletal dysplasia. We are currently probing the interaction of mutant versions of FGFR3 to determine how these interactions change relative to that of the wild type FGFR3. These interactions are quantified via QI-FRET. In this approach, CHO cell-derived plasma membrane vesicles are prepared to mimic the native environment for the expressed FGFR3 constructs, which are linked to fluorescent proteins for direct visualization. Two important attributes of this approach over conventional whole-cell imaging are the low background noise and the strong intensity of the obtained vesicles. This results in the ability to fit the intensity profile with a Gaussian distribution and facilitate automated processing of images such that large numbers of vesicles with varying protein concentrations can be analyzed. From which, changes in interactions between wild type and mutant FGFR3 can be quantitatively determined.

2978-Pos Board B83

Kinetics of the Cytochrome C Oxidase from *R. Sphaeroidis* Under Turn-Over Conditions by Time-Resolved Surface-Enhanced Infrared Absorption Spectroscopy (SEIRas)

Renate C. Naumann, Christoph Nowak, Dieter Walz, Robert B. Gennis, Shelagh Ferguson-Miller, Wolfgang Knoll.

Cytochrome c Oxidase (CcO) is investigated under conditions of electronic wiring to a gold electrode modified with Au nanoparticles, designed for use with SEIRA spectroscopy in the ATR mode. In the presence of oxygen cyclic voltammetry had indicated that the enzyme is catalytically active when it is immobilized in the orientation with the first electron acceptor Cu_A directed toward the electrode. After immobilization CcO was protected by a lipid bilayer generated by in-situ dialysis. The full catalytic activity was obtained only after the enzyme had been subjected to a succession of several turn-overs. Thereafter SEIRA spectra measured under static conditions had indicated that the enzyme was in an ¯activated¯ state considered equivalent to the pulsed state found in biochemical assays.

Time-resolved (tr) SEIRA spectra recorded in the step-scan mode of the CcO were initiated by periodic potential pulses changing between an oxidizing and reducing potential thus varying the redox state of the enzyme many times. This allowed us to measure the kinetics of electron transfer at different frequencies. Moreover, amino acids correlated with electron transfer (ET) to the redox centers Cu_A, heme a, heme a_3 and Cu_B were identified. Particularly useful in this context proved 2D IR auto-correlation maps, which also allowed us to identify the sequence of conformational changes regarding different amino acids involved in ET and proton transfer as well as the reorientation of the transition dipole moments of various groups relative to each other.

Christoph Nowak, M. Gabriella Santonicola, Denise Schach, Jiapeng Zhu, Robert B. Gennis, Dieter Baurecht, Thamara Laredo, Jacek Lipkowsky, Dieter Walz, Wolfgang Knoll, Renate L. C. Naumann, Soft Matter, 2010, DOI:10.1039/C0SM00160K.

2979-Pos Board B84

Structure-Based Design of Phospholamban Mutants for Treatment of Heart Failure

Simon J. Gruber, David D. Thomas.

Ca^{2+} cycling through the SR in muscle cells is largely controlled by the Ca-pump (SERCA). SERCA transports Ca^{2+} into the SR, allowing muscles to relax, and is inhibited by phospholamban (PLB) at submicromolar [Ca^{2+}]. PLB inhibition can be relieved by adrenergic stimulation, leading to PLB phosphorylation. Heart Failure (HF), which contributes to 12% of US deaths, can be caused by a variety of genetic or environmental factors, but a common symptom is decreased SERCA activity. We are using EPR and NMR to study the relationships among structure, dynamics, and function of PLB, with the goal of designing LOF-PLB mutants (PLB_M) that can compete with WT-PLB and thus relieve SERCA inhibition. Several studies have shown that a pseudophosphorylated PLB (S16E-PLB) is effective for gene therapy in rodents and sheep, and we are using spectroscopic methods to refine this approach. We have developed a system for examining the function and interactions of SERCA and PLB in HEK cells. Active SERCA is expressed and cells are co-transfected with WT-PLB and/or PLB_M to measure SERCA inhibition in living cells. Effects of PLB/PLB_M on SERCA specific activity (s^{-1}), as well as PLB oligomeric states are characterized in stable cells lines. We can also measure a mutant's ability to compete with WT-PLB by measuring fluorescence resonance energy transfer (FRET) between labeled SERCA and WT-PLB. If PLB_M displaces WT-PLB, less energy is transferred between fluorophores and a decrease in FRET is observed. Preliminary results have led to rAAV-mediated expression of a PLB_M (P21G) in cardiomyocytes of a rat HF model, increasing contractility to near WT levels.

2980-Pos Board B85

Analyzing the Role of NCKX2 in Hippocampal Long Term Potentiation

Yuntian Zhang, Ray W. Turner, Jonathan Lytton.

Na+/Ca2+ exchangers control clearance of cytosolic Ca2+ following a signaling event when Ca2+ is elevated due to their low-affinity/high capacity transport properties. NCKX2 is a member of the family of K+-dependent Na+/Ca2+-exchangers, and is abundant in brain neurons. Targeted knockout of the NCKX2 gene results in a profound loss of long term potentiation and an increase in long term depression at hippocampal Schaffer/CA1 synapses. We examined the expression of a variety of synaptic molecules when NCKX2 is knocked out to disclose the role of NCKX2 in hippocampal plasticity. Co -localization experiments using confocal and electron microscopy were conducted to define the location of NCKX2 in hippocampus. Immunoblot results from whole brain lysates showed that GluR2/3 and NMDA-receptor 1 were reduced in NCKX2 knockout mice. There was no statistical difference in immunoblot for CamKII, PSD95, or GluR1 between wild type and the knockout. In hippocampus phospho-CamKII was upregulated, and small but insignificant changes were found in the expression of other synaptic marker proteins. Co-localization analyses showed minimal overlap of NCKX2 with either the post synaptic marker CamKII or the presynaptic markers synapsin, synaptophysin or VGLUT-1. Immunocytochemistry revealed a decrease in net MAP-2 label in the CA3 region of knockout animals that correlates to a reduction in the number of neuronal profiles and increase in DAPI-labeled nuclei, suggesting neuronal loss and glial cell proliferation. From the above experiments, we can for first time approach the idea of the exact location of NCKX2. Expression change for various synaptic molecules in hippocampus is not obvious, but rather loss of CA3 neurons and the associated Schaeffer collateral projection to CA1, potentially resulting from changes in calcium dynamics when NCKX2 is knocked out.

Protein Ligand Interactions: Receptors & Small Molecules

2981-Pos Board B86

Anesthetic Modulation of Signal Transduction Pathways in the α4β2 nAchR Revealed by the Perturbation-Based Markovian Transmission Model

Lu Tian Liu, Mingzhu Li, David Mowrey, Hsiao-Mei Lu, Jie Liang, Yan Xu, Pei Tang.

The gating mechanism of ligand-gated ion channels and anesthetic modulation of channel gating remain to be determined. In this study, we used the perturbation-based Markovian transmission model to investigate the time-dependent signal propagation in the neuronal nicotinic acetylcholine receptor (α4β2 nAChR) under initial perturbations by agonist binding. Both open- and closed-channel α4β2 nAChR conformations in the presence and absence of the anesthetic halothane, from our previous computational studies, were examined. We found that signal transduction in α4β2 resembles the conformation wave mechanism. In all systems, the perturbation signal flows from the agonist-binding sites up toward the main immunogenic region, then down to the bottom of the beta barrel, followed by the extracellular (EC)/transmembrane (TM) interface, and finally to the transmembrane domain, as measured by the time dependence of the maximum probability flux. The EC domain of the open- and closed-channel α4β2 conformations showed different dynamic responses to the perturbation at the agonist-binding site: many more residues in the EC domain of the open-channel α4β2 nAChR exhibited frequent fluctuation. In the system with halothane, the signal transduction within pre-TM1 (R207), Cys-loop (F137, P138, F139), and TM2-TM3 linker (L271) slowed down in some of the subunits, but speeded up in others. The changes in signal transduction at the EC/TM interface may underlie the effects of anesthetics on the α4β2 nAChR. Supported by NIH (R01GM066358, R01GM056257, R37GM049202).

2982-Pos Board B87

Catharanthine Alkaloids are Noncompetitive Inhibitors of Muscle-Type Nicotinic Acetylcholine Receptors

Ruin Moaddel.

This is an attempt to characterize the binding sites and the mechanisms of action of several catharanthine alkaloids including ibogaine, vincristine, and vinblastine, on muscle-type nicotinic acetylcholine receptors (AChRs), by comparing their pharmacological properties with that for the well characterized high-affinity noncompetitive antagonist (NCA) phencyclidine (PCP). In this regard, structural and functional approaches were used including radioligand equilibrium and competition binding assays using [^{3}H]ibogaine and the analog of PCP, [piperidyl-3, 4-^{3}H(*N*)]-*N*-(1-(2 thienyl)cyclohexyl)-3,4-piperidine ([^{3}H]TCP), Ca^{2+} influx determinations, thermodynamic and kinetic measurements using column-immobilized *Torpedo* AChRs, and molecular docking and dynamics studies The results established that: **(a)** the alkaloidsinhibit (±)-epibatidine-induced Ca^{2+} influx in embryonic muscle AChRs with the following potencies (in μM): ibogaine (17 ± 3) > vinblastine (20 ± 5) > vincristine (25 ± 4), that are slightly higher than that for PCP (31 ± 2), **(b)** the alkaloids inhibit [^{3}H]TCP binding, and ibogaine and PCP inhibit [^{3}H]ibogaine binding, to the desensitized *Torpedo* AChR with higher affinity compared to the resting AChR, **(c)** ibogaine binds to the *Torpedo* AChR by an entropy-driven process, and **(d)** ibogaine interacts with a binding domain located between the serine (position 6') and valine (position 13') rings, by a network of van der Waals and polar interactions. Collectively our data indicate that catharanthine alkaloids block agonist-activated ion channels by interacting with a binding domain that is shared with PCP located between the serine and valine rings. This supports the view that the catharanthine moiety, which is shared by ibogaine and vinca alkaloids, is a minimum structural requirement for the interaction of these molecules with the ion channel. In addition, ibogaine and vinca alkaloids may induce and maintain the desensitized state by a mechanism where their dissociation rates are decreased.

2983-Pos Board B88

A Combined Experimental and Simulation Approach to Develop Selective High-Affinity Small-Molecule Inhibitors of Cannabinoid Receptors CB1/CB2

Irene Meliciani, Nicole Volz, Viktor Rempel, Sonja Hinz, Tadeusz Karcz, Christa E. Müller, Stefan Bräse, Wolfgang Wenzel.

The cannabinoid receptors belong to the membrane-bound G protein-coupled receptor superfamily and are predominantly coupled via Gi/o proteins. The CB1 receptor subtype is known to play an essential role in analgesia, memory-impairment, spasmolysis and regulation of appetite. Selective agonists for CB2 receptors show antiinflammatory and analgesic properties in animal models [1]. Cannabinoid receptors are activated by three major groups of ligands, mammalian endocannabinoids, plant and synthetic cannabinoids (e.g. THC from the plant Cannabis sativa). Here we investigated the interactions between the cannabinoid receptors type 1 and 2 (CB1/CB2) with a novel set of coumarin derivatives.

Rational drug design for many GPCRs is complicated by the lack of receptor crystal structures. To aid interpretation of the experiments we have therefore constructed a model for the CB1 and CB2 receptors based on homology to bovine rhodopsin (pdb-code 1U19) and performed ligand binding simulations for a family of 39 coumarin derivatives applying an all-atom docking protocol using Flexscreen [2].

We rationally designed, synthesized and tested a novel set of ligands to exploit a hydrophobic cavity in the vicinity of the docking pose of known ligands. All novel ligands showed improved, affinities with respect to their reference compounds, in good quantitative agreement between experiment and simulation, some of them reaching nanomolar affinities. Studying a series of site-specific mutations, we could computationally rationalize the receptor selectivity of specific compounds to either preferentially bind CB1 or CB2, respectively.

[1] S.H. Burstein and R.B. Zurier (2009) Cannabinoids, Endocannabinoids, and Related Analogs in Inflammation,
AAPS J. 11(1), 109-119.
[2] H. Merlitz, B. Burghardt and W. Wenzel (2003) Application of the Stochastic Tunneling Method to High Throughput Database Screening,
Chem. Phys. Lett. 370, 68-73.

2984-Pos Board B89

Field-Modulated Magnetic Birefringence Relaxation to Assay b-Adrenergic Receptor-Ligand Association

Louis H. Strong, Daniel B. Hall, Hiep-hoa Nguyen, **Gyula Varadi**.

We developed a platform for monitoring the association between biologically active molecules and their cognate receptors based on measuring rate changes of magnetic birefringence relaxation of superparamagnetic nanoparticles. The method is particularly designed for rapid screening of display libraries and mutant receptor libraries expressed in bacteria and yeast. The magnitude of birefringence rate change after particle orientation in a magnetic field reflects the difference of nanoparticle hydrodynamic volume upon formation of the ''receptor-ligand complex''. The rationale for using nanoparticle birefringence to identify ligand and receptor interactions is that it eliminates the need for removing unbound ligands. We have previously demonstrated that maghemite nanoparticles, decorated with ligand molecules, exhibit longer relaxation times when associated with proteins, viruses and small size microorganisms. We utilize magnetic field-modulated birefringence to monitor association between a ligand (alprenolol) immobilized on the surface of magnetic nanoparticles and β-adrenergic receptor overexpressed on the cell surface of bacteria and yeast. Upon association of the ligand with the receptor, we observed an increase in the birefringence rate constant, an effect that was fully reversible by adding β-adrenergic competitor ligands. Rate constant distributions were reconstructed using the Phase Function Method. We show that birefringence signals can be used to monitor the dynamics of particle rotational alignment as well as rotational relaxation. Alignment dynamics are characteristic of the number of accessible receptor sites while relaxation characterizes the aggregate size. This novel approach is applicable in systems where the interaction of ligand with cognate receptor does not activate intracellular pathways and thus are difficult to monitor with a ratiofluorometric platform. This method will be useful for a broad range of applications, including discovery research to develop small molecule drugs and for identification of orphan receptors and biologically active peptides and proteins from display libraries.

2985-Pos Board B90

Transient Kinetics of Nucleotide Binding to the P-glycoprotein Multidrug Transporter

Miguel R. Lugo, Joseph W.K. Chu, Frances J. Sharom.

The P-glycoprotein multidrug transporter (Pgp) is a member of the ABC (ATP-binding cassette) superfamily of proteins, and contains two highly conserved cytosolic nucleotide-binding domains (NBDs). These domains couple ATP hydrolysis to the export of a variety of hydrophobic natural products, chemotherapeutic drugs and peptides. Pgp ATPase activity has been extensively characterized, but many details of the catalytic cycle of ATP hydrolysis remain unexplored. The fluorescent nucleotide analogue, TNP-ADP, interacts with the NBDs of Pgp, and the stoichiometry and affinity of binding were previously determined in our laboratory. Transient kinetic methods are commonly used to investigate the mechanism of molecular processes over a time-scale from milliseconds to hundreds of seconds. In this work, we studied the binding of TNP-ADP to Pgp using rapid stopped-flow kinetics. In these experiments, the binding reaction was monitored by following different fluorescent signals, under pseudo-first-order conditions (excess ligand). The time course of TNP-ADP binding displayed five relaxation times (τ_i's) over a time-span of 300 sec, which correspond to at least five different transitions. All the relaxation times presented a strong temperature-dependence. The time course of the reaction was analyzed by the computational tool Global Kinetic Explorer (KinTek, USA), using several models of sequential isomerizations after/before the fast bimolecular binding reaction. Also, the parameters were analyzed using the matrix projection operator technique for kinetic data (Bujalowski *et al.*, 2000, J. Mol. Biol. 295:831). Both approaches provide, for the first time, information about the rate constants and fluorescent properties of the diverse intermediates formed during binding of TNP-ADP to Pgp. Elucidation of the details of the interaction of nucleotides with Pgp is of prime importance for formulation of a detailed mechanism of action of the transporter.

This research is supported by a grant from the Canadian Cancer Society.

2986-Pos Board B91

Identification of an Efficacy Pharmacophore for μ Opioid Receptor Ligands Using the Conformationally Sampled Pharmacophore (CSP) Method

Jihyun Shim, Andrew Coop, Alexander D. MacKerell Jr.

μ opioid receptor agonists and antagonists play a critical role in the treatment of severe pain and as treatments for drug abuse. Their structure activity relationships (SAR) have been extensively investigated followed by lead optimization. However, challenges remain in improving the utility of m ligands with respect to reducing adverse effects such as tolerance, dependence, constipation, etc. while maintaining the potency of current medicines. To facilitate the meeting of these challenges, consensus pharmacophore models for diverse classes of μ opioid receptor ligands were established and we constructed predictive model differentiating agonists and antagonists activities using the conformationally sampled pharmacophore (CSP) method. The predictability of the models was validated against a number of classes of opioids including 4,5-Epoxymorphinans, Diels-Alder adducts of thebaine, Benzomorphans, Methadone, Fentanyl, and, notably, non-nitrogenous opioids; a collection of compounds which have eluded a consensus SAR of opioids for decades. The consensus model was derived by virtue of CSP method incorporating flexibility of molecules through using all-accessible conformers in model development and by eliminating any limitations associated with alignment procedures. The procedures to develop and features of the CSP model will be presented.

2987-Pos Board B92

Probing Binding of Apelin to the Extracellular Loops of the Apelin Receptor (APJ) in Lipid Mimetic Environments

Pascaline Ngweniform, Jan K. Rainey.
[a] Department of Biochemistry & Molecular Biology and [b] Department of Chemistry, Dalhousie University, Halifax, NS B3H 1X5.

The apelin receptor, previously called APJ, is a G protein-coupled receptor highly expressed in the central nervous system (CNS), cardiovascular system, the adipoinsular axis and the mammary glands, among other tissues and organ systems. The apelinergic system plays important biological functions in the regulation of blood pressure, blood glucose, drinking behavior and food intake. The action of this system is also implicated in tumour angiogenesis, diabetes and cardiovascular diseases. In addition, the apelin receptor is a co-receptor for human immunodeficiency virus type 1 (HIV1) and simian immunodeficiency virus (SIV). Despite these roles, the mechanism of activation of apelin receptor by its cognate ligand has not been studied at the molecular level. Following the ''divide and conquer'' approach for membrane protein characterization, we present the biophysical characterization of the interaction of two extracellular loops of the apelin receptor (extracellular loops 1, EL1 and 3, EL3) with a fluorescently-tagged apelin analogue in lipid environment. Peptides were synthesized by solid phase peptide synthesis and purified by high-performance liquid chromatography. Characterization both of the peptides in isolation and of the binding between apelin and EL peptides is provided using circular dichroism spectroscopy, fluorescence resonance energy transfer and nuclear magnetic resonance spectroscopy. These results provide insight into understanding of the apelinergic system at the molecular level and provide the first structural information on the apelin receptor for the development of therapeutics targeting this system.

2988-Pos Board B93

Design and Biophysical Characterization of a Single Chain Four-alpha-helix Bundle Protein Which Binds Volatile General Anesthetics

Lucia M. Morstadt, Qing Cheng Meng, Jonas S. Johansson.

In order to investigate the interaction of volatile general anesthetics with their putative membrane protein targets, we designed a four-alpha-helix bundle protein in a single protein chain. The four alpha helices, connected by three 8 glycine loops, had the sequence A, B, B', A'. The DNA sequence was designed with the goal of making helices with the same amino acid sequence (helix A and A', B and B', respectively) as different as possible in their

DNA sequence, while using codons which are favorable for expression in E.coli. Restriction enzyme sites were added on both ends. The synthesized DNA sequence was cloned into an expression vector. The protein was bacterially expressed and purified to homogeneity using reverse-phase HPLC. Protein identity was verified using MALDI-TOF mass spectroscopy. Near UV circular dichroism spectroscopy confirmed the strongly alpha helical nature of the protein. Guanidinuium chloride denaturation showed that the single chain four-alpha-helix bundle protein is twice as stable as the dimeric dihelical protein. The sigmoidal character of the unfolding reaction was conserved, the sharpness of the transition increased. Our single chain four-alpha-helix bundle protein bound halothane with a dissociation constant of 1.2 mM, as shown by tryptophan fluorescence quenching. This single chain four-alpha-helix bundle protein can now be used as a scaffold to incorporate natural membrane protein sequences to examine general anesthetic interactions in detail.

2989-Pos Board B94

Binding Profiles Based on Normal Mode Analysis as a Foundation for a Unified Approach to Allosteric Activation of Prolactin Receptor

Adam D. Schuyler.

Two of the most fundamental biological processes are ligand binding and allosteric signaling. Despite their (often) direct linkage, a unified model of the underlying dynamics is not well established. The harmonic motions identified by normal mode analysis (NMA) provide a natural coordinate system for conformation space. Binding profiles and allosteric profiles based on NMA allow for a unified model which describes the propensity for various structure motions to promote/inhibit binding and allosteric activation. The authors have recently developed the allosteric model; the current work presents the binding model.

The normal modes describe local motions accessible to a conformation. Each of the modes is followed over a small displacement, leading to a set of new conformations. This procedure is repeated to generate an ensemble, where each conformation is defined by its sequence of normal modes. Ensembles are generated around a receptor and ligand. Each receptor conformation is paired against each ligand conformation and scored for: (1) compatibility of interface shape; and (2) compatibility of interface dynamics. These scores are attributed to the normal mode sequences associated with each candidate conformation. The scores are summed over all possible conformation pairings, producing a binding profile that defines each normal mode's propensity to contribute to compatible interface shape and interface dynamics.

The prolactin receptor dimerizes and preferentially binds prolactin at one binding site, and then binds another prolactin at the second binding site - activating the receptor. Binding profiles are generated for prolactin and prolactin receptor, isolated from the various complexes along the activation pathway. The goal is to identify the dynamics that regulate binding site preference and allosteric activation. Future work will incorporate NMR studies to validate and refine the initial results.

2990-Pos Board B95

Solid-State NMR Study of Ligand Binding to Human Peripheral Cannabinoid Receptor CB2

Tomohiro Kimura, Alexei Yeliseev, Mihaela Mihailescu, Kejun Cheng, Kenner C. Rice, Klaus Gawrisch.

The peripheral cannabinoid receptor CB2 belongs to the family of G protein coupled receptors (GPCRs). Ligand binding studies on CB2 are complicated by high affinity of the endogenous or exogenous cannabinoid ligands for the lipid matrix that hosts the GPCR. Here we show that solid-state NMR distinguishes between specific ligand-binding to CB2 and nonspecific interactions with the lipid matrix. Experiments were conducted with recombinant, human CB2 expressed in *E. coli*, purified and functionally reconstituted into unilamellar liposomes. Location, structure, and dynamics of ligands in the lipid matrix were probed by NMR as well as neutron diffraction. The synthetic agonist CP-55,940 locates near the hydrophobic/hydrophilic interface of bilayers with its bond linking hydroxyphenyl and hydroxycyclohexyl rings perpendicular to the bilayer normal, while the endogenous agonist 2-AG orients parallel to the bilayer normal with the glycerol moiety near the hydrophobic/hydrophilic interface and the arachidonoyl chain in the hydrophobic region. Both ligands maintain a high level of conformational flexibility and have lateral diffusion rates in membranes comparable to those of lipids. Ligand binding to CB2 drastically shortens transverse relaxation times of the ^{2}H-labeled ligands which distinguish between specific and non-specific binding events. Competition binding experiments with protonated and selectively deuterated CP-55,940 showed that ~90% of the reconstituted CB2 was ligand-binding competent and formed a one-to-one complex with the ligand. Activation of G protein by agonist-bound CB2 was confirmed in a G protein activation assay. The endogenous 2-AG has a binding affinity to CB2 that is orders of magnitude lower compared to CP-55,940. The possibility that cannabinoid ligands approach the receptor from the lipid matrix will be discussed. Experiments are underway to gain structural insights into specific binding interactions based on selective isotope-labeling of both ligand and recombinant CB2.

2991-Pos Board B96

Fluorescence Guided Force Microscopy (FGFM) Used to Measure Receptor Ligand Interactions in Live Mammalian Cells

Jeremy C. Bonor.

Fluorescence Guided Force Microscopy (FGFM) is a new technique that was developed in order to measure and quantify ligand surface interactions on the cell surface in living cells. Using this method we can determine the binding affinity of ligands with surface receptors and their spatial distribution by combining force volume measurements, confocal microscopy and atomic force microscopy into one new instrumental setup. In order to validate this new method we covalently linked a ligand, Bone Morphogenetic Protein 2 (BMP2) to an Atom Force Microscopy (AFM) probe and acquired topographical and force binding information. To visualize caveolae by confocal microscopy, membrane domains known to co-localize with BMP receptors on the cell surface, Caveolin-1 was fused to green or red fluorescent protein and used as a marker. We transfected C2C12 cells with plasmids encoding Caveolin-1 isoforms alpha and beta (fused to green fluorescent protein) and Caveolin-1 alpha (fused to red fluorescent protein). Detecting the unbinding forces, surface topography and fluorescent protein location on the live cell surface, required combining Force Volume measurements, AFM and confocal imaging; which we achieved through the integration of the Veeco Bioscope2 AFM module, equipped with a closed loop scanner and a Zeiss LSM510 NLO confocal. The collection of high resolution confocal images, AFM images and unbinding force curve data on live cells allowed us to resolve the spatial distribution of binding events on the plasma membrane of C2C12 cells. This data showed that BMP 2 bound with the highest affinity inside Caveolin-1 isoforms.

2992-Pos Board B97

Nanoparticles Masquerade as "Self" to Inhibit Phagocytosis

Pia L. Rodriguez, Takamasa Harada, Dennis E. Discher.

A major challenge for injecting particles or implanting biomaterials into the body is that they activate immune cells such as macrophages, the cells that normally function to clear invading pathogens. Interestingly, macrophages have a surface receptor mechanism which prevents them from phagocytosing our own "self" cells. During initial macrophage engulfment, macrophages recognize foreign and self targets because they both have antibodies or plasma complement proteins on their surface. However, before the macrophage engulfs the target, self cells are checked for the presence of the surface protein CD47 which will bind to the macrophage receptor SIRPα (CD172), and we show that CD47-SIRPα interactions in cell-cell adhesion, with human macrophages in sparse culture, produce phagocytosis inhibition. Whether the CD47 interaction is functional with small targets of phagocytosis is unclear and relevant perhaps to nano-sized targets. We show that CD47 coupled to a series of synthetic beads can inhibit uptake by macrophages. However, we need to test this interaction and observe how these results are consistent with in vivo systems. We are currently testing whether nanoparticles that have surface immobilized hCD47 or a portion of it will not be phagocytosed in nobese diabetic (NOD) mice, we believe that hCD47 will bind to this mSirpa strain and that could bring a better understanding of the interaction at a nanoscale.

2993-Pos Board B98

In Vivo Binding Kinetics and Stoichiometry of Toll-Like Receptor 9 and CpG DNA Resolved by Multiparametric Single Molecule Techniques

Jiji Chen, Suman Nag, Joseph Irudayaraj.

Toll-like receptor 9 (TLR9) activates the innate immune system in response to oligonucleotides rich in CpG whereas DNA lacking CpG could inhibit its activation. Although in vitro experiments demonstrate TLR9 binding to nucleic acids, the mechanism of how this receptor interacts with nucleic acid and becomes activated in live cells is far from behind understood. Here, we report on the successful implementation of single molecule tools, constituting fluorescence correlation spectroscopy (FCS), fluorescence cross-correlation spectroscopy (FCCS), photon count histogram (PCH) and fluorescence lifetime imaging (FLIM) to study the interaction of TLR9-GFP with Cy5 labeled oligonucleotide containing CpG or lacking CpG in live cells.

We found that TLR9 predominantly forms homodimers (80%) before binding to a ligand and addition of CpG or non CpG DNA does not necessarily increase the proportion of TLR9 dimers. Experiments in living cells reveal that CpG DNA has a lower dissociation constant (62 ± 9 nM) compared to non CpG DNA (153 ± 26 nM) upon binding to TLR9 in live cells, suggesting that a motif specific binding affinity of TLR9 could be an important factor in its conformational change-dependant activation. Furthermore, it was observed that the CpG-TLR9 has a slower mobility compared to non CpG-TLR9 complex and both CpG and non CpG DNA bound to TLR9 with a 1:2 stoichiometry in vivo. Collectively, our findings establish an in vivo model for TLR9 activation by CpG DNA and highlight the significance of the need for an integrated and sensitive approach to obtain quantitative investigation of biomolecular interactions in live cells.

2994-Pos Board B99

Regulation of Integrin Activation in Acidic Extracellular Microenvironments

Ranjani K. Paradise, Douglas A. Lauffenburger, Krystyn J. Van Vliet.

It is well known that extracellular pH (pHe) becomes acidic in the tumor and wound microenvironments, and that acidic extracellular pH can have profound effects on cell adhesion and migraation processes integral to metastasis and wound healing. However, the molecular mechanisms underlying cellular responses to acidic pHe are largely unknown. Integrin receptors form a physical linkage between cells and the extracellular matrix, and are thus capable of modulating cell adhesion and migration in response to extracellular conditions. Here, we examine the role of acidic pHe in regulating activation of integrin $\alpha_v\beta_3$, as well as downstream consequences for cell-level processes. Employing atomistic molecular dynamics simulations, we find that acidic pHe promotes opening of the $\alpha_v\beta_3$ headpiece, indicating that acidic pH can promote integrin activation via an outside-in mechanism. In agreement with these simulations, flow cytometry and atomic force microscope-mediated force spectroscopy assays of integrin $\alpha_v\beta_3$ on live cells demonstrate increased levels of integrin activation when cells are exposed to acidic pHe. Finally, cell morphology and migration measurements demonstrate that cells respond to acidic pHe in a manner that is consistent with increased integrin activation. These multiscale computational and experimental results suggest a new mechanism of integrin activation regulation in regions of acidic extracellular pH, with associated implications for cell adhesion and migration in wound healing and cancer.

2995-Pos Board B100

Unraveling Key Features of the Beta-Galactoside Binding Protein Galectin-1 in Interplay with Ligand Binding and Dimerization Equilibria

Santiago Di Lella, Julio J. Caramelo, Carlos M. Guardia, Marcelo A. Martí, Gabriel A. Rabinovich, Darío A. Estrin.

Galectin-1 is a multifunctional β-galactoside-binding protein associated with critical biological processes such regulation of immune responses and cellular differentiation. Upon binding to the disaccharide lactose, a model study ligand, subtle changes may be responsible of modulating its function.

In this work, structural changes occurring upon binding of galectin-1 to its specific glycans and under different experimental conditions are tested by experimental (i.e. circular dichroism and fluorescence spectroscopy) tools. On the other hand, we studied dimerization as another factor that may induce structural changes. The results are then complemented with molecular dynamics simulations followed by a detailed computation of thermodynamic properties, including the internal energy, solvation free energy, and conformational entropy. In addition, an energetic profile of the binding and dimerization processes is also presented, under different conditions. Whereas binding and cross-linking of lactose only subtly alter galectin-1 structure, the interactions lead to substantial changes in the flexibility and internal energy of the protein which confer new properties to this endogenous lectin. Furthermore, key features determining ligand binding at different experimental conditions are analyzed.

Provided these physicochemical properties of galectin-glycan interactions, a discussion will be presented on possible biological connotations and prediction of their potential therapeutic applications.

2996-Pos Board B101

Characterization of the Phosphatidylinositol 3-Phosphate Binding Mechanism of the *Phytophthora Sojae* Effector Avh5

Furong Sun, Dan Li, Brett M. Tyler, Daniel G.S. Capelluto.

Phytophthora sojae is an oomycete pathogen of soybean plants. The economic damage mediated by this pathogen is estimated in the tens of billions of dollars. *P. sojae* encodes effector proteins to perform pathogenesis, and the major function of these effectors is to reduce the signal transduction pathways of the defense system of soybean plants. The mechanism of entry is still unclear, although two conserved N-terminal motifs of these effectors, the RXLR and dEER motifs, are indispensable for entry. We have recently demonstrated that phosphoinositides are ligands for effector proteins, and particularly, phosphatidylinositol 3-phosphate (PI3P) is the specific ligand for one of these effectors, the *A*virulence *H*omolog *5* (Avh5) protein. NMR spectroscopy analysis indicates that the protein interacts with the PI3P head group in a fast-exchange regime and that phosphorylation at the position 3 in the inositol ring is critical for protein recognition. The large number of chemical shift changes observed throughout Avh5 suggests that conformational changes accompany binding. By completion of the NMR resonance assignments of Avh5, we will be able to precisely map the PI3P-binding site. Conformational changes of Avh5 were further confirmed by the observation that Trp70 becomes solvent-exposed in the presence of the PI3P head group. Spectroscopy analysis reveals that Avh5 exhibits an alpha-helical and compact tertiary structure and that PI3P head group binding induces structural changes in the protein. Thermal stability studies indicate that Avh5 presents two-state melting transitions and that thermal unfolding is highly cooperative. Thus, the identification of the PI3P-binding site and the resultant structural changes of Avh5 may provide the structural basis to understand the role of the lipid in providing entry of the effector into plant cells.

2997-Pos Board B102

Relative Affinities of Fatty Acid Binding Sites on Human Serum Albumin Probed by 2D-NMR

Eileen Krenzel, Zhongjing Chen, James A. Hamilton.

In circulation HSA is the principal carrier for endogenous lipophilic compounds, primarily non-esterified long chain fatty acids (FA). Since FA bind to multiple binding sites with varying affinities, it would be useful to probe the relative affinities for these FA binding sites with a method that distinguishes individual binding sites. As visualized in crystal structures FA binding distributes asymmetrically throughout the protein. In the physiologically relevant solution state, these sites were partially distinguished by 1D-^{13}C-NMR spectroscopy and subsequently correlated with crystal structure sites. Here we show nine, well-resolved peaks in ^{1}H-^{13}C-NMR spectra of 18-^{13}C-oleic acid (OA) / HSA complexes. Different NMR signals represent FA bound at different sites throughout the protein, with the varying intensities corresponding to the different affinities HSA has for OA. This investigation probes the relative affinities of FA with three approaches: (i) addition of different FA molar ratios to HSA, to observe the order of filling of binding sites; (ii) addition of FA acceptors to observe the dissociation of FA from HSA; and (iii) addition of drugs that are known to bind to low affinity FA sites. From the order of filling, the three highest affinity-binding sites are clearly differentiated from the six lower/medium affinity-binding sites at the physiologically relevant FA:HSA molar ratio- 4:1. Methyl-β-cyclodextrin (MβCD) extracted FA from individual sites, in a concentration dependent manner, with the highest concentrations removing FA from the highest affinity sites. Relative affinities determined as above were consistent with the binding of drugs to Sudlow's drug binding sites, which displaced bound FA from specific lower affinity sites. 2D-NMR spectroscopy is a powerful approach for studying interactions of FA with HSA and FA-competitive drugs in a site-specific manner, providing a unique view of HSA-ligand binding.

2998-Pos Board B103

Solution NMR Spectroscopy and Protein Interaction Studies of Membrane Proteins in Nanodiscs

Julian M. Glück, Marc Wittlich, Sophie Feuerstein, Dieter Willbold, **Bernd W. Koenig**.

Insolubility of integral membrane proteins (IMPs) in buffer often prevents their investigation with biophysical methods developed for soluble proteins. First, solution NMR of large proteins or complexes is limited by slow rotational diffusion. IMPs in cellular membranes or liposomes are beyond the size limit of solution NMR. Therefore, detergent micelles or bicelles are often used for solubilization and NMR studies of IMPs. Unfortunately, detergents may destabilize the native structure or compromise the activity of proteins. Nanodiscs are a lipid-based, detergent free, relatively small and very promising new model membrane system. We inserted a recombinantly produced and ^{15}N, ^{13}C-labeled fragment of human CD4 into nanodiscs. This polypeptide comprises the membrane-spanning and the cytoplasmic domains of CD4. Our NMR data demonstrate the feasibility of solution NMR spectroscopy on IMPs in nanodiscs. Second, surface plasmon resonance

(SPR) is predominantly utilized in interaction studies of soluble proteins. Incorporation of IMPs into nanodiscs provides a close to native environment to the membrane protein and results in a water-soluble proteolipid particle that might be amenable to standard SPR-based methodology. We reconstituted a decahistidine-tagged IMP into nanodiscs and studied binding between the nanodisc-inserted IMP and a PentaHis monoclonal antibody (mAb) immobilized on the surface of a CM5-sensorchip. For comparison, we also determined the affinity of the decahistidine-tagged soluble domain of the same IMP toward the immobilized PentaHis mAb. Binding affinities were almost identical in both cases. However, the association and dissociation rate constants were found to differ, which is in agreement with the distinct diffusion coefficients of the soluble analyte particles. Our data indicate that nanodisc-inserted IMPs can serve as analyte in interaction studies of membrane proteins.

2999-Pos Board B104

^{31}P NMR Studies of Active Site and Activator Site Ligands Binding to PTEN

Yang Wei, Mary F. Roberts.

PTEN, a tumor suppressor mutated in a large variety of human tumor cells, antagonizes the PI3K signaling pathway by dephosphorylating the $PI(3,4,5)P_3$ at the 3 position of the inositol ring. $PI(4,5)P_2$, the product of $PI(3,4,5)P_3$ hydrolysis, has been shown to activate PTEN, possibly by binding to the N terminus of the protein. However, the mechanism for this activation is still in dispute. ^{31}P NMR, both fixed field and field cycling methods, was used to study the binding of PTEN to different diC_8PI derivatives. There were distinct differences in motional parameters for active site ligands (e.g., D-diC_nPI species) versus those for activator molecules (D-$diC_nPI(4,5)P_2$). Molecules binding in the active site exhibited a significant increase in linewidth consistent with intermediate exchange that was not observed for activator molecules. Spin-labeled protein was also used to interrogate active and activator sites. Modeling studies of the catalytic domain of PTEN indentified a hydrophobic pocket formed by the loop containing Arg47 that appeared to play an important role in substrate and substrate analog binding. Mutations of this residue (R47G, R47K, R47L and R47W) exhibited dramatically decreased activity. ^{31}P NMR analyses of these mutants and short-chain PI ligand binding together with kinetics are used to propose a model for the two sites on PTEN.

3000-Pos Board B105

β-Lactamase Inhibition: Mechanistic Details and Novel Inhibitors

Elizabeth A. Rodkey, Jared M. Sampson, Matthew Kalp,
Christopher R. Bethel, John D. Buynak, Paul R. Carey, Robert A. Bonomo, Focco van, den Akker.

Bacteria that are resistant to β-lactam antibiotics by producing β-lactamases are a significant public health threat. These β-lactamases hydrolyze β-lactams and render them inactive. To combat these resistant strains, β-lactams are often administered with β-lactamase inhibitors. Unfortunately, β-lactamases are beginning to acquire mutations which confer resistance to these inhibitors as well. Therefore, a clear need exists to identify novel inhibitors to ensure continued antibiotic efficacy.

We used a synergistic X-ray and Raman crystallographic approach to investigate the mechanisms of inhibitor binding and to further the development of new inhibitors of the β-lactamase SHV-1. To this end, we first engineered an acylation deficient mutant to capture the pre-acylation complex of β-lactamase and inhibitor. Our 1.45 Å structure, as well Raman measurements, reveals an unreacted sulbactam species in the active site of the mutant SHV enzyme and represents the first pre-acylation structure between inhibitor and β-lactamase. The structure identifies key interactions that are made immediately before acylation.

The second project involves a series of derivative compounds designed to improve upon the novel C2 penam sulfone inhibitor, SA2-13, which forms a stabilized trans-enamine conformation in the active site. Structures of the derivative compounds suggest that the C2 chain length is important in SA2-13 stabilization. Exploring a series of C2 derivatives by X-ray and Raman spectroscopy permitted deeper insight into more favorable inhibitor conformations. Understanding the interactions which occur in the steps immediately prior to and during covalent complex formation will allow for design of better β-lactamase inhibitors against these important drug targets. Using Raman and protein crystallography allow us to track and trap reaction intermediates inside protein crystals.

3001-Pos Board B106

Ligand-Binding Domain of Type 1 Metabotropic Glutamate Receptor is Fully Functional in iTs Monomeric Form

Eugene Serebryany, Ewa Folta-Stogniew, Elsa C.Y. Yan.

The type 1 metabotropic glutamate receptor (mGluR1) is an archetypal class C G-protein coupled receptor (GPCR) that modulates neurotransmission and synaptic plasticity in the brain. It has been demonstrated that mGluR1 carries out its biological function as a covalently linked dimer. All class C GPCRs investigated to date undergo dimerization, yet the precise biological significance of this phenomenon remains unclear. We sought to test the effect of dimerization on the activation properties of the ligand-binding domain (LBD) of mGluR1, expressed in HEK293 cells as a truncated soluble domain. Two variants of the protein were created: a wild-type construct and the C140S mutant, which lacks covalent linkage between subunits. The extent of dimerization in solution under non-denaturing conditions was examined by using static light scattering (SLS) to measure weight-average molecular weights for both constructs. These measurements support full dimerization in the wild type and permit quantification of the monomer-dimer equilibrium in the C140S mutant. Structural rearrangements of the purified LBDs were probed in vitro by monitoring changes in intrinsic tryptophan fluorescence; fluorescence was titrated with the native ligand L-glutamate to quantify biological activity. These titrations were carried out at low protein concentration at which preliminary SLS results show that the C140S mutant exists in its monomeric state, in contrast to the covalently linked wild-type dimer. We found that the monomeric mGluR1 LBD has equal or greater activity compared to the wild type. Our results indicate that dimerization is not a prerequisite of function, but likely plays a modulatory role in the ligand-binding domain of this receptor. This approach will allow future investigations to reveal emergent properties arising from dimerization in mGluR1 and similar GPCRs, with implications for our understanding of chemical signaling in the nervous system.

3002-Pos Board B107

The Response of Enzymatic Parameters to the Presence of Osmolytes

Mikhail Sinev, Joerg Roesgen.

Cytosolic conditions can strongly fluctuate under various conditions, including stress and normal cell function. This applies particularly to an important group of molecules called osmolytes. Changes in the concentrations of such osmolytes are known to affect both protein stability, and enzyme activity. There is already remarkable progress in the field of osmolyte-dependent protein stability. However, the understanding of the osmolyte effect on enzyme function remains poor. This is due to the absence of detailed experimental studies, and the complexity of enzyme reactions.

Here we quantify the reaction kinetics in adenylate kinase, which catalyzes the conversion between 2 ADP and ATP + AMP. We show how osmolytes (urea and TMAO) affect nucleotide affinities, and microscopic rate constants. The selected osmolytes present the two extremes on the denaturant-stabilizer continuum, affecting protein stability in different directions. We find that urea and TMAO have opposite effects on nucleotide affinities. However, the magnitude of the osmolytes' impact drastically varies among rate constants.

Our results demonstrate the intricacy of osmolyte-effects on enzyme kinetics as compared to protein conformational changes. Cells have to maintain the integrity of cytoplasmic processes against such disturbances. This now turns out to be a much more difficult task in the case of enzyme reactions than for protein folding.

3003-Pos Board B108

Role of Electrostatic and Hydrogen Bonding Environment in Sequestering Lipids from Membranes Into the Sec14 Protein Cavity

Tatyana I. Smirnova, Thomas G. Chadwick, Vytas A. Bankaitis,
Gabriel Schaaf, Oleg G. Poluektov, Alex I. Smirnov.

Sec14p is a major yeast phosphatidylinositol/phosophatidylcholine (PtdIns/PtdCho) transfer protein that promotes transfer of PtdIns or PtdCho between lipid bilayers in vitro in energy-independent manner. The exact biophysical mechanism of such a process is unknown at this moment. Here we report on employing an arsenal of advanced spin-labeling EPR methods to probe local electrostatic and hydrogen bonding environment that govern binding of lipids by Sec14 protein. n-doxyl PtdCho (where n=5,7,10,12, and 16 reflects position of nitroxide along the acyl chain) were used as EPR active probes. The local polarity and hydrogen bonding profile inside the lipid binding cavity of Sec14p were assessed from characteristic changes in high field EPR at 130 GHz (D-band). The data indicate that the phospholipid-binding cavity of Sec14p with the likely sequestered water molecules provides a close match

for the polarity profile along the bound PtdCho molecule and the one determined for membrane bilayers. This polarity match rationalizes the efficient energy-independent partitioning of a lipid molecule from a bilayer into the Sec14p phospholipid-binding pocket. Further, we have developed a direct method for observing formation of a hydrogen bond between sequestered water molecules and a spin-labeled site by applying pulsed Hyperfine Sub-level Correlation (HYSCORE) spectroscopy. Funded by: NSF-0843632 to TIS and NIH 1R01GM072897 to AIS.

3004-Pos Board B109

A Study of Traditional Chinese Medicine in Modulations of EGFR-EGF Interaction by Using Spr

Guo-Chung Dong.

Epidermal growth factor receptor (EGFR) is an important target on cancer therapy. One of the approaches is to modulate EGFR induced ligand-binding affinity change. In order to understand the correlation between ligand-binding change and EGFR modulation, we try to get some small molecular agents from traditional Chinese medicines (TCMs) to modulate EGFR activity on the biosensor system. Among 60 of TCMs, we find that some samples exhibit different influence on EGFR modulation. Among these, 051 showed a more inhibitive property due to decreasing EGF-affinity, -binding to EGFR and existed an anti-EGFR activity to A549 cells. On the other hand, 040 exist opposite function to 051. 040 is a most powerful enhancer that can increase the affinity and quantity of EGF binding to EGFR and a pro-EGFR activity on cell culture system. In our study, we can regulate the EGFR-mediated cell proliferation and anti-apoptosis by modulating the affinity of EGF-EGFR interaction. This way will be a useful method to apply on the therapy of human diseases.

3005-Pos Board B110

Targeting the NADPH Binding Site of Nitric Oxide Synthase by a Ligand with Two-Photon Absorption Properties

Etienne Henry, Yun Xu-Li, Huan Wang, Patrick Tauc, Jean-Luc Boucher, Anny Slama-Schwok, **Eric Deprez**.

Synthesis of nitric oxide is performed by NO-synthase. The catalysis is initiated by the combined transfer of electrons/proton from NADPH to the flavin FAD. We have previously characterized one photoactive compound (named Nanotrigger)1,2 allowing to trigger and synchronize NOS activity upon light illumination. Here, we described a new compound (C1) with two-photon absorption properties suitable to assess the binding to the NOS protein. This family of compounds combines a docking moiety (NADPH analog) and a chromophore moiety responsive for light illumination. C1 was characterized in DMSO by an absorption maximum at 460nm and was found to be fluorescent with an emission peak centered at 740nm upon one-photon excitation. However, the fluorescence emission was strongly sensitive to solvent polarity as evidenced by the significant decrease in the emission intensity in polar solvents. The same behaviour was observed under two-photon excitation (Exc, 940nm). One- and two-photon fluorescence approaches were used to assess the binding of C1 to the neuronal NOS. Under one-photon excitation, the emission properties of the complex were rather difficult to interpret due to the overlapping between the intrinsic fluorescence of nNOS and C1 fluorescence. As the two-photon fluorescence of nNOS protein is very weak, the complex formation was measured by monitoring the two-photon fluorescence recovery of C1 upon binding to nNOS. The calculated Kd value was found to be consistent with the value characterizing NADPH binding. However, competition experiments suggest that the competition between C1 and NADPH is more complex than expected from a one-binding site model. Our results suggest that C1 represents a promising compound for cellular applications in two-photon fluorescence imaging.

1 Beaumont et al., J. Am. Chem. Soc. 2007, 129, 2178-2186.
2 Beaumont et al., ChemBioChem 2009, 10, 690-701.

3006-Pos Board B111

Fluorescent Binding Studies of Phosphofructokinase from Bacillus Stearothermophilus Using a Tryptophan-Shifted Mutant

Amy M. Knutson, Gregory D. Reinhart.

Phosphofructokinase from Bacillus stearothermophilus (BsPFK) is an allosteric, homotetrameric enzyme containing one tryptophan per subunit. Unlike the homologous PFK from E. coli (EcPFK), the fluorescence of the native tryptophan is unresponsive to ligand binding. This study utilizes a tryptophan-shifted mutant, in which W179 has been mutated to phenylalanine, and F240 has been mutated to tryptophan. The variant is functionally similar to wild-type, however a decrease in the fluorescence of 6.5% is associated with substrate fructose 6-phosphate (Fru-6-P) binding and a decrease of 16% is associated with inhibitor PEP binding. Dissociation constants of $1.9 \pm 0.3\mu M$ for Fru-6-P and $107 \pm 13\mu M$ for PEP were thereby determined. This dissociation constant for PEP is in good agreement with that determined by kinetic assays ($128 \pm 5\mu M$). Due to the absence of known ATP antagonism, the dissociation constant for Fru-6-P in the absence of MgATP is lower than with steady-state kinetic assays determined at saturating MgATP ($36 \pm 1\mu M$). The coupling between PEP and Fru-6-P has also been determined and increases with temperature as observed with steady-state kinetic assays using wild-type BsPFK. Like wild-type PFK, the coupling free energy results from compensating enthalpy and entropy components. The sign of the coupling free energy is opposite that of the enthalpy and is therefore determined by the larger absolute value of the entropy term. This is opposite the thermodynamic basis of the allosteric response in EcPFK, where the sign is established by the enthalpy component. The functional and thermodynamic similarity of the mutant enzyme to wild-type, together with the added ability to follow ligand binding with fluorescence, make it a good candidate for further studies probing a deeper understanding of the thermodynamics involved in PFK allosterism. Funding provided by the following: NIH-GM33216, NIH-CBI, and the Welch Foundation.

3007-Pos Board B112

Characterizing Riboflavin Antagonists for Targeted Drug Delivery Applications

Anna Plantinga, Amanda Witte, Seok-Ki Choi, Kumar Sinniah.

Riboflavin ligands present an alternative pathway for targeted drug delivery as riboflavin receptors are over-expressed in breast and prostate cancer cells. We have examined riboflavin and several riboflavin mimicking molecules (antagonists) for targeting the riboflavin binding protein, which acts as a model protein for the riboflavin receptor. Isothermal titration calorimetry (ITC) was used for determining the binding constant of riboflavin (RF) and RF antagonists to chicken riboflavin binding protein (RfBP). The equilibrium dissociation constants determined for riboflavin (Kd = 1.4 nM) and lumiflavin (Kd = 64.2 nM) in 0.1 M phosphate buffer (pH 7.4) by the microcalorimetric method are in close agreement with the binding data previously determined by fluorescence quenching spectrometry. Several of the RF antagonists screened showed dissociation constants in the micromolar range while some exhibited no binding. The RF antagonists will be used in future studies to target riboflavin receptors for cellular uptake as a potential route for the selective delivery of drug molecules to cancer cells that over-express riboflavin receptors.

3008-Pos Board B113

Aluminum Phosphate Adsorption of Proteins Using Isothermal Titration Calorimetry

Ronan O'Brien, **Verna Frasca**, Mark Arsenault, Mary Jo Wojtusik.

Isothermal titration calorimetry (ITC) is widely used for measuring the affinity and thermodynamics of biomolecular interactions. These instruments measure the 10^{-7}°C change in temperature that occurs when micromolar concentrations of biological molecules interact in solution. Recently it has become apparent that the technique can also be used for studying heterogeneous systems such as the interaction between proteins in solution and the largely insoluble aluminum phosphate, the only FDA approved adjuvant used in vaccine formulations. Here we will describe results of measuring the adsorption of a number of proteins to aluminum phosphate, using ITC, highlighting the possible applications in vaccine development.

3009-Pos Board B114

Characterizing the Interaction Between Phthalocyanine Tetrasulfonates and Mammalian Prion Protein

Iveta Sosova, Abhilash Vincent, Amarnath Gupta, Max Anikovskiy, Angela Brigley, Michael T. Woodside.

Phthalocyanine tetrasulfonates are known to interact with mammalian prion protein, having the ability to act as anti-prion agents and help prevent the conversion of native isoform PrPc to the scrapie isoform PrPsc. However, the interaction between phthalocyanines and PrP remains poorly characterized. We explore the phenomenology of this interaction in detail by examining the binding of phthalocyanines to monomeric native Syrian Hamster prion protein using multiple complementary assays: surface plasmon resonance, FCS, fluorescence quenching, calorimetry, and CD spectroscopy. We determine binding constants, kinetics, stoichiometry, structural and spectroscopic effects of binding, and the influence of buffer ionic strength.

Local Calcium Signaling

3010-Pos Board B115

Familial Alzheimer's Disease Mutations in Presenilin-1 and Store-Operated Calcium Entry

Maria Ryazantseva, Lyubov Glushankova, Ilya Pozdnyakov, Ilya Bezprozvanny, Elena Kaznacheyeva.

Alzheimer's disease (AD) is a progressive and irreversible neurodegenerative disorder. Familial AD (FAD) mutations in presenilins have been linked to Ca^{2+} signaling abnormalities. Presenilins (PS) are 50 kDa proteins in the endoplasmic reticulum (ER) membrane. The cleaved presenilins are well known as catalytic components of a gamma-secretase, which cleaves the amyloid precursor protein (APP) and releases the amyloid beta-peptide. In addition uncleaved presenilins function as passive ER Ca^{2+} leak channels which control steady-state ER Ca^{2+} levels. It was found that many FAD mutations in presenilins result in loss of ER Ca^{2+} leak function, leading to ER Ca^{2+} overload and supra-normal Ca2+ release from the ER. The ER Ca^{2+} leak function of presenilins is independent of their gamma-secretase activity. We suggested that presenilins affect store-operated calcium influx (SOC) by controlling the filling state of ER Ca^{2+} stores. To determinate the influence of FAD presenilins mutations on SOC we performed a series of patch-clamp experiments in whole-cell mode. PS1-M146V and PS1-ΔE9 mutants have been shown to have loss and gain of ER Ca^{2+} leak channel function respectively. A decrease in maximum amplitude and speed of SOC current activation was observed in SK-N-SH neuroblastoma cells and primary culture of rat hippocampal neurons transfected with PS1-M146V mutant comparing to wild type PS1 transfected cells. An increase in maximum amplitude and speed of SOC current activation was observed in cells transfected by PS1-ΔE9 mutant comparing to wild type PS1. In experiments with triple transgenic AD mice hippocampal neurons (3XTg mice; KI-PS1M146V, Thy1-APPKM670/671NL, Thy1-tauP301L) the maximum amplitude of SOC were decreased comparing to WT, but the speed of activation was the same for 3XTg and WT hippocampal neurons. Electrophysiological properties of all impaired SOCs suggest that TRPC1 is the main target of presenilins FAD mutations affect.

3011-Pos Board B116

Application of Designed Calcium Sensors with Fast Kinetic Responses

You Zhuo, Shen Tang, Yusheng Jiang, Chen Zhang, Florence Reddish, Jenny Jie Yang.

Transient change of cytosolic calcium level leads to physiological actions, which are modulated by the intracellular calcium store, as well as membrane calcium channels. To probe fast calcium responses in high calcium environments, there is a pressing need to develop calcium sensors to overcome the limitation of relatively slow kinetics of current GECIs with τ value around several hundred milliseconds. We have developed single green fluorescence protein-based calcium sensors, with tunable calcium binding affinity and fast kinetics. In this study, we first report our further development of a red calcium sensor using our design strategy. We then report our applications of the developed calcium sensors to monitor endoplasmic reticulum (ER) calcium release in several cell lines responding to perturbations of extracellular calcium signaling. The effects of various drugs as channel and pump inhibitors and activators have also been examined using our developed calcium sensors targeted to calcium channels in the ER membrane.

3012-Pos Board B117

Rational Design and Structural Analysis of Calcium Biosensors and their Application to the Study of SR/ER Calcium Dynamics

Shen Tang, You Zhuo, Yusheng Jiang, Hing-Chueng Wong, Zhong-min Wang, Osvaldo Delbono, Jenny J. Yang.

Quantitative, real-time detection of Ca2+ fluctuations in intracellular organelles is essential to determining the mechanism of Ca2+-dependent signaling. Here, we developed genetically encoded Ca2+ indicators by creating a Ca2+-binding site in the enhanced green fluorescent protein (EGFP). These novel biosensors allow real-time measurement without perturbing the cells' Ca2+ signaling. Upon binding to Ca2+,these biosensors exhibit single-wavelength fluorescence enhancement and Kd values from 0.1 mM to 1 mM, which are optimal for detecting signaling in the skeletal muscle SR. Excessive biological metal ions, such as K+ or Na+, do not alter their ability to sense Ca2+. In particular, our CaratER can respond to various agonists and antagonists in C2C12, HeLa, and HEK-293 cells. It was expressed in the SR of FDB fibers and successfully monitored Ca2+ signaling under voltage-clamp and application of SR agonists. Its fluorescence decrease in response to sarcolemmal depolarization indicates its fast Ca2+ dissociation rate. These results match our stopped-flow kinetic analysis showing that 40-50% of the fluorescence change finished within the 2.2 ms deadtime, when EGTA rapidly mixed with Ca2+- saturated CaratER. We investigated our sensors' optical and conformational properties using various spectroscopic methods, including high-resonance resolution NMR, and designed red fluorescent protein-based Ca2+ biosensors, which exhibit metal selectivity and large fluorescent changes in response to Ca2+. The pH stability was dramatically enhanced with apparent pKa below 5, so they can monitor Ca2+ signaling in deep tissues and small animals and detect simultaneous Ca2+ changes in various subcellular compartments with multiple colors. In conclusion, our molecular design method achieved biosensors that can reliably monitor Ca2+ signaling in high [Ca2+] environments.

3013-Pos Board B118

Evoked Centripetal Ca^{2+} Activation in Cardiac Purkinje Cells: CICR or Ca^{2+} Diffusion?

Kazi T. Haq, Rebecca Daniels, Sharene Bungay, **Bruno D. Stuyvers**.

In large mammals, cardiac Purkinje cells (**Pcells**) lack transverse tubules (**T-tubules**). However, Pcells respond to stimulations by massive Ca-releases from the sarcoplasmic reticulum (**SR**) similar to those of ventricular myocytes (**VMs**) with T-tubules. Ca-imaging revealed a wave of elevated Ca-concentration (**Cai**) propagating from the sarcolemma (**SL**) toward the centre of Pcells upon stimulation. Ca-diffusion was proposed to explain this centripetal propagation. A thin layer of SR expressing RyR3 was found ~5μm below the SL while other SR-regions expressed RyR2. *Ca-Induced Ca-Release* (**CICR**) from RyR3-SR-region could relay Ca-signal from Ca-entry to RyR2-Ca-release sites in the core, playing equivalent role as T-tubules in VMs. Our **objective** wasto examine whether centripetal Ca-signaling results exclusively from Ca-diffusion or involved intermediate RyR3-CICR. **Methods:**Pcells were prepared from Yucatan swine (30-40kg) and incubated with Fluo4-AM. Ca-dynamics was assessed by 2D-confocal microscopy (30-100fps); pH7.3,35oC. 26 cells were field stimulated at various external Ca-concentrations (**Cao**). Ca-data were compared with those from a model of Ca-propagation across 3 virtual adjacent SR-Ca-release regions. **Results**: In stimulated Pcells, Ca-increase first happened under SL with amplitude increasing from 0.1 to 0.5μmol/L with Cao from 1 to 4mmol/L. A Ca-wave then propagated uniformly from the SL toward cell center at 100-250μm/s. An overall Ca-transient appeared when Ca-wave reached the core region. When the model included intermediate CICR-region, predicted data were consistent with Pcells observations: minimal amplitude (**minAmp**) of peripheral Ca-increase mediating a central Ca-transient similar to that of Pcells, was 130nmol/L; this generated Ca-propagation with velocity (**propVel**) of 160μm/s; propVel was independent on Cao. In contrast, minAmp and propVel were 220nmol/L and 40μm/s respectively, and propVel increased with Cao when only diffusion was considered. **Conclusion**: Our data were consistent with an intermediate CICR-mechanism which ''boosts'' Ca-propagation between SL and core of Pcells.

3014-Pos Board B119

Local Control of Cardiac Sodium-Calcium Exchanger by PMCA in Submembrane Microdomain in Mouse Heart Cells

Takao Shioya.

OBJECT: This study aimed at unveiling functional interaction between the Na/Ca exchanger (NCX) and the plasma membrane Ca^{2+}-ATPase (PMCA) on the sarcolemmal membrane of heart cells. METHOD: The Na/Ca exchange current (I_{NCX}) was recorded from whole-cell clamped mouse ventricular myocytes under physiological conditions at 37°C. Functions of the ryanodine receptor and SERCA Ca^{2+}-pump on the sarcoplasmic reticulum were abolished by using ryanodine and thapsigargin. The I_{NCX} was isolated as Ni^{2+}-sensitive current component, under the conditions that eliminate other major membrane current systems. RESULTS: With the $[Ca^{2+}]_i$ strongly buffered with 10 mM-BAPTA, the I_{NCX} was recorded as a time-independent current. However, with the $[Ca^{2+}]_i$ only weakly buffered with 0.1 mM-BAPTA, the I_{NCX} showed a small current amplitude and a slow activation time-course. This was not observed when the $[Ca^{2+}]_i$ was strongly buffered (with 10 mM-BAPTA). Inhibition of PMCA by intracellular administration of orthovanadate (VO_4^{3-}) dramatically increased the amplitude of I_{NCX} and accelerated its activation kinetics. At the same time, orthovanadate shifted the $[Ca^{2+}]_i$-dependence of the I_{NCX} amplitude (EC_{50} = 0.97 μM) to lower levels (EC_{50} = 0.40 μM). Moreover, similar effects were observed by intracellular application of a selective PMCA inhibitor 5(6)-carboxyeosin. CONCLUSION: The PMCA regulates the operation of the NCX by altering local $[Ca^{2+}]_i$ level around the NCX molecule. Because PMCA is driven by ATP, this functional coupling might serve as a mechanism that the intracellular metabolic status to the $[Ca^{2+}]_i$ regulation and Ca^{2+} signaling in heart cells.

3015-Pos Board B120

$InsP_3$ Triggered Calcium Release Events in Mouse Atrial Myocytes

Tamara Horn, **Marcel Egger**.

In the heart, the dominant mechanism of intracellular Ca^{2+} release is Ca^{2+}-induced Ca^{2+} release (CICR) via sarcoplasmic reticulum (SR) Ca^{2+} release channels (RyR's). Recently, a second mechanism, Ca^{2+} release through channels sensitive to the intracellular second messenger Inositol-1,4,5-trisphosphate ($InsP_3$) has been described. The contribution and significance of $InsP_3$-induced Ca^{2+} release in cardiac excitation-contraction coupling (EC-coupling) is still a matter of debate. However, recent reports have emphasized the importance of $InsP_3$ signaling for EC-coupling in atrial myocytes, for excitation transcription coupling and embryogenesis. Investigating $InsP_3$ signaling is challenging because adequately selective pharmacological tools or fluorescent indicators are not available and the specific activation of highly localized intracellular $InsP_3$ receptors ($InsP_3R$) is hampered due to experimental inaccessibility. We are using UV-flash uncaging approaches of caged $InsP_3$ to study the interplay of $InsP_3R$ Ca^{2+} release and CICR based on the activation of RyR under whole-cell conditions. UV-flash photolysis of caged $InsP_3$ was accompanied by an increase in the number of local Ca^{2+} release events that show larger FDHM and/or smaller amplitude. In the presence of $InsP_3R$ blocker xestospongin C the frequency of $InsP_3$ evoked Ca^{2+} events was reduced and suggest coexistence of spontaneous SR-Ca^{2+} release events (Ca^{2+} sparks) and $InsP_3$ evoked SR-Ca^{2+} release events (Ca^{2+} puffs). In addition, photorelease of $InsP_3$ in PM loaded cells induced global Ca^{2+} release events suggesting that $InsP_3$ facilitation of Ca^{2+} release may be linked to RyR mediated Ca^{2+} release in atrial cells. Two-photon excitation photolysis (TPP) of caged $InsP_3$ was used to study $InsP_3$ signaling in a highly targeted way. TPP triggered $InsP_3$-induced Ca^{2+} release exhibiting spatio-temporal characteristics corresponding to elementary Ca^{2+} signals, such as Ca^{2+} waves and Ca^{2+} ''puffs'' and seems to be promising tools for studying $InsP_3$ signaling on the sub-cellular scale. Supported by SNF.

3016-Pos Board B121

Effects of Mitochondrial Membrane Depolarization on Cellular Function in Cardiac Myocytes

Aristide Chikando, Joseph P.Y. Kao, W.J. Lederer.

Mitochondria are the primary sites of ATP generation in heart cells. The voltage gradient across the mitochondrial inner membrane ($\Delta\Psi_{mito}$) is a critical feature and this in turn is controlled in part by the mitochondria permeability transition pore (mPTP), whose molecular identity remains elusive. Here we used used illumination-dependent subcellular mitochondrial depolarization to investigate cardiac mitochondrial function in cells exposed to low (nM) concentrations of the fluorescent mitochondrial reporter tetramethyl rhodamine methyl ester (TMRM). The relationship between mPTP gating (as measured by $\Delta\Psi_{mito}$ depolarization) and subcellular myocyte function was examined in single cardiac myocytes. ROS production was measured using dichlorofluorescin (DCF). $[Ca^{2+}]_i$ was measured with intracellular fluo-4. There was a time-dependent increase in the depolarization of those mitochondria exposed to visible light but nearby mitochondria in the same cell but kept in the dark remained normally polarized. Only rarely did the illuminated and depolarized mitochondria repolarize following the cessation of illumination. We have also investigated the hypothesis that the illuminated mitochondrial depolarization is due to a ROS-dependent mechanism. How Ca^{2+} signaling, ROS, $\Delta\Psi_{mito}$ are inter-related will be discussed. Additionally the mitochondrial depolarization dependent actions on other myocyte functions (contraction, $[Ca^{2+}]_i$ transients, Ca^{2+} instability, membrane currents) will be discussed.

3017-Pos Board B122

A Comparative Assessment of Fluo Ca^{2+} Indicators in Rat Ventricular Myocytes

Brian M. Hagen, Liron Boyman, Joseph P.Y. Kao, W. Jonathan Lederer.

Improvements in the fluo series of fluorescent Ca^{2+} indictors routinely used to measure cytosolic free Ca^{2+} concentration ($[Ca^{2+}]_i$) have increased signal-to-noise ratio, enabling more quantitative $[Ca^{2+}]$ measurements. The improved fluo derivatives show increased cellular loading efficiency, reduced pH sensitivity, and excitation maxima that better match the wavelengths of common lasers. Nevertheless, the extent to which these indicators interfere with native intracellular Ca^{2+} homeostasis has not been systematically characterized. Here, we have examined three different fluo derivatives (fluo-2, fluo-3 and fluo-4) in freshly isolated rat ventricular myocytes. Cells were loaded with a fluo indicator either by incubation with the acetoxymethyl (AM) ester or by introducing the K^+ salt of the indicator through a whole-cell pipette (injection-loaded).

Fluorescence changes in cardiomyocytes were measured using confocal microscopy during field simulation or current injection. Three significant differences were identified among the three indicators and two loading methods. 1. Ca^{2+} kinetics in AM-loaded cells were slower than in injection-loaded cells; thus the decay of the cardiac $[Ca^{2+}]_i$ transient appeared to be slower. In AM-loaded cells, fluo-3 reported the fastest response while fluo-2 and fluo-4 gave comparable, slower responses. When injection-loaded as the K^+ salt, all three indicators reported comparable responses that were faster than any of the AM-loaded indicators. 2. When AM-loaded, all three indicators showed apparent spatial inhomogeneities in cellular fluorescence, in contrast to injection-loaded cells. Thus diverse cellular structures appear brighter in AM-loaded cells than in injection-loaded cells. 3. For each indicator, the calibrated signals (F/F_o) in the AM-loaded cells were higher than in injection-loaded cells.

We conclude that injection-loaded cells produce more accurate $[Ca^{2+}]_i$ measurements and spatially resolved signals. If AM loading is needed, the use of fluo-3 would appear to provide more accurate calibrated signals.

3018-Pos Board B123

Impaired Local Calcium Signaling in Primary Cultured Adult Rat Ventricular Myocytes

Joon-Chul Kim, Min-Jeong Son, Yuhua Li, Suk-Han Jung, Sun-Hee Woo.

Although cultured adult cardiac myocytes have been adopted in studying protein functions in combination with cell-level genetic modifications, cellular alterations by culturing itself need to be clarified to understand real function of the protein genetically altered. We systematically compared contractile properties, calcium ion (Ca^{2+}) signaling, transverse (t)-tubules, ryanodine receptor distributions between freshly isolated and two-days cultured adult rat ventricular myocytes. Density of t-tubules was remarkably decreased by culture. In cultured myocytes, cell shortenings were attenuated by ~60% and relaxation was slowed. Consistently, magnitudes of action potential-induced Ca^{2+} transients were decreased to ~50% and decays of the Ca^{2+} transients were retarded by culture. In cultured cells, density of L-type Ca^{2+} current was reduced to ~40% and its inactivation was retarded. The latter is consistent with smaller Ca^{2+} transients in cultured group. However, sarcoplasmic reticulum Ca^{2+} contents were not different between two groups. To know the mechanism for smaller Ca^{2+} transient in cultured cells we examined Ca^{2+} sparks in these two groups of cells. The frequency of spontaneous Ca^{2+} sparks was significantly decreased by culturing. The amplitude, duration, and time-to-peak of individual Ca^{2+} sparks were not different between the two groups. Mean spark width was two-fold larger in cultured cells compared with freshly isolated cells. Quantitative analysis of immunofluorescence revealed shortening of longitudinal spacing between RyR2 clusters, and less dense and disorganized distributions of RyR2 clusters in cultured cells, which may be related to lower frequency of sparks in these cells. These results provide evidence on significant difference in Ca^{2+} sparks as well as excitation-contraction coupling in primary cultured adult ventricular myocytes. (This work was supported by National Research Foundation of Korea grants funded by the Ministry of Education, Science and Technolgy (2010-0000070).)

3019-Pos Board B124

A Caveolin Targeted L-type Calcium Channel Antagonist Inhibits Hypertrophic Signaling without Reducing Contractility of Cardiac Myocytes

Catherine A. Makarewich, Hui Gao, Hongyu Zhang, Nathan Correll, Jeffrey D. Molkentin, Steven R. Houser.

The source of Ca^{2+} to activate pathological hypertrophy is not thought to involve the $[Ca^{2+}]$ that activates contraction. We hypothesize that Ca^{2+} influx through a subpopulation of L-type Ca^{2+} channels ($Ca_V1.2$; $I_{Ca,L}$) localized in caveolin (Cav) containing membrane signaling microdomains locally activates calcium/calmodulin and calcineurin-mediated NFAT nuclear translocation to induce hypertrophy. Rem-GTPase is known to inhibit $Ca_V1.2$ which requires a membrane association c-terminal. We truncated the c-terminal of Rem ($Rem^{1\text{-}265}$) which eliminated $Ca_V1.2$ inhibition and fused $Rem^{1\text{-}265}$ to a canonical caveolin binding domain to create $Rem^{1\text{-}265}$-Cav. **Results**: Adenoviral-mediated expression of normal Rem in adult feline myocytes almost fully eliminated $I_{Ca,L}$ while non-membrane targeted $Rem^{1\text{-}265}$ had no significant effect on $I_{Ca,L}$. $Rem^{1\text{-}265}$-Cav exhibited a small inhibition (less than 15%) of the normal $I_{Ca,L}$. Myocytes expressing $Rem^{1\text{-}265}$-Cav responded normally to isoproterenol while those infected with normal Rem failed to respond. Myocytes infected with normal Rem had markedly reduced fractional shortening (2.4+/-0.7% resting cell length) while those infected with the truncated $Rem^{1\text{-}265}$ (7.8+/-1.8) and $Rem^{1\text{-}265}$-Cav (5.9+/-1.4) had contractions not significantly smaller than controls (7.4+/-2.1). Sucrose density gradient experiments revealed that $Rem^{1\text{-}265}$-Cav cosedimented with caveolin-3 enriched low-density fractions. These experiments suggest $Rem^{1\text{-}265}$-Cav inhibits caveolin-associated $Ca_V1.2$. To investigate the effects of our Rem constructs on NFAT nuclear translocation (hypertrophic signaling) myocytes were also infected with NFAT-GFP. Bath $[Ca^{2+}]$ was elevated to induce NFAT nuclear translocation measured by nuclear to cytoplasmic NFAT-GFP ratio. Normal

Rem fully inhibited $[Ca^{2+}]$-induced nuclear NFAT translocation and truncated $Rem^{1\text{-}265}$ had no effect. $Rem^{1\text{-}265}$-Cav inhibited more than 80% of $[Ca^{2+}]$-induced NFAT nuclear translocation. **Conclusion**: These results suggest that $Ca_V1.2$ within Cav3 signaling microdomains is a major source of hypertrophic $[Ca^{2+}]$ signaling and it can be blocked with little or no effect on excitation-contraction coupling.

3020-Pos Board B125

Dantrolene Restores Altered RyR2-Mediated Ca Signaling in Heart Failure

Joshua T. Maxwell, Timothy L. Domeier, Lothar A. Blatter.

In heart failure (HF) arrhythmogenic Ca release and chronic $[Ca]_{SR}$ depletion arise due to altered function of ryanodine receptors. Dantrolene, a therapeautic agent used to treat malignant hyperthermia associated with mutations of the type 1 ryanodine receptor (RyR1), is purported to be without effects on the cardiac type 2 ryanodine receptor (RyR2). However, recent investigations suggest that dantrolene may correct abnormal RyR2-mediated calcium release associated with HF. In this investigation, we tested if dantrolene exerts anti-arrhythmic effects on heart failure ventricular myocytes by examining the intra-SR Ca threshold for arrhythmogenic Ca waves. Using the low-affinity calcium indicator fluo-5N entrapped in the SR, direct measurement of $[Ca]_{SR}$ showed that in normal rabbit myocytes dantrolene (1 microM) had no effect on SR Ca content, the amplitude of action potential induced intra-SR Ca depletions, or on the threshold for spontaneous Ca wave initiation (i.e., the SR Ca content at which spontaneous waves initiate). Furthermore, in field stimulated (0.5 Hz and 1.0 Hz) normal cardiomyocytes loaded with indo-1, dantrolene treatment had no effect on Ca transient amplitude, SR Ca load, or post-rest decay of SR Ca content. In cardiomyocytes from failing rabbit hearts, SR Ca content and the wave initiation threshold were decreased compared to normal myocytes. Interestingly, treatment of HF cardiomyocytes with dantrolene restored the SR Ca content and increased the wave initiation threshold. Together, these data suggest that dantrolene may exert anti-arrhythmic effects in heart failure cardiomyocytes by increasing the intra-SR Ca threshold at which spontaneous Ca waves occur.

3021-Pos Board B126

A Stochastic Model of the Ryanodine Receptor Featuring Coupled Gating and Competitive Binding of Luminal and Cytosolic Ca^{2+} and Mg^{2+}

Johan Hake, William E. Louch, K Haugen, Ivar Sjaastad, Ole M. Sejersted, Andrew McCulloch, Anushka Michailova, Glenn T. Lines.

During the last fifteen years, a number of computational models of local control of Ca2+ induced Ca2+ release have been presented. Recently, models for the activation of the ryanodine receptor (RyR), have been suggested which, include competitive binding of cytosolic and luminal Ca2+ and Mg2+. These models reproduce experimental spark frequency data obtained under different luminal and cytosolic Ca2+ and Mg2+ concentrations. However, they are steady-state models which cannot be used to study detailed spark kinetics, or they have only been used to fit RyR kinetics from bi-layer experiments. Here we present a stochastic and discrete model of the RyR featuring allosteric activation by competitive binding of luminal and cytosolic Ca2+ and Mg2+. The model also includes allosteric coupling between neighboring RyRs. We couple the model of the RyR with diffusional domains for both the junctional sarcoplasmic reticulumn and the dyadic cleft using a finite element model of diffusion. The allosteric coupling is modeled using a symmetric free energy approach, which keeps the number free parameters low. The model is fit to spark data from failing and SHAM-operated mice. The failing myocytes were aquired from a murine model of congestive heart failure (CHF). Myocardial infarction was induced by left coronary artery ligation, and at 10 weeks post-MI, mice exhibited symptoms of CHF. We use the computational model to explore the effect of phosphorylated RyRs in the failing myocytes.

3022-Pos Board B127

Determinants of the Site of Ca^{2+} Wave Initiation in Smooth Muscle

Marnie L. Olson, John G. McCarron.

Many smooth muscle activities including contraction, transcription and apoptosis are regulated by inositol 1,4,5-trisphosphate ($InsP_3$)-mediated increases in cytosolic Ca^{2+} concentration ($[Ca^{2+}]_c$). Activation of surface receptors, such as muscarinic acetylcholine M3 receptors (mAChR3), leads to the production of $InsP_3$ to evoke Ca^{2+} release via receptors ($InsP_3R$) present on sarcoplasmic reticulum. Ca^{2+} release usually begins in a single 'eager' region and regeneratively propagates along the length of the cell as a Ca^{2+} wave. The Ca^{2+} wave repeatedly originates at the same 'eager' site. We addressed the mechanisms which determine the Ca^{2+} wave initiation site. One possibility is that the 'eager' site has a higher sensitivity to $InsP_3$ to evoke larger Ca^{2+} release. This does not appear to be the case because the site where waves initiated was not the site of largest Ca^{2+} release (as determined by local photolysis of caged $InsP_3$). The expression patterns of mAChR3 and $InsP_3R$ may provide an explanation. Although, there was no apparent regional receptor clustering, dual labelling of mAChR3 and $InsP_3R$ showed some receptor co-localization. Ca^{2+} wave initiation site may be determined by regions where the proximity of mAChR3 and $InsP_3R$ generate higher local $[InsP_3]$ and $[Ca^{2+}]_c$. To explore this possibility the adaptability of the Ca^{2+} wave initiation site was examined by changing the local Ca^{2+} buffer capacity using the caged Ca^{2+} buffer diazo-2. Photolysis of diazo-2, at the site of wave initiation, during agonist application prevented initiation at this location. Yet, after a time lag the Ca^{2+} wave initiated at a new 'eager' site. These results indicate that the Ca^{2+} wave initiation site may be determined by co-localisation of mAChR3 and $InsP_3R$ and that the 'eager' site is altered when the $[Ca^{2+}]_c$ increase is prevented. Supported by the Wellcome Trust and British Heart Foundation.

3023-Pos Board B128

Sustainable TRPM4 Channel Activity Following Restoration of Cytosolic Calcium Buffering in Freshly Isolated Cerebral Smooth Muscle Cells

Albert L. Gonzales, Scott Earley.

The melastatin transient receptor potential (TRP) channel TRPM4 is a critical regulator of smooth muscle membrane potential and arterial tone. Activation of the channel is Ca^{2+}-dependent, but prolonged exposures to high intracellular Ca^{2+} causes rapid desensitization under conventional whole-cell patch clamp conditions. Using amphotericin B perforated whole-cell patch clamp electrophysiology which allows for minimal disruption of cytosolic Ca^{2+} dynamics, we recently showed that Ca^{2+} release from inositol trisphosphate receptors (IP_3R) activate TRPM4 channels, producing Transient Inward Cation Currents (TICCs). The coupling of IP_3R-mediated Ca^{2+}-release with activation of TRPM4 channels has not been fully characterized. We hypothesized that under conventional whole-cell conditions, loss of intrinsic cytosolic Ca^{2+} buffering following cell dialysis contributes to desensitization of TRPM4 channels. With the Ca^{2+} buffer ethylene glycol-bis(2-aminoethylether)-N,N,N′,N′-tetraacetic acid (EGTA, 10mM) included in the pipette solution, we were able to restore cytosolic Ca^{2+} buffering and record sustained TICC activity in freshly isolated cerebral smooth muscle cells. The total open probability for TICC activity was reduced following the administration of the TRPM4 inhibitor 9-phenanthrol and by siRNA-mediated knockdown of TRPM4, strongly suggesting that TICC activity is mediated through TRPM4. Lower concentrations of EGTA were not sufficient to restore TRPM4 activity. We further examined the spatial and temporal coupling between Ca^{2+} released through IP_3R and the activation of TRPM4 channels using the fast Ca^{2+} buffer bis-ethane-N,N,N',N'-tetraacetic acid (BAPTA) in the pipette. This study demonstrates our ability to restore Ca^{2+} buffering to physiological levels and allows for further examination of the coupling between IP_3R and TRPM4 activity in arterial smooth muscle cells RO1HL091905; F31HL094145-01.

Calcium Fluxes, Sparks, & Waves

3024-Pos Board B129

Modeling the Mechanisms of Calcium-Mediated Cardiac Arrhythmias

M. Saleet Jafri, W. Jonathan Lederer, George S.B. Williams, Joseph L. Greenstein, Raimond L. Winslow.

Dysfunction of normal calcium dynamics has been implicated in the generation of cardiac arrhythmias. It is thought that spontaneous calcium release events in the myocyte lead to the formation of intracellular calcium waves. These calcium release events occur through opening of the ryanodine receptors (RyRs) in the sarcoplasmic reticulum. In order for this to lead to an arrhythmia, these waves need to depolarize the cardiac myocyte in events know as early afterdepolarizations (EADs) and delayed afterdepolarizations (DADs). These aberrant depolarizations must spread to adjacent cells in a propagating wave of depolarization to disrupt the normal pattern of electrical excitation of the heart. Computational compartmental ventricular myocyte models have shown that EADs and DADS can be generated by certain conditions consistent with experiments. We have developed a spatio-temporal computational model of a chain of cardiac myocytes based on the Jafri-Rice-Winslow model of the guinea pig ventricular myocyte. The model includes spatial resolution of the individual myocyte as well as a network of myocytes, calcium dynamics, and the sarcolemmal electrical activity. We use the model to explore how factors such as calcium overload, RyR calcium sensitivity, and other factors affect the generation of calcium waves. Furthermore, we also explore under what conditions the calcium wave can depolarize the myocyte and induce

a propagating wave of depolarization to adjacent myocytes. These insights can be used to better understand the basic mechanisms of calcium-entrained cardiac arrhythmias.

3025-Pos Board B130

Self-Organization of Pacemaking Sites for Calcium Waves and Oscillations in Cardiac Myocytes

Michael Nivala, Chris Ko, Alan Garfinkel, James N. Weiss, Zhilin Qu.

Calcium (Ca) sparks are elementary events of intracellular Ca signaling, which tend to occur randomly. Ca waves and whole-cell Ca oscillations occur under Ca overload and disease conditions. How Ca waves emerge from Ca sparks is not completely understood. We developed a three-dimensional model for Ca cycling which contains 100x20x10=20,000 identical Ca release units (CRUs), simulating the CRU network corresponding to a complete cardiac myocyte with dimensions of 100x20x10 micrometers. Using this model, we can generate the well known Ca signaling hierarchy: Ca quarks, Ca sparks, macro-sparks, abortive waves, and full Ca waves. We can also induce spiral waves within the cell, a wave phenomenon widely observed in myocyte experiments. Besides the well known experimental observation that increasing Ca loading promotes these wave dynamics, we also make the following observations: 1) The diffusion rate of Ca is a key parameter. Spontaneous Ca waves occur only when the diffusion rate is above a critical value. 2) When the model is homogeneous, Ca waves originate from different locations via a self-organizing process. This self-organizing process is influenced by, but does not require, heterogeneity. 3) When the model contains heterogeneities, such as heterogeneous Ca release channel distribution, Ca waves can originate from different locations or occur repeatedly from the same location. In real cardiac rabbit ventricular myocytes loaded with Fluo-4 AM to image intracellular Ca, Ca waves typically originate from different locations after successive rapid pacing episodes. In conclusion, our results indicate that Ca waves in cardiac myocytes originate predominantly as a result of self-organizing processes rather than pre-existing heterogeneities.

3026-Pos Board B131

Ca^{2+} Leak and Ca^{2+} Sparks in Mammalian Heart: Insights from a Computational Model

George S.B. Williams, Aristide C. Chikando, W. Jonathan Lederer, Eric A. Sobie, Hoang-Trong M. Tuan, M Saleet Jafri.

Calcium (Ca2+) signaling in muscle, neuronal, and non-excitable cells has benefited significantly from advances in biological tools and imaging technology, however, the molecular interactions of nanoscopic molecules, structures and compartments has been challenging to study under physiological conditions. Here, we exploit novel computational modeling techniques to examine real-time molecular and cellular physiology in cardiac ventricular myocytes. The model focuses on local and cell-wide Ca2+ signaling phenomena related to calcium induced calcium release from intracellular calcium channels, ryanodine receptors (RyR2s), located on the sarcoplasmic reticulum (SR) membrane. This work is informed by the latest molecular investigations and recent characterizations of channels, transporters, and buffers located in mammalian heart. We have created a detailed, whole-cell model of Ca2+ signaling using a realistic number of calcium release units (CRU) each containing a cluster of stochastically gating RyR2s. During systole the opening of these RyR2s is triggered by Ca2+ entry via voltage gated L-type Ca2+ channels. The synchronized opening of the RyR2 cluster leads to localized elevations of [Ca2+]i known as Ca2+ sparks. During diastole Ca2+ sparks are still observed and are attributed to the finite opening rate of the RyR2. RyR2s are also believed to display unsynchronized or non-spark openings where only a few channels in the CRU open without triggering the remainder of the RyR2 cluster. This non-spark Ca2+ release would be below current experimental detection thresholds and therefore ''invisible.'' These spark and non-spark openings of RyR2s constitute a molecular basis for Ca2+ leak from the SR. The computational model suggests that a significant fraction of SR Ca2+ leak is due to RyR2s openings that fail to trigger a ''visible'' Ca2+ spark. Additionally, the fraction of non-spark or ''invisible'' SR Ca2+ leak increases as SR Ca2+ content declines.

3027-Pos Board B132

GPU-Enabled stochastic Spatiotemporal Model of Rat Ventricular Myocyte Calcium Dynamics

Tuan M. Hoang-Trong, George S.B. Williams, Jonathan W. Lederer, Saleet Jafri.

The dysfunction of the normal calcium dynamics is a major factor in certain types of cardiac arrhythmias. These cardiac arrhythmias are thought to result from Ca^{2+} waves which occur when Ca^{2+} release propagates from one release site to another outside of the normal time during systole resulting in depolarization of the cell's outer membrane. Experimental results suggest that the elementary event underlying calcium release at these sites is the Ca^{2+} spark and the summation of these Ca^{2+} sparks result in the global $[Ca^{2+}]_i$ transient that causes contraction. We have developed a model of the cardiac myocyte that includes the spatial organization and microsecond level resolution of clusters of ryanodine receptor (RyR) that are Ca^{2+} release channels responsible for the generation of Ca^{2+} sparks. We use this model to explore how Ca^{2+} overload, RyR Ca^{2+} sensitivity, RyR coupling, and other factors that affect the propagation of Ca^{2+} release between release sites. We will utilize our newly developed Ultrafast Markov chain Monte Carlo method which allows the rapid simulation of a whole-cell model containing 20,000 release sites, each containing 7 L-type Ca^{2+} channels and 50 RyRs. This algorithm greatly reduces computation time by using adaptive time step approach and a compact representation of the Markov chain state space. Hence, this novel method provides a powerful tool for performing stochastic cellular simulation with realistic Ca^{2+} dynamics. Also, with the availability of the next generation graphics processing units (GPU) computing architecture - codename Fermi from NVIDIA - model solution is greatly accelerated allowing the implementation of such a detailed model for the first time.

3028-Pos Board B133

Contributions of Structural t-Tubule Heterogeneities and Membrane Ca^{2+} Flux Localization to Local Ca^{2+} Signaling in Rabbit Ventricular Myocytes

Peter M. Kekenes-Huskey, Yuhui Cheng, Johan Hake, Frank Sachse, John Bridge, J.A. McCammon, Anushka Michailova.

The micro-architecture of the transverse tubular system (t-system) and the arrangement of associated proteins are central to the function of ventricular cardiomyocytes. Recently, confocal imaging and image processing was used to characterize the geometry of the t-system in rabbit ventricular cells [1]. The average diameter of single t-tubules was estimated to be 448+-172 nm with constrictions occurring every 1.87+-1.09 um along their principal axis. Here, we used mathematical modeling to investigate how local variations in t-tubular cross-sectional area and the distribution of membrane Ca^{2+}flux regulate Ca^{2+}-entry, diffusion and buffering in rabbits [2]. The current model includes a realistic geometry of a single t-tubule, its surrounding half-sarcomeres, the spatially distributed Ca^{2+}transporting proteins along the cell membrane (L-type Ca^{2+} channel, Na^{+}/Ca^{2+} exchanger, sarcolemmal Ca^{2+} pump) as well as stationary and mobile Ca^{2+} buffers (troponin C, ATP, calmodulin, Fluo-3). A finite element software package CSMOL was used to solve the coupled reaction-diffusion PDE system describing the time-dependent concentration profiles of the above-listed species.[3]. The model was parameterized according to voltage-clamp data in rabbit ventricular myocytes with Ca^{2+} release at the sarcoplasmic reticulum disabled pharmacologically [4]. The results indicate that the constrictions and spatial arrangements of membrane Ca^{2+} proteins may cause local inhomogeneities in Ca^{2+} concentration. In addition, we examined the activation of a catalytic Ca^{2+}-binding site on Na^{+}/Ca^{2+} exchanger on local Ca^{2+} gradients in the presence or absence of fluorescent dye.

[1]Savio-Galimberti *et al.*, *Biophys J* 95:2053-2062,2008.
[2]Cheng*et al.*, *PLoS CompBiol* 2010, (in press).
[3]SmoluchowskiSolver (CSMOL), http://mccammon.ucsd.edu/smol/
[4]Sobie et al., *Biophys J: Biophys Lett*:L54-L56,2008.

Supported by NBCR (NIH grant 2 P41 RR08605), NIHGM31749, NSFMCB-0506593,MCA93S013, Center for Theoretical Biological Physics, HHMI, SDSC, W. M. Keck foundation, and the Nora Eccles Harrison Cardiovascular Research and Training Institute

3029-Pos Board B134

How Does RyR2-Mediated SR Calcium Leak Fail to Cause Sparks?

Daisuke Sato, Donald M. Bers.

Recent experiments have shown that Ca leak from the sarcoplasmic reticulum (SR) can occur via spontaneous Ca sparks, non spark ryanodine receptor (RyR) mediated leak, and RyR independent pathways (Zima *et al.BJ,* 94:104a, 2008). Opening of a single RyR is expected to increase local [Ca] in the cleft space rapidly (<< 1 ms) to levels that are expected to activate neighboring RyR in that cleft via Ca induced Ca release. Our question is how and why RyR-mediated SR Ca leak becomes mainly non-spark mediated at moderate to low SR Ca loads. To answer this question, we analyze Ca flux through RyRs using a physiologically detailed mathematical model of junctional SR Ca release in which RyR gating is regulated by intra SR and cleft [Ca] ($[Ca]_{SR}$ & $[Ca]_{Cleft}$). In this model, there are one hundred RyR channels in one Ca release unit. Each RyR opens stochastically depending on $[Ca]_{Cleft}$ and $[Ca]_{SR}$. We

find that several factors contribute to the failure of one RyR channel opening to opens adjacent RyRs as $[Ca]_{SR}$ declines: 1) the lower $[Ca]_{SR}$ reduces driving force and thus limits local $[Ca]_{Cleft}$ (both absolute level and rate of rise), 2) low $[Ca]_{SR}$ can inhibit RyR open time (τ_O) which further reduces local $[Ca]_{Cleft}$ attained, 3) the low τ_O and fast $[Ca]_{Cleft}$ dissipation after closure shorten the opportunity for neighboring RyR activation, 4) at low $[Ca]_{SR}$ the RyR2 exhibits reduced $[Ca]_{Cleft}$ sensitivity. We conclude that all of these factors conspire to reduce the probability of Ca sparks as $[Ca]_{SR}$ declines, despite continued RyR-mediated SR Ca leak.

3030-Pos Board B135

Mitochondrial-SR Ca^{2+} Cycling Modulates Normal Automaticity of Rabbit Cardiac Sinoatrial Nodal Pacemaker Cells

Yael Yaniv, Harold A. Spurgeon, Alexey E. Lyashkov, Bruce D. Ziman, Edward G. Lakatta.

A coupled-clock system within sinoatrial node cells (SANC) confers robustness and regulates their normal automaticity: basal cAMP-mediated, protein kinase A-dependent phosphorylation of Ca^{2+} cycling-proteins enables sarcoplasmic reticulum (SR) to generate spontaneous rhythmic Local, subsarcolemmal Ca^{2+}Releases (LCRs) (''Ca^{2+} clock''). LCRs activate an inward Na^+-Ca^{2+} exchange current that accelerates the diastolic depolarization promoting the ensemble of surface membrane ion channels (''membrane clock'') to generate the next action potential (AP). Intracellular Ca^{2+} enters mitochondria through the mitochondrial uniporter and is extruded by the mitochondrial Na^+-Ca^{2+} exchanger. We hypothesized that mitochondrial Ca^{2+} cycling is coupled to SANC-clocks via its impact on the intracellular Ca^{2+} cycling.

Specific inhibition of Ca influx into and efflux from mitochondria in intact single isolated SANC was effected by Ru360 and CGP-37157, respectively. Changes in mitochondrial Ca^{2+} content (Ca_m) were indexed by selective quenching of the fluorescent Ca^{2+} probe, Indo-1 in the cytosol by Mn^{2+}. Ru360 decreased Ca_m to $80 \pm 8\%$ control and increased the spontaneous SANC AP firing rate to $111 \pm 1\%$. Conversely, CGP-37157 increased Ca_m to $119 \pm 7\%$ control and reduced the spontaneous AP firing rate to $89 \pm 2\%$. Blocking Ca influx into mitochondria increased the average LCR size (measured via confocal linescans images of fluo-4) from 4.2 ± 0.1 to $6.1 \pm 0.2\mu m$ and reduced the normal LCR period from 317 ± 5 to 274 ± 6ms. In contrast, inhibition of Ca efflux from mitochondria reduced LCR size to $3.6 \pm 0.1\mu m$ and increased LCR period to 389 ± 7ms. Changes in LCR period by specific inhibition of Ca^{2+} influx or efflux into and from the mitochondria from 274 ± 6 to 389 ± 7ms predicted (R^2=0.84) the concomitant changes in the spontaneous SANC AP cycle length from 349 ± 5 to 462 ± 6ms.

We conclude that Ca^{2+} cycling into and out of mitochondria interact with the SANC coupled-clock system to modulate normal automaticity.

3031-Pos Board B136

Stochastic Beat-To-Beat Variation in Periodicity of Local Calcium Releases Predicts Intrinsic Cycle Length Variability in Single Sinoatrial Node Cells

Oliver J. Monfredi, Larissa A. Maltseva, Mark R. Boyett, Edward G. Lakatta, Victor A. Maltsev.

Abstract: In sinoatrial nodal cells (SANC), spontaneous, rhythmic, submembrane sarcoplasmic reticulum (SR)-generated local Ca2+ releases (LCRs) that occur during diastolic depolarization (DD) activate inward Na+/Ca2+-exchange currents that accelerate the DD rate. LCRs are roughly periodic, 'LCR period' being the time from the preceding AP-induced Ca2+-transient peak to their subsequent appearance. Previously, we demonstrated that in a given steady-state, the average LCR period of multiple AP cycles predicts concurrent average steady-state AP cycle length. We tested whether variation in LCR periods also predicts the beat-to-beat cycle length within a given steady-state. Methods: We imaged single rabbit SANC using a fast 2D-camera to capture almost all LCRs (in contrast to the relative few LCRs captured by line scan images), and in selected cells we also simultaneously measured APs by perforated patch clamp. Results: LCRs begin to occur very early during diastole, on the descending part of the prior AP-induced Ca2+ transient, shortly after the maximum diastolic potential (MDP). About 40 ms after the MDP, the ensemble of waxing LCR activity causes a late diastolic Ca elevation accompanied by a notable DD acceleration. On average, SANC (n = 9) generated 13.2 ± 3.7 LCRs per cycle, varying in size (7.1 ± 4.2μm) and duration (44.2 ± 27.1 ms). The LCR size and duration were greater for later-occurring LCRs. The average LCR period for a given cycle ranged from 70-460ms, and closely predicted (R2=0.89) the time of occurrence of the next AP, i.e. the duration of that cycle (220 to 470 ms). Numerical modeling simulations closely reproduce this experimental result. Conclusion: Intrinsic cycle length variability in single SANC is linked to cycle to cycle stochastic variations in roughly periodic LCRs.

3032-Pos Board B137

Spatially Complex Diffraction-Limited Photolysis of Caged Calcium and IP3 Combined with High-Speed Confocal Imaging

Vyacheslav M. Shkryl, Joshua T. Maxwell, **Lothar A. Blatter**.

The novel Mosaic digital illumination system (Photonic Instruments/Andor Group) integrated into a Nikon A1R confocal microscope was used to uncage Ca (DM-nitrophen, NP-EGTA) or IP_3 from multiple geometrically complex (Fig.) diffraction-limited subcellular regions and simultaneously measure $[Ca]_i$ with high-speed 2-dimensional confocal imaging (430 fps). The Mosaic System uses a computer controlled spatial light modulator to map a diffraction limited mask onto the specimen plane. A Digital Micromirror Device, consisting of a high speed array of hinge-mounted individually addressable, tiltable microscopic mirrors, directs continuous wave laser light (405 nm) onto the image plane according the user-defined diffraction limited mask. Local uncaging of Ca from multiple small regions of interest (0.63 micrometer diameter) generated artificial Ca sparks outside the cell and produced CICR inside permeabilized cardiac myocytes. Uncaging Ca from a 0.63x10 micrometer region triggered CICR and propagating Ca waves. Subsarcolemmal uncaging of IP_3 initiated propagating Ca waves that originated within the region of uncaging, and caused increased peak amplitude of electrically evoked Ca transients and Ca alternans, suggesting that in cardiac myocytes Ca release from IP_3 recpetors primes ryanodine receptor Ca release channels and enhances CICR.

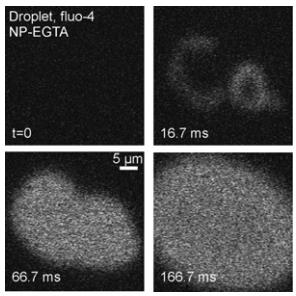

3033-Pos Board B138

Calcium Spark Termination: Ryanodine Receptor Unitary Flux Dependent Mechanism

Tao Guo, Dirk Gillespie, Michael Fill.

Spontaneous sparks seem to terminate at a fixed free sarcoplasmic recticulum Ca concentration ([Ca]SR) indicating that the SR luminal Ca level is a key factor in terminating Ca sparks. In principle, such luminal Ca control could be achieved by different mechanisms. One is that luminal Ca may alter RyR2 gating by acting at intra-SR sites. Another is that, as luminal Ca falls, RyR2 unitary release flux (iCa) may become insufficient to support continued inter-RyR2 Ca-induced Ca release within a RyR2 cluster (a cytosolic process). To date, it has been virtually impossible to experimentally distinguish these possibilities in cells. We have overcome this obstacle by devising a means to manipulate iCa independently of [Ca]SR. This was accomplished by exploiting RyR2 permeation properties. Briefly, sparks and [Ca]SR were simultaneously recorded in permeabilized rat myocytes. Unitary RyR2 iCa in the tested cellular solutions was defined using single RyR2 measurements in bilayers as well as a well-established RyR permeation model. Preliminary data reveal that reducing RyR2 iCa (at a relatively constant [Ca]SR) dramatically decreases spark frequency. We believe this method is the first to experimentally delineate the contribution of RyR2 iCa flux in the SR luminal Ca control of sparks in cardiomyocytes.

3034-Pos Board B139

4-D Scanning of Calcium Sparks in Cardiomyocytes Reveals their In-Focus Amplitude

Vyacheslav M. Shkryl, Lothar A. Blatter, Eduardo Ríos.

Ca sparks, puffs and related discrete events of intracellular Ca release have so far been studied by imaging fluorescence of a suitable monitoring dye over one or two spatial coordinates and time (xt or xyt modes). By missing the vertical (z) coordinate either technique is susceptible to the out-of-focus error. This error corrupts every measurement, especially altering the measurement of amplitude, which is crucial for evaluation of numbers of contributing channels and other features with mechanistic implications. Existing theory of spark scanning (Izu et al.1998; Ríos et al. 2001) allow correction of the out-of-focus error, but only in a statistical sense, leading to correct distributions rather than accurate amplitudes of individual sparks. We now use a fast confocal slit scanner (5-LIVE; Zeiss) to image sparks in x, y and z as they evolve in time, and take advantage of the added dimension to characterize those sparks that are in focus. The distribution of amplitudes of 1196 such sparks (33 cat atrial cells) was not a sum of decaying exponentials, indicating that their Ca sources are non-Markovian channels (in agreement with Ríos et al. 2001, Wang et al. 2002), due for instance to interactions within the cluster. The directly determined distribution of amplitudes was similar to that obtained by correction, according to the theory of spark scanning, of the distribution in a larger sample imaged in xt linescans (xt-to-xyzt correction). The theory is generalized to

provide the relationship between the distribution of amplitudes in focus and in xyt images (xyt-to-xyzt correction), thus unifying the three possible modes of spark sampling. The relative merits and shortcomings of the three modes will be discussed from this unified viewpoint.
Funded by NIAMS, NHLBI and NCRR (NIH).

3035-Pos Board B140
Isoproterenol Widens the Source of Release Flux Underlying Ca Sparks
Demetrio J. Santiago, Eduardo Rios, Thomas R. Shannon.
Our previous work [Biophys. J. 98(10):2111-20; Biophys. J. 98(3):102a] suggested that the diastolic ryanodine receptor (RyR) mediated leak (Jleak) from the sarcoplasmic reticulum (SR) of intact ventricular myocytes occurs in spark and non-spark forms. We further showed that the fraction of spark-mediated Jleak increases upon isoproterenol treatment in intact rabbit ventricular myocytes, suggesting that the effective sensitivity to cytosolic Ca is increased by RyR phosphorylation [Biophys. J. 98(3):102a]. We now present an extension of this work, focused on aspects of individual sparks taken from cells at matched [Ca] and SR load. Events were wider in isoproterenol (8.5% greater FWHM of the F/F0 profile) but had similar amplitudes than control. A backward reconstruction of the release flux density, when applied to average sparks assumed to be spherically symmetric, rendered a source that was wider for the isoproterenol event, indicating the recruitment of peripheral RyRs. A forward release flux reconstruction which recapitulates the steps of spark formation could not simultaneously fit the amplitudes and sizes of any of the two average sparks when using realistic radii for the junctional SR. This result may be interpreted as implying the existence of RyRs, peripheral to and perhaps outside the couplon. Compounded with the increased CICR sensitivity upon isoproterenol treatment (see above), the greater spark width of isoproterenol events may increase the probability of Ca wave generation.

3036-Pos Board B141
Activation of Calcium Sparks in Resting Cardiomyocytes by β-Adrenergic Stimulation May Involve CaMKII and nNOS
Daniel Gutierrez, Jakob Ogrodnik, Ernst Niggli.
It has been reported that during β-adrenergic stimulation of cardiac myocytes, phosphorylation of Ca^{2+} release channels (ryanodine receptors, RyRs) by PKA and/or CaMKII may result in arrhythmogenic diastolic Ca^{2+} leak (as elementary Ca^{2+} release events, Ca^{2+} sparks) from intracellular Ca^{2+} stores (the sarcoplasmic reticulum, SR). Using confocal Ca^{2+} imaging, we have recently shown that β-adrenergic stimulation by 1 μM isoproterenol (ISO) increases the Ca^{2+} spark frequency several-fold in quiescent, whole-cell voltage-clamped guinea-pig myocytes, without altering SR Ca^{2+} content. As this occurs without variations of the diastolic intracellular Ca^{2+} concentration, this observation suggests a sensitization of the RyRs. Experiments with protein kinase inhibitors (KN-93 and H89) indicated an involvement of CaMKII in the change of spark frequency. Surprisingly, but in line with the kinase inhibitor experiments, increasing cAMP production and PKA activity by direct stimulation of adenylate cyclase with forskolin (1 μM) did not significantly elevate Ca^{2+} spark frequencies under the same experimental conditions. Further experiments revealed that the change in sensitivity of the RyRs upon β-adrenergic stimulation may be linked to nitric oxide (NO), as pre-incubation of the cells with the NOS inhibitor L-NAME (500 μM) prevented the increase of the Ca^{2+} spark frequency without dramatic changes of SR Ca^{2+} content. Using the nNOS specific inhibitor AAAN (100 μM) resulted in analogous observations, suggesting that the nNOS isoform, located in close proximity of the RyRs, may be involved in this signaling pathway. Taken together, the results suggest the presence of a non-classical pathway linking β-adrenergic stimulation of cardiac myocytes to enhanced activity of the RyRs. Preliminary pharmacological evidence indicates that the pathway includes both, CaMKII and nNOS as important components. Supported by SNF.

3037-Pos Board B142
B-Adrenergic Stimulation Accelerates Local Recovery of Cardiac Ca^{2+} Release
Ona Liu, Hena Ramay, Eric A. Sobie.
In cardiac myocytes, Ca^{2+} sparks terminate reliably and exhibit time-dependent refractoriness after termination. Compelling evidence suggests that dynamic local changes in SR [Ca^{2+}] play an important role in the control of these processes. We examined Ca^{2+} spark refractoriness by exposing fluo-3 loaded quiescent rat ventricular myocytes to 50 nM ryanodine, recording Ca^{2+} sparks with a confocal microscope, and analyzing the repeated sparks that were produced at a limited number of ryanodine receptor (RyR) clusters. Previous experiments showed that altering RyR sensitivity (caffeine or tetracaine) influenced the time between consecutive sparks but did not affect the recovery of spark amplitude (time constant = ~100 ms in all cases). Here we examined repeated Ca^{2+} sparks after application of 100 nM isoproterenol to determine how β-adrenergic stimulation influences spark restitution. Isoproterenol dramatically decreased the median interval between consecutive sparks (192 ms vs. 280 ms in control) and led to faster recovery of Ca^{2+} spark amplitude (time constant = 58 ms). Mechanisms underlying these results were explored through simulations with an established mathematical model of the Ca^{2+} spark. Simulations showed that faster SR refilling led to earlier triggering of Ca^{2+} sparks due to the greater flux of Ca^{2+} through each open RyR, but this effect was insufficient to explain the experimental data. The results could be reproduced if we assumed that isoproterenol both increased the rate of local SR refilling and increased RyR sensitivity. Together, our results indicate that β-adrenergic stimulation influences both: 1) Ca^{2+} spark amplitude recovery, through changes in the time course of local SR refilling; and 2) Ca^{2+} spark triggering, through changes in both refilling and RyR sensitivity.

3038-Pos Board B143
Beta-Adrenergic Stimulation Increases the Intra-Sarcoplasmic Reticulum Ca Threshold for Spontaneous Ca Waves
Timothy L. Domeier, Joshua T. Maxwell, Lothar A. Blatter.
Beta-adrenergic signaling induces positive inotropic effects on the heart that frequently associate with spontaneous arrhythmogenic Ca release events including Ca waves. It remains unclear if the greater incidence of Ca waves is due to increased sarcoplasmic reticulum (SR) Ca content ([Ca]SR) or a change in the function of ryanodine receptors. To address this controversy we utilized dynamic [Ca]SR measurements (fluo-5N) to test if beta-adrenergic stimulation alters the [Ca]SR level where Ca waves initiate (wave threshold) during rest after action potential stimulation. Under control conditions [Ca]SR was progressively increased to the wave threshold via incremental increases in pacing frequency in a high extracellular Ca (7 mM) environment. In the presence of the beta-adrenergic agonist isoproterenol (ISO, 1 microM) [Ca]SR increased and Ca waves were observed. When [Ca]SR was subsequently lowered using low extracellular Ca (1 mM) and SERCA inhibition (3 microM cyclopiazonic acid), Ca waves were no longer observed, even at [Ca]SR levels above the control wave threshold. In parallel experiments we found that resting cytosolic [Ca] (indo-1) was similar between the respective experimental conditions. Indirect assessment of [Ca]SR using the amplitude of the cytosolic Ca transient induced by 10 mM caffeine confirmed our observation that in the presence of ISO Ca waves only occur when [Ca]SR is above the control wave threshold. Furthermore, spontaneous Ca spark measurements (fluo-4) showed a tendency towards spark inhibition in the presence of ISO at experimentally matched [Ca] SR. Together, these data show that acute beta-adrenergic stimulation increases the [Ca]SR threshold for Ca waves, and therefore the primary cause of Ca waves is the robust increase in [Ca]SR above this higher threshold level. Elevation of the [Ca]SR wave threshold may be interpreted as a protective mechanism against pro-arrhythmogenic Ca release during beta-adrenergic stimulation.

3039-Pos Board B144
β-Adrenergic Receptor Stimulation of ROS Production Generates Spontaneous Ca^{2+} Waves in Rabbit Ventricular Myocytes
Elisa Bovo, Stefan R. Mazurek, Stephen L. Lipsius, **Aleksey V. Zima**.
Stimulation of β-adrenergic receptors (β-AR) leads to positive inotropic effects, but also can generate pro-arrhythmogenic spontaneous Ca^{2+} waves. We investigated the role of reactive oxygen species (ROS) production in the generation of Ca^{2+} waves during β-AR stimulation in rabbit ventricular myocytes. In electrically stimulated myocytes, isoproterenol (ISO; 0.1 μM) increased Ca^{2+} transient amplitude during systole, sarcoplasmic reticulum (SR) Ca^{2+} load and the occurrence of spontaneous Ca^{2+} waves during diastole. These effects, however, developed at different time points during ISO application. While SR Ca^{2+} release and load reached maximum after 3 min, Ca^{2+} waves did not appear until 6-12 min after ISO application. Measurements of intra-SR free Ca^{2+} ($[Ca^{2+}]_{SR}$) with Fluo-5N showed an initial increase of SR Ca^{2+} load from 0.9 to 2.1 mM followed by a gradual decline to 1.4 mM after 12 min of ISO application. This decline of $[Ca^{2+}]_{SR}$ was not due to decreased SERCA activity, but instead was the result of increased SR Ca^{2+} leak in the form of Ca^{2+} waves. SR Ca^{2+} leak, measured as a decline of $[Ca^{2+}]_{SR}$ after SERCA inhibition, was increased by 30% after 6-12 min of ISO application. Moreover, ISO significantly increased ROS production. ROS scavenger Tiron and superoxide dismutase mimetic MnTBPA abolished the ISO-mediated ROS production. Tiron (10 mM) or MnTBPA (20 μM) significantly decreased the occurrence of Ca^{2+} waves during ISO application and partially prevented ISO-mediated SR Ca^{2+} leak, but did not affect ISO-mediated increase in SR Ca^{2+} load or Ca^{2+} transient amplitude. ROS donor t-butyl peroxide (100 μM) elicited Ca^{2+} waves that were dependent on elevated SR Ca^{2+} load. These results demonstrate that β-AR-mediated ROS production acts in

conjunction with elevated SR Ca^{2+} load to generate spontaneous Ca^{2+} waves in rabbit cardiomyocytes.

3040-Pos Board B145

Regulation of Sarcoplasmic Reticulum [Ca^{2+}] during Rest in Rabbit Ventricular Myocytes

Elisa Bovo, Aleksey V. Zima.

During diastole, ryanodine receptor Ca^{2+} release channels are not completely quiescent, thus providing a pathway for significant sarcoplasmic reticulum (SR) Ca^{2+} leak. Cytosolic Ca^{2+} can be pumped back into the SR by the SR Ca^{2+}-ATPase (SERCA) or extruded by Na^{+}-Ca^{2+} exchanger (NCX). Therefore, the activity of Ca^{2+} transport systems during diastole plays a critical role in setting SR Ca^{2+} load under normal conditions and in disease states. Using confocal microscopy, we studied mechanisms that control intra-SR free Ca^{2+} ($[Ca^{2+}]_{SR}$) at rest in rabbit ventricular myocytes. We compared the rate of $[Ca^{2+}]_{SR}$ decline (with Fluo-5N) after rest from electrical pacing in control conditions and after SERCA inhibition with thapsigargin (TG; 10 μM). We found that the rate of $[Ca^{2+}]_{SR}$ decline increased only ~30% after SERCA blockade compared to control conditions (from 10.9 in control to 14.1 μM/s in the presence of TG). Similar results were obtained by measuring the rate of decline of total SR Ca^{2+} content, estimated from caffeine-induced Ca^{2+} transient amplitude (with Fluo-4). Inhibition of NCX by Ni^{2+} (5 mM) or by 0 $[Na^{+}]$/0$[Ca^{2+}]$ solution significantly slowed $[Ca^{2+}]_{SR}$ decline during rest (by 3.4 times), but did not prevent it. Simultaneous inhibition of NCX with 0 $[Na^{+}]$/0$[Ca^{2+}]$ solution and plasmalemmal Ca^{2+} ATPase with La^{3+} (1 mM) completely prevented $[Ca^{2+}]_{SR}$ decline during rest. These results indicate that in rabbit ventricular myocytes the predominant mechanism for cytosolic Ca^{2+} removal during rest is NCX but not SERCA-mediated Ca^{2+} uptake. These data are compatible with a model in which the majority of SR Ca^{2+} leak occurs through clusters of ryanodine receptors in the junctional SR that closely oppose NCX in the dyadic cleft.

3041-Pos Board B146

Increased Myofilament Ca^{2+} Sensitivity Decreases Sarcomere Length and Increases Spark-Spark Interactions

Ye Chen-Izu, Tamas Banyasz, Shaden Khabbaz, Stephanie Edelmann, Charles Payne, Jil C. Tardiff, **Leighton T. Izu**.

People with familial hypertrophic cardiomyopathy (FHC) harboring mutations of cardiac troponin T (cTnT) are often at a high risk of sudden cardiac death. Transgenic mice harboring some of these cTnT mutations show increased myofilament sensitivity to Ca^{2+} and also shortened diastolic sarcomere length (SL). Our computational studies predicted that decreasing the distances between Ca^{2+} release units (CRUs) of the sarcoplasmic reticulum (SR) by decreasing SL can destabilize the Ca^{2+} control system and increase the probability of spontaneous Ca^{2+} waves. Destabilization results from enhanced crosstalk between neighboring CRUs. In this study we mimic the greater myofilament Ca^{2+} sensitivity conferred by cTnT mutations using the myofilament Ca^{2+} sensitizer EMD 57033 (EMD). At concentrations up to 3 μM, EMD had no effect on either the peak Ca^{2+} transient or the diastolic Ca^{2+} levels and did not alter the SR Ca^{2+} load. To test the prediction that SL shortening increases the coupling between CRUs, we loaded myocytes with Di8-ANEPPS and Fluo-4 and simultaneously measured SL and Ca^{2+} sparks in 2 spatial dimensions using the Zeiss 5 Live high-speed 2-D scanning confocal microscope. EMD (1.5 μM) decreased SL significantly compared to the control cells in normal Tyrode (1.58 μm vs.1.69 μm, $p<0.05$). The spark coupling strength measures the influence of one CRU on another and is derived from an analysis of the spatiotemporal distribution of Ca^{2+} sparks. EMD treatment significantly increased the spark coupling strength 2.5 fold. The enhanced spark-spark coupling as diastolic SL decreases may contribute to increased frequency of spontaneous Ca^{2+} waves during diastole that can lead to triggered arrhythmias and sudden cardiac death in FHC.

3042-Pos Board B147

RyR2 Channel Activity Determines the Potency of State-Dependent RyR2 Blockers for Suppressing Arrhythmogenic Calcium Waves

Eleonora Savio Galimberti, Bjorn C. Knollmann.

Mutations in ryanodine receptors (RyR2) or calsequestrin (casq2) cause catecholaminergic- polymorphic ventricular tachycardia (CPVT). We previously reported that the RyR2 open-channel blocker flecainide (FLEC) suppresses Ca2+ waves and prevents CPVT in mice and humans. Here we test the hypothesis that the open-state block by FLEC significantly contributes to FLEC efficacy in CPVT. We reasoned that FLEC would preferentially affect myocytes lacking casq2 (casq2-/-), which have higher rates of spontaneous RyR2 channel openings compared to WT channels. To test this hypothesis, we compared FLEC with tetracaine, a RyR2 channel blocker that has no state dependence and binds equally well to closed RyR2 channels. We found that FLEC reduced the incidence, amplitude and frequency of Ca2+ waves with significantly higher potency in casq2-/- myocytes compared to WT myocytes (Figure). In contrast, tetracaine did not suppress Ca2+ waves and had equal potency in WT and casq2-/- myocytes (Figure). Conclusion: RyR2 channel activity likely determines the potency of open-state RyR2 blockers such as FLEC for suppressing arrhythmogenic Ca2+ waves, a mechanism likely relevant to FLEC antiarrhythmic efficacy in CPVT. NIH HL88635 & HL71670.

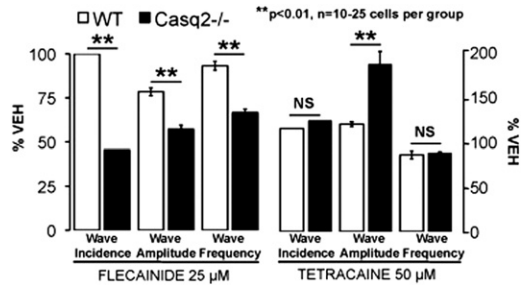

3043-Pos Board B148

FKBP12.6 'Stabilises' Cardiac SR Ca^{2+}-Release by Antagonising High-Affinity Reversible Activation of RyR2 by FKBP12

Elena Galfrè, Mano Sitsapesan, Samantha J. Pitt, Elisa Venturi, Stephen O'Neill, Rebecca Sitsapesan.

FKBP12.6 is thought to play an important cardioprotective role, however, the underlying mechanism is not understood. Since FKBP12 is structurally similar to FKBP12.6 but is found at much higher levels (1-3 μM), we investigated the effects of both FKBP12 and FKBP12.6 on RyR2 single-channel function and on SR Ca^{2+}-release in rat isolated permeabilised cardiomyocytes. FKBP12 increased RyR2 open probability (Po) in a concentration-dependent, reversible manner (EC_{50} 51 nM). Physiological levels of FKBP12 (3 μM) increased Po from 0.187 ± 0.051 to 0.657 ± 0.111 (SEM; n=14; $P<0.001$). FKBP12.6 (200 nM), itself, did not significantly alter RyR2 Po, but was a very effective antagonist of FKBP12, shifting the FKBP12 EC_{50} to 4 μM. In permeabilised myocytes perfused with Fluo-5F, spontaneous waves of Ca^{2+}-induced Ca^{2+}-release were induced by 234 nM Ca^{2+} in the mock cytosolic solution. Perfusion with FKBP12 (3 μM) increased wave frequency from 0.34 ± 0.04 Hz to 0.52 ± 0.07 Hz (SEM; n=14; $p<0.03$). 10 mM caffeine produced a larger Ca^{2+}-transient in control (2.21 ± 0.11; F/Fo) than in FKBP12 (1.47 ± 0.16; n=6; $p<0.003$) indicating lower SR Ca^{2+}-content. Perfusion with FKBP12.6 (200 nM) alone, had no significant effect yet it reduced the ability of FKBP12 to increase wave frequency (49.9 ± 5.8% increase over control in the absence of FKBP12.6 vs. 16.2 ± 2.1% in the presence). Our single-channel experiments demonstrate that FKBP12 is a high affinity, potent activator of RyR2. FKBP12.6 acts as an antagonist of FKBP12 at RyR2 but itself possesses minimal efficacy. Our cellular experiments suggest that this is the underlying mechanism by which FKBP12.6 acts to 'stabilise' or reduce SR Ca^{2+}-release in cardiac cells. Thus, the balance between the opposing actions of FKBP12 and FKBP12.6 on RyR2 gating may be crucial for normal EC-coupling in cardiac cells.

British Heart Foundation Funding

3044-Pos Board B149

Increased Levels of Micrornas miR-1 and miR-133 in Failing Heart Underlie Dissociation of Phosphatase Activity from RyR2 Complex Resulting in Enhanced RyR2 CaMKII-Dependent Phosphorylation and Cardiac Arrhythmias

Andriy E. Belevych, Sarah E. Sansom, Radmila Terentyeva, Mickey M. Martin, Cynthia A. Carnes, Terry S. Elton, Sandor Gyorke, **Dmitry Terentyev**.

Increased propensity of ventricular myocytes to arrhythmogenic spontaneous SR Ca release and afterdepolarizations in heart failure (HF) has been linked to abnormally high activity of RyR2. Growing evidence supports hyperphosphorylation of RyR2 at the CaMKII site S-2814 as a potential mechanism for altered RyR2 function. However, the specific molecular mechanisms underlying RyR2 hyperphosphorylation remain poorly understood.

MicroRNAs are small noncoding RNAs that regulate protein expression by interfering with mRNAs of target genes. We recently reported that 2-fold overexpression of microRNA miR-1 enhances CaMKII-dependent RyR2 phosphorylation by disrupting protein phosphatase 2A scaffolding to the RyR2, resulting in increased activity of the channel and Ca-dependent afterdepolarizations in myocytes. In the present study, we used a canine model of nonischemic HF to test the hypothesis that the HF-related alterations in RyR2 phosphorylation levels are caused by a decrease in phosphatase activity localized to RyR2 due to enhanced expression of two most abundant muscle-specific microRNAs miR-1 and miR-133. qRT-PCR studies revealed that the

levels of miR-1 and miR-133 were significantly increased in HF myocytes compared to controls (2 and 1.6 fold accordingly). Western blotting showed that PP2A regulatory (b56alpha) and catalytic subunits, specific targets of miR-1 and miR-133 validated by luciferase-reporter assay, were decreased in HF cells. Analysis using phospho-specific antibodies confirmed that RyR2 phosphorylation at Ser-2814 was significantly increased in HF myocytes compared to controls. CaMKII inhibitory peptide reduced the frequency of spontaneous Ca waves in paced current-clamped HF myocytes to low control values. These finding suggest that altered levels of major muscle-specific microRNAs contribute to abnormal RyR2 function in HF by depressing localized phosphatase activity to the channel, thus leading to excessive phosphorylation of RyR2s.

3045-Pos Board B150

Voltage-Dependent Anion Channel 2 modulates Resting Calcium Sparks, but not Action Potential-Induced Global Calcium Signaling in Cardiac Myocytes

Krishna P. Subedi, Joon-Chul Kim, Moonkyung Kang, Yeon-Soo Kim, **Sun-Hee Woo**.

Voltage-dependent anion channels (VDACs) are pore forming proteins predominantly found in the outer mitochondrial membrane and is thought to transport calcium ion (Ca^{2+}). In this study, we have investigated the possible role of type 2 VDAC (VDAC2) in cardiac Ca^{2+} signaling and Ca^{2+} sparks using a lentiviral knock-down (KD) technique and two-dimensional confocal Ca^{2+} imaging in immortalized autorhythmic adult atrial cells, HL-1. We confirmed high expression of VDAC2 protein in ventricular, atrial and HL-1 cells using Western blot analysis. Infection of HL-1 cells with VDAC2-targeting lentivirus reduced the level of VDAC2 protein to ~10%. Comparisons of autorhythmic Ca^{2+} transients between wild type (WT) and VDAC2 KD cells showed no significant change in the magnitude, decay, and beating rate of the Ca^{2+} transients. Caffeine (10 mM)-induced Ca^{2+} release, which indicates sarcoplasmic reticulum (SR) Ca^{2+} content, was not altered by VDAC2 KD. Interestingly, however, the intensity, width, and duration of the individual Ca^{2+} sparks were significantly increased by VDAC2 KD in resting conditions, with no change in the frequency of sparks. These results suggest that VDAC2 may suppress focal Ca^{2+} releases through ryanodine receptors in atrial myocytes under resting conditions. The results also indicate that VDAC2 may not regulate action potential-induced global Ca^{2+} signaling and SR Ca^{2+} loading.

3046-Pos Board B151

African Trypanosomes Increase Calcium Wave Frequency in Isolated Adult Rat Cardiomyocytes via Secretion of Cathepsin L

Elspeth B. Elliott, Liam J. Morrison, Hisashi Hasumi, Christopher M. Loughrey.

African trypanosomes are blood-borne extracellular parasites which have recently been linked to cardiac dysfunction in ~70% of sleeping sickness patients. Although this may result from an indirect effect of the parasite (e.g. myocarditis), a direct effect of the parasite on the heart has not been investigated. Adult rat cardiomyocytes were incubated with trypanosome growth media containing *Trypanosoma brucei* Lister427 (30min). A population assay assessed the percentage of cells demonstrating Ca^{2+} waves within a 1min period. Incubation with live trypanosomes led to a significant increase in the percentage of cells demonstrating Ca^{2+} waves ($54.8 \pm 2.8\%$ *vs.* $79.2 \pm 5.1\%$; media *vs.* live trypanosomes, $P<0.05$; n=4294 and 3006 cells respectively). This effect was maintained when cells were incubated with supernatant (trypanosomes removed from media by centrifugation) ($77.3 \pm 2.9\%$; n=2131 cells). Separate experiments showed the supernatant effect was lost upon boiling ($83.7 \pm 1.8\%$ *vs.* $66.3 \pm 2.4\%$; supernatant *vs.* boiled supernatant, $P<0.05$; n=527 and 612 cells respectively). Results were confirmed in Fura2AM loaded, field stimulated (1Hz) rat cardiomyocytes perfused with media (37°C). Following 4 min supernatant perfusion, the frequency of Ca^{2+} waves in the inter-stimuli interval was significantly increased (0.02 ± 0.01 *vs.* 0.44 ± 0.07 waves/s; media *vs.* supernatant, $P<0.05$; n=10). Since the parasite induces a similar phenomenon in brain mono-epithelial cells via cathepsin-L cysteine protease, we examined the role of cathepsin-L in the above effect on cardiomyocytes. In separate experiments, supernatant+K11777 (specific inhibitor of cathepsin-L) completely abolished the ability of supernatant to increase Ca^{2+} wave probability (56.3 ± 5.1 *vs.* $49.1 \pm 5.7\%$; media *vs.* supernatant+K11777, $P>0.05$), whereas CA074 (specific inhibitor of cathepsin-B) had no effect on Ca^{2+} wave frequency. These data suggest trypanosomes interact with cardiomyocytes leading to increased Ca^{2+} wave production via cathepsin-L. This may contribute to the cardiac abnormalities observed in patients with trypanosomiasis.

3047-Pos Board B152

Calcium Handling in Human Induced Pluripotent Stem Cell-Derived Cardiomyocytes

E. Michelle Capes, Randall E. Loaiza, Roberto Ramos, Jianhua Zhang, Timothy J. Kamp, Hector H. Valdivia.

Fibroblasts from human skin biopsies can be reprogrammed into pluripotent stem cells (iPSC), which can then be coaxed to differentiate into myocytes with cardiac-specific properties (iPSC-CMs). The field of iPSCs is still in its infancy, but it is increasingly clear that the excitation-contraction coupling (ECC) machinery of differentiating CMs undergoes proportionally incremental complexity and it remains to be seen whether it reaches complete maturity in cultured cells. We used patch-clamp and confocal Ca^{2+} imaging for a comparative assessment of ECC in human iPSC-CM and adult cardiomyocytes. In the latter, entry of Ca^{2+} through the L-type Ca^{2+} channel (I_{Ca}) triggers rapid, uniform release of Ca^{2+} from the sarcoplasmic reticulum (SR) via CICR. In iPSC-CMs at early stages of differentiation, the current-voltage relationship for I_{Ca} is remarkably similar to that of adult cardiomyocytes, indicating that the appearance of a "trigger" for contraction is an early event in the ontogenesis of ECC that doesn't hinder efficient generation of Ca^{2+} signals. However, primitive iPSC-CMs commonly exhibit a poorly developed SR, as assessed by their variegated response to caffeine and their great dependence on extracellular Ca^{2+} for contraction. Cells are mostly rounded and t-tubules are absent. As a result, $[Ca^{2+}]_i$ transient waveforms appear non-uniform and start at the periphery of the cell, as is expected of a Ca^{2+} front with focal initiation that propagates later to the interior of the cell. At more advanced stages of differentiation, iPSC-CMs display fairly uniform Ca^{2+} fronts, suggesting fast propagation of external Ca^{2+} signals to the interior of the cell. Thus, by this coarse functional estimate, it is expected that iPSC-CMs become accurate models of cardiomyopathies at late stages of differentiation, but the developmental characteristics of ECC is unclear and warrants a systematic approach, which we are currently performing.

3048-Pos Board B153

Impaired Calcium Signaling Refractoriness Contibutes to Increased Rate of Diastolic Calcium Waves in Myocytes from Post-Myocardial Infarction Hearts

Andriy E. Belevych, Dmitry Terentyev, Radmila Terentyeva, Hsiang-Ting Ho, Cynhtia A. Carnes, George E. Billman, Sandor Gyorke.

Spontaneous Ca^{2+} waves (SCWs) are recognized as important contributors to triggered arrhythmia. SCWs waves are thought to arise when $[Ca^{2+}]_{SR}$ reaches a certain threshold level, which might be reduced in cardiac disease as a consequence of sensitization of ryanodine receptors (RyR2s) to luminal Ca^{2+}. We investigated the mechanisms of SCW generation by simultaneous measurements of cytosolic and luminal Ca^{2+} in myocytes from normal and diseased hearts using a canine model of post-myocardial infarction (MI) tachyarrhythmia. The frequency of SCW, recorded during periodic pacing in the presence of β-adrenergic receptor agonist isoproterenol, was significantly higher in MI myocytes than in control. Rather than occurring at once upon reaching a final $[Ca^{2+}]_{SR}$, SCWs arose with a distinct time delay from the attainment of the maximum $[Ca^{2+}]_{SR}$ in both experimental groups. While the rate of $[Ca^{2+}]_{SR}$ recovery following the SR Ca^{2+} release was similar between the two myocyte types, the maximally attainable $[Ca^{2+}]_{SR}$ was lower, and the latency to SCW was shorter in MI myocytes compared to control. Both phosphorylation at the CAMKII site Ser-2814 and the level of oxidized thiols were higher in RyR2s from MI hearts than in control. The CAMKII inhibitor, KN93, or the reducing agent, mercaptopropionylglycine, reduced SCW frequency in MI myocytes. The MI-related alterations in myocyte Ca^{2+} cycling were mimicked by the RyR2 agonist, caffeine. These results indicate that attainment of a certain threshold $[Ca^{2+}]_{SR}$ is not a sufficient condition for the generation of SCWs and that Ca^{2+} signaling refractoriness that develops following release critically influences SCW occurrence in the diastolic period. We conclude that shortened Ca^{2+} signaling refractoriness due to RyR2s phosphorylation and oxidation is responsible for the increased rate of SCWs observed in MI myocytes.

3049-Pos Board B154

Inositol 1,4,5 Triphosphate (IP3) Receptors Activate Type 1 ryanodine Receptors to Mediate Ca^{2+} Sparks Signaling in Adult Mammalian Skeletal Muscle

Andoria Tjondrokoesoemo, Na Li, Noah Weisleder, Jianjie Ma.

Ca^{2+} sparks are the elemental event of Ca^{2+} induced Ca^{2+} release (CICR) that originate from clustered ryanodine receptor Ca^{2+} release channels (RyR1) in mammalian striated muscles. Previously we found that application of transient osmotic stress to the intact skeletal muscle leads to a robust Ca^{2+} spark response that is restricted to the periphery of sarcolemmal membrane. Here we

determine the fundamental mechanism for CICR activation in mammalian skeletal muscle. Transient osmotic stress increases PI(4,5)P2 and inositol 1,4,5 triphosphate (IP3) levels. Application of wortmannin or xestopongin C significantly reduces osmotic stress-induced Ca^{2+} spark activity in intact muscle fibers, suggesting the role of IP3 receptor in Ca^{2+} spark signaling. Western blot shows that both IP3 receptor type 1 and 2 are present in adult skeletal muscle, and immunostaining reveals that both IP3 receptors are distributed along the sub-sarcolemmal region of the muscle fiber (with some concentrated to the perinuclear area). Using electroporation mediated transfection to deliver short hairpin (sh)RNA that targets IP3 receptors, we are able to knockdown the expression of both IP3 receptors 1 and 2 in the muscle of viable adult mice. We find that reduced expression of IP3 receptors ablates osmotic stress-induced Ca^{2+} spark activity, indicating Ca^{2+} sparks activity in skeletal muscle requires activation of IP3 receptor. Thus, osmotic stress-induced Ca^{2+} spark signaling in skeletal muscle requires two cellular events: first, uncoupling of the inhibitory role of the voltage sensor on the RyR1 channels, and second, production of the IP3 second messenger near the sarcolemmal membrane. These results represent the first description of IP3 receptors producing CICR from RyR1 in mammalian skeletal muscle and provide essential clues to the function of these Ca^{2+} sparks in skeletal muscle physiology.

3050-Pos Board B155

Recovery of the Compromised Ca^{2+} Spark Signaling in Aged Skeletal Muscle Through Restoration of MG29

Xiaoli Zhao, Norio Takizawa, KiHo Park, Kyoung-Han Choi,
Hilary A. Wilkinson, Dennis M. Zaller, Noah Weisleder, Jianjie Ma.

Sarcopenia is a degenerative loss of skeletal muscle function associated with aging. Our previous results identify reduced MG29 expression in aged skeletal muscle, and mirroring phenotypes of the young MG29 knockout and aged wild type muscles in that both show reduced Ca^{2+} spark response to osmotic-stress. Thus, compromised intracellular Ca^{2+} homeostasis due to reduced MG29 expression may be one of the underling mechanisms for aging-related skeletal muscle dysfunction. Here we explored the effects of MG29 rescue on Ca^{2+} spark signaling in aged skeletal muscle. Electroporation-based method was used to introduce MG29 into *flexor digitorum brevis* (FDB) muscle and adeno-associated virus (AAV)-based method was used to deliver MG29 gene into the hindlimb of the living mice. Confocal microscopic imaging revealed increased Ca^{2+} spark events in aged FDB muscle following transient overexpression of MG29. These Ca^{2+} sparks showed plastic response to osmotic stresses, similar to those observed in the young wild type muscle. 2-3 weeks following AAV-mediated delivery of MG29, the aged skeletal muscle showed only marginal increase in contractile force as compared to the contralateral controls. Our data suggest that transient restoration of MG29 expression in aged muscle has beneficial effects on improvement of intracellular Ca^{2+} signaling. Since MG29 is involved in maintenance of the transverse-tubule network, restoration of contractile force in aged muscle may require sustained elevation of MG29 to allow for remodeling of the disrupted membrane network.

3051-Pos Board B156

Hypersensitive Intracellular Ca^{2+} Signaling Precedes Deterioration of Cardiac Functions in Muscular Dystrophy

Sergii Kyrychenko, Eva Poláková, Krisztina Poscai, Nina D. Ullrich,
Ernst Niggli, Natalia Shirokova.

Duchenne muscular dystrophy (DMD) is a severe form of striated muscle disease. Although respiratory failure remains a leading cause of death, a number of patients succumbs from cardiac manifestations of the disease. The *mdx* mouse, an animal model of DMD, develops progressive dilated cardiomyopathy. Several studies associated changes in Ca^{2+} homeostasis with the disease. Here we investigated whether these changes were causal for or a consequence of the pathology. Ca^{2+} handling was studied in intact and patch-clamped cardiomyocytes isolated from 1 to 4 month old mice. According to several reports, young *mdx* mice show no significant changes in cardiac performance. However, even myocytes from 1 month old *mdx* mice produced exaggerated Ca^{2+} signals in response to osmotic shock, and exhibited ''hypersensitive'' excitation-contraction coupling (ECC gain was more resistant to a reduction in $[Ca^{2+}]_{ex}$ in *mdx* than in WT cells). Ca^{2+} transients induced by osmotic shock were nearly abolished by the super-oxide dismutase mimetic Mn-cpx3, substantially reduced by a CaMKII inhibitor (KN-93) and partially diminished by PKA inhibitors (KT5720, H89). No significant changes in SR Ca^{2+} load as well as in resting $[Ca^{2+}]_i$ were found in young *mdx* compared to WT cells. Together with our previous results, these data suggest that 1) increased sensitivity of RyRs to Ca^{2+} precedes and probably contributes to the development of cardiomyopathy in dystrophy and that 2) there is a synergistic interaction among several pathomechanisms which hypersensitize the RyR. This includes a) abnormal Ca^{2+} influx resulting in b) cellular Ca^{2+} overload, c) elevated ROS generation leading to RyR redox modification and sensitization, and d) activation of protein kinases with subsequent RyR phosphorylation and even further sensitization. Thus, future pharmacological strategies should preferably target several of these mechanisms contributing to abnormal Ca^{2+} signals in DMD.

3052-Pos Board B157

A Novel Role for Polyphosphate in Astrocyte Signalling

Kira M. Holmstrom, Alexander V. Gourine, Andrey Y. Abramov.

Inorganic polyphosphate exists in nature in varying lengths from tens to thousands of orthophosphates linked by high energy bonds similar to ATP. The polymer is highly conserved from bacteria to human, but although its role has been extensively studied in bacteria, its function in the mammalian cell is only slowly coming to light. Polyphosphate has been detected in the rodent brain at micromolar concentrations and has been shown to regulate ion channels in neurons, suggesting that polyphosphate may play a role in neuronal signalling.

We used fluorescent live cell imaging to investigate the response to polyphosphate in primary astrocytic and neuronal co-cultures. For the experiments three different lengths of polyphosphate (short −14, medium −60, and long −130, orthophosphates) were used. Further, using the ratiometric Ca^{2+} indicator fura-2, we were able to identify a transient Ca^{2+} signal, mainly in astrocytes, in response to polyphosphate in the range of 10-100μM for all three lengths of the polymer. Interestingly, inhibiting phospholipase C by U73122 abolished the Ca^{2+} transient, as did emptying the endoplasmic reticulum of Ca^{2+} before addition of polyphosphate, using the sarco/endoplasmic reticulum Ca^{2+} ATPase inhibitor thapsigargin. On the other hand, removal of Ca^{2+} from the extracellular recording medium did not alter the signal, suggesting that the Ca^{2+} signal stems from the endoplasmic reticulum and is mediated through phospholipase C and IP_3 activation. Further characterisation, using different cell surface receptor inhibitors, suggests that the signal is mediated through purinergic receptors, as the broad spectrum P2 inhibitors PPADS and suramin both block the signal.

These novel findings highlight the possible importance of polyphosphate in signal transmission in the brain.

3053-Pos Board B158

Dynamic Control of Neuronal Firing Threshold by Calcium Buffering: A New Role for Calcium Binding Proteins

Patrick Bischop, Céline Roussel, David Orduz, Serge N. Schiffmann,
David Gall.

We have investigated the detailed regulation of neuronal firing threshold by the cytosolic calcium buffering capacity using a combination of mathematical modeling and patch clamp recording in acute slice. Theoretical results show that, at similar free calcium concentration, increased calcium buffer concentration lowers the firing threshold of cerebellar granule cells. We show that this effect is a direct consequence of the major slowdown of calcium dynamics. Patch clamp recordings on cerebellar granule cells loaded with a high concentration of the fast calcium buffer BAPTA (15 mM) reveal alterations in the excitability threshold as compared to cells loaded with 0.15 mM BAPTA. In high calcium buffering conditions, granule cells exhibit a significative lower firing threshold. These results suggest that cytosolic calcium buffering capacity can tightly modulate neuronal firing threshold and therefore that calcium-binding proteins may play a critical role in the information processing in the central nervous system.

Intercellular Communications & Gap Junctions

3054-Pos Board B159

Single Hemichannels Recorded in Lipid Bilayers and Artificial Gap Junction Formation with Cells

Mohamed Kreir, Christoph Methfessel, Christian Carnarius,
Claudia Steinem, Niels Fertig.

Connexins (Cx) are members of a multigene family of membrane-spanning proteins that form gap junctions, which are composed of two hexameric hemichannels, called connexons. These gap junctions, organized in so-called gap junctional plaques, span the extracellular space/matrix of adjacent cells and thus allow a passive exchange of small molecules up to about 1 kDa. Connexins are widely distributed with various subtypes of connexin and are involved in different biological processes such transmission of information and propagation of action potential for e.g. Recent studies indicates that hemichannels do open under physiological and pathological conditions.

In our study, we investigated the biophysical properties of hemichannels Cx26 and Cx43 which were isolated biochemically and reconstituted into synthetic lipid membranes. Both hemichannels are present in different tissues and involved in different pathologies. The results on a study of the Cx26 are presented. Reconstitutions of functional Cx26 and mutant hemichannels were performed. Secondly, Cx43 was purified and reconstituted into bilayers. The hemichannel Cx43 properties were compared to previous studies and showed similarities of conductance on single channel recordings of Cx43 in cells. Our focus was then to form artificial gap junctions, first between two unrelated cells and then between cells and bilayers containing functional hemichannels. This was done using Cx26 or Cx43. The bilayer-cell configuration allows to measure electrophysiological properties of the cells indirectly via gap junctions. Single channel recordings of gap junctions were recorded using a bilayer containing Cx43 and Cardiomyocytes expressing Cx43. Macroscopic currents were as well recorded between bilayers and cell lines expressing Cx26 or Cx43.

3055-Pos Board B160

Asparagine175 of Cx32 is a Critical Residue for Docking and Forming Functional Heterotypic Gap Junction Channels with Cx26

So Nakagawa, **Xiang-Qun Gong**, Shoji Maeda, Yuhua Dong, Yuko Misumi, Tomitake Tsukihara, Donglin Bai.

Gap junctions result from the docking of two hemichannels. Depend on the connexin(s) in the hemichannels, homotypic and heterotypic gap junction channels can be formed. Previous chimera studies with domain exchange between different connexins indicated that the extracellular loop2 (E2) is important molecular domain to heterotypic compatibility. Based on the high resolution structure of Cx26 gap junction channel and homology models of heterotypic channels, we analyzed docking selectivity for several hemichannel pairs, and found that the hydrogen bonds between E2 domains are conserved in several heterotypically compatible hemichannels, e.g. between Cx26 and Cx32. According to our model analysis, Cx32 mutation, Cx32N175Y, destroys three hydrogen bonds in the E2-E2 interactions at the heterotypic docking interface. Our model predicts that the Cx32N175Y hemichannel is unlikely to dock with Cx26 hemichannel properly due to steric hindrance at the docking interface. Experimentally, we tagged GFP and RFP to the carboxyl terminals of Cx32 and Cx26 to generate Cx32GFP (Cx32N175YGFP) and Cx26RFP, respectively. Our data showed that tagged Cx26 and Cx32 were able to traffic to cell interfaces forming gap junction plaque-like structures in transfected HeLa/N2A cells. However, Cx32N175YGFP exhibited mostly intracellular distribution and rarely seen in cell-cell interfaces. Double patch clamp analysis demonstrated that this Cx32 mutant did not form functional homotypic channels. When wild-type or mutant Cx32GFP expressing cells were cocultured with Cx26RFP expressing cells, Cx32GFP and Cx26RFP were frequently colocalized at the cell-cell interfaces and formed functional Cx32/Cx26 heterotypic channels. No colocalization was found at the cell-cell interfaces between Cx32N175Y and Cx26 expressing cells, also no functional Cx32N175Y/Cx26 heterotypic channels were identified. Our modeling and experimental data indicate that N175 of Cx32 is a critical residue for heterotypic docking between Cx32 and Cx26 hemichannels.

3056-Pos Board B161

Calcium Permeability of Purified and Reconstituted Hemichannels formed by Connexin 26 and the Deafness-Causing Mutant R75W

Mariana C. Fiori, Maria E. Zoghbi, Guillermo A. Altenberg.

Gap-junctional channels are connexin oligomers (dodecamers) formed by head-to-head docking of two hemichannels (each one a connexin hexamer). Mutations of connexin 26 (Cx26) are the most frequent cause of genetic deafness. A single amino-acid mutation at position 75 (R75W) causes autosomal dominant deafness, and we have shown that this mutant is incapable of forming gap-junction channels, but forms functional hemichannels. Here, we studied the permeability of purified Cx26 and R75W hemichannels to Ca^{2+} and large hydrophilic solutes to further our understanding of the deafness associated with R75W expression. Cx26 and R75W were purified based on the affinity for Co^{2+} of a poly-histidine tag fused at the C-terminal end of the proteins overexpressed using the insect cell/baculovirus expression system, and the Cx26 and R75W affinity for the strong cation exchanger Mono S. Essentially all Cx26 and R75W solubilized in dodecylmaltoside were hexamers, and were functional when reconstituted in liposomes, as demonstrated by sucrose- and fluorescent-probe permeability assays. Cx26 and R75W hemichannels were permeable to sucrose, Alexa Fluor 350 and Cascade Blue, but not to Calcein, Fluo-5N or Alexa Fluor 647. Ca^{2+} permeability was evaluated in liposomes containing Cx26 or R75W hemichannels. In the proteoliposomes with the low-affinity calcium-sensitive probe Fluo-5N trapped inside, intra- and extra-liposomal free calcium equilibrated rapidly upon increasing free-[Ca^{2+}] from $<$ 10 nM to ~400 μM. These studies directly show permeability of Cx26 and R75W hemichannels to Ca^{2+}, but failed to identify permeability differences between hemichannels formed by Cx26 and the deafness-causing mutant. This work was supported in part by NIH grants R01GM79629 and R21DC007150, American Heart Association Grant-in-Aid 0755002Y, and a grant from the Center for Membrane Protein Research of TTUHSC.

3057-Pos Board B162

Origin and Dynamics of Calcium Waves in the Islet of Langerhans

Richard K.P. Benninger, Troy Hutchens, W. Steven Head, David W. Piston.

Interactions between cells in the islet of Langerhans are critical for the regulation of insulin secretion. Here, we study the electrical coupling and electrical dynamics between β-cells in the islet. We focus on quantitatively measuring multi-cellular calcium oscillations and waves, describing the emergence of these dynamics with a multi-cellular mathematical model, and experimentally testing predictions given by this model.

A key prediction is that calcium waves emerge from sub-regions of the islet with elevated excitability, due to endogenous β-cell heterogeneity in cellular excitability [Benninger et al. *BiophysJ* **95:**p5048 (2008)]. To test this we utilize a 2-channel microfluidic device [Rocheleau et al. *PNAS* **101:**p12899 (2004)] which allows a precise pattern of glucose stimulation to be applied. If glucose is elevated on one side of the islet, calcium waves consistently originate from this region, as predicted. Subsequently, upon uniform glucose stimulation, the wave direction is independent of where glucose was initially elevated: consistent with an intrinsic β-cell heterogeneity that determines calcium wave propagation.

We further explore the balance of β-cell excitability and coupling by describing the calcium activity upon a glucose gradient. In normal islets, a sharp transition in calcium activity occurs midway across the islet. In the absence of gap junction coupling this transition point is shifted towards the quiescent side of the islet. Interestingly following elevated glucose, the initial calcium elevation propagates further across the islet than subsequent calcium waves. We can explain this given a measured glucose dependence of gap-junction coupling.

This gives us further insight into the role of electrical coupling in determining the overall spatiotemporal electrical response. Furthermore the application of mathematical models to predict phenomena which can be experimentally verified to yield new functional insight is a significant advance in understanding emergent multi-cellular behavior.

3058-Pos Board B163

Transcriptional Suppression of Connexin 43 by Tbx18 Undermines Cell-Cell Electrical Coupling in Postnatal Cardiomyocytes

Nidhi Kapur, Eduardo Marbán, Hee Cheol Cho.

During embryonic development, critical steps in cardiac lineage specification are guided by T-box transcription factors. Mesenchymal precursor cells expressing Tbx18 give rise to the heart's pacemaker, the sinoatrial node (SAN). We sought to identify targets of Tbx18 transcriptional regulation in the heart by forced adenoviral overexpression in postnatal cardiomyocytes. Monolayers of neonatal rat cardiomyocytes (NRCMs) transduced with GFP alone showed sarcolemmal, punctate Cx43 expression. In contrast, Tbx18-transduced NRCMs exhibited sparse Cx43 expression. Both the transcript and protein levels of Cx43 were greatly downregulated within 2 days of Tbx18-transduction. Injection of Tbx18 in the guinea pig heart *in vivo* markedly suppressed Cx43 expression similar to what was seen in Tbx18-NRCMs. The repressor activity of Tbx18 on Cx43 was highly specific: protein levels of Cx45 and Cx40, which comprise the main gap junctions in the SAN and conduction system, were unchanged by Tbx18. A reporter-based promoter assay demonstrated that Tbx18 directly represses the Cx43 promoter. Phenotypically, Tbx18-NRCMs exhibited slowed calcein dye transfer kinetics (421 ± 54 vs. control 127 ± 43 ms). Intracellular Ca^{2+}-oscillations in control NRCMs monolayers were highly synchronized. In contrast, Tbx18-overexpression led to episodes of spontaneous, asynchronous Ca^{2+}-oscillations demonstrating reduced cell-cell coupling. The decreased electrical coupling led to slow electrical propagation; conduction velocity in Tbx18-NRVMs slowed by more than 50% relative to control (4 ± 1 vs 9 ± 2 cm/s). Taken together, Tbx18 specifically and directly represses the transcript and protein levels of Cx43 in NRCMs *in vitro* and in adult ventricular myocardium *in vivo*. Cx43 suppression led to significant electrical uncoupling, but the preservation of other gap junction proteins (Cx45 and Cx40) permitted action potential propagation at slower velocity. Thus, Tbx18 overexpression recapitulates a key phenotypic hallmark of the SAN, namely the characteristic loose electrical coupling.

3059-Pos Board B164

Cardiac Myofibroblast-Myocyte Gap Junction Coupling Promotes After Depolarizations

Thao P. Nguyen, Yuanfang Xie, Alan Garfinkel, Zhilin Qu, James N. Weiss.

Tissue fibrosis, as seen in diseased and aged hearts, promotes ventricular arrhythmias. We hypothesize that de novo gap junction coupling between myofibroblasts, which proliferate following cardiac stress injury, with neighboring ventricular myocytes may facilitate arrhythmia triggers such as early afterdepolarizations (EADs). A novel hybrid computational and biological approach was employed: virtual fibroblasts with programmable properties embedded in the dynamic clamp were coupled to a real patch-clamped rabbit ventricular myocyte exposed to oxidative (0.1 mM H_2O_2) or ionic (2.7 mM K^+_o) stressors. A virtual gap junction current of programmable conductance was added in real time to myocyte currents and their combined effects on myocyte action potentials and EAD genesis were evaluated. Exposure of myocytes to basal conditions failed to induce EADs, whereas exposure to stress led to 'bradycardia-dependent' EADs that occurred only during slow, but not during fast, pacing. However, when stressed myocytes were then coupled to a virtual fibroblast, EADs emerged independently of pacing rates. Fibroblast coupling alone to unstressed myocytes failed to induce EADs at any pacing rate. The virtual gap junction current has 2 components, but the earlier transient outward component was most critical for EAD generation; EADs disappeared when the virtual fibroblast was uncoupled from the myocyte during the initial 100 ms of the AP, but not when uncoupled for all but the first 100 ms of the AP. Our findings demonstrate that gap junction coupling of ventricular myocytes to myofibroblasts may directly induce EADs and the probability of EAD induction correlates with the myofibroblast-myocyte gap junction coupling strength. Elucidating the mechanism of myofibroblast-induced arrhythmogenesis may suggest new therapeutic strategies for preventing ventricular arrhythmias based on inhibiting fibroblast proliferation and/or uncoupling fibroblasts from myocytes.

3060-Pos Board B165

Targeted Inhibition of Connexin 43 Hemichannels Blunts Ca^{2+}-Induced Intercellular Dyssynchrony and ATP Efflux in Hl-1 Cardiomyocyte Syncitia

Nicole C. Silvester, Hala Jundi, Archana Jayanthi, Steven R. Barberini-Jammaers, W Howard Evans, Christopher H. George.

Gap junctions (GJ) are essential conduits that underpin cell-to-cell coupling between cardiomyocytes and are formed from the coalescence of connexin (Cx) hemichannels from two close opposed cells. However, there is evidence supporting a (patho)physiologic role for 'unpaired' Cx hemichannels as they traffic through the plasma membrane (PM) to the GJ. We used beating HL-1 cardiomyocyte monolayers as a model system for GJ intercellular communication (GJIC) and to investigate the functional role of Cx hemichannels in syncitial behaviour. GJIC was quantified as an index of intercellular Ca^{2+} release synchrony and was reconciled with detailed spatio-temporal analysis of intracellular Ca^{2+} signalling. Ouabain-evoked Ca^{2+} perturbation inhibited GJIC in a dose-dependent manner and was associated with reduced cell viability. We hypothesised that the intercellular dyssynchrony and cell death linked to ouabain-induced Ca^{2+} dysfunction was exacerbated by aberrant Cx hemichannel opening that may also compromise cellular metabolism. Consistent with this concept, the magnitude of intracellular Ca^{2+} flux dysfunction correlated with ATP release from cells. Trans-PM ATP leak was attenuated by Gap20, a peptide corresponding to an intracellular loop motif in Cx43. Moreover, Gap20 reduced intracellular Ca^{2+} perturbation, improved intercellular synchrony and reduced cell death in ouabain-treated syncitia. The lack of efficacy of a peptide corresponding to a similar epitope in Cx26, and also following the conjugation of Gap20 to a high molecular weight dextran confirmed i) the specificity of this approach and ii) that peptide bioactivity is dependent on its entry into cells and interaction with the intracellular face of Cx. Our data provides evidence that altered cellular Ca^{2+} homeostasis opens Cx hemichannels and that this may accelerate the metabolic deterioration of cardiomyocytes and exacerbate cardiac dysfunction in situ.

3061-Pos Board B166

Binding Kinetics of Inter-Connexon Interaction

Felix Rico, Atsunori Oshima, Yoshinori Fujiyoshi, Peter Hinterdorfer, Simon Scheuring.

Gap junctions are pairs of hexameric half-channels called connexons, which coaxially dock to connect two adjacent cells, mediating both adhesion and channeling between cells in many types of tissue. Connexons are formed of six connexin proteins (Cx). Gap junctions form by interdigitating the two extracellular loops of each connexin. While gap junction structure and function has been widely characterized using different techniques, the binding affinity of the inter-connexon interaction remains unknown. The goal of this work was to determine the binding affinity of gap junctions using dynamic force spectroscopy atomic force microscopy (AFM). Among the residues that mediate interconnexon interaction, an exposed stretch of conserved amino acids 'NTVD' within the extracellular loop 2 (E2) has been identified. For dynamic force spectroscopy, we covalently linked mimetic peptides 'NTVD' that mimic loop E2 of Cx26 to the AFM tip, while Cx26 two-dimensional (2D) crystals were immobilized on a mica substrate. We report the first characterization of the binding strength of the gap junction interaction. Force curves at various retraction speeds were acquired to determine the dissociation kinetics of the peptide-Cx26 interaction, while adhesion probability measurements at different contact times revealed the binding kinetics. The relatively fast intrinsic dissociation rate (k_{off}) inferred a rather dynamic inter-connexon interaction, while the slow association rate (k_{on}) probably reflects the restricted mobility and degrees of freedom of the connexons in the densely packed organization observed in native gap junction plaques and the reduced flexibility and dimensions of the extracellular loops. Our results suggest that gap junction formation may occur before plaque formation.

3062-Pos Board B167

A Stochastic Model of Voltage-Gating of Connexin-Based Gap Junction Channels Containing Fast and Slow Gates

Nerijus Paulauskas, Henrikas Pranevicius, **Feliksas Bukauskas**.

Connexins (Cxs), a family of membrane proteins, form gap junction (GJ) channels that provide a direct pathway for electrical and metabolic cell-cell interaction. Each hemichannel in the GJ channel contains fast and slow gates sensitive to transjunctional voltage (V_j). The fast gate operates between open and residual states with conductances of $\gamma_{F,o}$ and $\gamma_{F,res}$, while the slow gate operates between open ($\gamma_{S,o}$) and fully closed ($\gamma_{S,closed}$=0) states; all γs rectify but at different degree. We developed a stochastic 16-state model (S16SM), which extends earlier reported S4SM (*Paulauskas et al., 2009*) and accounts operation of four gates in series, instead of two, to describe the gating properties of homotypic and heterotypic GJ channels. Operation of each gate depends on the state of three other gates in series do to their effect on the fraction of V_j that falls across the gate (V_G) and is determined by equilibrium constants, $K_i=e^{Ai\cdot(\Pi i\cdot VG-V0)}$, where A_i characterizes the sensitivity to voltage, V_0 is the voltage for K_i=1 and Π_i is gating polarity. S16SM allows to simulate kinetics of junctional current and junctional conductance (g_j) dependence on V_j for several frequently used experimental protocols: 1) consecutive V_j steps rising in amplitude, 2) slowly rising V_j ramps, and 3) series of V_j steps of high frequency. In addition, we have developed *universal* V_j protocol simulating freely selected forms of V_j consisting of an unlimited number of consecutively combined pulses and ramps of variable durations and amplitudes. The model was used to evaluate parameters of fast and slow gates of homo- and heterotypic GJs for experimentally measured g_j-V_j dependencies under normal/control and pathological conditions. The proposed S16SM was also used to evaluate gating properties of unapposed hemichannels residing in the non-junctional plasma membrane.

Voltage-gated K Channels - Permeation

3063-Pos Board B168

Ion Conduction in a Shaker Potassium Channel Mutant Having an Unusually High Single Channel Conductance

David Naranjo, Ignacio Valencia, Cristian Moscoso, Katherine Stack, Valeria Márquez, Ariela Vergara, Marcos Sotomayor, Fernando González-Nilo.

K-channels are endowed of a highly K^+ selective pore but are very diverse in single channel conductance, ranging from 3 to 300 pS. Because the selectivity filter is so conserved among K-channels, the origin of this diversity must be searched for in other parts of the pore. We studied the single-channel behavior of the Shaker K-channel with the P475D point mutation located at its internal entrance. In 100 mM K^+ solution, this variant has a unitary conductance 8-10 fold larger than wild type (Sukhareva et al. 2003. J. Gen. Physiol. 122:541,). We did single channel recording of the variants expressed in Xenopus oocytes and molecular dynamics simulations of channels modeled by homology with the Kv1.2-Kv2.1 chimera structure (Long et al. 2007. Nature. 450:376). Single channel conductance was measured in the interval −100/+150 mV between 50-1000 mM KMES. Below 300 mM KMES, single channel currents exhibit significant inward rectification, but at 1000 mM the I-V relation is nearly symmetrical. This channel is blocked by Mg^{2+} ions in a voltage independent fashion ($z\delta$ ~zero) at 50 mM KMES, but at 1000 mM KMES, $z\delta$ approaches ~0.5. These results suggest that internal K+ ions lock in Mg^{2+} inside the pore. To test, indirectly, the physical dimensions of the channel internal entrance, we

recorded voltage ramps in the interval ±200 mV in the presence of 2 M internal sucrose. In these conditions, outward currents become voltage independent at voltages >150 mV, providing size estimates consistent with the size of the internal mouth derived from the crystallographic structure. The ion density profile obtained from molecular dynamics simulations using an applied voltage reveals a high density of K+ ions near P475D.
Funded by Conicyt 190493. IV is a Conicyt fellow

3064-Pos Board B169
Calculating Conductance and Size of the Entrance to the Inner Cavity of BK Channels with Side-Chain Replacement and a Two-Resistor Model
Yanyan Geng, Karl L. Magleby.
BK channels have the largest conductance (~250 pS) of all K+ selective channels. Previous studies suggest that residues E321/E324 in BK channels are located at the entrance to the inner cavity. We find that attachment of thiol reagents MPA and MTSET to E321C/E324C altered outward single-channel currents, suggesting that 321/324 face the ion conduction pathway. Therefore, substituting E321/E324 with different sized amino acids should change the size of the entrance to the inner cavity. We find that decreasing the size of the entrance decreases the conductance, whereas increasing the size of the entrance has little effect. Increasing [K+]i from 0.15 to 2.5 M negates differences in single-channel current associated with different side-chain volume. Plots of conductance vs. side-chain volume are approximated with a simple two-resistor model, where the ion conduction pathway is described by two resistors in series. R2 is a variable resistor, with resistance inversely proportional to the volume of the entrance to the inner cavity. R1 is a fixed resistor arising from the other parts of the conduction pathway including the selectivity filter. Fitting the data indicates that R1+R2 is ~5.4 gigaohm for glycine substitution, with an R1/R2 ratio of ~17, and effective radius and length of the entrance to the inner cavity of ~9.0 and 5.4 Å, respectively. (The volume of K+ and water are not taken into account.) The calculated size of the entrance to the inner cavity of BK channels is consistent with the crystal structure of large conductance bacterial MthK channels. These observations suggest that a large entrance to the inner cavity is required for the large conductance of BK channels, as decreasing the entrance size decreases the outward single-channel currents. Support: NIH-AR32805.

3065-Pos Board B170
Mechanism for Selectivity-Inactivation Coupling in KcsA Potassium Channels
Jason G. McCoy, Wayland Cheng, Ameer N. Thompson,
Crina M. Nimigean, Colin G. Nichols.
Potassium channels containing the GYG motif often diverge in their selectivity for monovalent cations, but the molecular basis is unknown. Using the prokaryotic potassium channel KcsA as our model, we have investigated the role of the interaction between glutamate 71 and aspartate 80, located behind the selectivity filter, in determining the selectivity of the channel as well as its influence on the conformation of the filter. In E71A KcsA channels, Na+ permeates at higher rates in both the presence and absence of K+, as seen with 86Rb+ and 22Na+ flux measurements. Single channel recordings indicate that Na+ ''punches through'' E71A KcsA channels at lower voltages than wild-type KcsA, and in the punchthrough regime the Na+-blocked current appears significantly larger. A crystal structure of E71A KcsA reveals that in contrast to what was seen for wild type KcsA, the selectivity filter does not collapse in the absence of K+, but instead assumes a ''flipped'' conformation. This flipped conformation is the same one observed in previous E71A KcsA structures in the presence of K+. The data reveal the importance of this E71-D80 interaction in both favoring inactivation and maintaining high K+ selectivity. We propose a molecular mechanism by which inactivation and K+ selectivity are linked, a mechanism that may also be at work in other channels containing the canonical GYG signature sequence.

3066-Pos Board B171
Structural Characterization of the Voltage Sensor Domain of the KvAP Channel Vectorially-Oriented within a Phospholipid Bilayer Membrane
Sanju Gupta, J. Liu, A. Tronin, J. Strzalka, J. Krepkiy, K. Swartz,
J. Kent Blasie.
Voltage-gated cation (Na^+, K^+) channels are responsible for the generation and propagation of action potentials in neurological signal transmission. Kv-channels are transmembrane proteins consisting of a homo-tetramer of 4 subunits that assemble about a 4-fold axis normal to the membrane plane to form the K^+ ion-selective pore. Each of the four subunits is comprised of six transmembrane helices, the S1-S4 helices forming the voltage-sensor domain (VSD) and the S5-S6 helices contributing to form the pore domain (PD). Despite several advances in the field, a complete understanding of the mechanism of electromechanical coupling interconverting the closed-to-open states is yet to be achieved. Positively charged arginine residues predominately in the S4 helix of the VSD are responsible for voltage sensing and the VSD's are arranged around the periphery of the PD in extensive contact with the lipid bilayer. This prompted us to focus initially on the structure of VSD itself within a phospholipid bilayer environment for the present study. A hydrated, phospholipid bilayer membrane environment has been reconstituted for the VSD of KvAP, vectorially oriented on the surface of inorganic multilayer substrates. This has been established by X-ray and neutron reflectivity (enhanced by interferometry), the latter employing a specifically deuterated phospholipid and water contrast variation, for the reconstituted membrane at both the solid-vapor and solid-liquid interfaces. This accomplishment now allows an investigation of the profile structure of the VSD within the lipid bilayer as a function of the applied transmembrane electric potential via x-ray reflectivity with millisecond time-resolution, employing high energy x-rays (> 20KeV) & pixel array detectors, and neutron reflectivity, employing selectively deuterium-labeled VSD proteins achieved via semi-synthesis. The same approach can be extended to the intact KvAP channel.

3067-Pos Board B172
KcsA Ion Affinity at an External Site Probed by Barium Block
Kene N. Piasta, Christopher Miller.
Block by Ba^{2+} is a distinctive property of K^+ channels since Ba^{2+}, a doubly charged analog for K^+, is electrostatically stabilized in the permeation pathway. Ba^{2+} block was used in BK channels as a tool to determine the equilibrium binding affinity for various ions at specific sites in the selectivity filter. In this work, we applied this approach to discrete block of single E71A KcsA channels, a non-inactivating mutant, in order to determine a thermodynamic measure of selectivity in a channel with abundant high-resolution structural information. We find at high concentrations of external K^+ the block time distribution is described by two distinct populations of Ba^{2+} block events. This argues there are at least two Ba^{2+} sites in the selectivity filter, fitting well with the published Ba^{2+} containing structure of KcsA where a Ba^{2+} ion resides approximately in S2 and S4. Utilizing a kinetic analysis of the blocking events as a function of external K^+, we determined the equilibrium dissociation constant of K^+ and other monovalent cations in an extracellular site, presumably S1, to arrive at a selectivity sequence for this particular site: Rb^+ (1 M) > K^+ (19 M) >> Na^+ (>1M). This represents an unusually high selectivity for K^+ over Na^+ with a $\Delta\Delta G^0$ of at least -7 kcal mol^{-1}. We are currently determining affinities for Li^+, NH_4^+, and Cs^+ at this site. The results fit well with other kinetic measurements of selectivity as well as with the many structures in various ionic conditions.

3068-Pos Board B173
QM/MM Modeling of Ba^{2+} Blockades in Potassium ion Channels
Christopher N. Rowley, Bogdan Lev, Sergei Noskov, Benoit Roux.
The robust selectivity of potassium channels for K^+ over Na^+ ions is a major component of the regulation of intracellular K^+ concentrations. The selectivity for K^+ was quantified through experiments measuring the Na^+ and K^+ dependence on Ba^{2+}-blockades,(1) indicating that K^+ has greater permeability by at least 150 fold. In thermodynamic terms, the relative binding free energy of Na^+ to the pore must be at least 3 kcal/mol less favorable than K^+. Na^+ vs K^+ free energy perturbation (FEP) simulations are consistent with this, although no simulations to date have modeled the actual Ba^{2+} blockade experiment. We have used MD simulations to calculate the relative binding energies of Na^+ and K^+ in the KcsA ion channel when the S4 site is occupied by Ba^{2+}. As Ba^{2+} is a strongly polarizing ion, we have used QM/MM FEP calculations using CHARMM interfaced to the deMon DFT code (2), as well as the polarizable Drude force field to correctly model the Ba^{2+}-filter interactions, with the aim of better interpreting the original selectivity experiments.

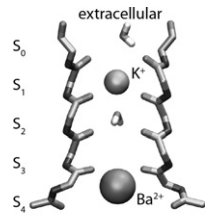

Schematic of ion binding in the selectivity filter.

1. J. Neyton, C. Miller, *J. Gen. Physiol.* 92: 549-567.
2. B. Lev et al., *J. Comp. Chem.*, 31: 1015-1023.

3069-Pos Board B174
Human *ETHER-A-Go-Go*-Related Gene (HERG) K^+ Channel Inhibition by the Antidepressant Paroxetine
Hee-Kyung Hong, **Su-Hyun Jo**.
Paroxetine is a selective serotonin reuptake inhibitor (SSRI) for psychiatric disorders that can induce QT prolongation, which may lead to *torsades de*

pointes. We studied the effects of paroxetine on human *ether-a-go-go*-related gene (hERG) channels expressed in *Xenopus* oocytes and on action potential in guinea pig ventricular myocytes. The hERG encodes the pore-forming subunits of the rapidly-activating delayed rectifier K^+ channel (I_{kr}) in the heart. Mutations in hERG reduce I_{kr} and cause type 2 long QT syndrome (LQT2), a disorder that predisposes individuals to life-threatening arrhythmias. Paroxetine induced concentration-dependent decreases in the current amplitude at the end of the voltage steps and hERG tail currents. The inhibition was concentration-dependent and time-dependent, but voltage-independent during each voltage pulse. The S6 domain mutation Y652A did not affect the drug-induced hERG current block. In guinea-pig ventricular myocytes held at 36°C, treatment with 0.4 μM paroxetine for 5 min decreased the action potential duration at 90% of repolarization (APD_{90}) by 4.3%. Our results suggest that paroxetine is a blocker of the hERG channels, providing a molecular mechanism for the arrhythmogenic side effects during the clinical administration of paroxetine.

3070-Pos Board B175

Quinidine Block of Shab K Channels: Irreversible Collapse of the K^+ conductance, and Characterization of an External Selectivity Filter K^+ binding Site

Froylan Gomez-Lagunas, Elisa Carrillo.

Quinidine is a commonly used antiarrhythmic agent and a useful tool to study ion channels. We will show that: (1) quinidine (Qd) equilibrates within seconds across the plasma membrane of Sf9 insect cells, blocking the open pore of Shab K channels from the intracellular side of the membrane in a voltage-dependent manner with 1:1 stoichiometry. (2) On binding to the channels Qd interacts with pore K^+ ions in a mutually destabilizing manner. As a result, (3) when the channels are blocked by Qd with the cell bathed in an external medium lacking K^+, the Shab conductance G_K collapses irreversibly, despite the presence of a physiological [K^+] in the intracellular solution. (4) The Qd-promoted collapse of Shab G_K resembles the collapse of Shaker G_K observed with 0 K^+ solutions on both sides of the membrane: thus the extent of G_K drop depends on the number of activating pulses applied in the presence of Qd, but it is independent of the pulse duration. Taken together the observations indicate that, as in Shaker, the Qd-promoted collapse of Shab G_K occurs during deactivation of the channels, at the end of each activating pulse, with a probability of 0.1 per pulse at −80 mV. (5) Finally, we will compare the Ki (inhibition constant) with which different external cations destabilize the binding of Qd against the potency with which the same cations inhibit the collapse of G_K, in an attempt to characterize both the selectivity of the external K^+ binding sites (s1/s2) and their role in the stability of G_K.

3071-Pos Board B176

Effect of MTS Reagents on Wildtype and *h*Kv1.3_V417C Mutant Channels and its Implications for C-Type Inactivation

Sonja I. Schmid, Stephan Grissmer.

The voltage-gated *h*Kv1.3 channel, member of the *Shaker*-related potassium channels, is involved in T-cell activation and is characterized by its typical C-type inactivation. To characterize the three-dimensional structure of the C-type inactivated state a cysteine was introduced at position 417 (*Shaker* position 467) in the *h*Kv1.3 channel and a putative involvement in C-type inactivation was determined using MTS-reagents. MTSEA application led, in contrast to wildtype channels, to a fast and irreversible current reduction through *h*Kv1.3_V417C channels in the open or inactivated state indicating that a modification of both states was possible. This modification could be prevented by verapamil. In contrast, the closed state of this mutant channel could not be modified by MTSEA. Furthermore a current reduction was observed only when the positively charged MTSET was applied intracellularly and not when applied extracellulary to *h*Kv1.3_V417C channels. These experiments indicated that the binding site for MTS-reagents is intracellular and that a modification of the cysteine at position 417 in the *h*Kv1.3_V417C mutant channel was possible in the open and also inactivated state of the channel. In addition, the fact that the inactivated state of the *h*Kv1.3_V417C mutant channel could be modified by MTSEA indicated also that the activation gate must be open during inactivation, the side chain of the cysteine at position 417 does not move during inactivation in a way that it is not available for modification any more and the channel is, using the model by Cuello et al. (2010, *Nature* **466**:203), in the open-inactivated state.

This work was supported by a grant from the Deutsche Forschungsgemeinschaft (Gr 848/14-1) and by the International Graduate School in Molecular Medicine Ulm.

3072-Pos Board B177

Discrimination Among Heteromeric Potassium Channels by Pore-Blocking Conotoxins

Rocio K. Finol-Urdaneta, Stefan Becker, Baldomero M. Olivera, Heinrich Terlau, Robert J. French.

Screening of specificity of drugs affecting K channels commonly uses homotetrameric channels assembled following expression of a single monomer. However, in many tissues, voltage-gated K currents may reflect the properties of heteromeric channels. Recently, we described a cardioprotective action of the Kv1.2-blocking conopeptide κM-RIIIK, but concluded that this was unlikely to result from an interaction with homomeric Kv1.2 channels (Chen et al., 2010, J.Biol.Chem. 285:4882). Here, we examine target discrimination, among heteromers, of the related conotoxins κM-RIIIJ and κM-RIIIK by testing their activity on 12 different Kv1.2-containing channels, each formed after expression of a single dimeric construct. Expression of homodimeric Kv1.2 yielded channels with toxin sensitivity similar to homotetramers, suggesting that dimerization, *per se*, does not affect toxin sensitivity. κM-RIIIK was most potent against Kv1.2 homotetramers and 1.2/1.7 heteromeric channels, but did not discriminate based on the order of connectivity in the latter. κM-RIIIJ was most potent against 1.1/1.2 constructs, without regard for connectivity, but showed significant discrimination based on connectivity between the two constructs for both 1.5/1.2 and 1.6/1.2 heteromers. Preliminary data for two Kunitz family conopeptides Conkunitzin-S1 and Conkunitzin-S2 suggest that each of these peptides can also discriminate among targets based on their order of connectivity. In conclusion, peptide inhibitors are able to select among heteromeric K-channel targets based on both identity of the component monomers, and on their order of connectivity. Thus, the toxins may bind across monomeric boundaries. This may account for the wide variety of selectivity "fingerprints" observed for intact cells and tissues and maybe of major relevance for the physiological action of a given peptide.

3073-Pos Board B178

Scorpion Toxins Modify C-Type Inactivation in a Mutant Potassium Channel

Azadeh Nikouee Ghadikolaei, Stephan Grissmer.

The amino acid at position 399 in the outer vestibule of *h*Kv1.3 channels (in *Shaker* 449) critically determines the C-type inactivation time course. In the present study we generated an *h*Kv1.3_H399N mutant channel with asparagines in the outer vestibule. This mutant channel showed faster inactivation and recovery time courses compared to the wild-type channel. We investigated the effect of MgTX and CTX on C-type inactivation of the mutant channel in $NMDG^+$ (K^+:4.5 mM) solutions using the whole-cell patch-clamp technique. Our results showed that the inactivation time course of the mutant channel increased around 10-fold in the presence of MgTX and 3-fold in CTX. In both cases the toxin affinity to the mutant channel is much lower compared to the wild-type channel. Other peptide toxins (NTX, AgTX2 and KTX) did not show any remarkable effects on C-type inactivation. We think that MgTX and CTX can bind to the outer vestibule of the mutant channel thereby impeding the structural changes in the outer mouth of the channel that are involved in the inactivation process. Rearrangement of the outer vestibule during C-type inactivation has been proposed earlier (Grissmer et al., 1989, *BiophysJ* **55**:203; Choi et al., 1991, *PNAS* **88**:5092; Liu et al., 1996, *Neuron* **16**:859).We conclude that C-type inactivation in voltage-gated potassium channels induce structural changes in the outer vestibule and therefore differs from the C-type inactivation in *KcsA* channels (Cuello et al., 2010, *Nature* **466**:203), which shows little changes in the outer vestibule of the *KcsA* channel.

This work was supported by a grant from the Deutsche Forschungsgemeinschaft (Gr-848/14-1).

3074-Pos Board B179

Quantification of Non-Conducting Kv2.1 Channels in Transfected HEK Cells and Cultured Hippocampal Neurons

Philip D. Fox, Robert Loftus, Emily Deutsch, Michael M. Tamkun.

Kv2.1 potassium channels retained within cell-surface clusters in transfected HEK cells are incapable of conducting potassium. Expression of GFP-tagged Kv2.1 reveals two distinct populations of channels, those retained within clusters and those freely diffusing throughout the membrane. We hypothesized that all whole-cell current is derived from non-clustered channel. The goals of our present work were to 1) determine how the number of freely diffusing Kv2.1 channels in transfected HEK cells relates to the number of channels conducting K+, and 2) compare levels of endogenous Kv2.1 and Kv current in cultured hippocampal neurons. To quantify GFP-tagged Kv2.1

expression density in HEK cells high resolution TIRF microscopy was used to measure the intensity of individual fluorescent channels. Based on individual Kv2.1 intensity the average number of freely diffusing, non-clustered channels was ~200,000/cell whereas electrophysiological recordings of peak Kv currents corresponded to ~100,000 channels (n = 11), suggesting only 50% of the non-clustered channels are conducting K+. Endogenous Kv2.1 expression in cultured E18 hippocampal neurons at 20 days in vitro (DIV) was determined by immunocytochemistry, standardized to the GFP-Kv2.1 in HEK cells, and compared to total Kv current. Average immunofluorescence corresponded to ~60,000 channels (n = 11) in DIV 20 neurons while the ratio of clustered to non-clustered channels in DIV 20 neurons was 2:1 resulting in ~20,000 non-clustered channels. Steady-state Kv current magnitude in these neurons averaged 15 nA at +60mV (n = 4). Since 60% of this outward current is Kv2.1 mediated, there are 9,000 conducting Kv2.1 channels present. Thus, less than 50% of non-clustered Kv2.1 channels in cultured neurons conduct K+. These data also suggest that the endogenous Kv2.1 channels trapped within the cell surface clusters are held in a non-conducting state as observed in HEK cells.

3075-Pos Board B180

Effects of Electric Field on Channel Proteins Through Dipole Perturbation and Network of Signal Transmission

Gamze Gursoy, Larisa Adamian, Hsiao-Mei Lu, Jie Liang.

Kv1.2 voltage-gated and MlotiK1 cyclic nucleotide-gated K+ channels belong to the family of tetrameric cation channels and share a similar protein fold in the transmembrane region. Kv1.2 channel is activated by the changes in the transmembrane potential, while MlotiK1 channel is activated upon the binding of cyclic nucleotides to its intracellular domain. We use a perturbation-based markovian transmission model [Lu and Liang,PLoS Comp. Biol. 2009] to study allosteric activation pathways in both channels. The initial perturbation on residues, e.g., ligand binding or conformational change, is converted to flow of probability, which allows studying of the time-course of signal transmission and propagation of probability flow through the protein molecule. As dipoles in channel proteins respond to the external electric field, change in energy and introduction of torque arise for individual residues. We postulate residues that experience large energy change and torque are those responding first to the membrane depolarization in ion channels. To identify regions of initial perturbation, we build structural models by embedding channel proteins in the POPC lipid bilayer, with surrounding slabs of water molecules on both sides of the membrane. Our calculations identified S1 helix of voltage sensing domain, linker, and filter regions in Kv1.2 channel, as well as helix S1 and linker in MlotiK1 channel as the regions of initial response, as they contain the majority of strongly polarizable dipoles. Our results show that dipole perturbation results in a strong signal transmittion to the charged arginine residues of S4 in Kv1.2, whereas no significant signal transmission is observed under the same perturbation for MlotiK1 channel. This suggests dipole perturbation is a mechanism how voltage gated channel proteins respond to external electric field. This mechanism, however, is not employed by ligand-gated channels.

Voltage-gated Ca Channels

3076-Pos Board B181

Cav3.1/α1G T-Type Ca^{2+} Channels are Involved in the Heart Rate Regulation

Yingxin Li, Fang Wang, Xiaoying Zhang, Zhao Qi, Christopher Szeto, Mingxin Tang, Yinzheng Guan, Xiaojie Ai, Hongyu Zhang, Jeffery D. Molkentin, Xiongwen Chen.

T-type Ca^{2+} channels (TTCCs) are expressed in cardiac pacemaker cells and conduction system of mammals. However, the role of TTCCs in heart rate (HR) generation and regulation is not well understood. In the mouse, the major TTCC expressed in the heart is Cav3.1/α1G, and therefore we used Cav3.1/α1G transgenic (TG) and knockout (KO) mice respectively to define the role of TTCC in the heart rate generation and regulation. **Methods:** Telemetric (conscious) and surface (anesthetized) ECG were used to determine the effect of isoproterenol (ISO) on the HR *invivo*. To reduce the complication of *in vivo* HR regulation, Langendorff ECG was used to measure the response of the HR to ISO. Whole cell voltage clamp was used to measure the $I_{Ca\text{-}T}$ before and after ISO application on TG myocytes. **Results:** At baseline, telemetric ECG recording showed no significant difference in HR between the Cav3.1/α1G TG mice (536.3 ± 24.8bpm vs. FVB control: 550.6 ± 15.3bpm), Cav3.1/α1G KO mice (614.4 ± 39.9bpm vs. c57/bl6 control: 603.1 ± 64.5bpm) and control mice was detected. ISO increased the HR rate in conscious mice to the same extent in both TG (41.2 ± 6.9% vs. FVB control: 34.0 ± 3.6%) and KO (22.6 ± 8.8% vs. c57/bl6 control: 22.8 ± 8.5%) mice. However, when the central regulation is depressed (anesthetized) or removed (ex-vivo Langendorff perfusion), the percentage of HR increase after ISO application were significantly enhanced in the TG mice but reduced in KO mice. Cav3.1/α1G T-type Ca^{2+} currents ($I_{Ca\text{-}T}$) in sinoatrial nodal cells was significantly increased by 43 ± 16 % by ISO. **Conclusions:** Cav3.1/α1G TTCC might not play a major role in basal HR generation but it may play an important role in sympathetic/adrenergic regulation of HR, in which PKA could be an important mediator.

3077-Pos Board B182

Cav1.3 L-Type Calcium Channels-Mediated Ryanodine Receptor Dependent Calcium Release Controls Heart Rate

Angelo Torrente, Pietro Mesirca, Patricia Neco, Martina Sinegger-Brauns, Joerg Striessnig, Joël Nargeot, Sylvain Richard, Ana Maria Gomez, Matteo E. Mangoni.

Pacemaker activity of the sino-atrial node (SAN) controls heart rate. However, the mechanism underling SAN pacemaker activity is not completely understood and in particular, the respective physiological importance of ion channels and ryanodine receptor (RyR)-dependent Ca2+ release in pacemaking is hotly debated. We have investigated Ca2+ handling in SAN pacemaker cells of wild-type (WT) and mice lacking L-type Cav1.3 (Cav1.3-/-) channels. In isolated Cav1.3-/- SAN cells the frequency of Ca2+ transients was reduced by 45% compared to WT pacemaker cells. Loss of Cav1.3 channels also blunted by about 47% the positive chronotropic effect induced by 0.01 μM isoproterenol (ISO). Furthermore, in Cav1.3-/- pacemaker cells, local Ca2+ release (LCR) occurring during the diastolic phase was reduced by 71%. In SAN cells from mice in which L-type Cav1.2 channels have been rendered insensitive to dihydropyridines (Cav1.2DHP-/-), application of 0.3 μM isradipine decreased diastolic LCR by 78 %, thus showing that Cav1.3 channels are major regulators of RyR-dependent LCR during the diastolic phase. In individual cells of isolated intact SAN, pacemaking of Cav1.3-/- cells was characterized by reduced (37%) frequency of Ca2+ transients and an increase in Ca2+ waves. Normal pacemaking in Cav1.3-/- isolated SAN cells and intact tissue could be observed only after direct activation of RyR-dependent Ca2+ release by low doses of caffeine (200 μM). Experiments with high doses of caffeine (10 mM) in Cav1.3-/- cells, showed that the reduction in diastolic LCR and in the frequency Ca2+ transients could not be ascribed to a decrease in sarcoplasmic reticulum (SR) Ca2+ content. Our results show that in SAN pacemaker cell, LCR Ca2+ release is tightly controlled by Cav1.3 channels and that such a control is critical for promoting the formation of whole-cell Ca2+ transients.

Support: FWF (P20670, P22528), ANR-06-PHYSIO-004-01.

3078-Pos Board B183

Evidence for a Role for the Cytoskeleton in Communication Between the L-Type Calcium Channel and the Mitochondria in Isolated Cardiac Myocytes

Helena M. Viola, Livia C. Hool.

Cytoskeletal proteins stabilize cell structure but also regulate subcellular distribution of mitochondria and cardiac L-type Ca^{2+} channel (LTCC) activity. We have previously demonstrated that mitochondrial function can be regulated by alterations in LTCC activity. This effect was attenuated when the cytoskeleton was disrupted with latrunculin A. To further explore this, we determined whether regulation of mitochondrial function by the LTCC is altered in a murine model of Duchenne Muscular Dystrophy(*mdx*). Mitochondrial membrane potential (Ψ_m) and metabolic activity was assessed after activation of the LTCC in cardiac myocytes isolated from C57BL/10ScSn-Dmdmdx/Arc (*mdx*) and C57BL/10ScSnArc (control) mice. Exposure of control myocytes to 10μM BayK(-) (LTCC agonist) caused a 11.4 ± 1.7% increase in Ψ_m assessed as alterations in JC-1 compared to myocytes exposed to inactive BayK(+) (n=8, $p<0.05$). The response was attenuated when myocytes were exposed to LTCC antagonist nisoldipine (n=7). However BayK(-) did not induce any significant alteration in JC-1 signal in myocytes from *mdx* mice (n=6). In control myocytes BayK(-) caused a 105.4 ± 7.4% increase in metabolic activity assessed using an MTT assay (n=8, $p<0.05$). The response was attenuated when myocytes were exposed to nisoldipine (n=8) or mitochondrial calcium uniporter inhibitor Ru360 (n=8) but unaltered when exposed to ryanodine receptor antagonist dantrolene (n=4). Exposure of *mdx* myocytes to BayK(-) did not induce any significant alteration in metabolic activity (n=8). These data confirm that alterations in LTCC activity can modulate mitochondrial function and that the cytoskeleton plays an important role in mediating this response. Since the LTCC is the initiator of contraction it has been proposed that a functional coupling between the LTCC and mitochondria may assist in meeting myocardial energy demand on a beat to beat basis.

3079-Pos Board B184

The Cardiac L-Type Ca^{2+} Channel is Downregulated by Ischemic and Pharmacological Preconditioning

Jorge A. Sanchez, German González, Daniel Zaldívar, Elba D. Carrillo, Maria C. García.

Ischemic preconditioning (IP) is a phenomenon in which briefs periods of ischemia activate endogenous mechanisms that protect cardiomyocytes from subsequent ischemia. Pharmacological Preconditioning (PPC) with mitochondrial ATP-sensitive K^+ channel (mitoK_{ATP}) openers such as diazoxide mimics IP. However, changes in Ca^{2+} homeostasis during IP and PPC, particularly in Ca^{2+} channel activity, are poorly understood. We investigated the effects of IP and PPC on cardiac L-type Ca^{2+} channels.

IP was achieved by four cycles of ischemia-reperfusion in isolated hearts**.** PPC was induced in isolated hearts and in dissociated cardiomyocytes from adult rats by preincubation withdiazoxide. We measured reactive oxygen species (ROS) production and Ca^{2+} signals associated with action potentials usingfluorescent probes. L-type currents were measured with the whole-cell patch-clamp technique. Levels of the $alpha_{1c}$ subunit of L-type channelsin the cellular membrane were measured by Western blot.

IP produced a 20% reduction in $alpha_{1c}$ subunit levels. PPC was accompanied by a 50% reduction in $alpha_{1c}$ subunit levels, and by a reversible fall in L-type current amplitude and Ca^{2+}transients. These effects were prevented by the ROS scavenger N-acetyl-L-cysteine (NAC) or by the mitoK_{ATP} channel blocker5-hydroxydecanoate (5-HD). PPC significantly reduced infarct size, an effect blocked by NAC and 5-HD. Nifedipine alsoconferred protection against infarction when applied during the reperfusion period. Downregulation of the $alpha_{1c}$ subunit andCa^{2+} channel function were prevented in part by the protease inhibitor leupeptin.

We conclude that IP andPPC downregulate the $alpha_{1c}$ subunit by a proteolytic process in which ROS are involved. This in turn leads to a reduced Ca^{2+} influx and attenuates Ca^{2+} overload during reperfusion.

Grants: CONACYT: 60880 (J.S) and 102100 (M.C.G).

3080-Pos Board B185

Expression Pattern of L-Type Calcium Channel Subunits in Human and Murine Atherosclerosis

Ann Kristin Boehnke, Margarete Odenthal, Michael Gawenda, Jan Matthes, Peter Hein, Stefan Herzig.

Cardiovascular L-type Ca^{2+}-channels (LTCC) are heteromeric protein complexes consisting of a pore-forming $Ca_v1.2$ (α_{1C}) and several auxiliary subunits. Major determinants of channel function include the composition of the heteromeric complex, but also subunit transcript regulation by splicing. This is of particular importance since splicing patterns may change under pathophysiological conditions, such as atherosclerosis. In human atherosclerosis, arterial smooth muscle $Ca_v1.2$ isoforms containing exon 21 were reported to be replaced by a single isoform containing the alternative exon 22. We have recently shown that this splice shift has major effects on LTCC: co-expressing a β_3-subunit together with α_{1C70} (containing exon 21) led to markedly reduced current density compared to α_{1C77} (containing exon 22). Co-expression of a β_2-subunit with either α_{1C70} or α_{1C77} had the opposite effect.

In the present work we sought to determine the expression pattern of LTCC subunits in both murine and human atherosclerotic arterial tissue. Murine aorta was isolated from wild-type and atherosclerotic apoE-knockout mice. Samples of human atherosclerotic arteries were obtained from patients undergoing arterial bypass surgery, and vascular smooth muscle cells were isolated by laser microdissection. qRT-PCR was used to determine LTCC subunit expression.

In murine aortic tissue we were able to detect exon 21- as well as exon 22-containing $Ca_v1.2$ subunit mRNA. Furthermore, we detected β_1-, β_2- and β_3-subunit mRNA with expression of β_1-subunits being significantly reduced in atherosclerotic aortic tissue compared to non-atherosclerotic tissue. In human atherosclerotic tissue samples, we found mRNA expression of all four β-subunits, $\beta_{1\text{-}4}$, with a trend towards β_2-subunit mRNA being more abundant than that of other β-subunit isoforms.

Given the functional impact of LTCC composition, our data support the idea that altered expression profiles of b-subunits might affect channel function in atherosclerosis.

3081-Pos Board B186

Novel Blockers of T-Type Calcium Channels Modify Gating

Pamela Bergson, Victor N. Uebele, John J. Renger, Dorothy A. Hanck.

Physiological and biophysical studies of T-type calcium channels, a subclass of voltage gated ion channels with a characteristically low voltage threshold for activation, have been hampered by a lack of selective antagonists, and no specific blockers of T-type calcium channels are currently clinically available. Several compounds have recently been identified that block calcium entry into cells expressing T-type calcium channels (Uebele et al, Cell Biochem Biophys 55:81). These compounds include an amide (TTA-A2) and a quinazolinone (TTA-Q4). We used whole cell patch clamp to examine block by these two experimental drugs in HEK 293 cells heterogeneously expressing $Ca_V3.1$. When holding potential was −110 mV, the TTAs blocked resting T-type channels with sub-micromolar affinity (ED_{50}=890nM for TTA-A2 and 560nM for TTA-Q4). Block was voltage dependent, and the affinity rose by approximately 5-fold when tested at −20 mV (ED_{50}=200nM for TTA-A2 and 130nM for TTA-Q4). Although the extent of block was voltage dependent, the kinetics were not. Neither the rate of development of block (τ=100ms for TTA-A2 and 178ms for TTA-Q4) nor the recovery from block (τ=1.2 sec for TTA-A2 and 4 sec for TTA-Q4) changed with voltage, consistent with a guarded receptor model. An examination of gating current revealed that both TTA-A2 and TTA-Q4 inhibited the movement of gating charge at depolarized potentials, without shifting the half-point of activation. These findings suggest that TTA-A2 and TTA-Q4 inhibit T-type current by restricting the movement of one or more voltage sensors, which may prevent the opening of the channel.

Support: T32HL007381 (PB), RO1HL065680.

3082-Pos Board B187

Amiloride Docking to T-Type Calcium Channels

Manuel Rivera, Osbaldo López-Charcas, Juan C. Gomora.

Amiloride and its analogues are small molecules frequently used as potassium-sparing diuretics. These drugs have been utilized for decades in the treatment of diseases like hypertension. They are known for interacting with the sodium/hydrogen antiporter, sodium/calcium exchanger, and mainly with the epithelial sodium channel (ENaC). However, amiloride has also served as a pharmacological tool for the study of T-type calcium channels. The structural basis for these interactions has not been elucidated as crystal structures of these proteins are not known yet. Nevertheless, a possible interpretation of the amiloride blocking effects is that these proteins share common structural homologies. In this work we examined the interaction of amiloride with T-type voltage-gated calcium channels (Ca_V3), whose protein structure was available by computational modeling approach. Using molecular docking software, amiloride and related molecules were docked to Ca_V3 channels model structures in order to unveil potential interaction sites. The resulting predictions were experimentally validated by assessing the effect of amiloride on Ca_V3 channels expressed in HEK-293 cells, with the use of the whole-cell patch-clamp technique. The results showed differential sensitivity of Ca_V3 family members to amiloride, being $Ca_V3.2$ the most sensitive to the diuretic. The difference with $Ca_V3.1$ and $Ca_V3.3$ was more than an order of magnitude. These results offer the possibility to propose a model of electrostatic interactions of the putative sites with members of Ca_V3 family, which interact with drugs that share a similar structure with amiloride.

Supported by CONACYT J50250Q and ICYTDF PICDS08-28.

3083-Pos Board B188

Interaction of Diltiazem with an Intracellularly Accessible Binding Site on $Ca_V1.2$

Stanislav Beyl, Waheed Shabbir, Eugen Timin, Denise Schellmann, Thomas Erker, Annette Hohaus, Gregory H. Hockerman, Steffen Hering.

Diltiazem inhibits $Ca_V1.2$ channels and is widely used in clinical practiceto treat cardiovascular diseases. Binding determinants for diltiazem are located on segments IIIS6, IVS6 and the selectivity filter of the pore forming α_1 subunit of $Ca_V1.2$. Here we elucidate the access path of Diltiazem to its binding site making use of membrane impermeable quaternary derivative qDil and mutant α_1 subunits. qDil was synthesized and applied to the intracellular side (via the patch pipette) or to the extracellular side of the membrane (by bath perfusion). qDil inhibits $Ca_V1.2$ when applied to the intracellular side of the membrane in a use-dependent manner ($59 \pm 4\%$ at 300 μM) and induced only a low level of tonic (non use-dependent) block ($16 \pm 2\%$ at 300 μM) when applied to the extracellular side of the membrane. Mutations in IIIS6 and IVS6 reduced sensitivity to intracellularly applied qDil.Our study demonstrates intracellular access of quaternary diltiazem and its interaction with previously identified determinants of BTZ binding pocket. Recovery from block by diltiazem was found to be voltage independent, which is in contrast with the pronounced voltage dependent recovery from block by phenylalkylamines.

3084-Pos Board B189

Thermodynamic Linkage with Voltage Sensing Explains the Large Variability of Inactivation in L-Type Ca Channels with γ1 Subunit

Anna Angelova, **Roman Shirokov**.

The voltage-dependence of steady-state inactivation (a.k.a. the inactivation curve) is an important determinant of functional availability of calcium channels. Some experimental and pathological conditions change the half-inactivation voltage ($V_{1/2}$) but not the slope of the inactivation curve. We observed that the $V_{1/2}$ varies from cell to cell by as much as 40 mV when $Ca_V1.2$ channels are co-expressed with γ1 subunit in tsA-201 cells. This parallel shift cannot be explained by a simple mixing of channels with different $V_{1/2}$ values (e.g., with and without the γ1).

We found that the γ1 subunit had a relatively small effect on inactivation assessed at the level of gating currents. It caused the voltage-dependence of the intramembrane charge movement in inactivated channels to shift by about −10 mV, and this effect did not vary from cell to cell. Therefore, the large shift of the inactivation curve seen at the level of ionic currents appears to be unrelated to the small changes observed at the level of the voltage sensor for activation/inactivation gating. We explain this paradox in the framework of a minimal four-state model of inactivation, in which the $V_{1/2}$ parameter of the inactivation curve is determined by both the voltage-dependence of gating currents and the maximal extent (efficacy) of inactivation. The parallel shift of the inactivation curve may result solely from a change in the efficacy.

Therefore, we propose that functional availability of $Ca_V1.2$ channels with the γ1 subunit is controlled by a cell-specific molecular modification that affects similarly all channels in a particular cell. This modification primarily alters the efficacy of inactivation and, thus, leads to large changes of the availability of channels to activate.

Supported by NIH R01MH079406.

3085-Pos Board B190

Physicochemical Properties of Pore Residues Predict Activation Gating of Cav1.2: A Correlation Mutation Analysis

Katrin Depil, Stanislav Beyl, Annette Hohaus, Anna Stary-Weinzinger, Eugen Timin, Waheed Shabbir, Michaela Kudrnac, Steffen Hering.

Mutations of gating sensitive amino acids in pore-forming S6 segments may transform a high-voltage-activated into a low-voltage-activated calcium channel. Resulting disturbances in calcium entry can cause channelopathies. Here we analyze the role of physico-chemical properties of residues in the 'bundle-crossing-region' of helices IS6, IIS6 and IIIS6 in activation gating of Cav1.2. Gating sensitive L434, I781 and G1193 were substituted by residues of different size, hydrophobicity and polarity. Descriptors characterizing the various amino acid properties were calculated using the software package MOE or taken from literature. Most mutations induced leftward shifts of the activation curves and decelerated current activation and deactivation suggesting a destabilization of the closed and a stabilization of the open channel state. A selection of 17 physico-chemical parameters (descriptors) was calculated for these residues and examined for correlation with the shifts of the midpoints of the activation curve (V_{act}). V_{act} correlated with local side chain flexibility in position L434 (IS6), with the polar accessible surface area of the side chain in position G1193 (IIIS6) and with hydrophobicity in position I781 (IIS6). Combined descriptor analysis for positions I781 and G1193 revealed that additional amino acid properties may contribute to conformational changes during the gating process. The identified physicochemical properties in the analyzed gating sensitive positions predict the shifts of the activation curves of $Ca_V1.2$. Correlation analysis emerges as a useful tool to identify the impact of the different properties of amino acids on channel gating.

3086-Pos Board B191

Mutational Analysis in the Bundle Crossing Region Guides the Design of Cav1.2 Homology Models

Anna Weinzinger, Katrin Depil, Stanislav Beyl, Eugen Timin, Steffen Hering.

In continuation of our previous work (Stary et al. 2007, Beyl et al. 2010) we have analyzed the functional role of gating determinants in the bundle crossing region of Cav1.2. G432 (IS6), A780 (IIS6), G1193 (previous data, IIIS6) and A1503 (IVS6) were substituted with residues of different physicochemical properties. This 'G/A/G/A' motif was identified in a conservation analysis showing that Cav, Nav, TRP and many K channels contain glycines or alanines in equivalent positions. Most 'G/A/G/A' mutations shifted the activation curve in the hyperpolarizing direction, suggesting a destabilization of the closed and a stabilization of the open channel state. Mutations G432A/V, G1193A and A1503V did, however, stabilize the closed channel conformation as evident from rightward shifts of the activation curves. A comparison with the closed KcsA structure revealed that the 'G/A/G/A' motif ('A/A/A/A' in KcsA) is located at the narrowest point of the interface between two S6 (M2) helices, tightly packed in a hydrophobic environment. Our analysis suggests that size and hydrophobicity might be important for channel gating. We found that mutations to methionine or tryptophan either destabilize the closed channel or result in non-conducting channels. Small hydrophobic residues like alanine or valine stabilize the resting state. A comparison between resting and open state KcsA structures indicates that the 'G/A/G/A' motif and surrounding residues in Cav1.2 undergo large conformational changes upon gating, resulting in a displacement of more than 7 Å.

1 Stary, A., Shafrir, Y., Hering, S., Wolschann, P., Guy, H.R. (2007) Channels 2 (3), 210-215.

2 Beyl, S., Depil, K., Hohaus, A., Stary-Weinzinger, A., Timin, E., Shabbir, W., Kudrnac, M., Hering, S. (2010) Pflugers Arch, in press.

3087-Pos Board B192

Modulating Recovery of N-Type Calcium Channels from Voltage-Dependent Inactivation: A Novel PKC-Independent Effect of Phorbol Esters

Lei Zhu, Sarah M. McDavid, **Kevin P.M. Currie**.

N-type voltage-gated calcium channels play key roles in many cellular functions including the regulation of neurotransmitter and hormone release. Ca^{2+} influx through these channels is tightly regulated by second messenger pathways and intrinsic channel properties including voltage-dependent and calcium-dependent inactivation. Less is known about the recovery of calcium channels following inactivation, or if the kinetics of recovery can be modulated by signaling pathways. Recombinant N-type channels ($Ca_V2.2$ (α_{1B}), $\alpha_2\delta$, and β_{1b}) were expressed in HEK293 cells and barium used as the charge carrier to isolate voltage-dependent inactivation. An individual step depolarization lasting 1-10s, or trains of brief step depolarizations were used to produce inactivation, and recovery was tracked using brief steps at given intervals following the stimulus. Following ''short'' (<2s) stimuli, recovery was clearly biphasic, but the faster component became minimal after longer duration stimuli (>10s). Acute application of the phorbol ester PMA (50-200nM) had little effect on the resting amplitude of I_{Ba} or inactivation during 5-50Hz stimulus trains. However, the slower time constant of I_{Ba} recovery was significantly prolonged by PMA. This action of PMA was not blocked by inhibitors of PKC that target the catalytic domain of the enzyme (bisindolylmaleimide I, Go6983, PKC inhibitory peptide 19-36), but was blocked by calphostin-C which targets the diacylglycerol binding C1 domain of PKC and other proteins. Intracellular dialysis with GDP-β-S also blocked the actions of PMA on recovery from inactivation. PMA had a similar effect on endogenous I_{Ca} recorded from bovine adrenal chromaffin cells. Our data identify a novel PKC-independent mechanism by which PMA (and perhaps diacylglycerol signaling) modulates the availability of N-type calcium channels during sustained or repetitive activity.

Supported by NIH/NINDS (NS052446) and VUMC Discovery grant.

3088-Pos Board B193

Competition of Ca_Vβ-Subunits for Cardiac L-Type Calcium Channels

Wanchana Jangsangthong, Elza Kuzminkina, Stefan Herzig.

Cardiac L-type Ca^{2+} channels are composed of a $Ca_V1.2$ pore-forming subunit and auxiliary $Ca_V\beta$- and $Ca_V\alpha_2\delta$- subunits. $Ca_V\beta$-subunits are independently involved in chaperoning of channels to the plasma membrane and modulation of channel gating. Here, we investigated whether and how competitive replacement of different $Ca_V\beta$-subunit isoforms affects gating properties of $Ca_V1.2$. We studied competition between a $Ca_V\beta_{1a}$-subunit conferring rather low open probability, and a strongly activating $Ca_V\beta_{2b}$-subunit. Patch-clamp measurements were performed on recombinant human cardiac L-type Ca^{2+} channels expressed in HEK293 cells.

In whole-cell competition experiments, we found that higher amount of $Ca_V\beta_{1a}$-subunits in relation to $Ca_V\beta_{2b}$-subunits resulted in faster inactivation of $Ca_V1.2$ channels. Moreover, the voltage dependence of the steady-state inactivation was shifted to more negative potentials.

Inspection of single-channel recordings suggested that channel gating switched between low-$P_{(O)}$ and high-$P_{(O)}$ modes on a minute time-scale. To provide statistical evidence for this gating switch, we used a custom-made software segmenting data based on clusters of similar channel activity. To exclude that temporal clustering of high and low channel activity is an artifact, we repeatedly analyzed the data after randomly reordering the originally recorded traces. We found that with either $Ca_V\beta_{1a}$- or $Ca_V\beta_{2b}$-subunits alone, channels stayed predominantly in the low-$P_{(O)}$ or high-$P_{(O)}$ modes, respectively. Expressing

both, $Ca_V\beta_{1a}$- and $Ca_V\beta_{2b}$-subunits, fraction of low-$P_{(O)}$ mode periods increased when more $Ca_V\beta_{1a}$-subunits in relation to $Ca_V\beta_{2b}$-subunits were expressed. As expected, when recordings were split into low-$P_{(O)}$ ($Ca_V\beta_{1a}$-like) and high-$P_{(O)}$ ($Ca_V\beta_{2b}$-like) periods, the extent of inactivation was higher for the low-$P_{(O)}$ ($Ca_V\beta_{1a}$-like) mode.

Our results illustrate a functionally effective competition between $Ca_V\beta$-subunits, suggesting that in cells that express different $Ca_V\beta$ isoforms, activity of a given channel can be dynamically regulated.

3089-Pos Board B194

Biophysical Properties of a Human Disease-Causing Mutation in $Ca_V1.3$ L-Type Calcium Channels

Andreas Lieb, Shahid M. Baig, Mathias Gebhart, Claudia Dafinger, Jutta Engel, Martina J. Sinnegger-Brauns, Matteo E. Mangoni, Habib U. Khan, Peter Nürnberg, Hanno J. Bolz, Alexandra Koschak, Jörg Striessnig.

Mice lacking functional $Ca_v1.3$ L-type Ca^{2+}-channels show sinoatrial node dysfunction and are congenitally deaf. Here we investigated the functional consequences of a homozygote mutation (insertion of an amino acid residue in a pore-forming S6-helix) in the alpha1-subunit encoding the CACNA1D gene which causes bradycardia and deafness in humans.

We expressed human wildtype (WT) and mutant channel complexes (MUT) in tsA-201 cells (with $alpha_2delta$ and $beta_3$-subunits) and recorded ON-gating (Q_{on}) and ionic Ca^{2+}-currents (I_{Ca}) using the whole-cell patch-clamp technique. Full length WT and MUT channel alpha1 subunit proteins were expressed at equal levels in tsA-201 membranes. In contrast to WT, MUT channels did not conduct significant I_{Ca}, but gave clear rise to Q_{on}. WT and MUT Q_{on} exhibited a typical nonlinear voltage-dependence of activation. Under identical experimental conditions (block of I_{Ca} by replacing Ca^{2+} with Mg^{2+} and addition of La^{3+} and Cd^{2+} in the recording solution) the half maximal activation voltage (V_h) of MUT Q_{on} was significantly shifted by 16.2 ± 2.8 mV (n=6-8, $p<0.0001$) to more negative voltages compared to WT. Inward I_{Ca} of WT activated 11.5 ± 2.9 mV more positive than WT Q_{on} (n=7-8; p=0.0016). In addition, MUT Q_{on} kinetics were significantly faster than for WT evident e.g. as shorter time constants for gating current decay over a large voltage range (-10 to $+50$ mV).

The presence of charge movement in the absence of ionic currents implies that voltage-sensors in MUT channels move, but either fail to trigger pore opening or prevent conduction through opened channels. The mutation is not located within voltage-sensing S4-helices, but within a region of S6 predicted to interact with the voltage-sensor. Compromising this functional module may uncouple voltage-sensor function from pore opening and allow voltage-sensor movements to occur faster and at more negative voltages.

3090-Pos Board B195

Role of the Putative Glycines Hinge of Cav3.3 Channels

Ricardo K. Sepúlveda-Hirose, Juan M. Arias-Montaño, Clara E. Díaz-Velásquez, Manuel Rivera, Juan C. Gomora.

Voltage-gated ion channels (VGIC) are proteins that form transmembrane pores in cell membranes. Based on the crystal structure of an open potassium channel (K_V) that reveals the bending of a glycine residue in the inner helix that lines the pore (M2 or S6), and the conserved pore sequences in many members of the VGIC superfamily, is thought that the opening mechanism might be quite similar within the family. In fact, this has been demonstrated for a bacterial sodium channel (Na_V). However, in LVA calcium channels, the mid-S6 hinge glycine residue is present only in IS6 and IIS6, suggesting a likely different opening mechanism. Here, we explored this possibility in the $Ca_V3.3$ member of LVA channels by performing a mutational analysis of the two conserved glycines (Gly385 and Gly814), and a valine (Val1383) in IIIS6 which, according to sequence similarity, corresponds to a hinge glycine in K_V and Na_V channels. Substitution of Gly814 for proline (G814P) or alanine (G814A), as well as the mutant V1383G, drastically decreased whole-cell current density, with discrete effects on the voltage-dependence of activation. However, the mutant G814P displayed a 10 mV shift in the steady-state inactivation curve to hyperpolarized potentials; the current inactivation kinetics was slowed down by 50%, and the recovery was also more than two-fold slower. The substitution by proline also increased the channel closing time constant by 60%; this effect was also displayed by mutant V1383G, which in addition induced the strongest effect on the inactivation kinetics slowing ($\geq$ 2-fold). Our preliminary results suggest that residues Gly814 and Val1383 are mostly involved in the inactivation gating and, in a lesser degree, stabilizing the open state of $Ca_V3.3$. Additional mutations, including double and triple substitutions, are currently under investigation.

Supported by CONACYT México J50250Q.

3091-Pos Board B196

Mechanical Induced Inhibition of L-Type Calcium Channels

Angelo O. Rosa, Naohiro Yamaguchi, Martin Morad.

L-type calcium channels are modulated in different fashions by Ca2+ (Ca2+ dependent inactivation, Ca2+ dependent facilitation), cytosolic proteins (CAM, CAMKII, PKA, PKC, etc) and voltage (voltage dependent inactivation). Here we describe a novel modulation of Ca2+ channel exerted by pressure/flow (PF) forces where 35-60% inhibition of IBa occurs when cells were exposed to 30 cm of PF forces. Only brief periods (300ms) of high PF applications were required to activate the response, but the effect was reversible and had a latency of ~500-700 ms. Similar data was obtained in HEK cells expressing all the recombinant subunits of Ca2+ channel. To determine the mechanism underlying the PF effect, the current through the channel was measured in cells treated with 10μM of thapsigargin, or IP3R blocker APB-2 (10μM), or mitochondrial protonophore, FCCP + oligomycin, or high concentrations of BAPTA. We found no significant difference in effectiveness of PF pulses to inhibit IBa, or ICa in cell exposed to, thapsigargin, APB-2, FCCP, BAPTA or a mixed cocktail of them. We concluded that native Ca2+ channel of rat ventricle myocytes or recombinant human variants of L-type Ca2+ expressed in HEK cells can be modulated by PF forces. This mechanism may represent a different physiological regulation of calcium channels in the heart and blood vessels.

3092-Pos Board B197

A Model of the Inner Pore of Ca Channels in the Open State

Gregory M. Lipkind, Harry A. Fozzard.

Known open state structures of K channels do not provide a useful template for open Ca channels, because the latter do not contain the hinge residues Gly and Pro. We, therefore, began with the closed KcsA structure (Doyle et al, Science 280:69, 1998) and sequentially outwardly displaced amino acids near the bundle crossing (Thr107-Ala111) and optimized the structures (restrained minimization with distance constraints). We then populated open channel structures with amino acid residues of T and P/Q channels and re-optimized. The Ca channel structures with openings of ~11 Å were similar and allowed both symmetrical TEA and verapamil to enter and block from inside. However, simulations were in disagreement with the MTSET accessibility data for the P/Q channel (Zhen et al, JGP 126:193, 2005). Noting that amino acid residues near C-terminal ends of S6 helices of Ca channels have side chains facing the inner pore that are quite different from those in K channels, we speculated that these segments might contain intra-molecular deformations that lead to the reorientation of their side chains. We modeled these deformations by π-bulges, which produced wide turns, containing an additional amino acid residue. The very conserved Asn residues of Ca channels initiated the formation of π-bulges in the direction of the C-ends in all 4 S6 α-helices. Introduction of π-bulges achieved agreement between amino acid residues predicted to face the pore and MTSET accessibility data. Formation of π-bulges would be expected to stabilize the open state of the Ca channel, and MTSET modification of single cysteines at the C-ends of S6's could produce physical occlusion of the inner pore, i.e. full block of Ca current as observed experimentally. Supported by RO1HL065680.

3093-Pos Board B198

Signaling Complex of Calcium/Calmodulin-Dependent Protein Kinase II Associated with the C-Terminal Domain of $Ca_V2.1$ Channels

Venkat G. Magupalli, Xin Jiang, Ruth E. Westenbroek, Todd Scheuer, Thomas R. Soderling, Angus C. Nairn, William A. Catterall.

Abstract:

Ca^{+2}/calmodulin-dependent protein kinase II (CaMKII) forms a major component of postsynaptic density, where its functions are well established but the presynaptic actions of CaMKII are poorly defined. We show that CaMKII constitutively binds and modulates presynaptic voltage-gated calcium ($Ca_v2.1$) channels that conduct P/Q type calcium currents. Using co-immunoprecipitation methods, we isolated a signaling complex of $Ca_v2.1$ with bound CaMKII. The pore-forming $_1$ subunit of $Ca_v2.1$ channels offers a unique platform for association of CaMKII at the C-terminal domain. The $Ca_v2.1$/CaMKII signaling complex operates as a network of multiprotein machines by recruiting other protein components and processing information by a series of protein interactions and protein phosphorylation reactions. Using GST pulldown assays we dissected the preferential binding of the inactive kinase to the $Ca_v2.1$ channel and mapped the binding site. Binding of CaMKII at this site *per se* is sufficient to slow voltage-dependent inactivation and shift the voltage dependence of inactivation to more positive membrane potentials, thereby greatly enhancing $Ca_v2.1$ channel activity. Using transfection assays, we show that the bound kinase is autophosphorylated at Thr286 and phosphorylates synapsin 1. We observed more than a six-fold increase in the synapsin 1

phosphorylation by CaMKII bound to the C-terminal domain $Ca_v2.1$ channel. Synapsin phosphorylation at Ser603 by CaMKII leads to formation of stable higher order oligomers. Our studies reveal a signaling complex of $Ca_v2.1$/CaMKII at the C-terminal domain of the $Ca_v2.1$ channel. Association of CaMKII with this signaling complex generates rapid response to calcium entry, recruitment of protein components, and phosphorylation of nearby proteins. Hence, kinase couples calcium influx to the downstream pathways for rapid, localized signal transduction and regulation.
Supported by R01 NS22625

3094-Pos Board B199

Targeting of Protein Phosphatases PP2A and PP2B to the C Terminus of L-Type Calcium Channel $Ca_V1.2$

Hui Xu, **Kenneth Ginsburg**, Duane Hall, Maike Zimmermann, Mingxu Zhang, Samvit Tandan, Joseph Hill, Mary Horne, Donald M. Bers, Johannes Hell.

The L-type Ca^{2+} channel $Ca_V1.2$ lies within a macromolecular complex including β_2- adrenergic receptor, trimeric G_S protein, adenylyl cyclase, and cAMP-dependent protein kinase (PKA). This complex mediates highly spatially and temporally regulated signaling, both acute (cardiac excitation contraction coupling, synaptic transmission, neurosecretion) and long-term (gene expression). Protein phosphatases PP2A (PPP2CA) and PP2B (PPP3CA; calcineurin) are also constitutive complex members. Acutely, either phosphatase counteracts PKA-dependent increase in Ca current by PKA. We here report that PP2A binds independently to two separate specific regions in the C-terminus of the central pore-forming α_1 subunit of $Ca_V1.2$: one region spans residues 1795-1818 and the other residues 1965-1971. PP2B binds independently to a distinct region immediately downstream of residue 1971. To determine the binding regions for these phosphatases we assayed their ability to bind α_1 C-terminal fragments with appropriate subregions cleaved. Further, we assayed a pallette of small peptides and identified those able to compete with PP2A and PP2B binding in pull-down assays. With these interfering peptides, we investigated PP2A and PP2B function, assayed by recording I_{Ca}(L) in acutely isolated rabbit cardiomyocytes. Using whole-cell β-escin perforated patch, which allowed pipette introduction of peptides while limiting rundown, we found that the PP2B competing peptide increased both basal and isoproterenol-stimulated I_{Ca}(L), while a PP2A competing peptide had no effect vs a control peptide or no peptide. Together, the biochemical and electrophysiological results suggest that while PP2A and PP2B are anchored at their respective binding sites on cardiac $Ca_V1.2$ α_1 and negatively regulate I_{Ca}(L) (in this case by counterbalancing PKA-mediated phosphorylation), a fine dynamic balance between phosphorylation and dephosphorylation responses exists. This would be important to the ability of I_{Ca}(L) flux to efficiently regulate end effects.

3095-Pos Board B200

Departure of Calmodulin from the IQ Domain of $Ca_V1.3$ Channels During Calcium-Dependent Inactivation

Hojjat Bazzazi, Manu Ben Johnny, David T. Yue.

Studies of calmodulin (CaM) regulation of Ca_V channels have long focused on an IQ domain in the carboxy-terminus of channels. Strong evidence indicates that Ca^{2+}-free CaM (apoCaM) preassociates with the IQ domain before Ca^{2+} entry through channels (e.g., Liu *et al*Nature **463**:968), and that Ca^{2+}/CaM has the potential to bind the IQ. Hence, Ca^{2+}-dependent inactivation (CDI) of channels has been proposed to result from Ca^{2+}-dependent conformational changes of CaM, all while bound to the IQ. Yet, analysis of Ca^{2+}/CaM complexed with the IQ domain of $Ca_V2.1$ (Structure **16**:607) hints that Ca^{2+}/CaM *departs* from the IQ domain during channel regulation. To generalize this hypothesis, we here alanine scanned the entire IQ domain of $Ca_V1.3$, a prototype channel homologous to long-studied $Ca_V1.2$. Surprisingly, CDI was strongly diminished at only three residues: the signature isoleucine (I[0]), an alanine situated four residues upstream (A[-4]), and a downstream phenylalanine (F[4]). How do these mutations decrease CDI? If CDI were suppressed by inhibiting Ca^{2+}/CaM binding to an IQ effector site, then Ca^{2+}/CaM binding to this domain should exhibit commensurate disruption. However, FRET two-hybrid assays indicated no such decrease in binding. Alternatively, mutations could attenuate CDI by inhibiting apoCaM preassociation with the channel. Indeed, binding assays revealed strong mutational effects on apoCaM interaction with the IQ domain, consistent with the observed CDI deficits. Indeed, overexpression of wild-type CaM largely restored CDI of mutant channels, fitting with recovery of apoCaM preassociation via mass action. Thus, while the IQ domain appears to be important as a preassociation locus for apoCaM, CDI is likely triggered by the departure of Ca^{2+}/CaM to interact with effector sites elsewhere on the channel (Ben Johny, Yang, and Yue, this meeting). This departure would fundamentally transform our understanding of CaM/channel regulation.

3096-Pos Board B201

An Improved Model of Voltage- and Ca-Dependent Inactivation of the L-Type Ca Channels

Stefano Morotti, Eleonora Grandi, Aurora Summa, Kenneth Ginsburg, Stefano Severi, Donald M. Bers.

The L-type Ca^{2+} current (I_{Ca}) contributes to the action potential plateau and initiates excitation-contraction coupling in cardiac myocytes. Here we present a kinetic model of L-type Ca^{2+} channels (LTCCs), based on the Mahajan et al. 7-state Markov model, incorporated into the Shannon et al. model of the rabbit ventricular myocyte, which includes a subcellular restricted space where Ca^{2+}-induced Ca^{2+} release occurs. LTCC inactivation is both voltage- and Ca^{2+}-dependent (VDI and CDI), the latter being due to Ca^{2+} binding to calmodulin that is pre-bound to the LTCC. To discriminate between these mechanisms, existing experimental data from our group and others were used. First, we implemented a model for I_{Ba} accounting for both divalent cation- and V-DI. This was based on the evidence that complete substitution of Ba^{2+} for Ca^{2+} reduces, but does not abolish, ion-dependent inactivation. The model was constrained to recapitulate a wide set of experimental data including steady-state and kinetics of activation, inactivation and recovery from inactivation. Next, we tuned the model, by adjusting the ion-dependent transitions rates only, to reproduce experimental I_{Ca} measured when sarcoplasmic reticulum (SR) Ca^{2+} release is abolished (by exogenous buffers or SR Ca^{2+} depletion) or during physiological Ca^{2+} transients (when SR Ca release amplifies Ca^{2+} influx). Finally, we validated the I_{Ca} model against action potential clamp data obtained with and without Ca^{2+} transients. Our model provides an important tool to dissect relative contributions of different Ca^{2+} sources (SR vs. LTCCs) to total CDI, and the relative roles of CDI and VDI in normal function and pathophysiology (e.g., to analyze I_{Ca} kinetics during normal and diseased action potentials and its contribution to arrhythmogenesis).

3097-Pos Board B202

RyR(R4496C) Mutant Mice Model Reveals a New Paradigm on Local Ca^{2+} Control of I_{CaL}

Maria Fernandez-Velasco, Gema Ruiz-Hurtado, Angelica Rueda, Patricia Neco, Carlo Napolitano, Silvia G. Priori, Sylvain Richard, **Ana M. Gomez**, Jean-Pierre Benitah.

The Ca^{2+}-dependent inactivation (CDI) of the widely distributed L-type Ca^{2+} channels is a major intrinsic feedback mechanism for Ca^{2+} homeostasis. CDI manifests by the time-dependent current decay during prolonged depolarization but also the voltage-dependent availability of Ca^{2+} channel during double-pulse protocols. Whereas the first one has received most of the attention cumulating with the identification of calmodulin (CaM) as an important Ca^{2+} sensor that mediates CDI, the latter has not received extensive investigation. Here we evidence that Ca^{2+} sparks control L-type Ca^{2+} current (I_{CaL}) availability in cardiomyocytes and consequently the steady-state window current. Comparing RyR^{R4496C} catecholaminergic polymorphic ventricular tachycardia (CPVT) mutant mice to wild type (WT) littermates, we show that whereas peak density of I_{CaL} and global $[Ca^{2+}]_i$ transient are not modified, $RyR2^{R4496C}$ myocytes demonstrated a significantly lower I_{CaL} density at −30 and −20 mV. This decrease is the consequence of a depolarizing shift in steady-state activation and a hyperpolarizing shift of steady-state inactivation that result in a decreased window current. These differences are eliminated in presence of fast the Ca^{2+} buffer BAPTA and by depleting the sarcoplasmic reticulum (SR) with thapsigargin, pointing out to a local control by the observed increase in Ca^{2+} spark occurrence at low voltages in CPVT mice. Somewhat surprisingly, CaM antagonists did not have any effect on CPVT cells but altered the inactivation and activation curves in the WT cells to make these similar to the CPVT. Our data echo the retrograde coupling of RyR and L-type Ca^{2+} channel observed in skeletal muscle, representing a novel mechanism to counteract excessive SR Ca^{2+} leak and to preserve CPVT mice from arrhythmic trigger activity such as early afterdepolarization due to enhancement of I_{CaL} window current.

3098-Pos Board B203

Glucose Inhibits Glucagon Secretion from Pancreatic Alpha-Cells by Closure of K_{ATP}-Channels

Quan Zhang, Reshma Ramracheya, Orit Braha, **Patrik Rorsman**.

Glucose inhibits glucagon secretion but the mechanisms involved are not known. We performed whole-cell perforated patch membrane potential recordings on alpha-cells in intact mouse pancreatic islets. Alpha-cells are electrically active at low glucose concentrations (<1 mM) and generate overshooting action potentials that peak at +10 mV. These action potentials result from activation of voltage-gated Na^++ and A-type K^+-channels. The most negative interspike membrane potential is approx. −45 mV. Application of 6 mM glucose reversibly depolarized the alpha-cell by approx. 5 mV and reduced peak voltage of the action potentials by up to 15 mV. We estimated the impact

this decrease in action potential amplitude on alpha-cell exocytosis by capacitance measurements of depolarization-evoked exocytosis. We found that exocytosis is reduced by approx. 7% for every mV reduction of spike height. Thus, the glucose-induced reduction of spike height is sufficient to account for the 70-80% inhibition of glucagon secretion measured biochemically. We also measured alpha-cell electrical activity elicited by current injection and found that small depolarizations above the normal interspike voltage mimic the effects of glucose on action potential height. In parallel measurements of glucagon secretion, the inhibitory effect of glucose could be mimicked by tolbutamide (a blocker of K_{ATP}-channels) and antagonized by diazoxide (an activator of K_{ATP}-channels). We conclude that glucose inhibition of glucagon secretion involves closure of plasmalemmal K_{ATP}-channels. The resulting membrane depolarization leads to voltage-dependent inactivation of the ion channels involved in action potential firing and a lowered action potential amplitude. This culminates in reduced activation of the N-type Ca^{2+}-channels mediating the Ca^{2+} entry required to trigger exocytosis of the glucagon-containing secretory vesicles. Thus, alpha-cells provide an example where reduced K^+-conductance is associated with lowered rather than increased (as seen in most other cell types) membrane excitability.

Channel Regulation & Modulation II

3099-Pos Board B204

Tmem16a Ca^{2+} Activated Chloride Channels in Sensory Neurons can Discriminate between Different Intracellular Ca^{2+} Sources

Xin Jin, Hailin Zhang, **Nikita Gamper**.

Proteins of Tmem16 (anoctamin) family are the candidate subunits for Ca^{2+}-activated Cl^- channels (CaCC). Both Tmem16a expression and CaCC currents were reported in small (predominantly nociceptive) sensory neurons from dorsal root ganglia (DRG). In contrast to CNS neurons, nociceptors accumulate high intracellular Cl^- concentration and thus activation of CaCC in these neurons was shown to be excitatory and to contribute to the inflammatory nociceptive responses. We show that CaCC in nociceptors is activated by the release of Ca^{2+} from the IP3-sensitive intracellular stores in response to bradykinin (BK; 44/47 responsive neurons) or proteases (through PAR-2 receptors; 8/12 responsive neurons). This current was attenuated by 48% by siRNA knock-down of the Tmem16a (n=7). Interestingly, while in the majority of small DRG neurons CACC was induced by Ca^{2+} release from the stores, only in 12/58 neurons CaCC was activated by the Ca^{2+} influx through the voltage-gated Ca^{2+} channels triggered by the voltage pulse. Chelating intracellular Ca^{2+} with the slow Ca^{2+} buffer EGTA did not affect CaCC activation by PAR2-AP (5/7 responsive neurons) while the fast buffer BAPTA abolished such activation (1/9 responsive neurons) suggesting a close proximity of the Ca^{2+} release sites and CaCC. Acute treatment of DRG neurons with lipid raft disrupting agent methyl-beta-cyclodextrin (MBCD) partially restored coupling of CaCC to VGCC but disrupted coupling with the intracellular stores. Thus, after the MBCD treatment activation of VGCC by voltage pulse induced -106.5 ± 51.4 pA CaCC currents in 17/25 neurons while BK and PAR2-AP failed to induce measurable CaCC in 4 and 8 tested neurons respectively (PAR2-AP induced -100 ± 20 pA CaCC in 9/13 MBCD-untreated neurons). Or data suggest that Tmem16a/CaCC channels in small DRG neurons are functionally coupled to the IP3-sensitive Ca^{2+} stores.

3100-Pos Board B205

Cardiac Background Potassium Channels Change ion Selectivity and Conduct Inward Leak Sodium Currents in Hypokalemia

Liqun Ma, Xuexing Zhang, **Haijun Chen**.

Hypokalemia refers to lower-than-normal blood potassium (K^+) levels, which often result in cardiac arrhythmias. In lowered extracellular K^+ concentrations ($[K^+]_o$) under hypokalemia, the resting membrane potential of human cardiomyocytes can paradoxically depolarize inconsistent with the Nernst equation. Such a well-known paradoxical depolarization is the key to understanding thepathological mechanism of hypokalemia-induced cardiac arrhythmias. An inward leak sodium (Na^+) current was implied to cause cardiac paradoxical depolarization, but its molecular mechanism is not yet understood. Background K^+ channels primarily maintain normal cardiac resting membrane potentials at around -80 mV, close to the K^+ equilibrium potential. A fundamental characteristic of K^+ channels, the ion selectivity, is generally considered to be static and independent of physiological regulation. None of over 80 mammalian K^+ channels shows dynamic ion selectivity in response to physiological or pathological stimuli, but several voltage-gated K^+ channels conduct Na^+ currents in the absence of intracellular K^+, implying that the selectivity filter of K^+ channels can be dynamic. Here we show that 1) a cardiac background K^+ channel exhibits dynamic ion selectivity, becomes permeable to Na^+, and conducts inward leak Na^+ currents in hypokalemia or lowered $[K^+]_o$; 2) a specific residue within the selectivity filter determines dynamic ion selectivity of the K^+ channels; 3) in lowered $[K^+]_o$, over-expression of the K^+ channels results in acquired paradoxical depolarization in mouse HL-1 cardiomyocytes and inhibits hyperpolarization in rat primary hippocampal neurons, and knockdown of the K^+ channels eliminates paradoxical depolarization in human primary cardiomyocytes. These findings demonstrate that ion selectivity of the K^+ channels is regulated by a pathological stimulus, elucidate a molecular basis of inward leak Na^+ currents that may contribute to hypokalemia-induced cardiac paradoxical depolarization, and indicate a novel mechanism that regulates potentially cardiac excitability.

Cardiac Electrophysiology II

3101-Pos Board B206

Pharmacological IKs Activation Slows Cardiac Conduction and Exacerbates the Effect of INa Blockade

Rengasayee Veeraraghavan, Anders Peter Larsen, Steven Poelzing.

Background: The Kv7.1 channel underlies the IKs current and plays a key role in cardiac repolarization. Loss of IKs function can lead to the type 1 long QT syndrome (LQT1). The Kv7.1 activator R-L3 has been suggested as a potential antiarrhythmic therapy in LQT1. Having previously demonstrated that other K+ currents can modulate cardiac conduction, we tested here the effects of pharmacological IKs activation on cardiac conduction and its dependence on the sodium current (INa).

Methods and Results: Conduction velocity (CV) was quantified by optical mapping during LV or RV pacing. Under control conditions transverse CV (CVT) was significantly greater (15 ± 1 %, $p<0.05$) in RV than LV with no difference in longitudinal CV (CVL) between ventricles. During partial blockade of INa (flecainide, 1 μM), RV CVT decreased by 36 ± 5 % while LV CVT decreased by 24 ± 5 %. These data demonstrate greater RV conduction dependence on sodium channel availability. Partial IKs blockade by R-L3 (10 μM) significantly decreased both CVT (by 15 ± 4 % in RV & 8 ± 2 % in LV) and CVL (by 11 ± 2% in RV & 6 ± 1 % in LV) relative to control. Further, R-L3 exacerbated the effects of INa blockade: 1 μM flecainide now decreased CVT by 45 ± 3% and 28 ± 4% in RV and LV respectively.

Conclusion: Pharmacological IKs activation by R-L3 slows cardiac conduction and shifts the conduction velocity - INa relationship downward. These findings may have significant implications for the use of Kv7.1 activator as antiarrhythmic drugs.

3102-Pos Board B207

Evidence for Functional SK Channels in Isolated Atrial Myocytes

Jane M. Hancock, Andrew F. James, Jules C. Hancox, Neil V. Marrion.

Atrial fibrillation (AF) is the most common sustained arrhythmia and contributes to cardiac morbidity and mortality. Extension of the atrial effective refractory period through the block of cardiac potassium channels is a therapeutic strategy for the prevention of re-entrant arrhythmias and AF. However, many conventional potassium channel blockers carry an increased risk of potentially lethal ventricular arrhythmias such as *torsades de pointes*. Atrial selective compounds may offer attractive therapeutic alternatives. Small-conductance calcium-activated potassium (SK) channels have recently been suggested as a promising atrial selective target for the treatment of AF. Although there is growing evidence for SK channel expression in the mammalian heart, there is little consensus concerning SK function and it is possible that species differences may contribute to the controversy. We have investigated the expression and function of SK channels in atrial myocytes from mouse and rabbit. Immunocytochemistry using confocal microscopy showed the presence of SK2 protein in mouse atrial myocytes, with clear localization of staining along the z-lines. Whole-cell voltage clamp recordings from mouse and rabbit atrial myocytes, using a pipette solution with limited Ca^{2+} buffering capacity, revealed the presence of apamin-sensitive currents positive to -30 mV. In mouse cells, the apamin-sensitive difference currents slowly decayed during the sustained depolarization. In contrast, a rapidly decaying apamin-sensitive current that inactivated within 50 ms was observed in a proportion of rabbit atrial myocytes . These data suggest that both mouse and rabbit atrial myocytes exhibit functional SK channels, with the presence of SK2 protein confirmed in mouse cells. The apparent kinetic differences

of apamin-sensitive current between species may underlie different physiological roles.

3103-Pos Board B208

Plasticity in KCNQ1 Subcellular Distribution and Partnership with Different KCNE Subunits Contribute to Variations in IKs Channel Function in the Heart

Dimitar P. Zankov, Min Jiang, Mei Zhang, Yuhong Wang, Gea-Ny Tseng.

Background: KCNQ1 can associate with KCNE1 - KCNE5 subunits, singly or in combination, and assume different channel phenotypes in current amplitude and gating kinetics. In the heart, KCNQ1 is known to partner with KCNE1 to form the slow delayed rectifier (I_{Ks}) channel, a major contributor to cardiac electrical heterogeneity and stabilizer of heart rhythm. It is unclear whether KCNQ1 can partner with other KCNE subunits expressed in the heart, and how these potential partnerships impact on I_{Ks} channel function. **Methods:** We study the above issues by patch clamping, immunoblotting, and immunofluorescence/confocal microscopy. **Results**: (1) I_{Ks} current density is higher in guinea pig (GP) atrial (A) than ventricular (V) myocytes. There are 2 contributing factors: KCNQ1 protein level is higher in A than in V, and KCNQ1 is colocalized with KCNE1 in the peripheral cell surface to a higher degree in A than in V. (2) I_{Ks} current density in V myocytes is much lower in spontaneously hypertensive rat (SHR) than in GP, despite abundant expression of KCNQ1 and KCNE1 in SHR. This coincides with a higher degree of KCNQ1 colocalization with KCNE2 in SHR than in GP V myocytes, and the current-suppressing effect of KCNE2 on I_{Ks}. (3) I_{Ks} is *upregulated* during aging in SHR V myocytes. This correlates with a modest increase in KCNQ1 protein expression and, importantly, a prominent redistribution of KCNQ1 and a higher degree of colocalization with KCNE1 on the peripheral cell surface. **Conclusion**: We propose that the KCNQ1 channel exhibits plastic subcellular distribution patterns and dynamic partnerships with KCNE1 and KCNE2 in the heart. These factors contribute to I_{Ks} channel remodeling in response to variations in work load or changes in the heart rate.

3104-Pos Board B209

Sialytransferase ST3Gal4 Deficient Mice Demonstrate Left Ventricular Action Potential Extension and Attenuated IK

Andrew R. Ednie, Eric S. Bennett.

Extracellular protein glycosylation is a ubiquitous cellular process that is vital to normal physiology. Aberrant glycosylation of both genetic and acquired etiologies are observed in severe disease states including congenital disorders of glycosylation and Chagas disease, which afflict millions. Cardiomyopathies including altered electrical signaling are a hallmark of these glycosylation disorders; although, little of the underlying mechanisms are understood. Cardiac conduction and contraction is dependent on various types of voltage-sensitive ion channels that are extensively modified by protein glycosylation. Our lab and others have demonstrated an isoform-specific role of glycosylation in channel gating. Protein glycosylation is a sequential process that involves hundreds of genes that are regulated throughout development and our lab showed that regulated glycosylation alters cardiac electrical signaling. One such glycogene, ST3 beta-galactoside alpha-2,3-sialyltransferase 4 (ST3Gal4), adds negatively charged sialic acids to many membrane proteins including voltage gated ion channels that likely contribute to the extracellular surface charge. Myocytes isolated from the left ventricular apex of ST3Gal4 deficient mice (n=5) demonstrated a 30 % ($p<0.05$) increase in the APD_{90} compared to gender and age matched controls (n=8). The current densities of both the peak and the slowly inactivating sustained (I_{Kslow}) repolarizing voltage-sensitive potassium currents were attenuated ($n<0.05$) at all depolarizing potentials in the ST3Gal4 mice (n=6) compared to controls (n=13). This reduction in potassium current should act to extend the action potential, as observed. The fact that the absence of a single gene involved in protein glycosylation can lead to such deleterious effects on cardiac electrical signaling may provide insight into other diseases of glycosylation that affect millions world-wide.

3105-Pos Board B210

A KCNE1 C-Terminus Long QT Mutation Disrupts a Crucial Interaction with the Kv7.1 Coiled-Coil Helix C and Reduces I_{KS} Channel Expression

Meidan Dvir[1], Dana Shaham[2], Yoni Haitin[1], Enbal Ben-Tal Cohen[1], Joel Hirsch[2], Bernard Attali[1].

[1]Department of Physiology, Sackler Faculty of Medicine and [2]Department of Biochemistry, Faculty of Life Sciences, Tel Aviv University, 69978 Israel.

Kv7.1 α-subunit assembles with the KCNE1 auxiliary subunit to form the cardiac I_{KS} K^+ channel. Mutations in these subunit genes produce the long QT syndrome, a life-threatening ventricular arrhythmia. We recently explored the direct interactions between the C-termini of Kv7.1 and KCNE1 using purified recombinant proteins in a series of *in-vitro* pull-down experiments. We found that the KCNE1 C-terminus physically interacts with the coiled-coil helix-C of the tetramerization domain. Here we show that the missense LQT5 mutation (P127T) located in the KCNE1 distal C-terminus and previously found to produce a dominant Romano-Ward LQT syndrome, disrupted the physical interaction of KCNE1 with the Kv7.1 coiled-coil helix C. When co-expressed in CHO cells with WT Kv7.1, the KCNE1 LQT mutant P127T dramatically reduced I_{KS} current density, without altering channel gating properties. Our results show that deletion of the proximal KCNE1 C-terminus (KCNE1Δ69-77) significantly enhanced the binding of KCNE1 to Kv7.1 C-terminus. In contrast, deletions of the more distal regions of KCNE1 C-terminus (KCNE1Δ78-129 and KCNE1Δ109-129) totally prevented its binding to the Kv7.1 C-terminal region. Our data suggest that the most distal region of the KCNE1 C-terminus (aa.109-129) is crucial for the KCNE1 interaction with the Kv7.1 coiled-coil helix-C and that the missense LQT5 mutation P127T located within this domain affects I_{KS} channel expression by disrupting this coiled-coil interaction and possibly disturbing channel trafficking.

3106-Pos Board B211

Evolution of KChIP2 Gene Function is Localized Within the Core Promoter and 5' UTR

Qinghong Yan, Rajeev Masson, Maria Magdalena Pritz, Barbara Rosati, David McKinnon.

The primary means by which different electrophysiological phenotypes are produced in different species is through the evolution of the cis-regulatory function of ion channel genes. The specific changes underlying this evolutionary process have proven elusive. We have begun to understand this process through analysis of the KChIP2 gene.

The KChIP2 gene encodes an auxiliary subunit obligatory for the expression of the transient outward current (I_{to}) in heart. KChIP2 mRNA expression levels are strongly correlated with the level of I_{to} expression in ventricular myocytes. I_{to} and KChIP2 mRNA expression is high in small rodents, such as mouse and rat, intermediate in larger mammals, such as human and canine, and largely absent in a few species, including guinea pig.

Gene function was studied using three species: mouse, human and guinea pig, representative of high, low and close to zero KChIP2 mRNA expression levels in heart, respectively. The KChIP2 promoter is a CpG island promoter and the transcription start site (TSS) maps to the same homologous region in all three species. The function of equivalent regions of the KChIP2 proximal promoter from mouse, guinea pig and human genomic sequences were compared using an in vitro transcription assay in cultured myocytes. There was a remarkably good correspondence between the transcriptional activity of this region of DNA and the relative level of mRNA expression in vivo. A series of deletion and swapping experiments demonstrated that the large differences in promoter activity were primarily due to sequence differences located within the core promoter and 5' UTR of the gene.

Surprisingly, evolution of core promoter function, rather than cardiac specific enhancer elements, primarily accounts for the large differences in KChIP2 expression in the ventricle of different mammalian species.

3107-Pos Board B212

Temperature Dependence of Herg Blocker Pharmacology - an Automated Patch Clamp Study

Cristian Ionescu-Zanetti, **Qin Chen**.

The hERG ion channel (Kv11.1) is at the center of preclinical cardiac safety assessment. Historically, patch clamp measurements that are used to assess hERG block of candidate compounds have been done at room temperature. While recording at physiological temperatures is challenging in terms of establishing and maintaining a high sealing resistance, recordings at elevated temperature are feasible using recently introduced automated patch clamp systems are capable of controlling temperature.

In this study we compare hERG current voltage relations and kinetics at different temperatures, and report observed changes in the pharmacology of known blockers using a next generation automated patch clamp platform.

3108-Pos Board B213

Combination In Vitro and in Silico Methodology for Risk Assessment of Long QT Type 1 Patients

John J. Rice, Matthias Reumman, Coeli Lopes.

There is a long history of simulating the effects of channelopathies on the cardiac action potential (AP) in diseases like Long QT (LQT) Syndrome. While an important proof of concept, studies have been limited because the number of mutants considered was small and correlation with the phenotype was anecdotal. This study seeks to address such limitations by including 17 Long QT type 1 (LQT 1) mutations for which both *in vitro* characterizations have been performed and detailed clinical outcome data are known. The IKs channel (KCNQ1 and KCNE1 subunits) were expressed in both *Xenopus* oocytes and HEK-293T cells, and G_{max}, V_{half} and the τ of activation and deactivation were measured. The properties were then incorporated into a humanized version of the Flaim-Giles-McCulloch reconstruction of canine cardiomyocytes. The model also included beta-adrenergic stimulation that is known to modulate IKs and is thought to contribute to exercise-induced sudden death in some LQT patients. Both single cell and 1-D cable models were investigated. The simulated QT prolongation in the cable model correlated well with the QTc in patients carrying the 17 mutations studied. The cable model including beta-adrenergic stimulation showed early afterdepolarizations (EADs) and T-wave alternans for mutants. The presence of T-wave alternans correlated with cardiac risk for these patients. Correlation of electrophysiology and clinical phenotype showed that slow activation rates for LQT1 mutations are risk factors for these patients independent from QT prolongation. Incorporation of slow IKs activation into the model produced a more severe to response to β-adrenergic-mediated EADs as compared to responses with reduced IKs conductance only. Our results suggest that cellular electrophysiology in combination with 1-D cable models is a good methodology to predict cardiac risk associated with Long QT1 mutations.

3109-Pos Board B214

SERCA2 Knockout Mice Exhibit Impaired Control of Ca^{2+} Current but not Ventricular Arrhythmias

Halvor K. Mørk, Sylvain Richard, Mathis K. Stokke, Ivar Sjaastad, Kristin B. Andersson, Geir Christensen, Ole M. Sejersted, **William E. Louch**.

Impaired Ca^{2+} handling by the sarcoplasmic reticulum (SR) and Ca^{2+}-dependent arrhythmias are hallmark features of human heart failure. We investigated the control of L-type Ca^{2+} current ($I_{Ca,\ L}$) when SR function is reduced and the consequences for arrhythmogenesis. Experiments were performed on cardiomyocytes isolated from conditional SERCA2 KO mice (KO) which had developed heart failure 7 weeks following gene disruption. $SERCA2^{flox/flox}$ (FF) mice served as controls. SR Ca^{2+} content was reduced to 4% ($P<0.05$) of FF values in KO cardiomyocytes, and SR Ca^{2+} release did not occur on a beat-to-beat basis. Marked up-regulation of the L-type Ca^{2+} channel in KO (α_{1C} subunit= 178% FF, α_2/δ_1= 147% FF, $P<0.05$) was accompanied by a 40% increase in peak $I_{Ca,\ L}$ ($P<0.05$). Loss of SR function resulted in slower Ca^{2+} current inactivation, prolonged duration of current activation, and loss of frequency-dependent facilitation. The larger magnitude and prolonged $I_{Ca,L}$ in KO resulted in AP prolongation, which was not observed in the presence of nifedipine or upon removal of extracellular Ca^{2+}. AP prolongation was associated with prolonged QT intervals corrected for heart rate in KO mice compared to FF (5.63 ms vs 4.90 ms, $P<0.05$). While AP prolongation is expected to be arrhythmogenic, incidence of early afterdepolarizations in KO cardiomyocytes was not increased (FF= 2/13 cells, KO= 0/10 cells, P=NS). Telemetric ECG surveillance during pharmacological stress also revealed a similar incidence of ventricular arrhythmias in FF and KO mice. In conclusion, loss of SR function results in greater L-type Ca^{2+} entry, loss of Ca^{2+}-dependent inactivation, and prolonged APs and QT interval. While such alterations would be expected to pro-arrhythmic in larger species, the relatively brief AP in failing mice may preclude occurrence of early after-depolarizations.

3110-Pos Board B215

Non-Genomic Effects of 17beta-Estradiol on Cardiomyocytes

Rebecca C. Stratton, Charlotte Poile, Nina M. Storey.

Pre-menopausal women have a reduced risk from ischemic heart disease compared to men; this protection is lost after ovariectomy or menopause. Estrogen has been found to confer protection in whole-heart studies in animal models. ATP-sensitive K^+ (K_{ATP}) channels act as metabolic sensors, opening when cellular energy levels fall and are thought to play a role in cardioprotection. We investigated whether the cardiac K_{ATP} currents play a role in the cardioprotective effects of 17β-estradiol in isolated cardiomyocytes.

Ventricular myocytes were isolated from adult male Wistar rats by enzymatic digestion. The ability of myocytes to recover contractile function after simulated ischaemia/reperfusion injury was calculated by video microscopy. Contracting myocytes (1Hz) were continuously superfused with Tyrode solution, then subjected to 7 minutes of similated ischaemia by perfusion with a metabolic inhibition solution, comprising substrate-free Tyrode with cyanide (2mM) and idoacetic acid (1mM), followed by 10 minute reperfusion with Tyrode to simulate reperfusion. A 5 minute pretreatment of 17β-estradiol (500nM) significantly increased contractile recovery; control 30% n=100, 17β-estradiol 68% n=185, DPN (ERβ agonist) 53% n= 111.

Using the whole-cell patch-clamp mode we investigated the effect of estrogen on K_{ATP} channel activity. P1075 (10μM) elicited a K_{ATP} current which was completely blocked by bath application of estradiol (500nM). Both the classical estrogen receptors; ERα and ERβ have been implicated in several rapid effects of 17β-estradiol. DPN is a specific agonist of ERβ and application of DPN (500nM) following opening of K_{ATP} by P1075 (10μM) also resulted in 100% decrease in K_{ATP} current.

We show that rapid estrogen signalling has a cardioprotective effect in isolated ventricular myocytes. Application of estradiol resulted in complete loss of K_{ATP} current recorded in cardiomyocytes; therefore questioning the role of K_{ATP} in estrogen-dependent cardioprotection.

This work was supported by funding by The British Heart Foundation.

3111-Pos Board B216

Extracellular Proton Modulation of Peak and Late Sodium Current in the Canine Left Ventricle

Lisa Murphy, Danielle M. Renodin, Charles Antzelevitch, Jose M. Di Diego, **Jonathan M. Cordeiro**.

Background: Cardiac ischemia produces a reduction in excitability in ventricular tissue. Acidosis (one component of ischemia) affects a number of ion currents. We examined the effects of extracellular acidosis on Na^+ current in canine ventricular cells. **Methods:** Epicardial (Epi) and endocardial (Endo) myocytes were isolated from the left ventricle. Voltage clamp methods were used to record I_{Na}. Peak I_{Na} was recorded in low external Na^+ to ensure voltage control. Late I_{Na} was recorded in full external Na^+ and defined as the TTX-sensitive current. **Results:** Action potential recordings from left ventricular wedges exposed to pH=6.6 showed a widening of the QRS complex indicating slowing of transmural conduction. In myocytes, exposure to acidic conditions caused a $17.3 \pm 0.9\%$ reduction in upstroke velocity at pH=6.6 versus 7.4. Patch clamp analysis of fast I_{Na} showed current density was similar in Epi and Endo cells at normal pH (68.1 ± 7.0 pA/pF versus 63.2 ± 7.1 pA/pF respectively at −35 mV). Extracellular acidosis reduced fast I_{Na} magnitude by 22.7% in Epi cells and 23.1% in Endo cells. In addition, a slowing of the decay (τ) of fast I_{Na} was observed at pH=6.6. Acidosis did not affect steady state inactivation of I_{Na} or recovery from inactivation. Analysis of late I_{Na} during a 500 ms pulse showed acidosis reduced late I_{Na} at 250 and 500ms into the pulse but no reduction was observed 50ms into the pulse. **Conclusions:** We demonstrate that acidosis reduces the size of peak I_{Na} and slows the decay without affecting Na^+ channel availability or recovery. Acidosis also reduced the TTX-sensitive late I_{Na}. The reduction in peak and late I_{Na} observed during acidosis may contribute to the depression in cardiac excitability observed under ischemia.

3112-Pos Board B217

Normalizing Action-Potential Morphology in Long-Term Cultures of Adult Guinea-Pig Ventricular Cardiomyocytes by Ca_VBETA Expression

Rosy Joshi-Mukherjee, Ivy E. Dick, Ting Liu, Brian O'Rourke, Leslie Tung, David T. Yue.

Adult guinea-pig ventricular myocytes (aGPVMs) exhibit enduring action-potential plateaus similar to those in humans, making this system advantageous for investigating human phase 2 phenomena. Long-term cultures of aGPVMs (Canadian J Physiol Pharmacol**7**:740) further offer the promise of genetic manipulation by somatic gene transfer,

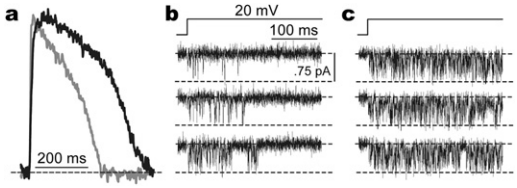

but have been infrequently exploited. Here, we confirm that aGPVM cultures form monolayers featuring organized myofibrils and robust contraction. Beyond this, we now demonstrate that point pacing of di-4-ANEPPS stained monolayers enable optical measurements of action potentials. At 2-Hz pacing, action potentials indeed lasted ~250 ms, but displayed attenuated plateau phases (**a**, gray trace). To normalize phase 2, and to demonstrate genetic manipulability, we virally expressed Ca^{2+} channel $Ca_V\beta$ subunits that enhance L-type channels in heterologous systems. $Ca_V\beta$ expression in fact restored a full-bore plateau phase, as shown by the black trace in **a**. To confirm a role of Ca^{2+} current, we obtained single-channel recordings of native L-type channels. $Ca_V\beta$ subunits strikingly increased open probability, while decreasing inactivation (**b**, control; **c**, $Ca_V\beta$ expression), thus explaining the normalization of action-potential morphology. Overall, long-term cultured aGPVMs offer a powerful model system for electrophysiological exploration.

3113-Pos Board B218

Effects of Voluntary Exercise on Viability and Electrical Remodeling in DCN Model Mice

Masami Sugihara, Takeshi Suzuki, Fuminori Odagiri, Yuji Nakazato, Takashi Sakurai, Hiroyuki Daida, Sachio Morimoto, Nagomi Kurebayashi.

A moderate amount of exercise has been reported to improve the symptom of heart failure (HF). Dilated cardiomyopathy (DCM) is one of major causes of HF characterized by ventricular dilatation and contractile dysfunction, and often associated with sudden death (SD) by lethal arrhythmia. Applicability of exercise to DCM patients is not established yet. In this study, we evaluated effects of voluntary exercise on arrhythmogenic changes in a mouse model of inherited DCM that closely mimics human phenotype. Mice with a deletion mutation of K210 (ΔK210) in cardiac troponin T, which decreases Ca^{2+} sensitivity in myofilaments, were used as DCM model. Wild type (WT) and DCM mice at various ages were housed with free access to a running wheel and their voluntary running activity was measured. Ventricular muscles were excised and gene expressions of ion channels were determined by real-time PCR analysis.Membrane potential signals were optically determined to detect functional changes in myocardium. Homozygous ΔK210 mice developed cardiac enlargement and showed frequent SD with t1/2 of 70 days. Down regulation of multiple types of K+ channels was detected in DCM mice. In parallel, prolongation of action potential duration and frequent spontaneous activity were observed. At 2-month of age, DCM mice showed similar wheel-running activity to WT. Some of DCM mice at 3 months or later decreased running activity with lung edema. In DCM mice with high activity, down-regulation of K^+ channels was less marked. The DCM mice that started running at a young age showed significantly improved survival rate. These results indicate that (1) running wheel was useful to detect sign of HF, and that (2) voluntary exercise is beneficial to DCM mice. Potential mechanisms contributing to the improved survival rate will be discussed.

3114-Pos Board B219

Possible Roles of Cannabinoid Receptors in Cardiac Myocytes

Emma L. Bolton, Derek A. Terrar.

Anandamide is an endogenous ligand of G-protein coupled cannabinoid CB_1 and CB_2 receptors, which has been shown to have complex effects on the cardiovascular system culminating in a hypotensive response and a reduction in cardiac contractility. The aims of this study were to investigate electrophysiologically the effects of anandamide on cardiac ventricular action potential (AP) parameters and accompanying cell contractions, and to explore the involvement, if any, of CB_1 and CB_2 receptors.

Guinea pig ventricular myocytes were stimulated to fire APs by a 2 ms depolarising current pulse applied via an intracellular microelectrode at a frequency of 1 Hz using an Axoclamp 2 (Axon Instruments) amplifier (bridge mode). Myocyte contraction was measured using an edge detection system.

Anandamide (1, 3, 10 μM) caused a concentration-dependent reduction in AP duration (APD) at 90, 50 and 20 % repolarisation, which was accompanied by a reduction in the amplitude of myocyte contraction. At a concentration of 10 μM, anandamide reduced APD 90 by 38 ± 8 % (n = 7, $p < 0.001$). In addition, 10 μM R-(+)-methanandamide (a non-hydrolysable analogue of anandamide) similarly reduced APD and amplitude of contraction. In the presence of the CB_2 receptor antagonist AM 630, but not the CB_1 receptor antagonist AM 281, the magnitudes of these reductions in response to 10 μM anandamide were partially but significantly reduced.

This study confirms that anandamide causes a reduction in ventricular myocyte contractility and may modulate ventricular cell Ca^{2+} handling. Since these effects appear only to be partially inhibited by CB_2 receptor blockade, it is likely that anandamide has actions which are independent of CB_1 and CB_2 receptors.

3115-Pos Board B220

Human Heart Slices - a Novel Multicellular System Suitable for Electrophysiological and Pharmacological Studies

Patrizia Camelliti, Sara A. Al-Saud, Ryszard T. Smolenski, Samha Al-Ayoubi, Nicholas R. Banner, Christopher T. Bowles, Magdi H. Yacoub, Cesare M. Terracciano.

Electrophysiological and pharmacological data from the human heart are limited due to the absence of simple but representative experimental model systems of human cardiac tissue. Here, we describe and characterise a novel, simple and reproducible preparation suitable for studying human cardiac tissue at the multicellular level, the living human cardiac slice.

Vibratome-cut slices (350 μm thick) were prepared from left ventricular transmural biopsies (5x5 mm) obtained from end-stage heart failure patients undergoing transplant or left ventricular assist device implantation. One biopsy was sufficient to generate >15 slices. Histology revealed that slices cut in parallel to the epicardial surface had predominantly longitudinal muscle fibre orientation. ATP/ADP and phosphocreatine/creatine ratios (3.32 ± 0.61 & 1.37 ± 0.31; n=5 slices/3 hearts) measured by HPLC were comparable to intact organ values.

Electrical activity and its propagation in response to electrical stimulation (1Hz) were recorded using a multi-electrode array system. Field potential duration (FPD) remained stable and could be recorded for up to 8h.Mean FPD was 467 ± 4 ms (n=42/10), similar to previously reported data using ventricular wedges.

Longitudinal conduction velocity (CV) was faster than transversal CV (51 ± 3 & 20 ± 1 cm/sec, n=19/7, $p<0.0001$), with an anisotropic ratio of 2.5:1.

Ikr blocker E4031 (1 μM) and Iks blocker Chromanol 293B (20 μM) prolonged FPD by $64 \pm 3\%$ (n=20/7, $p<0.001$) and $22 \pm 2\%$ (n=12/5, $p<0.001$) respectively, similar to previous results using intact papillary muscles. The non-specific K^+ channel blocker 4-aminopyridine (1mM) prolonged FPD by $47 \pm 2\%$ (n=6/2, $p<0.001$).

Our results show that cardiac slices from human biopsies are a reproducible preparation that remains stable for several hours *in vitro* and has structural, electrophysiological, pharmacological and metabolic properties of native myocardium. Cardiac slices offer a novel multicellular system suitable for the study of heart failure and therapy.

3116-Pos Board B221

Voltage Sensitive Protein 2.3: A Novel Tool to Study Sarcolemmal Structure and Electrical Activity in Mouse Hearts

Mei-Ling Chang Liao, Hiroki Mutoh, Yuka Iwamoto, Nour Raad, Viacheslav Nikolaev, Stefan Luther, Stephan Lehnart, Stefan Wagner, Lars Maier, Walter Stühmer, Thomas Knöpfel, Wolfram-Hubertus Zimmermann.

Optical imaging of cardiac electrical activity is of considerable interest, especially in cardiac pathophysiology and pharmacology studies. Voltage sensitive fluorescent dyes are widely used in this context, but have a limited applicability in long-term studies. We hypothesized that novel genetically encoded voltage sensitive fluorescent proteins (VSFPs) can be stably expressed in mouse hearts to (1) specifically label sarcolemmal membranes and (2) monitor membrane voltage transients. **Methods:** cDNA encoding for the VSFP2.3 voltage probe (see W. Akemann et al., 2010 Nat Methods) was placed under the control of the cardiomyocyte-specific alpha myosin heavy chain (αMHC) promoter. Transgenic mice were generated by pronuclear injection. Myocardial structure and performance were assessed by echocardiography (in 16-week old mice). Myocyte- and sarcolemma-restricted transgene activity was studied in isolated cardiomyocytes using confocal laser scanning microscopy and FRET-imaging. **Results:** We established 4 independent αMHC-VSFP2.3 mouse lines (TG#97, #107, #108, #123). Heart morphology and function did not differ in transgenic and wildtype mice with an average heart-to-body weight ratio of 4.3 ± 0.5 (n=26) and 4.2 ± 0.2 (n=8), respectively. Fluorescent imaging of intact hearts showed homogeneous pattern of CFP and YFP expression throughout the ventricles. Fluorescence intensity varied between the established lines (#123>#97>#108>#107). On a single cell basis, prominent sarcolemmal targeting was observed. Interestingly, the T-tubular system was clearly labeled with a predicted periodicity of 1.88 ± 0.02 and 1.82 ± 0.02 μm (from 7/11 cells) in wildtype and transgenic mice, respectively. Voltage transients could be readily detected using optical imaging at the level of intact hearts and isolated myocytes. **Conclusion:** We have established the first mouse model with cardiac-restricted VSFP-expression. αMHC-VSFP2.3 mice demonstrated unimpaired myocardial structure and function. We

anticipate that myocyte-specific VSFP-based voltage imaging will facilitate studies of cardiomyocyte and whole-heart functionality under minimally invasive conditions.

3117-Pos Board B222

Sinoatrial Nodal (SAN) Cells from Center or Peripheral SAN Area are not Functionally Different

Dongmei Yang, Ihor Zahanich, Alexey E. Lyashkov, Edward G. Lakatta.

SAN cells (SANC) determine the rate and rhythmicity of action potentials (AP) that emanate from the SAN to drive the heartbeat. Perspectives gleaned from SAN tissue have been interpreted to indicate that cells from the central SAN, i.e. smaller cells, control the SAN AP firing rate, while data from both SAN and isolated SANC argue that calcium cycling protein density is independent of SAN area and SANC size, and that spontaneous AP cycle length is independent of cell size. Since it is well documented that the gap junction protein, Connexin 43 (Cx43), is largely expressed in the peripheral vs. central SAN areas, we measured the properties of single SANC, employing Cx43 immunolabeling to distinguish cells isolated from the central (Cx43-negative) or peripheral (Cx43-positive) SAN areas.

Freshly isolated adult rabbit SANC from the central area (Cx43-negative) are, on average, smaller ($612.9 \pm 2.5 \mu m^2$, n=340) than peripheral SANC ($818.6 \pm 23.7 \mu m^2$, n=188, $p<0.001$), but there is no difference in the spontaneous AP firing rate (3.07 ± 0.13Hz, n=13, for Cx43-negative and 3.28 ± 0.12Hz, n=23, for Cx43-positive). The AP amplitude and Maximum Diastolic Depolarization also did not differ, but compared to Cx43-positive SANC, the AP of Cx43-negative SANC has a slower AP upstroke (dV/dt_{max} (V/S): 8.12 ± 1.31 *vs.* 13.4 ± 0.62, $p<0.001$) and a longer repolarization time (APD75 (ms): 120.7 ± 4.9 vs. 102.4 ± 2.9, $p<0.01$). Linear regression analyses failed to detect any significant correlations between any AP parameter and the cell size for both. Preliminary data does not show significant differences between Cx43-positive or negative SANC in the AP triggered global Ca^{2+}-transient or spontaneous diastolic Local Ca^{2+} Releases. Our results indicate that although different in size, single isolated central and peripheral SANC, in the basal state, are not functionally different from each other in respect to average spontaneous AP cycle length.

3118-Pos Board B223

Cellular Basis of Phase 2 in Mouse Ventricular Action Potentials

Marcela Ferreiro, Ariel L. Escobar.

Ventricular action potentials (AP) are characterized by a fast depolarizing phase followed by a second upstroke known as phase 2 (Ph2). However, mouse cardiac AP is well known for a lack of Ph2. Recently, we have shown that epicardial AP measured with a large diameter optical-fiber Pulsed Local Field Fluorescence Microscope (PLFFM) display a prominent Ph2. The aim of this work is to understand why most of published electrophysiological studies did not show Ph2. Furthermore, we evaluated several hypotheses to explain these paradoxical differences. First, we evaluated if electrical and optical recordings in different regions of the epicardial layer could differentially display Ph2. We performed simultaneous and colocalized recordings by means of PLFFM and intracellular microelectrodes in different regions of the epicardial layer. Although we found that the contribution of Ph2 to the action potential was dissimilar for different positions all of them show a noticeable Ph2 in both the optical and the electrical recordings. Second, we tested if different pharmacological and physiological intervention that on other mammal hearts modifies Ph2 were able to change this late depolarizing component in mice. Interestingly, Nifedipine and Ryanodine can significantly reduce Ph2. Moreover, when Langenforff perfused hearts were cooled down to 22°C, Ph2 was dramatically reduced. Finally, we tested if Ph2 was an emergent property of the tissue and not a characteristic of a single ventricular myocyte. Surprisingly, ventricular myocytes current clamped with sharp microelectrodes display a large Ph2 (71 ± 3 % of the total AP). This Ph2 was significantly decreased at 22°C and when the membrane potential was hyperpolarize to −100 mV. We conclude that mouse ventricular APs display Ph2 under physiological conditions and changes in the intracellular Ca^{2+} dynamics and thermodynamic parameters can abolish Ph2. Supported by NIH-R01-HL-084487 to AE.

3119-Pos Board B224

Comparison of Action Potential Characteristics from Intact Rabbit Myocardium Using 2-Photon Excitation, Widefield Epifluorescence and Microelectrode Recordings

Allen Kelly, Ole J. Kemi, Iffath A. Ghouri, Francis L. Burton, Rachel C. Myles, Godfrey L. Smith.

2-photon excitation of voltage-sensitive dyes enables determination of sub-cellular electrical activity within intact myocardium at a range of depths. The investigation aimed to compare action potential (AP) characteristics derived from sub-cellular 2-photon imaging in an intact cardiac preparation using Di-4-ANEPPS with epifluorescence and microelectrode voltage recordings. Hearts from male New Zealand white rabbits were Langendorff-perfused at 37°C and paced at a cycle length of 350ms. Preparations were loaded with Di-4-ANEPPS and optical APs recorded using widefield epifluorescence and 2-photon (2P) microscopy. BDM (10mM) and Blebbistatin (10μM) were used to eliminate motion artefacts. Membrane potentials were recorded at 26KHz before and after perfusion of mechanical uncouplers.

Using surface microelectrodes V_{max} values of up to 120 $V.s^{-1}$ were recorded. Mean 10-90% AP rise times were 2.78 ± 0.29 ms (mean ± S.E.M) using microelectrodes (n=3), compared with 3.91 ± 0.30 ms recorded at 50 μm below tissue surface with 2P imaging (at 2.6KHz). Matching sampling frequency between microelectrode and 2P recordings abolished this difference. Perfusion of mechanical uncouplers did not significantly alter rise time (2.44 ± 0.20 ms *vs.* 2.78 ± 0.29 ms; before *vs.* after, $P=0.4$) or APD_{90} (134.90 ± 4.13 ms *vs.* 130.25 ± 2.93 ms; before *vs.* after, $P=0.4$). Mean AP rise times for 2P recordings lengthened with increasing tissue depth (3.91 ± 0.30 ms *vs.* 5.35 ± 0.23 ms; 50 *vs.* 250μm from surface, $P<0.05$, n=7) while epifluorescence rise times were consistently longer (7.85 ± 0.32 ms, n=7). Composite images from multiple depths using 2P microscopy displayed rise times approaching those recorded from widefield epifluorescence. These data suggest that tissue light-scattering at increasing depths results in lengthening of measured AP rise times without significantly altering APD. Slower rise times combined with more diffuse images obtained at depths greater than 200μm suggests optical aberrations cause loss of signal resolution at these depths.

3120-Pos Board B225

Cardiac Vortex Dynamics: From Cell to Tissue

Ashley E. Raba, Jacques Beaumont.

We address issues related to the construction of multiscale models used to investigate the molecular mechanisms of bioelectric disorders.

We construct a channel gating model of the sodium current from simulated data generated with the Ebihara and Johnson model. Three cases are considered, the simulated data set is: complete and noiseless, complete and noisy, and incomplete. The gating model parameters are obtained with an inversion methodology which allows to: determine, *a-priori*, whether the data set constrains the model, avoid local minima of the objective function, and address the ill-posed nature of the problem if present.

Using this model we simulate excitation in a portion of the left ventricular free wall of a pig heart. The Bidomain Equations are solved with a Finite Element Method (resolution: 50 mm, 100 ms).

We show that 5 complementary stimulation protocols are necessary to fully constrain the sodium gating model. Data collection should be iterative, so stimulation parameters are adjusted to generate independent currents. When the data set is complete, the inversion recovers parameters and functions without ambiguity. However, the estimation is ill-posed with respect to sodium activation. A 5% white noise on the current generates up to 50% change on the time constant. When the data set is incomplete, the inversion identifies many models that can reproduce the data set. We come to realize that such models generate erroneous predictions. Varying the inactivation time constant within the range prescribed by the inversion, due to ill-posedness, predicts a variety vortex dynamics behaviors.

Biophysics of Ion Permeation

3121-Pos Board B226
Molecular Dynamics Studies of Ion Permeation in VDAC
Huan Rui, Kyu Il Lee, Richard W. Pastor, Wonpil Im.
The voltage dependent anion channel (VDAC) in the outer membrane of mitochondria serves an essential role in transport of metabolites and electrolytes between the cell matrix and mitochondria. To examine its structure, dynamics, and mechanisms underlying its electrophysiological properties, we have performed a total of 1.77 μs molecular dynamics simulations of human VDAC isoform 1 in DOPE/DOPC mixed bilayers in 1M KCl solution with transmembrane potentials of 0, ±25, ±50, ±75, and ±100 mV. The calculated conductance and ion selectivity are in good agreement with the experimental measurements. In addition, ion density distributions inside the channel reveal possible pathways for different ion species. Based on these observations, a mechanism underlying the anion selectivity is proposed; both ion species are transported across the channel, but the rate for K+ is smaller than that of Cl- because of the attractive interactions between K+ and residues on the channel wall. This difference leads to the anion selectivity of VDAC.

3122-Pos Board B227
Effects of Divalent Cations on the Single-Channel Conductance of the OmpF Channel: Linearity, Saturation and Blocking
M. Lidón López, Elena García-Giménez, Vicente M. Aguilella, Antonio Alcaraz.
Previous studies on the bacterial porin OmpF (Biophys. J. 96 (2009) 55-66) have shown that the channel moderate cationic selectivity of OmpF in NaCl and KCl solutions is reversed to anionic selectivity in solutions of $CaCl_2$ and $MgCl_2$. We study here the effect of salts of divalent cations on the channel conductance with a particular emphasis in dissecting the role of the electrolyte, the role of the counterion accumulation induced by the protein channel charges and any other effect not found in salts of monovalent cations. Single-channel conductance measurements are performed over a wide range of salt concentrations (up to 3 M).
We find that the change of channel conductance with salt activity in bulk solution exhibits different features in salts of monovalent cations and in salts of divalent cations. In order to separate channel and electrolyte effects we analyse the correlation between channel conductance and bulk solution conductivity. While one scales with the other in solutions of NaCl and KCl over the whole concentration range studied, the conductance for $CaCl_2$ and $MgCl_2$ has two regimes. At salt concentrations below 1 M we found the same pattern as in solutions of NaCl and KCl. However, for higher concentrations such linearity between conductivity and conductance vanishes. Moreover, surprisingly, at high concentrations of $MgCl_2$ and $CaCl_2$ the conductance decreases as conductivity increases. Once, one accounts for the big variation of activity coefficients of divalent salts at high concentrations, the experimental results suggest that at low concentrations the pore conductance is controlled mainly by the electrolyte properties. The current recordings in salts of divalent cations reveal the existence of substates of lower conductance as one of the causes of the conductance decrease in the high concentration regime.

3123-Pos Board B228
Sialic Acid Transport in E. coli: Role of Outer Membrane Porin NanC
Janhavi Giri, John M. Tang, Christophe Wirth, Caroline M. Peneff, Tilman Schirmer, Bob Eisenberg.
Sialic acid is a nutrient of bacteria important in host-pathogen interactions. The mechanism of transport of sialic acid from outer membrane to periplasmic space of *Escherichia coli* is not known. N-acetylneuraminic acid (Neu5Ac) - the most abundant form of sialic acid - induces a specific porin NanC (**N-a**cetyl**n**euraminic acid **C**hannel) in the outer membrane of *E. coli*. Recently, a high resolution structure of NanC (Wirth et al., J.Mol.Biol., (2009) 394:718) revealed unique structural features that support Neu5Ac transport. However, patch-clamp experiments seemed to show that NanC conductance is unaffected by sialic acid (Condemine et al., J.Bacteriol., (2005) 187:1959). We report single channel current measurements of NanC in bilayers in the presence of Neu5Ac. Neu5Ac changes gating and considerably increases the ionic conductance of NanC in 250 mM KCl, pH 7.0. (See our other NanC poster.) The unitary current through NanC increases when 7-12 mM of Neu5Ac is added to the grounded side of the bilayer. A distinct steady voltage dependent current (sublevel) is observed that seems to add to the unitary current. The single channel slope conductance of NanC increases by 51% in the presence of 7 mM Neu5Ac and by 74% in 55 mM. The effect of Neu5Ac on the unitary current through NanC seems to saturate at higher Neu5Ac concentrations. The unit conductance of NanC also increases when 20 mM Neu5Ac is added to both sides of the bilayer. It is likely that some of the current is carried by Neu5Ac. Interestingly, Neu5Ac reduces the ionic conductance of trimeric OmpF (Outer membrane porin F) under the same conditions: frequent, long closures are seen. Thus, we provide evidence that sialic acid translocation is specifically facilitated by NanC, and not by the general porin OmpF.

3124-Pos Board B229
Measurement and Interpretation of Ion Selectivity in Wide Channels: Merging Information from Different Approaches
Antonio Alcaraz, Elena García-Giménez, María L. López, Vicente M. Aguilella.
The ion selectivity of a channel can be quantified in several ways by using different experimental protocols. A wide, mesoscopic channel, the OmpF porin of the outer membrane of E. Coli, serves as a case study to compare and analyze several measures of the channel cation-anion permeability in chlorides of alkali metals (LiCl, NaCl, KCl, CsCl). We show how different insights can be gained and integrated to rationalize the global image of channel selectivity. To this end, reversal potential, channel conductance and bi-ionic potential (two different salts with a common anion on each side of the channel but with the same concentration) experiments are discussed in the light of an electrodiffusion model based on the Poisson-Nernst-Planck (PNP) formalism. Measurements and calculations based on the atomic crystal structure of the channel show that each protocol displays a particular balance between the different sources of selectivity.

3125-Pos Board B230
Numerical Simulation of Molecular Delivery via Electroporation
Hao Lin, Mohamed Sadik, Jianbo Li, Jerry W. Shan, David I. Shreiber.
A numerical simulation to study molecular delivery via electroporation is presented. The Nernst-Planck equations for species transport are solved in both the intra- and extra-cellular spaces, and are coupled at the cell membrane through an asymptotic Smoluchowski equation for membrane permeabilization. The delivery of calcium ions into a Chinese Hamster Ovary cell is simulated. To facilitate comparison with fluorescence measurement, the simulation includes three species (Ca2+, Fluo-3, and CaFluo) and their reactive kinetics. The results agree well with experimental data from the literature (Gabriel and Teissié, Biophys. J., 1999), and reveal that ion electrophoresis plays an important role in the process. Furthermore, the maximum achievable concentration within the cell is reciprocally correlated with the extracellular electrical conductivity. This observation corroborates well with both previous data (Djuzenova et al., Biochim. Biophys. Acta, 1996) and our own recent measurements. The root-cause of this behavior is an electrokinetic mechanism known as field-amplified sample stacking. Through this mechanism, the intracellular ion concentration can reach a level higher than the extracellular one provided that the intra-to-extra-cellular conductivity ratio is greater than unity. This work is a step toward the quantification of electroporation-mediated molecular delivery.

3126-Pos Board B231
A Pressure-Polish Setup to Fabricate Patch Pipettes Yielding Low Access Resistance and Efficient Intracellular Perfusion
Mascia Benedusi, Alberto Milani, Marco Aquila, **Giorgio Rispoli**.
When performing whole-cell configuration recordings, it is very important to minimize series resistance. This goal is achieved here by using a method able to enlarge the cone-shape section of the pipette, without increasing the tip opening diameter, by using a calibrated combination of heat and air pressure. The heat was produced by passing current in a glass-coated platinum wire, shaped appropriately to ensure an homogeneous heating of pipette shank, connected to a regulated high-current generator. The pressurized air (~4 atm) was applied to the pipette lumen through a 0.2 μm filter (to avoid pipette clogging), via the pressure port of a modified commercial holder. The pipette reshaping was viewed on an LCD monitor (and recorded on-line on a computer), connected to a contrast-intensified CCD camera coupled to a bright-field stereomicroscope. The hot halogen lamp of the microscope illuminator was replaced with a variable white LED source, to avoid the loss of fine control of the platinum wire temperature. By pressurizing the pipette lumen during fire-polishing, the pipette shank was widened as desired, without increasing the tip opening diameter: these pressure-polished pipettes, tested on many cell types, yielded routinely access resistances ~4-fold smaller than the ones attained with conventional pipettes. The pressure-polished pipettes minimized therefore intracellular ion accumulation or depletion, and errors in membrane potential control, in the presence of large membrane currents. Moreover, they allowed to study rapid voltage-activated currents (by reducing the time constant of charging the cell membrane capacitance), the efficient incorporation in the cytosol of large molecules (that was followed with fast fluorescence imaging), and to position pulled quartz capillaries inside the pipette very close to its tip, resulting in fast intracellular perfusion.

3127-Pos Board B232
Recreating Ion Channel IV Curves using Specific Frequency Components
John Rigby, Steven Poelzing.
INTRODUCTION: Impedance spectroscopy cannot distinguish between ion channel families. We hypothesized that amplitudes of specific characteristic frequencies will correlate with the current amplitude passed by a specific ion channel families. Previously, we demonstrated the feasibility of this technique using the inward rectifying potassium channel, $K_{IR}2.1$. In this study, $Na_V1.5$ is used to demonstrate that the technique is applicable to other families of ion channels.
METHODS: IV curves were generated using a standard voltage step protocol performed in whole-cell voltage clamp mode on HEK293 cells transiently transfected with SCN5A (encodes $Na_V1.5$). Noise functions containing 1-50 kHz frequencies were inserted into each voltage step. The real component of the Fast Fourier transform (FFT) was then calculated for each trace. Each frequency magnitude as a function of voltage step was correlated with the IV curve.
RESULTS: The magnitude of 22.5 and 24.5 kHz correlated well with the IV curve of $Na_V1.5$ in the presence of the noise function ($R>0.8$), and poorly in the absence of noise ($|R|<0.3$). Two nodes of zero correlation were also found (11.36 +/- .08 kHz and 36.23 +/- 4.79 kHz. For $K_{IR}2.1$, current and frequency amplitudes did not correlate well between 11 and 36 kHz, suggesting that this correlation may be unique to $Na_V1.5$. On the other hand, frequencies were identified below 10 kHz whose amplitudes highly correlate with either one or both channels.
CONCLUSIONS: These data suggest that specific frequencies exist which can re-create the shape of both $K_{IR}2.1$ and $Na_V1.5$ IV curves. Furthermore, the correlation at some frequencies is channel specific, while others are not. This methodology could be a powerful tool for assessing the behavior of multiple ionic currents simultaneously during a freely running action potential.

3128-Pos Board B233
Mapping the Importance of 4 factors in Creating Monovalent Ion Selectivity in Biological Molecules
Michael Thomas, Dylan Jayatilaka, Ben Corry.
The ability of macrocycles, enzymes, ion channels, transporters and DNA to differentiate between ion types is often crucial to their function. Using molecular dynamics simulations on both detailed systems and simple models we quantify the importance of four factors which affect the ion selectivity, including the number of coordinating ligands [1], their dipole moment [2], the cavity size [3] and their vibrational motion. The information resulting from our model systems is distilled into a series of 'selectivity maps' that can be used to 'read off ' the relative free energy associated with binding of different ions, and to provide an estimate of the importance of the various factors. While our maps cannot capture all elements of real systems, it's remarkable that our simple model produces differential site binding energies in line with experiment and more detailed simulations for a variety of systems. This makes our maps a very useful tool for assisting in understanding the origins of selective binding and transport. Our studies show that the various suggested mechanisms of ion selectivity can be important in various situations. The chemical nature of the coordinating ligands is essential for creating thermodynamic ion selectivity in flexible molecules, but as the binding site becomes more rigid the number of ligands and the reduction of thermal fluctuations can become important.
[1] Thomas M, Jayatilaka D, Corry B (2007). The predominant role of coordination number in potassiumm channel selectivity.
*Biophys J***93**, 2635-2643
[2] Noskov S, Berneche S, Roux B (2004). Control of ion selectivity in potassium channels by electrostatic and dynamic properties of carbonyl ligands. *Nature***431**, 830-834
[3] Doyle D et al. (1998). The structure of the potassium channel: molecular basis of K^+ conduction and selectivity. *Nature***280**, 67-77

3129-Pos Board B234
Testing the Applicability of Nernst-Planck Theory in Ion Channels
Chen Song, Ben Corry, Bert de Groot.
The question of whether Nernst-Planck (NP) theory, which is a macroscopic method for calculating ion flux, is still valid in microscopic narrow ion channels has been remaining a mystery for some years. Recently, we tested the ability of the NP theory to accurately predict channel currents by combining and comparing the results with those of Brownian dynamics (BD) simulations. The extensive tests for simplified and realistic ion channels indicate that the NP theory is still applicable in narrow ion channels provided that accurate concentrations and potentials can be input into the NP equation properly, as the currents obtained from the combination of BD and NP match well with those obtained directly from BD simulations. Here, we show first results comparing NP calculations and molecular dynamics (MD) simulations that show promising agreement, further confirming the validity of the NP theory at the microscopic scale. This finding opens a door to utilizing the results of microscopic simulations in continuum theory which can provide an efficient way to calculate the ion flux in ion channels, and might stimulate further effort in this direction.

3130-Pos Board B235
A New Poisson-Nernst-Planck Equation (PNP-FS-IF) for Charge Inversion Near Walls
YunKyong Hyon, James E. Fonseca, Bob Eisenberg, Chun Liu.
The plasmas of biology are interacting mixtures of ions - often charged spheres - that do not behave like the ideal solutions of textbooks. Interactions are always present because of strong electrical forces. Flows are usually present. Life without flow is death. We analyze ionic solutions as complex fluids with an approach that has successfully analyzed complex systems like liquid crystals that are dominated by interactions between composite components. The finite size of ions is particularly important in biology in crowded environments like channels, active sites of enzymes, or charged surfaces. We here deal with surfaces and try to capture the essential features of charge inversion (layering) near a charged wall. Charge inversion (layering) near walls is a characteristic phenomenon resulting from the electrostatic interactions in systems with charged walls. The mathematical model is derived by the energy variational approach (*EnVarA*) – J.Chem.Phys. (2010) 133:104104 – that combines the action of conservative (Hamiltonian) systems and the dissipation of Onsager and Rayleigh. Both are written in the same laboratory coordinates after variational derivatives of variables are taken. The generalized energy and dissipation include entropic and electrostatic components, and repulsion between spheres. An interfacial electroneutrality constraint between bulk and charged wall captures some essential features of charge inversion. Taking variational derivatives yields a field theory of partial differential equations and boundary conditions that are appropriate for life's solutions – that interact and flow – as well as thermodynamic equilibrium. The new equations, PNP-FS-IF, include (1) a nonlocal contribution of finite size (FS) and (2) an interfacial constraint (IF) of electroneutrality. PNP-FS-IF produces charge inversion near walls. We compare the charge inversion seen with PNP-FS-IF and Monte-Carlo simulations.

3131-Pos Board B236
How Interactions Control Molecular Transport in Channels
Anatoly B. Kolomeisky, Karthik Uppulury.
The motion of molecules across membrane channels and pores is critically important for understanding mechanisms of many cellular processes. Here we investigate the mechanism of interactions in the molecular transport through nanopores by analyzing discrete stochastic models. According to this approach the channel transport is viewed as a set of chemical transitions between discrete binding sites along the pore. It is shown that the strength and spatial distribution of molecule/channel interactions can strongly modify the molecular fluxes. Our analysis indicates that the most optimal transport is achieved when the binding sites are near the entrance or exit from the channel depending on the sign of the interaction potential. This observation allows us to explain recent single-molecule experimental results on translocation of different polypeptides. It also agrees with available information on distribution of binding sites in many membrane channels. In addition, we studied the role of intermolecular interactions during the channel transport, and it is argued that an increase in the flux can be observed for some optimal interaction strength. The mechanisms of these phenomena are discussed.

3132-Pos Board B237
Investigating Co-Transport Mechanisms in the AmtB Ammonium Transporter using QM/MM Molecular Dynamics
Shihao Wang, Sefer Baday, Simon Bernèche, Guillaume Lamoureux.
AmtB from Escherichia coli is a transmembrane protein with an important role in ammonium transport, especially at low external ammonium concentrations. However, whether AmtB is a channel that permeates NH_3 or an NH_3/H^+ co-transporter is still an open question. An extensive series of hybrid Quantum Mechanical(QM)/Molecular Mechanical(MM) simulations has been performed to investigate the mechanism of ammonium transport through AmtB. Focus has been placed on the deprotonation of ammonium and the possible co-transport of H^+ and NH_3. Constraint dynamics simulations have been used to obtain the potentials of mean force for the possible NH_4^+ deprotonation paths involving water molecules and/or protein side chains. Further investigations on the transport pathways of H^+ and NH_3 have shown the details of the co-transport mechanism. The distribution of solvent and ammonia inside the pore is also analyzed

and the possible mechanisms of ammonia re-protonation and how side chains are reset back to original state are presented.

3133-Pos Board B238
Permeation Mechanism in the AmtB Ammonium Transporter: Putative Electrogenic Co-Transport of NH3 and H+
Shihao Wang, Sefer Baday, Esam A. Orabi, Simon Bernèche, **Guillaume Lamoureux**.
Despite the growing amount of structural information, the molecular details of the mechanism by which membrane proteins of the Amt/Rh family mediate ammonium transport remain elusive. For instance, in protein AmtB from Escherichia coli, it is not known whether NH3 is diffusing passively through the protein pore or is involved in an NH3/H+ co-transport mechanism.
Using state-of-the-art computational methods (polarizable force fields and hybrid QM/MM molecular dynamics simulations combined with free energy calculations) we investigate the thermodynamics and kinetics of various mechanisms for proton co-transport. Based on these simulations we propose a plausible NH3/H+ co-transport mechanism in which the twin-histidines dyad lining the pore plays a central role.

3134-Pos Board B239
Investigating Ammonium Transport Mechanisms in AmtB and RhCG by Molecular Dynamics Simulations
Sefer Baday, Shihao Wang, Guillaume Lamoureux, Simon Bernèche.
Membrane proteins of the ubiquitous Amt/Rh family mediate the transport of ammonium. Despite the availability of different X-ray structures that provide many insights on the ammonium permeation process, the molecular details of its mechanism remain controversial. Functional experiments on plant ammonium transporters and rhesus proteins suggest a variety of permeation mechanisms including the passive diffusion of NH3, the antiport of NH4+/H+, the transport of NH4+, or the cotransport of NH3/H+. The X-ray structures have revealed that the pores of the prokaryotic AmtB and the eukaryotic RhCG proteins share a similar architecture suggesting that they might both catalyze the diffusion of NH3. However, molecular mechanics simulations of both proteins reveal that small differences in the pore lining residues might actually alter the properties of the pore. We notably find that the pore of the AmtB transporter can stabilize water molecules at much greater extent than the pore of RhCG. The possible presence of water molecules in the pore lumen of AmtB opens the door to alternative permeation mechanisms, notably involving the co-transport of H+. We discuss the possible permeation mechanisms in both the AmtB and RhCG proteins in light of some recent functional studies, and illustrate how closely related proteins can support quite different mechanisms.

3135-Pos Board B240
A View of Hydrogen/Hydroxide Flux Across Lipid Membranes
J. Wylie Nichols, **Ronald F. Abercrombie**.
A topic emerging roughly thirty years ago and engendering an incompletely resolved controversy is addressed: the relatively high permeability and pH independence associated with H^+/OH^- passive movements across lipid membranes. The expected characteristics of simple H^+/OH^- diffusion and those of a reaction between H^+ and OH^- being attracted from opposite surfaces and condensing in an interfacial region of the membrane are considered. An interfacial H^+/OH^- reaction mechanism predicts the experimentally observed behavior of a H^+/OH^- flux that is independent of the pH measurement range. In order to obtain the correct magnitude of flux, it is assumed that H^+ and OH^- within the interfacial zone become electrostatically aligned on opposite sides of the hydrophobic membrane core. Electrostatic attraction combined with charge delocalization among a small cluster of water molecules surrounding the ions sufficiently reduce the Born energy for insertion into lipid, accounting for the experimentally determined magnitude of this flux. The pH independence associated with H^+/OH^- passive movements across membranes could have satisfied a requirement for pH homeostasis in emerging life forms and provided stability for natural selection.

3136-Pos Board B241
Single Channel Measurements of N-Acetylneuraminic Acid-Inducible Channel (NANC) in E. coli
Janhavi Giri, **John M. Tang**, Christophe Wirth, Caroline M. Peneff, Tilman Schirmer, Bob Eisenberg.
Escherichia coli can use *N*-acetylneuraminic acid (Neu5Ac) as its sole carbon source even if the general outer membrane proteins OmpF and OmpC are not expressed: NanC - a monomeric outer membrane channel - allows Neu5Ac to move into the bacterial periplasm. Recently, a high resolution structure of NanC in two different crystal forms was reported by Wirth et al., J.Mol.Biol., (2009) 394:718 (PDB codes: 2WJQ and 2WJR). Our goal is to determine appropriate 'baseline' ionic conditions to study the transport of Neu5Ac through NanC using single channels in lipid bilayers. Measurements of single channel currents showed that NanC has two modes of time dependent behavior ('gating'). In the many situations we have tested, the modes are not induced or changed by surrounding ionic conditions or voltage. Single channels of NanC at pH 7.0 have: (1) a large conductance (around 100 pS to 800 pS in 100 mM KCl to 3M KCl) that varies with the polarity of the applied voltage; (2) anion over cation selectivity ($V_{reversal}$ around +16 mV in 250 mM KCl || 1 M KCl); (3) voltage-dependent gating (channel closures above ±200 mV). Single channel conductance of NanC decreases about 50% when HEPES concentration is increased from 100 μM to 100 mM in 250 mM KCl at pH 7.4, consistent with the two HEPES binding sites observed in the crystal structure (PDB code: 2WJR). Studying alternative buffers, we found that phosphate interferes with the channel conductance, whereas TRIS could not be used because it reacts with Ag/AgCl electrodes producing artifacts even in the presence of Agar-KCl bridges. Our further studies of NanC will use no pH buffers, but low concentration (250 mM) salt solutions adjusted to neutral pH 7.0.

3137-Pos Board B242
Blebbistatin Protects Rodent Myocytes from Death in Primary Culture via Inhibiting Na/Ca Exchange
Yinzheng Guan, Xiaoying Zhang, Yingxin Li, Chris Szeto, Xiajie Ai, Xiongwen Chen.
Introduction: It has been long recognized that rodent myoyctes die during long-term primary culture, which limits the use of genetically altered myocytes for signaling studies. Blebbistatin (BLB), a myosin II ATPase inhibitor, has been used to protect rodent myocytes. However, the mechanisms underlying the protective effects of this drug are not clear and are the topics of this study.
Materials & Methods: Adult rat ventricular myocytes (ARVM) were isolated and cultured with or without BLB (10μM) and BDM(10mM) for 72 hours. Myocyte death was evaluated by trypan blue staining. The effects of these two drugs on myocyte contraction, intracellular Ca transient ([Ca]i, Indo-1,410/480), SR Ca content, L-type calcium and Na/Ca exchanger currents were studied acutely.
Results: 1, Both BDM (61.5 ± 6.4%) and BLB (74.0 ± 3.2%) promoted myocyte survival in culture at 72 hours (control: 7.0 ± 1.8%); 2. ARVM fractional shortening was reduced by BLB (1.7 ± 0.4%) and BDM (0.5 ± 0.1%, control: 6.5 ± 0.7%); 3, Acutely, the amplitude of $[Ca]_i$ ($\Delta[Ca]_i$) was depressed by both BDM (0.038 ± 0.005) and BLB (0.065 ± 0.008) comparing to control (0.130 ± 0.010). 4, Diastolic Ca was significantly increased by BLB (0.90 ± 0.06) but not by BDM (0.73 ± 0.06) comparing to control (0.70 ± 0.05). 5. BLB and BDM significantly reduced the SR Ca content(Δ[Ca]i in BLB vs. BDM vs. control: 0.16 ± 0.016, 0.09 ± 0.01, 0.24 ± 0.03). 5. The mechanisms of the protective effect of BDM and BLB are different in that BDM mainly reduced Ca influx through the L-type Ca channel (85% reduction) and Na/Ca exchanger (60% reduction) while BLB inhibited Na/Ca exchanger (100% inhibition) without altering the LTCC(<5% reduction).
Conclusion: These results suggest both BDM and BLB protects rodent myocytes in culture by preventing cytosolic and SR Ca overload by both common and different mechanisms: both BDM and BLB inhibit NCX while BDM, but not BLB, reduces $I_{Ca\text{-}L}$.

3138-Pos Board B243
On Conduction and Gating in K^+-Channels
Carmen Domene, Simone Furini.
Potassium channels can conduct passively K^+ ions with rates of up to ~ 10^8 ions per second at physiological conditions, and they are selective to these species by a factor of 10^4 over Na^+ ions. Ion conduction has been proposed to involve transitions between two main states, with two or three K^+ ions occupying the selectivity filter separated by an intervening water molecule. The largest free energy barrier of such a process was reported to be of the order of 2-3kcal mol^{-1}. Here, we present an alternative mechanism for conduction of K^+ in K^+ channels where site vacancies are involved, and we propose that coexistence of several ion permeation mechanisms is energetically possible. Conduction can be described as a more anarchic phenomenon than previously characterized by the concerted translocations of K^+-water-K^+. Experiments also suggest that local structural changes in the selectivity filter may act as the a gate referred to as C-type inactivation. An extensive computational study on KirBac, is presented which supports the existence of a physical gate or constriction in the selectivity filter of K^+ channels. Our computations identify a new selectivity filter structure, which is likely associated with C-type inactivation.

3139-Pos Board B244

Sodium-Potassium ion Channel Selectivity can be Modeled by Thyrofluidic Channel Gating

James P. Barger, **Patrick F. Dillon**.

Current views hold that the primary barrier to ion diffusion through a narrow pore is the energy required to dehydrate the transiting ion. The standard model for the selectivity filter of potassium channels consists of four carbonyls coordinating with the K+ ion, replacing the energy of ion hydration. Sodium ions, however, have diminished free energy due to their smaller radii, causing an increase in steric repulsion between the coordinating carbonyl groups. It has been recognized that this model does not completely account for experimentally measured selectivity, however.

In the thyrofluidic ion channel model, the gating mechanism for a channel is the ion hydration state. A sufficient membrane electric field at the ion pore entrance will strip water molecules from the ion, facilitating ion entry. The electric field decays exponentially away from the membrane within several nanometers. If the ion channel extends too far from the membrane negligible hydration stripping will occur, and the hydration shell will remain around the ion, inhibiting entry. In addition to regulating channel gating, this mechanism also helps to account for the selectivity exhibited by Na+ and K+ channels. Our measurements of ion mobility in an electric field show that hydration stripping occurs at 400 V/cm, the field 6-7 nm from the membrane. Potassium channels tend to extend past this distance, where hydrated Na+ ion radii exceed hydrated K+ radii. As such, ion coordination energy transfer for ion flux would be significantly greater for Na+. Sodium channels tend to lie within this boundary, however, so they will be exposed primarily to dehydrated ions. As such, sterically unfavorable ion coordination becomes unnecessary to allow ion flux. Thus, the effects of membrane electric field hydration stripping and channel extension create differential ion states at channel entry sites.

Voltage-gated K Channels - Gating: BK Channels

3140-Pos Board B245

A Proton Pathway in the Voltage Sensing Domain of K_V Channels, with a Possible Relation of Gating to the Pore Cavity and to the T1 Moiety

Alisher M. Kariev, **Michael E. Green**.

Voltage gating of a channel is complex. Strong evidence links the activation gate to the intracellular T1 moiety (Minor et al, 2000, *Cell,***102**,657), and to slow inactivation (Panyi and Deutsch, *J. Gen'l. Physiol*.,2007,**129**,403, and other references). Using quantum calculations (B3LYP with mixed basis set, plus frequency corrections to reach room temperature), we have found a large entropic barrier (81kJ) between pore cavity and selectivity filter. This barrier may relate to slow inactivation, but it could be overcome, allowing ion transport, by electrostatic interactions either with an incoming ion, or protons that move during gating. Some additional calculations are presented in the context of specific interactions of S6 and S3 with T1 and the S4-5 linker. Possible electrostatic relation to the pore, and slow inactivation, requires further calculations. The residues for relevant amino acid linkages include (numbering, 3LUT structure, K_v1.2 channel): 1) E420(S6):Q315(S4-S5):[possible water]:N253(S3):E142(T1) 2) Q319(S4-S5):E136(T1):R419(S6):Y415(S6) 3) E422(S6):K134(T1). Also involved: D259, and N256 (S3: the latter may require one water for network linkage). Moving protons would, in this hypothesis, neutralize charges on acid residues, breaking links in the network, leading to gating. The complete proton pathway forms a ''box'' with defined boundaries; limited water connects sections of the network, which reaches the S4 positively charged residues to continue the path. Unless there is a mutation RàH, protons do not exit the VSD. The residues comprising the proton pathway are conserved not only in K_v1.2 channels from multiple organisms, but in Kcna, K_v1.3 and K_v1.5 from chicken.

3141-Pos Board B246

"Must Channels Open Before Inactivating?" Redux

Jeffrey D. Fineberg, Manuel Covarrubias.

Voltage-gated ion channels may adopt four distinct conformations - resting, activated, open and inactivated - and can achieve inactivation from either the closed (activated) or open states (CSI or OSI, respectively). Kv4.x channels are subthreshold-operating K+ channels exhibiting A-type, rapidly-inactivating phenotype, and are responsible for the Ito in the heart and ISA in the nervous system. While previous studies from our lab and others strongly suggest CSI in Kv4.x channels, there is no conclusive evidence for this autoregulatory pathway; and the molecular mechanism of CSI remains unsolved. To shed light on the inactivation pathways of native Kv4.x channels, we expressed the ternary Kv4.2 channel complex including auxiliary Beta-subunits (KChIP and DPP6) in mammalian tsA-201 cells and investigated the resulting A-type currents in the whole-cell configuration of the patch-clamp method. Specifically, we implemented model-independent kinetic analyses to test whether the channels must open before they inactivate (Bean. Biophys J 35, 595-614, 1981; Horn, et al. Nature 291, 426-427, 1981). The main results demonstrate that the development of inactivation induced by a conditioning voltage pulse begins without a significant lag and follows an exponential profile. Consequently, this time course does not reflect the trajectory of the change in open probability induced by a step depolarization to the same voltage. Furthermore, contrary to a prediction of conventional OSI, the rate of macroscopic inactivation slows gradually as the membrane is progressively depolarized. The latter indicates that as the voltage-dependent open probability increases, the rate of inactivation decreases. These observations yield strong model-independent support for a mechanism of preferential CSI in the Kv4.2 channel complex. We are testing this hypothesis at the unitary current level and probing the pathways of inactivation in neuronal Kv4.x channels (cerebellar granule and primary sensory neurons). Supported by NIH grant R01 NS032337 (MC).

3142-Pos Board B247

The Nature of the Energy Barrier for the Charge Movement in Voltage-Sensors

Jerome J. Lacroix, Fabiana V. Campos, Francisco Bezanilla.

Voltage-sensors (VS) are protein domains which transduce changes in membrane potential into conformational changes thereby controlling the opening of a pore or the activity of a phosphatase domain. This operation creates measurable gating currents (Ig) by a local rearrangement of charged groups in the VS. Although there is high conservation of these gating charges among VS, the kinetics of Ig varies greatly, spreading over several orders of magnitudes. These kinetic differences explain the temporal separation of Na^+ and K^+ conductances in excitable cells, critical for the generation and propagation of the action potential. Despite its fundamental importance, the molecular mechanism underlying this phenomenon is not well understood. Here, we identified in the Shaker K^+ channel two hydrophobic residues Ile241 and Ile287 located in S1 and S2 respectively which directly interact with S4 arginines during gating charge movement. We show that Shaker gating kinetics can be speeded up ~ 3 fold by mutating Ile287 to more hydrophilic residues threonine or serine. Interestingly, voltage-dependent sodium channel (Nav) possesses threonines in domains I-III at positions homologous to Ile287 and exhibit Ig ~ 10 times faster than that of Shaker. Mutating these threonines to isoleucines in Nav1.4 slows down Ig 2-3 times. Moreover, the sensing currents of the voltage-sensitive phosphatase Ci-VSP, which are ~ 8 times slower than that of Shaker, can be speeded 3-4 fold by substituting Ile126, (homologous to Ile241 in Shaker) to threonine. Taken together, our data indicate that the side chains of these two key positions form a hydrophobic plug separating the external and internal media. This plug constitutes the main energy barrier for charge crossing and its amplitude is modulated by its degree of hydrophobicity, thus controlling the kinetics of the sensor. Support: NIH-GM030376.

3143-Pos Board B248

Gate Closure Strictly Follows Voltage-Sensor Movements in K_V Channels

Alain J. Labro, Jerome J. Lacroix, Carlos A. Villalba-Galea, Dirk J. Snyders, Francisco Bezanilla.

Kv channels are voltage-dependent potassium pores that shape the action potential duration and are critical for cell excitability. Detection of membrane potential (V) is done by a charged (Q) voltage sensor domain (VSD) whose reorientations generate a transient gating current (I_Q). Prolonged depolarization of *Shaker* Kv channels pushes the VSD into the relaxed state, characterized by a slowing in I_QOff. Kv channels also have two gates (in series) that seal off K^+ permeation: the S6 bundle crossing (BC), directly tied to the VSD, and the selectivity filter (SF). Direct comparison of K^+-conduction in *Shaker*, reflecting the status of the BC gate, with I_Q shows a strong correlation between both. As I_QOff slowed down with prolonged depolarizations, BC gate closure displayed a similar 2-fold slowing when the duration of a +20mV pre-pulse was increased from 0.2 to 10 seconds. Simultaneous monitoring of the VSD movement (fluorescence recordings) and channel gate closure (ionic recordings) in the TMRM-labeled *Shaker* mutant M356C showed that the slowing in I_QOff and gate closure occurs simultaneously. This indicates that the gate is strictly controlled by the movements of the VSD and most importantly that the BC gate remains open even when the VSD relaxes. Consequently, K^+ conduction continues as long as the SF gate does not close (inactivation). Interestingly, in Kv3.1 - a channel that regulates high frequency firing *in-vivo* - the opposite behavior was observed: prolonged depolarization speeded up both I_QOff and gate closure. Thus, the effect of VSD relaxation differs between different subtypes of Kv channels suggesting that relaxation affects the excitability of cells differently depending on their depolarization history, either reducing excitability in

cells expressing *Shaker* or increasing it in case of Kv3.1. (Support: NIH-GM030376, FWO-G025608)

3144-Pos Board B249

Use of Tethered Spectroscopic Probes as Chemical Calipers to Measure Molecular Distances

Brian W. Jarecki, Suquing Zheng, Xiaoxun Li, Alessandro Senes, Weiping Tang, Baron Chanda.

Fluorescence based techniques have the advantage of being able to probe dynamic structural changes in a physiological milieu. Here we describe the development of a novel approach to estimate molecular level distances between two sites in a protein structure. Distance information was inferred by measuring accessibility of a fluorescent tag on one site to a variable length collisional quencher covalently affixed to a second site. The functionalized variable length quenchers therefore act as ''tape measures'' which can be utilized to obtain point-to-point distance information in the protein structure. We validated our approach using model proline polypeptide substrates of varied lengths (n = 6 or 10). Polyproline substrates were flanked with an N-terminal fluorophore and a C-terminal cysteine. Cysteine reactive tailed quenchers of varying lengths were attached at the C-terminal end. The quenching compounds contained two reactive tails, one that includes a maleimide group to cross-link with the free sulfhydryl of cysteine and a second that has a nitroxide radical quenching moiety, joined by a polyethylene glycol (PEG) spacer of known lengths (n = 3-8). Our results demonstrate that variable length tethered quenchers are able to estimate molecular distances between two attachment sites by exploiting bimolecular quenching. Quenching efficiency closely matched the predicted average conformation length and sampling radius of the PEG spacer as determined by Monte Carlo simulations. Our findings establish the feasibility of using these tools to determine nanometer scale distances between two sites in a protein structure in real time.

3145-Pos Board B250

Ca^{2+} Dependent Activation of Large Conductance Ca^{2+} Activated Potassium (BK) Channels by Binding to the RCK1 Domain

Guohui Zhang, Shenyou Huang, Junqiu Yang, Jingyi Shi, Xiao Yang, Alyssa Moller, Xiaoqin Zou, Jianmin Cui.

BK channels sense intracellular Ca^{2+} and are important modulators of muscle contraction, neuronal spike frequency adaptation, neurotransmitter release and circadian pacemaker output. The cytosolic domain (CTD) of BK channels contains two structural sub-domains, RCK1 and RCK2. Mutagenesis studies have identified a series of Asp residues in the RCK2 domain (termed as the Ca^{2+} bowl) and Asp367 in the RCK1 domain as two putative Ca^{2+} binding sites. A recently published crystal structure of the BK CTD showed Ca^{2+} binding to the Ca^{2+} bowl but, surprisingly, provided less further information about the Ca^{2+} binding site in RCK1. We have performed mutational scan in the RCK1 domain to search for the residues that are necessary for Ca^{2+} binding in addition to Asp367. Here we show that the mutations of Glu535 in the RCK1 domain produce nearly identical functional consequences on the Ca^{2+} dependent activation as the mutations of Asp367. Therefore, Glu535, same as Asp367, may be one of binding coordinators for Ca^{2+} binding in RCK1. We also show that mutations of Met513, some of which have been previously shown to reduce Ca^{2+} sensitivity, result in a different pattern of functional consequences than those of Glu535 and Asp367, which suggest that Met513 is not part of the Ca^{2+} binding site. Molecular modeling and experimental data suggest that the binding of Ca^{2+} by the side chains of Glu535 and Asp367 changes the conformation around the binding site and turns the side chain of Met513 into a hydrophobic core, thereby opening the activation gate of BK channels. We have also investigated Cd^{2+} dependent activation of BK channels and found that Ca^{2+} and Cd^{2+} interact with different sets of residues to activate BK channels.

3146-Pos Board B251

Calcium-Dependent Operation of the Human BK Channel Gating Ring Apparatus

Taleh Yusifov, Anoosh Javaherian, Chris Gandhi, **Riccardo Olcese**.

The large cytoplasmic C-terminal domain (CTD) of the human BK channel forms a gating ring structure composed by two tandem RCK domains serving as a signal transducer for intracellular Ca^{2+} and other ligands. However, the mechanism of the gating ring's operation remains unknown. We have used steady-state and time-resolved spectroscopy in combination with dynamic light scattering to the Ca-induced conformational changes of the purified CTD of human BK channel. The CTD domain of the human BK channel assembles as a tetrameric gating ring structure (MW~310 kDa) with a hydrodynamic radius (R_H) ~10.5 nm. In the presence of 35 μM free Ca^{2+}, R_H reversibly decreases to ~7.5 nm. The modulation of the gating ring hydrodynamic shape suggests that it undergoes Ca^{2+}-induced conformational transitions, which we further, characterized using time-correlated single-photon counting spectroscopy. Increasing free [Ca^{2+}] up to 35 μM shortened the average Trp fluorescence lifetime (τ_{avg}) of the wild-type gating ring from ~2.6ns to ~1.9ns, while the neutralization of the high-affinity Ca-binding site within RCK2 (Ca bowl, D894-898N) attenuated the effect of Ca^{2+}. Steady-state fluorescence analysis revealed that these ligand-dependent structural rearrangements of the gating ring possess strong divalent cation selectivity. The gating ring exhibited i) high-affinity Ca^{2+}-binding (K_{half_1} ~0.3μM and K_{half_2} ~4μM); ii) significantly lowered affinity for Mg^{2+} (K_{half} ~200μM) and iii) no Ba^{2+} sensitivity up to 13mM, consistent with the lack of Ba^{2+}-dependent BK channel activation. Interestingly, Ca^{2+} bowl neutralization eliminated Mg^{2+} sensing up to 12mM. In summary, under physiologically-relevant conditions, these ligand-induced conformational transitions are strongly ion-specific and associated with changes in the hydrodynamic properties of the BK gating ring and likely represent the ligand-induced molecular events underlying channel activation.

3147-Pos Board B252

On the Properties of the RCK1 Domain of the Human BK *(SLO1)* Channel

Taleh Yusifov, Anoosh Javaherian, Antonios Pantazis, Chris Gandhi, Riccardo Olcese.

In BK channels, four RCK1 and four RCK2 domains assemble into a cytosolic ligand-sensing superstructure known as the gating ring. While electrophysiological data suggest that both RCK1 and RCK2 contain high affinity Ca^{2+}-sensing sites, recent crystallographic data (Wu et al., 2010) has revealed Ca^{2+} binding only within the RCK2 domain. Does the RCK1 domain bind Ca^{2+}? What is the role of the high-affinity Ca^{2+} sensing residues D362/D367 (Xia, et al 2002) located in RCK1 domain? To address these questions, we expressed and purified the region of the human BK channel C-terminus corresponding to the amino acid sequence ^{322}IIE¼HDP^{667}. We have probed the structure and Ca^{2+} sensing properties of the RCK1 domain in solution, under physiologically relevant conditions. In addition to the α/β fold shared with its bacterial counterparts and human BK RCK2 domain, the RCK1 domain preferentially self-assembles into a homo-octameric structure. We recently reported that RCK1 undergoes Ca^{2+}-dependent conformational changes similarly to the RCK2 domain (Yusifov et al., 2008 and 2010). The neutralization of residues D362/D367 altered the secondary and quaternary structure of the RCK1 domain and prevented Ca^{2+}-induced structural transitions in RCK1. $^{45}Ca^{2+}$ overlay assay suggested that the neutralization of D362/367 did not abolish the Ca^{2+}-binding activity of RCK1 in the range of 2.1-115 μM free Ca^{2+}. While it cannot be excluded that D362/D367 are elements of a Ca^{2+} binding site with multiple coordinating residues, our results favor the view that D362 /D367 have a predominantly structural role. Possibly, these mutations set RCK1 domains in a conformational state that hampers the propagation of structural changes caused by ligand binding.

3148-Pos Board B253

Probing the Dynamic Structure of the BK_{Ca} Voltage Sensor: Relative Motion of Segments S0 & S4 During Activation

Antonios Pantazis, Azadeh Kohanteb, Riccardo Olcese.

Voltage- and Ca-activated, Large-conductance Potassium (BK_{Ca}) channel α subunits (Slo1) possess the transmembrane helix S0 at their N-terminus, which is absent in other members of the voltage-gated channel superfamily. S0 mediates the interaction between pore-forming α and modulatory β subunits, while it is thought to pack closely to voltage-sensing segment S4 (Liu *et al.*, 2010). We previously reported that conformational rearrangements relevant to voltage-dependent activation occur in the proximity of the BK_{Ca} N-terminus, by using voltage clamp fluorometry (Pantazis *et al.*, BPS meeting 2010). In this work, we have identified the principal molecular source of the fluorescence signal reported from the extracellular flank of S0 (positions 17, 18 or 19 labeled with the fluorophore TMRM) in W203, at the extracellular tip of S4: Substitution of W203 with a Valine reduced the amplitude of voltage-dependent ΔF/F reported from the extracellular portion of S0 by ≈90%. Accordingly, we demonstrate that the tryptophan side-chain is able to efficiently quench TMRM fluorescence with a Stern-Volmer constant K_{SV} = 41.3 M^{-1}. Considering this data, we suggest a model for the dynamic structure of the BK_{Ca} voltage sensor domain: at rest, S0 is in collisional proximity with S4, so that TMRM labeling S0 is quenched by W203. Upon depolarization, a relative motion between the two segments increases the distance between them, relieving TMRM quenching. Regarding the relevance of the relative motion between S0 and S4 to channel activation, we propose that S0 acts as a pivot, against which the voltage-sensitive S4 moves to actuate channel gating. We speculate that the modulation of the relative positions of S0 and S4 by β subunits could mechanistically explain their effects on voltage-dependent activation.

3149-Pos Board B254
Modular Allosterism in Potassium Channels
Daniel M. Sigg, Riccardo Olcese.
Allosteric interactions in ion channels serve to sharpen the control of environmental influences on conductance. We investigated the thermodynamic and kinetic properties of a multi-allosteric K^+ channel model possessing three distinct regulatory sites on each of four homologous subunits. Each site was characterized by a bistable free energy landscape with equilibrium constant *J,K*, or *P* that was sensitive to a particular environmental variable, as well the activation state of neighboring domains (see figure). The **P** domain comprising the central pore domain was defined by strong nearest-neighbor interactions that, combined with a counter-balancing bias in *P*, raised the energy and significantly shortening the dwell times of subconductance states. The mean number of activated regulatory sites was derived from the partition function through linkage analysis. A numbering scheme based on subunit occupancies of the 2^3 single-subunit activation states generated 330 energetically distinct kinetic states. Solutions to the rate equations simulated unique features attributed to different voltage-dependent K^+ channels (for example, intermediate pore activation states in the BK channel, and the rising phase and relationship with activation charge displacement observed in Shaker gating currents), supporting the feasibility of using a modular allosteric approach to K^+ channel activation.

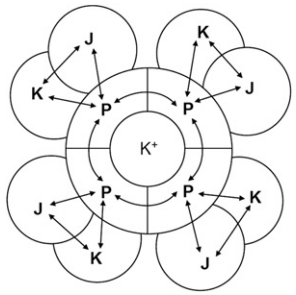

3150-Pos Board B255
Voltage Sensor Deactivation Inhibits BK Channel Opening by Mg^{2+}
Ren-Shiang Chen, Yanyan Geng, Karl L. Magleby.
Functional and structural studies suggest that intracellular Mg^{2+} activates BK channels through interaction with the voltage-sensing domain (Yang et al. 2007, 2008; Horrigan & Ma 2008; Yuan et al. 2010; Wu et al. 2010). To further explore the mechanism of activation of BK channels by Mg^{2+} through the low affinity E374/E399 Mg^{2+} sites located beneath the voltage sensors, we use single-channel analysis to study BK channels mutated to remove the high affinity Ca^{2+} sites. We find that 10 mM Mg^{2+} shortens the latency to first channel opening after a voltage jump to +100 mV from −100 mV, consistent with the hypothesis that Mg^{2+} can bind to the closed channel and shorten the latency. However, it is not clear whether the closed-channel binding occurs when the voltage sensors are deactivated (down) or activated (up). We therefore recorded single-channel activity in macro-patches held at constant −50 mV, where voltage sensors occasionally activate. Under this condition, 10 mM Mg^{2+} decreases mean closed duration and increases mean open duration. These effects are attenuated at −100 mV, and become negligible at −150 mV, where the voltage sensors are mainly deactivated. For BK channels modified to have deactivated voltage-sensors (R167E), 10 mM Mg^{2+} has little effect on mean closed and open durations at −50 mV. In contrast, for BK channels modified to have constitutively activated voltage sensors (R210C), 10 mM Mg^{2+} shortens the mean closed durations and lengthens the mean open durations at −200 mV. The above observations are consistent with a model in which voltage sensor deactivation inhibits BK channel opening by Mg^{2+}. Supported by NIH grant AR32805 and AHA 10POST4490012.

3151-Pos Board B256
Influence of Hydrophobic Residues on BK Channel Gating
Guido Gessner, Toshinori Hoshi, Stefan H. Heinemann.
Large-conductance calcium- and voltage-activated potassium (Slo1 BK) channels participate in the control of vascular tone and neurotransmitter release. A neuronal splice variant of BK channels with altered sequence in the S6/RCK1 linker exhibits increased open probability in 100 μM calcium at −150 mV (PoC) compared to "wild-type" BK channels (Soom et al. 2008, Channels 2:278-282). To identify amino-acid residues underlying this notable change in gating behavior, we expressed wild-type and mutant human Slo1 BK channels in HEK 293 cells and analyzed their calcium- and voltage-dependent gating in the inside-out configuration of the patch-clamp technique. Mutation G327L, located in the linker connecting the S6 helix to RCK1, most strongly increased PoC from 0.02 to 0.24. Systematic substitution at that site revealed that hydrophobicity is most important for channel opening at low voltages. PoC for G327F and G327Y were 0.19 and 0.01, respectively; addition of a single hydroxyl group ("F327Y") decreased PoC by 0.18. The same change in hydrophobicity by mutation F315Y within S6 has qualitatively opposite effects (Lippiat et al. 2000, J Physiol 529:131-138). Phenylalanine scanning mutagenesis of the S6/RCK1-linker region revealed that the mutation K330F most strongly increased PoC to around 0.5. Introduction of an additional hydroxyl group at this site ("F330Y") decreased PoC by 0.37 down to 0.13. We conclude that hydrophobicity within the S6/RCK1-linker region is a critical determinant of the calcium-dependent gating.

3152-Pos Board B257
Voltage-Dependent Inactivation Gating at the Selectivity Filter of the MthK K+ channel
Andrew S. Thomson, Brad S. Rothberg.
Voltage-dependent K+ channels can undergo a gating process known as C-type inactivation, which involves entry into a non-conducting state through conformational changes near the channel's selectivity filter. Here we report on a form of voltage-dependent inactivation gating observed in MthK, a prokaryotic Ca2+ -gated K+ channel. In single-channel recordings, we observe that Po decreases with depolarization, with a half-maximal voltage of 96 ± 3 mV. This gating is kinetically distinct from blockade by internal Ca2+ or Ba2+, suggesting it may arise from an intrinsic inactivation mechanism. Inactivation gating was shifted toward more positive voltages by increasing external [K+] (47 mV per 10-fold increase in [K+]), suggesting that K+ binding at the extracellular side of the channel stabilizes the open-conductive state. The open-conductive state was stabilized by other external cations, and selectivity of the stabilizing site followed the sequence: K+ ≈ Rb+ > Cs+ > Na+ > Li+ ≈ NMG+. Selectivity of the stabilizing site is weaker than that of sites that determine permeability of these ions, suggesting that the site may lie toward the external end of the MthK selectivity filter. We could describe MthK gating over a wide range of positive voltages and external [K+] using kinetic schemes in which the open-conductive state is stabilized by K+ binding to a site that is not deep within the electric field, with the voltage-dependence of inactivation arising from both voltage-dependent K+ dissociation and transitions between non-conducting (inactivated) states. These results provide a quantitative working hypothesis for voltage-dependent, K+-sensitive inactivation gating, a property that may be common to other K+ channels.

3153-Pos Board B258
C. Elegans Slo-2b uses its RCK1 Domain as a Ca^{2+} Sensor and does not Exhibit Cl^- Dependence
Zhe Zhang, Qiong-Yao Tang, Diomedes E. Logothetis.
Slo-2 channels play an important role in the adaption of neuronal firing rates and have been implicated in protection against ischemia. Slo-2 channels belong to the family of high-conductance potassium channels but their gating mechanism is unique and has been reported to exhibit species differences. The rat Slo2 (Slack) channel is activated by Na^+ and Cl^-, whereas the *C.elegans* Slo-2a has been reported to be sensitive to Ca^{2+} and Cl^-. Here, we report isolation of a novel isoform of the *C. elegans* channel Slo-2b (F08b12.3c) that was cloned from ESTs (YK1522e1, YK1193) of *C.elegans*, which has a distinct N-terminal region (by 18 amino acids) compared to the previously reported Slo-2a (F08b12.3b) (Yuan et al, 2000). This new clone shows voltage- and Ca^{2+}-activated macroscopic currents when expressed in *Xenopus* oocytes. We find that the *C. elegans* Slo-2b channel isoform exhibits a unitary conductance consistent with Slo-2a but it is not activated by Cl^-. Furthermore, the current characteristics of Slo-2b can be described well by the Horrigan-Aldrich model, which had been developed to describe Slo1 current properties. Mutagenesis screening revealed that the Slo-2b channel with mutation of a critical Glu residue in the RCK1 domain largely controls Ca^{2+} sensitivity. In contrast, mutations of negatively charged residues around the region corresponding to the Na^+ sensitive site of Slack channels in the RCK2 domain do not affect Ca^{2+} sensitivity of the Slo-2b channel. Thus, we conclude that the Ca^{2+} sensor of the Slo-2b in the RCK1 domain is largely sufficient to confer Ca^{2+}-sensitivity to the Slo-2b channel isoform.

3154-Pos Board B259
An Epilepsy/Dyskinesia-Associated Mutation in BK Channel Enhanced Channel-PIP_2 Apparent Affinity
Qiong-Yao Tang, Zhe Zhang, Vasileios I. Petrou, Diomedes E Logothetis.
Large conductance, Ca^{2+}- and voltage-gated BK (Slo1) channels are critical for neuronal functions. A previous study has shown that BK channels are regulated by membrane phosphatidylinositol 4,5-bisphosphate (PIP_2). However, the mechanism of such regulation remains largely unknown. Here we show that an Asp-to-Gly mutation (D369G) associated with the human syndrome of generalized epilepsy and paroxysmal dyskinesia (GEPD) enhanced channel-PIP_2 sensitivity in BK channels. With 106 mM Ca^{2+} in the bath, the inside-out patch G-V curve of D369G was leftward shifted by ~ −28mV, suggesting enhanced channel activity for the mutated channel. Following depletion of endogenous PIP_2 by poly-lysine, PIP_2 activated D369G in a dose- and voltage-dependent manner. The EC_{50} for diC8-PIP_2 activation of D369G decreased ~4-fold compared to the WT channel, suggesting an enhanced channel-PIP_2 interaction. Structural models of the BK channel place D369 near the membrane, where it could interact directly with PIP_2. To study the mechanism of BK channel regulation by PIP_2, we also used neomycin, a polycation that binds PIP_2, as an indirect assay of channel-PIP_2 affinity. We tested whether the D362G and D367G

mutants, sites previously shown to be involved in BK Ca^{2+}-sensitivity and located closely to D369, also affected channel-PIP_2 affinity. Our results show that the IC_{50} values for neomycin effects on both D362G and D367G were largely decreased (~100-fold), indicating that the mutations weakened channel-PIP_2 interaction. In contrast, the D369G mutation increased the IC_{50} for neomycin in a voltage-dependent manner, suggesting an enhanced channel-PIP_2 interaction. Taken together, these results suggested that mutation of the negatively charged residues D362 and D367, which lowers Ca^{2+} affinity, also decreases channel-PIP_2 affinity, while the mutant D369G, which increases Ca^{2+} affinity also enhanced channel-PIP_2 interaction. Thus Ca^{2+} and PIP_2 affinities are interrelated down to the single site interaction level.

3155-Pos Board B260

Structure-Function Studies of the Large Conductance Voltage-and Calcium-Activated Potassium Channel BETA1 Auxiliary Subunit

Bin Wang, Aleksandra Gruslova, Iurii Semenov, Robert Brenner.

BK channels are large conductance, voltage- and calcium-activated potassium channels. In smooth muscle, these channels maintain a polarized negative membrane potential and therefore deactivate calcium influx through voltage-gated calcium channels and reduce contraction. The smooth muscle-specific auxiliary β1 subunit confers increased BK opening and therefore plays an essential role in limiting smooth muscle contraction. β1 has at least two opposing gating effects: reducing intrinsic opening and stabilizing voltage-sensor activation. The goal of this research was to identify residues and structural domains that mediate these gating effects. Here, we performed an Alanine-scanning mutagenesis of β1 residues identical between β1, β2 and β4 based on the assumption that functionally important residues are likely to be conserved among family members. Effects of the Alanine mutants were categorized based on steadystate and kinetic effects on gating at 60, 4 micromolar and nominal 0 calcium. We found that 17 mutants display moderate or no effects at all calcium. 10 Class I mutants reduce conductance-voltage shifts at both high and nominal 0 calcium. Interestingly, all Class I residues are non-polar, and reside in the extracellular loop. This suggests that extracellular key residues may promote opening by providing a non-polar environment to the activated voltage senor. The only Class II mutant, G171A, abolished β1's ability in reducing opening in the absence of calcium. This suggests that G171 plays a critical role in reducing intrinsic opening. Finally, the mutagenesis data suggests that 2 evolutionarily conserved Cysteine pairs and their disulfides may play an important role in the extracellular β subunit structure. Combining single and double mutations, we found that the two amino acid pairs C53-C135 and C76-C103, may serve to form disulfide bonds that bring key extracellular Class I residues in close approximation.

3156-Pos Board B261

Investigation of BK Channel Gating using Mallotoxin

Janos Almassy, Ted Begenisich.

While large-conductance, BK K^+ channels are activated by both voltage and by Ca^{2+} in the microM range, the channels can be activated by voltage even in the absence of Ca^{2+}. BK channel β-subunits, several chemicals, and mutations can shift voltage activation toward more hyperpolarized potentials but in a rather complex manner. In contrast the accessory protein leucine-rich repeat containing protein 26 (LRRC26) and mallotoxin each appears to produce a simple shift. We have investigated the functional basis for the gating shift produced by mallotoxin in the absence and presence of the LRRC26 protein in the context of the Horrigan-Aldrich (HA) model. In the absence of intracellular Ca^{2+}, we found that, in addition to a hyperpolarizing shift of BK activation, mallotoxin produced a large, hyperpolarizing shift of channel activation kinetics. This result suggests that a major action of mallotoxin is to sensitize the BK channel voltage sensors. We also found that the degree of gating shift of mallotoxin was significantly decreased when co-expressed with the LRRC26 protein or in native parotid acinar cells that endogenously express this accessory protein. These results suggest that there is limit to the degree of sensitization of the BK channel voltage sensors.

3157-Pos Board B262

Cholesterol Regulates the Basal Functions and Ethanol Sensitivity of Large Conductance, Ca^{2+}-Sensitive K+ channel through Specific Cholesterol-Protein Interaction

Chunbo Yuan, Steven N. Treistman, Douglas F. Covey, Maohui Chen, Linda J. Johnston.

Membrane cholesterol plays an important role in regulation of a variety of ion channels and in maintaining the normal functions of cell membranes. The mechanism underlying this influence on ion channels, however, remains poorly understood. Cholesterol can act on ion channel proteins through either: 1) direct interaction with the protein, or 2) indirect effects on the biophysical properties of lipid bilayer. To differentiate between these alternatives, we used a synthesized enantiomer of cholesterol (ent-CHS). Enantiomeric forms of cholesterol have been used in the study of cholesterol-protein interaction, based upon the assumption that the effect on the lipid bilayer will be identical to that of natural cholesterol (nat-CHS), steric interaction directly with the protein will be abolished. We employed planar bilayer recording techniques to study the interaction of nat-CHS and ent-CHS with the large conductance, calcium-sensitive potassium channel (BK) in lipid bilayers of POPE/POPS (3/1, weight) and DOPE/SPM (3/2, weight), and examined how the presence of nat-CHS and ent-CHS affected the basal function and ethanol sensitivity of the BK channel. We found that ent-CHS increased BK channel conductance in both lipid bilayers similarly to that of nat-CHS. However, they are strikingly different in their effects on BK channel gating and ethanol sensitivity. In the POPE/POPS bilayer, nat-CHS dramatically reduced the open probability (Po) while ent-CHS did not. Both ent-CHS and nat-CHS reduced the ethanol sensitivity of the BK channel, but ent-CHS did so to a lesser extent. In the DOPE/SPM bilayer, nat-CHS dramatically changed the ethanol response of BK, depending on cholesterol concentration in the membrane. However, ent-CHS had little effect on ethanol sensitivity. We conclude that membrane cholesterol has a specific interaction with the BK channel that can directly influence ethanol's actions.

3158-Pos Board B263

The Slo1 C-Tail Domain Confers Cholesterol-Sensitivity to Arterial Smooth Muscle BK Channels

Aditya K. Singh, Anna N. Bukiya, Alejandro M. Dopico.

Large conductance, voltage- and calcium-gated potassium (BK) channels are known to cluster in cholesterol-rich cell membrane domains. Furthermore, cholesterol-BK channel interaction usually results in reduced channel activity (Po), as reported with native (Bolotina et al., 1989) and recombinant (Crowley et al., 2003) channels. We previously communicated that cholesterol-inhibition of BK channels cloned from rat cerebral artery myocytes (cbv1; AY330293) and reconstituted into POPE:POPS (3:1) bilayers displayed enantiospecificity and stereoselectivity, strongly suggesting that the decrease in Po involved cholesterol-recognition by a protein surface (Bukiya et al., Biophys. Soc. 2010). Using a similar system, we now demonstrate that cholesterol (16-33 mol%) inhibition of cbv1 channels is similar whether the channel is open by positive voltage or increased intracellular calcium, suggesting that the cholesterol-protein(s) interaction leads to altered channel function independently of the signal that gates the channel. Because the channel phenotype was characteristic of homomeric slo1, we hypothesize that regulation of BK gating by cholesterol involves an interaction between the steroid and the cbv1 subunit. One of the motifs that favors cholesterol-protein interactions is CRAC: -L/V-(X)(1-5)-Y-(X)(1-5)-R/K-, where X denotes any residue (Epand, 2008). We used CRAC sequence patterning and found ten CRAC motifs in cbv1, three in the core (S0-S6) and seven in the C-tail (S7-C end) domain. Thus, we next evaluated the cholesterol sensitivity of cbv1 channels truncated immediately after S6 (trS6cbv1). Remarkably, trS6cbv1 was consistently resistant to cholesterol-induced modulation (n=11) under conditions where *wt* cbv1 remained sensitive. Therefore, the C-tail domain confers cholesterol-sensitivity to cbv1 channels. We are currently using a combination of computational dynamics, sequential cbv1 truncation, and point mutagenesis in CRAC motifs to determine the relative contribution, if any, of these motifs to the cholesterol-sensitivity of BK channels.

Support: HL104631 (AMD), UTHSC Neurosci. Postdoc. Fellowship (AKS).

3159-Pos Board B264

A Functional Analysis of NaK at the Single Channel Level

Raymond W. Bourdeau, Valeria Vasquez, Julio F. Cordero-Morales, Eduardo Perozo.

NaK is a non-selective monovalent cation channel from *Bacillus cereus*. Despite being unable to discriminate between Na^+ and K^+, NaK shows high sequence similarity to other K^+ channels. Based on recently solved crystal structures in the closed and putatively open state, NaK exhibits an overall architecture similar to that found in the pore domain of tetrameric K^+ channels. Rb^+ influx studies suggest the channel conducts cations, however net flux is unusually low for a channel. The absence of electrophysiological data from NaK precludes significant understanding of it's functional behavior. Using a random mutagenesis approach together with a K^+ transport based screen, we have identified gain-of-function mutants in an attempt to develop a system for electrophysiological studies. One of these purified and reconstituted mutants was further studied by liposome patch-clamp. The channel displays non-selective conductances at 25 and 91 pS and is characterized by a low probability spiking

behavior. In addition, we show that NaK undergoes a voltage-dependent inactivation process, which is functionally similar to that seen in K^+ channels. This inactivation may contribute to the low flux of Rb^+ through NaK. Our functional characterization, along with the known crystal structures, now allows us to use NaK as a model system to further investigate structure-function correlations in non-selective channels and related selectivity filters.

3160-Pos Board B265
Engineering the hERG1 Selectivity Filter into the NaK Pore Domain
Julio F. Cordero-Morales, Vishwanath Jogini, Valeria Vasquez, Raymond W. Bourdeau, Haibo Yu, Benoit Roux, Martin Tristani-Firouzi, Eduardo Perozo.
Comparison of the hERG1 selectivity filter sequence and pore helix with a variety of prokaryotic ion channels revealed an unusually high sequence identity (63%) with the non-selective cation channel NaK (~19 amino acids). Taking advantage of this remarkable similarity, we have used NaK as a template to carry out a structural analysis of a hERG1-like NaK selectivity filter in K+. To engineer the NaK filter into that of hERG1, we substituted two critical residues, V59S in the pore helix and D66F at the selectivity filter (equivalent to positions Ser620 and Phe627 in hERG1, respectively). The final construct shares 73% sequence identity with the hERG1 selectivity filter, equivalent to the closest orthologue of hERG1, the bovine ether-a-go-go channel (bEAG1). Crystals of this engineered hERG-NaK diffracted to 2.8 Å resolution and were solved by molecular replacement using closed NaK as template. The crystal structure of hERG1-like NaK in 100 mM K+ revealed a striking similarity to the all canonical K+ channel filters in the conductive conformation (RMSD= 0.5 Å with the KcsA filter) and shows three major differences compared to WT NaK. First, hERG1-like NaK filter revealed four equivalent K+ binding sites. Second, the side chain of Phe66 residue establishes critical packing interactions with the adjacent aromatic residues from the pore helix. Third, hERG1-like NaK shows hydrogen bond interactions through a water molecule behind the selectivity filter, which is absent in WT NaK, but present in KcsA. We suggest that the hERG-NaK construct represents a unique tool to investigate the properties of the hERG1 channel selectivity filter at atomic level.

Muscle: Fiber and Molecular Mechanics & Structure II

3161-Pos Board B266
Radial Motion of Myosin Heads in Isolated Intact Rat Myocardium in Diastole
Gerrie P. Farman, HsiaoMan Hsu, David Gore, Edward J. Allen, Kelly Q. Schoenfelt, Younss Ait Mou, Thomas C. Irving, **Pieter P. de Tombe**.
The main cellular mechanism that underlies the so-called ''Frank -Starling Law of the Heart'' is an increase in the responsiveness of cardiac myofilaments to activating Ca^{2+} ions at longer sarcomere lengths (SL). The fundamental mechanism responsible for this increase in responsiveness has been elusive, despite considerable experimental scrutiny. Here we tested the hypothesis that the increase in calcium sensitivity upon increasing SL is correlated with a radially outward movement of the myosin heads during diastole. 2D x-ray diffraction patterns were obtained from electrically stimulated intact, twitching papillary muscle isolated from rat hearts during a 10 ms time window in diastole just prior to electrical stimulation. A range of sarcomere lengths was compared either at L_{max} (SL= ~2.3 μm) or following a quick release to slack length (SL=~1.9μm). The relative position of myosin heads was first assessed by the I_{11}/I_{10} equatorial intensity ratio. To our surprise, I_{11}/I_{10} was negatively correlated with SL, i.e. I_{11}/I_{10} was less at L_{max} vs. slack length. A more direct measure of the radial position of the myosin heads can be estimated from the position of the first maxima on the unsampled myosin layer lines, which are prominent in diastole. The intensity maxima, when examined pair-wise, moved outwards to a maximum of 5-6% for a 0.4μm change in SL indicating that the heads must be moving radially outward at slack length. Our data suggest that myofilament length dependent activation does not derive from a radial extension of the myosin heads at the long SL and must, therefore, involve some other mechanism. Supported by NIH HL75494 and RR08630.

3162-Pos Board B267
Electron Tomography of Thick Sections of Insect Flight Muscle
Claudia L. Vargas, Anthony Warrington, Kenneth A. Taylor, Susan Hester, R.J. Perz-Edwards, Michael K. Reedy.
Insect flight muscle (IFM) is a good model system within which to visualize actin-myosin interactions due to its highly ordered lattice of actin and myosin filaments. Lethocerus flight muscle is perhaps the best ordered muscle in nature. Electron tomography (ET) of Lethocerus IFM has recently resulted in a model for the weak to strong transition that incorporates large azimuthal changes in the position of the lever arm compared to that predicted from crystal structures of myosin subfragment 1 in both the nucleotide free and transition states (Wu et al. PLoS-ONE, Sept. 2010). Those studies did not visualize the S2 domain in either the raw tomogram or in subvolume averages which would clarify the crossbridge origin. Here we have used ET of IFM fibers in rigor in which the filament lattice has been swollen in low ionic strength buffer to view where S2 emerges from the thick filament backbone as a test of the weak to strong transition. Previous ET on myac layers (single filament layers containing alternating myosin and actin filaments) of these same swollen rigor fibers revealed the S2 domain with clarity. In the present work, we are examining 80 nm thick transverse and longitudinal sections of swollen rigor IFM fibers in order to visualize all of the crossbridges originating from each 14.5 nm crown on the thick filament, but especially the so-called lead bridges, which bind the thin filament within the same target zone of isometric contraction. Class averages of both thick filaments as well as myac layers are being pursued. The thick filaments show subfilaments in the backbone and many of the myac layer raw repeat subvolumes show S2. Progress on this study will be presented. Supported by NIGMS and NIAMSD.

3163-Pos Board B268
Vanadate Responses of Insect Fight Muscle
Robert J. Perz-Edswards, Rebecca L. Porter, **Michael K. Reedy**.
When exposed to sodium orthovanadate (Vi), permeabilized insect flight muscle (IFM) from *Lethocerus* water bugs behaves differently in three ways from vertebrate skeletal muscle (VSkM) under similar conditions.
Weak binding of Vi in RLX: IFM treated 5-10 min with 250 μM Vi in Lo-μ RLX buffer (= Vi-RLX) (pCa ~9.0; μ ~90 mM), then washed free of Vi in Lo-μ RLX, and placed in Lo-μ ACT buffer (pCa ~4.5; μ ~105 mM) rises to maximal isometric tension far more slowly (fives of minutes) than untreated IFM, suggesting a weak-binding, slowly reversible interaction with (presumably) myosin.
IFM 100x more sensitive to Vi than VSkM: Exposing maximally Ca-activated IFM to 250 mM Vi in Lo-μ ACT (= Vi-ACT) quickly suppresses active-state tension 97-100% and induces relaxed-state X-ray diffraction structure. Vi-ACT-exposed IFM recovers little or no active-state tension during 30-60 subsequent minutes in Lo-μ ACT. Vi-trapping in IFM is so strong that just 2 μM Vi ultimately (30-50 min) suppresses active tension in Lo-μ ACT by ~75%, suggesting that 50% IFM force inhibition would require 1 μM or less Vi, versus 45-94 μM in VSkM.
Only crossbridges opposite target zones are Vi-trapped: Despite 97-100% paralysis of Ca-activated isometric force production by Vi-ACT, Vi trapping only affects myosin crossbridges opposite actin target zones. When stretched 2-4%, fibers recover active tension capability. Post-Vi washout with RLX, followed by 2-4% stretch, followed by Lo-μ ACT exposure, generates significant Ca-activated tension, because at the longer sarcomere length target zones have moved toward myosin heads that at rest length were unable to reach the 2/7 fraction of IFM actin monomers (Wu *etal*, PLoS One **5**: e12643 (2010)) that accept strong-binding crossbridges, ATPase cycling and tight Vi trapping. Slow 3% length-cycling in Vi-ACT Vi-traps **all** accessible IFM crossbridges. (Support: NIH, MDA).

3164-Pos Board B269
N-Benzyl-P-Toluenesulfonamide (BTS) Traps the Myosin Head in a Conformation Associated with Strong Myosin Based Layer Lines and Weak, Rapidly Reversible Actin Binding even in the Absence of Nucleotide
Theresia Kraft, Ante Radocaj, **Bernhard Brenner**.
During its working cycle myosin proceeds through several structural changes coupled to changes in the state of the nucleotide. Details of the coupling between nucleotide state and myosin conformation are still unclear. Several lines of evidence suggest that for the same nucleotide state several conformations of the myosin head coexist while the state of the nucleotide may only determine their relative proportions (e.g., Xu et al., Biochemistry 2003; Nesmelov et al., Biophys J. 2008).
We were particularly interested whether with ADP or without nucleotide, i.e., when myosin binds tightly to actin, we can find experimental interventions for which (1) strong myosin based layer lines (MLLs) can be seen in 2D-X-ray diffraction patterns as sign of the closed, pre-power stroke conformation, and (2) binding kinetics of myosin to actin can be determined by fiber stiffness. While we were unsuccessful with blebbistatin, we found N-Benzyl-p-toluenesulfonamide (BTS) to accumulate myosin heads, both without nucleotide and with ADP, in structural states that generate strong MLLs. While BTS had no effect on MLLs in the presence of ATP, with ADP or no nucleotide BTS generated MLLs as strong as seen with ATP at high temperature. This suggests that

essentially all myosin heads can be trapped in a closed, pre-power stroke conformation by BTS even in the absence of nucleotide. Dependence of fiber stiffness on speed of applied stretches showed that nucleotide free myosin heads in the presence of BTS not only generate strong MLLs but also have much lower affinity for actin than seen without BTS and show rapid reversibility of binding to actin similar to that previously seen by us for weak binding states.

3165-Pos Board B270

A Reinvestigation of the Source of Compliance of Muscle Cross-Bridges

Massimo Reconditi, Marco Linari, Gabriella Piazzesi, Malcolm Irving, Vincenzo Lombardi.

In the X-ray diffraction pattern from skeletal muscle the 3rd order myosin-based meridional M3 reflection originates from the axial repeat of myosin cross-bridges along the thick filament. Changes in the intensity (I_{M3}), spacing (S_{M3}), and fine structure (R_{M3}) of the M3 reflection in contracting muscle have been measured in many different protocols (Linari *et al. PNAS***97**:7226, 2000; Piazzesi *et al. Nature***415**:659,2002; Reconditi *et al. Nature***428**:578**,** 2004; Huxley *et al.J. Mol. Biol.***363**:743, 2006). The results are explained with model simulations based on (1) the crystallographic structure of the myosin head (subfragment-1, S1), integrated with the tilting lever arm hypothesis (Rayment *et al. Science***261**:50, 1993), (2) the presence of a fixed periodic mass attributed to detached myosin heads and (3) the assumption that all the compliance of the cross-bridges resides in S1 (Seebohm *et al. Biophys. J.***97**:806, 2009). Here the possibility that a substantial proportion of the cross-bridge compliance is provided by the subfragment-2 (S2) link between the head and the thick filament (Knupp *et al. J. Mol. Biol.***390**:168, 2009) is analyzed by adding a variable compliance in S2 and testing the resulting model in the different mechanical protocols mentioned above and, moreover, against I_{M3} changes induced by rapid length changes imposed on the muscle fibre in rigor (Dobbie *et al.Nature***396**:383, 1998). The results show that S2 does not significantly contribute to the cross-bridge compliance.

3166-Pos Board B271

Multiscale Model Predictions of X-Ray Diffraction Patterns in Contracting Skeletal Muscle

Srboljub M. Mijailovich, Boban Stojanovic, Thomas Irving.

In order to explain time-resolved x-ray diffraction data, enabled by recent advances in synchrotron small-angle diffraction instruments, we explored the feasibility of using dynamic 3D models of muscle contraction to predict x-ray diffraction patterns. This approach differs radically from previous attempts, which merely aimed to provide a ''best fit'' structure for defined quasi-static states, by providing a tool to generate families of structures that evolve in time that explains both the structural (x-ray) and the mechanical data simultaneously. Specifically, we exploit the computational platform MUSICO which was developed originally to model muscle mechanics data, by extending this framework to simulate x-ray diffraction patterns using 3D multiscale models. These models take into account (i) biochemical states of myosin interacting with actin; (ii) rate constants in the actomyosin ATP hydrolysis cycle; (iii) function of myosin molecular motors in a 3D sarcomere lattice; (iv) Ca^{2+} regulation of myosin binding to actin; (v) extensibility of actin and myosin filaments; and (vi) multiple sarcomeres in series and in parallel. The platform is conceived primarily as a hypothesis-testing tool in which model predictions are tested against the best available mechanical and x-ray diffraction data on the same system. Our preliminary simulations provided dynamic x-ray diffraction patterns during force development and relaxation in skeletal muscle. The simulated patterns generally predicted well changes in repetitive molecular spacings and displayed similarity with experimental data. Once fully developed, this tool will enable extraction of maximum information from the x-ray patterns, in combination with the physiological data, and therefore provide a template to test hypotheses concerning crossbridge and regulatory protein action in working muscle. Our approach can be extended to any muscle system, and it could ultimately provide an interpretive framework for studying the mechanisms of inherited or acquired diseases.

3167-Pos Board B272

Effects of Cardiac Myosin Binding Protein-C and its Domains on the Rotational Dynamics of Actin Filaments

Brett A. Colson, Inna N. Rybakova, Ewa Prochniewicz, Richard L. Moss, David D. Thomas.

Cardiac myosin binding protein-C (cMyBP-C) is a multi-domain thick filament-associated modulator of contraction, but it remains unknown whether cMyBP-C alters myosin S1 access to the thin filament by its interaction with myosin S2 and/or by its interaction with actin. Recently, actin binding properties of baculovirus-expressed full-length mouse cMyBP-C and its domains (i.e., C0-C10), assessed by cosedimentation, showed that cMyBP-C interacts with F-actin via a single moderate-affinity site localized to the C-terminal half of cMyBP-C, with no effect on binding due to phosphorylation (Rybakova *et al.*, 2010, *J Biol Chem.*, in press). Here, we have determined the effects of cMyBP-C and its domains on the microsecond time-scale rotational dynamics of actin labeled at C374 with erythrosine iodoacetamide, using time-resolved phosphorescence anisotropy (TPA). The interaction of cMyBP-C with actin increased the final anisotropy ($r_{infinity}$) of the TPA decay in a concentration-dependent manner, indicating restriction of the rotational amplitude of actin dynamics. The N-terminal domains C0C1 had no detectable effect to on the final anisotropy of actin, probably due to its inability to bind actin, whereas C0C4 moderately increased final anisotropy. Fragments containing the C-terminal domains, such as delta-C0C1, increased final anisotropy to a similar extent as full-length cMyBP-C, suggesting that the C-terminal domains are important for restricting rotational dynamics of actin. Protein kinase A (PKA) phosphorylation of cMyBP-C or delta-C0C1 reduced, but did not eliminate, the effects of these proteins to increase the final anisotropy of the TPA decay. Increased anisotropy was not caused by actin bundling, as shown by electron microscopy observation. These cMyBP-C-induced changes in actin dynamics may play a role in the known effects of cMyBP-C on the functional actin-myosin interaction.

3168-Pos Board B273

Similar Regions of Instability in Tropomyosin and Myosin Coiled Coils

Douglas D. Root, Nakiuda Hall, Lee Chen, Yuxiao Qian, Nasrin Taei.

Tropomyosin shares sequence similarities with the N-terminal portion of the striated muscle myosin subfragment-2 (S2) coiled coil domain. Hypotheses of the instability of tropomyosin coiled coils may also be relevant to the myosin S2 coiled coil. Gravitational force spectroscopy indicates that the S1/S2 junction can be separated by forces applied through the rigor actomyosin bond which illustrates the low stability of this region of myosin. A comparison of the Langevian dynamics simulations on these two long coiled coils of tropomyosin and myosin suggests some similarities in the dynamics of these structures as well. An atomic model of full length tropomyosin was constructed by fusing existing crystallographic structures of tropomyosin fragments. Dynamics simulations of up to 10 nanoseconds at physiological temperatures yielded traces demonstrating regions where the coiled coil structure readily separates. Similar regions of instability are observed during dynamics simulations of human myosin S2 both in the existing crystallographic structure and in a full length myosin S2 predicted atomic model. Interestingly, mutations that give rise to familial hypertrophic cardiomyopathies appear to cluster in some of these regions of instability. Dynamics simulations on mutated atomic models of both tropomyosin and myosin S2 indicate that the mutations can impact the structure of these unstable regions. In myosin, a deletion mutation, del930, has a particularly strong structural impact and is known to cause a high incidence of sudden death clinically. These data suggest that such structural instabilities of homologous regions of tropomyosin and myosin might be a target for disease causing polymorphisms and could well be of important functional significance to the contractile functions in muscle.

3169-Pos Board B274

Orientation of the Calcium Sensitizing Agent dfbp-o, when Bound to Troponin in a Muscle Fiber as Determined by Solid-State NMR Spectroscopy

Samuel S.W. Szeto, **Ian M. Robertson**, Yin-Biao Sun, Brian D. Sykes.

Heart failure is characterized by the inability of the heart to supply the body with oxygenated blood. There is a large range of treatment strategies employed by physicians; however, many of these options are limited in their ability to improve mortality during acute heart failure. A more recently identified therapeutic option involves a class of pharmaceuticals termed ''calcium sensitizers''. These molecules enhance the contractile apparatus's response to calcium, instead of increasing the concentration of cytosolic calcium. Levosimendan is the most widely used calcium sensitizer, but since it is unstable, its exact mode of action has yet to be identified. Recently, we have determined that the stable structural analog of levosimendan, dfbp-o, functions as a calcium sensitizer in a similar manner as levosimendan [Robertson *et al*., J Mol Cell Cardiol. 2010 Aug 27. [Epub ahead of print]]. Two fluorine atoms are present on dfbp-o which can be used to elucidate useful structural information via ^{19}F-NMR spectroscopy. ^{19}F is a particularly attractive nucleus for study by NMR spectroscopy because like ^{1}H it is ~100% naturally abundant, has a spin of 1/2, and possesses a large gyromagnetic ratio. We have used ^{19}F solid-state NMR spectroscopy to study the orientation of dfbp-o in demembranated rabbit psoas muscle fibers. Upon incubating the muscle fiber in relaxing solution containing dfbp-o, the length of the fiber decreased approximately three fold, presumably due to the calcium sensitizing nature of dfbp-o. This approach will allow us to establish the orientation of the dfbp-o:troponin complex with respect to the thin filament axis. In addition, the results give us further evidence that dfbp-o binds muscle fibers to elicit its calcium sensitization effect.

3170-Pos Board B275
Cardiac-Specific Helical Structure in Troponin I Imparts Unique, Cardiac-Specific Contractile Function
Steven J. Ford, Ranganath Mamidi, Murali Chandra.
A coiled-coil between helical motifs of cardiac troponin I (cTnI) and cardiac troponin T (termed cH2(I) and cH2(T), respectively) forms a centrally positioned interface within the core domain of cardiac troponin. The centralized position and cardiac-specific structure of cH2(I) suggest an important, cardiac-specific regulatory role for this region of troponin I. However, whether the cardiac-specific structure of cH2(I) imparts unique, cardiac-specific function to cardiac myofilaments is not currently known. To better understand the functional significance of the structure of cH2(I), we studied the effects of replacing native troponin in detergent-skinned rat cardiac muscle fiber bundles with complexes containing chimeric cTnI in which cH2(I) was replaced with the corresponding helix from rat slow skeletal (ssH2(I)) or fast skeletal (fsH2(I)) troponin I. Ca^{2+}- and length-mediated myofilament force, ATPase activity, and length-dependent contractile dynamics were estimated at different levels of activation in muscle fibers reconstituted with wild-type or chimeric cTnI. Our preliminary work demonstrates that fiber bundles containing chimeric cTnI produced the same maximal force and ATPase activity, but exhibited significant differences in myofilament responsiveness to Ca^{2+} and changes in muscle length, when compared to bundles reconstituted with wild-type cTnI. Fiber bundles containing chimeric cTnI exhibited altered cooperativity and sensitivity of force production to Ca^{2+}. For example, myofilament cooperativity was lower and the sarcomere length-dependent change in myofilament Ca^{2+} sensitivity was less pronounced in fiber bundles reconstituted with ssH2(I) chimeric cTnI. Furthermore, length-dependent recruitment dynamics and the nonlinear effect by which crossbridge distortion influences crossbridge recruitment were both blunted in fiber bundles containing chimeric cTnI. These results indicate that replacing cH2(I) with either ssH2(I) or fsH2(I) results in aberrant cardiac contractile function, and suggest that the structure of cH2(I) is important to impart unique, cardiac-specific function in cardiac myofilaments.

3171-Pos Board B276
Deletions in the N-Terminus of Troponin T Reveal a Region Important for Ca^{2+}- and Length-Dependent Cardiac Myofilament Activation
Ranganath Mamidi, Steven J. Ford, Murali Chandra.
Interactions between the N-terminus of cardiac troponin T (cT1), a region rich in negatively charged amino acids, and the head-to-tail overlapping region of tropomyosin are responsible for localizing the troponin complex on the thin filament. Thus, cT1 is uniquely positioned on the thin filament to modulate cardiac contractile activity. Previous studies have demonstrated that truncations of cT1 result in severe inhibition of Ca^{2+}-activated force development and ATPase activity of cardiac myofilaments, indicating that cT1 is essential for cardiac myofilament activation. However, the specific region of cT1 that plays an important role in cardiac contractile activation remains unknown. To determine the specific region of cT1 that plays an important role in cardiac contractile activation, we progressively deleted cT1 in rat cardiac troponin T (RcTnT) to generate four deletion mutants, RcTnT 1-29 deletion, 1-43 deletion, 30-43 deletion, and 44-73 deletion. Cardiac contractile activity and crossbridge recruitment dynamics were studied in detergent-skinned rat cardiac papillary bundles reconstituted with either wild-type (control) or the deletion proteins. Our preliminary studies show that the Ca^{2+}-dependent force development, ATPase activity, myofilament Ca^{2+} sensitivity, and rate of crossbridge recruitment were significantly depressed in reconstituted fibers containing RcTnT 1-43 deletion. Fiber bundles reconstituted with RcTnT 44-73 deletion exhibited an increase in myofilament Ca^{2+} sensitivity. Another significant finding is that both RcTnT 1-43 and RcTnT 1-29 deletions resulted in an ablation of length-dependent increase in myofilament Ca^{2+} sensitivity, an important component of the Frank-Starling mechanism of healthy heart function. Thus, our data indicates that the region of cT1 comprising 1-43 amino acids plays an important role in Ca^{2+}- and length-dependent cardiac myofilament activation. Furthermore, our findings suggest that other regions of cT1 have specific roles in mediating cardiac myofilament activation.

3172-Pos Board B277
Flexibility Change in Human Cardiac α-Tropomyosin E180G Mutant: Possible Link to Cardiac Hypertrophy
Campion Loong, Huan-Xiang Zhou, P. Bryant Chase.
α-Tropomyosin (αTm) is the predominant tropomyosin isoform in adult human heart and constitutes a major component in Ca^{2+}-regulated systolic contraction of cardiac muscle. The familial hypertrophic cardiomyopathy (FHC)-related αTm E180G mutant is associated with decreased thermal stability and enhanced Ca^{2+}-sensitivity in functional assays. A mechanistic relationship between the E180G missense mutation and functional changes has not been established. We present here the first direct probe images of WT human cardiac and E180G mutant αTm by atomic force microscopy, and demonstrate that the mutant is more flexible than WT. Single molecules of bacterially-expressed human cardiac αTm were imaged on poly-lysine coated mica and their contours were analyzed. Analysis of tangent correlation along molecular contours yielded values of persistence length (L_p), which showed 27% increase in flexibility of the E180G mutant. Increased flexibility of the mutant was confirmed by shorter mean end-to-end length and fitting end-to-end length distributions to the worm-like chain model. Corresponding to increased flexibility, it is expected that less mechanical moment, and hence a lesser extent of Ca^{2+}-induced conformational change of troponin, are required to perturb αTm to initiate thin filament activation during systole, thus explaining enhanced Ca^{2+}-sensitivity of function. Hypersensitivity to Ca^{2+} could overwork cardiac muscle resulting in hypertrophy in FHC. Support: NIH and American Heart Association.

3173-Pos Board B278
Atomic Model of F-Actin-Tropomyosin
Xiaochuan Edward Li, Larry S. Tobacman, Ji Young Mun, Roger Craig, Stefan Fischer, **William Lehman**.
The presence of tropomyosin on the surface of actin filaments governs the access and hence the interactions and activity of numerous actin-binding proteins in muscle and non-muscle thin filaments. Electron microscopy and fiber diffraction studies of native and reconstituted F-actin-tropomyosin filaments reveal the azimuthal position of end-to-end linked tropomyosin molecules on the surface of actin. However, the longitudinal z-position and pseudo-rotation of tropomyosin along F-actin is still uncertain. Without this information, atomic models of F-actin-tropomyosin, unconstrained by troponin in striated muscle or other actin-binding proteins in smooth muscle or somatic cells, cannot be formulated, and thus the optimal interfacial contacts between actin and tropomyosin remain unknown. We have carried out a computational search assessing electrostatic interactions for multiple azimuthal locations, z-positions and pseudo-rotations of αα-tropomyosin on F-actin. The information gleaned was used to localize tropomyosin on F-actin, yielding an atomic model characterized by protein-protein contacts that primarily involve clusters of basic amino acids on actin subdomains 1 and 3 juxtaposed against acidic amino acids on successive quasi-repeating units of tropomyosin. A virtually identical model generated by docking F-actin and tropomyosin atomic structures into EM reconstructions of F-actin-tropomyosin validated the above solution. Here, the z-position of tropomyosin alongside F-actin was defined by matching the ''broad'' and ''narrow'' faces typifying tropomyosin's twisting superhelical coiled-coil to the twisting contours of the tropomyosin densities seen in F-actin-tropomyosin reconstructions. Our computational search indicates that, in the absence of troponin or other actin-binding proteins, tropomyosin occupies an optimal z-position and rotation in the surrounds of the closed C-state location on actin. However, no specific electrostatic minima were noted when tropomyosin was shifted computationally toward the open or blocked states on the troponin/myosin-free structure. The functional implications of the F-actin-tropomyosin model that has been determined will be discussed.

3174-Pos Board B279
Structural Simulations of Troponin-Regulated Tropomyosin Movement on F-Actin
Marek Orzechowski, Stefan Fischer, William Lehman.
Contraction of striated and cardiac muscles is regulated by a mechanism involving two major components: tropomyosin and troponin. Tropomyosin strands that run along the actin filaments block the myosin-binding sites in resting muscle. However, when concentration of Ca^{2+} ions is increased, the position of tropomyosin on actin is shifted and the myosin-binding sites are unblocked. This leads to myosin-crossbridge cycling on actin and, as a result, muscle contraction. The unblocking of myosin-binding sites is triggered by troponin. Troponin itself is a complex of three proteins: Ca^{2+}-binding troponin-C, inhibitory troponin-I and troponin-T, which links the complex to tropomyosin on the actin filament. To investigate the thin filament regulatory process, we are applying the Conjugate Peak Refinement (CPR) technique to determine energetics of the transition of tropomyosin on actin from the closed to the open state. CPR should also help to refine the precise position of tropomyosin in the open state. Results from the CPR calculations are verified by comparison with observations from EM experiments. In addition, corresponding structural transitions associated with troponin are being addressed. In particular,

interactions of the mobile C-terminal domain of TnI with TnC and actin are being examined. One of the objectives is to determine the location and orientation of the troponin complex on F-actin both at low and high concentration of Ca^{2+} ions, which are still uncertain. Additionally, Sykes and colleagues have proposed in a recent ''fly-casting'' model that the latter part of TnI competes with tropomyosin for access to a binding site on F-actin. Molecular Dynamics simulation of TnI, tropomyosin and actin performed at atomic resolution is being used to define relationships among the proteins involved in this regulatory process.

3175-Pos Board B280

Molecular Dynamics of Tropomyosin Bound to F-Actin

Xiaochuan Edward Li, Stefan Fischer, William Lehman.

We have previously studied the structural mechanics of isolated tropomyosin molecules by electron microscopy and Molecular Dynamics protocols. We found that single tropomyosin molecules bend anisotropically without showing any signs of kinks or joints. We observed that, even in the absence of actin, tropomyosin, on average, has a shape matching the helical curvature of F-actin filaments. Moreover, isolated tropomyosin is semi-rigid with an apparent persistence length (an estimate of curvature) of 104 nm and dynamic persistence length (a measure of flexibility) of 423 nm (Li et al., 2010). In order to determine the likely position of tropomyosin on F-actin, we docked theMD structure of tropomyosin into EM reconstructions of F-actin-tropomyosin. The location found is the same as that computed for tropomyosin on F-actin following a search to optimize their intermolecular electrostatic contacts. We have initiated NAMD MD simulations of this structure of F-actin-tropomyosin at 300°K in explicit water including 150mM NaCl. Here tropomyosin fluctuates locally around the closed C-state position on F-actin, maintaining its initial electrostatic contacts as well as hydrophobic interactions with actin residue Pro333. Over the current 25 ns MD run, the apparent and dynamic persistence lengths of the tropomyosin on F-actin are 113 nm and 3318 nm, demonstrating that tropomyosin maintains a comparable degree of curvature either when bound to F-actin or when unbound, but that its flexibility is restricted by the presence of F-actin. Any azimuthal movement of tropomyosin on F-actin that is induced by troponin and/or myosin may require perturbation of the weak stabilizing interactions noted between tropomyosin and F-actin. We are continuing the current MD run and are also planning to run simulations at higher temperatures in attempting to detect transitions of tropomyosin to the open and blocked M- and B-states of the thin filament.

3176-Pos Board B281

Thin Filament Length in Mouse Skeletal Muscle and its Relationship to Differential Splicing of Nebulin

Danielle Buck, Paola Tonino, Adam Hoying, Henk Granzier.

Nebulin is a large actin binding protein (600-800 kDa) which undergoes differential splicing to yield proteins of various sizes in different skeletal muscles. This giant protein has been proposed to function as a molecular ruler to determine the length of the thin filament in skeletal muscle. Using electron microscopy, we measured the length of the thin filament in mouse skeletal muscle. It was found that the length of the thin filament was greatest in the soleus (1.25 $\pm$ 0.004, N=136), shortest in the psoas major muscle (1.20 $\pm$ 0.011, N=102), and intermediate in the tibialis cranialis muscle (1.22 $\pm$ 0.005, N=161). Next, we estimated the molecular weight of nebulin in these tissues to assess if nebulin size correlates with thin filament length. In mice, nebulin size was found to vary between 700kDa in the psoas major, extensor digitus longdum and gastrocnemius to 750kDa in the soleus and diaphragm muscle while intermediate lengths were found in quadriceps and tibialis cranialis muscle. Since there was a positive correlation between thin filament length and nebulin size, we next sought to determine if the differences in nebulin size could be explained by differential splicing of nebulin between mouse skeletal muscles. Using a home-made nebulin exon microarray, we compared the exon composition between these muscles and found that the soleus muscle nebulin isoforms contains M-repeats in the Z-disk (exons 153-155) while nebulin isoforms in other muscle types do not contain these repeats. This data has been confirmed by qPCR. In conclusion, the changes in nebulin size between mouse skeletal muscles can partially be explained by differential splicing of the nebulin gene, and further studies are needed to ascertain in the mouse the correlation between nebulin size and thin filament length.

3177-Pos Board B282

The Function of Obscurin in Regulating Assembly and Symmetry of the Sarcomere in Drosophila Flight Muscle

Anja R. Katzemich, Kevin R. Leonard, John C. Sparrow, **Belinda Bullard**.

Obscurin is a 400 kDa protein in the M-line of insect flight muscle (IFM). The protein has 21 Ig domains, two Fn3 domains and two kinase domains near the C-terminus. The effect of reducing the expression of obscurin on the structure of the sarcomere was investigated. A P-element inserted into the first intron of the gene resulted in reduced protein expression and homozygotes were unable to fly. Sarcomere length was normal, but the M-line was missing and the H-zone shifted from the middle of the sarcomere. Obscurin RNAi mutants had a similar but more extreme phenotype. Electron micrographs of mutant sarcomeres showed that thin filament length and the polarity of crossbridges was dependent on the position of bare zones in adjacent thick filaments: shifted bare zones resulted in abnormally short or long thin filaments. Isolated thick filaments were asymmetrical with displaced bare zones and in RNAi mutants, some thick filaments were up to three times the normal length. The kinase domains of obscurin are predicted to be inactive. Ligands binding to the two domains have been identified. Kinase 1 binds ball, itself a kinase, and kinase 2 binds MASK, which contains ankyrin repeats. MASK is present in both Z- and M-lines. RNAi mutants of ball and MASK had IFM with abnormal sarcomere structure: H-zones were shifted, thick filaments asymmetrical, and Z-discs irregular. Surprisingly, expression of obscurin was normal in RNAi mutants of both ligands, and MASK was present in obscurin RNAi mutants. Therefore, correct assembly of the sarcomere needs obscurin, ball and MASK. Obscurin is likely to form a scaffold binding ball and MASK. The two ligands are genetically linked to the same signalling pathway in the development of muscles in Drosophila.

3178-Pos Board B283

Effect of Confinement on Titin Conformation and Elasticity

Tannie B. Liverpool, **Larissa Tskhovrebova**, John A. Trinick.

Elasticity in muscle sarcomeres results largely from the mechanical properties of the giant protein titin. The I-band parts of titin molecules form filamentous connections between thick filaments and the Z-line, and behave as semi-flexible polymers, passively coiling and uncoiling during changes in sarcomere length. Important questions about titin mechanics *in vivo* concern effects of confinement, due to the surrounding actin filament lattice and to the high local concentration of titin. The actin lattice changes across the I-band, from hexagonal near the A-band to tetragonal towards the Z-line. At resting sarcomere length, a single hexagonal unit cell has radius ~27 nm (Millman, 1998) and contains the six titin molecules that emerge from each thick filament, with a space of radius R ~11 nm available to each molecule. The tetragonal lattice has average side length ~24 nm and contains three titin molecules, with radius ~7.8 nm for each molecule. Taking into account the condition for transition from weak to strong confinement $2R < R$F (De Gennes, 1979), or $2R \sim L$p (Cifra, 2009), and the average persistence length of titin (Lp, 9-19 nm), it can be concluded thatI-band titin is confined towards the Z-line. We analysed the effect of cylindrical confinement on the force-extension relationship of a polymer chain and showed it to lead to stiffening of the chain. This result, together with the above estimates, indicates that values of titin stiffness *in situ* derived from the interpolation formula for an unconfined worm-like chain (Marko & Siggia, 1995) are likely to be underestimates, even if titin molecules cross the I-band independently.

3179-Pos Board B284

Free Fall Force Spectroscopy of Nebulin Suggests Improved Folding after Repeated Stretching

James W. Dunn, Jeffrey G. Forbes, Kuan Wang, Douglas D. Root.

The gravitational force spectrometer (GFS) is capable of applying physiological forces from femtonewtons to the nanonewtons that single molecules might experience in their native environments. While macromolecules are under such loads, the instrument is also capable of measuring the absolute molecule length with a resolution of $\pm$ 5 nm. In order to measure a range of forces on the same single molecule, the GFS was attached to a spring system and dropped at up to free fall conditions which varied the force stretching the molecule from zero to greater than the weight of the attached glass microsphere. To apply this method to full length nebulin, the nebulin molecules were attached between two microspheres coated with antibodies to the N-terminus of nebulin on one microsphere and to the C-terminus on the other microsphere. Nebulin's structure is far less ordered than the coiled coil motif of the myosin rod, however, its properties are believed to include a function as an actin ruler in the sarcomere. By extending from the Z line to the end of the thin filament, it would measure approximately a micron, and it is thought to act as a compression spring to keep the actin under load. The force spectra of nebulin molecules acquired by this instrumentation indicated that upon repeated stretching, the nebulin displayed greater range of extension and less hysteresis in its force distance curve, and this change was maintained for at least one hour after the initial stretching. This result is consistent with the recent stretch-to-match ruler hypothesis (Langmuir 25:7496), and it also demonstrates that nebulin could be extended to near full length (800 nm) by forces of only 80 pN when the force is applied repeatedly to the same single molecule.

3180-Pos Board B285
New Obscurins Play a Role in Cardiac Electrochemical Signaling
Maegen A. Ackermann, Jane Valenti,
Aikaterini Kontrogianni-Konstantopoulos.
Obscurins are a family of modular proteins expressed in striated muscle cells. Alternative splicing events give rise to various isoforms containing a combination of adhesion modules and signaling motifs. The prototypical obscurin (obscurin-A) is a giant (~720 kDa) multidomain protein that intimately surrounds sarcomeres at the level of M-bands and Z-disks where it is appropriately positioned to participate in their assembly, stability and integration with other sarcoplasmic elements.
Our laboratory has recently identified a novel isoform of obscurin (referred to as obscurin-D), that results from complex differential shuffling at the 3' end of the OBSCN gene leading to the usage of an alternate initiation codon within exon 82. The obscurin-D transcript encodes a protein that contains tandem rho-guanine nucleotide exchange factor (Rho-GEF) and pleckstrin homology (PH) motifs followed by two immunoglobulin (Ig) domains and non-modular sequences. Using immunofluorescence combined with confocal microscopy and Z-stack sectioning, we found that obscurin-D localizes at the intercalated disc (ICD), the unique membrane microdomain of cardiomyocytes that contributes to the electrical and mechanical coupling of neighboring cells. This finding was further confirmed by immunoelectron microscopy, which indicated the presence of obscurin-D throughout the length of the ICD, at the transitional zone. Consistent with this, biochemical assays demonstrated that obscurin-D is in a complex with major ICD proteins, including N-cadherin, vinculin and connexin-43, and may bind to membranes through its PH domain, following activation of phosphoinositide 3 kinase (PI3K). Experiments are currently under way to examine the roles of obscurin-D at the ICD by manipulating its expression levels through adeno-associated mediated viral gene delivery in whole animals.

3181-Pos Board B286
How to Catch Moby Dick: Systematic Identification of Binding Partners for UNC-89 (Obscurin)
Hiroshi Qadota, Ge Xiong, Kristy Wilson, M. Berenice Duran,
Emily Swartzbaugh, John Nahabedian, **Guy Benian**.
Mutations in *unc-89* result in adult *C. elegans* with reduced motility and disorganized, thinner sarcomeres. UNC-89-B (8,081 residues) has 53 Ig domains, 2 Fn3 domains, SH3, DH and PH domains at its N-terminus, and 2 protein kinase domains (PK1 and PK2) at its C-terminus. The human homolog is called ''obscurin''. Antibodies localize UNC-89 to the M-line. To understand how UNC-89 is localized and how it performs its functions, we are systematically identifying its binding partners. UNC-89-B is entirely represented as 16 overlapping segments in 2-hybrid vectors. All 16 have been used to screen ~23 known components of the nematode M-line. 7/16 have been used to screen a 2-hybrid library. We have identified 6 partners, each with human homologs, and all but one localized to M-lines. Both PK1 and PK2 interact with SCPL-1, a CTD-type protein phosphatase. *scpl-1* mutants display defective egg laying muscles, and ''hyper-bending'' during locomotion. PK1 and the ''interkinase region'' interact with LIM-9 (FHL). *lim-9(RNAi)* show aggregates of myosin. Ig50-Ig51 interacts with HIF-1 (hypoxia inducible factor), and Fn1-Ig52 interacts with HUM-6 (class VII myosin). Ig1-Ig2-Ig3 interacts with CPNA-1, a copine domain containing protein. Loss of function for *cpna-1* results in a Pat embryonic lethal phenotype, characteristic of mutations in 19 other genes, most of which encode products associated with integrin associated muscle adhesions. Three segments, Ig9-Ig11, Ig18-Ig23, and Ig50-Ig51 interact with CUL-1, a cullin, known to act as a scaffold for assembly of the ubiquitylation protein degradation machinery. *cul-1(RNAi)* shows disorganization of thick filaments in a pattern similar to that of *unc-89(su75)*, an allele lacking all CUL-1 binding sites. My talk will focus on the role of CPNA-1 in localizing UNC-89, and the UNC-89/CUL-1 interaction as a novel means of regulating protein degradation in muscle.

3182-Pos Board B287
Interaction of Obscurin a with Small Ankyrin 1
Robert J. Bloch, Ben Busby, Taiji Oashi, Chris Willis, Maegen Ackermann,
Aikaterini Kontrogianni-Konstantopoulos, Alexander D. Mackerell Jr.
We have studied the binding of a small product of the ankyrin 1 gene (sAnk1; Ank1.5), a ~17.5 kDa integral protein of the sarcoplasmic reticulum, to the C-terminus of obscurin A, a ~720 kDa protein that envelopes sarcomeres at Z-disks and M-bands. Alanine scanning mutagenesis identified several lysines and arginines in the cytoplasmic sequence of sAnk1 that mediate binding to obscurin, and several glutamates in the high affinity site of obscurin that mediate binding to sAnk1. Complementary K- or R-to-E and E-to-K mutations identified specific pairs of residues involved in binding; mutagenesis of several of these eliminates binding. Molecular and Brownian dynamics simulation suggested several possible models for the docked complex but predicted only one in which D111 of sAnk1 and K6338 of obscurin interact. We confirmed their interaction by complementary mutagenesis. We tested the model further by using similar approaches to examine the hydrophobic residues involved in binding, with results consistent with the predictions of a representative structure of the docked complex selected from cluster analysis of structures generated from molecular dynamics simulations. Our studies indicate that the obscurin-binding region of sAnk1 is comprised of two ankyrin-like repeats, which establish specific electrostatic and hydrophobic contacts with the high affinity site on obscurin, composed of an 18-residue α-helical polypeptide. We identify structures similar to this polypeptide in the binding regions of proteins that interact with other ankyrin repeat proteins. We propose that the 18-mer in the high affinity binding site on obscurin for sAnk1 represents a prototypical ankyrin binding motif.
Supported by grants to ADM from the NIH (CA120215; GM051501) and the University of Maryland Computer-Aided Drug Design Center, and from grants to AKK and RJB from the MDA and the NIH (RO1 AR052768 to AKK; RO1 AR056330 to RJB).

3183-Pos Board B288
Novel Insights in the Function of the Giant Sarcomeric Proteins Titin and Nebulin
Henk Granzier.
The striated muscle sarcomere contains two giant proteins: titin and nebulin. Titin is a giant elastic protein (3-4 MDa) that spans the half sarcomere from Z-disc to M-band, and is responsible for a large fraction of passive stress that develops when muscle is stretched. Alternative splicing results in large fetal isoforms and smaller adult isoforms that differ mainly in the size of their extensible I-band region. Differences in the mechanical properties of these isoforms and how these properties are altered by excision of specific spring elements have been recently established using novel knockout models. Findings show that titin mechanics can be tuned by phosphorylation, including the recently discovered PKG and PKC phosphorylation pathways. Furthermore, titin-binding proteins that interact with titin along the full length of the sarcomere play a role in protein turnover, and in sensing mechanical stresses that initiate hypertrophic signaling. Nebulin is a giant 600-900 kDa filamentous protein that is an integral component of the skeletal muscle thin filament. Recent improvements in the field, especially the development of mouse models deficient in nebulin (NEB-KO mice), indicate that nebulin functions, in addition to its role in thin filament length specification, in the regulation of muscle contraction. Muscle fibers deficient in nebulin have a higher tension cost, and develop less force due to reduced myofilament calcium sensitivity and altered crossbridge cycling kinetics. These novel functions indicate that nebulin might have evolved in vertebrate skeletal muscles to efficiently develop high levels of muscle force. The NEB-KO mouse models also highlight nebulin's role in the assembly and alignment of the Z-disks. Importantly, rapid progress in understanding nebulin's in vivo roles provides clinically important insights in how nebulin deficiency in patients with nemaline myopathy contributes to debilitating muscle weakness.

3184-Pos Board B289
Deciphering the Functional Properties of Nebulin: It is a Stabilizer!
Chris T. Pappas, Paul A. Krieg, **Carol Gregorio**.
Striated muscle cells display one of the most extreme examples of molecular organization found in nature. Efficient muscle contraction requires precise regulation of actin (thin) filament lengths. In one highly cited model, the giant protein nebulin (~750-900 kDa) has been proposed to function as a ''molecular ruler'' specifying filament lengths. We directly challenged this hypothesis by constructing a unique, small version of nebulin (mini-nebulin). When endogenous nebulin was replaced with mini-nebulin in skeletal myocytes, thin filaments extended beyond the end of mini-nebulin; an observation that is inconsistent with a strict ruler function. However, under conditions that promote actin filament depolymerization, filaments associated with mini-nebulin were remarkably maintained at lengths either matching or longer than mini-nebulin. This indicates that mini-nebulin is able to stabilize portions of the filament it has no contact with. Knockdown of nebulin also resulted in more dynamic populations of thin filament components, while expression of mini-nebulin decreased the dynamics at both ends of the filament (i.e., efficiently recovered loss of endogenous full-length nebulin). Taken together, our data reveals that nebulin regulates thin filament architecture by a mechanism that includes stabilizing the filaments and preventing actin depolymerization.

3185-Pos Board B290
A Novel Assay of Mechano-Transduction in Single Muscle Cells
Christopher W. Ward, Benjamin L. Prosser, Maura Greiser,
Håkan Westerblad, Ramzi Khairallah, W.J. Lederer.
In striated muscle the tight integration of contractility and biomechanical properties with electrical, metabolic and hormonal signaling are defined as mechano-transduction signaling pathways. The great interest to define the molecular basis for mechano-transduction is underpinned by the growing number of loss-of-function disorders and diseases in which altered mechano-transduction has been identified.
Intact, single cell preparations are attractive for studying mechano-transduction, however the mechanical loading of single cells requires technically challenging methods. We have recently developed MyoTak, a tenacious biological adhesive, which enables us to attach single dissociated striated myocytes (skeletal and cardiac) to force transducer and length controller units. The myocytes thus prepared can be readily imaged using an inverted microscope equipped with confocal, widefield and multiphoton fluorescence imaging systems. With this preparation we have been able to control myocyte length while assaying passive tension and electrically evoked contractility. In recent experiments we have explored the interaction of myocyte stretch and contractility with Ca^{2+} signaling, mitochondrial function and ROS production. We will present these new findings, the novel methods and additional experiments examining the role of microtubules as mechano-transducer elements that contribute to these interactions.
Supported by RC2 NR011968 to CWW, and to WJL (NHLBI P01 HL67849 and R01-HL36974; Leducq North American-European Atrial Fibrillation Research Alliance; European Union Seventh Framework Program (FP7) ''Identification and therapeutic targeting of common arrhythmia trigger mechanisms'' and support from the Maryland Stem Cell Commission).

3186-Pos Board B291
Dynamic Interactions between the Myocyte and Extracellular Matrix Promote Myocyte Differentiation and Myofibril Assembly
Maide O. Raeker, **Mark W. Russell**.
During development, skeletal myoblasts differentiate into myocytes and skeletal myotubes with mature contractile structures that are precisely oriented with respect to surrounding cells and tissues. Establishment of this highly ordered structure requires reciprocal interactions between the differentiating myocytes and the surrounding extracellular matrix to form correctly positioned and well organized connective tissue attachments from the skeletal muscle to the bony skeleton. Using the developing zebrafish embryo as a model, we examined the relationship between new myofibril assembly and the organization of the membrane domains involved in cell-extracellular matrix interactions. We determined that apical clustering of integrins was associated with changes in cell morphology which included myoblast elongation along the body axis. Through the analysis of zebrafish embryos depleted of obscurin A that have impaired formation of the myotendinous junctions, we determined that cell elongation and, as a result, new myofibril formation was delayed in regions that lacked integrin clustering and fibronectin matrix organization. In addition, it was noted that striated myofibrils first form at the cell periphery and are associated with the early patterning of the lateral sarcolemma. These specialized membrane domains will ultimately form mature lateral connections between the myofibril and the extracellular matrix at the costameres. We have also determined that the giant cytoskeletal and sarcomeric protein obscurin has an important role in the organization and maturation of the MTJ and in the maturation of the costamere. As myocyte-extracellular matrix connections have critical roles in force transduction and tension-mediated signaling defining the processes that promote and sustain these connections will have important implications for the understanding the pathogenesis of, and developing new treatment strategies for, a range of myopathies and muscular dystrophies.

3187-Pos Board B292
Muscle Giants Create Order from Chaos with Force
Kuan Wang, Jeffrey G. Forbes.
Titin and nebulin possess perhaps the longest span of intrinsically disordered protein segments in the human proteome. We have implemented an integrated platform of nanomechanics to investigate the elasticity of intrinsically disordered segments and its functional manifestations. Our titin studies have indicated that the titin PEVK region is an elastic spring, with charge pairing as a new mechanism of creating diversity and modulating molecular elasticity. Significantly, PEVK also serves a dual role as a giant scaffold for SH3-containing signaling proteins. Many novel hybrid and overlapping motifs for SH3 domains are embedded in the seemingly random proline-rich sequences throughout the titin molecule. We now propose that titin PEVK directly couples the force sensing and response, by controlling the accessibility of SH3 receptor proteins via the opening and closing the access to binding sites upon mechanical stress, reversibly and elastically. In other words, titin's elastic PEVK appears to act both as an analog force sensor and as a transducer that converts the force input directly into biochemical signals of the SH3 pathways. Our nebulin studies indicated that native full length nebulin and nebulin modules are intrinsically disordered and elastic. We proposed that that nebulin is an "elastic or adjustable ruler" that has to be stretched and lengthened properly to interact and stabilize actin filaments. The continued presence of compressive force exerted by stretched nebulin may well be a requirement for thin filament assembly, integrity and maintenance. Additionally, since skeletal muscle thin filaments is thought to be "dually-regulated" where calcium activates contraction by targeting both troponin and nebulin-bound calcium sensor proteins (Root and Wang 1994), we envisage that nebulin tethers elastically myosin heads to actin in the inactivated state and then releases and de-inhibits myosin heads upon calcium activation.

Excitation Contraction Coupling II

3188-Pos Board B293
Electron Microscopy of Cryo-Sectioned Skeletal Muscle by Focused ion Beam Milling
Terence Wagenknecht, Chyong-ere Hsieh, Michael Marko,
Clara Franzini-Armstrong.
Knowledge of the detailed three-dimensional architecture of the couplon, the fundamental functional unit of excitation-contraction coupling (ECC), is essential for understanding the mechanism of ECC in striated muscle. Transmission electron microscopy of conventional thin-sectioned skeletal muscle resolves some structural features of the couplon: (1) the sarcoplasmic reticulum (SR) -associated ryanodine receptors whose cytoplasmic regions (''foot'' structures) bridge the junctional gap between the transverse (T-) tubule, and (2) density in the SR lumen attributable to calsequestrin. However, many structures are surely not resolved due to resolution and specimen preparation limitations. To advance further, we propose to image the native ECC machinery by cryo-electron microscopy and tomography of vitreously frozen thin sections of muscle. Obtaining suitable vitreous sections by ultramicrotomy is difficult and artifact-prone, and so we are investigating the application of focused ion beam (FIB) milling to obtain cryo-sections of 200 nm or less in thickness. The first cryo-micrographs of FIB-milled skeletal muscle from toadfish swimbladder (glutaraldehyde fixed) have been obtained, and they show structural features seen previously, as well as some additional ones (e.g., mass densities within the T-tubule lumen, densities associated with the T-tubule in the vicinity of RyRs). The micrographs obtained from FIB-milled specimens appear comparable to those obtained by cryo-ultramicrotomy, but without the defects, such as specimen compression, associated with the latter technique. Our goal is to extract many RyR-containing sub-volumes from tomograms of cryo-sectioned muscle, and then to average them so as to reproducibly resolve additional fine structure within the couplon.

3189-Pos Board B294
Inducible Silencing of Junctophilins in Skeletal Muscle Leads to Reversible Remodeling of the Triad Junction Structure and Compromised Store-Operated Calcium Entry
Jae-Kyun Ko, Kyoung-Han Choi, Xiaoli Zhao, Shinji Komazaki, Zui Pan,
Noah Weisleder, Jianjie Ma.
Junctophilins (JPs) play an essential role in muscle excitation-contraction (E-C) coupling by contributing to the formation of junctional membrane complexes (JMCs). However, the lethality associated with germ-line ablation of either JP1 or JP2 prevents physiological evaluation of their function in the maintenance of calcium homeostasis in adult muscle fibers. To investigate the physiological role of JP genes, we developed a novel transgenic system for tissue-specific and inducible control of gene expression in mouse models. This system employs a Tet-response CMV promoter that controls expression of a small-hairpin (sh) RNA against JP1 and JP2, which is non-functional until an interrupting reporter gene cassette is excised by the Cre recombinase. Insertion of the natural *Dicer* and *Drosha*-RNAse processing sites within the shRNA sequence allows for generation of specific siRNA probe for efficient knockdown of JP1 and JP2. Under the tight control of doxycycline (Dox), tissue- or lineage-specific expression of siRNA is achieved by the use of inducer mice that expresss Cre in a given tissue. Transgenic mice with muscle-specific expression of shRNA against JP showed no apparent change of JP expression before treatment with Dox; inducible and reversible knockdown of JP in skeletal muscle

was achieved through feeding of animals with diet containing Dox. Dox-induced reduction of JP expression led to abnormal membrane structure and compromised store-operated Ca^{2+} entry in adult muscle fibers, consistent with JP's essential role in muscle development and function. This transgenic system can be applicable for inducible and reversible knockdown of different genes and in different tissues, as well as for control of transgene overexpression in an inducible and tissue-specific manner, thus providing a versatile system for eluciding the physiological gene function using viable animal models.

3190-Pos Board B295

Extrusion of Ca^{2+} Across the Tubular System Membrane is Dependent on Membrane Potential and the Cytoplasmic Ca^{2+} in Rat Skeletal Muscle

Joshua N. Edwards, **Bradley S. Launikonis**.

Little is known about the ability of the tubular (t-) system membrane in skeletal muscle to extrude Ca^{2+} from the fibre, which is presumably due mostly to the activity of the Ca^{2+}-pump. Therefore we aimed to characterise t-system Ca^{2+} translocation properties by changing the steady-state $[Ca^{2+}]_{cyto}$ and resting membrane potential. To do this, we imaged fluo-5N in the t-system of rat mechanically skinned extensor digitorum longus fibres bathed in a K^+- or Na^+-based internal solution on a confocal microscope. Fluo-5N was calibrated *in situ* and had a Kd of ~320 μM. Following depletion of $[Ca^{2+}]_{t\text{-}sys}$ by chronic activation of store-operated Ca^{2+} entry (SOCE) in a solution containing 10 μM Mg^{2+}, 5 mM BAPTA and 5 mM caffeine, the fibre was exposed to an internal solution containing 1 mM Mg^{2+}, 1 mM EGTA and either 100, 200 or 800 nM Ca^{2+}. $[Ca^{2+}]_{t\text{-}sys}$ increased to hundreds of μM and mM levels in polarized and depolarized fibres, respectively, in seconds due to the different driving forces for Ca^{2+} across the t-system. In some fibres, vacuolated longitudinal tubules (Edwards & Launikonis, 2008, J Physiol) were observed with a high $[Ca^{2+}]$. Under conditions of chronic SOCE activation, the transverse tubules rapidly depleted of Ca^{2+} (seconds) while high $[Ca^{2+}]$ persisted in the vacuolated longitudinal tubules for $>$ 20 min (n=3). Subsequent exposure to an internal solution with 1 mM Mg^{2+} and 800 nM Ca^{2+} saw a rapid (seconds) increase in transverse tubular $[Ca^{2+}]$ that was trailed by a similar Ca^{2+} increase in longitudinal tubules by at least 5 min.

3191-Pos Board B296

Using Superfast Confocal Microscopy to Measure the Ca^{2+} Release Waveform and Spread of Excitation throughout the Tubular Network in Mammalian Skeletal Muscle

Joshua N. Edwards, Tanya R. Cully, Thomas R. Shannon,
Bradley S. Launikonis.

In skeletal muscle, uniform release of Ca^{2+} is dependent on the rapid spread of excitation across the sarcolemma and throughout the tubular (t-) system. The t-system primarily consists of transverse, but also longitudinal tubules, interconnected throughout to form an extensive membranous network along the fibre. Both tubules can conduct action potentials, however, the rapid rising phase of the action potential-induced Ca^{2+} transient and underlying release flux as well as any longitudinal spread of excitation between sarcomeres cannot be adequately measured with conventional imaging techniques. Therefore, we imaged Ca^{2+} transients with Oregon Green Bapta 5N (OGB5N) at 15.5 μs $line^{-1}$ on a Zeiss 5 LIVE confocal system from electrically stimulated mechanically skinned fibres from rat. We resolved the rising phase of Ca^{2+} release from the SR during field stimulation, lasting some 1.5 to 5ms. From the OGB5N fluorescence signals that displayed a very uniform release of SR Ca^{2+} upon stimulation, we derived the release flux to rise to a peak of 120mM/s in about 0.6ms and continue at a rapidly decreasing rate for a further 2ms. Following field stimulation in some skinned fibres, we observed that in areas where transverse tubules failed to be excited by the initial stimulus Ca^{2+} release propagated in from the adjacent regions at a rate of ~16 μm ms^{-1}. The areas where depolarization via the field pulse failed to depolarize transverse tubules could be up to 50 μm along the long axis of the fibre. This area was subsequently always excited by action potentials propagating inward along longitudinal tubules to initiate Ca^{2+} release.

3192-Pos Board B297

Differential Recording of Voltage Changes at the Surface and Transverse Tubular System Membranes of Mammalian Skeletal Muscle Fibers using Di-8-Anepps and Global and TIRFM

Joana C. Capote, Marino DiFranco, Julio L. Vergara.

Aiming to investigate the distribution of ClC-1 and K_{IR} channels at the sarcolemma and transverse tubular system (TTS) membranes of mammalian skeletal muscle fibers, we used global and total internal reflection fluorescence microscopy (TIRFM) to monitor voltage changes in these compartments, respectively. Enzymatically-dissociated fibers from murine *FDB* and *interosseus* muscles were stained with the potentiometric dye di-8-ANEPPS, and voltage-clamped with a two-microelectrode system. Ion substitutions were used to isolate and characterize the specific ClC-1 (I_{Cl}) and K_{IR} (I_{KIR}) currents: 70 mM internal $[Cl^-]$ and 120 mM external $[K^+]$, respectively. Also, 9-ACA and TEA were used to, respectively, block these currents. Global di-8-ANEPPS signals report, early after the onset of large hyperpolarizing pulses, I_{Cl}-dependent attenuations with respect to those recorded in the presence of 9-ACA. Peak attenuation levels of ~35% were observed for I_{Cl} of ~900 μA/cm^2. Large attenuations were similarly observed in global signals recorded the presence of large I_{KIR}'s with respect to those in TEA. In contrast, TIRFM di-8-ANEPPS signals demonstrate only minor current-dependent attenuations ($<$10%) under conditions in which global signals evidenced much larger attenuations. Overall, our results demonstrate that voltage changes at the TTS membranes display prominent current-dependent attenuations while the sarcolemma is largely under voltage-clamp control. A radial cable model of the TTS, including equations for each current pathway and luminal accumulation/depletion of ions, was used to quantitatively predict the ionic currents and to assess their effects on average TTS voltage changes. Comparative analysis of global optical data with model predictions of voltage changes in the TTS suggests that both ClC-1 and K_{IR} channels are equally distributed in both membrane compartments. Supported by NIH grants AR047664, AR041802, and AR054816.

3193-Pos Board B298

Fatigue-Induced Kinetic Changes in Tetanic Ca^{2+} Transients in Enzymatically Dissociated Mouse Fibers

Juan C. Calderón, Pura Bolaños, Carlo Caputo.

We used enzymatically dissociated FDB and *Soleus* fibers loaded with the fast Ca^{2+} dye Magfluo-4 AM (Calderón et al. 2010), to test whether repetitive stimulation induces progressive changes in the kinetics of Ca^{2+} release and reuptake in a fiber type-dependent fashion. Control experiments applying repetitive stimulation to FDB fibers loaded with Fluo-3 AM demonstrated that the preparation reproduced the main previously published findings on Ca^{2+} transients during fatigue, namely the tetanic Ca^{2+} transient amplitude decrease and the basal Ca^{2+} increase (Westerblad & Allen, 1991). When loaded with Magfluo-4 AM, a subgroup of MT-II fibers (fMT-II) showed significant reductions, of 28,1 and 29% (n=7), of the amplitude and the amplitude/rise time relationship of the first peak of the tetanic transient, respectively, after 40 tetani. A subgroup of more resistant MT-II fibers (rMT-II) showed reductions of 21,6 and 28,8% (n=6) only after 60 tetani. MT-I fibers (n=5) showed significant changes in both variables only after 80 tetani. fMT-II fibers also showed an increase of 33,6% in the half width value of the first peak. MT-I fibres did not show kinetic changes in the decay phase of the tetanic transients, while significant changes of 29,3 and 13,3% in the first time constant of decay (t_1) values were seen after only 20 tetani in fMT-II and rMT-II fibers, respectively. These changes were reversed after an average recovery period of 10 min. Further experiments ruled out the possibility that the differences in the kinetic changes of Ca^{2+} release between fibers MT-I and MT-II could be related to the inactivation of Ca^{2+} release mechanism. In conclusion, we show that a fatiguing protocol induces important kinetic alterations of both Ca^{2+} release and reuptake, which are larger in fibers MT-II than in fibers MT-I (FONACIT G-2001000637).

3194-Pos Board B299

Role of C-Term Tail of DHPR β1A in the DHPR/RyR1 Interaction

Feng Wei, Kim Truong, Paul D. Allen, Isaac N. Pessah, **Claudio F. Perez**.

Although the mechanism by which the DHPR β1a subunit supports EC-coupling is still debatable it is apparent that C-terminal domain of β1a (β-Ct) is an intricate component of the interaction between the DHPR complex and RyR1. To characterize the molecular components of β-Ct involved in DHPR/RyR1 signaling we tested the effect of progressive truncation of β1a subunit on EC-coupling and RyR1 activity. To do this cDNA constructs carrying truncations of either the 52 (β-52), 38 (β-38) or 14 (β-14) most C-terminal amino acid residues of β1a were expressed in β-null myotubes and then tested for their ability to restore depolarization-induced Ca^{2+} release in Fluo-4 loaded cells. Whereas β-null myotubes expressing constructs β-52 and β-38 were unresponsive to K^+ depolarization the cells expressing β-14 displayed EC-coupling that was indistinguishable from that of cells expressing wt-β1a (K^+EC_{50}: β1a = 23mM, β-14 =21mM). Thus, these results identify a segment of β-Ct of up to 24 amino acids that appears to be critical for the functional interaction between DHPR and RyR1 during EC-coupling. To test for specific interactions between the β-Ct and RyR1 we then studied the effect of purified β subunits on RyR1 activity. Using ^{3}H-ryanodine

binding to SR vesicles from skeletal muscle we found that purified wt-β1a subunit had an inhibitory effect in RyR1 activity in a dose-dependent manner (IC_{50}=38nM). However, purified β-38, a construct that failed to restore EC-coupling in myotubes, failed to inhibit ^{3}H-ryanodine binding to RyR1. Overall, these results are consistent with the hypothesis that DHPR β1a subunit functionally interacts with RyR1 through a domain in the final 38 amino acids in its C-terminal tail.

Supported by NIH Grants 5K01AR054818-02 (to CFP) and 1P01AR044750 (to PDA)

3195-Pos Board B300

Hydrophobic Residues that Determine *In Vitro* Activation of RyR1 by the $Beta_{1A}$ Subunit of DHPR

Robyn T. Rebbeck, Yamuna Karunasekara, Esther M. Gallant, Nicole A. Beard, Philip G. Board, Marco Giovani Casarotto, **Angela F. Dulhunty**.

Excitation-contraction (EC) coupling in skeletal muscle depends on physical interactions between two calcium ion channels: the dihydropyridine receptor (DHPR) in the transverse tubule membrane and ryanodine receptor (RyR1) in the sarcoplasmic reticulum membrane. Although the molecular components of this interaction are still being identified, both the DHPR α_{1S} and β_{1a} subunit are essential. The C-terminal 35 residues of β_{1a} (V490-M524) and a hydrophobic heptad repeat (L478, V485, V492) are claimed to contribute to mammalian EC coupling (1, 2), but the heptad repeat is not important in a zebrafish model (3). We investigated the importance of the heptad repeat using two peptides: β_{1a}490-524 (containing only one hydrophobic heptad repeat residue) and β_{1a}474-508 containing all repeat residues.

Both biotinylated β_{1a} peptides bound RyR1 in streptavidin-agarose affinity chromatography. Peptide binding to the cytoplasmic side of RyR1 channels in lipid bilayers and in [^{3}H]ryanodine binding experiments showed that β_{1a} 490-524 (100pM-500nM) increased RyR1 activity at cytoplasmic Ca^{2+} concentrations between 1 and 10μM, in the absence of Mg^{2+} inhibition. The action of β_{1a} 474-508 at 10 and 100nM was indistinguishable from that of β_{1a} 490-524, indicating that the heptad repeat is not crucial for this *in vitro* interaction. In addition we find that three hydrophobic residues on one surface of an α-helix between L496 and W503 are essential for β_{1a}490-524 to activate RyR1 channels. Therefore hydrophobic residues in the C-terminus of the β_{1a} subunit activate RyR1 activity under cytoplasmic Ca^{2+} and Mg^{2+} inhibition conditions found during EC coupling, but the hydrophobic heptad repeat is not essential for this action.

1. Beurg M et al. (1999) *Biophys J***77**: 2953.
2. Sheridan DC et al. (2004) *Biophys J***87**: 929.
3. Dayal A et al. (2010) *Cell Calcium* **47**: 500.

3196-Pos Board B301

Intramolecular $Ca_v1.1$ Chimeras Reveal the Molecular Mechanism Determining the Characteristic Gating Behaviour of the Skeletal Muscle Calcium Channel

Petronel Tuluc, Manfred Grabner, Bernhard E. Flucher.

The Ca^{2+} channel $Ca_V1.1$ is the voltage sensor of skeletal muscle excitation-contraction coupling. The classical skeletal muscle $Ca_V1.1$ isoform has poor voltage sensitivity and conducts a small, slowly activating Ca^{2+} current. In contrast, a splice variant lacking exon 29 (α_{1S}-ΔE29) (Tuluc *et al*.,2009) has an 8-fold higher current amplitude, fast activation-kinetics, and a 30mV left-shifted voltage-dependence of activation. Therefore, the extracellular loop in repeat IV (IVS3-IVS4) mainly coded by exon 29 is a critical determinant of the characteristic gating properties of $Ca_V1.1$. Here we used intramolecular chimeras between repeats I and IV to characterize the structural basis of the gating properties of $Ca_V1.1$.

Inserting exon 29 (alone or in combination with IVS3) into the corresponding region of repeat I was ineffective. However, in combination with the voltage sensor (IVS4) it fully restored α_{1S}-like amplitude and voltage-sensitivity to α_{1S}-ΔE29. Interestingly, all three chimeras exhibit faster activation kinetics. Secondary structure predictions showed that the long IVS3-IVS4 loop contains a beta-sheet while the short loop forms a coil. Point mutations in exon 29 which abolish the beta-sheet fully mimic the effects of deleting exon 29 regarding the kinetic properties and increase the current amplitude by 3-fold and left-shift the voltage dependence by −15mV. Together with previous findings (Nakai *et al*., 1994) our data suggest that the S3-S4 loop of the first repeat determines activation kinetics, while the corresponding loop plus voltage sensor in the fourth repeat with its unique secondary structure dictate the voltage-dependence, amplitude, and kinetics of skeletal muscle Ca^{2+} currents.

Grants: PT (MFI-2007-417), BEF (FWF-P20059-B05).

3197-Pos Board B302

Electrophysiological Analysis of Two Malignant Hyperthermia-Linked Mutations in the 1,4-Dihydropyridine Receptor α_{1S} Subunit

Roger A. Bannister, Ong Moua, Jose M. Eltit, Paul D. Allen, Kurt G. Beam.

Malignant hyperthermia (MH) is a pharmacogenetic Ca^{2+}-handling disorder of skeletal muscle, for which three identified causative mutations reside in the α_{1S} subunit of the skeletal muscle 1,4-dihydropyridine receptor (DHPR). In this study, we investigated the effects of two of these mutations (R174W, R1086C) on the ability of the DHPR to function as an L-type Ca^{2+} channel. To do so, we introduced the respective mutations into α_{1S} subunits amino-terminally tagged with yellow fluorescent protein (YFP-α_{1S}), and expressed the fusion proteins in *dysgenic* (α_{1S} null) myotubes. Confocal imaging of the YFP tags indicated that both YFP-R174W and YFP-R1086C were efficiently targeted to plasma membrane junctions with the sarcoplasmic reticulum. Measurement of intramembrane charge movements showed no significant difference in YFP-R174W or YFP-R1086C expression relative to YFP-α_{1S} ($p > 0.05$, *ANOVA*). However, L-type Ca^{2+} currents in YFP-R1086C-expressing myotubes were substantially reduced relative to myotubes expressing YFP-α_{1S} ($p < 0.05$, *t*-test). Strikingly, YFP-R174W failed to produce inward Ca^{2+} current during 200-ms test depolarizations under standard recording conditions (n = 7; $p < 0.005$, *t*-test) or in the presence of the L-type channel agonist ± Bay K 8644 (10 μM; n = 2; $p < 0.05$, *t*-test). In addition, exogenous expression of YFP-R174W reduced (~85%) L-type currents in myotubes cultured from normal mice, indicating that the R174W mutation may potentially interfere with functional expression of the wild-type allele. Supported by NIH AR44750 and MDA 4319 to K.G.B.,and MDA 4155 to R.A.B.

3198-Pos Board B303

Effects of Cav1.1 Mutation (S4-II-R528H) Causing Hypokalemic Periodic Paralysis on L-Type Calcium Current and Voltage Dependent Calcium Release in Isolated Muscle Fibers

Erick O. Hernández-Ochoa, Vicky Fu, Wentao Mi, Martin F. Schneider, Stephen C. Cannon.

Hypokalemic periodic paralysis (HypoPP) is an inherited muscle channelopathy which has been linked to mutations in the L-type (Cav1.1) Ca2+ channel alpha 1 subunit. Remarkably, 6 of 7 HypoPP mutations in CaV1.1 are at arginines in S4 voltage sensors, as are all 8 HypoPP mutations in NaV1.4. Here, we generated a genetically engineered mouse with one amino acid substitution causing HypoPP located in the S4 voltage sensor of the second domain of the Cav1.1 alpha subunit (S4-II R528H). Homozygous mutant mice (S4-II R528H) were viable, and while spontaneous attacks of weakness were not observed, tetanic force was reduced during low K challenge for in vitro contractions. Single isolated flexor digitorum brevis (FDB) muscle fibers from S4-II R528H mice exhibited 80% reduction in the amplitude of fluo4 Ca2+ transients compared to fibers from wild type (WT) mice when subjected to single or repetitive (30 Hz) field stimulation. In voltage-clamped FDB fibers from S4-II R528H mice, charge movement was not significantly altered in amplitude or voltage dependence whereas calcium current density was significantly reduced by 50%. Depolarization-induced fluo4 transients (F/F0) were also reduced in FDB fibers from S4-II R528H mice when compared to WT counterparts, as were the Ca2+ transients and Ca2+ release calculated from F/F0. Fibers form S4-II R528H mice exhibited a reduction in the amplitude of maximum Ca2+ release rate (Rmax) by ca 80 % when compared to WT fibers. It is concluded that the S4-II R528H mutation of CaV1.1 channel significantly reduces the whole-cell Ca2+ channel current amplitude, and is crucial for Cav1.1/RyR coupling during voltage dependent Ca2+ release in skeletal muscle. Supported by NIAMS (AR42703) and NIAMS (R01-AR055099) of the NIH, and the Muscular Dystrophy Association.

3199-Pos Board B304

Regions of the DHPRβ1A Subunit Responsible for DHPR Voltage-Sensing in Skeletal Muscle Excitation-Contraction Coupling

Vinaya Kumar Bhat, Anamika Dayal, Manfred Grabner.

In the DHPRβ_1-null zebrafish strain *relaxed* the lack of β_{1a} results in reduced DHPRα_{1S} membrane expression, in impediment of tetrad formation, and also in the elimination of α_{1S} charge movement (*Schredelseker* et al., 2005, PNAS). Recently we postulated a model describing the β_{1a} subunit as an allosteric modifier of proper α_{1S} conformation (*Schredelseker/Dayal* et al., 2009, JBC) and thus enabling full DHPR functionality in skeletal muscle excitation-contraction (EC) coupling.

To investigate if distinct regions of β_{1a} might be responsible for inducing the voltage-sensing function of the DHPR, we expressed different β isoforms and chimeras in isolated myotubes of *relaxed* larvae for patch clamp (charge movement) analysis. Quantitative immunocytochemical analyses showed that all four β isoforms (β_1-β_4) were able to fully target α_{1S} into triads.

Interestingly, despite full triad targeting, β_3 was unable to restore considerable charge movement (Q_{max}, 2.53 ± 0.50 nC/μF) in contrast to the other β isoforms (Q_{max}, 8.86 ± 0.93 to 9.94 ± 2.06 nC/μF) upon expression in *relaxed* myotubes. Systematic exchanges of variable regions and conserved domains of β_{1a} with corresponding β_3 sequences revealed significantly reduced Q_{max} restoration with SH3 and C-terminal chimeras (Q_{max}, 4.02 ± 0.28 and 5.57 ± 0.74 nC/μF, respectively). In contrast, β_{1a}/β_3 chimeras with the N-terminus, HOOK and GK domain exchanged showed complete restoration of charge movement.

Together, our data suggest an essential role of the conserved SH3 domain and the variable C-terminus of β_{1a} in the induction of the voltage-sensing function of the DHPRα_{1S} in skeletal muscle EC coupling.

Grants: FWF-DK-W1101-B12, FWF-P23299-B09

3200-Pos Board B305

Troponin T3 Regulates Calcium Channel Beta1a Subunit Nuclear Translocation in Skeletal Muscle

Tan Zhang, Jackson Taylor, Zhongmin Wang, Osvaldo Delbono.

Voltage-dependent calcium channel (VDCC) beta subunits (CaVβ) are critical for CaVα subunit membrane expression and gating properties. While CaVβ interacts with a variety of other molecular partners, nonchannel functions of skeletal muscle CaVβ1a have not been reported. In a yeast two hybrid (Y2H) screening of the mouse tibialis anterior (TA) muscle cDNA library, troponin T3 (TNNT3), specific to fast skeletal muscle, was identified using full-length CaVβ1a as the bait. Further studies revealed that TNNT3, but not the slow skeletal muscle TNNT1, co-immunoprecipitated with CaVβ1a in the mouse skeletal muscle cell line C2C12 and mouse skeletal muscle. Consistently, both CaVβ1a and TNNT3 were highly expressed in mouse fast, but not slow, skeletal muscle. Surprisingly, when DsRed-tagged TNNT3 and YFP tagged CaVβ1a (CaVβ1a -YFP) were transiently co-expressed in C2C12 cells or the mouse flexor digitorum brevis (FDB) muscle, both showed a punctuate distribution pattern in the cytoplasm and nucleus. In comparison, CaVβ1a-YFP alone localized uniformly in the cytoplasm. Further truncation analysis revealed that TNNT3 C-terminus (aa 161-244) localized exclusively in FDB nuclei and enriched CaVβ1a -YFP accordingly. In contrast, the TNNT3 middle region (aa 55-160) localized only in the cytoplasm, while the N-terminus (aa 1-54) was found in both cytoplasm and nucleus. Note that the N-terminus could also recruit CaVβ1a-YFP in the nucleus. Y2H assay verified that the TNNT3 C-terminus has the strongest interaction with CaVβ1a. Immunoblotting with an antibody targeting the TNNT3 N-terminus detected an increased TNNT3 fragment in the aging mouse skeletal muscle. We conclude that TNNT3 interacts with CaVβ1a and regulates its nuclear translocation mainly through its TNNT3 C- or N-terminus. These findings strongly support a transcription-regulation function for CaVβ1a and TNNT3.

3201-Pos Board B306

ATP Sensitivity and IP_3-Dependent Calcium Transients Which Regulate Gene Expression in Adult Muscle Fibers are Altered in Mdx Mice

Denisse Valladares, Mariana Casas, Reinaldo Figueroa, Alejandro Leyton, Sonja Buvinic, **Enrique Jaimovich**.

ATP has been shown to be released from muscles during exercise and after tetanic electrical stimulation (ES) and induces IP_3 dependent slow calcium transients involved in gene expression in myotubes. The aim of this study was to characterize these signals in adult fibers and to establish differences between normal and mdx mouse.

Experiments were performed in cultured isolated muscle fibers obtained from normal and mdx adult mice. The release of ATP induced by ES was measured using luciferin-luciferase and for calcium release studies the fibers were loaded with fluo-3. The location and expression of the nucleotide receptors were determined by immunofluorescence and western blot.

Slow, post tetanic calcium signals were partly inhibited by pharmacological agents targeting pannexin-1 (a pathway for ATP release), purinergic receptors and extracellular ATP. These signals had slower decay constants in mdx fibers. ES induced significant ATP release in normal fibers but this release was not detected in mdx fibers. The cellular location of ATP receptors was similar in both fiber types but their level of expression was higher in mdx fibers. Pannexin-1 expression was significantly augmented in mdx fibers. External ATP induced Ca^{2+} signals in both, normal and mdx muscle fibers, but the sensitivity to ATP was much higher in mdx fibers. This study demonstrates that ATP signaling is profoundly altered in mdx fibers and could be implicated in the calcium disturbance described in DMD; a compensatory mechanism may be involved in the reduced ATP extrusion apparent in dystrophic cells.

FONDAP 15010006, AFM 14562, FONDECYT 1080120, CONICYT PhD fellowship (DV)

3202-Pos Board B307

The Role of Ryanodine Receptor Phosphorylation in Skeletal Muscle Excitation-Contraction Coupling

Matthew J. Betzenhauser, Daniel C. Andersson, Steven Reiken, Andrew R. Marks.

Activation of the type 1 ryanodine receptor (RyR1) during skeletal muscle excitation-contraction (EC) coupling allows the release of stored Ca^{2+} required for muscle contraction. While RyR1 is a well-known substrate of protein kinase A (PKA), the physiological significance of this phosphorylation event is poorly defined. PKA is known to increase the open probability of the channel in lipid bilayers by inducing phosphorylation of a specific residue (S2844). Knock-in mice harboring phosphorylation site deficient (RyR1-S2844A) and phosphomimetic (RyR1-S2844D) mutations were generated in order to probe the consequence of this phosphorylation event in skeletal muscle EC coupling. Specific force measurements were performed on extensor digitorum longus (EDL) muscles and intracellular Ca^{2+} release was examined in isolated flexor digitorum brevis (FDB) muscle fibers using confocal microscopy. While isoproterenol (ISO) enhanced both Ca^{2+} release and muscle force in wild type (WT) mice, the positive effects of ISO were abrogated in samples from RyR1-S2844A mice. This demonstrates the enhancing effects of RyR1 phosphorylation during adrenergic stimulation in skeletal muscle. While transient phosphorylation of RyR1 exerts positive effects, chronic phosphorylation, as occurs in animal heart failure models, is thought to be detrimental to muscle function. We tested this hypothesis by measuring muscle force production and intracellular Ca^{2+} in RyR1-S2844D mice. At 3-months of age, muscle function and Ca^{2+} release were similar to WT controls. However, muscle force production and intracellular Ca^{2+} release were both blunted by 6-months of age suggesting that a pathological Ca^{2+} leak induced by the S2844D mutation impairs muscle function.

3203-Pos Board B308

Nox2 Dependent Modulation of Skeletal Muscle EC Coupling

George G. Rodney, Guoli Shi.

Generation of reactive oxygen species (ROS) under physiological conditions is required for normal force production in skeletal muscle. However, high levels of ROS promote contractile dysfunction, resulting in muscle weakness and fatigue. Our recent studies suggest that sub-cellular site-specific ROS production governs the beneficial vs. damaging effects of ROS. NADPH oxidase (Nox2) is an enzyme complex that generates ROS. In this study we investigated the role of Nox2 in skeletal muscle EC coupling. Using sub-cellular site-specific redox probes we show that cytosolic glutathione redox potential becomes more oxidized during contractile activity while mitochondrial redox potential does not change. We show that increased contractile activity promotes Nox2 dependent ROS production. Interestingly, we have found that the non-tyrosine kinase Src is activated in response to increased contractile activity. These data support a hypothesis in which Src acts as a redox switch to activate Nox2. Increased ROS production during strenuous exercise would decrease sarcolemmal Ca^{2+} influx and decrease sarcoplasmic reticulum refilling, which could contribute to the development of fatigue. As trials of general antioxidant therapy to combat increased ROS production have not been convincingly beneficial, understanding the sub-cellular signaling pathways by which oxidants influence muscle function will allow for the development of targeted therapeutic interventions to combat the deleterious effects of sustained contractile activity as well as skeletal muscle diseases.

3204-Pos Board B309

Pathological RyR1 Mutations to Identify RyR1 Functional Domains

Marine Cacheux, Julien Fauré, Julie Brocard, Nicole Monnier, Joël Lunardi, **Isabelle Marty**.

Muscle contraction is achieved when an efficient excitation signal at the plasma membrane triggers intracellular calcium release. This process called ''excitation-contraction (E-C) coupling'' relies on a multimolecular protein complex, the calcium release complex. This complex, spanning the plasma membrane and the sarcoplasmic reticulum (SR), is organized around the calcium channel of the SR, the ryanodine receptor (RyR1).

Mutations in RyR1 lead to a number of muscle diseases: Central core disease (CCD), Multi mini core disease (MmD), centronuclear myopathy, Malignant hyperthermia¼ Nevertheless, the functional consequences of each mutation are largely unknown because of the lack of information on the functional domains in RyR1. For the present study, we use the mutations identified in RyR1 to decipher functional regions in RyR1. We have identified more than 200 RyR1 mutations in the course of clinical diagnosis. We have recently shown that RyR1 interacts with caveolin-3, via the transmembrane part of the channel (Vassilopoulos et al, 2010, Biochemistry, 49, 6130). Caveolin-3, which is a structural protein involved in intracellular trafficking, could therefore regulate RyR1 targeting. We are now searching for mutations in RyR1 which could affect the

RyR1/Caveolin-3 interaction, to analyze the functional consequences of the disruption of this interaction, and the possible origin of the pathology.

3205-Pos Board B310

Sarcoplasmic Reticulum Ca^{2+} Release in Mouse Muscle Fibers Expressing Pathological Mutant Forms of the Type 1 Ryanodine Receptor

Romain Lefebvre, Claude Legrand, Estela Gonzalez-Rodriguez, Linda Groom, Robert T. Dirksen, Vincent Jacquemond.

Mutations of the gene encoding type 1 ryanodine receptor (RyR1) are associated with susceptibility to malignant hyperthermia (SMH) and/or central core disease (CCD). We used in vivo expression of EGFP-RyR1 DNA constructs to study the function of pathological forms of RyR1 in fully differentiated muscle fibers. The Y522S, R615C, R2163H and I4897T mutant RyR1s were separately expressed in mouse *flexor digitorum brevis* muscles, using plasmid injection and electroporation. All EGFP-RyR1s were present within restricted regions of the transfected fibers with a pattern consistent with triadic localization. Confocal measurements of voltage-activated rhod-2 Ca^{2+} transients demonstrated spatially confined alterations of SR Ca^{2+} release closely correlated with the presence of the mutant channels; in fiber regions expressing Y522S-RyR1 channels, Ca^{2+} release was specifically enhanced at low and moderate levels of depolarization: for instance peak Ca^{2+} release in response to pulses from -80 to -30 mV and -10 mV was 3.0 $\pm$ 0.6 and 1.5 $\pm$ 0.3 (n=9) times larger in the Y522S-positive fiber regions than in adjacent negative ones, respectively. When expressing wild-type EGFP-RyR1s, the corresponding ratio value was 0.86 $\pm$ 0.1 (n=9) at the two same voltages. Results similar to the ones with Y522S were observed with R615C and R2163H RyR1s. Conversely, expression of I4897T-RyR1s tended to be associated with a reduced SR Ca^{2+} release: for instance peak value at -10 mV was depressed by 45 $\pm$ 10 % (n=6). Results are thus consistent with an inherent increased sensitivity to activation by the voltage sensor of SMH-associated RyR1 mutant channels and an inherent functional failure of the CCD-associated I4897T ones. Overall, the present strategy proves to be highly effective to reveal the dysfunction of SR Ca^{2+} release due to mutant-RyR1s in differentiated muscle fibers.

3206-Pos Board B311

Modulation of Sarcoplasmic Reticulum Ca^{2+} Release by Phosphatidylinositol-Phosphate Lipids in Isolated Mouse Skeletal Muscle Fibers

Estela Gonzalez-Rodriguez, Romain Lefebvre, Karine Poulard, Claude Legrand, Anna Buj-Bello, **Vincent Jacquemond**.

Previous results from ryanodine binding and single ryanodine receptor (RyR) channel measurements suggested that RyR1 activity may be modulated by phosphatidylinositol-phosphate lipids (PtdInsPs). Possibly related, recent data showed that skeletal muscle e-c coupling is altered in several models of PtdInsPs phosphatase deficiency. We measured intracellular Ca^{2+} in fibers from *flexor digitorum brevis* (fdb)muscles microinjected with a solution containing a given PtdInsP lipid (PtdIns(3,5)P2, PtdIns(3)P, PtdIns(5)P or PtdIns) together with the calcium dye indo-1. Following equilibration, fibers were stimulated by short voltage-clamp depolarizations of increasing amplitude from -80mV. Resting [Ca^{2+}] did not differ between control fibers and any group of PtdInsPs-injected fibers; it was though ~1.5 larger in fibers injected with PtdIns(3,5)P2 or PtdIns(3)P than in fibers injected with PtdIns(5)P or PtdIns. Peak SR Ca^{2+} release was specifically depressed in fibers injected with PtdIns(3,5)P2 or PtdIns(3)P with maximum values of 34.8 $\pm$ 3 $\mu M.ms^{-1}$ in control fibers (n=15) and of 24.4 $\pm$ 2 and 17.4 $\pm$ 2 $\mu M.ms^{-1}$ in fibers injected with PtdIns(3,5)P2 (n=8) and PtdIns(3)P (n=8), respectively. There was no concurrent effect on the membrane current measured during the pulses and the voltage dependence of Ca^{2+} release inactivation was also unaffected. These results highlight the possibility that SR Ca^{2+} release may be physiologically regulated by certain PtdInsPs. A plasmid coding for a wild-type form of the PtdIns phosphatase MTM1 tagged with the red fluorescent protein mCherry was transfected in fdb muscles. The protein was found distributed within the entire volume of the transfected fibers and to reproducibly yield a striated transversal expression pattern consistent with localization within the triadic area. Preliminary measurements of voltage-activated Ca^{2+} transients in these cells indicated that under these conditions over-expression of MTM1 had limited effects on SR Ca^{2+} release.

3207-Pos Board B312

Culture Methods and Initial Characterization of Calcium Homeostasis in Intercostal Skeletal Fibers Isolated from the Adult Mouse

Patrick Robison, Erick O. Hernández-Ochoa, Martin F. Schneider.

Primary cultures of single adult skeletal muscle fibers dissociated from locomotor muscles adhered to glass coverslips are routine models which allow monitoring of functional processes in living cultured fibers under controlled conditions. To date, such isolated fiber cultures have not been established for respiratory muscles, despite the critical function of these muscles and their role in mortality of many muscular diseases. We have developed an adherent culture system for single adult intercostal muscle fibers from the adult mouse. This system allows for monitoring functional properties of these living muscle fibers in culture exposed to various conditions (pharmacological agents, electrical field stimulation to drive muscle fiber contraction, etc.). We also provide initial characterization and demonstrate several common electrophysiological, Ca2+ imaging techniques and over-expression of foreign fluorescent fusion proteins in this new model system with comparisons to the established Flexor Digitorum Brevis muscle primary culture model. Supported by NIH-NIAMS Grants R01-AR055099, R01-AR056477 and T32-AR007592.

3208-Pos Board B313

Muscle Performance and Electrically Evoked Ca^{2+} Release are Compromised in Calsequestrin-1 Null Mice

Rotimi Olojo, Erick O. Hernández-Ochoa, Paul D. Allen, Martin F. Schneider, Christopher W. Ward.

In skeletal muscle the sarcoplasmic reticulum (SR) Ca2+ release channels (i.e., ryanodine receptor; RyR1) are critical determinants of contractile filament activation. Recent evidence suggests that several SR proteins may modulate RyR dependent SR Ca2+ release and thus could alter overall function. Recent attention has been focused on the SR luminal protein calsequestrin (Casq) as a SR Ca2+ buffer as well as its potential role in modulating the RyR1, the DHPR and other sarcolemmal channels. In our current work, we tested the hypothesis that mice null for Casq1 will have functional impairments reflecting the role of Casq1 in fast type skeletal muscle. Here we examined functional measures of overall muscle performance in vivo and of fast muscle in vitro, and identified significant deficits in functional performance that indicate an inability to sustain repetitive contractile activation. We then used measures of voltage dependent SR Ca2+ release and SR Ca2+ release flux in single fast type skeletal muscle fibers. Here we demonstrate a decrease in voltage dependent RyR Ca2+ release with single action potentials and a collapse of the Ca2+ release with repetitive trains of pulses. Finally in single voltage clamped muscle fibers we show that SR Ca2+ release flux as well as total SR Ca2+ release is markedly reduced in the Casq1 null myofibers. The voltage dependence of the Ca2+ release flux was not shifted but showed about 50% decrease in the maximum peak Ca2+ release flux in the Casq1 null fibers when compared to the WT counterpart. Taken together we have revealed that the genetic depletion of Casq1 results in significant deficits in contractile activation consistent with alterations in SR Ca2+ release. Supported by RC2 NR011968, R01-AR055099, and T32- AR007592.

3209-Pos Board B314

Measurement of Intra-SR [Ca^{2+}] Reveals Changes in SR Ca^{2+} Permeability During Intracellular Ca^{2+} Release in Skeletal Muscle

Monika Sztretye, Jianxun Yi, Leandro Royer, Jingsong Zhou, Lourdes Figueroa, Paul D. Allen, Eduardo Rios.

In skeletal muscle, Ca2+ release from the SR is under strong regulation. While this regulation has well known Ca2+-dependent components acting from the cytosolic side of the channels (CICR and CDI), putative effects of luminal calcium are not well defined. Combining imaging of $[Ca^{2+}]_{SR}$ by the cameleon D4cpV targeted with calsequestrin 1 or its Ca^{2+}-impaired variant ''Delta-Asp'', with measurements of cytosolic [Ca^{2+}] (X-rhod 1) in single mouse FDB fibers, we directly monitored the evolution of Ca^{2+} permeability (P) of the SR membrane during long-lasting voltage clamp depolarizations. These depolarizations were intended to both elicit the release response and substantially deplete the SR of calcium, so that P could be evaluated as the SR calcium decreased. Against our expectations (Royer 2007; 2010) P was found to decrease significantly during depolarization. Consequently, depletion was never complete, and $[Ca^{2+}]_{SR}$ reached on average 40% of the resting content after long pulses. This gating effect of depletion is similar to that which in cardiomyocytes is believed to terminate Ca^{2+} release and be associated with the presence of calsequestrin. Similar measurements in cells from casq1-null mice showed instead $>$ 90% depletion during long-lasting pulses. Permeability remained essentially constant, at a high value, for the duration of the pulses. This was confirmed under various compositions of cytosolic and external solutions, with different calsequestrin-derived targeting sequences and widely varying biosensor expression densities. An inhibitory effect on Ca^{2+} release is evidently lost in the casq1-null mouse. Whether this reflects allosteric gating by calsequestrin remains to be established. The observation goes a long way towards explaining the modest effect of calsequestrin KO in the maximal amount of SR calcium that can be released by depolarization (Royer, 2010).

Funded by NIAMS (NIH) and MDA.

3210-Pos Board B315

The SR Calcium Content of Fast Muscle Fibres Lacking Calsequestrin is Reduced and not Sufficient for Sustained Contractions

Carlo Reggiani, Ger Stienen, Marco Quarta, Marta Canato, Michele Scorzeto, Luana Toniolo, Feliciano Protasi.

Calsequestrin (CASQ) is an acidic, high capacity Ca^{2+}-binding protein located within the terminal cisternae of the sarcoplasmic reticulum (SR). CASQ1 is the major SR Ca^{2+}- buffer in fast muscle fibers, whereas CASQ2 predominates in cardiomyocytes and slow muscle fibers. Mice devoid of CASQ were generated by crossing mice lacking CASQ1 (Paolini et al J Physiol 2007, 583, 767) and mice lacking CASQ2 (Knollman et al J Clin Inv 2006, 116, 2510).

When studied ex vivo, fast muscles (EDL) showed an earlier decline in tension during tetanic stimulation than WT fibers. This was not the case in slow muscle, soleus. Such decline of the developed tension was compatible with the decay of free cytosolic calcium during repeated stimulation observed using Fura-2 in single intact fast FDB muscle fibers.

Single permeabilized fibers from EDL and tibialis anterior showed a reduction of the amount of calcium released by 30 mM caffeine, which is supposed to release about 80% of SR calcium (Murphy et al. J Physiol 2009, 587, 443), thus suggesting a depletion of SR. The depletion was confirmed by measurements of SR fee $[Ca^{2+}]$ using a FRET-based indicator (D1ER) genetically targeted to the SR. During contraction a massive/marked reduction in intraluminal free $[Ca^{2+}]$ was observed to a level close to full depletion.The results are consistent with the function of CASQ as a intraluminal SR buffer. CASQ1/2 null mice lack sufficient compensation for the loss in buffering power by other SR proteins. The diversity between slow and fast muscles might be attributed to the presence of parvalbumin as a relevant sink of calcium in cytosol of fast but not slow muscles (Celio et al Nature 1982, 297, 504).

3211-Pos Board B316

Activity-Dependent Regulation of Mitochondrial Superoxide Flashes in Skeletal Muscle

Lan Wei, Gheorghe Salahura, Karl A. Kasischke, Shey-Shing Sheu, Robert T. Dirksen.

Reactive oxygen species (ROS) are a class of molecules that oxidize diverse cellular proteins/lipids and are generated mainly in mitochondria by the electron transport chain (ETC). We previously discovered a novel biosensor for superoxide, circularly permutated YFP (cpYFP). Using mitochondrial-targeted cpYFP (mt-cpYFP), localized bursts of superoxide in individual or clusters of mitochondria, termed "superoxide flashes," are observed in quiescent cells across a wide range of cell types [Wang, W. et al., *Cell* 134:279-290, 2008]. Here, we examined the properties of superoxide flashes in *flexor digitorum brevis* muscle fibers from newly generated transgenic mice expressing skeletal muscle-specific mt-cpYFP. A new flash detection and analysis software ("Flash Collector") was developed to enable automated quantification of flash frequency, amplitude, kinetics, and area. Results demonstrate that skeletal muscle fibers exhibit higher basal mitochondrial superoxide flash frequency, but similar amplitude, kinetics, and area as those observed in cardiac myocytes. Rotenone (5υM) and oligomycin (5υM) reduced flash frequency to ~20% of control, confirming the ETC dependence of superoxide flash generation. Inhibition of adenine nucleotide translocase by bongkrekic acid (100υM) decreased flash frequency by 50%. Incubation in Ringer's containing 10mM glucose or mitochondrial substrates did not significantly alter flash frequency, but increased flash amplitude and duration by 10-15%. Importantly, superoxide flash activity was enhanced (frequency increased from 18.1 ± 1.6 to 22.3 ± 2.0 flashes/100s·100υm^2) following five consecutive brief tetani (500ms, 100Hz, 0.2 duty cycle), but was markedly suppressed following a prolonged fatiguing stimulation (40 tetani; frequency reduced from 17.6 ± 2.2 to 7.7 ± 1.6). These results demonstrate skeletal muscle activity regulates mitochondrial superoxide flash production. In adition, muscle-specific mt-cpYFP transgenic mice will be a powerful tool for assessing the physiological role of superoxide flash activity and how this activity is altered and contributes to skeletal muscle aging and disease.

Actin & Actin-binding Proteins II

3212-Pos Board B317

Allosteric Effects within the Catalytic Domain of Dictyostelium Myosin on Interaction with Actin and Nucleotide

Piyali Guhathakurta, Ewa Prochniewicz, Joseph M. Muretta, David D. Thomas.

To understand molecular features of myosin critical for its functional interaction with actin, we studied two constructs of Dictyostelium myosin II, which differ in cysteine content and length: (i) Cys-lite catalytic domain (M758-S619C) and (ii) fusion of wild type catalytic domain with two α-actinin repeats (M761-2R), which has been shown to be kinetically identical to full-length Dictyostelium myosin S1. In the absence of ATP, both constructs bound actin stoichiometrically. However, marked differences in interaction of each construct with actin were observed in the presence of ATP. Actin-activated ATPase of M758-S619C was very sensitive to the presence of an ATP regenerating system (i.e., elimination of free ADP), which increased activity by a factor of 2.5, while M761-2R was not affected. The ATP regenerating system greatly decreased actin binding of M758-S619C, as measured by cosedimentation. Fluorescence resonance energy transfer between IAEDANS-actin and IAF-M758-S619C showed that this interaction was strong in the presence of ATP, independent of ionic strength, and structurally indistinguishable from that of the strong-binding complex. These results indicated that M758-S619C has an altered relationship between the binding of actin and nucleotide. Binding of MantADP confirmed this hypothesis: actin had no significant effect on the tight binding ($K_d \sim 1$ μM) of MantADP to M758-S619C, while actin substantially decreased the affinity of MantADP for M761-2R, as for muscle S1. We conclude that the structural alterations of the M758-S619C construct (Cys content and/or the structure of the converter domain) allosterically modulates the reciprocal affinity of myosin for nucleotide and actin, which in turn changes the distribution of actomyosin states within the actomyosin ATPase cycle.

3213-Pos Board B318

Expression and Characterization of Full Length Nonmuscle Myosin IIs

Aibing Wang, Neil Billington, Robert S. Adelstein, James R. Sellers.

The nonmuscle myosin IIs (NMIIs) are filamentous myosins which are involved in a wide variety of cellular processes from cytokinesis to control of cell morphology. There are 3 isoforms of the NMII heavy chain in humans, NMIIA, IIB and IIC which are expressed at varying levels according to cell type. Owing to the difficulty of expressing the full length proteins, previous studies on this myosin have used tissue purified protein or expressed fragments of the molecule and in both cases this presents potential drawbacks for characterizing the protein *in vitro*. To circumvent current limitations and approach their native properties, we have successfully expressed full length wild type and mutated NMII proteins using the Sf9-baculovirus system. We also expressed two chimeric NMII proteins (one with the amino-terminal globular head of the IIA heavy chain fused to the rod of IIB; another with the IIB globular head preceding the IIA rod). We have begun characterizing the 3 human isoforms, along with their alternatively spliced counterparts and also mutants which are known to be associated with disease states in humans. Here we show that although full length NMIIA, IIB and IIC exhibit differences biochemically, the structure of the filaments determined by negative stain electron microscopy is essentially indistinguishable between the three isoforms. The ability of all 3 isoforms to adopt the 10S compact conformation in the presence of ATP is demonstrated. We also show using the chimeric constructs that the tail domains of different isoforms are interchangeable in terms of filament formation and formation of the 10S compact conformation.

3214-Pos Board B319

Mouse Models of Human *MYH9*-Related Diseases

Yingfan Zhang, Mary Anne Conti, Patricia Zerfas, Yelena Shmist, Sachiyo Kawamoto, Chengyu Liu, Jeffrey Kopp, Chi Cho Chan, Michael J. Kelley, Robert S. Adelstein.

Point mutations in *MYH9*, the gene encoding nonmuscle myosin heavy chain IIA (NMHC IIA), underlie autosomal dominant syndromes in humans (incidence 1 in 500,000). The abnormalities can manifest as macrothrombocytopenia, granulocyte inclusions, progressive proteinuric renal disease, cataracts, and sensorineural deafness. To gain insight into the pathological mechanism of *MYH9*-related diseases in humans, we generated mouse models of three disease-associated mutations, Arg702Cys in the amino-terminal domain of NMHC IIA which controls myosin motor activity, and Asp1424Gln and Glu1841Lys in the carboxyl-terminal rod domain, which regulates filament formation. Heterozygous Asp1424Gln and Glu1841Lys mutant mice produce homozygous mutant offspring at close to normal ratios. By contrast, homozygous Arg702Cys mice die at embryonic day E10.5 to E11.5 which though early, is considerably later in development than knockout NMHC IIA mice (E6.5). These results indicate that the motor domain function of NMHC IIA is critically important during the latter phase of mouse embryonic development. Giant platelets accompanied by decreased platelet counts and prolonged bleeding times are found in adult heterozygous and homozygous mice from all three mutant mouse lines. Bone marrow histology is consistent with failure of platelet release into the circulation. Some adult heterozygotes from all three mouse lines and homozygotes from Asp1424Gln and Glu1841Lys mouse lines have higher urine albumin/creatinine ratios than those of wild type

controls. Light and transmission electron microscopy reveals focal segmental glomerulosclerosis with thicker basement membranes and abnormal podocytes. Some of the mutant mice also have lens abnormalities consistent with early cataract formation. Our results show that even heterozygous mutations in the mouse *Myh9* gene can reproduce human *MYH9*-related diseases. These mouse models should be useful in understanding the pathophysiology of human *MYH9*-related diseases and also in designing and developing therapeutic stratagies.

3215-Pos Board B320

Force Amplification Response of Actin Filaments under Confined Compression

George W. Greene.

Actin protein is a major component of the cell cytoskeleton and its ability to respond to external forces and generate propulsive forces through the polymerization of filaments is central to many cellular processes. The mechanisms governing actin's abilities are still not fully understood due to the difficulty in observing these processes at a molecular level. Here we describe a new technique for studying actin-surface interactions using a Surface Forces Apparatus which is able to directly visualize and quantify the collective forces generated by adsorbed layers of non-interconnected, end-tethered actin filaments confined between two (mica) surfaces. We also identify a new force-response mechanism in which filaments stiffen under compression to produce an increase in the filament bending modulus and an amplification in the elastic opposing forces. This elastic stiffening mechanism enables actin filaments to both sense and respond to compressive forces without additional mediating proteins providing insight into the potential role compressive forces play in many actin and other motor protein based phenomena.

3216-Pos Board B321

Structure and Mechanical Properties of Actin Networks Crosslinked with Mutually Interacting Crosslinkers

Brian Grooman, Ikoku Fujiwara, Carol Otey, Arpita Upadhyaya.

Cells regulate their movement and mechanical properties by adjusting the concentrations and compositions of actin crosslinking proteins. Reductionist approaches where purified components are isolated from the cell and studied in vitro have yielded insights into how crosslinkers determine the structure and mechanics of actin networks. In this way, the viscoelastic properties of an actin network with one or more cross-linkers can be explored, and the behavior of the cross-linkers can be better understood. Despite a large body of work on singly crosslinked actin networks, few experiments have been carried out with multiple cross-linkers, and of these, none have used two cross-linkers that can bind to each other as well as actin filaments. Alpha-actinin and palladin are two such mutually interacting actin crosslinking proteins that are abundant in stress fibers and focal adhesions in cells. In this series of studies, we measure the dependence of the morphology and rheology of actin - palladin - alpha-actinin networks on the crosslinker concentrations. We use confocal microscopy to image crosslinked actin networks in three dimensions and determine the pore size distributions of these networks. Using bulk rheometry, we measure the linear as well as non-linear response of crosslinked actin gels to imposed shear stresses. We find that under certain conditions, these two proteins can enhance network stiffness and that the presence of alpha-actinin can affect the network's concentration dependence on palladin and vice versa. These studies reveal the conditions under which mutually interacting actin crosslinkers act redundantly or synergistically to determine the mechanical integrity of the cell and its ability to sense the physical environment.

3217-Pos Board B322

Strain Stiffening Induced by Molecular Motors in Active Crosslinked Biopolymer Networks

Peng Chen, Vivek B. Shenoy.

We have studied the elastic response of actin networks with both compliant and rigid crosslinks by modeling molecular motors as force dipoles. Our finite element simulations show that for compliant crosslinkers such as filamin A, the network can be stiffened by two orders of magnitude while stiffening achieved with incompliant linkers such as scruin is significantly smaller, typically a factor of two, in excellent agreement with recent experiments. We show that the differences arise from the fact that the motors are able to stretch the compliant crosslinks to the fullest possible extent, which in turn causes to the deformation of the filaments. With increasing applied strain, the filaments further deform leading to a stiffened elastic response. When the crosslinks are incompliant, the contractile forces due to motors do not alter the network morphology in a significant manner and hence only small stiffening is observed.

3218-Pos Board B323

Filamin a Segments Respond Force Differently

Hu Chen, Xiaoying Zhu, Michael Sheetz, Fumihiko Nakamura, Jie Yan.

Although the magnetic tweezers has many unique advantages in terms of specificity, throughput and force stability particularly for studying protein refolding, magnetic tweezers has had limited application because accurate measurement of force has been difficult for short tethers. Here, we report a novel method that allows us to apply magnetic tweezers to stretch short biomolecules with accurate force calibration over wide range up to ~ 100 pN. We apply this method to study unfolding and refolding dynamics of protein Filamin A.

Filamin A protein cross-links actin fiber and binds with many transmembrane and cellular signaling proteins. By using magnetic tweezers, it was found that domains 16-23 can response to force smaller than 10 pN, while domains 1-8 needs force bigger than 20 pN to be unfolded. As some structures in segment domains 16-23 can be unfolded by forces smaller than 10 pN, it indicates that the auto-inhibited binding site can be exposed by physiological relevant forces. The possible force sensor function of Filamin A is supported by the experiment. After Filamin A was unfolded, its refolding process was recorded as sudden drop of extension under force ~ 5 pN.

3219-Pos Board B324

Measurement and Origin of a Force that Pushes and Pulls the Plasma Membrane

Brenda Farrell, Feng Qian, Anatoly B. Kolomeisky, Bahman Anvari, William E. Brownell.

We report the measurement of a dynamic force that pulls and pushes the plasma membrane in a living cell. We form long F-actin filled membrane tubes from a cell and monitor the axial membrane force by use of laser tweezers where the optically trapped bead is attached to the end of the tube. We observe a sawtooth force (up to 75 pN in magnitude) that rides on top of the stationary force (~10-15 pN). The sawtooth force increases slowly (tens of seconds) and decays rapidly back (tens of ms) to the stationary value. This sawtooth force was not detected after addition of drugs that bind to the barbed end of actin filaments, but it was insensitive to drugs that affect microtubules and myosin II. We determine the force per working object is 3 to 5 pN, with 15 to 30 working objects in the tube, from the magnitude and direction of the discrete force. We calculate a length of ~ 3 to 6 nm from the measured force per working object and the time course of the force; this is equivalent to G-actin subunit half- and full-lengths. We propose the detected objects are working-actin filaments and the rise and decay phases of the sawtooth force are due to depolymerization and polymerization of actin. Our data supports a type of end-tracking motor model that operates in both the forward (polymerization) and reverse (depolymerization) directions; linker proteins attach the actin filaments to the membrane and transduce the chemical energy of polymerization and depolymerization to the mechanical motion of the membrane. Theory predicts that the actin motor should work in both directions. Our data provides experimental evidence that depolymerization of actin pulls the plasma membrane.

3220-Pos Board B325

An Autocatalytic Activator-Inhibitor Model of Actin Polymerization at the Leading Edge of Fibroblast Lamellipodia

Gillian L. Ryan, Matthew B. Smith, Heather Petroccia, Naoki Watanabe, Dimitrios Vavylonis.

Crawling animal cells are driven by lamellipodia – thin, dynamic, sheet-like projections consisting of a dense network of branched actin filaments. Arp2/3 complex mediated actin polymerization near the leading edge drives protrusion required for cellular motility. Actin filaments polymerize near the leading edge and undergo retrograde flow towards the main body of the cell. Both random fluctuations and travelling waves of protrusion and retraction have been observed during cell spreading. To characterize the protrusion rates of XTC fibroblasts we use active contours to track the leading edge of cells. We then calculate the correlation between local actin and Arp2/3 complex accumulation and cell protrusion rate as measured from conventional fluorescent microscopy. We also use quantitative fluorescent speckle microscopy, which allows us to track the dynamics of individual proteins within the actin network and measure quantities such as the retrograde flow rate. We present a noise-driven model of these actin-mediated protrusion events in which a diffusive, autocatalytic activator mediates actin polymerization, while actin saturation in turn inhibits further activator accumulation. Using analytic theory we find that our model captures both excitable and oscillatory behaviors, and can be tuned between the two behaviors by adjusting model parameters. Using computer simulation we are able to produce patterns of actin

polymerization that are quantitatively similar to those observed along the leading edge in live cell experiments.

3221-Pos Board B326
Myosin Motor Dynamics in Filopodia
Pavel I. Zhuravlev, **Maria Minakova**, Yueheng Lan, Garegin A. Papoian.
ATP-driven molecular motors are ubiquitously used for various cellular transport processes. Myosin motors that walk on actin filaments have been detected in both filopodia and stereocilia. Myosin X plays an important role in filopodial formation and growth, however, the specific mechanisms and cargo of various myosins remain unclear.
To address these issues, we have developed a comprehensive stochastic computational model of a filopodium, incorporating active transport by motors. Our model indicates that efficient motor mediated transport is hindered by sequestration of G-actin cargo by motors, as well as clogging of the actin filaments by multiple motors. Our work suggests potential mechanisms for overcoming these transport bottlenecks.
Furthermore, experimentally measured motor concentration profiles along the filopodial tube are difficult to explain. This motivated us to look into the details of this distribution. We created a theoretical model describing the steady-state concentration profile of the motors and compared it with the computer simulations. The theoretical results semi-quantitatevly agree with the numerical data. In the stationary state, the model shows a quick saturation of actin filaments with walking motors as a function of distance from the filopodial base. This adversely affects the flux of motors and their cargo to the filopodial tip, as space for motors to step into runs out. Thus, the clogging problem is at least as important as the sequestration one, and the cell would probably need to employ special facilities for solving it in order to achieve efficient active transport, and thus longer filopodia.

3222-Pos Board B327
Model of the Role of Actin Crosslinker Proteins during Contractile Ring Assembly in Fission Yeast
Nikola Ojkic, Dimitrios Vavylonis.
Actin cross linkers play a crucial role in various processes during cell cycle. Contractile ring formation in fission yeast is one of the processes where the role of two actin crosslinkers fimbrin and alpha actinin is important. In fission yeast contractile ring assembles from a broad band of cortical nodes. Fission yeast nodes are macromolecular complexes containing several myosin-II heads and a few formin dimers. The condensation of the broad band of nodes into a ring has been described by a search, capture, pull and release (SCPR) model. In this model, formin nucleates filaments along random directions parallel to the cell membrane. When a growing filament comes in close proximity to a myosin of a neighboring node, myosin grabs the filament and exerts force that moves nodes toward one other. Using analytical calculations and numerical simulations, we have shown that the SCPR model predicts that nodes coalesce into rings or clumps (i.e. disconnected aggregates), depending on the values of parameters. In experimental images of fission yeast, myosin nodes appear to get stabilized into linear elements towards the late stages of ring assembly, presumably due to crosslinkers. This process may assist ring formation by preventing the formation of clumps. To study this possible role of crosslinkers, we incorporated a short-range aligning force to the SCPR model, representing a short range aligning mechanism. We used simulations and scaling arguments to quantify the resulting dynamics and morphology of myosin aggregates. We describe regions in parameter space in which local alignment prevents clump formation. We compare the results to experiments on fission yeast cells in the process of contractile ring formation.

3223-Pos Board B328
Fluctuation-Dissipation Relations in Minimal Models for Active Driving
Yair Shokef, Eyal Ben-Isaac, Nir S. Gov.
Biological systems exhibit fluctuations driven by active (energy consuming) processes, such as molecular motors in the cytoskeleton and flagella propelling bacteria. It is tempting to treat these fluctuations in the same manner that thermal fluctuations are treated in equilibrium systems. Recent experiments have compared these inherent fluctuations with the response to small external perturbations. From these measurements, an effective temperature may be defined using the fluctuation-dissipation formalism of equilibrium statistical mechanics. In active systems, this effective temperature is frequency dependent (unlike the thermal case), and is higher than the ambient temperature. Another parameter that is useful for characterizing deviations from equilibrium of such fluctuations is the kurtosis of their distribution function; deviations of the kurtosis from its value for a Gaussian distribution indicate that the system may not be mapped onto an equilibrium ensemble.
We address these issues theoretically by examining simple model systems of randomly kicked "particles", with a variable number of kicking "motors". Our generalized particles and motors represent different objects in different real systems, and we make specific choices when comparing to experimental observations. We exactly calculate the non-equilibrium fluctuation-dissipation relations and resulting effective temperatures. We show that their frequency dependence is model dependent and generally non-monotonous. We investigate the non-Gaussianity of the velocity distribution functions by a combination of numerical simulations and theoretical estimates. We show that the kurtosis has a non-monotonous dependence on the motor activity. We identify situations in which these two indicators of non-equilibrium behavior contradict. In particular, in the presence of multiple motors, the kurtosis of the distribution recovers its Gaussian value, while the effective temperature may still exhibit strong frequency dependence. We compare our results with two recent measurements of oscillations of the red-blood cell membrane, where these two indicators where independently measured.

3224-Pos Board B329
Investigating Function of *Nck* Adaptor in Tyrosine Kinase Signaling to the Actin Cytoskeleton
Sofya Borinskaya, Jon A. Ditlev, Les M. Loew, Bruce J. Mayer.
Many extracellular signals are transduced through Receptor Tyrosine Kinases. We investigate RTK signaling to the actin cytoskeleton through the *Nck* adaptor protein. The SH2 domain of *Nck* binds phosphorylated tyrosine residues of RTK and then SH3 domains of *Nck* bind and activate N-WASP (Neural Wiskott-Aldrich Syndrome Protein). Activation of N-WASP involves release of the VCA domain (verprolin-homology, central and acidic domains). Simultaneous binding of G-actin monomer and actin nucleation factor Arp2/3 to the VCA domain initiates nucleation of a new actin branch.
Aggregation of the *Nck* SH3 domains on plasma membrane *in vivo* results in the formation of long, dynamic, moderately dense actin comet tails. We utilize a variety of techniques to study this artificially induced localized actin polymerization: cell culture and quantitative western blotting, confocal fluorescent microscopy and quantitative image analysis, biochemical modeling in the Virtual Cell environment. Our model recapitulates important features of *Nck* actin comets: length of the comet tails, F-actin concentration within the tails, distance from the head of the aggregate to the maximum F-actin concentration location, and dependence of these parameters on comet velocity and the number of *Nck* molecules in the membrane cluster. However the model does not account for the fact that *Nck* binding proteins (WIP, PAK, Abl) can have an effect on actin polymerization. The VCA domain of N-WASP is directly responsible for Arp2/3 activation and can be used in our experimental system to bypass the need for adaptor proteins such as *Nck* to initiate actin polymerization. Aggregation of VCA domains on the membrane *in vivo* produced actin ''blobs'' - short thick structures. Understanding the differences between the *Nck* and VCA induced localized actin assemblies will advance our knowledge of RTK signaling to mobilize and direct actin cytoskeleton.

3225-Pos Board B330
Nck Function in Tyrosine Kinase Signaling to the Actin Cytoskeleton
Jonathon A. Ditlev, Bruce J. Mayer, Leslie M. Loew.
Tyrosine kinase signaling leads to the post-translational modification of proteins and their binding partners. These modifications lead to the membrane recruitment of signaling proteins, promoting an increase in their local concentration, which results in a cellular response to the phosphorylation of tyrosine residues. Nck, an SH2/SH3 adaptor protein, functions in tyrosine kinase signaling by linking tyrosine phosphorylation on the membrane with binding partners, such as N-WASp, that function in facilitating actin nucleation and polymerization. Recent *in vitro* studies have demonstrated that N-WASp dimers bind to and activate N-WASp far more efficiently than individual N-WASp molecules. Because Nck has been shown to induce actin comet tail formation in an N-WASp dependent manner, we manipulate this molecular interaction to test the effect of N-WASp dimerization on actin polymerization. To manipulate the pathway, we vary the concentration of Nck within antibody-induced aggregates on the cellular surface and then use precise quantitative analysis of Nck density and induced actin polymerization to analyze the system. Using the *Virtual Cell*, we have built a comprehensive, quantitative actin cycle model. With this model we have tested 2 mathematical expressions for dimerized N-WASp activation of Arp2/3, which produce different experimentally testable predictions. These results demonstrate a nonlinear relationship between the density of Nck aggregates and actin polymerization and also demonstrate that a quadratic-based formula describing dimerized N-WASp activation of Arp2/3

most accurately predicts experimental observations. The combination of biochemical modeling and precise experimental manipulation and quantification provides unique insights into the relationship between the density of increased local concentrations of Nck and resulting localized actin polymerization. (Supported by NIH grants P41 RR013186 and U54 RR022232)

3226-Pos Board B331

Transcriptional Regulation of Mouse H2-Calponin Gene by Mechanical Tension

Wenrui Jiang, J.-P. Jin.

The importance of mechanical signaling in life process has long been recognized, however, it remains to be established that how mechanical signals is transduced in cells to regulate gene expression. Our previous studies have demonstrated that the gene encoding h2-calponin (*Cnn2*) is regulated by mechanical tension (Hossain et al., *JBC*, 2005). To investigate the regulatory mechanism, mouse genomic DNA containing the *Cnn2* promoter was cloned and 5'-serial deletion constructs were made in reporter plasmid vectors. By transfective expression in NIH3T3 fibroblasts and HEK293 cells that express endogenous h2-calponin, we tested the activity of the epigenetic *Cnn2* promoter constructs and their responsiveness to the stiffness of cultural substrates. The results showed that while the −0.6-kb construct had only near background activity, significant levels of transcriptional activities were observed for the −1.0-kb, −1.6-kb and −2.1-kb promoter constructs. The −1.6-kb and −2.1-kb constructs were both responsive to substrate stiffness that produce different mechanical tensions in the cytoskeleton, whereas the −1.0-kb construct showed no such regulation. The dada indicated that *cis*-regulatory element(s) located between −1596 and −1016 of the mouse *Cnn2* gene is responsible for the mechanical tension-regulated expression of h2-calponin. By establishing a novel experimental system to study mechanical cell signaling, the characterization of *Cnn2* promoter activity allows us to identify *trans*-regulatory factors involved in the cellular signaling pathway that transmits mechanical tension stimuli to the regulation of h2-calponin gene expression.

3227-Pos Board B332

Loss of Regeneration in Mammalian Ears Parallels the Accumulation and Stabilization of Junctional Actin in Supporting Cells

Joseph Burns, Jeffrey T. Corwin.

Humans and other mammals are vulnerable to permanent deficits of hearing and balance that arise when inner ear hair cells (HCs) are killed; however, non-mammals can recover sensory function after supporting cells (SCs) give rise to replacement HCs. Marked differences exist between non-mammals and mammals in an age-dependent reinforcement of junctional F-actin belts within vestibular SCs. In non-mammals, belts remain thin into adulthood, but their counterparts in humans and rodents dramatically thicken with age and nearly fill the adult cell at the level of the junction. In mice belts grow ~1300% thicker between E18 and P83, closely paralleled by declines in the ability of SCs to spread ($r = -0.989$), proliferate ($r = -0.975$), and generate new HCs ($r = 0.91$). Here, we used pharmacological agents and FRAP to investigate stability and turnover in belts at different stages of reinforcement. In adult mouse utricles cultured with 10nM-2μM Cytochalasin D, the circumferential belts in SCs exhibited an 80% reduction in thickness by 24hrs compared with controls, but no further reductions were observed thereafter, and sequestering actin monomer with 100nM-1μM Latrunculin A had no effect on reinforced belts. We tested the hypothesis that filament stabilization accompanies reinforcement by photobleaching belts in SCs of utricles from knock-in mice that express a GFP-actin fusion protein and measuring fluorescence recovery. By 2.5hrs after photobleaching, normalized fluorescence recovered 81.8 ± 4.5% in P0 mouse utricles, compared to just 37.7 ± 4.2% in >P20 mouse utricles. The results indicate that as regenerative capacity declines postnatally in mammals, the F-actin that accumulates in belts at SC junctions becomes increasingly stabilized. Future experiments will target actin filament dynamics in SCs to assess the role of reinforced belts in limiting HC regeneration.

3228-Pos Board B333

Modulation of the Actin Filament Reorganization Alters Cellular Calcium and Surface Adhesion in Wharton's Jelly Cells

Ying-Ming Liou, Kang-Wei Peng.

Wharton's jelly cells (WJCs), the mesenchymal stem cells derived from umbilical cord, require extensive remodeling of actin filaments by the action of a multitude of actin-binding proteins for their biological functions of self-renewal and differentiation. In this study, molecular approaches by specific siRNAs for caldesmon (CaD), and profilin (Pro) and by gelsolin (GSN) overexpression were used to alter those gene expressions and their subsequent controls of actin polymerization in WJCs and to investigate the effects of modulation of the actin filament reorganization on cellular Ca^{2+} levels and surface adhesion force in the cell. Ca^{2+} levels were measured as the fura-2 F340/F380 fluorescence ratio in the cells. Silencing of CaD and Pro by siRNAs raised intracellular Ca^{2+} and rendered the resistance of decreasing Ca^{2+} levels by a protein kinase inhibitor, genistein. The similar change in cellular Ca^{2+} was also found in GSN-overexpressed cells. To determine whether changes in cellular Ca^{2+} associated with modulation of the actin filament reorganization will affect surface adhesion of the cell, atomic force microscopy (AFM) force-distance measurements were applied to measure the stiffness and the adhesion force in si-control, si-CaD, si-Pro, and GSN overexpressed cells. Results obtained indicate that disturbing actin filament polymerization significantly increase in cell adhesion force but do not alter the stiffness in the cells. Apparently, modulation of the actin filament polymerization might alter cellular Ca^{2+} and cell adhesion that is important for determining the capacity of cell differentiation in WJCs.

3229-Pos Board B334

Molecular Motors at the T Cell Immunological Synapse

Yan Yu, Alex Smoligovets, Jay T. Groves.

Signal transduction in living cells via cascades of chemical reactions generally begins on the cell membrane and is regulated by the large-scale spatial arrangement of cell surface receptors. This phenomenon is particularly striking in the antigen recognition by T cells. Signaling through discrete T cell receptors (TCRs) in the context of immunological synapse, involves the orchestrated movement and reorganization of TCR microclusters. The frictional coupling between the actin cytoskeleton and protein microclusters has been proposed to be essential for the spatial organization of signaling receptors at all length scales, but the role of molecular motors in this process is largely unknown. By using the hybrid live T cells-supported membrane system, we study the dynamics of myosin motors and actin cytoskeleton during the synapse formation of primary T cells. The mechanical roles of myosin and actin cytoskeleton have been explored.

3230-Pos Board B335

Diamagnetic Levitation Causes Changes in Actin Architecture and Actin-Binding Proteins in Bone Cells

Ai-Rong Qian, Xiang Gao, Wei Zhang, Li-Fang Hu, Peng Shang, Jian-Ping Jin.

Diamagnetic levitation technology is a novel approach for simulated weightlessness and has only recently been applied in biological research. We have developed a superconducting magnet platform with large gradient high magnetic field (LG-HMF), which can provide three apparent gravity levels, namely μ-g (diamagnetic levitation), 1-g, and 2-g for diamagnetic materials. Here we studied the effects of LG-HMF on the morphology of actin cytoskeleton and the expression of actin-binding protein vinculin, paxillin, talin and MACF1 (microtubule actin crosslinking factor) in bone cells. The results showed that LG-HMF treatment of 48 hours had no acute lethal effects on both osteoblast-like and osteocyte-like cells. Compared to the nature 1-g control, μ-g significantly altered the cell shape, actin cytoskeleton structure (Fig 1), and the distribution and expression of actin-binding proteins in bone cells. In contrast, LG-HMF-produced 1-g and 2-g apparent gravity did not have such effects on bone cells. The results indicate that bone cells are sensitive to microgravity and vinculin, paxillin, talin and MACF1 may be involved in the mechanosensation and adaptation of bone cells. The diamagnetic levitation system provides a novel ground-based microgravity simulator for cell biological studies.

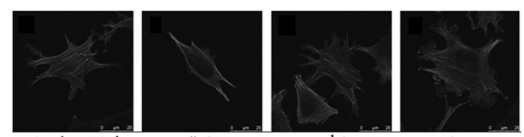

Fig 1. Rhodamine-phalloidin staining showed that diamagnetic levitation affects morphology and actin cytoskeleton structure of MLO-Y4 cells. Bar: 25 μ m

Cell and Bacterial Mechanics & Motility III

3231-Pos Board B336

Thermodyanmic Control on the Torque Generation of Bacterial Flagellar Motors

Manabu Hasumi, Masahide Terazima, **Masayoshi Nishiyama**.

Bacterial flagellar motor is an ion-driven molecular machine that is composed of a rotor and stator units. At least 11 stator units simultaneously associate with a single rotor, and the rest units diffuse in the inner membrane. The stator units exchange rapidly with the rotor and are concerned in the torque generation. Little is understood about the detailed energy conversion mechanism. Here, we demonstrate a novel assay that controls the intermolecular interaction between rotor and stator units with high-pressure techniques [1]. The strain was enclosed in the specially designed high-pressure chamber, which could be available up to 2,000 bar. The torque-speed relationship of the motor was measured by tracking of polystyrene beads attached to flagellar filaments at pressure range of less than 800 bar. At ambient pressure (1 bar), the torque is approximately constant (at ~1500 pN nm) from stall up to a ''knee'' speed of ~150 Hz, and then falls linearly with speed, extrapolating to zero torque at ~280 Hz. As the pressure increased, both the knee and zero-load speeds decreased significantly, while the zero-speed torque was not affected. Similar relations were obtained by decreasing intracellular pH [2]. Thus, our results suggest that applied pressure decreases the rate of proton translocation in the mechanochemical energy translation, but not the actual torque generation step within the cycle by the stator-rotor interactions.

[1] Nishiyama et al., Biophys. J. 96(3) 1142-1150 (2009).
[2] Nakamura et al., J. Mol. Biol. 386(2), 332-338 (2009).

3232-Pos Board B337

Are Biomechanical Changes Necessary for Tumor Progression? - The Impact of Cell Mechanics on Cancer Progression

Mareike Zink, Anatol Fritsch, Tobias Kiessling, Kenechukwu D. Nnetu, Steve Pawlizak, Franziska Wetzel, Josef A. Käs.

Biophysics established a new research area which described the progression of cancer from a materials science perspective. It has been know for a long time that malignant transformation is associated with significant changes in the cellular cytoskeleton. If the cytoskeleton's alterations are necessary for malignant transformation, they have to trigger biomechanical changes that impact cellular functions. In all cancers malignant neoplasia - uncontrolled growth, invasion into the surrounding tissue and metastasis occurs. Our results indicate that all these three phenomechanisms of malignancy require changes in the active and passive biomechanics of a tumor cell. Optical stretcher experiments with tumor cell lines and primary cells clearly show that malignant transformation causes cell softening for small deformations which correlates with an increased rate of proliferation compared to normal cells. However, tumor spheroids confined in agar gel proliferate until a gel stiffness of 10^4 Pa is exceeded which results in strain-hardening of cytoskeletal filaments at larger deformations. Furthermore, cell softening of the actin cortex can increase individual cell speed for lamellipodial motion of malignantly transformed fibroblasts and breast cancer cell lines. However, all cells can migrate and the motion of epithelial cells is mainly determined by their environment, whereas fibroblasts have the capability to move freely. Thus, it is the ability of single epithelial cells to overcome the tumor barrier to metastasize. The barrier that cells feel when they try to leave their cell compartment can be lowered by reducing cell adhesion. In breast tumor samples, small numbers of cells can be found that actively contract when laser light tries to stretch them. These could play a key role in metastasis because contraction can pre-strain and thus stiffen the cells to reduce adhesion sides to adjacent cells.

3233-Pos Board B338

Dual Mechanical Signal Integration Reveals Non Linear Cell Behavior

Robert L. Steward Jr., Chao-Min Cheng, Philip LeDuc.

Cell signaling is a complex, dynamic process, that requires precise coordination between internal signaling cascades and pathways and external environmental cues. One such external cue is mechanical stimulation which is known to influence a variety of cell responses including motility and proliferation. While mechanical stimulation may come in the form of tension, compression, or shear via a static or cyclic mode it may also occur separately or simultaneously reflecting the diversity of mechanical signals that cells may be required to integrate into cell behavior. For example, one cell type that experiences coupled mechanical influences are endothelial cells, which undergo three mechanical stresses: parallel shear flow, perpendicular radial stretch, and circumferential wall stress. Both normal and abnormal physiological processes result from the interplay between these forces. To probe how the cell integrates multiple mechanical signals single cells were exposed to uniaxial stretching, shear fluid flow and both modes of stimulation simultaneously to examine how the cell processes multiple inputs of mechanical stimulation as a function of cellular orientation. Cells exposed to single modes of mechanical stimulation were observed to align along the direction of stress, but intriguingly when combined, the responses were out of phase where the cells aligned between the direction of applied stresses with an orientation that was neither vertical or horizontal. This signal integration was observed to be not simply an additive approach, which has been investigated for physiological processes, but rather a nonlinear combination between both modes of mechanical stimulation, which is interesting as this has implications in abnormal physiological implications. These results will help provide insight into the complexities of cell behaviour and have implications in a variety of fields including biophysics, mechanotransduction, and cell signaling.

3234-Pos Board B339

Substrate-Ligand Friction Controls Traction Force in Cell Adhesion

Tilo Pompe, Thomas Bischoff, Stefan Glorius, Stephanie Johne, Maria Kasimir, Martin Kaufmann, Ina Uhlmann, Manfred Bobeth, Wolfgang Pompe, Carsten Werner.

Extracellular matrices determine cell fate decisions through the regulation of intracellular force and stress. The mechanical properties of these matrices like stiffness and ligand anchorage cause a distinct signaling behavior of adherent cells in respect to adhesion receptor forces. This process is known to be tightly linked to downstream kinase activation and epigenetic events including cell proliferation and differentiation. We report now on a new mechanism controlling traction forces in cell adhesion originating from sliding friction between adhesion ligands and the supporting material.

Using polymer surfaces with a graded physicochemistry we were able to tune the non-covalent anchorage of adhesion ligands, namely fibronectin, to the materials surfaces. Traction force cytometry and in situ analysis of cell-driven ligand reorganization revealed a correlated dependence on the ligand-substrate anchorage. Ligand reorganization during the formation of fibrillar adhesions was characterized by a reaction-diffusion process with a surface mobility around 1e4 m/Ns. Based on these quantitative data we could describe the force-velocity equilibrium at the adhesion site with its extracellular and intracellular components, namely the nanoscale friction of adhesion ligands on the materials surface and the myosin motor activity at the actin stress fibers. The correlation of a linearized Tomlinson model of ligand friction on the materials surface with the characteristics of myosin motors in the actin stress fibers revealed a control mechanism of traction forces of around 1pN per receptor-ligand pair by the ligand-substrate friction.

These findings elucidate a novel mechanism in force regulation at adhesion receptors, which is proposed to be highly relevant for cell behavior on natural and artificial scaffolds in vivo and in vitro, as many adhesion ligands are found non-covalently anchored to scaffold surfaces.

3235-Pos Board B340

Engineering the Mechanobiological Oscillations of Single Cells

Tianzhi Luo, Douglas N. Robinson.

Recently, we found that cytoskeletal proteins, such as myosin-II and cortexillin-I, cooperatively accumulate to highly deformed regions in Dictyostelium cells and the accumulation extent increases with increasing forces. Accompanying the protein accumulation, the cellular deformation decreases even as the external forces are kept constant. We argue that the accumulation of cytoskeletal proteins sense the mechanical stimuli and accumulate locally to enhance the local mechanical resistance of the cell, i.e. the cortical stiffness, which leads to diminishing cellular deformation. We suggest that the underlying mechanism of the cooperative accumulation could be that the binding of myosin to actin enhances cortexillin binding to actin filaments. Especially, myosin, undoubtedly a force sensor, binds to actin filaments in a force-dependent manner. On the other hand, cortexillin maintains the mechanical integrity of the whole actin network and anchors it to the cell membrane. Additionally, we found that cells are able to repeat the "increased deformation-protein accumulation-decreased deformation" cycle while the external force does not change. We propose two mechanisms for the restarting of the cycles. The first is that the myosin accumulation itself leads to less force experienced by each myosin, which results in the falloff of the accumulated myosins and the subsequent cortical softening, leading to larger deformation again. The second is that blebs, which behave as increased deformation, are sometimes formed when either the cortex-membrane linkage is too weak or the local myosin associated contractility is too strong. To test these hypotheses, we use chemicals, genetic tools and their combinations to modulate the expression level, the localization and function of cytoskeletal proteins and therefore tune the cortical stiffness, the cortex-membrane linkage and the period of the cellular oscillations in a quantitative way.

3236-Pos Board B341

Influence of Altered Local Effective Concentration on Cytoskeletal and Ecm Structure in Human Mesenchymal Stem Cells

Adam S. Zeiger, Felicia C. Loe, Michael Raghunath, Krystyn J. Van Vliet.

Mesenchymal stromal or stem cells (MSCs) are a type of pluripotent precursor cell found in bone marrow, which can be coaxed in vitro to express certain characteristics of differentiated mesenchymal tissue lineages. Many therapeutic applications of MSCs require isolation from a given patient, expansion to useful cell numbers in culture, and reimplantation. However, the in vivo and in vitro culture conditions remain in stark contrast, and confound interpretation of experiments and development of therapeutic uses for MSCs. For example, in vivo, the extracellular microenvironment is highly crowded with proteins; in vitro, the extracellular culture media is decidedly dilute. Here, we use multiple methods to consider whether this differential crowding can directly alter MSC structure and function. We consider a series of macromolecular crowders within the culture media of MSCs, expanded under basal (non-differentiating) conditions. We then quantify changes in population-level proliferation and migration, and in extracellular and intracellular protein structure and cortical cytoskeletal stiffness via immunocytochemistry, optical microscopy, and atomic force microscopy-enabled imaging and nanoindentation of living MSCs. We find significant effects of "crowded" culture conditions on cell architecture, extracellular matrix structure, and attendant cell properties. These results motivate the development of more physiologically relevant environments for both in vitro studies and biodevices, to ultimately answer fundamental questions of physiological and pathological behavior for MSCs.

3237-Pos Board B342

Regulating Cell-Substrate Adhesion via Prestress in the Cytoskeleton

Bin Chen, Huajian Gao.

Abstract

We investigate whether and how prestress in cytoskeleton influences cell adhesion with a stochastic-elasticity model of a stress fiber attached on a rigid substrate via molecular bonds. By comparing the variations in adhesion lifetime and observing the sequences of bond breaking with and without prestress in the stress fiber under the same applied force, we demonstrate that the effect of prestress is to shift the interfacial failure mode from crack-like propagation toward uniform bond failure within the contact region, thereby greatly increasing the adhesion lifetime. The present study suggests a feasible mechanism by which cell adhesion could be actively regulated via prestress due to cytoskeletal contractility.

3238-Pos Board B343

Tensile Mechanical Characterization of Cell Stiffness Improves Correlation to Metastatic Potential in Models of Osteosarcoma

Guido Bartalena, Yannick Loosli, Tomaso Zambelli, Roman Muff, Jess Snedeker.

A correlative link between decreased cancer cell stiffness and increased aggressiveness (metatstatic potential) has been established in a wide range of cancers, such as leukemia, breast cancer and chondrosarcoma. Nearly all studies establishing this link in adherent cells have utilized cell compression (indentation) or shearing (e.g. magnetic cyto-twisting). In this study we applied a novel tensile assay of cell stiffness to investigate the mechanical behavior of two osteosarcoma models (SAOS-2/LM5 and HUO9/M132), with each system comprising a parental cell line and its highly metastatic derivative form. The goal was to find a common trend linking cell stiffness and metastatic potential, further hypothesizing that a tensile assay could provide additional information compared to traditional compressive measures. Cells were therefore tested in two different mechanical configurations: in compression using atomic force micro-indentation; and in tension using a custom functional imaging platform that applies a controlled bi-axial deformation to the cell substrate while imaging and tracking substrate deformation at high spatial resolution. These measurements were coupled with an inverse finite element model to more precisely estimate cell tensile constitutive behavior.

Both parental lines proved to be significantly ($p<0.01$) stiffer than their metastatic variants in tension: 2.5 ± 1.6 kPa (SAOS-2) vs. 1.4 ± 1.0 kPa (LM5) and 5.3 ± 2.5 kPa (HUO9) vs. 2.5 ± 0.7 kPa (M132). Although a compressive characterization of the SAOS-2/LM5 model confirmed this trend (3.5 ± 1.7 kPa vs. 1.8 ± 0.8 kPa, $p<0.001$), the compressive (cytosolic) stiffness of the HUO9/M132 was unexpectedly higher in the highly metastatic cells (2.0 ± 0.7 kPa vs. 4.9 ± 2.1 kPa, $p<0.001$). These results indicate that the relationship between ''cell stiffness'' and phenotypic aggressiveness is not straight forward, and that tensional mechanical characterization provides additional, and perhaps more pertinent, information linking cell mechanical behavior to metastatic potential.

3239-Pos Board B344

Photobleaching Fluctuations Lead to Apparent Non-Exponential Decay, but can be used to Estimate Number of Fluorophores

Chitra Raju Nayak, Manfred H. Jericho, Andrew Rutenberg.

Intrinsic fluctuations are expected during photobleaching of a fixed number of fluorophores, such as inside a cell. We show that deterministic exponential fits of the stochastic photobleach curves lead to small but significant deviations from the true lifetime and, more significantly, to time-dependent residuals. These time-dependent (non-white) residuals should not be interpreted as evidence for non-exponential decay. We show however that the fluctuations can be directly used to estimate the number of fluorophores per cell, without requiring diffusive fluorophores, and we present an analytic estimate for the quantification error that is confirmed by stochastic simulations. Experimental tests of this fluctuation quantification with calibrated MESF beads leads to the surprising result that the MESF beads exhibit a clear multiexponential behavior that cannot be explained by intrinsic fluctuations. We cannot therefore use these calibrated beads to test our fluctuation-quantification approach.

3240-Pos Board B345

Tracking Bacterial Swimming Near a Solid or Air Surface

Liana Nisimova, James Bensson, Guanglai Li, Martin Maxey, Jay X. Tang.

Bacterial motility near a boundary has many implications in surface contamination, biofilm formation, and infection. We study the near surface swimming behavior of microbes using a monotrichous bacterium called Caulobacter crescentus. C. crescentus is a waterborne bacterium that progresses through a two-stage life cycle, alternating between a stationary stalked cell and a motile swarmer cell. The swarmer cell uses its flagellum to propel itself through fluid. We use a non-chemotactic, forward swimming mutant strain lacking pili, SB3860, to focus on near surface motility. Using defocused particle tracking to relate the radius of a dark field image of a swarmer cell to its height away from the microscope's focal plane, we track its motion in three dimensions as a function of time. With this approach, we measure the density distribution from the surface, the speed in relation to height, and the trajectories of bacterial motion. In investigating the behavior of the cells at two different interfaces (water-solid and water-air), we have discovered significant differences in speed, density distribution, and the trajectory shape. At the glass-water interface, a much higher density of cells is found within a micron from the surface, and the average speed reaches a maximum within a few micrometers. At the water-air boundary, however, there is a much wider spread of cell distribution, and the average swimming speed close to surface is significantly lower. Furthermore, most cells at the water-air interface swim in circular trajectories, whereas at the solid-water interface, most trajectories appear straight as the forward swimming cells tend to leave the surface within a fraction of a second. These intriguing properties may be relevant to a variety of microbial functions at the interface, such as accumulation, biofilm formation, and adhesion.

3241-Pos Board B346

The Integrins $\alpha5\beta1$ and $\alpha2\beta1$ Enhance Cell Motility

Claudia Tanja Mierke, Martin Herrmann, Ben Fabry.

Cell migration through connective tissue, or cell invasion, is a fundamental biomechanical process during metastasis formation. Cell invasion usually requires cell adhesion to the extracellular matrix through integrins. In some tumors, increased integrin expression is associated with increased malignancy and metastasis formation. Here, we studied the invasion of cancer cells with different $\alpha5\beta1$ and $\alpha2\beta1$ integrin expression levels into 3D collagen fiber matrices. Using a cell sorter, we isolated $\alpha5\beta1^{high}$ and $\alpha5\beta1^{low}$ as well as $\alpha2\beta1^{high}$ and $\alpha2\beta1^{low}$ expressing sub cell lines from parental MDA-MB-231 breast cancer cells. $\alpha5\beta1^{high}$ and $\alpha2\beta1^{high}$ cells showed increased cell invasiveness compared to $\alpha5\beta1^{low}$ and $\alpha2\beta1^{low}$ cells, respectively. Similar results were obtained for 786-O kidney and T24 bladder carcinoma cells, and in cells in which the $\alpha5$ integrin subunit was knocked down using specific siRNA. Knock-down of the collagen receptor integrin subunits $\alpha2$ did also reduce invasiveness, but to a lesser degree compared to the integrin subunit $\alpha5$. Fourier transform traction microscopy revealed that the $\alpha5\beta1^{high}$ cells generated 7-fold larger contractile forces compared to $\alpha5\beta1^{low}$ cells. Cell invasiveness was reduced after addition of the myosin light chain kinase inhibitor ML-7 in $\alpha5\beta1^{high}$ cells, but not in $\alpha5\beta1^{low}$ cells, suggesting that $\alpha5\beta1$ integrins enhance cell invasion through enhanced transmission and generation of contractile forces.

3242-Pos Board B347
The GPI-Anchored Receptor CD24 Increases Cancer Cell Invasion through Enhanced Contractile Forces
Claudia Tanja Mierke, Martina Fellner, Steffen Runz, Peter Altevogt, Ben Fabry.
The malignancy of a tumor depends on the capability of cancer cells to metastasize. The process of metastasis involves cell invasion through connective tissue and transmigration through endothelial monolayers. The GPI-anchored receptor CD24 expression is increased in several tumor types and is consistently associated with increased metastasis formation in patients. Furthermore, the localization of β1 integrins in lipid rafts depends on CD24. Cell invasion is a fundamental biomechanical process and usually requires cell adhesion to the extracellular matrix (ECM) through mainly β1 heterodimeric integrin receptors. Here, we studied the invasion of human lung A125 cancer cells with different CD24 expression levels in 3D ECMs. We hypothesized that CD24 expression increases the invasiveness of cancer cells by enhanced contractile force transmission or generation.
To analyze this, $CD24^{neg}$ cells (CD24-negative) were stably transfected with CD24 and sorted for high and low CD24 expression. The invasiveness of the $CD24^{high}$ and $CD24^{low}$ transfectants were determined in 3D-ECMs. The percentage of invasive cells and their invasion depth was increased in $CD24^{high}$ cells compared to $CD24^{low}$ cells.
Knock-down of CD24 and of the β1 integrin subunit in $CD24^{high}$ cells decreased their invasiveness, indicating that the increased invasiveness is CD24 and β1 integrin subunit dependent.
Fourier transform traction microscopy revealed that the $CD24^{high}$ cells generated 5-fold higher contractile forces compared to $CD24^{low}$ cells. To test whether contractile forces were functional related to cell invasion. Cell invasiveness was reduced after addition of myosin light chain kinase inhibitor ML-7 as well as Rho kinase inhibitor Y27632 in $CD24^{high}$ cells, but not in $CD24^{neg}$ cells, whereas an increase in prestress in $CD24^{neg}$ cells after addition of LPA increased cell invasiveness. Taken together, these results suggest that CD24 enhances cell invasion through increased transmission or generation of contractile forces.

Intracellular Cargo Transport

3243-Pos Board B348
Live-Cell Imaging of Colloidal Mesoporous Silica Nanoparticles for Drug Delivery: Drug Loading, Pore Sealing and Controlled Release
Anna M. Sauer, Axel Schlossbauer, Valentina Cauda, Hanna Engelke, Christian Argyo, Delphine Arcizet, Nadia Ruthardt, Joachim Rädler, Thomas Bein, Christoph Bräuchle.
Colloidal mesoporous silica (CMS) nanoparticles are promising candidates for drug delivery. However, after the drug is loaded into the pores, sealing of the pores against premature drug release and controlled intracellular drug release are challenging tasks. We studied the mechanisms of nanoparticle uptake into living cells, trafficking and intracellular delivery of drugs by highly-sensitive fluorescence microscopy and real-time single-particle tracking.
As an approach to seal the mesopores, we encapsulated CMS nanoparticles of 50 nm diameter with a supported lipid bilayer (SLB). We demonstrated the delivery of the microtubule-depolymerising drug colchicine from SLB-coated CMS nanoparticles into liver cancer cells. The microtubule network of the cells was destroyed within 2 h of incubation. With this method, colchicine is released directly into the cell showing characteristic effects at concentrations below the amount necessary for application in solution.
In another approach, we linked a fluorescently labelled model drug (cystein-ATTO633) via a redox-sensitive disulfide bridge inside the pores of CMS. For reduction of the disulfide bonds and release of the drug, the CMS nanoparticles need to reach the cytoplasmic reducing milieu after internalization. We showed that nanoparticles were endocytosed by HuH7 cells, but endosomal escape seems to be a bottleneck for drug release. Using a photosensitizer to induce endosomal escape, successful release of the drug was achieved. Additionally, we found that grafting of ATTO633 at high concentration in the pores of silica nanoparticles results in self-quenching of the ATTO633 fluorescence. Release of dye from the pores promotes a de-quenching effect with an excellent readout signal.
As the EGF-receptor is overexpressed on a variety of tumors, CMS particles were equipped with EGF as ligand for specific targeting. Internalization and cellular motion of the particles was studied by single-particle tracking.

3244-Pos Board B349
Internalization Pathways and Intracellular Fate of Poly(Lysine) Analogues
Zuzana Kadlecova, Laurence Abrami, Alessandra Griffa, Matthias Geissbühler, Theo Lasser, Florian M. Wurm, F. Gisou van, der Goot, Harm-Anton Klok.
Cationic peptides and polymers are widely used as nonviral transfection agents. A fundamental understanding of the relationship between structure and translocation mechanisms, intracellular trafficking and final targeting of these molecules is still lacking to date and mostly based on empirical observations.
In this contribution we systematically investigate the role of the structural parameters of the polycations on their endocytic pathway and intracellular fate in vitro. To cover all the structural parameters, a library of the polycations based on L-lysine monomer unit was constructed, covering a broad range of molecular weights and degree of branching. A new class of cationic polymers, prepared by polycondensation of L-lysine, was developed to explore the impact of very high molecular weights. The uptake pathways of the structural analogues were probed by specific inhibitors of endocytosis. The internalization kinetics was measured at a macroscopic scale by fluorescence intensity methods to identify the key structural parameters stimulating the translocation into the cytosol. The microscopic distribution and the trafficking kinetics were studied by two distinct methods: subcellular fractionation and confocal scanning laser microscopy with subsequent high throughput image analysis. The final localization in CHO cells was followed by indirect immunocytochemistry. In parallel a novel technique based on the sensitivity of the fluorescent probes to local microenvironment and assessed by triplet lifetime imaging is developed for this purpose.
We found that architecture and molecular weight of polycation have profound effects on intracellular trafficking and resulting localization. Hyperbranched polylysine with extremely high molecular weight posses a unique capacity in comparison to the linear and dendritic analogues to destabilize endosomes and to escape from lysosomes, which is generally the limiting step in gene delivery.

3245-Pos Board B350
GSK-3 Regulates Bidirectional Transport of Kinesin-1 driven Cargoes
Christina Leidel, Carole Weaver, Lukasz Szpankowski, Lawrence S.B. Goldstein, George T. Shubeita.
Abnormal deposits of amyloid plaques which characterize Alzheimer's disease have been linked to deficient transport of the Amyloid Precursor Protein (APP) by kinesin-1 motors. It is of great interest to identify the regulatory factors that enhance or inhibit axonal transport, thereby providing direction along the path of pharmaceutical treatments for neurodegenerative diseases. The serine/threonine kinase Glycogen Synthase Kinase 3 (GSK-3) has been proposed as a regulator of axonal kinesin-1 and has been linked to many aspects of the development of Alzheimer's disease. We use interdisciplinary techniques including force measurements and video tracking of individual cargos in *Drosophila* embryos, and kymographs of fluorescently labeled axonal cargos in *Drosophila* larvae to examine the role played in transport by dGSK-3, the GSK-3 homolog in *Drosophila*. Mutations in the Shaggy gene (sgg^1) which encodes for dGSK-3 allow us to probe the effects of loss-of-function and over-expression of dGSK-3 on transport parameters such as cargo velocity and run length. Our work indicates that GSK-3 is a required negative regulator of transport *in vivo* that directly affects the motion of APP in axons and lipid droplets in the embryos. *In vivo* measurements of the stall forces of motor-driven cargos enable us to differentiate between two possible mechanisms by which GSK-3 regulates transport: changes in the motor copy-number on the cargos or changes in motor activity.

3246-Pos Board B351
Coarse-Grained Modeling of Organelle Motility in Living Cells
Kristopher E. Daly, Kyle Lemoi, Yen-Chun Liu, Luis Vidali, **Erkan Tuzel**.
Organelle motility is essential for the functioning of the eukaryotic cell. Actively modifying intracellular structures allows cells to change and adapt to different conditions. In plants, reorganization of the chloroplasts is critical to adapt to changes in light quality and intensity. Our analysis of chloroplast motility in moss provides evidence that this active transport is facilitated by the microtubule cytoskeleton and molecular motors. We will present detailed in vivo measurements of organelle organization and motility, combined with coarse-grained mesoscale modeling. Our simulations take into account both thermal fluctuations and the topology of the microtubule network, and shed light into the molecular mechanisms at play.

3247-Pos Board B352
Novel Mechanisms of Cell Uptake in Lipid-Mediated Gene Delivery
Giulio Caracciolo, Daniela Pozzi, Cristina Marchini, Maura Montani, Augusto Amici, Michelle A. Digman, Susana S. Sanchez, Enrico A. Gratton, Anna Laura Capriotti, Aldo Laganà.
The mechanism of cell uptake in lipid mediated gene delivery was investigated in NIH3T3 and CHO cell lines. We show that different endocytic pathways are activated by shape coupling between lipoplex and membrane lipids. Our results suggest that tailoring the lipoplex lipid composition to the patchwork-like plasma membrane profile could be a successful machinery of coordinating the endocytic pathway activities and the subsequent intracellular processing. Transfection experiments performed at 4°C, when endocytosis does not take place, show that a novel class of highly efficient multicomponent lipoplexes enter cells by a temperature-independent fusion-like mechanism. In vivo, plasma proteins bind to lipoplex surface and create a rich 'protein corona' that is recognized by cells and other biological structures. The 'protein corona' associated to lipoplexes after interaction with human plasma was found to be much richer in basic immunoglobulins gamma proteins (Ig-Gs) than that of pure lipid vesicles in the absence of DNA. Because surface properties of lipoplexes may determine their interaction with cells and tissues, an accurate knowledge of lipoplex surface properties may be important for predicting biological responses. These findings also suggest the existence of hybrid structures made of multilamellar complexes either stuck together by DNA or coexisting with DNA-loaded intact vesicles.

3248-Pos Board B353
Lipid Trafficking in Neurons and Schwann Cells
James Matthew Love, Gunja Dave, Joshua Chetta, Sameer Shah.
Axons in the peripheral nervous system are capable of extending thousands of times the length of their cell bodies. These projections possess high surface area to volume ratios and thus require large quantities of lipids to maintain their membrane structure. During initial development this demand for lipids can be quite high as axons are capable of extending at rates of 1 mm/day. Studies suggest that long distance transport of lipids occurs in membranous vesicles with insertion occurring only at the growth cone. Other sources of membrane lipids have been demonstrated including locally synthesized lipids in axons, transfer of lipids from myelin, and addition of lipids internalized along the axon. Robust analysis and quantification of lipid trafficking has yet to be well characterized.
To quantify these phenomena, a model of developmental sensory axons utilizing dorsal root ganglia (DRG) of day 1 to 5 rats were used. Cells were harvested and plated overnight. Cultures were then treated with cytosine arabinoside to remove fibroblasts. Two days post-harvest, cultures were treated with a fluorescent ceramide analogue labeled with boron dipyrromethene difluoride (BODIPY). One hour post-treatment the cultures were observed for twenty minute time intervals using fluorescent microscopy. Preliminary results indicate multiple transport processes may play a role in the trafficking of lipids in the axons of neurons. At least two distinct populations seem to exist; one composed of bright, punctuate fluorescence that may be attributable to vesicles and a second diffuse fluorescence that may be attributable to labeled plasma membrane lipids. Quantification of the traffic patterns seem to initially suggest the bright, punctuate population are more motile than the diffusely fluorescent populations. Future experiments will compare patterns observed in neurons with those in Schwann cell projections, which may be a source of lipids transferred to axons.

3249-Pos Board B354
mRNA Transport in the Projections of Maturing Hippocampal Neurons
Gunja Dave, James Love, Joshua Chetta, Sameer Shah.
Translation of mRNA in axons and dendrites enables a rapid supply of proteins to specific sites of localization within the neuron. Distinct populations of mRNA-containing cargoes, including granules and mitochondrial mRNA, are transported with neuronal projections. The distributions of these cargoes appear to change during neuronal development, but details on the dynamics of mRNA transport during these transitions remain to be elucidated. The goal of this project is to characterize transport of mitochondrial and non-mitochondrial mRNA in neuronal projections during the development of hippocampal neurons. One day old rat hippocampal neurons were cultured for 1, 5, and 7 days, and mRNA transport was examined at each time point. The transport was observed via real-time imaging of SYTO14, a fluorescently labeled marker for mRNA. To differentiate between mitochondrial and granular mRNA, cells were also labeled with MitoTracker. Quantitative analysis was performed by kymograph which gives a graphical representation of spatial position over time. The results suggest differences in the transport pattern of mitochondrial and non-mitochondrial mRNA, and also indicate significant differences in transport parameters at different time points. Unexpectedly, increased bidirectional velocity of mRNA transport was observed from day 1 to day 7, which suggests altered demand for locally synthesized proteins even after maturity. To better understand the logic underlying altered mRNA transport, we are currently investigating whether changes in transport correlate with specific stages of neurite differentiation into axons or dendrites or synaptic contact with other neurons. This work has important implications for the regulation of neuronal plasticity during neuronal growth, maturity, and neurodegeneration.

3250-Pos Board B355
Microtubule Motors cannot Coordinate Bidirectional Transport of Lipid Droplets in the Absence of Cytosolic Components
Rafael A. Longoria Casasa, Hayley Manning, George T. Shubeita.
Long-range intracellular cargo transport is achieved by kinesins and cytoplasmic dyneins each of which moves mostly unidirectionally along microtubules. Similar to many other cargos, lipid droplets in *Drosophila* embryos exhibit global directionality with local bidirectional motion resulting from a biased engagement of the opposite polarity motors. Using Differential Interference Contrast microscopy, we examined purified lipid droplets from *Drosophila* embryos *in vitro*. Unlike lipid droplets *in vivo*, a large fraction of the purified droplets exhibit short distance transport. This suggests that, in the absence of cytosolic non-motor proteins, transport is impaired leading to opposite polarity motors engaging in a tug-of-war. This stalemate is consistent with previous *in vivo* force measurements that demonstrated equal force generation in both directions. Force measurements using an optical trap show that the motors on the purified lipid droplets are functional. We specifically alter this activity for the opposite polarity motors to resolve the stalemate.

3251-Pos Board B356
Dynamic Behavior of Intracellular Vesicles Probed with Two-Color Single Particle Tracking
Craig J. Szymanski, Christine K. Payne, William H. Humphries IV.
Understanding the dynamics of intracellular vesicles is essential for studies of cellular internalization, intracellular transport, and the movement of proteins between organelles. Of particular interest are the dynamics that result in the fusion of vesicles as extracellular cargo is transported through the endocytic pathway. We use two-color single particle tracking fluorescence microscopy to study populations of vesicles that exist as both isolated vesicles and fused hybrid vesicles. Specifically, we are interested in the relationship between Rab7-vesicles, LAMP1-vesicles, and Rab7-LAMP1-hybrid vesicles. The majority of these vesicles exist as hybrid vesicles, which limits the ability of static measurements and standard biochemical approaches to resolve differences between these three populations. We propose that while these vesicle populations are highly colocalized, they can be distinguished by their dynamics during the short periods when they are not colocalized. To this end, individual vesicles, labeled with distinct variants of GFP, were tracked and analyzed. An algorithm was developed to obtain the total and linear distance traveled by the vesicle, travel direction relative to its eventual fusion site, and efficiency in reaching its destination. Significant differences in these measurements suggest LAMP1-vesicles fuse more efficiently than Rab7-vesicles. This approach will prove useful in future studies for resolving the differences in highly colocalized populations of vesicles.

3252-Pos Board B357
Superresolution Studies to Reveal the Interactions between Motor Proteins and Individual Cargos in Chlamydomonas Flagella
Ziah Dean, Pamela Duboc, Ahmet Yildiz.
Our research aims to understand the molecular mechanism of cytoplasmic dynein, which is involved in the transport of cargo towards the microtubule minus end of eukaryotic cells. Specifically, we use intraflagellar transport (IFT) in Chlamydomonas cells as a model system to study interaction of IFT dynein with kinesin II, opposite polarity motor that moves cargos toward the plus end. To detect the distribution and cargo interaction of single motor proteins along the flagellum, we employed Stochastic Optical Reconstruction Microscopy (STROM) microscopy. This technique has proven to construct superresolution images of precisely positioned fluorophores from single-molecule images. In order to facilitate STORM imaging, photoswitchable cyanine reporter and an activator molecule were coupled to antibodies against kinesin II and IFT dynein. The quantitative analysis of the STORM images will allow us to determine how many kinesin and dynein motors actively work on a cellular cargo, and how the cargo direction is determined by kinesin-dynein interactions. IFT is a universal process in all eukaryotic cilia and flagella. Defects in this process are the primary causes of polycystic kidney disease and retinal degeneration.

Biomolecular NMR

3253-Pos Board B358

The His-75-Asp-97 Cluster in Proteorhodopsin: A DNP and Solid-State NMR Study

Franziska Hempelmann, Mirka-Kristin Verhoefen, Soraya Hölper, Lenica Reggie, Johanna Baldus-Becker, Sarah-Anna Fiedler, Andreas Wörner, Thomas Köhler, Josef Wachtveitl, **Clemens Glaubitz**.

The proteorhodopsin (PR) family found in bacteria near the ocean's surface to high abundance consists of hundreds of PR molecules which are colour-tuned to their environment. The green absorbing species has been shown to act as a light-driven proton pump in vitro and in non native host organisms. In contrast to bacteriorhodopsin, the pKa of the primary proton acceptor Asp-97 is highly elevated and a single His is found close to the active site. Here, we report a complete biophysical study of this His-75, which is highly conserved within the PR family but not found in other retinal proteins. 13C-13C dipolar correlation experiments did show, that both side chains are close enough to enable the formation of a H-bond. In addition, 15N-MAS NMR provides evidence, that indeed a neutral, H-bonded His-Asp complex is formed in which the protonation is shifted to D97 explaining its high pKa. Using the sensitivity enhancement provided by dynamic nuclear polarisation, we were able characterise the active site and especially the H-bonding character of the His-Asp coupling in great detail. Our study is complemented by site-directed mutagenesis in combination with black lipid membrane measurements, ultrafast optical spectroscopy and flash photolysis. Our data show, that His-75 forms a pH dependent complex with Asp-97 but replacing His-75 with Met, Trp or Asn accelerates PR's photocycle and does not prevent proton transfer. This raises the question of the true function of PR in vivo.

3254-Pos Board B359

Structural Dynamics of Phosphorylated Pentameric Phospholamban in Lipid Membranes using a Combination of Solution and Solid-State NMR Spectroscopy

Raffaello Verardi, Martin Gustavsson, Nathaniel J. Traaseth, Gianluigi Veglia.

Phospholamban (PLN) is a 52-residue membrane protein that regulates the cardiac sarcoplasmic reticulum Ca2+ATPase (SERCA). PLN is in equilibrium between monomeric and pentameric species. The monomer binds to and decreases the rate of Ca^{2+} transport of SERCA. This inhibitory action is relieved upon PLN phosphorylation at Serine-16 and Threonine-17. Here, we present the structural dynamics of fully phosphorylated pentameric PLN by a combination of solution and solid-state NMR spectroscopy. SDS-PAGE analysis revealed a higher thermal stability of the phosphorylated pentameric PLN (at Ser-16, Thr-17 and both) with respect to the unphosphorylated protein when reconstituted in different lipids and detergents.

Conventional T1, T2, and heteronuclear steady state NOEs experiments were used to probe fast (ps-ns) dynamics of the amide backbone upon phosphorylation at Ser-16, revealing a significant increase of the dynamics in this time scale. Slower (μs-ms) dynamics were probed by measuring rotating frame R (1rho) and R(2rho) dispersion curves using a new adiabatic irradiation scheme. The structural and topological effects of phosphorylation in pentameric PLN were investigated using solid-state NMR experiments on mechanically and magnetically oriented lipid systems. For the mechanically oriented samples, phosphorylated PLN was reconstituted in DOPC/DOPE lipid bilayers and uniaxially aligned between glass plates. For magnetically oriented samples, the protein was reconstituted in DMPC/Triton X-100 bicelles. Two-dimensional PISEMA and SAMPI4 experiments were used to determine the topology of PLN in lipid membranes. Chemical shifts anisotropy and dipolar coupling values were also used in combination with solution NMR restraints to determine a preliminary high-resolution structure of fully phosphorylated pentameric PLN.

These studies reveal residue-by-residue details of the pentameric PLN structure and topology upon phosphorylation.

3255-Pos Board B360

Solid State NMR Studies of Lung Surfactant Protein B Fragment, Mini-B, in Mechanically Oriented Lipid Bilayers

Dharamaraju Palleboina, Michael R. Morrow, Valerie K. Booth.

Lung surfactant, a lipid protein complex, prevents lung collapse by lowering the surface tension at the alveolar air-water interface. Surfactant protein B (SP-B) is an essential component of lung surfactant and is indispensable for life. Mini-B is a two-helix fragment of lung surfactant protein SP-B which retains significant biological activity compare to the full-length protein SP-B. Solid-state ^{2}H-NMR was used to characterize mechanically oriented lipid bilayers composed of POPC-$_{d31}$/POPG or DPPC-$_{d62}$ doped BLES, with and without associated Mini-B. The spectra were interpreted with the help from orientational order parameter profiles. The results indicated that 1) the order parameters were greater when the number of plates were increased 2) DPPC-$_{d62}$ in BLES is more ordered than POPC-$_{d31}$/POPG and 3) Mini-B tends to disrupt the orientation of bilayers and reduce the order in the fraction of the sample that remain oriented. Even in the presence of Mini-B, the lipid bilayers could be well oriented by optimizing plate dimension, amount of sample between the plates and volume of the solvent used to dissolve the organic solvent. These well-oriented samples are being used in further studies of lipid headgroup orientation, as indicated by 31P NMR, as well as for studies of 15N-lebled peptides, to indicate the tilt angle of the peptide's helices within the bilayer.

3256-Pos Board B361

The Selectivity Filter of the hERG Channel - NMR Study of its Structure and Interaction with Membranes and Drugs Involved in the Long QT Syndrome

Andrée Gravel, Alexandre A. Arnold, Érick J. Dufourc, Isabelle Marcotte.

The drug-induced (acquired) long QT syndrome (ALQTS) is a cardiac muscle dysfunction responsible for heart arrhythmia and failure. Virtually all cases of ALQTS are due to the blockage of the heart human ether-a-go-go-related-gene (hERG) potassium channels located in the myocardium cell membranes. The hERG channel is a unique member of the family of voltage-gated K^+ (K_v) channels because of its different selectivity filter (SF) signature and linker sequence between the last two pore helices (S5-S6) as compared to other bacterial, mammalian and *Drosophila* K_v channels. Recent work has shown that binding sites of LQTS-prone drugs could be found at the intracellular base of the SF. Considering the sequence particularities of the hERG channel's SF and the occurrence of potential drug binding sites, the objective of this work is to study the SF structure of the hERG channel and role in the ALQTS. Results obtained by liquid-state NMR experiments and circular dichroïsm suggest that the SF peptide has no defined secondary structure in water. However, changes in chemical shifts for the C-terminal end of the SF can be observed in the presence of a low concentration of K^+ ions (10mM), suggesting structural modifications. Using ^{2}H and ^{31}P solid-state NMR, we have investigated the interaction of the SF with model complex membranes and simple DMPC vesicles. The spectra reveal that both membrane systems are destabilized by the SF. Moreover, the presence of K^+ ions appears to reinforce this perturbing effect of the lipid bilayer. Our results, therefore, demonstrate a possible interaction for the hERG channel SF with the membrane environment. The interaction of bepridil, fluvoxamine and promethazine with the SF will also be discussed.

3257-Pos Board B362

Structural Studies of Mammalian Dynactin CAP-Gly Domain by Solid-State NMR

Si Yan, Shangjin Sun, Guangjin Hou, John C. Williams, Tatyana Polenova.

Microtubules and their associated proteins play essential roles in a broad range of physiological functions, including cell migration, mitosis, polarization, differentiation, and vesicle and organelle transport. Dynactin, an activator and the dominant cofactor of dynein, is a large (1.2 mD) multisubunit complex that bridges vesicles to the MT network and thus is central to dynein mediated retrograde transport. Its central subunit, p150^{Glued}, binds to microtubules via the CAP-Gly domain that is thought to be critical for +MT tip localization. Mutations in the p150^{Glued} subunit of the CAP-Gly domain have been implicated in predominantly in neurological disorders including dSMBA and Perry's Syndrome. Despite its critical role, the mechanism by which the CAP-Gly domain recognizes microtubules remains largely unknown, particularly at the atomic level. Herein, we report our recent progress in structural studies of CAP-Gly domain of dynactin by using solid-state NMR. For tertiary structure calculation, we acquired numerous medium- and long-range distance restraints from the DARR and R2$_1^1$ spectra of the ^{13}C sparsely enriched CAP-Gly.

References

1. S. Sun, A. Siglin, J. C. Williams, T. Polenova **(2009)** *J. Am. Chem. Soc.*, 131 (29), pp. 10113-10126.

2. S. Ahmed, S. Sun, A. E. Siglin, T. Polenova, J. C. Williams **(2010)** *Biochemistry*, 49 (25), pp. 5083-5085.

3258-Pos Board B363

Characterizing Recombinant Spider Wrapping Silk Monomers and Fibers by NMR and AFM

Marie-Laurence Tremblay, Lingling Xu, Paul X.-Q. Liu, Jan K. Rainey.

Spider silks are among the strongest and toughest naturally produced biomaterials. Despite these appealing properties, very little is known about the mechanisms by which these fibers form or about how fiber structure correlates to mechanical properties. Nuclear magnetic resonance spectroscopy (NMR) and far-ultraviolet circular dichroism (CD) spectroscopy were carried out in the solution-state on monomeric recombinant 13C and 15N labeled wrapping silk protein. This protein is a key constituent of egg case sacs, providing both flexibility and strength, produced in the aciniform spidroin with sequence

taken from the spider Argiope trifasciata. Atomic force microscopy (AFM) and fluorescence spectroscopy were performed on manually drawn fibers. Circular dichroism spectroscopy and an initial low-resolution NMR structure both indicate that monomeric aciniform spidroin protein is predominantly α-helical in solution but changes to β-sheet in the fiber, as indicated by thioflavin T fluorescence co-localized with fibers. AFM characterization provides nano-scale surface chemistry and mechanical information for the silk fiber. Our ongoing work is correlating structure to mechanical properties to elucidate the mechanism by which spider silk fibers form.

3259-Pos Board B364

Structural Analysis of the Pf1 Subunit of the Sin3S/Rpd3S Complex and its Implications in Chromatin Targeting and Complex Assembly

Senthil Kumar Ganesan, Tao Xie, Chetan Velagapudi, Yongbo Zhang, Ishwar Radhakrishnan.

Multi-protein complexes containing histone deacetylase (HDAC) activities play key roles in regulating eukaryotic gene transcription by altering 'the histone code' and modulating chromatin structure dynamics. The evolutionarily-conserved, HDAC-associated, ~0.5 MDa Sin3S/Rpd3S complex is implicated in repressing transcription from cryptic start sites in the intragenic regions of transcriptionally-active genes and in limiting DNA damage due to genotoxic stress. Unlike the related ~2 MDa Sin3L/Rpd3L complex, which is targeted to promoter regions of genes through interactions with sequence-specific DNA-binding repressors, the smaller Sin3S/Rpd3S complex is targeted to intragenic regions through interactions with H3 K36(me_2/me_3)-modified histones. The Sin3S/Rpd3S complex comprises at least five subunits of which the MRG15 and Pf1 subunits are unique to this complex and play important roles in chromatin targeting and complex assembly. Pf1 harbors two PHD zinc fingers of unknown function and two Sin3 interaction domains - SID1 and SID2 - that interact with the PAH2 and PAH1 domains, respectively, of Sin3. Pf1 SID1 overlaps with a segment that we recently identified as being critical for interactions with MRG15 - the subunit that is thought to interact directly with H3 K36(me_2/me_3). We have used solution NMR spectroscopy to investigate the network of protein-protein interactions involving Pf1 and to characterize the structure and potential functions of its PHD domains. These studies provide unexpected insights into the assembly of this co-repressor complex besides affording new insights into Sin3 PAH-SID interactions and into the structure and function of PHD fingers. The results of these studies will be presented and their implications in chromatin/transcription biology discussed.

3260-Pos Board B365

Structure-Function Analysis of MRG15, a Chromatin-Targeting Protein Invovled in Cell Growth and Aging

Tao Xie, Anand Patel, Arvind Krishnan, Yongbo Zhang, Ishwar Radhakrishnan.

MRG15 is a member of the mortality factor family of proteins that have been implicated in processes involving cell growth and aging and is found in at least two distinct chromatin-modifying complexes, a 5-subunit histone deacetylase (HDAC)-complex containing the Sin3 corepressor and the 11-subunit NuA4 histone acetyltransferase complex. At the molecular level, MRG15 has been implicated in targeting the Sin3 corepressor complex to histones enriched in H3 K36(me_2/me_3) found in actively transcribed chromatin via a N-terminus chromodomain. The MRG domain at its C-terminus is thought to link MRG15 with Pf1 and thereby to the Sin3 and HDAC proteins in the Sin3 complex. MRG domains are common to all the mortality factor proteins and although the structure of the MRG domain is known, there is no information about the nature of the targets and how it interacts with them.

We have characterized the interaction of the MRG15 chromodomain with its cognate chromatin target and also that of the MRG15 MRG domain with Pf1. Our results indicate a surprisingly low affinity interaction between the chromodomain and its chromatin target, but a much stronger interaction between the MRG domain and Pf1; interestingly, other H3 methylated lysine peptides display comparable affinities to H3 K36(me_2/me_3). We have identified and characterized the MRG-interaction motif in Pf1 using a combination of mutagenesis, biochemical assays, informatics, and solution NMR; an analogous motif is also found in other MRG-domain interactors such as PALB2 and PAM14. The motif binds to MRG15 MRG with high affinity and competitively inhibits the oligomerization activity of MRG15 MRG.

3261-Pos Board B366

NMR Dissection of the Detailed Mechanism for Antibiotic Binding to Asite RNA

Jeetender Chugh, Anette Casiano-Negroni, Hashim M. Al-Hashimi.

A growing number of studies are suggesting the importance of non-coding RNAs that play a variety of roles by undergoing conformational changes in response to a specific cellular signal. It has been increasingly believed that this predisposition of RNA conformational changes in a specific manner is encoded by the flexibility that in turn is encoded in RNA sequences. Base flipping is a conformational transition that occurs ubiquitously across diverse RNA functional and structural contexts. A prominent example is Asite ribosomal RNA that contains two highly conserved internal loop adenines A1492 and A1493, which serve to decode the mRNA message by looping out and stabilizing a codon-anticodon mini-helix when it is formed between mRNA and its cognate aa-tRNA. Asite is also known to bind to many antibiotics where drug binds the internal loop, flips the two adenines out and the adenines are forced to bind the codon-anticodon minihelix irrespective of correctness of tRNA.

In this study, we attempt to dissect the process of Asite drug binding further using NMR spin relaxation techniques. Site-specific measurement of fast dynamics (using transverse and longitudinal relaxation measurements) and slow dynamics (using R1rho dispersion measurements) on free and bound Asite RNA provide insights into the transition states of binding. Our results highlight the significance of various neighboring bases that dynamically encode the process of base flipping that is vital for an effective antibiotic binding.

3262-Pos Board B367

Enzymatic Synthesis of Site-Specific Labeled NTPS used for *In Vitro* Transcription of RNAs to Facilitate Multi-Dimensional Nuclear Magnetic Resonance Spectroscopic Studies

Luigi J. Alvarado, Kwaku Dayie.

RNAs, more than ever before, are increasingly viewed as biomolecules at the forefront of the life and chemical sciences, given their diverse functional capabilities and ability to adopt intricate three-dimensional folds. Structural biologists faced with two critical challenges of chemical shift overlap and fast signal decay for large RNAs (>15 KDa) have resorted to stable-isotope labeling to circumvent the overcrowding problem. In this work, we have developed a facile and streamlined means of producing eight non-commercially available recombinant enzymes from the pentose phosphate pathway for synthesizing such labeled nucleotides. The enzyme preparations were purified to >90% homogeneity by a one-step Ni-NTA affinity chromatography resulting in specific activities comparable to or higher than those previously reported. These new site-specific labeled nucleotides made by these enzymes can be used to transcribe RNAs of any sequence and length. To demonstrate the usefulness of the site selectively labeled nucleotides, the highly conserved 36-nucleotide domain 5 (D5) RNA structure, which is the heart of the group II intron ribozyme machinery, was transcribed and various multidimensional NMR experiments tailored for these labels were run. The availability and reliability of these constructs would render production of fully and site-specific labeled nucleotides for transcribing RNA more accessible and straightforward, and facilitate high-resolution NMR spectroscopic and other biophysical studies.

3263-Pos Board B368

Mapping Col E1 RNA I - RNA II Kissing Complex and ROM Binding Interface using Paramagnetic Relaxation Enhancement NMR

Raviprasad Aduri, John P. Marino.

The RNA II transcript of ColE1 plasmid acts as the primer of plasmid replication, while RNA I transcript, an RNA antisense to the 5' end of RNA II, acts as a suppressor of replication. The RNA I and RNA II interaction involves the formation of a kissing complex that is stabilized by plasmid encoded RNA One Modulator (ROM) protein. High-resolution structures of both the ROM protein and the RNA kissing complex have been determined. Alanine scanning mutagenesis experiments of ROM have shown that the surface residues Asn10, Phe14, Glu18, Lys25, and Lys3 of helix 1 interact with RNA loop residues. To date, there is no high resolution structure of the complex of ROM with the kissing complex and the details of this interaction remain unknown. Towards our effort to determine this RNA-protein complex, an RNA construct capable of forming a C2 symmetric kissing complex, to reduce NMR spectral complexity, has been designed by introducing a U-U mismatch into the kissing helix. 2D NMR spectra of the kissing dimer formed by this construct reveal a structural fold similar to the wild type. The challenge of elucidating a high resolution structure of this complex, however, lies in availability of few, if any, NOE contacts between ROM and RNA. To overcome this problem, the RNA UU kissing dimer construct has been 5′-end labeled with 3-(2-Iodoacetamido)-proxyl group so distance restraints could be measured using the paramagnetic relaxation enhancement (PRE) effect of the spin label on the protons in the protein. Using T1/T2 relaxation measurements, structural restraints for the complex are being pursued to enable a high resolution description of the how ROM specifically binds the RNA kissing complex.

3264-Pos Board B369

Early Biomineararalization of Mice Bone Studied by ^{31}P and ^{13}C Solid State NMR at Different Stage of Age

Peizhi Zhu, Jiadi Xu, Guisheng Zhao, Michael D. Morris, Ayyalusamy Ramamoorthy, Renny T. Franceschi.

Biomineralization in nearly all vertebrates is a complex process controlled by interactions of minerals and organic matrix. Several Studies have demonstrated that the size of mineral can also affect collagen microarchitecture. Although bone structure has been extensively studied, the early stages of bone mineralization and matrix formation still remain unknown. Bone is a highly heterogeneous material with a complex hierarchical structure. High-resolution solid-state NMR can probe selected magnetic nuclei and get structure information at the atomic-level that are difficult to obtain by other methods. Using ^{31}P and ^{13}C solid state NMR, we investigated the mineral and matrix change as a function of age. Our results show that there is a large amount of monohydrogen phosphates at early stage of mineralization. The experimental results indicate that apatite content increase while monohydrogen phosphates, phosphates and phosphouslipid decrease as mice matured. Our findings confirmed that with the increase of mineralization, the stiffness of collagen increases due to the interaction between the collagen and mineral.

3265-Pos Board B370

Speciation of Organic Phosphorus in P-Immobilizing Soils: A ^{31}P NMR Study

Johan E. Vestergren, Andrea Vincent, Per Persson, Mats Jansson, Juergen Schleucher, Reiner Giesler, Gerhard Gröbner.

Phosphorus (P) is globally a crucial nutrient and in many agricultural areas the limiting factor for plant growth. Over the past 30 years several studies have been made in order to completely understand the fate and cycle of P, but knowledge is still limited, especially in the area of overall speciation and the sorption processes and mechanisms of organic P in soils Here,solution ^{31}P NMR and solid state ^{31}P NMR were used on humus soils to describe the P composition in soils along two productivity gradients in a Fennoscandian boreal forest who simultaneously display sorption gradients due to differences in Al and Fe levels. Phosphorus composition changed significantly along the gradients. The abundance of phosphate diesters, their degradation products and polyphosphates are more abundant in low Al and Fe sites. Phosphate mono esters, like inositole phosphate has a more pronounced presence in high Al and Fe sites. It would seem that in low Al and Fe sites the difference in speciation of organic P more closely mirrors the input of P whereas the high Al and Fe sites shows the composition of P possibly being more governed by sorption affinity.

Our sampling sites include the wide range of soil properties expected to be found in boreal Fennoscandian soils and therefore provide an important view on the biogeochemistry and especially the organic P governing factors for this region.

3266-Pos Board B371

Structural Studies of an Immunoglobulin-Fibronectin Type III Domain Tandem from Titin

Andras Czajlik, Gary Thompson, Ghulam N. Khan, Arnout Kalverde, Steve W. Homans, John Trinick.

Abstract: Titin is a giant multidomain protein in muscle. Single molecules span half the sarcomere, from the Z-disk to the M-band, and are involved in sarcomere assembly and elasticity. In the A-band titin is attached to thick filaments and here the domain arrangement is in regular patterns of eleven, called large super-repeats. The large super-repeat occurs eleven times and forms nearly half the titin molecule. Interactions of the large super-repeats with myosin and C-protein suggest a role in thick filament assembly. We are determining the atomic structures, dynamical properties and the inter-domain arrangements of overlapping double and triple domain fragments of a large super-repeat (titin A59-A69 unit) by NMR spectroscopy. Ultimately, we hope to combine the data to reconstruct the overall conformation of the super-repeat. As reported earlier, we first studied a fibronectin type III domain tandem (A59-A60). Now we are investigating an immunoglobulin-fibronectin type III domain tandem (A67-A68). Assignment of the backbone atoms was completed using triple resonance NMR experiments. Initial structures for both domains were determined from either backbone chemical shifts using CS23D and CS-Rosetta software packages or homology modeling. We are refining the structures using NOE and RDC data to give atomic models and the orientation of the domains. These will be used as a basis for analysis of solution state 1H-15N relaxation data and dynamic models.

3267-Pos Board B372

Intrinsic Dynamics Prime Calmodulin for Peptide Binding: Characterizing Lowly Populated States by Paramagnetic Relaxation Enhancement

Nicholas J. Anthis, Marius Clore.

Many biomolecular processes, such as protein binding, proceed through transient lowly populated states. Because these intermediates comprise only a small fraction of the total population at equilibrium, they are inaccessible to traditional structural biological methods. However, recent developments in paramagnetic relaxation enhancement (PRE) have now made it possible structurally characterize these otherwise invisible states by NMR if they rapidly exchange with the major state. Here, we extend these methods to explore the lowly populated states adopted in solution by the calcium-sensing protein calmodulin. Calmodulin adopts a highly compact structure in its peptide-bound form, but X-ray studies indicate that the unbound form adopts a more extended ''dumbbell'' structure, comprised of two globular domains separated by a central helix, which has been indicated to be highly flexible. In order to characterize the lowly populated states adopted by calmodulin, we measured the transverse PREs induced by covalently attaching nitroxide spin labels at various sites within the protein. The PRE profiles measured for calmodulin bound to a myosin kinase peptide are fully consistent with the known X-ray structure. Unbound calmodulin, on the other hand, exhibits significant interdomain PREs that cannot be explained by the extended ''dumbbell'' model or any other known structure. However, the experimental PRE data were successfully fit by performing simulated annealing structure calculations in Xplor-NIH, starting from the ''dumbbell'' structure but allowing flexibility within the central helix for a minor population. Many members of the resulting ensemble cluster around the peptide-bound conformation, although calmodulin samples a wide range of conformations in the unbound state. Thus, flexibility in its central helix appears to prime calmodulin to bind to its various peptide targets. These findings illustrate the utility of PRE-based studies for exploring such dynamic systems.

3268-Pos Board B373

Dynamics Studies of HIV-1 CA Protein Assemblies by Solid-State MAS NMR Spectroscopy

Guangjin Hou, Yun Han, Christopher Suiter, In-Ja L. Byeon, Jinwoo Ahn, Jason Concel, Angela M. Gronenborn, Tatyana Polenova.

The capsids of mature retroviruses perform the essential function of organizing the viral genome for efficient replication. In mature HIV-1 virions, the 25.6 kDa CA protein assemblies into a fullerene cone, a closed shell. Tyrosine residues in the capsid proteins of retroviruses play important roles in protein folding and assembly packing[1]. In HIV-1 CA protein, Y145, which is located in the linker region between N- and C-terminal domains might play a pivot role in HIV-1 capsid assembly.[2,3] However, the molecular interactions involving Y145 that stabilize the assembly, including the dynamic behavior of this residue in the assembled and unassembled CA are unknown.

We have recently determined that MAS NMR spectroscopy can yield atomic-resolution information on assembled CA capsids and reported partial resonance assignments and secondary structure analysis of conical assemblies.[4] Herein, we present studies of the internal dynamics of the Tyr resiudes in CA as probed by various solid-state NMR methods. $^{15}N/^{1}H$ chemical shift anisotropies (CSA) and ^{1}H-^{15}N/^{1}H-^{13}C dipolar order parameters have been obtained in selectively labeled ^{13}C, ^{15}N -Tyr HIV-1 CA protein assemblies of conical morphologies, as well as in N- and C-terminal domains of CA. Our results demonstrate that Y145 exhibits reduced ^{15}N and ^{1}H chemical shift anisotropy, as well as smaller ^{1}H-^{15}N and ^{1}H-^{13}C dipolar order parameters, presumably due to its backbone mobility on nano- to microsecond timescales. Moreover, the NMR parameters of Y145 are strongly temperature dependent, another evidence of internal conformational dynamics. In contrast, the other three Tyr residues, Y130, Y164 and Y169, which are located in α-helical regions of CA, display rigid-limit chemical shielding anisotropies and dipolar order parameters.

References

1. T.Yamashita, et.al. **(2009)** *Proc.Natl.Acad.Sci.USA,*106, 12986-12991.
2. O.Pornillos, et.al. **(2009)** *Cell,*137, 1282-1292.
3. I.L.Byeon, et.al. **(2009)** *Cell,*139, 780-790.
4. Y.Han, et.al. **(2010)** *J.Am.Chem.Soc.*,132, 1976-1987.

3269-Pos Board B374

Characterizing the Interaction of Human CD4 and the HIV-1 accessory Protein VpU using Liquid State NMR

Sameer K. Singh, Luis Möckel, Marc Wittlich, Dieter Willbold, Bernd W. Koenig.

Human CD4 is a 433 residue transmembrane protein involved in the body's adaptive immune response. The extracellular domain of CD4 serves as primary receptor of the human immunodeficiency virus (HIV-1) and binds the viral glycoprotein gp120. The cytoplasmic domain of the 81 residue Virus protein U (VpU) plays an important role in downregulation of CD4. It directly binds the cytoplasmic domain of CD4 in the endoplasmic reticulum, which initiates a series of events resulting in CD4 degradation in the proteasome. We characterized the CD4 - VpU interaction by liquid state NMR spectroscopy utilizing paramagnetic relaxation enhancement (PRE). The PRE effect is a distance-dependent enhancement of the spin relaxation in magnetically active nuclei in the vicinity of a paramagnetic centre. PRE leads to line broadening or complete quenching of NMR signals and indicates spatial proximity to the probe. We recorded NMR spectra of the ^{15}N-labelled cytoplasmic domain of VpU in the presence of varying amounts of a single-cysteine-mutant of CD4(372-433), which was labelled with the active PRE-probe, methanethiosulfonate (MTSL). This CD4 polypeptide contains the single transmembrane and the C-terminal cytoplasmic domain of CD4. Experiments were conducted in membrane-mimicking dodecyl phosphocholine (DPC) micelles. Spectra recorded in the presence of paramagnetic MTSL show reduced NMR signal intensities of certain amino acids of ^{15}N-labeled VpU. Additionally, we studied chemical shift perturbations (CSP's) of VpU resonances observed on titrating increasing concentrations of unlabelled CD4. Such chemical shift changes are expected for residues in the binding interface but may also occur at remote sites due to allosteric effects. Our data reveal VpU residues involved in CD4 binding, provide insight into the exchange regime, and yield an estimate of the binding affinity.

3270-Pos Board B375

Structural Studies of RNase H Domain to Develop HIV-1 Reverse Transcriptase Inhibitors using Solution NMR

Lakshmi Menon, Qingguo Gong, Jinwoo Ahn, Michael A. Parniak, Rieko Ishima.

The Human immunodeficiency virus (HIV) reverse transcriptase (RT) is a bifunctional enzyme having DNA polymerase activity and the ribonuclease (RNase H) activity. Although inhibitors that target the polymerase site are clinically available, no effective RNase H inhibitor exists. To screen RNase H inhibitors, an isolated RT RNase H fragment, p15-EC, that has insertion of a alpha-helical substrate-binding loop derived from Escherichia coli RNase HI has been often used (Keck & Marqusee, 1995). It is important to structurally characterize interaction of the p15-EC with Mg2+ and/or inhibitors. In particular, the intact RT RNase H domain fragment has been expected to undergo significant conformational changes upon Mg2+ interaction and exhibits different dynamics upon slight mutations (Pari et al., 2003). Thus, we have used a series of 1H-15N Heteronuclear Single Quantum Coherence (HSQC) experiments in combination with three-dimensional solution NMR experiments to clarify whether the p15-EC shows similar structural features to that of the intact RT RNH domain. We also identified the binding site of one of inhibitors, and compared Mg2+ effects on the inhibitor interaction.

3271-Pos Board B376

Studies of HIV-1 Gag Protein Assemblies by Solid-State MAS NMR Spectroscopy

Christopher L. Suiter, Guangjin Hou, Yun Han, Jinwoo Ahn, Angela Gronenborn, Sherimay Ablan, Eric Freed, Tatyana Polenova.

During virus release from the infected cell, the Pr55Gag polyprotein is cleaved by the viral protease into the major structural Gag proteins of HIV-1. Gag is composed of three major domains: matrix (MA), capsid (CA), and nucleocapsid (NC). Gag also contains two small spacer peptides SP1 and SP2, and a C-terminal p6 domain. When assembled in the presence of RNA, Pr55Gag forms spherical assemblies that are structural analogous to immature virus-like particles (VLPs) 1. In this work we introduce solid state (MAS) NMR spectroscopy to study the structure of assemblies formed by a 40-kDa construct of the Gag polyprotein in which the p6 domain and a 75 amino acid stretch of the MA domain have been removed. This Gag PRR400 construct assembles into well-defined spherical VLPs very similar to those formed by the full-length Gag. The initial results demonstrate the feasibility of high-resolution structural studies of VLP assemblies by MAS NMR.

1. Stephen Campbell, Alan Rein. (1999), Journal of Virology, 73, pp. 2270-2279.

3272-Pos Board B377

Characterization of Functional and Structural Domains in the Adaptor Protein LMO7 and their Interactions with Proteins at the Adherens Junctions

Justin C. Baker, Jun Li, Shannon C. Banning, Pradeep R. Rajasekaran, Janelle M. Owens, Fernando F. Cuadrado, Yuanxiufu Cao, Justin M. Hennings, Mateo C. Houle, Tori L. Nosovitsky, Catherine A. Carney, **Gabriela C. Pérez-Alvarado**.

The adaptor protein LIM domain only-7 (LMO7) has a role in stabilizing the communication between the cadherin and nectin associated complexes in the cell-to-cell adherens junctions through its association with alpha-actinin and afadin.[1] In the nucleus, LMO7 interacts at the nuclear envelope with the protein emerin, and also regulates the transcription of genes important for heart, muscle and retina formation.[2] The structure of domains in LMO7 associated with the molecular recognition are being studied using Nuclear Magnetic Resonance (NMR) spectroscopy, molecular biological, biochemical and biophysical methods. These studies are providing information to further our understanding of the protein-protein assembly process.

The alpha-actinin-binding domain in LMO7 contains two subdomains that are N-terminal to a PDZ domain, and the afadin-binding domain consists of a LIM domain. SDS-PAGE electrophoresis, analytical reverse phase HPLC, mass spectrometry and NMR were used to characterize these domains. In order to determine the minimal regions of alpha-actinin and afadin that interact with LMO7, several proteins containing different domains of afadin and alpha-actinin were expressed and purified. The mechanism of protein-protein complex formation is being characterized using a combination of analytical gel filtration with NMR spectroscopy methods.

1. Ooshio et al. (2004) J. Biol. Chem. 279, 31365-31373.
2. Holaska et al. (2006) Hum. Mol. Genet. 15, 3459-3472.

3273-Pos Board B378

Backbone Dynamics Studies of Mammalian Dynactin CAP-Gly Domain by Solid-State NMR

Si Yan, Alexander J. Vega, John C. Williams, Tatyana Polenova.

Dynactin is a multisubunit microtubule-associated protein complex functioning in retrograde transport, and binds to microtubules via the CAP-Gly domain of its p150^{Glued} subunit. We have recently reported solid-state NMR investigations of CAP-Gly free and in complex with microtubules.[1] Mutations in the CAP-Gly domain of the p150^{Glued} subunit of dynactin are associated with neurological disorders, and little has been known about what gives rise to the pathogenicity associated with these mutations. We have discovered recently that several neurologically related mutants, surprisingly, do not show altered binding to microtubules while their global fold and stability are perturbed with respect to the wild type protein.[2] We hypothesize that backbone dynamics of CAP-Gly domain of dynactin may be an important determinant of its interaction with microtubules, and therefore understanding the internal motions in free CAP-Gly and in CAP-Gly/MT complex may provide insights into the regulation mechanisms of CAP-Gly function. Here, we present site-specific measurements of ^{15}N-^{1}H dipolar and ^{15}N CSA lineshapes of CAP-Gly by solid-state NMR spectroscopy at different temperatures, using $R18_1^7$ and ROCSA recoupling sequences.[3,4] The CSA and dipolar order parameters derived from lineshapes by numerical simulations indicate different backbone mobility for the different residues of CAP-Gly; strong correlation between the variation of dipolar order parameters with temperature and the secondary structure is observed.

References

1. S. Sun, A. Siglin, J. C. Williams, T. Polenova **(2009)** *J. Am. Chem. Soc.*, 131 (29), pp. 10113-10126.
2. S. Ahmed, S. Sun, A. E. Siglin, T. Polenova, J. C. Williams **(2010)** *Biochemistry*, 49 (25), pp. 5083-5085.
3. J. Yang, M. Tasayco, T. Polenova **(2009)** *J. Am. Chem. Soc*., 131 (39), pp. 13690-13702.
4. J. C. Chan, R. Tycko **(2003)** *J. Chem. Phys*. 128, pp. 8378-8389.

3274-Pos Board B379

Solution Structure Determination of Norwalk Virus 3C-Like Cysteine Protease

Daisuke Takahashi, Yunjeong Kim, Kyeong-Ok Chang, Asokan Anbanandam, Om Prakash.

Noroviruses are the leading cause of acute food- or water-borne gastroenteritis outbreaks in humans with an estimated 23 million annual cases in the US alone and show high diversity with at least five genogroups (GI-GV). Norwalk virus (NV) is a prototype strain classified as GI strain. Norovirus RNA genome is composed of three open reading frames (ORFs), and the ORF1 encodes a polyprotein that is cleaved by the viral 3C-like cysteine protease (Pro) into 6 non-structural proteins, which makes the Pro as an

essential component for the viral replication as well as an attractive target for antiviral drug development. The specificity of NV Pro depends on the primary sequence of the cleavage site where the Q/G at P1/P1' position of a polyprotein peptide is preferentially cleaved followed by E/A or E/G as a secondary sites. X-ray crystallographic studies also show that NV Pro adopts a serine protease-like fold containing two β-barrel domains separated by a cleft within which lie the active-site catalytic residues. In addition to the active site, it was suggested that mutual conformational rearrangement of Pro/peptide binding site plays a pivotal and common role in efficient substrate recognition of Pro from different genotypes, GI and GII. These findings lead us toward the development of substrate-based peptidemimetic inhibitors with broad-spectrum activity. We are using solution NMR spectroscopy to solve the solution structure of NV Pro and investigate the interaction mode of NV Pro and inhibitor(s) in parallel with in vitro assay using a fluorescent substrate derived from the natural cleavage site of NV. Here we will present the solution structure of NV Pro solved by NMR spectroscopy. Preliminary results on structural and dynamical characterization of the protease-inhibitor interaction will also be presented.

3275-Pos Board B380

Structural Characterization of the Zinc Finger Domain of Cytoplasmic Polyadenylation Element-Binding Protein

Daniel Merkel, Bryce Hilburn, Sarah Wells, Stephanie Geiser, Haley Hoover, Oluwatobi Ajoku, Brian Lee.

Cytoplasmic polyadenylation element-binding protein (CPEB) is an important factor in translational regulation of oogenesis, cellular senescence and synaptic plasticity. It does this by regulating a poly(A) tail elongation through interactions with a number of other proteins. The region of mRNA that CPEB binds to is a uracil rich region known as the cytoplasmic polyadenylation element (CPE). The carboxy terminal region of CPEB is composed of three regions that are required for CPE recognition and binding within the 3' UTR of mRNA. It has two RNA binding domains and a zinc finger motif. The zinc finger region contains six cysteine and two histidine amino acids that are highly conserved throughout many species. The conserved residues suggest the presence of a zinc finger structure containing two zinc ions. The zinc finger region of CPEB does not seem to be homologous with any know zinc fingers. We are currently in the process of structural characterization using NMR techniques.

3276-Pos Board B381

Domain Structure of the Major Allergen Ovomucoid by Solution NMR

Natalie E. Stenzoski.

Domain Structure of the Major Allergen Ovomucoid by Solution NMR

Natalie E. Stenzoski, Gugsa W. Gebriel, Bruce D. Ray, Horia I. Petrache

The interest in the ovomucoid protein is twofold. First it is a protein of interest for medical studies due to its potent allergen activity. Second, as a special variety of glycosylated protein (Kazal family), it allows us to explore the role of protein glycosylation for a particular or model case. Glycosylated proteins are commonly secreted by tissues as signaling agents. For example, the serpin family serine proteinase inhibitor, α-1 proteinase inhibitor (A1AT/ α-1 antitrypsin) regulates trypsin. Recent research in our laboratory indicates that A1AT interacts with lipid membranes and affects ionic currents through the membrane. In contrast, ovomucoids do not. This difference in membrane interaction is expected to have a structural cause. However, very little overall structural data is available. The nature, location, and orientation of the glycosyl groups are determining factors in protein-membrane interactions and are deeply involved biological effects of glycosylated proteins, including effects on ion transport. We use solution NMR spectroscopy to determine the structure of the chicken ovomucoid protein, taking advantage of the division of its structure into three stable domains of 55-65 amino acids each. We present results on the protein purification steps and isolation of separate domains and the models of individual domains and overall protein structure from the analysis of NMR spectra.

3277-Pos Board B382

Solution Structure of a Central Domain of the Conjugative Transfer Protein TraI

Nathan T. Wright, Joel F. Schildbach.

TraI, the F plasmid-encoded nickase, is a 1756 amino acid protein essential for conjugative transfer of F plasmid DNA from one bacterium to another. While crystal structures of N- and C-terminal domains of F TraI have been determined, central domains of the protein are structurally unexplored. These middle domains (between residues 306 and 1500) are known to both bind single-stranded DNA (ssDNA) and unwind DNA through a highly processive helicase activity. Of this central region, the more C-terminal portion (~900-1500) appears related to helicase RecD of the E. coli RecBCD complex. The more N-terminal portion (306-900), however, shows limited sequence similarity to other proteins. In an attempt to define the structure of well-folded domains of this middle region and discern their function, we have isolated stable regions of TraI following limited proteolysis. One of these regions, TraI (381-569), was identified and shown to be well-folded in solution via NMR. Here, we present the high resolution solution structure of this region. We show that, like the 900-1500 region, 381-569 is part of a RecD-like fold. We also show where the 381-569 region is located relative to the rest of the protein via a series of SANS and SAXS experiments. Together, these data provide structural explanations to several questions about the exact mechanism of TraI-dependant plasmid transfer.

3278-Pos Board B383

Application of Magnetic Resonance for Metabolomic Investigation of Mollusks

Andrey P. Tikunov, Haakil Lee, Michael K. Stoskopf, Jeffrey M. Macdonald.

Metabolites, as the end products of metabolism, represent the functional responses of a cell. Their characterization can provide insight into the underlying mechanisms of genomic or environmental actions on metabolism. The aquatic environment is varied and dynamic, providing a vast diversity of physical and chemical challenges to metabolism, making the study of the metabolites of mollusks particularly fruitful for scientists interested in comparative physiology, pharmacology and toxicology. Organ specific metabolic fingerprints can establish time dependent assessments for interpreting functional adaptations to environmental and nutritional challenges using either invasive tissue extraction from multiple individuals or non-invasive longitudinal observation of the same individual. NMR spectroscopy and magnetic resonance imaging (MRI) permit non-invasive monitoring of the metabolome.

The mollusks are a useful, robust model organism for tissue metabolism studies. Its relatively few organs are easily delineated and there is sufficient understanding of their functions based on classical assays to support interpretation of advanced spectroscopic approaches. Here we apply high-resolution proton and carbon nuclear magnetic resonance (1H and 13C NMR)-based metabolomic analysis to Eastern oyster C. virginica and freshwater mussel Eastern Elliptio E. Complanata to investigate the variation in the metabolic profile of different organ groups. MRI was used to non-invasively identify the morphology of the organs. In vivo MR spectra can be obtained from single region of interest (ROI or voxel) or multiple ROI simultaneously using the technique typically called chemical shift imaging (CSI). Here we also report applications of CSI to marine samples and describe the use of the technique to study in vivo glycine metabolism in oysters using 13C MRS.

A biochemical schematic is presented that relates metabolites to biochemical pathways correlated with physiological organ functions.

3279-Pos Board B384

Paramagnetic Contributions to Nuclear Spin-Lattice Relaxation in Proteins

Robert G. Bryant, Galina Diakova, Yanina Goddard, Jean-Pierre Korb.

Paramagnetic contributions to spin-lattice relaxation rate constants are very useful in providing long-range distance constraints for structural determinations by NMR and also for controlling image contrast in clinical MRI protocols. When a radical with a long electron-spin-relaxation time is bound to a protein, the paramagnetic contribution to the water-proton-spin-lattice-relaxation rate is larger than predicted by usual theory. We show that this excess nuclear spin relaxation efficiency results from long-lived-bound water molecules for which the electron-nuclear coupling is correlated with the long rotational correlation time of the protein. Because the correlation time is so long compared with the relative translational correlation times, even distant water molecules make significant contributions and increase the relaxation efficiency of the paramagnetic center. If the rotational motion of the protein is stopped, as in a solid protein, a protein gel, or a tissue, the paramagnetic contributions to relaxation are both qualitatively and quantitatively changed from the solution limit. The spin-lattice relaxation for different paramagnetic systems may be understood in terms of the intrinsic dynamics of the protein and the spin dynamics of the paramagnetic center, which depends on the identity and magnetic characteristics of the paramagnetic center. These different effects are important for applications to magnetic imaging and structure determination by solid state NMR.

Micro and Nanotechnology; Nanopores III

3280-Pos Board B385

A Multiplexed Electrochemical Microelectrode Array for High-Throughput Measurement of Quantal Exocytosis

Jia Yao, Kevin D. Gillis.

Electrochemical microelectrodes are commonly used to detect spikes of amperometric current that correspond to exocytosis of oxidizable transmitter from individual vesicles, i.e., quantal exocytosis. We are developing transparent multi- electrochemical electrode arrays on microchips in order to automate measurement of quantal exocytosis. Whereas patterning hundreds of electrodes in a small area is straightforward and cost-effective using photolithography, easily making connections between hundreds of electrodes and external amplifiers remains a bottleneck. Here we report a simple multiplexing approach using multiple fluidic compartments that can reduce the number of external connections by ~100-fold. In this approach the set of electrodes in every fluidic compartment are wired in parallel and connected to external amplifiers. Cell recordings are made from the set of electrodes in one fluidic compartment at a time. The fluidic compartment to be used is addressed by loading it with cells in a physiological electrolyte solution and connecting it to the ground / reference electrode. Measurements demonstrate that this approach attains current noise levels as low as that obtained with individual electrodes. However, if electrolyte solution is in more than one fluidic compartment the noise increases proportionately. An equivalent circuit model has been developed to quantify this noise as resulting from the thermal noise of the electrode / electrolyte junction. The new device will enable high-throughput studies of quantal exocytosis that can be combined with fluorescence microscopy. Supported by NIH R01 NS048826.

3281-Pos Board B386

Nano-Scale Surface Topology Improves Neuronal Development in Culture

Ghislain Bugnicourt, Jacques Brocard, Mariano Bisbal, Nora Collomb, Annie Schweitzer, Catherine Villard.

Neurons may be grown on opaque silicon surfaces covered with poly-L-lysine, the same way it is usually carried out on glass coverslips. Neuronal development may also be improved by structuring silicon surfaces with reactive ion etching. Here, we produced silicon samples by a classical photolithography process with an alternation of 1mm-wide bands, presenting atomically flat or rough topologies.

Hippocampal neurons from E18.5 mice, grown over these samples, developed faster on rough bands: they differentiated an axon more readily after 2 days in culture (75% neurons display an axon vs 60% on flat surfaces) and their total neuritic length was 50% larger whereas they developed 20% less neurites. Moreover, neurons with neurites in both areas preferentially differentiated an axon onto the rough surface (76% polarized neurons).

Finally, we characterized the topology of rough surfaces using Scanning Electron Microscopy. We observed 1µm-high silicon nano-peaks randomly distributed on the surface. Interestingly, our observations indicated that neurites grew on top of the nano-peaks with a typical distance between adhesion points of about 600nm. Neuron on rough silicon surface (bar, 5 µm), and zoom over a neurite (dark rectangle and inset; bar, 500 nm).

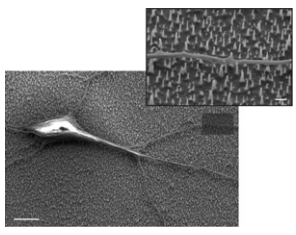

3282-Pos Board B387

Adaptive Mechanically Controlled Lubrication Mechanism found in Articular Joints

George W. Greene.

Articular cartilage is a highly efficacious water-based tribological system exhibiting low friction and wear over a lifetime despite its biological isolation and slow ability to regenerate. Hyaluronic acid (HA) is abundant in cartilage and synovial fluid and widely thought to play a principle role in joint lubrication and proper joint function although this role remains unclear. HA is also known to complex readily with the surface active glycoprotein lubricin (LUB) to form a cross-linked network and is also believed by some to be important to the lubrication and wear prevention mechanism of joints, although again it's role is unclear, especially the synergy in the actions of LUB and HA. Friction experiments on porcine cartilage using the surface forces apparatus, and enzymatic digestion, reveal an ''adaptive'' role for an HA-LUB complex whereby, under compression, nominally free HA diffusing out of the cartilage becomes mechanically, i.e., physically, trapped at the interface by the increasingly constricted collagen pore network. The mechanically trapped HA-LUB complex now acts as an effective (chemically bound) 'boundary lubricant' - reducing the friction force slightly but, more importantly, eliminating wear damage to the rubbing/shearing surfaces.

3283-Pos Board B388

Towards the World Smallest Chemical Reactors: On-Demand Generation and Fusion of Femtoliter Aqueous Droplets

Seung-Yong Jung, C. Patrick Collier, Scott Retterer.

Water in oil droplets has been an important research topic because of the possibility of small-volume biochemical reaction vessels in which the reaction time and chemical concentration can be precisely controlled. Here, a new method for producing *femtoliter-scale* (10^{-17} L) aqueous droplets on-demand has been developed based on pressure driven formation of droplets at the intersection of microchannels. Different aqueous solutions in two apposed microchannels with 1 micrometer in width were forced into an oil-filled microchannel to form two aqueous droplets, which then collided with each other to start biochemical reactions by diffusional/convectional mixing. These monodisperse micro-reactors can enable the characterization of catalytic or biochemical reaction dynamics in confined environments, as well as the development of reaction vessels for highly localized sampling and dosing.

3284-Pos Board B389

A Combined Surface Chemistry / Microwell Approach for Trapping Single Cells on Electrochemical Microelectrodes for Measurement of Quantal Exocytosis

Xin (Alice) Liu, Syed Barizuddin, Wonchul Shin, Cherian J. Mathai, Shubhra Gangopadhyay, Kevin D. Gillis.

Electrochemical microelectrodes are commonly used to detect spikes of amperometric current that correspond to exocytosis of oxidizable transmitter from individual vesicles, i.e., quantal exocytosis. We are developing transparent multi- electrochemical electrode arrays on microchips in order to automate measurement of quantal exocytosis. Here we report the development of an improved device to target individual cells to each microelectrode in an array. Efficient targeting (~75%) was achieved using cell-sized micro-well traps fabricated in SU-8 photoresist together with patterning of poly (L-lysine) in register with electrodes to promote cell adhesion. The surface between electrodes was made resistant to cell adhesion using poly (ethylene glycol) grafted to a poly (dopamine) adhesive in order to facilitate movement of cells to electrode microwells. We demonstrated the activity of the electrochemical microelectrodes using the test analyte ferricyanide and perform recordings of quantal exocytosis from bovine adrenal chromaffin cells on the devices. Dozens of cell recordings on a single device illustrated the consistency of recordings and multiple recordings from the same electrode demonstrated that the device could be cleaned and re-used without degradation of performance. The novel device will enable high-throughput studies of quantal exocytosis and may also have applications in rapidly screening drugs or toxins for effects on exocytosis. (Supported by NIH R01 NS048826.)

3285-Pos Board B390

Micro- and Nanoparticle Translocation through a Solid-State Membrane Pore Thinner than their Diameters

Ken Healy, Matthew Davenport, Sonia E. Letant, Zuzanna S. Siwy.

Micron-sized particles have been detected by the resistive-pulse or Coulter counting technique since the 1950's (Coulter, US Pat. 2656508) with 90 nm particle detection reported in 1970 (DeBlois and Bean, Rev. Sci. Inst. 41, 909). Due to the challenges of fabricating submicron pores in those times, the pores used were all several microns in length. Nanofabrication has advanced significantly since then, and in this poster we examine the interesting case of particles translocating through a membrane pore thinner than those particles.

With micron-long, high aspect ratio pores, a spherical particle will be entirely contained within the pore for the majority of the time it translocates. Thus, all but the beginning and end of the observed signal is due to the entire particle. In addition, pore resistance dominates over access resistance. In contrast, with low-aspect ratio pores thinner than the particle, the signal reflects the interactions of the particle with both the access resistance volumes and the pore volume. The signal is a complex combination of these interactions, that changes as the particle moves through the pore. Another advantage of shorter pores is that identical particles passing through longer pores give smaller modulations in current, because the proportional change in resistance due to the particle is smaller.

We use a focused ion beam to drill nanopores tens to hundreds of nanometers in diameter in silicon nitride membranes, with thicknesses in the same range. Polystyrene microspheres are driven through these pores by an applied electric field. As they pass through, they modulate the flux of ions through the pore, and thus the current flowing between the electrodes. We present experimental and

simulated studies of particle translocation, aimed at determining the optimum system for analyzing virus particles using this method.

3286-Pos Board B391

Electrical Cellular Interface by Nanoelectrodes

Chong Xie, Lindsey Hanson, Carter Lin, Yi Cui, Bianxiao Cui.

Interfacing cells with micro- and nano-electronic devices has been intensively studied over the last decade. However, a long-term and efficient electrical cell interface is yet to be accomplished. Here we report that vertically aligned nanoscale electrode arrays, which promote tight attachment to cell membrane, form good electrical coupling with cultured cardiomyocytes and neuron cells. Scanning electron microscopy (SEM) analysis shows that cells readily engulf nanoelectrodes by wrapping around them. The tight junction between cells and nanoelectrodes enables high quality and long-term electrical cell interface, which allows us to achieve non-destructive action potential recording with intercellular-like signal quality.

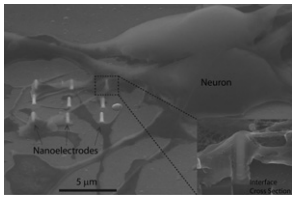

3287-Pos Board B392

Near Field Detection of Beta-Amyloid Proteins by the use of Olfactory Cells and Nano Particles in a Microfluidic Channel

Hee-Kyeong Sung, Jong-Il Ju, Chang-bum Kim, Jung-Dae Suh, Kwan-Soo Kim, Chul-Ju Chae, Hyo-Bong Hong, Ki-Bong Song.

It is well known that Alzheimer's disease (AD) is pathologically defined by the presence of amyloid-beta plaques and neurofibrillary tangles within the brain by advanced medical imaging technique such as computed tomography or magnetic resonance imaging. Currently, in AD-related olfactory sensory loss studies, early olfactory perceptual loss is likely contributed by nonfibrillar, versus fibrillar, amyloid-beta related mechanism in the olfactory system and nonfibrillar amyloid beta deposition is observed within the olfactory bulb. Therefore, the results of the olfactory dysfunction studies represents that if the amount of nano-sized amyloid beta proteins (nano-Abs) is quantified in *in vivo* olfactory system, *in vivo* early diagnosis of AD is possible. In this paper, we have measured the amount of nano-Abs by the use of olfactory cells and nano particles (100nm bead) in a micro-fluidic channel. For sample preparation, nanoparticles are sequentially conjugated with linkers (biotin, straptavidin and so on) and the particles are absorbed (or adhere) into *in vivo* olfactory system. The amount of the conjugated nano-Abs is measured by evanescent field-nano particle coupling effect where we use micro-fluidic channels. As results, in the *in vivo* olfactory system, the coupled optical power with single nanoparticle is around 1nW. The results of quantification with amyloid-related nano-particles in *in vivo* olfactory system will be briefly introduced.

3288-Pos Board B393

The Mechanisms of Decreasing Voltage-Gated Sodium Current by Nanosecond Electric Pulses

Vasyl Nesin.

The application of high-voltage nanosecond electric pulses (nsEP) causes the formation of nanopores in plasma membrane of mammalian cells, modifies function of voltage-gated ion channels. However, it is not known if nsEPs affect ion channels directly, or these effects are mediated in alternate method. We used the whole-cell patch-clamp technique to explore the effect of 300-nsEP on voltage-gated sodium current (INa) in NG108 neuroblastoma cells. Our data have shown that a single nsEP decreased the INa in dose-dependent manners; in parallel nsEP exposures induced a non-inactivating, voltage-sensitive inward current due to nanopore formation. At the same time, the recovery of INa after nsEP exposure took significantly longer than nanopore resealing. To check if the inflow of Na+ through nanopores was efficient enough to overcome the buffering capacity of the pipette, we measured changes of Na+ concentration in ''patched'' cells using the Na+-sensitive fluorescent dye (Sodium Green). These experiments showed that opening of nanopores increases the Na+ concentration in patched cells; however, the maximum increase the Na+ content, even with the most intense exposure (5.3 kV/cm), was only 2.7mM, which could unlikely cause INa inhibition. The measurement of submembrane fluorescence intensity of Sodium Green by nsEP didn't show significant increase of submembrane Na+ concentration too. The another potential pathway of reducing the INa is increasing the intracellular Ca2+ concentration after nsEP and Ca2+ mediated inhibition of INa. Our data showed that nsEP exposure in presence of high concentration Ca2+ buffer - BAPTA (20mM) in the intracellular solution caused reduce INa in NG108 cells. Our finding suggest that decreasing of INa by nsEP was not resulted of inward Na+ leakage through nanopores, as well as Ca2+ release from intracellular stores after nsEP exposure.

3289-Pos Board B394

High Resolution Single Molecule Analysis using Nanopore Recording on Microelectrode Cavity Arrays

Gerhard Baaken, Srujan K. Dondapati, Norbert Ankri, Jürgen Rühe, Jan C. Behrends.

Single molecule detection using biological nanopores in lipid bilayers is crucially limited by noise and bandwidth of the recording. We have tested a newly developed 16-channel microelectrode cavity array (MECA, Ref. 1) for single molecule detection using alpha-Hemolysin (alphaHL) nanopores. The device is based on subpicoliter cavities in a high-quality dielectric polymer adding less than 0.5 pF to the input capacitance of the amplifier (Axopach200B), thereby optimizing noise and bandwidth.

An example trace is shown in Fig.1A with an open state rms noise of 0.65pA at 0-5 kHz. Note that for the blocked state, there is no significant difference between an all points histogram of a 5 kHz filtered trace (black) and that of a event amplitudes defined by averaging (grey). Fig.1B shows 35 single PEG induced blockages superimposed and aligned in time. They are detected as square pulses down to durations<100μs and longer events seem to correlate with deeper blocks. The recording performance of MECAs with high integration densities and superior mechanical stability is expected to greatly facilitate single molecule nanopore analysis in the future.

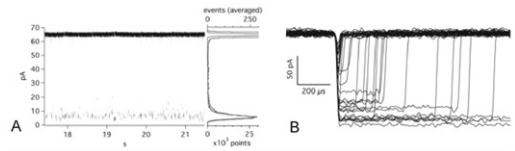

Fig.1. (A) Current trace of PEG induced blockages in a single HL pore **(B)** Single superimposed PEG blockages of a HL pore.

(1)Baaken et al.(2008),Lab Chip 8(6):938-44.

3290-Pos Board B395

Biophysical Properties of DNA Strands Attached Inside Single Nanopores

Gael H. Nguyen, Stefan Howorka, Zuzanna Siwy.

Single nanopores attract scientific interest as they serve as a basis for biosensors as well as a system to study interactions and behavior of molecules in a confined space. Nanopores with a particular geometry and surface chemistry can lead to devices that control the transport of ions and molecules in a solution. Here we present a new strategy for ionic and molecular control that is based on attaching single stranded DNA to the inside of a pore wall. The DNA attachment is restricted to the region next to the 10 nm wide small opening of a conical polymer pore. We find that the pore blockade caused by the DNA increases with lower ionic strengths of the electrolyte medium. The result can be explained by the distinct conformations of DNA at different concentrations of electrolyte solution. At low KCl concentrations (10 mM KCl) the DNA is expected to be extended and rigid and causes a greater blockade than the condensed strands at high ionic concentrations. In the future, the ability to tune the opening diameter of DNA-modified nanopores by experimental conditions may be applied to regulate transport of neutral species.

3291-Pos Board B396

Automated Lipid Bilayer Formation Facilitated by Solvent Extraction

You-Hyo Baek, Joongjin Park, Seunghwan Jeong, Wonyoung Kim, **Tae-Joon Jeon**.

Artificially created lipid bilayers(BLMs) play very important roles in ion channel studies and screening platforms, as well as biosensing applications. Although many applications with lipid bilayer platforms have been suggested, lipid bilayer formation is still based on conventional techniques invented by Montal and Mueller in 1960s. The creation of lipid bilayer membranes is labor intensive, often requiring expertise. The difficulties of lipid bilayer formation preclude a number of useful applications. In the work by Jeon, et al. (Lab Chip, 2008), a frozen membrane precursor was devised and a lipid bilayer membrane was spontaneously created when it was thawed. The frozen membrane precursor can be transported to any place and thawed when a membrane is needed, widening usability of lipid bilayer platforms. However, the film used in this work is a hydrophobic sheet, typically used in the conventional methods. Since membrane formation process driven by spontaneous assembly was unchanged, time required for membrane formation varied with a range of ~30 minutes to 24 hours. To ameliorate the variation of membrane formation time, other work using pin tools was conducted, significantly reducing the formation time by minimizing the solvent volume deposited on the aperture. Taking advantages of previously proposed platforms, we used a thin film made of Polydimethylsiloxane(PDMS) instead of using conventional films. PDMS absorbs organic solvent, thereby the thin film absorbs an excess solvent and

decreases thinning out time, keeping thinning out time more consistent (~30min). Lipid solution was deposited in a small aperture fabricated on a PDMS film and was frozen before use. Upon thawing a lipid bilayer is spontaneously reconstructed with the mean formation time of ~30 min with high success rate (>80%). We also show potential applications with lipid bilayers created in a PDMS film due to its versatility

3292-Pos Board B397
Noise Properties of Ion Current in Rectifying Nanopores
Matthew Powell, Ken Healy, Matt Davenport, Sa Niya, Lane Baker, Sonia Letant, Zuzanna Siwy.
Studying noise properties of ion currents in nanopores can improve detection limits for nanopore sensors as well as give insight into behavior of transport at the nanoscale. We focused on the 1/f⊥alpha noise that is observed in the low frequency regime of the ion current power spectra with the exponent alpha~1. We found that 1/f noise in single conically shaped nanopores in polymer films and glass nanopipettes exhibits asymmetric noise properties with respect to voltage polarity which are not observed for cylindrical and silicon nitride nanopores. The noise asymmetry is shown by the normalized power spectra, which present the noise amplitude at a given frequency, typically 1 Hz for these measurements, divided by the ion current squared. The conically shaped structures rectify the ion current and the currents for the forward bias exhibit noise that increases with voltage in an exponential manner, and are weakly KCl concentration dependent. The normalized noise of currents in the reverse bias is typically voltage-independent but increases with the increase of KCl concentration. The difference in noise properties of the currents is most pronounced when the pore diameter is comparable to the thickness of the electrical double-layer. We discuss two models, which could explain the observed effects: (i) presence of air bubbles, and (ii) crowding of ions at the pore entrance.

Fluorescence Spectroscopy III

3293-Pos Board B398
Tryptophan Fluorescence from G. Weber to the Present
Ludwig Brand.
Gregorio Weber (Symposium on Light and Life, W.D. McElroy and Glass, B. Eds., 1961) described the fluorescence of tryptophan in proteins. Since that time more than 12,000 papers have appeared related to tryptophan fluorescence. It is used to measure the folding of proteins and the interaction of proteins with each other, with nucleic acids, membranes and small molecules. Time-resolved fluorescence studies have revealed details regarding the excited-state of tryptophan in proteins. Ground-state and excited-state heterogeneity influence the fluorescence and its relation to protein conformation. Excited-state electron transfer, proton transfer, energy transfer, solvent and protein relaxation are among the processes that have been implicated in tryptophan fluorescence in proteins The availability of new experimental, computational and theoretical methods suggest that there are now opportunities for using tryptophan fluorescence for probing protein structure and dynamics. Femtosecond time-resolved techniques and molecular dynamics computations have been of particular value and should provide new information about folded and unfolded structural regions in proteins.

3294-Pos Board B399
Protein Hydration and Coulpled Water-Protein Fluctuations Probed by Tryptophan
Dongping Zhong.
Using tryptophan with site-directed mutagenesis, we can map out global hydration dynamics and water-protein fluctuations with femtosecond resolutions. We clearly demonstrated that tryptopahn is a powerful optical probe to study protein hydration.

3295-Pos Board B400
TDSS in Trp Fluorescence Reveals Multiple Protein and Solvent Relaxation Modes
Dmitri Toptygin, Thomas B. Woolf, Ludwig Brand.
The Time-Dependent Spectral Shifts (TDSS) in the fluorescence of solvatochromic dyes in polar solvents report solvent relaxation dynamics, which in water occurs on the femtosecond timescale. The TDSS in the emission of tryptophan and other solvatochomic fluorophores in proteins span a range of timescales from femtoseconds to nanoseconds. MD simulations of the GB1 protein in TIP3P water made it possible to separate five relaxation modes and to explain their physical origins. Two of these relaxation modes also contribute to the TDSS of dyes in polar solvents.
The ultrafast relaxation mode (τ~35fs) is due in part to the librational relaxation of water molecules and in part to the small adjustments in the local protein structure. This mode is responsible for about half of the total TDSS amplitude. Two collective rotational relaxation modes of water molecules are known. The longitudinal (τ_L~550fs) mode contributes to the TDSS of both dyes in water and tryptophan residues in proteins. The transverse (τ_D~8.3ps) relaxation cannot contribute to the TDSS of dyes in water, but it contributes to the TDSS in proteins having internal water channels or pockets. This can be used to study internal water. In MD simulations using TIP3P water both τ_L and τ_D are ~30% shorter than the experimental values.
A small (<0.25Å) adjustment of the GB1 tertiary structure occurs in MD simulations on the time scale of 130ps and results in a 140cm^{-1} contribution to the TDSS. A shift in the sidechain conformation of Glu-42 in close proximity to the fluorophore (Trp-43) is the main contributor to the slow TDSS amplitude (470cm^{-1}). This conformational change takes 2.6ns in MD simulations and only 80ps in the experiment, which reveals that in CHARMM22 the potential barriers separating sidechain conformations are too high.

3296-Pos Board B401
Nonradiative Processes in Constrained Trps and Model Compounds
Mary D. Barkley.
Constrained derivatives and model compounds were used to elucidate the nonradiative decay pathways of Trp. Fluorescence quenching by electron transfer from the excited indole to the amide backbone was studied in 7 cyclic hexapeptides.

3297-Pos Board B402
5-Fluorotryptophan as Fluorescent Probe to Characterize an Oligomeric Membrane Protein
Jaap Broos.
The mannitol transporter from *E. coli*, EII^{mtl}, belongs to a class of membrane proteins coupling the transport of substrates with their chemical modification. EII^{mtl} is functional as a homodimer and it harbors one high-affinity mannitol binding site in the membrane-embedded C domain (IIC^{mtl}). To localize this binding site, single Trp containing mutants of EII^{mtl} were mixed with azi-mannitol, a substrate analogue acting as a Förster resonance energy transfer (FRET) acceptor (R_0 of 10 Å). Due to the complex fluorescence decay of Trp, we could not establish whether one or both Trp residues showed FRET with azi-mannitol. To overcome this, we took advantage of the homogeneous decay of 5-fluorotryptophan and this analog was biosynthetically incorporated in 19 mutants. Typically, for mutants showing FRET, only one 5-FTrp was involved, while the 5-FTrp from the other monomer was too distant. This proves that the mannitol binding site is asymmetrically positioned in dimeric IIC^{mtl}. The FRET results localized the position of the binding site halfway the first transmembrane helix. Combined with available 2D projection maps of IIC^{mtl}, it is concluded that a second resting binding site is present in this transporter. This work demonstrates the potential in structural and mechanistic protein research of a donor-acceptor pair with a very short R_0, of which the donor shows homogeneous fluorescence decay kinetics.

3298-Pos Board B403
Time Resolved Fluorescence of the Single Tryptophan in R61, a DD-Carboxypeptidase from Streptomyces: Contributions of Dynamics and Heterogeneity
Abel Jonckheer, Marc De Maeyer, Anton J.W.G. Visser, Nina Visser, Olaf Rolinsky, Jean-Marie Frere, **Yves Engelborghs**.
The fluorescence emission of the single tryptophan (W233) of the mutant protein DD carboxypeptidase from *streptomyces* is characterized by a red edge excitation shift (REES). This phenomenon is an indication for strongly reduced dynamics in the environment of the tryptophan residue, which has a very low accessibility to the solvent. The Stokes shift however, shows an unusual temperature and time dependence. This, together with the fluorescence lifetime analysis, showing three resolvable lifetimes, can be explained by the presence of three rotameric states which can be identified using the Dead End Elimination (DEE) method. The three individual lifetimes increase with increasing emission wavelength. This is interpreted as each individual lifetime being an average lifetime on its own, indicating the presence of restricted protein dynamics within the rotameric states. This is confirmed by time resolved anisotropy measurements, which demonstrate dynamics within the rotamers but not among the rotamers and by maximum entropy analysis producing distributions that shift with the emission wavelengths. The maximum entropy distributions can also be fitted using a gamma-function analysis, again indicating a dynamic component next to a static heterogeneity. Advanced DEE calculations together with MD simulations indicate the existence of two minima (i.e. substates) within one particular rotamer, with frequent transitions. The global picture is that of a protein with a single buried tryptophan showing strongly restricted dynamics within three distinct rotameric states, one of which is further subdivided into two substates, with different emission spectra.

3299-Pos Board B404
Non-Exponential Decay: Understanding the Correlation of Wavelength and Lifetime caused by Heterogeneity
Patrik R. Callis.
We report work that leads naturally to the missing underlying universal physical principle accounting for the strong correlation between tryptophan (Trp) decay associated (DAS) fluorescence wavelength (λ_{max}) and lifetime (τ_f), *in the absence of solvent relaxation*. The familiar broad fluorescence spectrum of a solvent-exposed chromophore is actually an ensemble average of single molecular λ_{max} values, fluctuating on a femtosecond time scale typically over 4000 cm^{-1} or 40 nm. In this dynamic picture, those conformers having shorter wavelength emission spectra, i.e., higher average energy, have an increased probability for transient fast electron transfer (ET) during large fluctuations in environment that bring a high energy, non-fluorescent charge transfer (CT) state and the fluorescing state (S_1) into resonance. For Trp, the CT state lies well above the S_1 state, *and* the wavelength is quite sensitive to local electric field. In these cases, heterogeneity and relaxation *both* can lead to time dependent red shifting fluorescence, making heterogeneity difficult to prove. Studies using non-natural amino acids expose the reality of heterogeneity by contrasting behavior. The fluorescence decays of 5-fluoroTrp incorporated in proteins are much more nearly monoexponential. This probe is not as easily quenched by ET as Trp because of its higher ionization potential, but it retains full wavelength sensitivity. Abbyad et al.(2007), find that time resolved fluorescence spectra of Aladan behave *oppositely*. When incorporated at several sites in the protein GB1, λ_{max} shifts to *shorter* wavelength on the nanosecond time scale– unequivocally revealing ground-state heterogeneity, because relaxation always requires a red shift in time; this is consistent with the observation that τ_f for this probe *decreases* with increasing solvent polarity by an internal mechanism.

3300-Pos Board B405
Ultrafast ("Quasi-Static") Quenching of Trp in Proteins and Peptides
Jay R. Knutson, Arianna Biesso, Jianhua Xu.
Femtosecond UV Upconversion Spectrophotofluorometers have, in recent years, provided a very new look at the Trp environment within proteins. For any protein in water, one observes the ~2ps energy loss due to bulk water relaxation; moreover, in some proteins, the signatory risetime in emission intensity at redder wavelengths can include some slower (15-100ps) processes involving relaxation modes of either the protein or coupled water interface.
We have taken more interest, however, in the environmental ***heterogeneity*** that is visible even at these short times. Positive definite preexponential (DAS, decay-associated spectra) terms are seen associated with lifetimes of 20-300 ps ; these require very effective quenching partners. Since this ultrafast quenching process is invisible in regular lifetime instruments, we refer to it as ''quasi-static self quenching''- a loss in yield without apparent lifetime reduction. QSSQ is found even in simple Trp dipeptides, thus these potential quenchers are ubiquitous . In proteins like crystallins, strong QSSQ is apparently employed to limit lens photodamage from the excited Trp singlet.
These rapid quenching events are reconcilable with QM-MM simulation, and the heterogeneity appears to originate not only from local Trp orientation (i.e. rotamers), but also from more distant conformers that move the quencher (eg. creating more proximate and more distant subpopulations).
Unresolved QSSQ might complicate rotamer assignment and this population of ''dark'' conformers will often exceed the bright population. QSSQ rates and proportions vary as proteins change conformation.
Finally, we find some QSSQ is too fast for our current (~300fs) resolution; this implies Trp must either have intimate contact with a quencher or some alternative prompt deactivation channel; both potential mechanisms require further exploration.
In all, QSSQ provides a new set of handles on protein conformation and motions.

Computational Methods II

3301-Pos Board B406
Automated Umbrella Sampling Simulations for the Calculation of Multidimensional Potentials of Mean Force
Wojciech Wojtas-Niziurski.
The potential of mean force (PMF) describing the conformational changes of biomolecules is a central quantity that determines the function of biomolecular systems. Calculating a multidimensional PMF (free energy landscape) is a time consuming process. Each additional reaction coordinate drastically increases the required simulation time for conformation sampling, making calculations in four or more dimensions practically impossible. However, in most cases, only a small fraction of such multidimensional space is energetically relevant. PMF calculations in high dimensionality could thus be achieved if one could effectively focus the simulation effort on those region of high interest. We have developed a method based on umbrella sampling (US) that determines, using a feedback mechanism, which regions of the multidimensional space is worth exploring. The first aim of such application is to manage the creation and analysis of sampling windows for the calculation of PMFs involving up to four reaction coordinates. While this approach could in some cases be used to find the minimum free energy pathway underlying large conformational changes, it is not as general as other approaches that were specifically developed in that purpose. However, contrary to most other approaches, our method allows for the simultaneous characterization of several pathways, and not only the most probable one. The current implementation consists in a C++ application with a python interface that manages MD simulations performed with the biomolecular simulation program CHARMM. The feedback mechanism and final PMF calculation involves the unbiasing of simulations using the weighted-histogram analysis methods (WHAM).

3302-Pos Board B407
A Dynamic Model of Furrow Ingression during Cytokinesis
Christopher C. Poirier, Win-Pin Ng, Douglas N. Robinson, **Pablo A. Iglesias**.
Cytokinesis is one of the most elegant transformations in nature, whereby a mother cell is separated into two identical daughter cells. This complex process relies not only on biochemical reactions, but also on the mechanics and geometry. We create a computational model to examine the role geometry, cellular mechanics and forces influence cytokinesis. Using the level set method, an effective tool for studying shape changes, coupled with high fidelity, experimentally obtained stress profiles and material models, we model cell division under a variety of conditions. We carry out a systematic, reverse engineering of the cellular subsystems, and recreate experimentally measured furrow-thinning trajectories measured for several genotypes in Dictyostelim cells. In doing so, we identify the contributions of motor proteins, substrate adhesion and surface tension in shaping the furrow-thinning trajectory. This model allows for the modular addition and removal of cellular subsystems and provides an attractive framework for the study of altered genotypes and conceptual models. In particular, it provides an effective way to study the effects of temporally and spatially molecular and mechanical inhomogeneities have on the furrow trajectory.

3303-Pos Board B408
Maxwell Relations for Single-DNA Experiments: Monitoring Protein Binding and Double-Helix Torque with Force-Extension Measurements
Houyin Zhang, John F. Marko.
Single-DNA stretching and twisting experiments provide a sensitive means to detect binding of proteins, via detection of their modification of DNA mechanical properties. However, it is often difficult or impossible to determine the numbers of proteins bound in such experiments, especially when the proteins interact nonspecifically (bind stably at any sequence position) with DNA. Here we discuss how analogs of the Maxwell relations of classical thermodynamics may be defined and used to determine changes in numbers of bound proteins, from measurements of extension as a function of bulk protein concentration. We include DNA twisting in our analysis, which allows us to show how changes in torque along single DNA molecules may be determined from measurements of extension as a function of DNA linking number. We focus on relations relevant to common experimental situations (e.g., magnetic and optical tweezers with or without controlled torque or linking number). The relation of our results to Gibbs adsorption is discussed.

3304-Pos Board B409
Structural Mapping of MHCII-Eluted Peptides to their Source Proteins: A Preliminary Survey of the Effect of Structure on Immunodominance
Karen Katrina Manalastas, Denise Mirano-Bascos, Neil Andrew Bascos, Pablo Manalastas.
The prediction of which peptides would bind to major histocompatibility complex class II molecules (MHCII) has long been of interest as a method of predicting immunodominance. Most approaches for MHCII binding prediction have been sequence-based (i.e. predicting which amino acids are optimal binders to the MHCII binding groove). Alternatively, a structure-based view for MHCII-peptide binding may be taken. Recent studies suggest that the population of peptides available for binding MHCII may be dependent on exposed protease cleavage sites in the protein structure at different stages of antigen processing. Thus, we hypothesized that a survey of MHCII-binding peptides would reveal them to be clustered at a particular depth in their respective undigested source proteins as these areas would be exposed at appropriate times for loading into MHCII. A population of 127 documented MHC-II binding peptide sequences with available source protein structure files in the RCSB Protein Data Bank was used for this study. An algorithm was constructed to determine the relative position of these peptides in their source protein. The surface of each source protein was estimated by computing the convex hull of their

alpha-carbon coordinates. The distance of each eluted peptide from its hull was then computed (d: distance of peptide to protein surface) and normalized against the distance from the center of the hull (S: percent submergence in source protein). In our preliminary survey, 53% of the samples had d-values of 1A or less, with 51% having S-values of less that 15%, indicating that peptides that are selected as MHCII binders are relatively near the surface of their undigested source proteins. Our preliminary results indicate that timing, as well as affinity, may be equally important in MHCII binding.

3305-Pos Board B410

A Multiscale Approach for Path Sampling

Hiroshi Fujisaki, Motoyuki Shiga, Akinori Kidera.

Proteins often accompany conformational changes when they function in cells, and its characterization is one of the most important subjects in biophysics. The ability of theoretical and computational methods based on molecular dynamics simulations has been increasing due to the advance of hardware and algorithms, it is, however, still not feasible to simulate and clarify a biological role of conformational changes of (large) proteins. To address this time-scale problem from a different point of view, we proposed to use a statistical approach based on the Onsager-Machlup (OM) action [J. Chem. Phys. 132 (2010) 134101], where a path, not a configuration, is the most fundamental object to be studied, and its probability distribution is described by a path-integral representation using the OM action in the exponent. In the present study, we apply this formalism to a model polymer system considered by Micheletti and coworkers [J. Chem. Phys. 129 (2008) 074105], where they used the OM action to estimate the free energy landscape and the diffusion coefficient of a coarse-grained variable (end-to-end distance). We execute path sampling for the same model polymer with an Asakura-Oosawa-type interaction, and address some practical issues of path sampling when we apply it to a molecular system. We further discuss how coarse-grained variables can be used to accelerate the convergence of path sampling.

3306-Pos Board B411

In Silico Investigation of a Missense Mutation in CLIC2 Associated with Intellectual Disability

Shawn Witham, Kyoko Takano, Charles Schwartz, Emil Alexov.

While numerous nsSNPs (nonsynonomous SNP) have been reported in the CLIC2 gene in healthy individuals (indicating that the CLIC2 protein can tolerate amino acid substitutions while still being fully functional), we recently identified a missense mutation in CLIC2 on Xq28 in a male with X-linked intellectual disability (XLID). This mutation, c.303C>G (p.H101Q), was not observed in 1059 control X chromosomes, which indicates that it may contribute to intellectual disability. To test the possibility that p.H101Q is a disease-causing mutation, we performed extensive in silico simulations to calculate the effects caused by the p.H101Q mutation on CLIC2 stability, dynamics, and ionization states. We then compared the effects obtained for the (presumably) harmless nsSNPs. In silico analysis predicted that p.H101Q, in contrast with other nsSNPs, (a) reduces the flexibility of the joint loop which is important for the normal function of CLIC2, (b) makes the overall 3D structure of CLIC2 more stable and thus reduces the possibility of the large conformational change expected to occur from the soluble to membrane state of CLIC2, and (c) removes the positively charged residue, H101, from the joint loop which may be important for the membrane association of CLIC2. The results of the in silico modeling, in conjunction with the polymorphism analysis, suggest that p.H101Q is indeed a disease-causing mutation, which is the first one found in the family of the CLIC proteins. This work was supported by awards from NLM/NIH, grant numbers 1R03LM009748 and 1R03LM009748-S1.

3307-Pos Board B412

Automation of the Charmm General Force Field for Drug-Like Molecules

Kenno Vanommeslaeghe, Jayeeta Ghosh, Narendra K. Polani,
Michael Sheetz, Sudhakar V. Pamidighantam, John W.D. Connolly,
Alexander D. MacKerell Jr.

The CHARMM Force Field[1] is widely used for the study of biological macromolecules. Recently, we released the CHARMM General Force Field (CGenFF) which allows simulating drug-like molecules in an environment represented by the CHARMM biomolecular force field.[2] To facilitate the use of CGenFF, a computer program was developed that automatically assigns atom types, bonded parameters and charges to any organic molecule. The atom typing is rule-based and programmable, making it easy to update the atom typing scheme as the force field grows. Assignment of bonded parameters is based on substituting atom types in the definition of the parameter, and returns a ''penalty score'' as a measure for the accuracy of the approximation. Charges are assigned using an extended bond-charge increment scheme that should be able to capture short- and medium-range inductive and mesomeric effects.[3] This functionality is accessible on the web, which makes it possible to apply CGenFF on arbitrary molecules in a matter of seconds.[4] Although the program should ideally accept any molecule, the quality of the resulting parameters (as indicated by their ''penalty scores'') varies depending on whether a similar compound has been parametrized before. Therefore, an effort has been started to build a computational engine with the capability of automatically validating and/or optimizing parameters for drug-like model compounds of the user's interest in the framework of CGenFF, thus providing high-quality force field parameters for computer-aided drug design.[4]

1. A. D. MacKerell et al., J. Phys. Chem. B 1998, 102, 3586-3616
2. K. Vanommeslaeghe et al., J. Comput. Chem. 2010, 31, 671-690
3. K. Vanommeslaeghe et al., in preparation
4. NSF Award #0823198; https://www.paramchem.org/

3308-Pos Board B413

From Small Molecules to Macromolecules: Progress Towards a Charmm Drude Polarizable Force Field for the Nucleic Acids

Christopher M. Baker, Alexander D. MacKerell Jr.

Electrostatic interactions play a crucial role in determining the structure and function of biomolecules, and an important aspect of the electrostatic interaction is polarizability, the response of the molecular dipoles to an external electric field. Towards development of a comprehensive force field for biomolecules, initial work on the CHARMM Drude polarizable force field for nucleic acids focused on optimizing the theoretical model and developing parameters for small molecule analogs of the sugar, phosphate and base moieties.

With parameters for the small molecule analogs now in place, current work is focused on construction of the full nucleic acids, and details of this work will be presented here. Initial simulations of the full nucleic acids have demonstrated that the polarizable model is both robust and stable, and work is now underway to assemble the small molecule building blocks into the full nucleic acids. This procedure requires careful optimization of the parameters associated with covalent connections between the constituent moieties. Following initial optimization of the intramolecular connections, multiple simulations will be performed to provide a detailed assessment of macromolecular properties in comparison to experimental data. These results will be used to identify and correct any weaknesses in the force field, and are also an essential tool for validation of the model in condensed phase environments; they will give new insights into the importance of polarizability in nucleic acid simulations.

3309-Pos Board B414

Solid-State NMR Ensemble Dynamics as a Mediator between Experiment and Simulation

Taehoon Kim, Sunhwan Jo, Wonpil Im.

Solid-state NMR (SSNMR) is a powerful technique to describe the orientation of membrane proteins and peptides in their native membrane bilayer environments. Various SSNMR observables such as ^{2}H NMR quadrupolar splitting (DQS), ^{15}N chemical shift (CS), and ^{1}H-^{15}N dipolar coupling (DC) have been used to characterize the orientation of transmembrane (TM) helices with a static rigid-body model. In particular, TM helix orientational information is often related to membrane protein function and has been used to investigate the role of hydrophobic mismatch between TM helix and lipid bilayer. However, dynamic information of these TM helices can be missing or misinterpreted when a static model is used. We have investigated the orientation and dynamics of WALP23 in DMPC and GWALP23 in DLPC by determining ensemble of structures using multiple conformer models with various SSNMR restraint (DQS, CS, and DC) potentials. The resulting ensemble structures that satisfy the SSNMR observables are compared with those from MD simulations and free energy calculations in both explicit and implicit membrane. The good agreement illustrates that SSNMR-ensemble dynamics provides a means to extract the dynamic information from the SSNMR measurements and realistic explanation of the discrepancy between MD simulation and experimental interpretation based on a static model.

3310-Pos Board B415

An Integrative Approach using Numerical Models to Bridge Spatiotemporal Interactions of Subcellular Processes: Cell Spreading

Yannick Loosli, Reto Luginbuehl, Jess Snedeker.

After an initial phase of non-specific interactions with an adhesive substrate, cells enter a rapid phase of spreading. During this phase, unstable entities (focal complexes -FXs- and actin bundles) selectively mature into long lasting focal adhesions and associated actin stress-fibers. This process is regulated by complex signaling cascades involving mechano-sensation at the focal adhesions, and relies on the spatial and temporal coordination of a many proteins. This complexity presents a hurdle in elucidating the relationship between local stimuli and resultant global cellular behavior. Actual models have generally employed elaborate algorithms with many degrees of freedom precluding any insight into the modeled system behavior.

We propose an alternative modeling framework that drastically reduces the number of parameters by integrating discrete subcellular processes into a framework of weakly coupled functional modules. Module interaction is governed by few rules. In the case of cell spreading, we model the stochastic formation of FXs by discrete modules representing lamellipodial and filopodial activity, and consider the spatiotemporal interactions of these modules. These interactions are regulated by the top-level cellular objective. More specifically, maturation of nascent FXs and accompanying stress-fibers recruitment is driven by actin bundle bridging of overly-large distances between consecutive adhesions and the eventual spatial incorporation of stable filopodia by the lamellipodia. Based on this framework, an iterative and non-deterministic numerical algorithm was developed that enabled prediction of spread cell morphology (focal adhesion and stress-fiber layout), in a time dependent manner. Numerical outcomes were compared to a wide range of experimental evidence. For all tested substrates, the model provided robust replication of the experimental analog. We interpret this fact to imply that the selected functional modules and governing top-levels rules for their interaction were adequate to describe cell spreading.

3311-Pos Board B416

Developing a Fast Polarizable Force Field for Biophysical Simulations

George Kaminski.

Computer simulations have become very helpful in biophysical studies. It has been demonstrated by our and other groups that explicit treatment of the electrostatic polarization is crucial for obtaining biochemically accurate computational data in a variety of cases. For example, we have managed to calculate pKa values for protein residues within 0.6 - 0.7 pH units of the available experimental data. We have also shown that some experimentally known protein-ligand complexes have to be modeled with explicit polarization in order to reproduce the very existence of the complexes. Our results also allow to conclude that simulation of complexes with the Cu+ ion can have a ca. three-fold error in the magnitudes of the binding energies if the polarization is not included. We are now developing a complete polarizable force field for proteins using the second-order approximation formalism which permits to increase the computational speed by ca. an order of magnitude. Results of this ongoing development will be presented, and a number of relevant issues (including the relative importance of quantum mechanical and experimental data in fitting of torsional parameters) will be discussed.

3312-Pos Board B417

Compartmental Analysis of Intravaginal HIV Transport and Neutralization by Microbicides

David F. Katz, Jason A. Chen.

Microbicides are topically acting molecules intended to inhibit HIV-transmission by acting within luminal fluids and/or vaginal mucosa. Gels are a promising microbicide delivery modality, with clinical evidence that they can reduce the rate of sexually-transmitted HIV in women (Karim et al, 2010). We created a model of interacting vaginal co-transport of HIV virions and gel-introduced microbicides in four compartments: semen, gel, vaginal fluid, mucosa. Imaging studies of gel distribution have shown that mucosal surfaces has incomplete gel coating; there can be substantial surface area directly exposed to semen. HIV and microbicide transport occur by diffusion and convection, the latter modeled using Taylor dispersion theory. Here, the active microbicide is an HIV entry inhibitor that must collide with virions in sufficient numbers before they arrive at the mucosal surface to prevent transmission. Key model output is the time-dependent number of non-neutralized virions arriving at the tissue surface. Key inputs are: fraction of surface with coating; coating thickness distribution; viral load in semen; microbicide concentration in gel; parameters of HIV neutralization mechanism; HIV and microbicide diffusion coefficients in gel, semen and vaginal fluid; and time interval between gel application and semen deposition. Results show that infectious HIV transport to tissue is largely over uncoated regions, since HIV diffusion in gel is significantly restricted (Lai et al, 2010). If fractional coated area $>90\%$, most reasonable combinations of system parameters cause substantial HIV neutralization, with small numbers (~ 1000) of still-infectious virions reaching tissue. Lower fractional coated areas and increased HIV diffusion coefficients result in increased flux of infectious virions to tissue in a multivariate manner delineated by the model. This modeling helps improve our understanding of how HIV transmission can be reduced by rationally designed microbicides. [Support: NIH AI077289 and Duke CFAR].

3313-Pos Board B418

Deriving Effective Force and Moment due to Pairwise Interactions in Coarse Grain Simulations

Mohammad Poursina, Kurt S. Anderson, Jeremy Laflin.

We extend the approach used to approximate the long range gravitational force and the associated moments in spacecraft dynamics to calculate the pairwise forces in coarse grain simulations. First, we provide a relatively accurate approximation of the resultant force applied from an atom $\boldsymbol{P}$ to a rigidified superatom. Since this resultant force does not generally act through the center of mass of the superatom, it creates a moment about the center of mass of the body. This potentially valuable moment is completely neglected in bead model representations. We also calculate this moment which is very useful when the equations of motion are formed in articulated multibody-based framework. In this process, assuming each superatom as a discontinuous rigid body, we introduce the concept of the pseudointertia dyadic $\boldsymbol{I}_{\alpha}$. If the governing force field is the gravitational force, this pseudoinertia tensor represents the inertia matrix of the rigid body or system of particles. We show that the resultant force and moment applied to the superatom only depend on the location of the center of mass of the superatom with respect to the atom $\boldsymbol{P}$, and the pseudointertia tensor of the body. This tensor is calculated for each rigid domain of the system before starting the simulation; therefore, there is no cost associated with this tensor during the course of the simulation. Then, based on the results obtained in the previous step, we calculate the resultant force and moments between two rigid pseudoatoms due to the pairwise interactions among the individual atoms belonging to one superatom and the other one. We show that the resultant force and moments are functions of the relative location of the centers of mass of the bodies, and the pseudoinertia dyadic of the individual pseudoatoms.

3314-Pos Board B419

Relationship of the 2′-Hydroxyl Orientation in RNA to Watson-Crick Base Pair Opening

Elizabeth Denning, U. Deva Priyakumar, Alexander D. MacKerell Jr.

RNA molecules are one of the more versatile macromolecules within a cell as they have a variety of structures and functions. Thus, it is important when studying RNA using empirical force fields, to consider the models and methodologies used to study RNA, including the quality of force field parameters. CHARMM27 force field parameters exhibits Watson-Crick (WC) basepair opening in RNA molecules. Here, we present a series of new RNA force field parameters that improve the behavior of RNA molecules. The updates result in changes in the distribution of the 2'-hydroxyl torsion leading to a reduction the frequency and extent of WC base-opening events. As a result of the shift in the 2′-hydroxyl distribution, we observe results that are in improved agreement with experimental and RNA survey data. The optimal force field parameter was applied to study the behavior and folding mechanisms of different types of RNA molecules.

3315-Pos Board B420

Development of the Charmm Polarizable Force Field for Polypeptides Based on Drude Oscillators

Pedro E.M. Lopes, Xiao Zhu, Albert Lau, Benoit Roux,
Alexander D. MacKerell Jr.*.

Ongoing developments of polarizable CHARMM force field for proteins, based on the classical Drude oscillator, are presented. Inclusion of polarizability has the potential to describe physical properties of complex systems in a way not possible with current additive force fields. However, polarizable force fields are extremely sensitive to the environment and extreme care has to to be used in their development. For example, small changes of the electrostatic parameters result in large variations of the calculated properties relative to the reference QM values. In this work we describe the steps in optimization of the force field. The bonded parameters were developed based on the reproduction of QM and crystal structures and vibrational spectra of small models (ex. NMA, alanine dipeptide and proline dipeptide). Determination of the crucial electrostatic parameters was based on reproduction of QM electrostatic properties, dipole and quadrupole moments, of small (NMA and alanine dipeptide) and larger models (alanine 5-mer polypeptide) in different conformations. Determination of the electrostactic parameters pose a considerable challenge since ultimately, they have to be able to describe the electrostatic properties of small and extended compounds (ex. polypeptides) alike. VdW parameters were developed following the customary reproduction of condensed phase results (heats of vaporization and free energies of hydration). Finally, adjustments needed to fine tune the agreement between calculated and target properties of larger polypeptides are described.

3316-Pos Board B421

No New Islet Formation after Neonatal Islet Fission

Junghyo Jo, German Kilimnik, Abraham Kim, Manami Hara, Vipul Periwal.

Glucose homeostasis is regulated by the islets of Langerhans, a cluster of microorgans embedded in the exocrine pancreas. These pancreatic islets range in size from a few to several thousand endocrine cells independent of species over a range of body sizes, suggesting an optimal functional size. Humans have more but not larger islets than mice. To examine the developmental processes that produce this size range of islets, we used a novel method that images all the islets in an intact pancreas of the transgenic mice expressing a fluorescent protein specifically in beta cells. Based on changes of the islet size distribution from postnatal day 1 to week 20, we analyzed islet developmental processes such as birth, growth and fission with mathematical modeling. No new islets were formed after postnatal week 3. At early postnatal days, islet growth was size-dependent with more active cell

proliferation in smaller islets than in larger islets. In adulthood, however, every beta cell in an islet of arbitrary size ultimately has an equally small proliferation potential. In addition to this limited islet growth, fission of large islets occurred most actively at postnatal week 3, and contributed to maintaining a limited range of islet sizes. On the other hand, in a tumor (insulinoma) progression model, we found unlimited islet growth, with especially accelerated cell proliferation in larger islets. We conclude that islet size is constrained by preferential growth of small islets and fission of large islets in the early postnatal period, and a low rate of proliferation in maturity.

3317-Pos Board B422

In Silico Titration of Biomolecules: Explicit Solvent Constant pH Molecular Dynamics

Serena Donnini, Florian Tegeler, Gerrit Groenhof, Helmut Grubmüller.

The pH is an important parameter in macromolecular systems as it determines the protonation state of ionizable groups and consequently influences the structure, dynamics and function of molecules in solution. In most force field simulation protocols, however, the protonation state of a system (rather than its pH) is kept fix and cannot adapt to changes of the local environment. Here, we present a method to perform molecular dynamics simulations in explicit solvent at constant pH. During the simulation the protonation states of titratable groups are allowed to change dynamically, and the titration curves agree with experiment. Our method is based on the lambda-dynamics approach, in which the dynamics of the titration coordinate lambda is driven by generalized forces between the protonated and deprotonated states. Constant pH simulations can be achieved by accounting for the pH dependence of the hydration free energy. As a benchmark, titration curves of amino acid analogues and a di-peptide, as well as of turkey ovomucoid inhibitor protein were calculated.

3318-Pos Board B423

Estimating the Orientational Entropy of Water at Protein Interfaces

Stephanus M. Fengler, Helmut Grubmüller.

The entropy of solvents significantly contributes to the stability of the native state of proteins. However, obtaining solvent entropies from molecular dynamics simulations remains a computational challenge. Reasons for this are first, that the phase space of solvent molecules poorly converges because they sample a shallow free energy basin. Second, its dimensionality rapidly grows with the number of molecules.

To address the problem of phase space convergence, we apply the recently introduced approach of permutation reduction. Further, this method maps water molecules such that their resulting trajectories are restricted to a small region of space around a reference position without changing the physics of the ensemble. For density estimation, we adapted the efficient nearest neighbor (NN) method to the curved space of orientations. The NN method is entirely nonparametric and efficient on high-dimensional manifolds. For approximation of the total entropy, we apply the mutual-information expansion (MIE). The MIE is a systematic expansion of the entropy in mutual information terms by splitting the phase space into subsystems with reduce dimensionality.

Orientational entropies of water molecules are estimated by a the combination of these methods. Well-converged and spatially resolved many-body correlations of higher order are captured. The developed method was tested on specific distributions of orientations, the correlated orientations of water molecules from a pure water box, and the correlated orientations of water molecules around the small globular protein Crambin.

We found that orientational correlation is dominated by pair correlations between neighboring water molecules, and drops within the first two water shells. Further, the relative position of water molecules to each other plays an important role in three body-correlations, but their small mutual information suggests that higher order terms are not necessary to capture the orientational entropy of water.

3319-Pos Board B424

Charge Separation and Isolation in Water and Ice Particles on Strong Impacts

F. Wiederschein, E. Vöhringer-Martinez, A. Beinsen, R. Srama, S. Kempf, F. Postberg, B. Abel, H. Grubmüller.

Charge separation is a general phenomenon in nature. There has been vivid speculation and discussion about the mechanism of charge separation in condensed matter on strong impacts at small energies. Here we show that charge separation naturally occurs if water aggregates or particles with embedded charge carriers, e.g. ions, encounter a high energy impact even though no plasma occurs and the involved kinetic energies are much below any molecular ionization energy. We find that the charge distribution in the fragments resulting from a strong impact can simply be described by a three step model. The first level of the model is a simple statistical description of the resulting charge distribution at low salt concentrations by making usage of the Poisson distribution. The second step of describing the charge distribution of the dispersed fragments involves the mutual interaction between the charge particles in the condensed matter, which allows us to describe the charge process at higher salt concentrations. We achieved this by using implicit water Monte Carlo Simulation methods of the charged particles. Finally we included the full dynamics of the separation process into our model by using non-equilibrium Molecular Dynamics Simulations to describe the charge separation at high salt concentrations and high separation process velocities.

We present a microscopic model of the charging mechanism of fragments, that contributes to the understanding of a larger range of phenomena related to charges and charge separation in Nature. With this model we shed light on the charge mechanism of laser desorption experiments and discuss the impact of the current results for particle detection in space and possible implications for lightning formation in the atmosphere.

3320-Pos Board B425

Toward a Unified Model of Molecular Crowding: A Regression Approach to Predict Equilibria and Kinetics of Assembly Systems in Crowded Environments

Byoungkoo Lee, Philip R. LeDuc, Russell Schwartz.

Chemistry in living cells functions significantly differently from chemistry in a test tube. One defining characteristic of the intracellular environment is molecular crowding, which can dramatically alter the rates and equilibria of biochemical reactions, potentially either enhancing or inhibiting reactions depending on numerous physical parameters of a given system. However, it is extremely difficult to predict how crowding will quantitatively affect any particular reaction system or which physical factors of the system will be most critical. Sophisticated particle models provide a way to more accurately simulate chemistry in crowded systems, but at a computational cost that makes them infeasible for all but the most trivial reaction systems. With the goal of developing a unified model of molecular crowding, we developed a novel multi-scale approach to predict binding chemistry in crowded media using high-cost particle models of crowded conditions on simple test systems to train predictive regression models that can then be applied to low-cost differential equation or stochastic simulation models of more complicated systems. We show that a polynomial regression model can incorporate several interrelated parameters influencing chemistry under crowded conditions and accurately reproduce thermodynamic binding equilibria from stochastic off-lattice simulations of binding chemistry in crowded media. The model accurately reproduces the results of particle simulations over a broad range of variation of both independent and cross-dependent physical parameters expected to influence the crowding effect. We further show how the approach can be extended to efficiently capture the effects of molecular crowding on kinetic rate parameters. The work thus makes an important step toward the long-term goal of building computational models of reaction chemistry in the cellular environment that are both computationally tractable and predictive for large, complex systems.

3321-Pos Board B426

A Structurally Flexible Protein Backbone for the MARTINI Coarse Grained Force Field

Xavier Periole, Siewert-Jan Marrink, Peter Tieleman.

By reducing the level of description of a system as compared to atomistic models coarse grained (CG) molecular force fields allow simulating larger systems for longer time scales, thereby probing exciting properties of biological systems. It is our constant effort to improve their accuracy and range of applicability.

The MARTINI CG model defines a library of beads or super-atoms corresponding to chemical entities (defined by 3-6 non-H atoms) for which the interaction strengths are parameterized against thermodynamic (partitioning free energies) and structural data extracted from experiments and simulations. Virtually any molecular topology can be built from a combination of beads that reproduces structural and thermodynamic available data for that particular molecule. Molecular topologies are available for a large variety of molecules including lipids, amino acids and proteins, and sugars.

Here we present a refined version of the MARTINI force field for proteins in which restraining the secondary structure is not required anymore. This is achieved by restoring directionality in the backbone interactions. To do so a dipole (two net charges kept at a fix distance) is placed on the peptide bond of the backbone. We show that this simple representation coupled with a rigorous parameterization of the dipole and related bonded/non-bonded interactions is able to capture some essential mechanical and physicochemical properties of the polypeptide backbone. In particular the backbone may access both extended (β-sheet) and compact (α-helix) conformations using a single potential. A few simple test cases are shown to illustrate the structural flexibility of the new backbone and its ability to stabilize secondary structure elements in proteins. The potential is tested with both regular and polarizable MARTINI water models.

3322-Pos Board B427
Molecular Simulations of Sequence-Specific Association of Transmembrane Proteins in Lipid Bilayers
Manolis Doxastakis, Lorant Janosi, Anupam Prakash.
Association of membrane proteins is central in material and information flow across the cellular membranes. Amino-acid sequence and the membrane environment are two critical factors controlling association, however, quantitative knowledge on such contributions is limited. In this work, we study the dimerization of helices in lipid bilayers using extensive parallel Monte Carlo simulations with recently developed algorithms [1].
The dimerization of Glycophorin A is examined employing a coarse-grain model that retains a level of amino-acid specificity, in three different phospholipid bilayers. Association is driven by a balance of protein-protein and lipid-induced interactions with the latter playing a major role at short separations. In all bilayers, sequence-specificity is evident by the formation of a clear interface between the helices that is modulated by the lipid environment. Extracted estimates of the dimerization affinity are in excellent agreement with experimental data [2]. Following a different approach, the effect of amino-acid sequence is studied using the four transmembrane domains of the epidermal growth factor receptor family in identical lipid environments. Detailed characterization of dimer formation and estimates of the free energy of association reveal that these helices present significant affinity to self-associate with certain dimers forming non-specific interfaces. We present results that support the role of lipid-mediated contributions to such effects with major implications on protein function.
[1] Janosi L. and Doxastakis M., ''Accelerating flat-histogram methods for potential of mean force calculations'', J. Chem. Phys., 131, 054105 (2009)
[2] Janosi L., Prakash A. and Doxastakis M., ''Lipid-Modulated sequence-specific association of Glycophorin A in membranes'', Biophys. J., 99, 284-292 (2010)

3323-Pos Board B428
Low Order Physical Multipoles
Charles J. Baker, Ramu Anandakrishnan, Alexey Onufriev.
Point multipoles are a strong theoretical tool for studying fields due to a given charge distribution; they often provide simplifications that can be used to gain physical insight into systems. However, when used for practical calculations, such as the potential due to atomic charges in large biomolecules, both the required number of calculations and the complexity grows rapidly with each additional term kept in the expansion. We propose the use of physical multipoles, which consist of a set of point sources placed such that they optimally represent the multipole expansion of the original distribution. This method maintains the theoretical strength of point multipoles but allows for both fewer and simpler calculations. Most importantly, physical multipoles are always at least as accurate at describing the electrostatic potential as the corresponding point multipole of equivalent order and they can be substantially more accurate, especially in the most relevant regime where the distance from the charge distribution to the point of interest is no longer much smaller than the system size. We show that for some extreme charge distributions the RMS error in calculated potential for a physical dipole is 300-400 times lower than for point dipoles, at a distance of two system sizes from the origin. And for biologically relevant systems, such as certain amino acids, the RMS error in calculated potential for physical dipoles can be 4-5 times lower than a corresponding point dipole, at a distance of two times the size of the amino acid from its center. Thus physical multipoles offer a strong alternative to point multipoles, especially in practical computations.

3324-Pos Board B429
Multi-Scale Simulations of Proteins in Different Solvent Conditions
Dirar Homouz, Antonios Samiotakis, Margaret Cheung.
We developed a multiscale approach (MultiSCAAL) that integrates the potential of mean force (PMF) obtained from all-atomistic molecular dynamics simulations with a knowledge-based energy function for coarse-grained molecular simulation in better exploring the energy landscape of a small protein under chemical interference such as chemical denaturation. The two key features of this scheme are the Boltzmann inversion and a protein atomistic reconstruction method we previously developed (SCAAL). Using MultiSCAAL, we were able to enhance the sampling efficiency of proteins solvated by explicit water molecules. Our method has been tested on the folding energy landscape of a small protein Trp-cage with explicit solvent under 8M urea using both the all-atomistic replica exchange molecular dynamics (AA-REMD) and MultiSCAAL. We compared computational analyses on ensemble conformations of Trp-cage with its available experimental NOE distances. The analysis demonstrated that conformations explored by MultiSCAAL better agree with the ones probed in the experiments because it can effectively capture the changes in side chain orientations that can flip out of the hydrophobic pocket in the presence of urea and water molecules. In this regard, MultiSCAAL is a promising and effective sampling scheme for investigating chemical interference which presents a great challenge when modeling protein interactions in vivo.

3325-Pos Board B430
Macromolecular Crowding Effects on Multiprotein Binding Equilibria: Molecular Simulation and Theory
Jonathan Rosen, Young Chan Kim, **Jeetain Mittal**.
We present a coarse-grained model for studying the effects of macromolecular crowding on the thermodynamic and structural properties of multiprotein complexes. Residue-level interactions between proteins and crowding agents are incorporated in a recently developed transferable coarse-grained model of multiprotein complexes. The model is used to study the binding equilibrium between two protein complexes, ubiquitin/UIM and cytochrome c/cytochrome c peroxidase using replica exchange Monte Carlo simulations. We find that the change in binding free energy due to purely repulsive crowding can be quantitatively described by a scaled particle theory (SPT) model without any fitting parameters. The same SPT model can also be used to predict the effects of mixed crowding - a mixture of crowding particles with different sizes, using an additivity ansatz. We find that attractions between proteins and crowding molecules can not only change the crowding effects quantitatively but also qualitatively. For a critical attraction strength, stabilizing entropic effect due to excluded volume interactions are exactly cancelled by destabilizing enthalpic effects. We find that this critical attraction strength is largely independent of crowding packing fraction. A modified SPT model which includes the effect of protein-crowder attractions in a mean-field manner can predict the change in binding free energy due to crowding semi-quantitatively. Further, structural analysis suggests that crowding may significantly change the fraction of specific versus non-specific transient encounter complexes in a crowded environment.

3326-Pos Board B431
Classification of Projections in Single Particle Electron Microscopy using Common Line Similarity Measure
Hstau Y. Liao, Robert Langlois, Joachim Frank.
In single-particle reconstruction methods [1], projections of macromolecules lying in randomly unknown orientations are collected by a transmission electron microscope. Often, several classes of conformations or binding states coexist in the sample. To obtain structures with high accuracy, it is required to separate the classes before reconstruction of the molecules. In this work, we use a graph-theoretic criterion based on common lines, which measures both the dissimilarity between the classes and the similarity within the classes. Projections are then sorted by optimizing this measure, without need for a reference volume or for any intermediate reconstructions, as done in most classification methods.
The usefulness of this type of approach, via a combinatorial optimization of the measure, was first demonstrated in [2], but tested only on simulated projection data. We instead view the optimization as an eigen-decomposition problem, which makes it easy to account for different kinds of normalization of the measure. The work in [3] also uses eigen-decomposition, but the similarity is measured between 2D averages, and a reference volume is required to pre-sort the projections according to their angular orientation.
In this work we measure the similarity between the projection data themselves and show the results for both simulated and experimental data.
[1] J. Frank, Three Dimensional Electron Microscopy of Macromolecular Assemblies, Oxford, 2006
[2] G.T. Herman and M. Kalinowski, Classification of heterogeneous electron microscopic projections into homogeneous subsets, Ultramicroscopy 108:327-338, 2008
[3] M. Shatsky et al., Automated multi-model reconstruction from single-particle electron microscopy data, J. Struct. Biol. 170:98-108, 2010

3327-Pos Board B432
Monte Carlo Simulations of Absolute Binding Free Energy of Targeted Nanocarriers to Cell Surfaces
Jin Liu, Blaine Zern, Portonovo Ayyaswamy, David Eckmann,
Vladimir Muzykantov, Ravi Radhakrishnan.
We have developed a computational methodology based on Metropolis Monte Carlo (MC) and the weighted histogram analysis method (WHAM) to calculate the absolute binding free energy between functionalized nanocarriers (NC) and endothelial cell (EC) surfaces. The binding affinities are then calculated according to the free energy landscapes. The predictions quantitatively agree with the analogous measurements of specific antibody coated NCs (100 nm in diameter) to intracellular adhesion molecule-1 (ICAM-1) expressing EC surface in *in vitro* cell culture experiments. We then systematically explore the effects from a broad range of experimentally tunable parameters including the antibody surface coverage σ_s of NC, glycocalyx in both *in vivo* and *in vitro* conditions, shear flow and NC size. The simulation results agree remarkably well

with experimental data in all scenarios. Of particular biological significance, our model predicts a threshold σ_s value below which the NC binding affinities reduce drastically and drop lower than that of single anti-ICAM-1 molecule to ICAM-1; our results reveal that this is due to a change in the multivalency (or number of bonds formed per NC). The trend and threshold values are exactly recovered by the *in vivo* measurements of the endothelium targeting of NCs in the pulmonary vascular in mice [Liu *et al*. *PNAS* 107: 16530-16535 (2010)]. Increasing the shear flow rate enhances the NC binding affinities till a threshold value is reached; this quantitatively agrees with existing experiments and a novel mechanism is revealed based on our model results. On this basis, our computational protocol represents a quantitative and predictive approach for model driven design and optimization of functionalized nanocarriers in targeted vascular drug delivery.

This work is supported by NIH Grants: R01-EB006818 (D.M.E.), R01-HL087036 (V.R.M.), and NSF Grant: CBET-0853389 (R.R.).

Imaging and Optical Microscopy III

3328-Pos Board B433

Characterization of Binding Affinity and Epitope Dynamics of Anti-HIV-1 Antibodies

Meron Mengistu, Krishanu Ray, Joseph R. Lakowicz, Anthony L. DeVico.

A preventive vaccine is potentially the most effective way to control the HIV pandemic. Such a vaccine needs to successfully harness humoral immunity and produce cross-reactive anti-envelope antibodies that mediate direct virus neutralization and/or Fc receptor-dependent killing. For these antibodies to carry out their functions in clearing HIV infection, they must bind the virus and prevent it from infecting target CD4+ cells. The capacity of an antibody to do this is dependent on the timing, duration and extent of cognate epitope exposure before and during the attachment and entry processes. The goal of this study was (i) to quantify antibody binding to HIV, and (ii) to characterize when and for how long antibody epitopes are exposed before and during virus-cell fusion. We studied the binding properties and epitope dynamics of antibodies against HIV envelope gp120 [b12 (CD4 binding site), 2G12 (carbohydrate clusters), A32 (C1, C4, & C5 domains)], CD4-induced epitope of gp120 (17b & 19e), and the membrane-proximal external region (MPER) of gp41 (4E10). To directly quantify antibody binding to virus in solution, we developed a fluorescence correlation spectroscopy (FCS) methodology that uses fluctuations in fluorescent signals to measure diffusion and reaction kinetics of fluorescently-labeled anti-envelope Mabs as they attach to HIV-1-JRFL, HIV-1-Bal, and HIV-1-NL4-3 pseudoviruses and infectious molecular clones. We have also developed methods to visualize the temporal appearance and disappearance of cognate epitopes during virus-cell fusion using immunofluorescence and live-cell imaging techniques. In this case, viral particles were labeled with a novel SNAP-tag technology that permits tracking of particles during different stages of fusion with CD4+ target cells, and concurrent imaging of epitopes that become exposed on the HIV envelope.

3329-Pos Board B434

An Improved Method for Studying Single Proteins Trapped in Lipid Vesicles

Claudiu C. Gradinaru.

We report on an improved method to encapsulate proteins inside surface-tethered liposomes in order to reduce or eliminate environmental interference for single-molecule investigations. The liposomes are large enough for the molecule to experience free diffusion, but sufficiently small so that the molecule appears effectively immobile for fluorescence imaging. Various single-molecule fluorescence experiments were performed to fully characterize this anchoring method relative to direct immobilization via biotin-streptavidin linkers. Multidimensional histograms of intensity, polarization and lifetime reveal that molecules trapped in liposomes display a narrow distribution around a single peak, while the molecules directly immobilized on surface show highly dispersed values for all parameters. For instance, when TMR-labelled molecules were immobilized directly on surface, we recorded large intensity fluctuations (6.30 ± 4.91 emission states/molecule), whereas the fluctuations were much smaller for the vesicle-trapped molecules (1.37 ± 0.71 emission states/molecule). During sample preparation, by hydrating the lipid film at low volumes, high encapsulation efficiencies can be achieved with ~10 times less biological material than previous protocols. By measuring directly the vesicle size distribution, we found no significant advantage for using freeze-thaw cycles during vesicle preparation. On the contrary, the temperature jump can induce irreversible damage of fluorophores and it reduces significantly the functionality of proteins, as demonstrated on single-molecule binding experiments involving a peptidic inhibitor for the oncogenic protein STAT3. Our improved and biologically gentle molecule encapsulation protocol has a great potential for widespread applications in single-molecule fluorescence spectroscopy.

3330-Pos Board B435

In Vivo Structure of the E. coli FtsZ-Ring Revealed by Photoactivated Localization Microscopy (PALM)

Guo Fu, Tao Huang, Jackson Buss, **Carla Coltharp**, Zach Hensel, Jie Xiao.

The FtsZ protein, a tubulin-like GTPase, plays a pivotal role in prokaryotic cell division. In vivo it localizes to the midcell and assembles into a ring-like structure-the Z-ring. The Z-ring serves as an essential scaffold to recruit all other division proteins and generates contractile force for cytokinesis, but its supramolecular structure remains unknown. Electron microscopy (EM) has been unsuccessful in detecting the Z-ring due to the dense cytoplasm of bacterial cells, and conventional fluorescence light microscopy (FLM) has only provided images with limited spatial resolution (200-300 nm) due to the diffraction of light. Hence, given the small sizes of bacteria cells, identifying the in vivo structure of the Z-ring presents a substantial challenge. Here, we used photoactivated localization microscopy (PALM), a single molecule-based super-resolution imaging technique, to characterize the in vivo structure of the Z-ring in E. coli. We achieved a spatial resolution of ,35 nm and discovered that in addition to the expected ring-like conformation, the Z-ring of E. coli adopts a novel compressed helical conformation with variable helical length and pitch. We measured the thickness of the Z-ring to be ,110 nm and the packing density of FtsZ molecules inside the Z-ring to be greater than what is expected for a single-layered flat ribbon configuration. Our results strongly suggest that the Z-ring is composed of a loose bundle of FtsZ protofilaments that randomly overlap with each other in both longitudinal and radial directions of the cell. Our results provide significant insight into the spatial organization of the Z-ring and open the door for further investigations of structure-function relationships and cell cycle-dependent regulation of the Z-ring.

3331-Pos Board B436

Assessing the Cellular Uptake Pathway for Poly-Lysine Analogues using Triplet Lifetime Imaging

Matthias Geissbuehler, Zuzana Kadlecova, Iwan Märki, Mattia Matasci, Dimitri Van De Ville, Harm-Anton Klok, Theo Lasser.

Research on synthetic delivery vectors is of major interest for cell imaging and manipulation, as they allow an efficient transfer of nucleic acids, therapeutic proteins or small drugs into the cells. We have developed a library of L-lysine analogues that allow for highly efficient gene delivery with low cytotoxicity. However little is known on the exact mechanism of uptake and the final intracellular destination of the synthetic carriers. Therefore we have developed a novel optical technique based on a modulated excitation allowing for intracellular imaging of the triplet-lifetime and -yield of fluorophores attached to the delivery vector. Both these parameters are highly dependant on the intracellular environment thus provide insight into the subcellular localization of the labelled carrier. The method combines high temporal and spatial resolution and is compatible with a multiplicity of fluorophores.

We performed series of model experiments to compare the triplet lifetime and triplet yield behaviour during the natural uptake mechanism to a series of controlled conditions. The latter include microinjection of fluorescently labelled carriers directly into the cytoplasm and cell nucleus as well as in vitro measurements under conditions mimicking physiological, acidic, or DNA rich environments. To validate our technique the results from the triplet imaging were compared with two complementary methods: carrier localization by subcellular fractionation and confocal laser scanning microscopy.

— Reference —

Geissbuehler et al. Triplet imaging of Oxygen consumption during the contraction of a single smooth muscle cell (A7r5). Biophysical Journal (2010) vol. 98 (2) pp. 339-349

3332-Pos Board B437

Correlative EFTEM, Stem and Fluorescence Microscopy as a Tool for Chromatin Biology

Maria A. Aronova, Alioscka A. Sousa, Guofeng Zhang, Michael J. Kruhlak, Elissa P. Lei, Richard D. Leapman.

In eukaryotes, the highly coordinated gene expressions require sophisticated levels of regulation. One such mechanism regulates the spatial and temporal organization of genes and their associated sequences in higher-order chromatin domains. Chromatin insulators, specific gene regulatory assemblies, form large nucleoprotein complexes known as insulator bodies and are thought to influence the organization of higher-order chromatin domains. In order to test current models of insulator function and provide ultrastructural information about these chromatin based domains, we use a correlative microscopy approach based on light microscopy and electron microscopy operating in the mode of energy filtered transmission electron microscopy (EFTEM) and scanning transmission electron microscopy (STEM).

We explore the ultrastructure of the well-studied *Drosophilamelanogaster-gypsy* chromatin insulator by immunolabeling a key insulator protein CP190 using a fluoronanogold conjugated antibody probe. In our correlative method, fluorescent imaging is initially performed to identify nuclei that contain insulator bodies, which are rare within thin sections. A comparison of low-magnification EM image of a whole cell with the corresponding fluorescent image reveals the approximate location of the structure of interest. The fluorescence signal observed by light microscope guarantees the presence of the conjugated nanogold, which can be visualized using STEM, and used to locate precisely the labeled CP190 proteins. EFTEM is then performed to image the distribution of nitrogen and phosphorus and thus map the distributions of protein and nucleic acid. It is evident from these two elemental maps that the insulator body contains an abundance of protein but a small quantity of nucleic acid. Even though dense chromatin surrounds the insulator body, it is difficult to determine whether the low levels of phosphorus within the insulator body structures correspond to DNA or RNA, which requires further investigation.

3333-Pos Board B438

Dominant Vinculin Binding Angle in Podosomes Revealed by High Resolution Optical Microscopy

Susan Cox, Marie Walde, James Monypenny, Rainer Heintzmann, Gareth Jones.

Podosomes are dynamic actin-rich cell-matrix adhesion sites of migrating and invasive cells such as macrophages and osteoclasts, and are receiving increasing attention due to their possible involvement in physiological events such as monocyte extravasation and tissue transmigration, as well as pathological conditions such as atherosclerosis, osteoporosis and cancer metastasis. These structures were examined using three different fluorescence microscopy techniques which provide resolution below the diffraction limit: structured illumination microscopy, stimulated emission depletion microscopy and stochastic optical reconstruction microscopy have been used. In high resolution images, it is clearly visible that each podosome consists of an actin core surrounded by a protein-enriched ring, supporting the existing podosome model. However, these rings are polygonal structures rather than smooth circles. An analysis of the binding angles at corners reveals vinculin to have a dominant binding angle of around 115 degrees.

3334-Pos Board B439

Imaging Fluorescence Cross-Correlation Spectroscopy as a Tool to Study Cell-Membrane Organization

Jagadish Sankaran, Nirmalya Bag, Thorsten Wohland.

The structure of biological membranes has been investigated for many years. However, progress is hindered by the fact that putative domains are highly dynamic and their size is smaller than the optical diffraction limit and thus direct observations are difficult. Therefore, there is a need to develop new biophysical tools which can infer the existence of domains within membranes and can follow their development over time. We have introduced in the past a method called Imaging Total Internal Reflection-Fluorescence Correlation Spectroscopy (ITIR-FCS) using EMCCD or sCMOS cameras. ITIR-FCS allows the measurement of a large number (up to ~0.5 million) correlation curves at contiguous locations on cell membranes of live cells with millisecond time resolution. The spatial information within the data can be used to obtain information on the structure and organization of the membranes. This is achieved by calculating differences between the forward and backward cross-correlations between adjacent pixels A and B (CCF_{AB} - CCF_{BA}) or A, B, and C (CCF_{AB} - CCF_{CB}). The results can be depicted as histograms referred to as ΔCCF distributions. In this work we conduct measurements on supported lipid bilayers and cell membranes and perform simulations to demonstrate how ΔCCF distributions change characteristically with membrane complexity and structure. In particular, we demonstrate that domains with sizes below the diffraction limit have a characteristic broadening effect on the ΔCCF distributions. As an example we show that changes in membrane structure and organization of live neuroblastoma cells can be followed over the time course of an hour or more by way of ΔCCF distributions. To deal with large amount of data collected we developed an open source software, ImFCS, to calculate and fit the auto- and cross-correlation functions and depict the results in an imaging format.

3335-Pos Board B440

Probing Orientational Order of MHC Class I Protein and Lipids in Cell Membranes by Fluorescence Polarization-Resolved Microscopy Imaging

Alla Kress, Hubert Ranchon, Patrick Ferrand, Hervé Rigneault, Sophie Brasselet, Tomasz Trombik, Hai-Tao He, Didier Marguet.

Biomolecular orientational organization of lipids and proteins in plasma membrane is a crucial factor in biological processes where functions can be closely related to orientation and ordering mechanisms. The concept of transient nanosized phase separations in ordered and disordered domains, called ''lipid rafts'' is now widely accepted. Furthermore, the ordered domains are enriched in signalling proteins, which highlights the crucial impact of phase separation during the signalling processes. While this field has been so far largely addressed by studying the translational diffusion behaviour of membrane proteins by Single Molecule Tracking or Fluorescence Correlation Spectroscopy, only little is known about the orientational behaviour of signalling proteins in plasma membranes, mainly due to the lack of appropriate rigid fluorescent label which would be able to act as a proper orientation reporter. In this work we develop a fully polarization-resolved fluorescence imaging technique using a tuneable incident polarization state (''fluorescence polarimetry''), in combination with fluorescence anisotropy imaging, in order to provide orientational order information in very general cell membranes shapes.

We apply this technique to the measurement of quantitative orientational distribution of MHC Class I proteins in the plasma and nuclear membranes, benefiting from a rigidly attached GFP probe. The surrounding lipid orientational order in the plasma membrane is additionally probed using the fluorescent reporter di-8-ANEPPQ.The MHC Class I protein is found to be more ordered in the plasma membrane as compared to the nuclear membrane. Both MHC I and di-8-ANEPPQ orientational orders in the plasma membrane are furthermore seen to be highly affected by actin depolymerisation upon Latrunculin A treatment, with variations that indicate both a structural change in the membrane morphology and a disruption of MHC I - actin interactions.

3336-Pos Board B441

A Combined Confocal-Total Internal Reflection Fluorescence (TIRF) Single-Cell Microscopy Investigation of CEACAM1 Dynamics

Laura N. Poloni, Christopher M. Yip.

The carcinoembryonic antigen-related cellular adhesion molecules (CEACAMs) represent a subset of the immunoglobulin superfamily of cell adhesion molecules that mediate intercellular adhesion. One member of this subset, CEACAM1, is particularly interesting since it is down-regulated in tumourigenic cell lines. CEACAM1 exists as an equilibrium between monomers and dimers; however, the spatial and temporal distribution upon cell-substrate contact is not known.

In order to determine CEACAM1 dynamics, a coupled confocal-total internal reflection fluorescence (TIRF)-atomic force microscopy (AFM) platform was used. Live YFP-CEACAM1 labelled cells were isolated on AFM tips for controlled positioning of cells. Confocal microscopy was used to map CEACAM1 receptors over the entire cell surface. Coupled TIRF microscopy monitored the free cell surface as it was brought into contact with a substrate (i.e. another cell, a model membrane, modified glass). Confocal and TIRF microscopy homoFRET measurements were used to determine the distribution of monomeric and dimeric CEACAM1 receptors prior to and upon cell-substrate contact. Through this understanding of how molecular organization affects intercellular binding and signal transduction, it may be possible to identify peptide or pharmacological drug strategies to create CEA CAM-focused therapies for cancer.

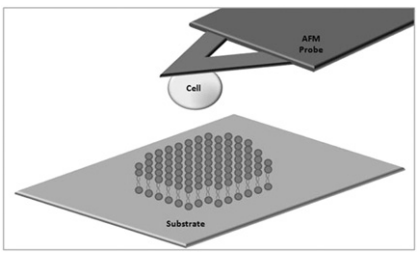

3337-Pos Board B442

Following Actin Fibers in 3D During Cell Migration in Collagen Matrices

Michelle A. Digman, Chi-Li Chiu, Jose S. Aguilar, Enrico Gratton.

Actin polymerization is a major mechanism for the production of the force necessary for cell migration in 2D. The polymerization of actin and its retrograde motion at the leading edge of cell moving in 2D has been studied in great detail as well as the interaction of actin with focal adhesions. When cells grow in 3D collagen matrices, the extending lamellipodial protrusion is more difficult to visualize and it is likely not relavent for the movement of the cell over large distances. We use the modulation tracking 3D method to accurately image the cell protrusion. This method is capable of producing detailed images of 3D structures at the nanoscale and at the same time measure diffusion and aggregation of molecules in these structures. In 3D, cells produce very long protrusions that presumably grab on the surrounding collagen fibers to propel the rest of the cell

body in a specific direction. What is unclear is if the cell is capable of forming stable adhesions with the collagen matrix and how the force is generated. Using the modulation tracking imaging method we can follow the changes in shape of the cellular protrusion and also image separately various proteins, including actin in the cytoplasm and in the membrane. In the thin long protrusion we observe both fast diffusing actin molecules and also relatively immobile species, presumably part of the actin cytoskeleton. We are developing a method to directly measure the movement of the entire actin bundle inside the very thin cells protrusions. The method is conceptually similar to speckle imaging; however, it works in 3D.

3338-Pos Board B443

Super-Resolution Imaging of Chromosomal DNA in Cells

Paul D. Simonson, Eli Rothenberg, Paul R. Selvin.

Super-resolution imaging is achieved by localizing diffraction-limited spots with high accuracy. Here we combined two powerful approaches to image the chromosomal DNA inside cells. In one method, the accumulated, stochastic binding of fluorescent labels to an imaging target are localized, while in the other the fluorophore transitions between dark and bright states (compatible with binding, photobleaching, photo-activation, blinking, etc.), even when fluorophore images overlap, are localized. Combining the two techniques results in a robust microscopy that is faster than what is possible with either technique alone, requires less optimization, and corrects for cell autofluorescence. In addition, background noise due to fluorescent labels in solution can be virtually eliminated by using labels that fluoresce only when bound to the target.

Many DNA-specific dyes show dramatic fluorescence enhancement upon binding to DNA, including SYTO, LOLO, and YOYO dyes. We used nanomolar concentrations of SYTO and LOLO to image lambda DNA attached to poly-L-lysine coated glass and chromosomal DNA in fixed HEK 293 and HeLa cells. We found average single-fluorophore localization errors of 36 nm and 24 nm on glass and in cells, respectively. These imaging techniques may prove useful in future studies of chromosomal DNA in cells, including chromatin structure and defects.

This approach was further applied to imaging microtubules in vitro. We used commercial Oregon Green 488 paclitaxel to achieve a 10 nm average fluorophore localization error, and streptavidin S45A to transiently label biotinylated microtubules with Atto647N, resulting in an average of 18 nm fluorophore localization error. Future work will involve simultaneous imaging of DNA and proteins to answer important biological questions.

3339-Pos Board B444

Investigation of Lysosomes as Enzyme Storage Vesicles using Single Particle Tracking Fluorescence Microscopy

William H. Humphries IV, Christine K. Payne.

Intracellular, vesicle-mediated, degradation of extracellular cargo is an essential cellular function. Of particular interest is the population of vesicles responsible for degradation of extracellular cargo. Previous work using low-density lipoprotein (LDL), a classic extracellular cargo, demonstrates that the enzyme-mediated degradation of LDL occurs in a hybrid late endosomal-lysosomal vesicle[i]. In addition, the degradation of LDL occurs within 60 s of the colocalization of LDL with a lysosomal protein, LAMP1. These observations suggest that lysosomes are responsible for delivering enzymes to late endosomes, forming a hybrid organelle in which degradation occurs. Using single particle tracking fluorescence microscopy, we investigate the hypothesis that lysosomes serve as enzyme storage vesicles. We test this hypothesis using two different approaches. The first approach uses cell-permeable drugs that inhibit specific enzymes known to degrade LDL; CA074ME, a cathepsin B inhibitor, and pepstatin methyl ester, a cathepsin D inhibitor. The second approach uses siRNA to knockdown expression of LAMP. Unique to these experiments is the ability to directly monitor, in intact live cells, LDL degradation utilizing a fluorescence labeling scheme that reports on the integrity of the LDL particle. This method involves conjugation of distinct fluorophores to the protein and lipid components of LDL. Upon degradation the protein reporter decreases in fluorescence intensity while the lipid reporter increases fluorescence intensity. Our experiments make it possible to describe the complete endocytic pathway of LDL from internalization to degradation and provide a more complete picture of the intracellular degradation of extracellular cargo.

[i] W.H. Humphries IV, N.C. Fay, and C.K. Payne, *Intracellular degradation of low-density lipoprotein probed with two-color fluorescence microscopy*, Integrative Biology, in press, (2010).

3340-Pos Board B445

Superresolution Imaging of Intact Microbial Communities Reveals Molecular Architecture of Biofilm Development and Bacterial Organization

Veysel Berk, Nicholas Fong, Graham Dempsey, Omer Develioglu, Xiaowei Zhuang, Fitnat Yildiz, Steve Chu.

Most bacteria live as a biofilm community in their natural habitat. This surface-attached social life form is commonly found in antibiotic-resistant infections and chronic diseases. For example, bacterial biofilms are a leading cause of lung infection and death among cystic fibrosis patients. Biofilms are also crucial for bioenergy research since cellulose degrading bacteria in the gut of termites are organized as heterogenic biofilms and believed to communicate throughout these tissue-like structures. To gain structural and molecular insight on biofilm formation, we imaged intact bacterial biofilms at different developmental stages without using any fixing agents by STORM microscope. These three-dimensional superresolution images revealed ten to twenty biofilm-promoting exopolysaccharide-rich regions that are sparsely distributed on the cell surface. A few hours after surface attachment of bacteria, these small globular structures expanded to ~100 nm in size and protruded from the cell surface. During the initial stage of biofilm formation, we observed extensive interactions among neighboring cells through these globular exopolysaccharides. Moreover, we identified straight cable-like cell-to-cell and cell-to-substrate connections, up to 5 microns in length, originating from globular structures. These physical interactions may explain how bacteria form initial microcluster on the surface, first stage of commitment to biofilm formation. Microcluster formation depends on bacterial twitching motility on the surface and exopolysaccharide synthesis.These results are shifting the paradigm in the biofilm field which states that bacteria are randomly embedded in an extracellular matrix in biofilms. Our data suggests that bacteria actively build their house similar to a spider web by synthesizing sticky globular polysachharides on the cell surface, which are then extended to cable-like structures by twitching motility on the surface.

3341-Pos Board B446

3D Tracking of Single Fluorescent Particles with Sub-Millisecond and Nanometer Resolution

Joerg Bewersdorf, Manuel F. Juette.

Observing dynamics at the nanoscale requires sub-millisecond time resolution. Notably, in studying biological systems, three-dimensional (3D) trajectories of fluorescently labeled objects such as viruses or transport vesicles often need to be acquired with high temporal resolution.

Here, we present a novel instrument (1) which combines scanning-free multiplane detection at 3.2 kHz frame rate and single photon sensitivity with optimized beam-steering capabilities. This setup enables ultrafast 3D localization with sub-millisecond time resolution and nanometer localization precision. We demonstrate 3D tracking of single fluorescent particles at speeds of up to 150 nm/ms over several seconds and large volumes. By focused excitation of only the particle of interest - while avoiding confocal pinholes - the system realizes maximum detection efficiency at minimal laser irradiation. These features, combined with the avoidance of stage movement, provide high live-sample compatibility for future biomedical applications.

Next to the characterization of the instrument, we will show first biomedical applications.

(1) Juette, M.F. and Bewersdorf, J., Nano Letters, in press

3342-Pos Board B447

Fluorinated Membrane Potential Probes

Ping Yan, Adrian Negrean, Huibert D. Mansvelder, Leslie M. Loew.

To explore the effect of fluorination on photophysical properties of membrane potential probes, we developed synthetic methods for ANEP dyes with fluorine substitutions at the donor, bridge, and acceptor sides. Fluorination on acceptor side induces red shifts in optical spectra while on donor side it induces blue shifts. The trend can be qualitatively rationalized as electron redistribution from donor in the ground state to acceptor in the excited state, and quantitatively predicted by quantum mechanical calculations using time-dependent density functional theory (TDDFT). Compared with parent ANEP dyes, fluorinated dyes generally show improved photostabilities in addition to similar fast response kinetics and high voltage sensitivities when tested in a voltage-clamped hemispherical lipid bilayer (HLB) apparatus. The characteristics of red-shifted absorption spectra, improved photostability, and high voltage sensitivity have enabled us to achieve a single trial resolution of 50 mV in two-photon imaging of cultured hippocampal neurons using 1100-1350 nm laser excitation, paving the way for in vivo imaging of spontaneous action potentials. (Supported by NIH grants EB001963).

3343-Pos Board B448
Combining DNA Nanotechnology and Fluorescence Polarization Microscopy to Determine the Orientation of DNA Bound Fluorophores
Deborah K. Fygenson, Christoph Schneider, Hunter Banks.
We determine the orientation of the transition dipole moment of a fluorophore bound to dsDNA using fluorescence polarization microscopy and compare with published results. We use DNA nanotubes to present the dsDNA in a known orientation and query a variety of intercalating (e.g., YOYO, TOTO), groove-binding (e.g. DAPI) and covalently linked (e.g., Fluorescein, Cy3, Cy5) dyes. We use a de Sénarmont prism in front of the camera to record simultaneous images of fluorescence polarized perpendicular and parallel to the DNA nanotube axis, making the associated polarization ratios insensitive to photobleaching. Our results suggest this technique can be used to detect helical supertwist, and possibly other nanoscale structural features, of DNA nanostructures.

3344-Pos Board B449
3D Visualization of Mitochondrial Network and Nucleoids of mtDNA in Ins1E and HepG2 Cells at 30 Nm Resolution by Biplane FPALM Microscopy
Andrea Dlaskova, Jitka Santorova, Michael J. Mlodzianoski, Tomas Spacek, Katarina Smolkova, Jan Tauber, Joerg Bewersdorf, **Petr Jezek**.
Three-dimensional (3D) super-resolution microscopy, using a biplane detection scheme, termed biplane photo-activated localization microscopy (Biplane FPALM), enables imaging of volumes as thick as whole cells and could reveal unknown details of cellular organization. Hence, we attempted to visualize mitochondrial reticulum via the matrix space loaded with mitochondria-addressed Eos, while transfecting cells by lentiviral expression. Our 3D images of single Eos molecules in the matrix space have proven the continuous character of mitochondrial reticulum tubules, i.e., an existence of a highly interconnected major mitochondrial reticulum in insulinoma Ins1E and oxidative-phosphorylation-dependent glutaminolytic hepatoma HepG2 cells (Fig.1). Also, using Eos-conjugate of mitochondrial transcription factor-A (TFAM), we have imaged nucleoids of mitochondrial DNA (mtDNA) in which TFAM represents a major assessor protein. Using PA-CFP2-TFAM and mitochondria-addressed Eos, the first 3D two color super-resolution images were obtained for mitochondrial reticulum together with the distribution of mt nucleoids in it. In intact cells we have found mt nucleoids of a narrow size distribution.

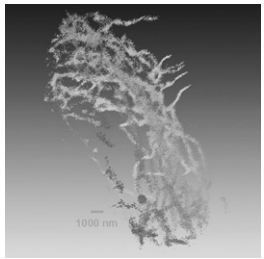

Supported by grants No. M200110902, IAA500110701, from Acad.Sciences, and AMVIS/ME09029 from Czech Ministry of Education.

3345-Pos Board B450
Photoactivatable Hemicyanine Chromophores as Fluorescent Lables
Na Liu, Stacy Wilson, Leslie M. Loew.
A series of photoactivatable hemicyanine chromophores containing azido group instead of the usual amino donor group has been designed and synthesized. Before photolysis, these compounds have negligible fluorescence. Upon photolysis, a molecule of nitrogen is lost from the azido group leaving behind a highly reactive nitrene moiety, which can react with and crosslink neighboring molecules to produce an amine. This fully restores the ''push-pull'' environmentally sensitive hemicyanine chromophore. If the molecule is in a cell membrane it will covalently crosslink lipid or protein molecules and remain relatively immobile. The photoactivity of the dyes was tested on neuroblastoma cells by selectively shining near UV or visible light on a small region of the cell and then observing the whole cell's fluorescence using a confocal microscope. This experiment shows strong fluorescence primarily in the illuminated area, which proves that we can selectively and stably stain a portion of the cell membrane using these photoactivatable hemicyanine dyes. The photoreleased dyes are fluorescent in the membrane because the amino-chromophore is similar to our voltage sensitive ASP and ANEP chromophores. These compounds are promising as targetable sensors of membrane potential. (This work is supported by Human Frontier Science Program grant RGP0027/2009 and NIH grant R01EB001963.)

3346-Pos Board B451
Nuclear Receptor (PXR), Ligand and Co-Activator Interactions Measured by Total Internal Reflection Fluorescence Microscopy
Punya Navaratnarajah, Bridgett L. Steele, Matthew R. Redinbo, Nancy L. Thompson.
The pregnane X receptor (PXR) is a member of the nuclear receptor family. PXR acts in a ligand-dependent manner, in concert with its dimerization partner, the retinoid X receptor, and co-regulators, to modulate the expression of proteins that metabolize endogenous and exogenous compounds. Here, we report the use of total internal reflection fluorescence microscopy (TIRFM) for examining interactions between the ligand-binding domain of PXR (PXR-LBD), its ligands, and a peptide derived from a co-activator. TIRFM is a surface-specific technique that enables us to study the behavior of fluorescent species close to or at interfaces. Our experimental system consists of biotinylated PXR-LBD immobilized on a fused silica substrate coated with NeutrAvidin and ovalbumin, a ligand (e.g., the antibiotic rifampicin) and a fluorescently labeled, 25 amino acid fragment of the steroid receptor co-activator-1 (F-SRC-1). Using TIRFM, we measured the surface-associated fluorescence as a function of the F-SRC-1 concentration at fixed ligand concentrations. These curves were fit to a model of single-site binding to obtain apparent equilibrium constants. The apparent equilibrium constants as a function of ligand concentration were fit to an appropriate model to obtain binding constants for the ligand/PXR-LBD interaction, F-SRC-1 binding to apo and ligand-bound PXR-LBD and ligand binding to F-SRC-1-bound PXR-LBD. The approach yielded four, previously unmeasured, binding constants. These values indicate that the increase in PXR's affinity for its co-activator peptide upon binding an activating ligand is modest. This observation implies that for gene expression to be significantly upregulated, the signal arising from the activation of PXR must be amplified downstream - possibly when co-activators like SRC-1 start recruiting the cell's transcription machinery. Kinetic data obtained by combining TIR illumination with fluorescence recovery after photobleaching and/or fluorescence correlation spectroscopy may also be discussed.

3347-Pos Board B452
Measuring Surface Binding Thermodynamics and Kinetics by using Total Internal Reflection with Fluorescence Correlation Spectroscopy: Practical Considerations
Xiang Wang, Punya Navaratnarajah, Nancy L. Thompson.
The combination of total internal reflection illumination and fluorescence correlation spectroscopy (TIR-FCS) is an emerging method useful for, among a number of things, measuring the thermodynamic and kinetic parameters describing the reversible association of fluorescently labeled ligands in solution with immobilized, nonfluorescent surface binding sites. However, there are many parameters (both instrumental and intrinsic to the interaction of interest) that determine the nature of the acquired fluorescence fluctuation autocorrelation functions. In this work, we define criteria necessary for successful measurements, and then systematically explore the parameter space to define conditions that meet the criteria. The work is intended to serve as a guide for experimental design; in other words, to provide a methodology to identify experimental conditions that will yield reliable values of the thermodynamic and kinetic parameters for a given interaction. In vitro experiments to verify the theoretical predictions will be also provided.

3348-Pos Board B453
Hyperspectral Raman and Fluorescence Microscopy of Individual Algal Cells for Biochemcial Analysis
Aaron M. Collins, Howland D.T. Jones, Thomas E. Beechem III, Ryan W. Davis, Qiang Hu, Anthony E. McDonald, Jerilyn A. Timlin.
Green algae are photosynthetic microorganisms, similar in many ways to plants, that fuel cellular processes with biochemical energy derived from sunlight. Algae are known to produce and accumulate triacyglycerol (TAG) or lipid under certain stress conditions. Subsequently, algae have garnered significant research interest as candidates to produce the next-generation of advanced biofuels because lipds are convertible into biodiesel. Therefore, there is significant interest to develop methodologies and analytical tools to characterize and understand lipid biosynthesis in living algal cells.
Raman spectroscopy offers excellent chemical and spatial resolution of the carotenoid, TAG and TAG precursor compounds, while fluorescence spectral information provides complimentary and confirmatory information about the photosynthetic pigments. The combination of Raman mapping and hyperspectral fluorescence imaging can provide critical insights into the spatial biochemical makeup of algal cells. Additionally, since each algal species has its own unique set of carotenoids, the carotenoid signatures present an opportunity for identifying algae at the taxonomic group and possibly even at the species level. Here, we present a novel use of confocal Raman mapping and hyperspectral confocal fluorescence microscopy paired with multivariate curve resolution to investigate carotenoid and lipid spectral signatures in several algal strains. We will 1) Identify algal species from mixed samples based on carotenoid spectroscopic signatures 2) localize, identify and quantify carotenoid distribution in individual algal cells and 3) determine the lipid content of individual cells from several algal species. This novel approach will demonstrate the feasibility of visualizing biochemical processes in live algal cells using spectroscopic imaging techniques.

*Sandia is a multiprogram laboratory operated by Sandia Corporation, a Lockheed Martin Company, for the United States Department of Energy's National Nuclear Security Administration under contract DE-AC04-94AL85000.

3349-Pos Board B454

Analyzing Aβ Aggregates with High Resolution Microscopy

Pia Zißmann, Aileen Susanne Funke, Stephanie Grabowski, Stefan Marawske, Lei Wang, Markus Richert, Ralf Kühnemuth, Eva Birkmann, Claus Seidel, Dieter Willbold.

In a world where more people grow older aging-related neurodegeneration like Alzheimer's disease (AD) affects more and more people.

Today, AD can be diagnosed with certainty only post mortem, detecting insoluble β-amyloid peptide (Aβ) aggregates and neurofibrillary tangles in the patient's brain tissue. Aggregates consisting of Aβ are a fundamental pathologic feature of AD. Today in many studies, concentrations of monomeric Aβ in body fluids are investigated, especially for diagnostic purposes. Nevertheless, for the detection, quantitation and qualification of aggregated pathologic Aβ forms, also in the course of aging, a highly sensitive detection assay system for aggregated Aβ species is necessary.

We developed an ultra-sensitive assay for the detection of aggregated protein species out of body fluids. This highly specific and sensitive assay uses confocal fluorescence spectroscopy methods and is sensitive enough to detect single aggregates. For the procedure, pathologic aggregates out of body fluids are immobilized on a glass chip, subsequently fluorescence labeled and detected via confocal spectroscopy.

Actually, we are optimizing the assay in concerns of instrumentation (imaging) and microscopy high-resolution and even super-resolution methods. We are developing methods to analyze aggregates via super-resolution microscopy. Setups like PAINT (Point Accumulation for Imaging in Nanoscale Topography) or STORM (Stochastic Optical Reconstruction Microscopy) allow resolutions in nanometer-range. PAINT is based on replacing the point-spread-function (PSF) of a fluorophore by a point in the middle of a 2D gaussian fit. First measurements show resolutions of 30 nm. STORM is based on high-accuracy localization of photoswitchable fluorophores. During one imaging cycle, only a small part of the fluorophores is turned on. This allows a high accuracy in determining the fluorophore position by replacing the PSF. The fluorophore positions obtained from a series of imaging cycles can be used to reconstruct the whole image.

3350-Pos Board B455

Real-Time Hyperspectral Imaging of Multiple Biosensors in Pancreatic Beta Cells

Amicia D. Elliott, Liang Gao, Alessandro Ustione, Tomasz S. Tkaczyk, David W. Piston.

Spectral imaging techniques are important for many biological experiments, particularly live-cell quantitative imaging of multiple fluorescence probes. Existing hyperspectral imaging systems require sequential techniques, limiting the data acquisition rate. A newly-developed snapshot device, the Image Mapping Spectrometer (IMS), acquires full spectral information simultaneously from every pixel in the field with image acquisition rates up to 10 frames/second. The IMS maps adjacent pixels from the object to create space between them in the image, and then uses a grating to spread wavelength content from each pixel into this space. Direct image re-mapping provides the final 3D (x, y, lambda) data cube.

Fluorescent protein (FP)-based biosensors are increasingly valuable tools for identifying subcellular dynamic processes in live cells. Many biosensors are based on FP-FRET, and measurements of the resultant small changes in FRET require high quality data. Tracking intracellular free Ca^{2+} levels is also crucial to elucidating signaling events, but the best Ca^{2+} indicator dyes overlap in the spectral emission range of the common FP-FRET biosensors. We have used the IMS system to simultaneously image multicolored FPs (i.e., CFP, GFP, YFP) in combination with extrinsic indicator dyes, such as Fluo-4.

To demonstrate the speed and resolution of the IMS approach, we monitored both intracellular Ca^{2+} oscillations and caspase-3 activity during hydrogen peroxide-induced apoptosis. Ca^{2+} activity was measured with Fluo-4 (emission peak at 517 nm) and caspase-3 activity was measured with SCAT3.1, a FRET biosensor based on the ECFP (emission peak at 484 nm) and EYFP (emission peak at 527 nm) pair. Using the IMS, the three fluorophores were imaged with sub-second temporal resolution and spectrally unmixed in real-time. This permits direct correlation of Ca^{2+} activity with other apoptotic signaling events and demonstrates the power of the IMS for measuring dynamic physiological processes.

3351-Pos Board B456

In Vivo Fluorescence Imaging of Blood Flow in Mouse Pancreatic Islets

Kurt W. Short, W. Steve Head, Michael McCaughey, David W. Piston.

Diabetes is a disease resulting from changes in pancreatic islets, which are insulin secreting micro-organs within the pancreas. With increased blood glucose, insulin is secreted from beta cells in the islets in a coordinated pulsatile manner. At the same time alpha cell glucagon secretion is inhibited. Mechanisms controlling these processes at the intercellular and at the inter-islet level remain unclear. We suggest that the three-dimensional organization of islet cells and the dynamics of islet blood flow have a role in regulating insulin and glucagon secretion. This is suggested by observation that the density of blood vessels within islets is much greater than in surrounding pancreatic tissue, and that most individual islet cells are adjacent to a blood vessel. As an initial test of our hypothesis, we have developed a high-speed in vivo fluorescence imaging method to track pancreatic blood flow in a living mouse. We are also developing methods necessary to analyze the large amounts of data generated. Using high speed line scan confocal microscopy the method has full frame sub-micron spatial and less than 10 ms temporal resolution. Islets are located within the pancreas by using mice with GFP-labeled beta cells. Blood plasma is labeled with a fluorescent dextran, allowing mapping of vascular dimensions and pathway. Individual blood cells are fluorescently labeled by osmotic shock loading with an Alexa dye, which allows tracking of the blood flow. We present current results for blood flow under different levels of blood glucose in clamping experiments. Our previous qualitative results have suggested that there are differences in blood flow parameters at different glucose levels. Here, a more quantitative analysis of blood flow velocity, any observed changes in vessel dimensions, and changes in blood flow coverage inside and outside islets is presented.

3352-Pos Board B457

Superresolution Optical Microscopy of Isolated Cardiac Mitochondrial Proteins

Harpreet Singh, Pedro Felipe, Gardeazábal Rodríguez, Rong Lu, Jean Chrisostome Bopassa, Yong Wu, Ligia Toro, Enrico Stefani.

To study the structural organization of mitochondrial proteins, we applied Stimulated Emission Depletion (STED) microscopy in isolated mitochondria. In STED microscopy, two laser beams are used: one for excitation of fluorophores and the other, with doughnut shape, to deplete them in order to allow fluorescence emission only from the excited volume located at the doughnut's center. With STED a lateral resolution of ~45 nm was achieved in images of isolated mitochondria. We investigated the localization pattern and distribution of MaxiKα, COX4 and VDAC1. After a combined analysis of classical confocal and STED images, we found distinct distributions for VDAC1, MaxiKα and COX4. COX4 distribution was consistent with localization in the cristae. We established that there are 7-15 clusters of MaxiKα, 10-15 clusters of VDAC1, and 15-20 clusters of COX4 per mitochondria. We have demonstrated that protein clusters in the mitochondria can be resolved with a separation power of ~45 nm, and that it is possible to retrieve quantitative information about the number of clusters and density of proteins in mitochondria. This approach can be extended to eins in mitochondria and subcellular organelles. Supported by NIH.

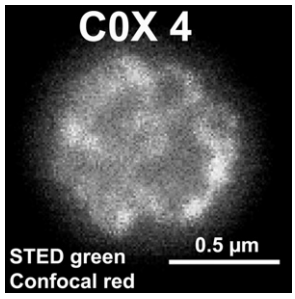

3353-Pos Board B458

Zero-Mode Waveguides: A Powerful Tool for Single-Molecule Optical Studies

Zhuangxiong Huang, Serge Donkers, Nynke H. Dekker.

Single-molecule fluorescence studies of enzymes that incorporate fluorescently labeled substrate nucleotides typically operate at substrate concentrations well below their K_m values. While this is inevitable in conventional fluorescence microscopy, the biological relevance of the insights gained into enzyme mechanism may be compromised. Zero-mode waveguides (ZMWs) provide an excellent solution to this problem by greatly reducing the observation volume. We report the nanofabrication of ZMWs, the surface treatment for controlled immobilization of biomolecules and the reduction of background noise. We also present the development of an assay to monitor in real time the incorporation of fluorescently-labeled nucleotides, which paves the way for the studies of nucleic acid polymerizing enzymes, e.g. DNA/RNA polymerase, reverse transcriptase, telomerase, etc.

Biotechnology & Bioengineering II

3354-Pos Board B459

Recombinant MG53 Binds Lipid Signals on Damaged Cell Membranes to Increase Membrane Repair Capacity

Noah Weisleder, Norio Takizawa, PeiHui Lin, Tao Tan, Pinjung Chen, Rosalie Yan, Xiaoli Zhao, Moonsun Hwang, Hiroshi Takeshima, Jianjie Ma.

Plasma membrane repair is a highly conserved mechanism that appears in most eukaryotic cells. While a simple lipid bilayer will reseal through thermodynamic principles, the presence of a cytoskeleton results in the native plasma membrane being held under tension, thus some disruptions the plasma membrane cannot spontaneously reseal. Previous studies established that plasma membrane repair is an active process involving translocation of intracellular vesicles to the injury site and fusion of these vesicles to form a repair ''patch''. An emerging concept in cell biology establishes this intrinsic membrane repair/regeneration process is a fundamental aspect of normal physiology and that disruption of this mechanism underlies the progression of many human diseases, including cardiovascular disease, neurodegeneration, ischemic injury and muscular dystrophy. We recently discovered that mitsugumin 53 (MG53/TRIM72) is an essential component of the cell membrane repair. In this study we tested the translational value of targeting MG53 function in tissue repair and regenerative medicine using in vitro cell based assays and animal models. While native MG53 protein is restricted to striated muscle, beneficial effects against cellular injuries are present in non-muscle cells with overexpression of MG53. In addition to the intracellular action of MG53, acute injury of the cell membrane leads to exposure of lipid signals that can be detected by MG53, allowing recombinant MG53 to repair membrane damage when provided in the extracellular space. Human MG53 protein retains dose-dependent protection against membrane disruption in both muscle and non-muscle cells. Intravenous delivery of MG53 protein is safe in rodent models, with suitable pharmacokinetic properties that are highly effective in restoring or preventing localized damage to muscle tissues. Our data indicate the MG53 protein is an attractive biological reagent for restoration of membrane repair defects in human diseases.

3355-Pos Board B460

Measurement of Platelet Activation with Anti-P-Selectin Coated Magnetic Microparticles

Loes van Zijp, Arthur M. de Jong, Nona Jongmans, Thijs C. van Holten, Mark Roest, Menno W.J. Prins.

Under normal conditions, platelets have very little interaction with each other or with other cells. However platelets become activated for instance, when they are exposed to collagen by vascular damage. Upon activation, several molecules get exposed on the cell membrane to support adhesion, spreading and aggregation of the platelets onto the damaged vessel. Platelet activation is involved in cardiovascular diseases. Traditionally, platelet activation is quantified with fluorescent markers in combination with flow cytometry. However flow cytometry requires complex and expensive equipment.

We are studying novel technologies for platelet activation biosensors that are inexpensive and require minimal sample preparation. We present a proof of principle measurement of platelet activation with magnetic particles. Particles coated with anti-P-selectin were used to remove activated platelets from samples stimulated with different concentrations of activation agonists. We analyzed the platelet activation level by measuring the remaining unbound cells in the solution. We compared our new approach to traditional flow cytometry and found good agreement (figure).

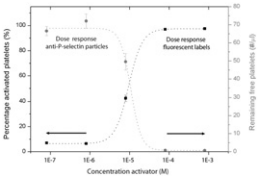

Our cell removal assay has the potential to be used in integrated cell biosensors which don't rely on fluorescent labeling and detection of cells.

3356-Pos Board B461

Highly Parallel Planar Patch Clamp for Ion Channel Screening

Andrea Brüggemann, Claudia Haarmann, Cecilia Farre, Juergen Steindl, Christian Patzig, Timo Stengel, Christian Grad, Johannes Stiehler, Michael George, Niels Fertig.

To meet the ever increasing demand for higher throughput in ion channel screening and safety testing, new platforms are being introduced allowing for yet more throughput whilst retaining data quality. A new platform recording from 96 cells at a time with giga-seals, with continuous recording during compound application and addition of multiple compounds to each of the 96 cells being recorded will be described. This new platform vastly increases throughput, while reducing the cost per data point. Borosilicate glass substrates containing microstructured apertures are used for parallel patch clamp experiments. In the figure below, a screenshot of an experiment on 96 cells in a parallel is displayed. Shown are raw current responses of $Ca_V3.2$ channels expressed in HEK293 cells to a current voltage relationship step protocol.

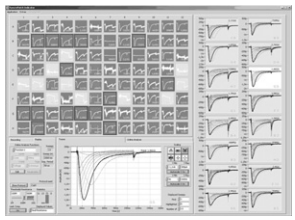

Recordings from various ligand- and voltage-gated ion channels on this platform will be shown.

3357-Pos Board B462

Piezoelectric Planar Patch Clamp System for Mechanically Actuating Ion Channels

Eric Stava, Minrui Yu, Hyuncheol Shin, Jonathan Rodriguez, Robert H. Blick.

Piezoelectric substrates enable the generation of mechanical forces with Angstrom resolution via an applied voltage. When using such a substrate for planar patch clamp experiments, these deformations will induce tension in the lipid membrane. This will, in turn, affect the conductive properties of any mechanosensitive ion channels in the membrane, as well as mechanically perturb any other proteins embedded in the cell membrane. We show that an applied electric field induces structural changes in our piezoelectric quartz substrates and, thus, to the micron-sized pores in the quartz. By affecting the electric field across the quartz substrate, we can precisely control the deformation of the pore. We also find that this field does not have an effect on the electric field across the pore. Therefore, it will not directly affect the electrical properties of the ion channels under test. Further, we have incorporated ion channels into this system, and demonstrate that the applied electric field alters the conductive properties of the ion channels. We, thus, show a device capable of actuating ion channels under a range of complex, finely-tunable mechanical stimuli.

3358-Pos Board B463

Multisuction Electrode Arrays to Investigate Multi-Sensory Integration in Neural Tissue

John M. Nagarah, Pieter Laurens Baljon, Daniel A. Wagenaar.

We are studying the neuronal basis of multisensory integration in the medicinal leech, a model animal with a well-characterized and relatively simple nervous system. We aim to discover how the leech's nervous system combines biologically relevant mechanical and visual sensory cues in order to come to a coherent decision about subsequent motion. One goal is to characterize the neural computation that occurs in the leech ganglion, where processing for most described leech behaviors occurs, while visually and mechanically stimulating the leech preparation. Specifically, we will interrogate all the neurons in the ventral side of the ganglion simultaneously at the single cell level by combining multielectrode array (MEA) recordings with voltage sensitive dye (VSD) imaging. The excellent spatial resolution of the VSDs combined with the temporal resolution of MEAs will provide a high level of detail of this computation in the ganglion. We enhanced the MEA design by fabricating optically transparent multi-suction electrode arrays (MSEAs). Each electrode in an array of 60 is constructed around a microfabricated suction pore. Directed suction holds neurons closer to the electrodes and immobilizes tissue without physical distortion, resulting in more stable recordings. The MSEA fabrication protocol builds upon a previously described batch-fabrication technique to make planar patch-clamp electrodes; thus, an entire array of an arbitrary number of pores and devices can be created simultaneously. We are exploiting this by making devices for our collaborators in parallel with our MSEA devices in order to study network behavior in mouse hippocampus slices, and ion channels in giant unilamellar vesicles (GUVs) and mammalian cells.

3359-Pos Board B464

Dual Micropores in Glass Substrates for Ion Channel and Gap Junction Recording

Brandon Bruhn, Stefan Schuhladen, Ran An, Michael Mayer.

Despite the commercial success of automated high-throughput patch clamp technologies, instruments on the market typically cannot match the quality of single-channel recordings obtained by traditional patch clamp experiments with glass micropipettes. In automated approaches that use suction to position a cell to a micropore, the inner surface of the pore can be contaminated with proteins in solution prior to seal formation. Traditional patch clamping avoids this problem by applying a positive pressure to the micropipette prior to contacting the cell membrane, which enables significantly higher electrical seal resistances. This research aims to develop a universal platform for high-quality transport assays on glass chips that circumvents the problem of surface contamination and takes advantage of the high seal resistances and low capacitive

current noise realized with glass substrates. Femtosecond laser ablation is used to fabricate a pair of micropores in close proximity to each other (distance < 5 μm) in glass, while the access channels to these pores are kept separate. This configuration makes it possible to use one pore for automated positioning of a cell by suction, while the other pore is kept clean by applying positive pressure. Once the cell is pre-positioned onto the first pore, suction may be applied to the second pore to establish a high quality seal that could be used to interrogate individual transmembrane transporter proteins and single ion channel proteins. In addition, this dual micropore configuration may enable the first automated gap junction recordings, bypassing the difficulties of manually positioning two micropipettes.

3360-Pos Board B465

A Device to Measure Ligand- or Voltage-Gated Channels Simultanously in 384 Wells

Xin Jiang, Trisha Tutana, David Yamane, Yuri Osipchuk, Edward Verdonk, **James Costantin**.

We have developed patch clamping instrumentation to measure ligand-gated or voltage-gated ion channels (LGICs or VGIC) simultaneously in a 384-well microplate. The apparatus combines a 384-well pipettor with 384 amplifier and digitizers for parallel recording in all wells at once, no multiplexing is performed. We use the perforated patch clamp technique on a polyimide substrate and are able to record stable currents over tens of minutes. Currents are measured using either a single hole at each recording site or an array of 64 holes at each site (Population Patch Clamp or PPC, Finkel et al. 2006). PPC measures the ensemble current through all 64 cells in an individual well using a single pair of electrodes. We present here data from LGICs including GABA chloride channels, acid sensing ion channels (ASIC), nicotinic acetylcholine (α1 nACh) receptors, and VGICs including Na_V, K_V and hERG channels. Data will be presented on 10 - 90% exchange rates for individual wells using high K^+ solutions. Pharmacological data will be presented on the blockade of several channel types listed above to validate this type of apparatus as being appropriate for screening ion channel targets in a drug discovery setting. Ref: Finkel, A. et al. (2006). J Biomol Screen **11**(5): 488-96.

3361-Pos Board B466

Development of a GPCR Based Electrophysiological Biosensor

Masato Suzuki, Shigeki Kiyonaka, Tomohiro Numata, Ken Shimono, Hiroaki Oka, Yasuo Mori.

G-protein coupled receptors (GPCRs), which can recognize various extracellular compounds, including hormones, neurotransmitters and chemical molecules such as odors and flavors, represent the largest superfamily of cell surface receptors. Moreover, it was estimated the 25 % of the 100 top-selling drugs targeted GPCRs. For these reasons, it is desirable to develop a robust, reliable, and cost-effective functional screening technique for compounds related to the GPCR in pharmaceutical industry.

We have developed a new platform to detect chemical compounds binding to a GPCR by using a hybrid G-proteins which could transmit the signal from the Gs/olf-coupled GPCRs to the inward rectifier potassium channels (Kir 3). To improve the receptor coupling profile, fifteen kinds of the hybrid G-proteins were designed by swapping some domains of Gαi protein to corresponding amino acids of Gαolf protein.

For evaluation of signal transduction from GPCR to ion channel, each hybrid G-protein was heterogeneously expressed in HEK-293T cells with mutated potassium channel (Kir 3.1 (F137S)) and β1 adrenergic receptor, which could not activate Kir 3. By utilizing of a hybrid G-protein, which was replaced with 94 amino acids from C-terminal, dramatically change of inwardly rectifying K^+ current was occurred in the presence of β1 agonist (30 nM isoproterenol). Moreover, the lower detection limit was possible to detect even 30 pM isoptoterenol (EC50 = 1 nM).

Thus, this new sensing platform based on a hybrid G-protein might provide a powerful method to screen drug compounds targeting for GPCR.

3362-Pos Board B467

Lowering Series Resistance in Whole-Cell Patch Clamp Experiments using the Pushpen Patch Clamp Electrode

Samsoon Inayat, Lawrence H. Pinto, John B. Troy.

Series resistance introduces voltage clamp errors in whole-cell patch clamp experiments and reduces the bandwidth of recordings by forming a low-pass filter with the cell membrane capacitance. The bulk of the series resistance is located at the pipette tip. During an experiment, cellular debris or membrane fragments can clog the tip and result in an increase in resistance. This effect is most notable when recording from small neural structures, as the pipette tip used is smaller than usual then. An increase in series resistance seriously limits the duration of recording and the reliability of the data recorded. The current procedure to lower series resistance is to apply gradual pulses of suction to clear the pipette tip of cellular debris or membrane, but this usually results in disruption of the gigaseal and ends the experiment. We introduce a new procedure for clearing clogged tips using our Pushpen patch clamp electrode.

The Pushpen patch clamp electrode is a novel electrode for whole-cell patch clamp experiments, in which a linear motor moves a conical tungsten wire wound with Ag/AgCl wire, linearly inside the pipette. The tungsten wire tip can protrude from the pipette tip like a push pen, the procedure we call the ''pushpen operation''. Using the pushpen operation, we obtain whole-cell configuration from cell-attached without applying suction but by impaling the cell membrane with the tungsten wire tip, while maintaining gigaseal. Currently we are working to demonstrate that we can lower series resistance during an experiment by using the pushpen operation to clear a clogged pipette tip and thus prolong the lifetime of experiments.

3363-Pos Board B468

Limitations of Equivalent Circuit Models in Data-Driven Simulation of the Neuron-Electrode Interface

Vaibhav Thakore, Peter Molnar, James J. Hickman.

Noninvasive neuroelectronic interfacing has important applications in the fields of neural prosthetics, biological computation and biosensors. Traditionally, neuron-electrode interfaces have been modeled as linear point or area contact equivalent circuits but such models have not been able to explain the shapes and magnitudes of the experimentally recorded extracellular signals. Also, previous work with Volterra-Wiener characterization of the planar neuron-microelectrode junction using bandlimited Gaussian white noise had shown that the mechanism of signal transduction across the nanoscale neuron-microelectrode cleft region might be nonlinear. In this optimization based study we compared and contrasted experimental and simulation data for point contact models of the extracellular 'on-cell' neuron-patch electrode and the planar neuron-microelectrode interface. The nonlinear contributions of the neurons to the dynamics of the equivalent circuit representation of the interfacial medium were systematically isolated by an independent estimation of the ion-channel parameters through a fitting of the simulated intracellular signals to the experimentally recorded voltage and current clamp signals. These ion-channel parameters were then employed in the optimization of the cell-electrode interface parameters based on extracellular recordings obtained from a neuron simultaneously interfaced to the 'on-cell' patch-electrode and the planar microelectrode using sub- and supra-threshold stimuli. An examination of the optimized model parameters for the experimental extracellular recordings from sub- and supra-threshold stimulations of the neuron-electrode junctions allowed us to draw important distinctions between the 'on-cell' neuron-patch electrode and neuron-microelectrode interfaces that could be attributed to the presence of electric double layer (EDL) and ionic electrodiffusion effects. Based on these results, we then discuss and point out the limitations of the equivalent circuit models in their failure to take account of the nonlinear EDL and ionic electrodiffusion effects occurring during the process of signal transduction at the neuron-electrode interface.

3364-Pos Board B469

Cardiac Excitation-Contraction Coupling Proteins: A 3D Spatial Analysis

Evan I. Blumgart, Isuru D. Jayasinghe, Michael J. O'Sullivan, Christian Soeller, Cameron G. Walker, Vijay Rajagopal.

The vital heart beat that pumps blood around the body is caused by millions of cardiac muscle cells exciting and contracting in concert. Cellular contraction is inextricably linked to the sarcoplasmic reticulum (SR) release event and subsequent binding of Ca^{2+} to myofibril binding sites. An integral protein in the release event is the SR membrane bound Ryanodine Receptor (RyR). Ca^{2+} enters the narrow spaces between transverse tubules and the termini of the SR via voltage-gated L-type Ca^{2+} channels. It then binds to RyR's to evoke the release of more Ca^{2+} from the SR, into the cytosol. Mathematical models examining this mechanism of excitation-contraction coupling (ECC) have thus far lacked anatomically realistic parameters for representing the ultrastructure and the distributions of key proteins in these myocytes. Our work has focused on producing an anatomically correct 3D model of a healthy cardiomyocyte that represents the spatial organization of the different cellular components involved in ECC. To this end, this study seeks to develop and perform statistical analyses on the 3D spatial distribution of RyR's and other ECC proteins in the healthy cell. Using immunofluorescence confocal microscopy images of rat ventricular muscle, we have carried out 3D spatial analyses which have enabled us to investigate the anisotropy, clustering, randomness and scatter of RyR's. We have also examined aspects of the spatial relationship between RyR's and myofibrils at Z-disks via the implementation of computational models. We have thus developed a novel anatomically based model of cardiomyocyte RyR distribution. This combined with models of other ECC component proteins, will enable us to gain new insights into the role of cardiomyocyte

ultrastructure in determining the spatiotemporal changes in intracellular Ca^{2+} which is central in ECC.

3365-Pos Board B470

Mechanisms Underlying Pulsed Infrared Stimulation of Cardiomyocytes

Gregory M. Dittami, Kenneth W. Spitzer, Suhrud M. Rajguru, Richard A. Lasher, Robert W. Hitchcock, Richard D. Rabbitt.

In this study, we investigated the origins of the endogenous cellular mechanisms underlying IR (1862 nm, 3-4 ms/pulse, 9.1 - 11.6 J/cm^2 /pulse, Capella, LHM Aculight) stimulation of neonatal rat ventricular and adult rabbit ventricular cardiomyocytes, *in vitro*. Confocal imaging (FV1000, Olympus; Fluo-4 AM, 4-6 μM, Invitrogen) of neonatal cardiomyocytes revealed IR-induced transient $[Ca^{2+}]_i$ responses consisting of a rapid $[Ca^{2+}]_i$ buffering component, discernable during periods of elevated $[Ca^{2+}]_i$, followed by consistent, subthreshold $[Ca^{2+}]_i$ rises that resulted in visible cell contractions with each IR pulse. Pharmacological block of the IR-evoked responses in neonatal cardiomyocytes with CGP-37157 (20 μM, N=12 cells) and Ruthenium Red (40 μM, N=13) suggested an integral role of the mitochondrial Ca^{2+} transporters in the IR-induced $[Ca^{2+}]_i$ cycling in neonatal cardiomyocytes. While initial results with adult cardiomyocytes during comparable IR stimulation also revealed visible contractile responses, the corresponding $[Ca^{2+}]_i$ transients were surprisingly not detected. To further investigate the response in adult cardiomyocytes, whole cell patch clamp measurements were performed to monitor sarcolemma membrane potential (V_m) changes during IR stimulation. Preliminary data revealed either depolarizing or hyperpolarizing V_m responses in the cells, the nature of which was determined by the relative timing of the IR pulse applications to threshold, electrically-induced cell depolarization. Based on these findings, additional efforts focused on resolving the extent and nature of this sarcolemmal involvement in the IR-evoked responses of both neonatal and adult cardiomyocytes.

3366-Pos Board B471

Macromolecular Crowding Facilitates Adipogenic Microenvironments for Human Mesenchymal Stem Cells

Felicia C. Loe, Krystyn Van Vliet, Michael Raghunath.

Mesenchymal stromal or stem cells (MSCs) are multipotent precursor cells in the bone marrow. The intended clinical applications of MSCs require ex vivo expansion to generate therapeutically relevant cell numbers, but extended propagation results in a loss of self-renewal capacity and multipotentiality. It is increasingly recognized that the microenvironment - including growth conditions and substrata - differ greatly from the original tissue microenvironments from which these cells are derived. The in vivo stem cell microenvironment is characterized by macromolecular crowding (MMC) due to the presence of extracellular macromolecules of molecular weight >50 kDa. In solution, it is known that such MMC generally accelerates macromolecular association kinetics, due to excluded volume effects. In contrast, current ex vivo culture systems are devoid of crowding. Here, we report the effects of a synthetic macromolecular crowder on the adipogenic differentiation of human MSCs. This MMC cocktail comprises a mixture of Ficoll70 and Ficoll400 with a hydrodynamic radius of ~4nm and ~13nm, respectively, resulting in a biologically relevant volume fraction occupancy of ~15%. We find that this maintenance of crowding more typical of in vivo environments substantially amplifies the adipogenic differentiation response, as compared to standard protocols of chemically induced differentiation. We show that this amplification was facilitated by the MMC-enhanced deposition and supramolecular assembly of extracellular matrix (ECM) components, and by more efficient lineage-specific remodeling of the ECM during differentiation. Further, decellularised ECM deposited by adipocytes under MMC drives naïve hMSCs into adipogenesis without chemical induction. This work demonstrates that in vivo levels of macromolecular crowding accelerate deposition of the ECM microenvironment, and that the application of MMC ex vivo can enhance hMSC differentiation potential via this matrix reciprocity.

3367-Pos Board B472

Effect of PDMS Nanopatterned Substrates on Embryonic Stem Cells Differentiation into Neuronal Lineage

Elisa Migliorini, Gianluca Grenci, Jelena Ban, Alessandro Pozzato, Maria Elisabetta Ruaro, Massimo Tormen, Vincent Torre, Marco Lazzarino.

Embryonic stem (ES) cell differentiation in specific cell lineage is a major issue in cell biology particularly in regenerative medicine. Differentiation is usually achieved by using biochemical factors which concentration and mechanism are not completely understood and with sides effects difficult to overcome. Using a substrate which mimics brain extracellular matrix it could be possible to induce ES-cells differentiation into neurons without adding any biochemical factors. Therefore, we produced patterns in polydimethylsiloxane (PDMS) consisting of groove and pillar arrays of sub-micrometric lateral resolution as substrates for cell cultures. Neuronal precursors from ES cells were obtained using a Stromal Cell-Derived Inducing Activity protocol and we analyzed the effect of different nanostructures on differentiation into neuronal lineage. Neuronal precursors adhered on PDMS more effectively than on glass coverslips. After 48 hours of culture on PDMS pillars with a 500nm period, neuronal differentiation increased and almost doubled with respect to flat PDMS substrates. Neuronal yield was enhanced by increasing pillars height from 35 to 400 nm. With pillars, 500nm period and 360nm height, the neuronal yield reached ~80% 96 hours after plating. However the largest differentiation enhancement of pillars over flat PDMS was observed during the first 6 hours of culture. These shown results that PDMS nanopillars accelerate ES cells differentiation into neurons.

3368-Pos Board B473

Wnt-Catenin Signaling System Functions in Embryoid Bodies Aggregated from Human Embryonic Stem Cell

Xuehong Xu, MengMeng Xu, Xunzhang Chen, Odell Jones, Harry Davis, Shangen Zheng, Joseph Bryant.

As an essential molecule in Wnt/β-catenin signaling, β-Catenin plays a crucial role in the decision making for tissue differentiation in embryogenesis and pathogenesis. The signaling was implicated in the development of skin. In mouse skin, the deferential fate of the skin stem cell depends on β-catenin, which organizes stem cells into follicular or epidermal lineages. These analyses indicate that Wnt/β-catenin signaling should also function in the development and differentiation of human embryonic stem cell. To study the function of β-catenin in early differentiation of human stem cells, we cultured H9 stem cell and aggregated them into embryoid bodies (EB). In this study, we revealed that in early EBs some guarding cells were first differentiated from EB stem cell aggregates. These early differentiated cells for guarding epithelial cells have strongest expression of β-catenin within EB. These cells were flattened on the surface of EB, covering the surface by connections formed through protein interactions. At certain confocal sections of EB, instead of a round boundary, a polygonal boundary was observed even though the EB appeared round under conventional microscope. In these polygonal boundaries, β-catenin positive guarding epithelial cells were positioned on every corner of the polygon. In the inner portion of the EB, undifferentiated β-catenin positive cells express β-catenin in the nucleus. As the initially simple shape of EB becomes more and more intricate during development, we revealed that more β-catenin positive cells were also observed in this complex structure. Based on these results, we predicted β-catenin to play different roles while guarding epithelial cells or undifferentiated stem cells in the inner portion of EB in *in vitro* culture system. Phosphorylation of β-catenin may be a critical factor for fate determination of the human stem cell.

3369-Pos Board B474

Interfacing Three-Dimensional Curved Structures and Cellular Adhesion

Mary E. Wilson, Nithyanand Kota, Burak O. Ozdoganlar, Yadong Wang, Donna B. Stolz, Philip R. LeDuc.

Curvature is a fundamental geometric design principle found in an array of biological systems, such as vasculature. Therefore, in studying cellular processes such as adhesion, proliferation and migration, it is important to consider the effects of curved 3D micro-topography as compared to flat 2D substrates, which are far more common. Creating these 3D curved systems requires novel approaches as well. Microfluidic devices would seem to be a good approach for this as they have often been utilized as a platform for studying cell adhesion and migration in vitro. However, the fabrication of curved, non-rectangular channels has been a major challenge to the field of microfluidics due to conventional fabrication methods. To overcome these limitations, we have developed a novel and robust approach using mechanical micromachining in combination with a two-step reverse polymer molding process to fabricate microfluidic channels with circular cross-sectional geometries. Here, we utilize these 3D microfluidic networks to study the effects of curvature on cell adhesion mechanics. Both fibroblast (NIH-3T3) and endothelial (HUVEC) cell lines were cultured within circular cross-section microfluidic channels and on reserve molded cylindrical curved polymers. Cell morphology on these curved versus flat substrates was then characterized via confocal and scanning electron microscopy. Furthermore, the formation of stable focal adhesions and cytoskeletal organization was analyzed by immunofluorescent confocal microscopy. We believe that this approach for fabricating bioinspired microfluidic systems provides a powerful platform for interfacing cellular interactions with curved 3D structures, which could be useful in a variety of fields from vascular biology and immune cell transmigration to cell mechanotransduction and tissue engineering.

3370-Pos Board B475

Hydrodynamic Trap for Single Cells and Micro- and Nanoparticles

Melikhan Tanyeri, Eric M. Johnson-Chavarria, Charles M. Schroeder.

Over the past twenty-five years, a diverse set of particle trapping and micromanipulation techniques have been developed to elucidate biological and biophysical mechanisms of proteins, nucleic acids, enzymes and cells. Many of the existing trapping methods rely on optical, magnetic or electric fields which are potentially perturbative to biological function. In this work, we present a novel flow-based confinement and manipulation method called the ''hydrodynamic trap'' which is based solely on hydrodynamic forces generated in a microfluidic device. The hydrodynamic trap is a non-contact confinement technique based on a stagnation point flow created at the junction of two perpendicular microchannels. In this way, the hydrodynamic trap enables free-solution trapping, manipulation, stretching and sorting of objects ranging from single molecules to individual cells. We successfully demonstrate trapping of single micro- and nanoscale particles (as small as 100 nm), single DNA molecules, and single cells for extended time scales with high resolution (within 1 μm for micron-sized particles) [1]. Trap stiffness was determined to be in the range $\kappa=10^{-4}$ -10^{-3} pN/nm, which compares favorably to magnetic and electrophoretic tweezers. Hydrodynamic trapping is feasible for any particle with no specific requirements on the material composition or the chemical/physical nature (optical, magnetic, surface charge) of the trapped object. The hydrodynamic trap inherently enables confinement of a single target object in dilute or concentrated particle or cell suspensions, due to the semi-stable nature of trapping potential. In summary, the hydrodynamic trap provides a new platform for observation of molecules, cells and particles without surface immobilization and offers the ability to vary the surrounding medium conditions of the trapped object in real-time.

[1] M. Tanyeri, E. M. Johnson-Chavarria, and C. M. Schroeder, ''Hydrodynamic Trap for Single Particles and Cells'' *Applied Physics Letters*, 2010, 96(22).

3371-Pos Board B476

A predicted Mechanism for Biological Effects of Radio-Frequency Electro-Magnetic Fields: Piezoelectric Rectification

William J. Bruno.

Currently, safety guidelines for exposure to radio-frequency radiation (RFR) from cellphones or other wireless devices consider only thermal heating. Although some non-thermal effects are well established experimentally (microwave hearing effect, cellular release of calcium and free radicals, stress response and DNA damage), for many effects the physical mechanism remains unclear.

It has long been known that bones, and in particular, the collagen in bones, exhibit the piezoelectric effect on the same scale (0.7 pC/N) observed in quartz crystals. It has been proposed that this effect is fundamental for regulating bone growth. Less well known is that piezoelectric substances have been shown to rectify RFR at frequencies up to at least 2.9 GHz. The rectified voltage is proportional to the power of the incident RF field. We claim, that exposures to cellphones, cordless phones, Wi-fi and microwave ovens may result in DC fields comparable to those used by the body to regulate growth of bones and possibly other tissues, given that collagens are found throughout the human body and throughout the kingdoms of life. The scale of such currents is a few milliamps or less, perhaps even less than a microamp. Applied DC electric fields of 1V/m can affect nerve firing rates.

In animal experiments, microwave exposure comparable to or weaker than a cellphone has caused permeabilization of the blood-brain barrier, an effect previously seen after brain stimulation with a DC current of 5 mA.

In the absence of a clear mechanism for explaining health effects (leukemia, Alzheimer's) associated with high-voltage transmission lines, biological rectification of RFR (present due to corona discharge and "dirty power") might play a role, as RFR is more penetrating than 60 Hz electric fields, and may induce more current than 60 Hz magnetic fields.

3372-Pos Board B477

Photothermal Poration of Cells using Carbon Nanoparticles

Ling Gu, Vijayalakshmi Varadarajan, Ali Koymen, Samarendra Mohanty.

Efficient and targeted delivery of impermeable exogenous material into cells in culture as well as in vivo is of great importance for drug and gene therapy. Traditional methods for drug delivery include viral vector, electroporation, ultrasound and chemical methods using liposomes, drug-loaded biodegradable polymer nanoparticles etc. However, highly spatial targeting of cells and efficient delivery of impermeable drugs can be achieved by laser microbeam. The only challenge has been to apply laser based poration for in vivo applications due to high peak power required for creating holes on the cell membrane. Here, we report efficient photothermal poration of cells using carbon nanoparticles (CNP) using very low power continuous wave laser beam. Scanning electron microscopy showed the localization of CNPs on membrane. For photothermal poration, a tunable (690-1040 nm) CW Ti: Sapphire laser beam was weakly focused on to the cell monolayer under an inverted fluorescence microscope. Irradiation of the CNPs near the desired cell(s) with near-infrared laser beam led to inject of impermeable dyes and YFP-tagged plasmids into the cells. Further, doping magnetic material into the carbon nanoparticles allowed localization of the nanoparticles in desired region by application of external magnetic field. This would be of high importance in minimizing the required number of injected nanoparticles. Due to significant absorption properties of the CNPs in the near-infrared spectrum of biological window, photothermal poration under in vivo condition is highly possible. Besides photothermal action, the CNPs can also be functionalized and used as controllable drug delivery vehicles because of their small size and interaction with biomolecules specific to cell membrane. The results of our study suggest that CNP based photothermal poration is a viable approach to remotely guide drug delivery offering high efficiency and significantly reduced cytotoxicity.

3373-Pos Board B478

Analysis of Single Cell Metabolic Behavior in Controlled and High throughput Microfluidic Culture Array

Qiong Pan.

The metabolic factor supply influences the cellular response. We have found based on bulk experiment that mouse embryonic stem (mES) cells have higher proliferation rates under lower metabolic factor supply while human carcinoma cells proliferate faster under higher metabolic factor supply. In terms of mES cells, the differentiation shows distinguished patterns of cell lines under different metabolic factor concentrations. These show the important role of extra-cellular metabolic factors on the fundamental modulation of cell growth and transcript gene expression. Single cell analysis shows the variation of individual cell response which could better demonstrate the true cellular phenomenon rather than the bulk experiments. However, which the conventional cell culture, the concentration effect cannot be addressed on a single cell level though the entire culture period, as well as the precise and time-dependent control of input doses, the immediate cellular responses cannot be obtained.

Here we have developed a high throughput microfluidic chip for single cell trapping and long term culture with refined control of perfusions, which enables various data collection for the statistical trend of cell population upon metabolic gradient and variation of individual cells' gene expression.

With this microchip, we are able to capture isolated single cells in 70 % of 1.2K chambers, and provide various metabolic gradients with refined control of the concentration and rate, perfusion time and intervals. With the convenient time-lapse observation of fluorescence probes addressing the mitochondria metabolic rate and observation of proliferation, we are able to quantitatively address the immediate response of cells as well as their long term behavior in regard of concentration effects on a single cell level.

3374-Pos Board B479

Microfluidic-Based Trap for Single Cell Micromanipulation and Analysis

Eric M. Johnson-Chavarria, Utsav Agrawal, Melikhan Tanyeri, Charles M. Schroeder.

We present a microfluidic tool for free-solution confinement and analysis of single cells using a recently developed hydrodynamic trapping technique. The hydrodynamic trap is a microfluidic-based device that enables confinement and manipulation of single ''target'' cells in concentrated and complex biological samples. In this work, we apply the hydrodynamic trap to confine single *Escherichia coli* cells in free solution for extended time scales. Using optical microscopy, we observe single *E. coli* cells growing and dividing both at room temperature and at 37^0C by incorporating a heat exchanger into the microfluidic device. We characterize cell proliferation in a variety of media conditions to ensure viability of single cells for long time scales, which is achieved by the gentle and non-perturbative action of hydrodynamic trapping at a fluid stagnation point. Our initial studies demonstrate that the hydrodynamic trap is a useful non-perturbative method for single cell trapping and may be used to study gene expression dynamics in real-time with precise control of the surrounding medium. Cell confinement is achieved using a free-solution hydrodynamic trap, which is constructed using a cross-slot microfluidic device where two opposing streams converge at the junction of orthogonal channels, thereby generating a flow field with a stagnation point. Using automated control of the stagnation point position with an on-chip valve, we confined cells to within 1 μm of the trap center for analysis. Overall, we anticipate that the microfluidic-based hydrodynamic trap will provide an ideal platform to study cellular regulation and gene network dynamics in single living cells for extended time scales.

3375-Pos Board B480
Retrieval of a Metabolite from Cells with Polyelectrolyte Microcapsules
Studer Deborah, Raghavendra Palankar, Sebastian Springer, **Mathias Winterhalter**.
To monitor cellular processes in individual cells, it is important to measure the concentrations of intracellular metabolites and to retrieve them for analysis. The use of functionalized polyelectrolyte microcapsules as intracellular sensors for in vivo reporting is persented. Capsules loaded with streptavidin-rhodamine, which was introduced into fibroblasts by electroporation, autonomously escaped from an endocytic compartment and effi ciently recruited biotin-fluorescein from the cytosol. This work demonstrates the utility of polyelectrolyte microcapsules for intracellular capture of metabolites and eventually for drug delivery on an organismic level.
D. Studer et. al. Small (2010) in press.
R. Palankar et. al. Small 5 (2009) 2168-76.

3376-Pos Board B481
UV Laser Patterning of Various Polymers for Biocompatibility Control of Chondrocyte Adhesion and Differentiation Grade
Marc Fahrner, Bettina Reisinger, Sergii Yakunin, Christoph Romanin, Johannes Heitz.
The control of cell adhesion at polymer surfaces is of great interest for applications in medicine and biotechnology research. Chondrocytes, which are the only cells found in cartilage, have proven to rapidly dedifferentiate to a fibroblastic phenotype when cultured under 2D conditions. The dedifferentiated phenotype is characterized by a change in cell morphology which is round in case of chondrocytes and spindle shaped in case of dedifferentiated chondrocytes. Furthermore, the fibroblastic phenotype shows increased expression of collagen I relative to collagen II and Integrin $\alpha 11\beta 1$ relative to Integrin $\alpha 10\beta 1$. The aim of this study was to treat the surface of polystyrene (PS), perfluoro ethylene propylene (FEP) and polyethylene terephthalate (PET) by UV laser irradiation for the improvement of adhesion and differentiation grade of human chondrocytes.
Depending on the type of polymer and the micro- or nano-structures at the surfaces induced by the surface pretreatment, the chondrocytes showed round morphology and high cluster formation, low cluster formation, or nearly no cluster formation. In contrast, chondrocytes cultured in well plates without foils showed progressive spreading and spindle shaped morphology. (supported by FFG - NSI3).

3377-Pos Board B482
Analyzing the Morphology of 3T3 Fibroblasts in Microenvironment
Keng-hui Lin, Wei-jung Hong, Wan-jung Lin, David Camarillo, Daniel Jones.
We have created 3D ordered gelatin scaffolds with monodisperse pores and cultured 3T3 fibroblasts inside. We are interested to explore the effect of microenvironment on the cell morphologies. The morphologies of cells are observed through labeling the F-actin inside the cells with fluorescent phalloidin and imaged by a confocal microscope. We compare the cell morphologies in the following microenvironment - on a 2D hard surface, on a 2D soft gelatin surface, in a 3D collagen gel, and scaffolds of different pore sizes. We found that the cells exhibit wide range of morphologies in different microenvironment. We classified cell shapes into three categories and measured the extension of cells by fitting with an ellipsoid. From the trend of cell extensions, a cell in a large pore resembles one on 2D soft gel surface. This result suggests a crossover in length from 2D-like to 3D-like morphology for cell cultured on a curved surface.

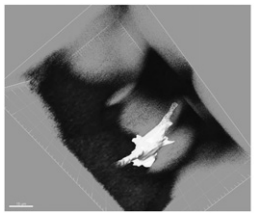

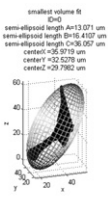

3378-Pos Board B483
Low Energy Laser Light (632.8 nm) Suppresses Amyloid-Beta Peptide-Induced Oxidative and Inflammatory Responses in Astrocytes
Xiaoguang Yang, Sholpan Askarova, Wenwen Sheng, JK Chen, Albert Y. Sun, Grace Y. Sun, Gang Yao, James C.-M. Lee.
Oxidative stress and inflammation are important processes in the progression of Alzheimer's disease (AD). Recent studies have implicated the role of amyloid β-peptides (Aβ) in mediating these processes. In astrocytes, oligomeric Aβ induces the assembly of NADPH oxidase complexes resulting in its activation to produce anionic superoxide. Aβ also promotes production of pro-inflammatory factors in astrocytes. Since low energy laser has previously been reported to attenuate oxidative stress and inflammation in biological systems, the objective of this study was to examine whether this type of laser light was able to abrogate the oxidative and inflammatory responses induced by Aβ. Primary rat astrocytes were exposed to Helium-Neon laser (λ= 632.8 nm), followed by the treatment with oligomeric Aβ. Primary rat astrocytes were used to measure Aβ-induced production of superoxide anions using fluorescence microscopy of dihydroethidium (DHE), assembly of NADPH oxidase subunits by the co-localization between the cytosolic $p47^{phox}$ subunit and the membrane $gp91^{phox}$ subunit using fluorescent confocal microscopy, phosphorylation of cytosolic phospholipase A_2 ($cPLA_2$), and expressions of pro-inflammatory factors including interleukin-1β (IL-1β) and inducible nitric-oxide synthase (iNOS) using Western blot Analysis. Our data showed that laser light at 632.8 nm suppressed Aβ-induced superoxide production, colocalization between NADPH oxidase $gp91^{phox}$ and $p47^{phox}$ subunits, phosphorylation of $cPLA_2$, and the expressions of IL-1β and iNOS in primary astrocytes. We demonstrated for the first time that 632.8 nm laser was capable of suppressing cellular pathways of oxidative stress and inflammatory responses critical in the pathogenesis in AD. This study should prove to provide the groundwork for further investigations for the potential use of laser therapy as a treatment for AD.

Membrane Structure III

3379-Pos Board B484
The Effects of Long-Chain Base Methylations on Ceramide Molecular Properties in Bilayer Membranes
Terhi Maula, Mayuko Kurita, Shou Yamaguchi, Tetsuya Yamamoto, Shigeo Katsumura, J. Peter Slotte.
Structural modifications have position-dependent effects on the molecular properties of ceramides in bilayer membranes. Ceramides with additional chemical groups, such as triple bonds or cyclic structures, in the long-chain base near the head group region induce similar thermal stabilization and displacement of sterol from sphingomyelin (SM)-enriched domains as unmodified ceramides[1]. However, the ability to thermally stabilize bilayers is significantly altered for ceramides with varying acyl chain length[2]. In addition, we have shown that methyl-branches in the amide-linked acyl chain markedly alter the lateral distribution of ceramides in bilayers, affecting the ability of the ceramides to interact with SM to form gel-phases that exclude sterol[3]. This study aims to determine the effects of yet another kind of structural modification on ceramide molecular properties, namely introduction of a methyl-group either to the amide-link or the hydroxyl-group of the sphingosine base, or both (yielding NMeCer, OMeCer, and NMeOMeCer, respectively). The analogs were prepared by enzymatic release of ceramides from corresponding N- or O-methylated SMs, and their membrane properties were studied with different fluorescence based methods. The ability of the analogs to interact with SM to form gel-phase domains, and the possible displacement of sterol from such domains was determined from the quenching susceptibility of *trans*-parinaric acid in gel phases, and cholestatrienol in sterol-enriched domains. In addition, the overall affinity of sterol for bilayers containing the ceramide analogs was determined from an equilibrium distribution of cholestatrienol between the bilayers and methyl-β-cyclodextrin. The results are discussed in relation to possible ceramide functions in cell membranes. [1]Megha *et al*., 2007 Biochim Biophys Acta 1768: 2205-12. [2]Nybond *et al*., 2005 Biochim Biophys Acta 1718: 61-6. [3]Maula *et al*., Chem Phys Lipids 163S1: S2-3, 2010.

3380-Pos Board B485
Phospholipid Headgroup Charge Modifies Condensing Effect of Gangliosides on Lipid Films
Karlina Kauffman, Matthew T. Davidson, **Shelli L. Frey**.
In model membrane mixtures that mimic lipid raft compositions, the more ordered domains are enriched in the ganglioside, G_{M1}, a glycolipid with a headgroup containing four neutral sugars and a negatively charged sialic acid. To understand the organization and partitioning of G_{M1} in cell membranes, the outer leaflet of the cell membrane was modeled using Langmuir monolayers of dipalmitoylphosphatidylcholine (DPPC), a phospholipid with a zwitterionic headgroup, and varying concentrations of G_{M1}. At low biologically relevant concentrations, G_{M1} condenses the DPPC monolayer while at higher concentrations, it fluidizes, with a switch-over point between the two behaviors at a ratio of 3:1 DPPC:G_{M1}.
To examine the role of electrostatics, lipids with negatively charged phosphatidylglycerol (PG) and positively charged trimethylammonium-propane (TAP) headgroups were combined with various ratios of G_{M1}. Fluidity of the monolayer was systematically altered by changing the hydrocarbon tail length. Additivity plots constructed for all mixtures show negative deviations from ideal mixing or condensation of the monolayer regardless of headgroup charge. For the zwitterionic and negatively charged lipids, the greatest condensation effect

compared to the pure lipid was seen at low G_{M1} concentrations. In binary mixtures containing positively charged lipids, a similar magnitude of condensation occurred at all G_{M1} ratios. For less fluid lipid nears their triple point temperature, the addition of G_{M1} caused minimal condensation suggesting the effect is specific to lipids that can be easily ordered.

3381-Pos Board B486

Disaccharides and Monosaccharides Exert Contrasting Effects on the Lamellar-Hexagonal Phase Transition

Thomas S. Wilhlem, Rachel R. Boerner, **Paul E. Harper**.

We have investigated how several disaccharides and monosaccharides affect the lamellar-hexagonal transition of the lipid SOPE (1-stearoyl-2-oleoyl-sn-glycero-3-phosphoethanolamine). The disaccharides sucrose and trehalose have similar effects, each lowering the lamellar-hexagonal phase transition temperature by about 9° C per molarity. Likewise, the monosaccharides fructose and glucose each affect the lamellar-hexagonal phase transition in a similar way to each other, but strikingly different than the dissacharides. The monosaccharides raise the phase transition temperature for concentrations up to about 0.5 molar, at which point increasing the concentration lowers the phase transition temperature.

3382-Pos Board B487

Sterol Affinity for Glycosphingolipid Containing Bilayer Membranes - effect of Sphingolipid Structure

Y. Jenny E. Isaksson, Max Lönnfors, Pia-Maria Grandell,
Thomas K.M. Nyholm, J. Peter Slotte.

Glycosphingolipids are major constituents of plasma membranes where they participate in the formation of ordered microdomains. These sphingolipid enriched domains are suggested to be involved in e.g. cellular signaling and toxin and viral entry. The membrane rafts are one type of ordered domains specifically enriched in cholesterol, whereas glycosphingolipids also may form sterol poor domains so called glycosynapses. The aim of this study was to investigate how the glycosphingolipid structure influences sterol partitioning into glycosphingolipid containing membranes. To assess this we analyzed sterol partitioning between methyl-β-cyclodextrin and large unilamellar vesicles of different composition. Sterol incorporation in the vesicles was determined by measuring fluorescence anisotropy of the cholesterol analog cholestatrienol. The sphingolipids studied include palmitoyl galactosylceramide and palmitoyl glucosylceramide, differing only in the stereochemistry of the sugar head group, and the corresponding glycosphingolipids containing 2-hydroxylated acyl chains. Preliminary results confirm our previous results that the stereochemistry of the sugar head group affects sterol affinity for the glycosphingolipids, being slightly higher for glucosylceramide than galactosylceramide. The ability of the different glycosphingolipids to form ordered, possibly sterol enriched, domains in multicomponent membranes was additionally analyzed with a fluorescence quenching approach.

3383-Pos Board B488

Investigating the Molecular Order of Mixures of Polyunsaturated Fatty Acids with Cholesterol

Iain M. Braithwaite, James H. Davis.

Cholesterol influences the fluidity of the membrane as well as other vital functions. The amount of cholesterol in a membrane is critical to ensure that the membrane works properly. Studies have shown that there are areas within the membrane bilayer where there is a higher concentration of cholesterol. These are known as rafts and may be important for the proper function of membrane proteins [Simons *et al*]. Despite this, we still do not fully understand how cholesterol circulates within the cells, and how it alters the molecular order of the membrane. We are investigating the molecular order of mixtures of 1,2-dimyristoyl (d_{54})-sn-glycero-3-phosphocholine (DMPC-d_{54}) and several polyunsaturated fatty acids with varying degrees of hydrocarbon chain unsaturation with and without cholesterol. Introducing cholesterol to the mixtures allows us to determine how it influences the membrane's molecular order and lets us probe the orientation of cholesterol within the bilayer. The experiments have been performed using solid state deuterium NMR techniques.

Simons, K., and E. Ikonen, 1997. Functional rafts in cell membranes. *Nature* 387:569-572

3384-Pos Board B489

In situ Monitoring of Structural Changes in Model Membranes upon Cholesterol Depletion via X-ray Diffraction

Kathleen D. Cao, Luka Pocivavsek, Niels Holten-Andersen,
Stephanie A. Harmon, Mati Meron, Binhua Lin, Ka Yee, C. Lee.

The importance of cholesterol in the molecular structure and organization of cell membranes is a topic of great research interest. It has been hypothesized that the lateral heterogeneity of cell membranes arises from the dynamic self-assembly of cholesterol enriched nanodomains. In order to elucidate the fundamental molecular interactions involved in the assembly of these nanodomains, binary lipid monolayers of dimyristoylphosphatidylethanolamine (DMPE) and dihydrocholesterol (DChol) were studied as model systems and probed using grazing incidence x-ray diffraction (GIXD). Mixed DMPE/DChol systems were shown to exhibit short-ranged lateral ordering consistent with previous data for a lipidic alloy of egg sphingomyelin and DChol that obeys Vegard's law [Phys. Rev. Lett 2009, 103, 028103]. In the presence of β-cyclodextrin (CD), DChol was selectively removed from the membrane. GIXD was used to monitor the changes of lipid ordering during CD mediated desorption of DChol to the subphase. The chemical of amount of CD to DChol was greater than a factor of 1000 and complete DChol depletion was expected. However, it was observed that a significant amount of DChol remains in the membrane during the experimental time frame of a couple of hours and this resistance to CD transfer could be due to the stability of condensed complexes formed between DMPE and DChol.

3385-Pos Board B490

The Maximum Solubility of Cholesterol in POPC/POPE Lipid Mixtures

Serkan Balyimez, Soyeun Park, Juyang Huang.

Cholesterol is a major constituent of cell membranes and has many important cell functions. The maximum solubility of cholesterol in a lipid bilayer is the highest mole fraction of cholesterol that can be incorporated into a lipid bilayer before cholesterol crystals precipitate. The maximum solubility can provide valuable information about cholesterol-phospholipid interaction. In this study, the maximum solubility of cholesterol in mixtures of POPE/POPC lipid bilayer has been investigated systematically using a cholesterol oxidase (COD) reaction rate assay. The maximum solubility of cholesterol was determined to be 67 mol % in POPC bilayers and 50 mol % in POPE bilayers. In mixtures of POPE/POPC, the maximum solubility of cholesterol increases linearly as a function of the ratio POPC/(POPE+POPC). The data indicates that cholesterol prefers the large headgroup lipid (POPC) over the small headgroup lipid (POPE) and the maximum solubility increases with the population of large headgroup lipid (POPC), which are consistent with the Umbrella Model. Previously, it has been suggested that cholesterol may form a ''hexagonal'' regular distribution pattern at the maximum solubility limit in POPE bilayers and a ''maze'' pattern at the maximum solubility in POPC bilayers. Whether such domains also exist at the maximum solubility limit in POPE/POPC mixtures is investigated using AFM.

3386-Pos Board B491

Orientation of Tie-Lines in the Phase Diagram of DOPC:DPPC: Cholesterol Molel Biomembranes

Pradeep Uppamoochikkal, Stephanie Tristram-Nagle, **John F. Nagle**.

We report the direction of tie-lines of coexisting phases in a ternary diagram of DOPC:DPPC:Cholesterol lipid bilayers, which has been a system of interest in the discussion of biological rafts. For coexisting Ld and Lo phases we find that the orientation angle α of the tie-lines increases as the cholesterol concentration increases and it also increases as temperature increases from T=15°C to T=30°C. Results at lower cholesterol concentrations support the existence of a different 2-phase coexistence region of Ld and So phases and the existence of a 3-phase region separating the two 2-phase regions. Our method uses the X-ray lamellar D-spacings observed in oriented bilayers as a function of varying hydration. Although this method does not obtain the ends of the tie-lines, it gives precise values ($\pm 1°$) of their angles α in the ternary phase diagram.

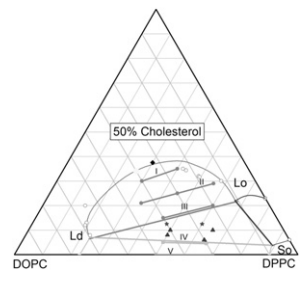

3387-Pos Board B492

Lipid Areas Obtained from the Simultaneous Analysis of Neutron and X-ray Scattering

Norbert Kucerka, Mu-Ping Nieh, John Katsaras.

Despite their importance to biophysical research, published lipid areas have been relatively scarce and for the most part, inconsistent. Noteworthy are the discrepancies between lipid areas as determined by standalone X-ray and neutron scattering experiments - arguably two of the most commonly used techniques in structural biology. Although they each have their advantages and disadvantages, when used in combination their advantages can be maximized. In particular, the large scattering contrast in the case of neutrons best resolves the overall bilayers thickness that is directly related to lipid lateral area. On the other hand, high resolution X-ray experiments yield detailed intra molecular structural information [Kucerka et al., Biophys. J. 95, 2356 (2008)].

We have utilized our recently developed method to characterize lipid areas of various phospholipids with varying numbers of carbons and double bonds. In the case of lipids with unsaturated fatty acid chains our results suggest that lipid areas change with increasing hydrocarbon chain length, but not linearly - lateral lipid area is the result of the fine balance between the hydrocarbon chain length and double bond position. Furthermore, we discovered that the most dramatic change in lipid area occurs after the introduction of the first double bond to the lipid's acyl chains.
Besides their importance in biology, lipid areas play a central role in molecular dynamics (MD) simulations, where their inconsistencies have been highlighted by the disparate results arising from MD simulations using different force fields. Since MD force fields are considered to be "well tuned" if they are able to reproduce experimental data, more reliable experimental information is necessary for their future development.

3388-Pos Board B493
Cardiolipin, a Key Component to Mimic the E. coli Bacterial Membrane in Model System Membranes
Sílvia Lopes, Cristina Neves, Peter Eaton, Paula Gameiro.
The phase transition temperatures of several lipidic systems were determined using two different techniques: dynamic light scattering (DLS) and steady-state fluorescence anisotropy, using two fluorescent probes that report different membrane regions (TMA DPH and DPH). Atomic force microscopy (AFM) was used as a complementary technique to characterize different lipid model systems under study. The systems were chosen due to the increased interest in bacterial membrane studies due to the problem of antibiotic drug resistance. The simpler models studied comprised of mixtures of POPE and POPG lipids, which form a commonly used model system for E. coli membranes. Given the important role of cardiolipin (CL) in natural membranes, a ternary model system, POPE/POPG/CL, was then considered. The results obtained in these mimetic systems were compared to those obtained for the natural systems E. coli polar and total lipid extract. DLS and fluorescence anisotropy are not commonly used to study lipid phase transitions, but it was shown that they can give useful information about the thermotropic behaviors of model systems for bacterial membranes. These two techniques provided very similar results, validating their use as methods to measure phase transitions in lipid model systems. The temperature transitions obtained from these two very different techniques and the AFM results clearly show that cardiolipin is a fundamental component to mimic bacteria membranes. The results suggest that the less commonly used ternary system is a considerably better mimic for natural E. coli membranes than binary lipid mixture.

3389-Pos Board B494
Bioenergetics Explains the Structures of Membrane Lipids: Cholesterol, Plant Sterols, Unusual Fatty Acid Chains and Polyisoprenes
Thomas H. Haines.
All living membranes support cation gradients, which they maintain by cation pumps: proton pumps or – for the animal plasma membrane – sodium pumps. This includes the organelle membranes of the eukaryote. The negative side of the gradient faces the cells' cytoplasm. Lipid bilayers leak both H+ and Na+ at rates that are equivalent in vivo (H+ is ~10-5 cm/sec without a membrane potential([H+] is ~10-7) whereas Na+ is ~10-12 cm/sec without a membrane potential ([Na+] is ~10-1). The resident membrane potential increases the rate of leakage. Cation leakage requires the cell to spend ATP energy pumping the cations back out. Resting cells spend 70 to 80% of their ATP on cation pumping. Cholesterol, found in animals, is the only lipid tested that inhibits Na+ leakage across phospholipid bilayers. It decreases leakage to 1/3 membranes w/o it. Meanwhile many membrane lipid structures inhibit H+ leakage by: 1) decreasing water diffusion through bilayers; 2) thickening the bilayer; 3) packing the bilayer cleavage with hydrocarbon.
1) sterols, hopanoids, tetrahymenol decrease membrane water permeability. 2) polyisoprenes, CoQ, squalene, dolichol, vitamin E., and carotenes thicken the membrane bilayer. 3) Iso- and anteiso-fatty acids, branched plant sterols, and chains in extreme acidophiles terminating with cyclohexane or cycloheptane groups.
A unique phospholipid, cardiolipin (CL), displays a high pK2 (~8.0) in bilayers. This appears to facilitate ATP synthesis in membranes that use the F0F¬1ATPase to make ATP. Except for the chloroplast with its CF0CF¬1ATPase, CL always accompanies the F0F¬1ATPase.
In sum, membrane lipid structures are uniquely designed to support membrane bioenergetics. This makes the structures of membrane lipids as biochemically functional as are the structures of amino acids, nucleotides and carbohydrates are for proteins, nucleic acids and CHO polymers.

3390-Pos Board B495
Material Properties of Matrix Lipids Determine Conformation and Intermolecular Reactivity of a Diacetylenic Phosphatidylcholine in the Lipid Bilayer
Anu Puri, Hyunbum Jang, Amichai Yavlovich, Alex Haber,
Athar M. Masood, Timothy D. Veenstra, Ulrich Baxa, Ruth Nussinov,
Robert Blumenthal.
Photopolymerizable phospholipid $DC_{8,9}PC$ (1,2-bis-(tricosa-10,12-diynoyl)-*sn*-glycero-3-phosphocholine) exhibits unique assembly characteristics in the lipid bilayer. Due to the presence of the diacetylene groups, $DC_{8,9}PC$ undergoes polymerization upon UV (254 nm) exposure and assumes chromogenic properties. Photopolymerization in a gel phase lipid matrix (DPPC) monitored by UV-VIS absorption spectroscopy occurred within 2 minutes after UV treatment, whereas no spectral shifts were observed when $DC_{8,9}PC$ was incorporated in a liquid phase matrix (POPC). Calcein release from DPPC/$DC_{8,9}PC$ liposomes was observed after a lag of 10 minutes following UV triggering, whereas no release occurred from POPC/$DC_{8,9}PC$ liposomes. LC-MS analysis showed a decrease in $DC_{8,9}PC$ monomer without any change in DPPC concentration in UV-treated samples. Cryo-electron microscopy revealed fiber-like structures in the UV-treated DPPC/$DC_{8,9}PC$ liposomes with few intact vesicles remaining indicating that the leakage of calcein was due to the disruption of liposomes. Molecular Dynamics (MD) simulations of DPPC/$DC_{8,9}PC$ bilayer indicate that lipid tails in the gel phase are more highly ordered than in the fluid phase of POPC/$DC_{8,9}PC$ bilayer, packing each other into close proximity. We speculate that well-packed fatty acyl chains can increase the probability of light-induced polymerization in $DC_{8,9}PC$. Further, MD simulations suggest that motions of $DC_{8,9}PC$ in the gel phase bilayer are more restricted than in the fluid bilayer. The restricted motional flexibility of $DC_{8,9}PC$ enables the reactive acetylenes in individual molecules to align and undergo the polymerization reaction, whereas the unrestricted motions in the fluid bilayer lead to a dampening of UV-triggered polymerization due to the lack of appropriate alignment of the fatty acyl chains. These studies may have implications for physicochemical effects at the nanoscale that may occur in biological membranes as a result of signaling, transport, and fusion.

3391-Pos Board B496
SANS Investigation of the Response of DMPC-DMPG Lipid Bilayers to Membrane-Active Peptides
Shuo Qian, William T. Heller.
Membrane-active peptides disrupt the integrity of cell membranes and form transmembrane pores in model lipid bilayers. Alamethicin and melittin are two extremely well-characterized examples of membrane-active peptides that are known to undergo a concentration-dependent transition from a surface-adsorbed state to a state in which transmembrane pores are formed, resulting in the death of the target cell. The action of these peptides strongly depends on the composition of the lipid bilayer membrane. In particular, charged lipids and cholesterol are thought to drive the cellular specificity of the cytotoxicity of these membrane active peptides. Further, lipid rafts, enriched domains in multi-component membranes, can concentrate or exclude proteins and peptides associated with lipid bilayers. SANS with contrast variation was used to probe the response of small-unilamellar vesicles (SUVs) composed of mixtures of the neutral lipid DMPC with the charged lipid DMPG to the presence of alamethicin and melittin. SUVs made of chain-deuterated d54-DMPC and DMPG at a molar ratio of 7: 3 were studied in the absence and presence of the two peptides in H2O/D2O mixtures containing 90% D2O solution. The measurements in 90% D2O, which is at the match point of the readily available d54-DMPC, greatly enhances the scattering from the hydrogenated components and ensure maximum signal for any in-bilayer aggregates or an asymmetric distribution between the leaflets of the bilayer of hydrogenated material that may form. The SANS experiments were performed using the BIO-SANS of HFIR at ORNL, which provided excellent signal for the dilute SUVs solutions. We found in both alamethicin and melittin, the asymmetric distribution of two lipids between the two monolayers increases with the peptide concentration. Interestingly, melittin was found to produce a stronger effect than alamethicin.

3392-Pos Board B497
Inclusion of Menaquinone in Lipid Membranes Decreases Susceptibility to Antimicrobial Peptides
Julia Nepper.
Most studies on the interaction of antimicrobial peptides with lipid bilayers have used unsaturated, fluid-state phospholipids to model bacterial membranes. However, unsaturated lipids are rarely found in cell membranes of gram-(+) bacteria, including *Staphylococcus aureus*. To maintain cell membrane

function, *S. aureus* uses fully saturated but terminally branched lipid acyl chains, which have a significantly lower phase transition temperature than their linear counterparts. We found that lipid vesicles composed of synthetic branched phospholipids are much more susceptible to attack by an amphipathic peptide than lipid vesicles composed of unsaturated phospholipids with the same headgroup composition. By contrast, natural membrane lipid extracts from *S. aureus* produce lipid vesicles that are as resistant to membrane-active peptides as those produced using synthetic, unsaturated lipids. We postulated that an unidentified component present in the *S. aureus* lipid extracts serves to stabilize the bacterial cytoplasmic membrane. A possible candidate is menaquinone, which participates in the bacterial electron transport chain but could, in addition, have a structural effect on the lipid bilayer. In the work presented here, we investigated the kinetics of dye efflux from lipid vesicles containing between 1 and 5 mol% menaquinone, induced by the antimicrobial peptide PMAP-23. PMAP-23 is a 23 amino acid, linear peptide of the cathelicidin family with the sequence RIIDLLWRVRRPQKPKFVTVWVR. We found that the presence of physiological concentrations of menaquinone had a notable effect on peptide-induce dye efflux.

3393-Pos Board B498

In Vivo ^{2}H-NMR Study of the Action of Antibacterial Agents on Escherichia Coli Membranes

Catherine Tardy-Laporte, Alexandre A. Arnold, Isabelle Marcotte.

Contrary to eukaryote membranes, bacterial membranes are negatively charged owing to the presence of phosphatidylglycerol (PG) or cardiolipin in their inner membranes. One of the action mechanisms of antibiotics such as antimicrobial peptides is to selectively interact with negatively charged lipids to create a breach in the bacterial membrane. The characterization of the cellular membrane integrity is, thus, a key element in understanding the mechanism of action of antimicrobial agents. Solid-state nuclear magnetic resonance spectroscopy (SS-NMR) is a useful tool that allows probing the organization and dynamics of phospholipids in a bilayer. In this work, we have performed an *in vivo* ^{2}H-NMRstudy of *Escherichia coli* membranes labeled with deuterated palmitic acid. More specifically, we have studied the effect of nanoparticles (NPs) and antibacterial molecules on the bacteria membrane. The ^{2}H-NMR spectra obtained on intact cells show that the *E. coli* membranes were successfully labeled according to previous work. A 10-hour exposure to the cationic detergent cetyltrimetylammonium chloride (CTAC) shows increased membrane fluidity at high detergent concentration (320μM). The study of the effect of fullerenol reveals that these NPs increase the lipid mobility in the membrane especially after 8 hours of exposure. The ^{2}H-NMR spectra obtained in the presence of polymyxin B show no fast-tumbling membrane fragments, although UV analysis indicates the leakage of the cell content. These results suggest that this antibiotic would perforate *E. coli* membranes without their complete disruption. Our work illustrates the use of *in vivo* ^{2}H NMR studies to understand the specific action of different substances on labeled biological membranes.

3394-Pos Board B499

Regulation of Antimicrobial Peptide Activity through Lipid Chain Order

Diego A. Ramirez, Daniel E. Otzen, Chad Leidy.

During changes in temperature, bacterial membranes present broad but cooperative lipid chain-melting events, where the membrane transitions from a solid-ordered state into a liquid-disordered state. For example, in Staphylococcus aureus, this melting event occurs at 15C. This transition has important implications. When temperature decreases near to the lipid melting event, cell division is inhibited. Gram-positive bacteria present cold-shock response mechanisms that shift the melting event to lower temperatures by varying the saturated fatty acids/unsaturated fatty acids ratio (SFA/UFA). It thus appears that the bacteria adaptatively strives to minimize the solid-ordered phase. However, the solid-ordered phase is not completely detrimental to cell viability. Recently we have shown that the solid-ordered phase induces resistance to PLA2-IIA, an innate human antibacterial agent that acts by disrupting membrane integrity. Therefore, we propose that adaptative modulation of the SFA/UFA ratio of bacterial membranes may alter the physical activity of antimicrobial agents that disrupt membrane integrity. To corroborate this, we studied, with the use of model systems, the activity of two antimicrobial peptides Magainin-2 and Novocidin (AMPs). Based on fluorescence spectroscopy, we measured calcein leakage potency on POPG (unsaturated) / DPPG (saturated) large unilamellar vesicles (LUVs). As we modified the SFA/UFA ratio we observe as expected a shift in the phase transition from ordered to disordered phase. This leads to 1) changes in the peptide needed to induce 50% leakage, and 2) changes in the leakage kinetic rate constant. Furthermore, we relate this kinetic rate to the energetics of a two state model in order to quantify the changes in the activation energy required for AMPs to perturb the bilayer as a function of the SFA/UFA ratio. We relate this change in activation energy to levels of lipid packing by measuring Laurdan generalized polarization.

3395-Pos Board B500

Lipid Bilayers of Ester-Modified Lipids

Diana Y. Villanueva, Joseph B. Lim, Jeffery B. Klauda.

Lipid membranes and bilayers essentially function as barriers for cells to control the transport of substances. Since phospholipid membranes consist of a hydrophilic surface and a hydrophobic inside, the center of a phospholipid bilayer is known to contain almost no water and to prevent the transport of water-dissolving substances, such as ions. These water soluble molecules take alternate routes via ion channel protein pumps to transverse the cell membrane. Typical lipid bilayers with saturated or moderately unsaturated chains show a bilayer with a water density that decreases to zero around 10Å and remains at zero at the center. Recent experimental work suggests that ester-modified lipids allow for ions and water to be present at the center of the bilayer (JACS, 128: 14034). These ester-modified phospholipid bilayers contain ester groups along their hydrocarbon chain at various positions. The addition of the ester groups to these lipids can occur naturally through a free radical reaction called lipid peroxidation. We are using molecular dynamics simulations to study two lipid bilayers with additional ester groups on the chain. One lipid contains ester groups in the upper half of the acyl chain (lipid E) and another contains ester groups towards the middle and the end (lipid G). The bilayers contain 15 lipid G (or E) and 35 POPC lipids per leaflet with a hydration of 70.5 waters per lipid. For lipid E, the water density reaches zero at ~7Å, as oppose to the standard 10Å. As for lipid G, water fully penetrates the bilayer. We are currently extending these simulations to at least 100 ns, to obtain good statistics on ion permeation where longer timescales are needed to further understand this water and ion permeation mechanism.

3396-Pos Board B501

Lipid-Soluble Hydroquinone Modifications Induced on Membranes

Sergio S. Funari, Vivian Rebbin, Liliana Marzorati, Claudio Di Vitta.

We synthesized new alkylthiohydroquinones (ATHs); in order to investigate different aspects of lipid-soluble hydroquinones interactions with phospholipids normally found in cell membranes. They have the same long hydrophobic alky chains found in many lipids forming the cell membranes. In these compounds the tails should share the inner of the membrane, while the hydroquinone, as polar head group should remain on the surface. One or more alkylthio chains attached to the aromatic ring, modifies its hydrophobicity and should alter the electron distribution. Moreover, the two OH groups become chemically distinguishable, e.g. NMR spectroscopy and also show different pKa values.

We investigate the interaction of ATHs with lipid membranes, POPE and POPC and observe the formation of structures with different morphologies, or curvature, of the lipid membrane, depending on temperature and pH. We attributed their formation to changes in the balance charge/polarity induced by the ATHs. Mixtures with POPE at pH=4 forms two cubic phases P4332 and Im3m that reach a maximum lattice size while in basic conditions they only expand upon heating from room temperature. They coexist with lamellar or hexagonal and have been associated with inhomogeneous distribution of the ATHs molecules over the lipid matrix. The zwitterionic POPC does not form cubic phases, but instead shows two lamellar structures up to a high temperature.

In all mixtures of lipid/ATHs we observed the formation of lamellar and hexagonal phases, similar to the behaviour of pure hydrated lipid e.g. POPC, while for POPE additional cubic structures, depending on the environment conditions.

3397-Pos Board B502

N-3 polyunsaturated Fatty Acids Disrupt Micron and Nanometer Scale Non-Raft Organization by Increasing Cell Size and Minimizing Molecular Interactions with Surrounding Rafts

Benjamin Drew Rockett, Andrew Franklin, Mitchel Harris, Heather Teague, Justin Williams, Stephen R. Wassall, Andrew H. Nguyen, Benjamin L. Stottrup, Saame Raza Shaikh.

N-3 polyunsaturated fatty acids (PUFAs), due to their unique molecular structure, modify plasma membrane organization; however, very few mechanistic details are known. Here we tested the hypothesis that n-3 PUFAs, in comparison to other fatty acids, can specifically disrupt the organization of non-rafts on several length scales using quantitative imaging. On a micron scale, EL4 cells treated with eicosapentaenoic (EPA) and docosahexaenoic (DHA) acid robustly increased accumulation of the non-raft probe FAST DiI. The increase in FAST DiI accumulation was dependent on the total cellular levels of EPA and DHA, as revealed by linear regression analysis across differing cell types

treated with n-3 PUFAs in vitro and in vivo. Unexpectedly, in vivo studies also revealed n-3 PUFAs disrupted rafts by increasing their size. On a nanometer scale, FRET imaging showed EPA and DHA increased the distance between non-raft molecules of EL4 cells. The increase in distance between non-raft molecules was due to an increase in cell size, driven by EPA and DHA's ability to promote cellular proliferation. Finally, we used model membranes to determine how EPA and DHA disrupted nonraft organization at a molecular level. NMR spectroscopy and quantitative microscopy revealed EPA and DHA acyl chains increased the nano- and micrometer size of non-raft domains by minimizing molecular interactions with surrounding rafts. Taken together, the data suggest a unifying model in which EPA and DHA target and disorder the organization of not only rafts but also non-rafts, which could serve as key intermediates to disrupt membrane architecture and cellular function.

3398-Pos Board B503

EPA and DHA Interact Differentially with Cholesterol: Solid State ^{2}H NMR of PUFA-Containing Phospholipids in Mixtures with Lipid raft Molecules

Justin A. Williams, Shawn E. Batten, M. Alan McCabe, William Stillwell, Saame Raza Shaikh, Stephen R. Wassall.

A plethora of health benefits accompany dietary consumption of ω-3 polyunsaturated fatty acids (PUFA) eicosapentaenoic (EPA, 20:5) and docosahexaenoic (DHA, 22:6) acids found in fish oils. An emerging view for one mechanism of action is that ω-3 PUFA incorporate into phospholipids of the plasma membrane and, due to their aversion for cholesterol, affect lateral organization. What is unclear is which component of fish oil drives the structural and concomitant functional changes. Here we test EPA vs. DHA in mixtures with the lipid raft molecules egg sphingomyelin (SM) and cholesterol. Our approach is to employ solid state ^{2}H NMR to characterize the molecular organization of EPA-containing 1-[$^2H_{31}$]palmitoyl-2- eicosapentaenoylphosphatidylcholine ([$^2H_{31}$]16:0-20:5PC) and DHA-containing 1-[$^2H_{31}$]palmitoyl-2-docosahexaenoylphosphatidylcholine ([$^2H_{31}$]16:0-22:6PC), and of oleic acid (OA, 18:1)-containing 1-[$^2H_{31}$]palmitoyl-2-oleoylphosphatidylcholine ([$^2H_{31}$]16:0-18:1PC) as a control. Spectra for mixtures with SM and cholesterol (1:1:1 mol) support our model according to which poor affinity of PUFA for the sterol promotes the formation of highly disordered PUFA-rich/cholesterol-poor (non-raft) domains on the nanoscale. The novelty of the results lies in the enhanced effect seen for EPA relative to DHA. Less interaction with cholesterol is indicated by the smaller increase in sterol-induced order measured for [$^2H_{31}$]16:0-20:5PC compared to ([$^2H_{31}$]16:0-22:6PC, and a larger domain size is implied with EPA than DHA. We speculate that these preliminary observations at the molecular level may reflect a more influential role for EPA.

3399-Pos Board B504

Role of Phospholipid Head Groups in Silver Nanoparticles Interaction with Membranes

Ramakrishnan Parthasarathi, S. Gnanakaran.

In order to understand the biocompatibility and cell affinity of metal nanoparticles for biosensing and drug delivering applications and also for nanotoxicity aspects, we investigate the different charged state phospholipid head groups interacting with silver (Ag) nanoclusters. Binding interactions of Ag, which serve as simple catalytic models of Ag nanoparticles with phospholipids, was studied using density functional theory (DFT). Geometries of neutral, anionic, and cationic phopholipid head groups with silver nanoparticle were optimized using the DFT-B3LYP approach with combined basis sets. The combined basis set used here for phospholipid and silver clusters was represented by 6-311++G (d,p) and LANL2DZ, respectively. This work demonstrates that the interaction of silver clusters with phospholipid head group is governed by two major bonding factors: (a) the anchoring phosphotidyl O−Ag, and (b) the nonconventional N−H···Ag and C−H···Ag hydrogen bonds. Role of different charge state within the membrane lipids and metal affinity on their interaction with Ag nanpoarticle is very crucial and will be discussed here in detail. DFT based global and local chemical reactivity descriptor analysis and natural bond orbital analysis was performed to calculate reactivity, charge transfer, and Wiberg bond indices of the nano-bio complexes. Bader's ''atoms in molecules'' theory is used to determine the nature of interactions that exhibit both electrostatic and covalent characters.

3400-Pos Board B505

Application of Neutron Diffraction for Localization of Specifically Deuterated Penetration Enhancers in Oriented Stratum Corneum Model Membranes

Tanja Engelbrecht, Thomas Hauss, Bodo Dobner, Reinhard N. Neubert.

The unique lamellar lipid matrix of the stratum corneum (SC) is known to play a key role in forming the main protecting barrier of the mammalian skin. This barrier function can be influenced e.g. by application of penetration enhancers. To learn more about their mode of action, the present study aimed at the characterization of the influence of lipophilic penetration enhancers like oleic acid (OA) on the bilayer structure of highly oriented SC model membranes. For exact localization of the enhancer molecules inside the bilayers of the studied quaternary SC models, we applied specifically deuterated penetration enhancers (e.g. OA-**9,10-D2** and isopropyl myristate-**14,14,14,13,13-D5**) to the samples which were investigated by means of neutron diffraction. Benefitting from the advantages offered by the neutron diffraction technique, we could evaluate the exact position of the deuterium labels inside the membrane. Furthermore, hydration properties of the membrane could be studied and the bilayer architecture was elucidated by calculating the neutron scattering length density (neutron SLD) profiles using Fourier transform.

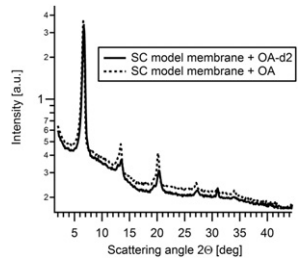

3401-Pos Board B506

The Effects of Sustained Hydrostatic Pressure on Human Bladder Smooth Muscle Cells Grown on Polymer Scaffolds

Hana Hanaee Ahvaz, Hamid Mobasheri, Mohamad Soleimani.

Monitoring the effect of different stationary and dynamic hydrostatic forces regimen imposed on bladder cells has achieved great consideration in bladder tissue engineering. In this study the effect of sustained hydrostatic pressure 10 cm water on smooth muscle cells grown on electo-spinned PLA-PLGA (60/40) polymer scaffold was studied. Gene expression changes were monitored for 3, 5, and 7 days. According to our quantitative PCR results the expression of Collagen Type I and III and IV as well as alpha actin smooth muscle, actin, elastin, calponin and caldesmon increased by day 5 and then decreased. Based on ELIZA results, at day 5 expression of both differentiation marker (desmin) and dedifferentiation marker (alpha actin smooth muscle) was increased. Collagen type I was up regulated but type III down regulated. Although mechanical stimulation has important effect on bladder function, pathologic condition such as outlet obstruction, disturbs both pattern of phenotypic markers and collagen type III to I ratio.

Reference :

1- Haberstroh KM, Kaefer M, Retik AB, Freeman MR, Bizios R. The effects of sustained hydrostatic-pressure on select bladder smooth muscle cell functions. J Urology. 1999 Dec;162(6):2114-8.

2- Haberstroh KM, Kaefer M, DePaola N, Frommer SA, Bizios R. A novel in-vitro system for the simultaneous exposure of bladder smooth muscle cells to mechanical strain and sustained hydrostatic pressure. J Biomech Eng-T Asme. 2002 Apr;124(2):208-13.

3402-Pos Board B507

Pulmonary Surfactant Membranes of Hibernating Ground Squirrels Possess Increased Fluidity but are Capable of Maintaining an Ordered Membrane Structure at Low Temperatures

Lakshmi N.M. Suri, Lynda McCaig, Victoria Picardi, Ruud Veldhuizen, James Staples, Fred Possmayer, Jesus Perez-Gil, Sandra Orgeig.

Pulmonary surfactant, a mixture of lipids and proteins, regulates the surface tension at the air-liquid interface of the lung. Reduced body temperature during hibernation is accompanied in 13-lined ground squirrels (*Ictidomys tridecemlineatus*) by an increase in fluid monounsaturated phosphatidylcholine (PC) species (e.g. PC 16:0/16:1, PC 16:0/18:1) and phosphatidylglycerol (PG) species (e.g. PG 16:0/18:1, PG 18:0/18:2), but fewer disaturated PC and PG species. Previously we speculated that altered surfactant lipid composition during metabolic depression states such as torpor or hibernation will reduce the phase transition temperature (T_m) of the mixture, enabling pulmonary surfactant to remain fluid over a broader range of temperatures and thereby maintaining respiratory function. Here we analyze thermodynamic properties and behavior of surfactant from hibernating and summer-active 13-lined ground squirrels in relation to natural porcine surfactant, using differential scanning calorimetry and LAURDAN fluorescence spectroscopy. In addition we conducted epifluorescence studies to visualize changes in phase coexistence of surfactant films of hibernating and summer-active animals. Surfactant membranes of hibernators showed gel-to-fluid transitions at lower T_m with reduced enthalpy relative to membranes from summer-active squirrels. Both exhibited lower enthalpy than porcine surfactant. LAURDAN fluorescence and epifluoresence suggested possible structural re-arrangements of surfactant membrane lipids and films, respectively, in hibernators. These exhibited a similarly dehydrated and condensed highly packed ordered phase as for summer active squirrels, despite differences in composition and T_m. In conclusion, pulmonary surfactant composition changes in hibernating squirrels to increase overall fluidity, but to maintain an ordered membrane structure at low temperature.

Membrane Dynamics & Bilayer Probes II

3403-Pos Board B508

Raft-Like Phase Coexistence Revealed by Solid-State Carbon-13 Separated Local Field Mas NMR

Avigdor Leftin, Klaus Beyer, Michael F. Brown.

Molecular interactions such as hydrogen-bonding and hydrophobic matching are observed for raft-like membranes using solid-state NMR [1]. We applied natural abundance separated-local field magic angle spinning ^{13}C NMR to study the components of a canonical raft-like membrane system. This method probes lipid structure at the headgroup, glycerol backbone, and acyl chains simultaneously for each membrane component. We resolved isotropic ^{13}C NMR chemical shifts and ^{13}C-^{1}H residual dipolar couplings (RDCs) for single-component, binary, and ternary membranes. These measurements are interpreted using a mean-torque model providing cross-sectional areas per lipid and volumetric hydrocarbon thicknesses [2]. The structural changes are related to mixing or de-mixing of lipids and cholesterol. In the single-component membranes, EYSM is highly ordered from hydrogen-bonding at the backbone, while POPC is highly disordered due to acyl chain unsaturation. The combination of these lipids leads to a reduction of EYSM order and an increase in POPC order due to inter-chain contacts. Addition of cholesterol yields a significant increase in hydrophobic matching in POPC and EYSM membranes [3]. From these structural results for single-component and binary systems, we evaluated the interactions contributing to lipid mixing in the ternary membrane system. EYSM exhibits a cross-sectional area and hydrocarbon thickness resembling the single-component system. In contrast, POPC exhibits a cross-sectional area and hydrocarbon thickness characteristic of the binary lipid-cholesterol mixture. This suggests a liquid-ordered phase is present in an ideally mixed ternary system. Our experimental results contribute to our understanding of raft-like membrane self-assembly, and can be used to interpret changes in membrane structure that occur during protein recognition events and membrane fusion.

[1] T. Bartels *et al*. (2008) *JACS* **130** 14521-14532. [2] H.I. Petrache *et al*. (2000) *Biophys. J.* **79**, 3172-3192. [3] G.M. Martinez *et al*. (2004) *Langmuir* **20** 1043-1046.

3404-Pos Board B509

First Observation of Dynamics in Lipid Multilayers using X-ray Photon Correlation Spectroscopy (XPCS)

Yicong Ma, Gang Chen, Curt DeCaro, Justin Berry, Mark Servantes, Lobat Tayebi, Zhang Jiang, Suresh Narayanan, Alec Sandy, Hyunjung Kim, Atul Parikh, Laurence Lurio, Sunil Sinha.

Collective modes of layer undulations in lipid multilayers are of considerable interest because they can be used to measure the elastic moduli and viscosity of the lipid bilayers as a function of interlamellar spacing, properties of the interlayer aqueous channels, and temperature. These are fundamental quantities required to calculate the configurations and fluctuations of lipid membranes, relevant in modeling many biomembrane functionalities (e.g., intermembrane interactions and polyvalent ligand recognition) that depend on elasticity and dynamics of membrane phases. However, only relatively few investigations have been made of lipid systems, with e.g. dynamical light scattering, neutron spin echo and inelastic neutron scattering. There remains a gap in time scales and length scales which the technique of x-ray photon correlation spectroscopy (XPCS) can fill.

We present here the first XPCS measurements of the dynamics of 1,2-dioleoyl-sn-glycero-3-phtosphocholine (DOPC) multilayers at relative humidity of 99% and temperature of 28°C. The measurements were done at and near the 1st Bragg peak of the multilayer, in which range the intensity-intensity autocorrelation function includes heterodyne oscillations [1] due to a large static component as well as homodyne oscillations predominated at q-values off the Bragg peak. According to de Jeu's theory [2], there are two different modes of relaxation time in the system: a slow and a fast one. Our experiment reveals the existence of the slow mode, which exhibits a plateau in relaxation time over a range of q (10e-5 Å-1~10e-4 Å-1). The results of the analysis of these correlation functions according to the model of de Jeu et al. will be presented.

1. C. Gutt et al, Phys. Rev. Lett. 91, 076104 (2003)
2. W. H. de Jue et al, Rev. Mod. Phys., 75, 181-235 (2003)

3405-Pos Board B510

Organization and Dynamics of Cholesterol Crystalline Domains using EPR Spin-Labeling

Laxman Mainali, Marija Raguz, Witold K. Subczynski.

EPR spin-labeling methods were used to study the organization and dynamics of cholesterol molecules in membranes formed from Chol/PL (cholesterol/phospholipid) mixtures. Membranes made from phospholipids with different cholesterol solubility thresholds (CST) were investigated. It was confirmed using the EPR discrimination methods that cholesterol crystalline domains (CCDs) were present in all of the membrane suspensions when the mixing ratio exceeded the CST. The behavior of phospholipids was monitored with phospholipid analogue spin labels (n-PCs), and cholesterol with the cholesterol analogue spin labels CSL and ASL. Results indicated that phospholipid and cholesterol mixtures can form a membrane suspension up to a mixing ratio exceeding significantly the CST. EPR spectra for n-PC indicated that phospholipids exist in these suspensions in the lipid-bilayer-like structures. Spectral characteristics of n-PCs (spin labels located outside the CCD) change with increase in the cholesterol content up to and beyond the CST. These results present strong evidence that the CCD forms an integral part of the phospholipid bilayer when formed from Chol/PL mixture up to a mixing ratio of 2 to 3. EPR spectra for CSL and ASL in the CCD and the PCD were very similar indicating that in both domains cholesterol exists in the lipid-bilayer-like structures. In the CCD cholesterol molecules are more ordered and sense more rigid environment than in the PCD. This difference is small and can be compared to that induced in the PCD by the ~10°C decrease of temperature. Thus, cholesterol molecules are unexpectedly dynamic in the CCD what should enhance their active interaction with the PCD. It is suggested that the EPR spin-labeling approach can discriminate the fraction of cholesterol that forms the CCD within the phospholipid bilayer from the fraction that forms the cholesterol structures outside the bilayer.

3406-Pos Board B511

Discrimination and Characterization of Cholesterol Crystalline Domains using EPR Spin-Labeling: Application to Lens Lipid Membranes

Laxman Mainali, Marija Raguz, Witold K. Subczynski.

Saturation-recovery EPR at X-band (9.4 GHz) and W-band (94 GHz) was used to discriminate cholesterol crystalline domains (CCDs) in model phospholipid membranes and membranes made of pigs lens lipids. We used dual-probe saturation-recovery EPR approach with cholesterol analogue spin labels, CSL or ASL, and oxygen (hydrophobic) or NiEDDA (polar) relaxation agents. The CCD was present in all of the phospholipid membranes when the cholesterol-to-phospholipid mixing ratio exceeded the cholesterol solubility threshold. Saturation-recovery curves show that spin labels detect a single homogenous environment in membranes made from cortical lipids. However, in membranes made from nuclear lipids, two domains were detected and were assigned to the bulk phospholipid-cholesterol domain and the CCD, respectively. Profiles of the oxygen transport parameter (oxygen diffusion-concentration product) across these domains contain significant structural information. These profiles also allow calculating the oxygen permeability coefficient across domain. The evaluated upper limit of the oxygen permeability coefficient across the CCD at 37°C (34.4 cm/s) is significantly lower than across the water layer of the same thickness (85.9 cm/s), indicating that the CCD can form a barrier for oxygen transport in the lens nucleus.

The new capabilities in measurements of the oxygen transport parameter at W-band are demonstrated and compared with results obtained at X-band. The loop-gap resonators used for W-band measurements have a sample volume of 30 nL, while the sample volume of the loop-gap resonator used for X-band is 3μL. These specifications ensure feasibility of experiments planned for samples with a limited sample volume. For example, the oxygen transport parameter profiles measured at X-band for lens lipid membranes were obtained for samples prepared from 50 - 100 eyes. Reliable profiles at W-band can be obtained based on samples prepared from one eye.

3407-Pos Board B512

Cholesterol Transport in Model Lipid Membranes

Sumit Garg, Lionel Porcar, Paul Butler, Francisco Castro-Roman, Ursula Perez-Salas.

Proper intracellular cholesterol transport is required for a healthy functioning of the cell and any disorder can lead to diseases, ranging from neurodegenerative Niemann Pick TYPE-C and Alzheimer, to cholelithiasis and atherosclerosis. However, the progress in the area of intra-cellular cholesterol transport is hampered by the huge inconsistencies in the reported value of cholesterol transport rates probably linked to the requirement of cholesterol tag or extraneous compounds such as cyclodextrine for such measurements. We recently reported a novel approach which employs Small Angle Neutron Scattering as a tool for in situ measurement of the cholesterol intra and inter-membrane exchange rates without recourse of cholesterol tags or extraneous compounds. Interestingly we found that cholesterol inter-membrane flipping is rather slow with half-life of a few hours. These results are in odds with the widely accepted belief that the presence of small hydrophilic group on cholesterol head should allow cholesterol to flip quickly through the hydrophobic acyl chain region of lipid membrane. In addition, we show that replacing cholesterol with the relatively benign dehydroergosterol or simply adding 2mM of cyclodextrine significantly affects and accelerates cholesterol flipping rates. To further develop the biophysical

mechanism for cholesterol trans-membrane flipping, transfer rates were measured for few cholesterol analogues with a slightly different molecular structure and thereby the geometrical and chemical compatibility with lipids. In addition, MD simulations were performed to measure the energetic and get the better understanding at molecular level for cholesterol transport. Overall, this work provides new insight in to cholesterol transport behavior in model lipid membrane.

3408-Pos Board B513

Unique Cholesterol Transport Behavior in Phosphoserine Vesicles: A Small Angle Neutron Scattering Study

Sumit Garg, Lionel Porcar, Paul Butler, Ursula Perez-Salas.

Cholesterol is critical for various cellular functions; however its excess is toxic. Cholesterol levels are maintained by various cholesterol metabolic pathways which depend critically on Intracellular cholesterol transport. Cholesterol is not homogeneously distributed in cell with 60-70% of cellular cholesterol present in plasma membrane and only 0.01-0.5% of cellular cholesterol present in endoplasmic reticulum. Any disruption in cholesterol distribution disorder has been linked to diseases such as Niemann Pick TYPE-C and Alziemers. It has been suggested that variable affinity of cholesterol for different lipids compositions could be one of the possible reason for the uneven distribution of cholesterol within cell. Traditionally the cyclodextrine or cholesterol oxidases have been used to measure the relative affinity of cholesterol for a particular lipid composition. However, the possible disruption of lipid-cholesterol interactions due to these molecules is unknown. This present study employs small angle neutron scattering to measure the cholesterol inter- and intra-membrane transport rate in model lipid vesicle without employing cholesterol tags and molecules such as cyclodextrine or cholesterol oxidase. The diffusion behavior was compared between two POPC vesicles and two POPS vesicles. Interestingly cholesterol exchange kinetics follows a non-continuous Arrhenius behavior in POPS membranes as compare to linear behavior in POPC membranes. Further cholesterol exchange kinetics was compared from POPC to POPS vesicles and POPS to POPC vesicles. Interestingly equilibrium cholesterol distribution changes with both cholesterol concentration and temperature. To our surprise we found that even a small amount of cyclodextrine can significantly shift the equilibrium distribution of cholesterol between POPS and POPC vesicles. Overall this wok provides insight in to POPS-cholesterol interaction and potential role of POPS is regulating intracellular cholesterol transport.

3409-Pos Board B514

Fluorogenic-Antioxidants: Novel Probes for Visualizing Reactive Oxygen Species in the Lipid Membranes of Live Cells

Katerina Krumova, **Gonzalo Cosa**.

We are pioneering the preparation of lipophilic fluorogenic antioxidant probes for the specific imaging of ROS in the membrane of live cells. Our strategy involves synthesizing a two segment receptor-reporter type free radical scavenger-fluorophore probe (an off-on fluorescent antioxidant indicator). The receptor segment in the probe mimics the structure and activity of the naturally occurring antioxidant α-tocopherol. A covalently tethered bodipy fluorophore serves the purpose of reporting, via emission enhancement, structural changes at the receptor end which result from the radical scavenging activity of the receptor.

Here we will present our most recent results involving the preparation of a second generation set of probes relying on newly synthesized bodipy dyes with improved redox properties. The new fluorogenic antioxidant probes undergo a 30 fold fluorescence enhancement upon reaction with peroxyl radicals in model lipid membranes. We will also illustrate a high-throughput fluorescence method enabled by the new probes, for the rapid determination of relative rates of free radical scavenging by α-tocopherol analogues. Rates are evaluated for tocopherol analogues with a modified lipophilic tail, when embedded in liposomes prepared from either unsaturated or saturated lipids, upon exposure to either hydrophilic or lipophilic peroxyl radicals. This work provides new insights and a quantitative understanding on the critical role of lipid diversity in modulating chemical reactions in the lipid milieu. Finally studies will be described where we utilize these new probes to image ROS in the lipid membrane of live cells.

3410-Pos Board B515

Relationships Between Bilayer Phase and Equilibration Rates of Patman and Laurdan

Hannabeth A. Franchino, John D. Bell.

Patman is a fluorescent membrane probe related to laurdan. The structural distinctions between the two probes are the lengths of the aliphatic tails (eleven carbons in laurdan and fifteen in patman) and the presence of a trimethylammonium forming a positively-charged head on patman. Studies exploring patman as a probe to detect membrane properties during apoptosis revealed that the two edges of the emission spectrum (435 and 500 nm) stabilize at different rates as the probe binds to the cell membrane. To test whether these differences represent dissimilarities in probe binding to ordered and disordered domains, experiments were conducted to monitor patman equilibration with bilayers composed of various mixtures of saturated and unsaturated phosphatidylcholines at temperatures above, at, and below the main thermotropic phase transition. In general, patman equilibrated more rapidly with bilayers in the liquid disordered phase than in the solid ordered phase. With solid phase membranes, the fluorescence stabilized faster at 435 nm than at 500 nm. Similar yet more subtle results occurred in the lipid disordered phase. In contrast, the situation was reversed at the phase transition temperature; equilibration was faster at 500 nm than at 435 nm. To determine whether these results reflected specific properties of patman, the experiments were repeated with laurdan, and several distinctions were observed. First, equilibration with solid phase lipids was faster than for patman and not different from equilibration with the fluid phase. Second, differences in rates between the two wavelengths were less than with patman for solid phase membranes but greater than with patman for melted bilayers. Third, at the phase transition temperature, equilibration rates favored 435 nm over 500 nm, the opposite of the result obtained with patman. Computer simulations were used to assist with interpretation of these results.

3411-Pos Board B516

Fluorescent Correlation Spectroscopy and Raster Image Correlation Spectroscopy as a Tool to Measure Diffusion in the Human Epidermis

Jonathan Brewer, Maria Bloksgaard, Jakub Kubiak, Luis Bagatolli.

Structural and dynamical characterization of skin tissue is vital for understanding the behavior of healthy and diseased skin tissue. Our objective is to develop protocols to measure the local diffusion of substances with different physical properties (for example amphiphilic or hydrophilic drugs) in the epidermis and dermis using fluorescent lipid analogs and hydrophobic dyes as model systems. As an example we use fluorescent labeled liposomes with a lipophilic dye in the bilayer and a hydrophilic dye inside. Using two color FCS (Fluorescent Correlation Spectroscopy) and two color RICS (Raster image correlation spectroscopy) we determine the diffusion and if intact liposomes penetrate the epidermis or if the burst before penetration. The experiments were preformed on a custom build multi-photon microscope[1]. Finally advantages and disadvantages of the different techniques for measuring diffusion in skin tissue are compared and discussed.

[1] J. Brewer, J. Bernardino de la Serna, K. Wagner and L.A. Bagatolli. Multiphoton Excitation Fluorescence Microscopy in planar membrane systems , Biochim Biophys Acta,doi:10.1016/ j.bbamem.2010.02.024 (2010).

[2] Susana A Sánchez and Enrico Gratton. Lipid-protein interactions revealed by two-photon microscopy and fluorescence correlation spectroscopy. Acc Chem Res 38(6): 469-77, 2005.

[3] Qiaoqiao Ruan, Melanie A Cheng,Moshe Levi, Enrico Gratton, and William W Mantulin. Spatial-temporal studies of membrane dynamics: scanning fluorescence correlation spectroscopy (SFCS). Biophys J 87(2): 1260-7, 2004.

[4] Claire M Brown, Rooshin B Dalal, B Hebert, Michelle A Digman, AlanR Horwitz, and Enrico Gratton. Raster image correlation spectroscopy (RICS) for measuring fast protein dynamics and concentrations with a commercial laser scanning confocal microscope. J Microsc 229(1): 78-91, 2008.

3412-Pos Board B517

Concentration Dependent Membrane Anchor Colocalization Study by Fluorescence Cross-Correlation Spectroscopy in Live Cells

Sara B. Triffo, Hector H. Huang, Adam W. Smith, Jay T. Groves.

Membrane anchors such as protein lipidations and glypiations have been proposed to play essential roles in the sorting and organization of plasma membrane-associated proteins, especially those involved in cell signaling. Here, we investigate the concentration dependence and variability of anchor colocalization in live cells by transfecting various cell types with pairs of fusion proteins created by replacing all but short tails of natively lipidated proteins with either red or green fluorescent proteins. These fusion proteins remove any native protein-protein interactions while fluorescently tagging membrane anchors in live cells. To observe sub-cellular organization, we use Fluorescence Cross-Correlation Spectroscopy (FCCS) to quantify the dynamic colocalization between green- and red-labeled anchors. FCCS allows observations of dynamic colocalization in live cells at a greater range of separation distances than is allowed by FRET, and because it is a dynamic measurement FCCS avoids ambiguous or false positive colocalization that can result from static studies. Fusion protein expression level, as determined by overall intensity of cell fluorescence, naturally varies in a population of transiently transfected cells. Using this to our advantage, we are able to observe cells within a wide range of protein expression and explore trends between concentration and fusion protein colocalization. We also analyze variation in the amount of colocalization and observe a difference between the variability from cell-to-cell and the variability from spot-to-spot within one cell across several anchor types and different cell lines.

3413-Pos Board B518

Dynamics of Red Blood Cells and Vesicles in Microchannels of Oscillating Width

Thomas Franke, Susanne Braunmueller, Schmid Lothar.

We have studied the dynamics of red blood cells and fluid lipid vesicles in hydrodynamic flow fields created by microchannels with periodically varying channels width. For red blood cells we find a transition from a regime with oscillating tilt angle and fixed shape to a regime with oscillating shape with increasing flow velocity. We have determined the crossover to occur at a critical ratio of channel width L_y and red blood cell velocity v_m approx. 10⊥-3s. These oscillations are superposed by shape transitions from a discocyte to a slipper shape at low velocities and a slipper to parachute transition at high flow velocities.

Ref.:
H. Noguchi, G. Gompper, L. Schmid, A. Wixforth, T. Franke, EPL (Europhysics Letters) 2010, 89, 28002
S. Braunmueller, L. Schmid, T. Franke J.Phys. Condens. Matt. accepted

3414-Pos Board B519

Modulation of the Solid-Ordered/Liquid-Disordered Melting Temperature in Staphylococcus Aureus during Biofilm Formation

Hector J. Ocampo Ariza, Johanna Chavez, Maria F. Contreras, Natalia Rodriguez, Catalina Arevalo, Chad Leidy.

Bacteria that interact with surfaces under hydrated conditions can form aggregated structures known as biofilms. Biofilms are characterized by having increased resistance to a variety of antibacterial agents. This resistance is responsible for the generation of persistent chronic infections, and represents a serious threat to human health. Several antimicrobial agents, including hydrolytic enzymes such as PLA_2-IIA and antimicrobial peptides (AMPs) such as Magainin-2, act by disrupting bilayer membrane integrity. Since these antimicrobial agents require physical disruption of the bilayer membrane, their activity is likely to be sensitive to lipid packing. This points to a possible mechanism for generating resistance during biofilm formation through the modulation of lipid packing. Bacterial membranes present broad but cooperative lipid chain-melting events, where the membrane transitions from a solid-ordered (so) state, characterized by a high level of lipid packing, into a liquid-disordered (ld) state. For example, for *Staphylococcus aureus* (*Sa*) in planctonic state, this melting event occurs at 15°C. We have recently shown that, for *Sa,* the solid-ordered phase provides resistance towards PLA_2-IIA. In this work we show, by measuring generalized polarization of Laurdan incorporated into lipid extracts, that the position of this melting event is shifted to 28°C during *Sa* biofilm formation. Additionally, we present evidence that this shift in the melting temperature modulates resistance towards PLA_2-IIA and magainin-2. These results point to a mechanism by which bacterial membranes can generate resistance towards membrane active antibacterial agents through the modulation of the so/ld chain melting event during biofilm formation.

3415-Pos Board B520

Outer Membrane Protein Dynamics in E.coli

Joseph Goose, Mark S.P. Sansom.

The vast majority of currently structurally characterised outer membranea proteins of E.coli are beta barrel porins that exist either as monomers or homo-oligomers. The function of these porins is varied and complex and is thought to depend not just on their structural dynamics but also on interactions both with other porins and with their lipid environment.

To provide an insight into these processes we study in detail the motion and arrangement of both lipids and proteins within a series of model systems.

We represent the outer membrane as a bilayer consisting of mixtures of phosphatidylglycerol (PG) and phosphatidylethanolamine (PE) lipids and examine by means of atomistic and coarse grained simulations the relative dynamics of a representative sample of outer membrane proteins. We consider the diffusive ability of both isolated, and multiple proteins within larger systems which more realistically reflects the density of porins within the outer membrane. The diffusive behaviour of proteins is related to protein characteristics such as size and localised bilayer deformation.

3416-Pos Board B521

Influence of Borna Disease Virus Matrix Protein on Model Membranes Investigated by Molecular Dynamics Simulations

Bjoern E.S. Olausson, Alexander Vogel.

Borna disease virus (BDV) is an infectious, neurotropic, enveloped RNA virus with a wide host range among the warm-blooded animals. It belongs to the *Mononegavirales* which also include Ebola and Marburg. Depending on the infected host species, BDVM can influence the behavior, neural plasticity, or trigger a immunopathological reaction with high mortality rates. Although the hypothesis that BDV can infect humans is discussed very controversially, it still serves as a model for persistent viral infections in the central nervous system. The BDV matrix protein (BDV-M) with ~16kDa is the smallest matrix protein among the negative stranded viruses. It plays an important role during the virus assembly and budding process by interacting with the host membrane and possibly the viral RNA. Studies, using a monolayer technique, showed that BDV-M condenses the lipid monolayer. Therefore, based on the 3D-structure, derived from X-Ray crystallography, a computer model was built to investigate the protein membrane interaction. The membrane consisted of POPS, POPC and Cholesterol (molar ratio 1:2:2) to closely match the brain lipid composition in terms of lipid head group charge distribution. The simulation was conducted at 303K in the NPγT ensemble and the membrane surface tension was adjusted to resemble the average order parameter measured by ^{2}H solid state NMR to ensure the correct area per lipid. Analysis of the MD simulation showed a distinct influence on lipid diffusion rates and lipid distribution in the BDV-M facing membrane leaflet. BDV-M quickly starts sorting charged lipids beneath itself and thereby partially separates POPS from POPC. This is accompanied by an increase in the POPS diffusion rate which for the proximal interface is higher (~1.4E-06 cm^2/s) compared to the distal interface (0.8E-06 cm^2/s) in the first few hundred ns.

3417-Pos Board B522

Dynamics of Multicomponent Lipid Membranes at Long Length and Time Scales: Domain Growth, Rheology, and Scaling Laws

Brian A. Camley, Frank L.H. Brown.

We present a simple continuum simulation method for multicomponent lipid bilayers that accounts for both the Saffman-Delbruck hydrodynamics of the membrane and the appropriate thermal fluctuations. We use this scheme to describe the dynamics of ternary model membranes on length scales from nanometers to microns and time scales of up to tens of seconds. Simulation results for phase separation, domain diffusion, and domain flickering are all in agreement with experimental results and well-established theory. Our results also provide a simple technique to extend fluorescence microscopy "flicker spectroscopy" to determine membrane viscosities. We also study the problem of phase separation (domain growth). Simple scaling theories, along with our simulations, allow us to explain the range of scaling exponents (0.15 - 0.67) previously reported by both experiments and simulations, and provide a framework for interpreting measured coarsening exponents. We briefly address some applications of this work to biophysical models of lipid rafts, as well as extensions to systems with embedded proteins and curvature-composition coupling.

3418-Pos Board B523

Peptide Transfer Energetics from Direct Water-To-Membrane Partitioning Simulations

Martin B. Ulmschneider.

Polypeptide partitioning properties are at the heart of biological membrane phenomena, and their precise quantification is vital for ab-initio structure prediction. However, this has proved difficult to measure experimentally. Recently the cellular translocon machinery has been employed to determine the insertion energetics for a series of systematically designed peptides. We show here that the insertion propensity, pathway and transfer energetics of these peptides into POPC bilayers can also be obtained by direct atomic resolution partitioning simulations. Remarkably, the results are in close agreement the translocon experiments, but reveal a systematic shift towards the insertion of shorter peptides. The insertion probability as a function of peptide length follows two-state Boltzmann statistics and reveal many hitherto unknown atomic-resolution details about the partitioning process. The method presented provides a powerful new tool for rapid determination of water-to-bilayer transfer properties of membrane active peptides.

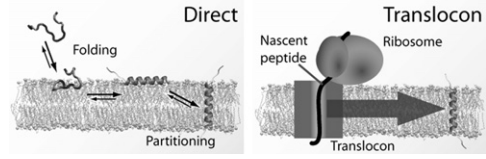

3419-Pos Board B524

Assessing Perturbations of a Fluorescent Lipid in a DPPC Bilayer with Molecular Dynamics

David Ackerman, Jonathan Amazon, Fred Heberle, Gerald Feigenson.

Fluorescent lipid analogs are a valuable tool for studying membranes, and in recent years a wide variety of fluorescence techniques have contributed significantly to our understanding of lateral heterogeneity in both model and cell membranes. Despite their usefulness, it is often overlooked that these fluorescent molecules are extrinsic to the system of interest, and a meaningful interpretation of data, e.g. properties of nanoscopic domains, local motion and order of the probe environment, or Forster resonance energy transfer, can

benefit from understanding probe location within the bilayer, and how the probe itself affects the native membrane state. We have conducted molecular dynamics simulations to investigate perturbations in a DPPC membrane of a family of commonly-used fluorescent lipids: the indocarbocyanine chromophore DiI attached to two alkyl chains, which vary in length and degree of unsaturation. In particular, we report on the order and dynamics of DPPC as a function of distance from the probe molecule, as well as the influence of probe acyl chains on the location and dynamics of the DiI chromophore.

3420-Pos Board B525
Self-Distribution of Dye and Isoflurane in the DPPC Bilayer
Brock Cardon, Eric Melonakos, **Neil Brasfield**, IlHeon Ha, John D. Bell, David D. Busath.
Volatile anesthetics are postulated to partition to the lipid-water interface. Lipid-soluble dyes, such as diphenylhexatriene (DPH) and its tetramethylammonium analog (TMA-DPH), have been measured, using quenching by tail-bound nitroxide spin labels, to span a bilayer leaflet, with the polar end of TMA-DPH residing ~4Å closer to the interface than DPH. Using empirical, non-polarizable force fields for the dyes and for isoflurane, and various starting positions, we assessed dye and anesthetic positions after 10-ns dynamics simulations at 330 K and isotropic pressure. Structural equilibration was evaluated by tracking tetragonal simulation cell dimensions. Dye molecules rapidly (<1 ns) migrated spontaneously into one of the 64-molecule dipalmitoylphosphatidylcholine leaflets. TMA-DPH resided closer to the surface of the bilayer with its axis parallel to the bilayer normal, whereas DPH often assumed tilted positions. Isoflurane molecules (4, 8, 32 or 128) were positioned in the bulk water (3363 molecules) near a bilayer with either a pair of DPH or TMA-DPH molecules, corresponding to anesthetic molalities of 0.06-1.94 m. In the high density simulations, they aggregated into a separate phase surrounded by water, and few molecules entered the lipid bilayer. This is consistent with the solubility of isoflurane in water, 0.0133 M at room temperature and declining with increasing temperature, ~2-fold/20 K. At the lower two densities, several or most anesthetic molecules were absorbed into the bilayer. First, they adsorbed to the headgroup region, where they paused briefly, but then they diffused to the tail region, where they typically stayed the remainder of the simulation. These studies lay the groundwork for assessment of the effect of anesthetics on the wobble motions of the dye molecules in the bilayer, for comparison to fluorescence anisotropy measurements.

3421-Pos Board B526
A computational Study of Gel Nucleation in Lipid Bilayer
Zun-Jing Wang, Markus Deserno.
Even though registration and anti-registration in lipid bilayers have been observed on the level of individual lipids experimentally in a nearest-neighbor recognition analysis and computationally in coarse-grained (CG) simulations, the switching mechanism from one matching to another between two leaflets remains unclear. In mean field analysis, coupling between domains was described by a composition-dependent surface tension or, in the case of small compositional changes, by a single coupling constant induced mainly by dynamic chain interdigitation, but the theory has not been tested. Here, we aim to provide a quantitative analysis of the coupling between gel domains at the early stage of nucleation by combining forward flux sampling (FFS) with molecular dynamics simulations of lipid bilayer membranes with a systematic solvent-free CG model. The combination of both techniques enables us to sample the rare events of gel domain nucleation in the lipid bilayers at moderate computational expense, while still preserving chemical specificity and quantitative accuracy. The FFS is implemented to capture the growing and shrinking scenarios of a gel nucleus in a bilayer. We first study gel nucleation in a fluid DPPC bilayer membrane to understand the coupling between domains independent of composition change. Afterwards, we study gel nucleation in a DPPC-DOPC binary membrane, which adds the complication of a composition-dependent surface tension of the gel domain. The free-energy of gel nucleation is computed as a function of gel domain size, and both intra- and inter-leaflet coupling between domains are analyzed.

Membrane Fusion II

3422-Pos Board B527
Mechanisms of Entry of Vaccinia Virus into Cells Studied by Photosensitized Labeling
Mathias Viard, Bernard Moss, Robert Blumenthal.
Vaccinia virus is a prototype member of the poxviruses that has a complex genome consisting of more than 200 genes. Along with this comes a complex assembly process giving rise to various forms of the virus whose topology needs to be further studied. To study fusion of intact virions with cells we have developed methodologies based on photosensitized activation by fluorescent lipid analogs of a hydrophobic probe, [^{125}I]5-iodonaphthyl-1-azide ([^{125}I]INA), that rapidly partitions into the membrane bilayer of cells. The photosensitized labeling methodology involves measurement of incorporation of [^{125}I]INA into the viral membrane-resident protein(s) as a result of virus-cell fusion. We can therefore assess the extent of membrane fusion at different times of interaction between the virus and its target cell and determine the sensitivity of this process to various compounds. We monitored vaccinia fusion with HeLa cells by assessing the incorporation of [^{125}I]INA into a vaccinia membrane protein D8L. Maximum labeling was observed upon 30 minutes incubation at physiological pH. This phenomenon was enhanced by the exposure of the prebound virus to a pH5 pulse. The measurements specificity was confirmed by the inability of the heat inactivated virus and entry-deficient mutants to induce D8L labeling. While supporting the hypothesis of a membrane fusion phenomenon, those observations also support a route of entry of the virus through internalization by endocytosis. However, comparison with influenza virus for endosomal entry indicates striking differences in their sensitivity to inhibitors of endosomal processes. To further assess endosomal entry we used a dynamin inhibitor, dynasore, which blocks vaccinia entry as measured using a gene reporter assay. Interestingly dynasore also inhibited the labeling of cells with fluorescent lipids. The multiple effects of dynasore are being further studied. Funded in part by NCI Contract HHSN26120080001E.

3423-Pos Board B528
Shallow Boomerang-Shaped Influenza Hemagglutinin G13A Mutant Structure Promotes Leaky Membrane Fusion
Alex Liqi Lai, Lukas K. Tamm.
Our previous studies showed that an angled boomerang-shaped structure of the influenza hemagglutinin (HA) fusion domain is critical for virus entry into host cells by membrane fusion. Since the acute angle of ~105 degree of the wild-type fusion domain promotes efficient non-leaky membrane fusion, we asked whether different angles would still support fusion and thus facilitate virus entry. Here, we show that the G13A fusion domain mutant produces a new leaky fusion phenotype. The mutant fusion domain structure was solved by NMR spectroscopy in a lipid environment at fusion pH. The mutant adopts a similar boomerang structure as wild-type, but with a shallower kink angle of ~150 degree. G13A perturbs the structure of model membranes to a lesser degree than wild-type, but to a greater degree than non-fusogenic fusion domain mutants. The strength of G13A binding to lipid bilayers is also intermediate between that of wild-type and non-fusogenic mutants. These membrane interactions provide a clear link between structure and function of influenza fusion domains: An acute angle is required to promote clean non-leaky fusion suitable for virus entry, presumably by interaction of the fusion domain with the transmembrane domain deep in the lipid bilayer. A shallower angle perturbs the bilayer of the target membrane so that it becomes leaky and unable to form a clean fusion pore. Mutants with no fixed boomerang angle interact with bilayers weakly and do not promote any fusion or membrane perturbation.

3424-Pos Board B529
Structure and Function of the Fusion Loop from Ebolavirus GP2
Sonia M. Gregory, Erisa Harada, Binyong Liang, Sue Delos, Judith M. White, Lukas K. Tamm.
Ebolavirus is an enveloped virus belonging to the *Filoviridae* family that causes hemorrhagic fever in humans. The mechanism of virus-host membrane fusion is not well characterized, but is mediated by the single viral glycoprotein, GP. Ebolavirus membrane fusion occurs from an endosomal compartment after proteolytic activation of GP by endosomal cathepsins and is governed by a patch of hydrophobic residues located within the internal fusion loop of the GP fusion subunit, GP2. Here we present liposome fusion data and NMR structures for the disulfide bound internal fusion loop (Ebov FL) at neutral and mildly acidic pH conditions. Membrane fusion activity of Ebov FL was measured in a liposome fusion assay after acidification to pH 5.5. Liposome fusion studies with varying lipid compositions showed that anionic lipids do not greatly contribute to lipid mixing, but the dependence on head group structure played a greater role. Replacement of POPG with POPS showed a decrease in lipid mixing whereas replacement with bis(monoacylglycero)phosphate (BMP) showed comparable lipid mixing. CD experiments indicated that moderate secondary structure was formed upon the addition of DPC at pH 7.0 reaching 14% α-helical structure, which further increased upon acidification to 23%. The NMR structures in DPC micelles at neutral and acidic conditions revealed a conformational change forming a bend in the fusion loop at the lower pH. The bend guides the reorganization of residues located in the hydrophobic patch. This rearrangement is thought to promote lipid disruption resulting in membrane fusion.

3425-Pos Board B530

Association of Transmembrane Helices in Viral Fusion Peptides Suggests a Protein-Centric Mechanism of Membrane Fusion

Giacomo Fiorin, Jason E. Donald, Yao Zhang, Vincenzo Carnevale, David R. Slochower, Feng Gai, Michael L. Klein, William F. DeGrado.

A broad range of biological functions, from neurotransmitter release to infection by enveloped viruses, is achieved by fusogenic proteins, which increase the intrinsically slow rate of membrane fusion by using their energetically downhill conformational changes. Among viral fusogenic proteins, many are identical trimers that feature a fusion mechanism reminiscent of the SNARE proteins responsible for vesicle fusion. In this mechanism, the N-terminal hydrophobic fusion peptide domains (FP) of the three protein chains insert into the host cell's membrane, and then zipper with the viral-membrane attached TM domains of the same protein, driving the two membranes together in the process. So far, only high resolution structures of the soluble portions exist, and the minimal number of trimeric proteins is also undetermined. By analytical ultra-centrifugation and polarized infrared spectroscopy, we proved that the FP of the parainfluenza virus (PIV) fusogenic protein forms hexameric helical bundles that lie transverse to lipid bilayers. We modeled the FP hexamer's structure and refined it by molecular dynamics simulations, observing an association mode mediated by water and a glutamine amino acid, frequently occurring in diverse fusion peptide sequences. This structure suggests that as few as two trimeric proteins may form a hexameric bundle of their FP domains, and induce curvature on the cellular membrane through a mechanism analogous to mechanosensitive channels. The FP hexamer is at the geometric center of such fusion mechanism at all times. By simulations at atomic detail of the fusion process, we identified the amino acids that control the associated hydration and dehydration events, and suggest new strategies to inhibit viral infections.

3426-Pos Board B531

High-Resolution Secondary and Tertiary Structure of the Membrane-Associated HIV Fusion Peptide by Itself and in Large gp41 Ectodomain Constructs: Correlation Between Beta Sheet Registry, Membrane Insertion and Perturbation, and Fusion Catalysis

Scott D. Schmick, Erica P. Vogel, Kaitlin M. Young, **David P. Weliky**.

The initial step of HIV infection is fusion between the viral and target cell membranes. Fusion is mediated by the HIV gp41 protein and its N-terminal ''fusion peptide'' (FP) which binds to target cell membranes. The FP by itself catalyzes membrane fusion and the secondary and tertiary structure of membrane-associated FP was probed at high-resolution using solid-state NMR spectroscopy. For membranes with biologically-relevant cholesterol content, the FP forms antiparallel β sheet structure with a wide distribution of antiparallel registries. The population of each registry was quantified and a good correlation was observed between registries that were populated and those which had negative free energies of membrane insertion. A very different registry distribution was detected for the non-functional V2E mutant which binds to membranes but is not membrane-inserted. These results support a general structure-function model which correlates β sheet FP registry, FP membrane insertion and membrane perturbation, and fusion catalysis. This model is currently being tested for large membrane-associated ectodomain constructs of gp41 that contain the FP.

3427-Pos Board B532

Individual Vesicle-Vesicle and Vesicle-Planar Bilayer Fusion Events Mediated by DNA

Bettina van Lengerich, Bob J. Rawle, Poul Martin Bendix, Minsub Chung, Steven G. Boxer.

We have previously reported that DNA-lipid conjugates, when inserted into lipid vesicles, can mediate interactions between vesicles such as docking and fusion*. These DNA-mediated interactions are a model for the biological machinery (SNARE proteins) employed in synaptic vesicle fusion. We can also use DNA-lipids to build model membrane platforms, such as tethered vesicles and tethered free-standing membranes, which are employed in these studies to observe individual fusion events using fluorescence microscopy. Two systems will be described: vesicle to vesicle fusion between mobile, tethered vesicles, and vesicle to planar bilayer fusion of small vesicles to a DNA-tethered free-standing bilayer. Fusion of individual vesicles is observed in real time using lipid and content mixing assays, as well as FRET upon hybridization of labeled DNA-lipids. These studies provide insight into the relative timescales and extents of docking, lipid mixing, and content exchange. In addition, using different sequences of fluorescently labeled DNA to mediate fusion gives insight into the importance of the rates and number density of hybrid formation at the fusion pore relative to the rate of fusion pore opening. This fusion machinery can also be used to deliver membrane proteins from small vesicles into GUVs or DNA-tethered planar bilayers, allowing membrane proteins to be studied in a free-standing bilayer.

*Chan et al, PNAS 2007 and 2009; Chan et al, Biointerphases 2008.

3428-Pos Board B533

DNA-Machinery for Delivering Membrane Proteins into Free Standing Lipid Bilayers

Minsub Chung, Poul Martin Bendix, Namdoo Kim, Steven G. Boxer.

Free standing lipid bilayers tethered to a glass surface by short DNA duplexes provide an excellent environment for studying transmembrane proteins free from any surface interactions. However, membrane protein dynamics in such model membranes are by far less studied due to the difficulty of protein incorporation into GUVs and tethered membranes while maintaining their function. Inspired by previous work on DNA-mediated membrane fusion study of our group*, we applied a DNA-machinery to achieve fusion of proteoliposomes containing photosyntethic reaction center to either GUVs or DNA-tethered lipid membrane patches formed by GUV rupture onto DNA coated glass surfaces**. The diffusion behavior of delivered proteins is measured and compared with those in supported bilayers. Also, the protein activity and orientation before and after fusion is analyzed. This will offer a feasible method to incorporate intact membrane proteins to already formed model membranes. In addition, the behavior of proteins during the fusion event will provide insight into the mechanism of DNA-mediated lipid membrane fusion.

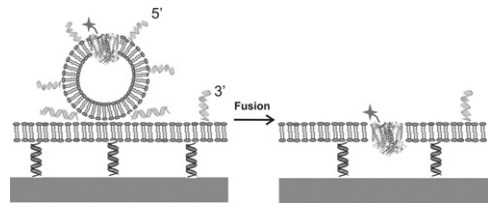

* Chan *et al., PNAS*, **106**, 4, 979-984 (2009)

** Chung *et al., Journal of Structural Biology*, **168,** 190-199 (2009)

3429-Pos Board B534

Interaction Forces Between Model Myelin Membranes

Xavier Banquy, Kai Kristianson, Dong Woog Lee, Joan Boggs, Cynthia Husted, Younjin Min, Joe Zasadzinski, Jacob Israelachvili.

Myelin dysfunctions vary from deterioration of signal transduction to demyelinating diseases such as multiple sclerosis (MS). MS is characterized by a change in the lipid composition of the myelin membrane which leads to the appearance of lesions reflecting loss of inter-membrane adhesion. We want to understand the molecular synergistic interaction between lipids responsible for a healthy myelin membrane structure.

We have performed Surface Force Apparatus measurements on supported myelin membranes, in order to study the effect of lipid composition and calcium on the interaction forces. Interaction forces between cytoplasmic healthy model membranes were found to be repulsive and electrostatic in nature at large separation distances. At smaller separation distances, steric forces due to the compression of the lipid headgroups and the hydration layer take over. Addition of calcium affected the effective surface potential of the membrane and its thickness. At high compressive loads and long contact time, adhesion forces appear but remain quite low (<2mN/m). Van der Waals and hydrophobic interaction forces are the main components of this adhesive force. Lipid composition of the membrane was changed to model the cytoplasmic membrane composition found in patients having MS. The interaction forces between the membranes in calcium depleted medium were found to be quite similar to healthy model. Addition of calcium in the medium resulted in a large increase of the adhesion force which magnitude appears to be time and load dependent. This enhancement of the adhesion energy is accompanied by a thinning of the membrane during contact time indicating that hydrophobic interaction is responsible for the increase in the adhesion force.

These results show how the molecular forces between model myelin membranes depend on the lipid composition which will allow us to develop a molecular model of the early stages of demyelination.

3430-Pos Board B535

The Accelerated Late Adsorption of Pulmonary Surfactant

Ryan W. Loney, Shankar B. Rananavare, Stephen B. Hall.

The rate at which surfactants lower surface tension (γ) during adsorption to an air/water interface normally slows progressively as γ falls. With vesicles of pulmonary surfactant, the slope of the γ-time isotherm initially decreases, but it then becomes steeper just before reaching the equilibrium γ. To determine the mechanisms that produce the accelerated drop in γ, we tested whether

the steeper slopes reflected later time or lower γ. Adsorption at constant γ and to preexisting films showed that the steeper slope depended on γ rather than time, indicating that the acceleration resulted from changes in the film rather than in the adsorbing material. Compositional studies tested how removing cholesterol, the anionic phospholipids, and the hydrophobic proteins affected the late acceleration. Only the absence of the proteins eliminated the late adsorption. Vesicles of phospholipid with dioleoyl phosphatidylethanolamine, however, which, like the surfactant proteins, promotes fusion between vesicles, also demonstrated the accelerated late adsorption. These results suggest that the late acceleration occurs when vesicles that adsorb by fusion with the nascent film can interact more readily with a more densely packed monolayer. (Small angle x-ray diffraction studies conducted at the Stanford Synchrotron Radiation Lightsource.)

3431-Pos Board B536

Dihydrosphingomyelin Impairs HIV-1 infection by Rigidifying Liquid-Ordered Membrane Domains

Catarina R. Vieira, Jose M. Munoz-Olaya, Jesús Sot, Sonia Jiménez-Baranda, Nuria Izquierdo-Useros, José-Luis Abad, Beatriz Apellániz, Rafael Delgado, Javier Martínez-Picado, Alicia Alonso, Josefina Casas, José L. Nieva, Gemma Fabriás, **Félix M. Goñi**.

The lateral organization of lipids in cell membranes is thought to regulate numerous cell processes. Most studies focus on the coexistence of two fluid phases, the liquid crystalline (ld) and the liquid-ordered (lo); the putative presence of gel domains (so) is not usually taken into account. We show that in phospholipid:sphingolipid:cholesterol mixtures, in which sphingomyelin (SM) promoted fluid lo domains, dihydrosphingomyelin (DHSM) tended to form rigid domains. Genetic and pharmacological blockade of the dihydroceramide desaturase (Des1), which replaced SM with DHSM in cultured cells, inhibited cell infection by replication-competent and deficient HIV-1. Increased DHSM levels gave rise to more rigid membranes, resistant to the insertion of the gp41 fusion peptide, thus inhibiting viral-cell membrane fusion. These results clarify the function of dihydrosphingolipids in biological membranes and identify Des1 as a potential target in HIV-1 infection.

3432-Pos Board B537

Cholesterol and Low Temperature Enhance Fusion of Vesicles to a Planar Bilayer

David E. Lee, Matthew G. Lew, Reed A. Doxey, Dixon J. Woodbury.

Lipid composition plays an important role in fusion of vesicles to membranes, an essential process for exocytosis. Lipid head group, tail structure, and sterol content all impact the complex phase behavior of membranes. To determine the effect of lipids on fusion rate, we utilized the nystatin/ergosterol (nys/erg) fusion assay and stimulated fusion with an osmotic gradient. Using PE/PC planar membranes with increasing concentrations of cholesterol, and keeping vesicle lipids constant (PE/PC/PS/ERG), we observed increasing fusion rates. We also observed that temperature affects fusion rates by forming DPPC membranes on 5ul glass capillary pipets. Planar membranes were painted with concentrated DPPC in decane. Significantly different fusion rates were observed at temperatures above and below the DPPC transition temperature (Tt) of 41C. Decreasing the temperature below Tt increased the fusion rate, while increasing the temperature above Tt reduced the fusion rate. These data are consistent with the hypothesis that vesicle fusion with a membrane is suppressed in a liquid disordered lipid phase, and shows how membrane fusion can be affected by lipid behavior.

3433-Pos Board B538

Cholesterol as a Modulator of the HIV-1 gp41 Fusion Domain's Function

Andrey Ivankin, David Gidalevitz.

The early steps in HIV-1 infection of cells involve fusion of the envelope with the host cell membrane. The N-terminal fusion domain of the viral envelope glycoprotein 41 subunit is widely accepted to play a key role in the fusion process facilitating membrane anchoring, destabilization, and bending. Ability of the fusion domain to perform these essential functions depends strongly on the structural and mechanical properties of the host cell membrane, which are defined by the lipid composition and cholesterol content. Here we present results of an X-ray study aimed at the understanding the effect of cholesterol concentration in model lipid membranes on the activity of the viral fusion domain. Lipid monolayers at the air-liquid interface composed of DPPC and cholesterol were used to model an approximate environment where the fusion domain comes into contact with the host cell membrane. The electron density profiles across the films, derived from X-ray reflectivity data, demonstrate that the fusion domain penetrates into all DPPC/cholesterol monolayers. The depth of membrane insertion and orientation/conformation of the fusion domain within the film, as well as lipid-to-fusion peptide ratio, depend strongly on the membrane cholesterol concentration. Distinct insertion modes also suggest that the fusion domain-induced membrane curvature is considerably different in bilayers with low and high cholesterol content. Finally, using grazing incidence X-ray diffraction we have demonstrated that the viral fusion domain possesses limited membrane destabilizing effect and is incapable to degrade the gel phase in the DPPC/cholesterol films.

3434-Pos Board B539

Destabilization of Highly Rigid Bilayers Enriched in Cholesterol by the Membrane-Proximal External Region of HIV-1 gp41

Beatriz Apellaniz, Andrey Ivankin, David Gidalevitz, **Jose L. Nieva**.

Current models for HIV fusion incorporate the induction of curvature stress and/or membrane defects by the membrane-proximal external region (MPER) of the envelope glycoprotein 41 subunit. The enrichment in aromatic residues predicts a highly favorable membrane-bound state for MPER, which would insert into the interface of the viral membrane external monolayer. However, the high levels of cholesterol found in the lipid envelope (Cholesterol-to-phospholipid mole ratio: ≈ 1) suggest that MPER insertion will be hampered in functional virions. Here, we have varied the membrane composition in order to test systematically bilayer area compressibility modulus (K_a) and monolayer spontaneous curvature (R_o) effects on binding and pore opening by MPER-derived peptides. In addition, we have assessed the degree of exposure to solvent, based on the reactivity to anti-MPER antibody. Finally, using grazing incidence X-ray diffraction (GIXD) and specular X-ray reflectivity (XR) we have studied the interactions of the MPER peptides with phospholipid monolayers containing low and high levels of Cholesterol. Our results support a role for MPER in destabilizing the highly rigid envelope, and suggest that the establishment of favorable MPER-cholesterol interactions may help overcoming the restrictions to the insertion process.

3435-Pos Board B540

Entry Pathways of an Avian Virus into Cells Expressing Transmembrane and GPI-Anchored Receptor Isoforms

Naveen Jha, Erik Martin, Olga Latinovic, Mariana Marin, Gennadiy Novitskiy, Kosuke Miyauchi, **Gregory Melikian**.

Avian Sarcoma and Leukosis Virus (ASLV) entry into cells proceeds through two major steps -priming by cognate receptors on the cell surface followed by low pH-induced fusion with endosomes. Subtype A viruses are able to utilize two naturally occurring isoforms of the TVA receptor for infection, the GPI-anchored (TVA800) and the transmembrane (TVA950) receptors, which are localized to different membrane domains. We monitored the consecutive steps of ASLV entry into cells expressing these receptor isoforms, including endocytosis, delivery into acidic compartments, and fusion with endosomes. Cells expressing TVA950 internalized ASLV much faster than those expressing the alternative receptor. In both cell lines, fusion occurred shortly after internalization, suggesting that virus uptake was the rate-limiting step of entry. We found that ASLV fusion with endosomes proceeded through two relatively long-lived intermediates, a hemifusion-like intermediate and a small fusion pore. The lifetime of these intermediates was dependant on TVA receptor isoforms and their expression levels. TVA950 supported more robust fusion intermediates compared to TVA800. These findings are consistent with ASLV trafficking by via TVA950 to endosomal compartments that are more conducive to fusion. Alternatively, transmembrane receptor might more efficiently prime the viral fusion proteins compared to the GPI-anchored receptor. This work has been supported by the NIH AI053668 grant.

3436-Pos Board B541

Trans-Membrane Domain of HIV gp41 Interacts with the Externally Added gp41 Fusion Peptide: TMD-FP Complex Inhibits Model Membrane Fusion

Hirak Chakraborty, David G. Klapper, Barry R. Lentz.

We report the effects of a complex between fusion peptide (FP) and transmembrane domain (TMD) of gp41, that separately promote fusion, on the kinetics of PEG-mediated fusion and on the structure of the bilayer. Circular dichroism (CD) measurements showed that FP in the membrane exists mostly in a beta sheet at L/P ratios 1200/1 to 200/1, while the gp41 TMD displayed ~32% helix, 23% beta, 21% turn and 24% other secondary structure content at L/P of 300/1. Adding FP to membranes containing TMD resulted in a TMD-FP complex with reduced helical content and increased beta and

turn content. DPH and TMA-DPH anisotropy measurements revealed that the FP-TMD complex reduced membrane order in both the interface and interior regions of the bilayer, whereas FP alone increased order in both regions. The complex also increased water penetration into the bilayer (lifetime ratio of TMA-DPH in H2O and D2O) much more than for the individual peptides. While the FP decreased membrane free volume (from partitioning of C6NBDPC from micellar to bilayer phase), the presence of TMD enhanced this effect enormously. The time courses of lipid mixing (LM), content mixing (CM) and content leakage (L) were fitted globally to 3-state or 4-state sequential models (Biophys. J., 2007, 92; 4012), providing estimates of rate constants for inter-conversion between states as well as probabilities of the occurrence of LM, CM or L in each state. The FP-TMD complex inhibited the rates of initial intermediate but especially pore formation. The effect on pore formation was predominantly due to a large increase in the activation enthalpy not matched by as large an increase activation entropy. Supported by NIGMS grant 32707 to BRL.

3437-Pos Board B542

Both Fusion Peptide and Trans-Membrane Domain of HIV gp41 Individually Reduce the Activation Barriers for the Fusion Process

Hirak Chakraborty, David G. Klapper, Barry R. Lentz.

Poly(ethylene glycol)- (PEG-) mediated fusion of 25 nm vesicles was examined in the presence of the HIV gp41 fusion peptide (FP) and trans-membrane domain (TMD) at temperatures between 17°C and 37°C. Membrane lipid composition was Dioleoylphosphatidylcholine (DOPC), dioleoylphosphatidylethanolamine (DOPE), bovine brain sphingomyelin (SM) and Cholesterol (CH) (35:30:15:20). Lipid mixing (LM), content mixing (CM) and content leakage (L) time courses were fitted globally to 3-state or 4-state sequential models (Biophys. J., 2007, 92; 4012), yielding estimates of rate constants for conversion between states as well as probabilities of the occurrence of LM, CM, or L in each state. Non-linear Arrhenius plots in control and peptide-containing vesicles implied that the nature of the barrier between states for all systems changed with temperature (i.e., activation enthalpy and entropy varied with temperature). In control vesicles, CM occurred earlier in the process at higher temperatures such that fusion shifts from a 4-state to a 3-state model above ($\geq$27°C). Mainly FP but also TMD enhanced the rate of initial intermediate formation. Above about 22°C, this resulted from a large increase in activation entropy overcoming an unfavorable large increase in activation enthalpy, suggesting that the peptides reduced exposure of water to hydrocarbon in the transition state relative to control vesicles. Both peptides enhanced the rate of final pore formation to such an extent that the fusion process followed a 3-state (single intermediate) model even at low temperature (170C). This effect was greatest for TMD and was also largely an entropic effect. Supported by NIGMS grant 32707 to BRL.

3438-Pos Board B543

The Trans-Membrane Domain of the SNARE Fusion Protein Syntaxin (SX) Enhances the Rate of Intermediate Formation

Suzanne E. Lynch, Michael J. Bruno, Barry R. Lentz.

During neurotransmitter release, synaptic vesicles fuse with the pre-synaptic plasma membrane, leading to the merger of two lipid bilayers and the release of neurotransmitters. This process requires formation of a complex between SNARE proteins in both membranes. One of the SNARE proteins required for membrane fusion is Syntaxin (SX), a membrane anchored protein in the pre-synaptic membrane. Since viral fusion peptides and trans-membrane domains (TMDs), which also insert into membranes, can affect rates of fusion, we hypothesized that the SX TMD may also affect fusion kinetics. Polyethylene glycol (PEG)-triggered fusion of highly curved 25 nm vesicles (SUVs) was examined in the presence of the TMD of SX (1:900 protein:lipid ratio) at temperatures between 17°C and 42°C. These SUVs were composed of a mixture of DOPC/DOPE/sphingomeylin/DOPS/cholesterol (32/25/15/8/20), which closely models the lipid composition of the natural membranes. Lipid mixing (LM), contents mixing (CM) and leakage (L) time courses were fitted globally to a 3 state sequential model (Weinreb, Biophys. J., 2007), from which we obtained estimates of rate constants for conversion between states as well as probabilities of LM, CM and L for each state. Results show that the SX TMD enhanced somewhat the rate of initial intermediate formation but had an even effect on the rate of pore formation. In addition, the probability of pore formation increased in the initial intermediate relative to the final fusion pore state. Since we have shown that uncomplexed SNARE proteins enhance PEG-mediated fusion roughly as effectively as does the complex, it may be that the SX TMD helps lower the activation barrier for fusion of closely juxtaposed bilayers in vivo. Supported by GM32707 to BRL and NIGMS grants GM000678 to UNC.

3439-Pos Board B544

Role of Anionic Lipids on Peg-Mediated Model Membrane Fusion

Pradip K. Tarafdar, Hirak Chakraborty, Barry R. Lentz.

Poly(ethylene glycol)- (PEG) mediated fusion of 25 nm vesicles composed of dioleoylphosphatidylcholine (DOPC), dioleoylphosphatidylethanolamine (DOPE), bovine brain sphingomyelin (SM), cholesterol (CH) and phosphatidylserine (PS) was examined in order to investigate the effects of phosphatidylserine (PS) on the fusion mechanism. Lipid mixing (LM), content mixing (CM) and content leakage (L) measurements were carried out with vesicles containing from 0 to 10 mol% PS and similar amounts of phosphatidylglycerol (PG) as controls. Fitting these time courses globally to a 3-state (aggregate, intermediate, pore) sequential model established the rate constants for each step as well as probabilities for the occurrence of LM, CM, or L in each state. Charged lipids inhibited rates of intermediate and pore formation, with inhibition of intermediate formation being directly proportional to negative surface potential for PG but greater for PS. Inhibition of pore formation was limited up to 4% PG or PS but increased dramatically above that. Even low PG content inhibited the rapid rate of PEG-induced aggregation (detected by turbidity) and led to smaller aggregates (detected by DLS), while a slower component of turbidity increase roughly tracked the dependence on PG content of the rate of pore formation. PS or PG content above 6% also inhibited lipid mixing in the initial intermediate. We conclude that, aside from an expected effect on the rate and extent of PEG-induced aggregation, PS at physiological membrane contents alters the nature of the initial intermediate such that lipid mixing between joined monolayers is considerably reduced prior to formation of a stable fusion pore. Supported by NIH grant GM32707 to BRL.

3440-Pos Board B545

Snare-Mediated Fusion Between Highly Curved and Un-Curved Membranes

Michael J. Bruno, Barry R. Lentz.

During neurotransmitter release, curved synaptic vesicles fuse with the uncurved pre-synaptic plasma membrane, leading to the merger of two lipid bilayers and the release of neurotransmitters, a process that requires SNARE proteins in both membranes. Our previous modeling of this system employed two populations of highly curved vesicles (SUV), while others have used two populations of vesicles having ill-defined but likely not high curvature. In our studies, the v-SNARE synaptobrevin (SB), the t-SNARE syntaxin (SX), and SNAP-25 linked vesicles via a SNARE complex, but were unable to promote fusion without poly ethylene glycol (PEG) to force close membrane contact. We hypothesized that the geometry of the membranes may contribute to native synaptic vesicle fusion. Here we reconstitute SB into SUVs and SX into relatively uncurved (LUV) vesicles, whose composition, DOPC/DOPE/sphingomeylin/DOPS/cholesterol (32/25/15/8/20), models that of the native membranes. Lipid mixing (LM), contents mixing (CM) and leakage (L) time courses were fitted globally to 3- or 4-state sequential models, from which we obtained estimates of rate constants for conversion between states as well as probabilities of LM, CM and L for each state (Biophys. J., 2007, 92; 4012). In the absence of SNAREs, the mismatched curvature of the LUV-SUV system promotes more efficient and productive fusion events than fusion between SUVs (Biophys. J., 2010, 98, S1; 674a). LUVs containing SX (1:2250 P/L) and SUVs containing SB (1:950 P/L) still did not fuse in the absence of PEG. However with 6% PEG, the probability of CM was greatly shifted to the first step in the fusion process. The results suggest that with mismatched curvature, SNAREs may enhance rapid transient pore formation that precedes fully LM and final pore formation.

Supported by NIGMS grants GM000678 to UNC and GM32707 to BRL.

Interfacial Protein-Lipid Interactions II

3441-Pos Board B546

Using Tyrosine to Anchor a Transmembrane Peptide

Nicholas J. Gleason, Denise V. Greathouse, Roger E. Koeppe II.

Due to the complexities of membrane proteins, synthetic model membrane peptides have proven useful for determining fundamental peptide-lipid interactions. A frequently employed peptide design has involved a hydrophobic core of Leu-Ala residues along with polar or aromatic amino acids flanking each side to ''anchor'' the transmembrane orientation. For example, WALP family peptides (acetyl-GWW$(LA)_n$LWWA-[ethanol]amide), anchored by four Trp residues, have received particular attention from both experimental

and theoretical perspectives. A recent modification proved successful in reducing the number of Trp anchors to one near each end of the peptide. The resulting GWALP23 (acetyl-GGALW^5(LA)$_6$LW^{19}LAGA-[ethanol]amide) displays greater sensitivity to lipid-peptide hydrophobic mismatch. Now we further modify GWALP23 to incorporate a single tyrosine, replacing W^5 with Y^5. The resulting peptide, Y^{5}GWALP23 (acetyl-GGALY^5(-LA)$_6$LW^{19}LAGA-amide) has now only a single remaining Trp residue which is accessible for fluorescence experiments. By labeling specific alanines in Y^{5}GWALP23 with deuterium, we were able to use solid-state ^{2}H-NMR spectroscopy to examine the peptide orientation in hydrated lipid bilayer membranes. The peptide orients well in membranes. The substitution of Y^5 for W^5 has remarkably little influence upon the GWALP23 apparent tilt or dynamics in bilayer membranes of DOPC, DMPC or DLPC. A second analogue with double Tyr anchors, Y^{4,5}GWALP23, was found to be generally less responsive to the bilayer thickness and to exhibit lower apparent tilt angles and possibly more extensive dynamics. Indeed the case with multiple Tyr anchors seems to be quite similar to the situation when multiple Trp anchors are present, as in the original WALP model peptides.

3442-Pos Board B547

Comparison of Proline Substitutions at Positions 8 and 10 in WALP19

Joseph M. Courtney, Vitaly V. Vostrikov, James F. Hinton, Roger E. Koeppe II.

Proline is often found in the transmembrane helices of naturally occurring membrane-spanning proteins. It is thought that proline introduces a kink and disrupts the helical structure, possibly causing an overall loosening of the helix, forming a "molecular hinge." The influence of proline at the center of the model peptide WALP19-P10 (acetyl-GWWLALALAP^{10} ALALALWWA-ethanolamide) has been characterized in several lipid bilayer membranes (see Biochemistry 48, 11883). In this research, we employ solution NMR spectroscopy to examine the structures of WALP19-P8 (acetyl-GWWLALAP^{8}ALALALALWWA-ethanolamide) as well as WALP19-P10 in SDS micelles. The spectral quality is better for WALP19-P8 than for the proline-10 peptide. Based upon >135 restricting NOE assignments throughout the sequence (including interactions that link residues L6 and A9, as well as A7 and L10, on either side of the proline), we have determined a kinked structure for WALP19-P8. Preliminary analysis suggests that some of the intrahelix hydrogen bonding is disrupted both near and far from the proline, indeed resulting in a general loosening of the helical structure. The spectra for WALP19-P10 are more difficult to interpret structurally, despite a high number of assigned NOE restraints (>220). Local dynamics near the hinge region and sparse NOE connectivity in the vicinity of proline permit multiple solutions for the WALP19-P10 backbone geometry. Conversely, local bond dynamics appear to be a minor factor in WALP19-P8. The interplay among proline location, spectral quality, and structure determination will be discussed.

3443-Pos Board B548

Influence of Glycine Substitutions on Designed Proline-Containing Transmembrane Peptides

Christopher D. DuVall, Vitaly V. Vostrikov, Denise V. Greathouse, Roger E. Koeppe II.

Membrane-spanning WALP peptides of general sequence acetyl-GWW(LA)$_n$LWWA-amide, in which ''n'' may range from about 3 to 12, have been well characterized. A kink induced by a central proline residue in WALP19-P10 (acetyl-GWWLALALAP^{10}ALALALWWA-ethanolamide) has also been characterized (see Biochemistry 48: 11883). It was furthermore observed that the ^{2}H-quadrupolar splittings from labeled alanine side chains in WALP19-P10 were especially sensitive to Leu-to-Ala substitutions elsewhere in the sequence. In this work, we examined the consequences of Leu-to-Gly substitutions within the proline-containing WALP19-P10, from a perspective that Leu-to-Gly substitutions could reasonably be expected to produce larger consequences than Leu-to-Ala substitutions. Circular dichroism spectra indicate small reductions in helicity for Gly substitutions in WALP19-P10, with the mean residue ellipticity values being similar for Leu-to-Gly substitutions on either side of the proline. Using ^{2}H-alanines as probes within the sequence, we have found from deuterium NMR spectroscopy of peptides incorporated within oriented lipid bilayer samples that the segment N-terminal to proline is generally more susceptible to Leu-to-Gly substitutions on both sides of the proline. In contrast, the C-terminal domain is largely unaffected by the glycine substitutions in either the N- or C-terminal segment. Substitutions near the C-terminus have little effect on either segment.

3444-Pos Board B549

Helix-Helix Interactions in Phospholipid Model Membranes as a Function of Acyl Chain Unsaturation

Bo Wang, Scott E. Feller.

Previous work in our laboratory has identified lipid-protein interactions that appear unique to the class of lipids having polyunsaturated fatty acids (PUFA). In this work we extend these studies to examine the effect of PUFA on lipid mediated protein-protein interactions. Specifically, we have used molecular dynamics (MD) computer simulation methods to compute the potential of mean force (PMF) between a pair of alpha helical peptides, i.e. the free energy as a function of separation. Constant pressure, constant temperature simulations of the identical peptides in phosphidylcholine bilayers with saturated chains (1,2-dipalmitoyl-sn-glycero-3-phosphocholine) and those containing PUFA (1-palmitoyl-2-docosahexaenoyl-sn-glycero-3-phosphocholine) have been carried out using the techniques of umbrella sampling and the weighted histogram analysis method. These lipids were carefully chosen for their near identical hydrophobic thicknesses so that the effect of unsaturation could be uniquely examined.

3445-Pos Board B550

RIP Pulchellin Isoforms: Biomembrane Models Showing Different Intoxication Mechanisms Between Them

Thatyane Morimoto Nobre, Ana Paula Ulian Araujo, Rosangela Itri, **Leila M. Beltramini**.

Pulchellin, a type-2 **R**ibosome **I**nactivating **P**rotein (RIP), whose action mechanism proposed would be initiate by B-chain binding on glycoconjugate onto the cell surface (lectinic chain). Into the cell, the A-chain (toxic chain) binding in ER lipids and stopping protein synthesis at ribosome inducing cell death. Was showed that Puchelin isoforms have different toxicity and were separated subgroups PI, PII, PIII, PIV based: toxicity, secondary structure, specificity for sugar binding. PII and PIV subgroups present structural identity above 70%, however PII is five-fold more toxic than PIV (Castilho, et al. FEBS journal, 2008). The present studies show results of interaction between model membranes and the two isoforms (PII and PIV) using Langmuir monolayers (LM) and giant unilamellar vesicles (GUVs). PII and PIV bond to LM-DPPC in the same extension, but when monolayers contented 5% of GalCer, PII remained strongly interacting with the mixed monolayer and PIV seems to be inhibited by the presence of the glycolipids. In GUVs-POPC, both PII and PIV destroyed the vesicles, however, in GUVs-POPC+5%GalCer, only PII induced vesicles decreased in their surface around 30% and some invaginations could be observed. After 20 minutes, small vesicles were observed inside of the GUV structure. For PIV, instead of invaginations, only fluctuations on the GUV surface were verified. Increasing PIV concentration the GUVs were destruction. In view of the results, one can conclude that the key for understanding differences in pulchellin isoforms toxicity is the interaction between B-chain lectinic and the glycosyl residues on cell surface.

Supported by Brazilian Agencies: FAPESP, CNPq

3446-Pos Board B551

A Putative Role for Lipid-Protein Interactions in the Localisation of Glycosyltransferases within the Cell?

Phedra Marius, Daniel A. Holdbrook, Syma Khalid, **Philip T.F. Williamson**.

Fukutin-I is a member of a family of putative O-linked glycosyltransferases involved in the glycosylation of the dystrophin complex. Mutations in this family of proteins have been linked to number of congenital muscular dystrophies and are characterised by the hypoglycosylation of the alpha-dystroglycan. The function of these proteins relies critically on their location within the endoplasmic reticulum (ER)/Golgi Apparatus (GA). The retention of proteins in these compartments is thought to be mediated by the interaction of the N-terminal transmembrane domain with the atypical lipid composition of these compartments although the molecular basis for this retention is far from clear. To address this question, we are currently studying how the composition of the lipid bilayer within the ER/GA modifies the structure, oligomeric state and lateral segregation of these proteins. Preliminary studies have established an expression system for the production and labelling of the transmembrane domains of these proteins. Using a combination of liquid and solid-state NMR we are characterising how the structure of the N-terminal transmembrane domain of Fukutin-I varies as a function of lipid/detergent composition. Solid-state NMR methods are revealing how the lipid bilayer composition changes the dynamics of the protein within the bilayer thus providing insights into the proteins oligomeric state. In conjunction with cross-linking and fluorescence resonance

energy transfer measurements these studies are revealing significant differences in the oligomeric state of the N-terminal transmembrane domain of Fukutin-I in response to bilayer composition with implications for the regulation of protein trafficking.

3447-Pos Board B552

The Intermembrane Ceramide Transport Catalyzed by CERT is Sensitive to the Lipid Environment

Peter Mattjus, Jessica Tuuf, Matti Kjellberg, Julian G. Molotkovsky, Kentaro Hanada.

The in vitro activity of the ceramide transporter, CERT has been studied using a fluorescence assay. CERT is responsible for the in vivo non-vesicular trafficking of ceramide between the endoplasmic reticulum and Golgi. In this study we have examined how the membrane environment surrounding the ceramide substrate, the membrane packing density and the membrane charge, are affecting the ceramide transfer activity. To examine this we have used an anthrylvinyl-labeled ceramide analogue. We found that if ceramide is in a tightly packed environment such as in sphingomyelin or dipalmitoylphosphatidylcholine containing membranes, the CERT transfer activity is markedly reduced. Ceramide in fluid membranes on the other hand are available for CERT mediated transfer. CERT also favors membranes that contain phosphatidylinositol 4-monophospate, due to its binding capacity of the pleckstrin homology domain towards phosphatidylinositol 4-monophospate. From this study we conclude that the membrane matrix surrounding ceramide, that is ceramide miscibility, is largely affecting the transfer activity of CERT.

3448-Pos Board B553

Membrane Thickness Dependence of Non-Mammalian Prestins

Chisako Izumi, Jonathan E. Bird, **Kuni H. Iwasa**.

Prestin is significant for voltage-dependent somatic motility of outer hair cells in the cochlea, which is important for mammalian hearing. This membrane protein undergoes conformational changes in response to changes in the membrane potential in a manner similar to piezoelectricity. Previously we have shown that mammalian prestin is sensitive to membrane thickness by changing membrane thickness by perfusion of gamma-cyclodextrin loaded with phosphatidylcholines with various hydrocarbon chain lengths. A reduction in membrane thickness led to a positive shift in the operating point of the membrane potential at which charge transfer associated with motile response takes place. The shift observed was up to 150 mV. An increase in membrane thickness had the opposite effect. Shifts were about +6 mV for 1% reduction in thickness. This result was interpreted as an indication that conformational change of prestin, namely the conformation with larger membrane area has thinner hydrophobic area that interfaces lipid bilayer. In the present study, we examined whether or not non-mammalian prestins are also sensitive to membrane thickness. We found that the membrane thickness dependence of platypus prestin was quantitatively similar to that of mammalian prestin. In contrast, chicken prestin did not show a systematic membrane thickness dependence. These results demonstrate that chicken prestin does not undergo conformational changes that are similar to those of mammalian or platypus prestin. These findings are therefore consistent with the presence of mechano-electric coupling in platypus prestin and the absence of such coupling in chicken prestin.

3449-Pos Board B554

A Systematic Approach Towards Elucidation of the Mode of Action of a Bacterial Thermosensor

Joost Ballering, Larisa E. Cybulski, Diego de Mendoza, J. Antoinette Killian.

The *Bacillus subtilis* membrane harbors the temperature sensing and signaling protein DesK. At low temperatures it triggers expression of a desaturase, which introduces double bonds into pre-existing phospholipids, thereby regulating membrane fluidity. Recently it was discovered [1] that both sensing and transmission of DesK, which has five transmembrane segments, can be captured into one single chimerical transmembrane segment, the so-called 'minimal sensor'. This simple system offers excellent perspectives to study the molecular detail of a biologically very important mechanism. As a first step here we analyzed membranes of *Bacillus subtilis* grown at different temperatures with several biophysical techniques including ^{31}P-NMR and Differential Scanning Calorimetry. We analyzed the membrane lipid headgroup and acyl chain composition and we identified transition temperature fluctuations related to the growth temperature. We found significant differences in membrane lipid composition and phase behavior for *Bacillus subtilis* membranes depending on growth temperatures. The next step is to synthesize the transmembrane segment of the minimal sensor and incorporate it in these membranes exploiting their properties to elucidate the molecular mechanism of thermosensing in *Bacillus subtilis.*

[1] Cybulski LE, Martin M, Mansilla MC, Fernandez A, de Mendoza D. Membrane thickness cue for cold sensing in a bacterium. *Curr Biol*. 2010 20 (17):1539-44

3450-Pos Board B555

Thermosensor Desk Measures Membrane Thickness

Larisa E. Cybulski, Mariana Martin, Diego de Mendoza.

The bacterium *Bacillus subtilis* adjusts the composition of membrane lipids to cope with temperature variations. The histidine kinase DesK is a five-pass transmembrane thermosensor suited to remodel membrane fluidity in *B. subtilis* according to temperature. To understand the mechanism of sensing, individual transmembrane segments (TMS) were fused to the cytoplasmic catalytic domain of DesK (DesKC) and the ability to respond to temperature analyzed. Surprisingly, a hybrid TMS composed of 17 aminoacids of the first TMS and the C-terminal 14-residue portion of TM5 fused to DesKC, fully retains *in vivo* and *in vitro* the sensing properties of full-length DesK [1]. Besides, when chimerical fusions of DesKC to either TMS1 or TMS5 are expressed *in vivo* individually in a desK- strain, thermosensing is lost. Nevertheless, when they are co-expressed thermosensing is recovered; suggesting that interactions between TMS1 and TMS5 are needed for signaling.

The N-terminus of TMS1 contains three hydrophilic aminoacids near the lipid-water interface creating an instability hot spot. We showed that this boundary-sensitive motif controls the sensing and transmission activity. Accordingly, we hypothesize that membrane thickness is the temperature agent that determines the signaling state of the cold sensor by dictating the hydration level of the meta-stable hydrophilic spot. This hypothesis is supported through biochemical studies including *in vitro* reconstitution of the MS in liposomes with different chain length.

[1] Cybulski LE, Martin M, Mansilla MC, Fernandez A, de Mendoza D. Membrane thickness cue for cold sensing in a bacterium. *Curr Biol*. 20: 1539-1544, 2010

3451-Pos Board B556

Modulation of the Activity of an Integral Membrane Protein by Phospholipids in Mixed Micelles

Martin M. Dodes Traian, Diego I. Cattoni, Valeria Levi, F. Luis González-Flecha.

Although the importance of lipid-protein interactions in determining the biological function of integral membrane proteins is well recognized, the underlying molecular mechanisms remain unclear. In this work we explore the modulation of the enzymatic activity of an integral membrane protein by phospholipids, using the Plasma Membrane Calcium Pump (PMCA) reconstituted in mixed detergent $C_{12}E_{10}$-phospholipid micelles as model system. Increasing amounts of phospholipids were added to purified PMCA preparations reconstituted in detergent micelles producing a reversible increase in activity reaching a maximum value. No major structural changes occur during this process neither in the protein as assessed by far UV circular dichroism (CD) and tryptophan fluorescence nor in the micellar system as determined by fluorescence spectroscopy and fluorescence correlation spectroscopy (FCS). In addition the relative affinities of phospholipids for the PMCA transmembrane region were evaluated by a FRET method using a pyrene labelled PC as fluorescent probe. These results were analyzed in terms of a macroscopic model that includes the affinities of the phospholipids covering the PMCA transmembrane region and a transduction parameter that correlates the composition of the boundary monolayer with the enzyme activity. The model predictions show good agreement with the experimental data, linking amphiphile/protein interactions with enzymatic activity.

3452-Pos Board B557

Small-Angle Neutron Scattering Reveals Colicin N Inserts into Clefts on the Outside of the OmpF Trimer

Christopher L. Johnson, Luke A. Clifton, Alexandra Solovyova, Phil Callow, Kevin L. Weiss, Helen Ridley, Anton P. le Brun, Stephen A. Holt, Jeremy H. Lakey.

We wish to understand the mechanism by which colicins translocate across the outer-membrane of competing bacteria to mediate cell death. Pore-forming colicin N hijacks *E. coli* outer-membrane protein OmpF and exploits it as both a receptor and translocator to cross the outer-membrane [1]. It is currently

a matter of debate if the translocation route taken by colicin N is through the OmpF internal pore or via the external protein-lipid interface. Recent electron microscopy data from our laboratory suggests the latter route for translocation [2]. In order to re-address this question we undertook small-angle neutron scattering experiments. By using a combination of deuterated OmpF and hydrogenated colicin N we were able to define the three dimensional structure of the colicin N-OmpF complex. This revealed that colicin N inserts into clefts on the outside of the OmpF trimer, supporting the case for translocation via the protein-lipid interface.

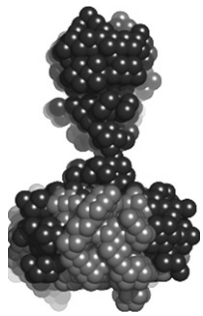

1. el Kouhen, R., et al., Eur J Biochem, 1993. **214**(3)
2. Baboolal, T.G., et al., Structure, 2008. **16**(3)

Fig1. The *ab initio* SANS model of OmpF (light grey) and colicin N (dark grey) complex.

3453-Pos Board B558

Analysis of Glycoprotein Interactions with Multichannel Membranes

Luis A. Palacio, Pat DeMoss, **Horia I. Petrache**.

We investigate the interaction of glycoproteins (including ovalbumin and alpha 1 antitrypsin) with lipid membranes by using a number of physical methods including light spectroscopy and ion current measurements. Glycoproteins are a class of proteins that are decorated with sugar (glycan) chains. Most known glycoproteins have been shown to play a role in intercellular interactions but the exact role of the glycan chains is still under investigation. The ion-current measurements involve the channel forming peptide gramicidin A (gA) which is used as a reporter. Alteration of gA activity indicates an interaction of the added glycoprotein with the membrane. For the analysis of such events, single channel recordings are preferable because the calculation of channel on and off times is straightforward. Obtaining single channel events however depends critically not only on the amount of gA present in the sample but also on the amount of the added glycoprotein. Therefore, the majority of the recordings exhibit multichannel events. We show how the multichannel events can be used (rather than discared) to calculate single channel parameters. This analysis allows us to characterize the interaction of glycoproteins with lipid bilayers which can help elucidate the role of glycosylation in cell signaling.

3454-Pos Board B559

Do Sphingolipids Control Viral Membrane Protein Activity?

John M. Sanderson, James A. Freeth, Helen K. McPhee, Harriette E. Foster.

The membrane-behaviour of the matrix (M) protein from respiratory syncytical virus, a prototypical enveloped virus, has been characterised by surface techniques (tensiometry, Brewster angle microscopy and atomic force microscopy) and experiments using lipid bilayers (FRET, light microscopy). Experiments have been conducted using both model lipid mixtures and reconstituted natural membranes.

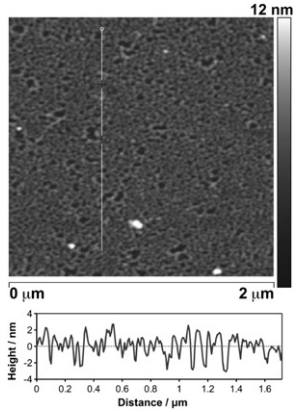

The protein is able to penetrate lipid monolayers and bilayers composed of phosphocholine/cholesterol or phosphocholine/phosphoethanolamine, inserting between lipid molecules. In contrast, in the presence of sphingomyelin, the protein exhibits a different behaviour, with a simple partitioning (i.e. penetration) at low concentrations, replaced by peripheral association at higher protein concentrations. A picture emerges of specific interactions between the protein and sphingomyelin influencing membrane behaviout. These findings are discussed in respect of the structure of the protein (PNAS, 2009, 106, 4441-4446), the formation of viral filaments during key stages of the infection cycle and the isolation of the protein from detergent-resistant membrane fractions.

3455-Pos Board B560

On the Treatment of Dynamics During Combined ^{2}H GALA and ^{15}N/^{1}H PISEMA Analysis of Transmembrane Peptide Tilt using Solid-State NMR Data

Vitaly V. Vostrikov, Christopher V. Grant, Stanley J. Opella, Roger E. Koeppe II.

Knowledge of transmembrane alpha-helix dynamics is important for interpretation of solid-state NMR observables. While precession of tilted peptides about the bilayer normal is commonly observed, additional dynamic features, such as anisotropic contributions from distributions of helix tilt or helix rotation, have the potential to influence the analysis. Previously, we compared independent analysis of ^{2}H-alanine (''GALA'') and ^{15}N/^{1}H-backbone data sets (''PISEMA'') as constraints for determining helix tilt. Here we report combined analysis of ^{2}H quadrupolar splittings together with ^{15}N/^{1}H dipolar couplings, using two methods to treat the dynamics, for the systematic evaluation of several membrane-spanning peptides based on the GWALP sequence (acetyl-GGALW(LA)$_{6}$LWLAGA-amide), which tilt by 2°-30° in lipid bilayer membranes.

By comparing individual and combined analyses of specifically ^{2}H or ^{15}N labeled peptides incorporated in mechanically or magnetically aligned lipid bilayers of differing thickness, we investigated the influence of data set size/identity, and of explicitly modeled dynamics, on the average apparent orientations of the peptides. We conclude that the peptides with small (less than ~10°) apparent tilt values can be fitted by extensive collections of solutions, which can be narrowed by incorporating additional ^{15}N as well as ^{2}H restraints. Conversely, peptides that exhibit larger tilt angles have a narrower range of distributions of tilt and rotation that are consistent with the experimental data. The resulting smaller range can then be fitted using smaller sets of experimental constraints, or even with ^{2}H or ^{15}N data alone. Importantly, for the peptides that tilt significantly more than 10° from the bilayer normal, the contribution from rigid body dynamics can be approximated by a simple scaling factor (principal order parameter), and the concomitant apparent peptide orientation remains reasonably accurate.

3456-Pos Board B561

Characterization of Chain Order of an Acylated-Lactoferricin Peptide by Solid-State NMR Spectroscopy and All-Atom Molecular Dynamics Simulations

Denise V. Greathouse, Tod D. Romo, Alan Grossfield.

The hexapeptide, LfB6 (RRWQWR-NH_2), derived from a cationic antimicrobial 25-residue fragment of bovine lactoferrin, retains broad spectrum activity. The two tryptophans and three arginines are thought to promote membrane interaction. Attachment of a short fatty acid to the N-terminus (C6-LfB6) further enhances membrane binding (Greathouse, et al. 2008. *J. Pept. Sci.* 14:1103). The mechanism by which antimicrobial peptides interact with bacterial cell membranes is proposed to depend on lipid composition. Mammalian membranes are comprised primarily of neutral lipids, whereas bacterial membranes contain a significant fraction of negatively charged lipids. We have shown using all-atom molecular dynamics simulations that association of C6-LfB6 with negatively charged membranes (3:1 POPE:POPG) begins with the arginines, followed by the tryptophans, with the C6 'tails' inserting last into the membrane (Grossfield, et al. 2010. *Biophys J.* 98:92a). By contrast, the association with a zwitterionic membrane (POPC) is led by the C6 tail, followed by the tryptophans and arginines. Solid-state ^{2}H NMR experimental results confirmed that the lipid order parameters are not significantly changed when C6-LfB6 is bound to negatively-charged membranes, while a slight decrease in order is observed with zwitterionic membranes. We now present the order parameters for a deuterated 6-carbon acyl chain (C6-d11) attached to either LfB6 or a single glycine control. Solid-state ^{2}H NMR results shown an increase in acyl chain order for C6-LfB6 in POPE:POPG compared to POPC, whereas the chain order for C6-Gly is the same in POPE:POPG and POPC. Additionally, the quadrupolar splittings of individual methylene deuterons are resolved at acyl chain carbons 2-4 in C6-LfB but not in C6-Gly, suggesting restricted motion for the membrane-embedded acyl-peptide. Results from all-atom molecular dynamics simulations will be compared with experimental data from solid-state NMR.

3457-Pos Board B562

How Transmembrane Model Peptides Affect Lipid Head Group Orientation: An Application of 14N NMR

Jacques P.F. Doux, Benjamin A. Hall, J. Antoinette Killian.

Studying interactions in lipid bilayers is not an easy task. It usually requires complex labeling strategies to answer specific questions, but sometimes such labels dramatically affect the subtle balance of interactions involved, especially at the membrane interface. One of the facile routes to study lipids in model membranes has been proposed to be 14N NMR.

In this study we used fully hydrated lipid vesicles of phosphatidylcholine, mixed with positively charged (DMTAP) and negatively charged (DMPG) amphiphiles, to monitor the effect of surface charge on the orientation of the phosphatidylcholine head group with 14N wide line NMR. The results showed

that the method is very sensitive to small variations in surface charge density. We then applied this method to probe the effect, on lipid head groups, of transmembrane model peptides consisting of a poly-(leucine-alanine) stretch flanked with either tryptophans (WALP) or lysines (KALP) and we could observe changes in orientation of the choline group, which were sensitive to peptide/lipid ratio and peptide length. For KALP peptides the results also indicated lipid demixing in the presence of DMPG in the bilayer, which was supported by molecular dynamics simulations. Since many natural membranes contain around 20 % of negatively charged lipids, these results might help to understand lipid interactions of membrane proteins in their native environment.

3458-Pos Board B563

Role of N-Myristoylation of Camp-Dependent Protein Kinase a in Recognition and Phosphorylation of Membrane-Bound Substrates

Ece C. Gaffarogullari, Emily E. Metcalfe, Larry R. Masterson, Nate Traaseth, Dan Mullen, Musa M. Musa, Erica Balatri, Mark Distefano, Gianluigi Veglia.

The catalytic subunit of cAMP-dependent protein kinase A (PKA-C), controls the activation and deactivation of over 100 unique cytosolic and membrane bound substrates. Nearly all the PKA-C in mammals is subjected to myristoylation and myristoylation can be dependent on cell/tissue type. Although the function of myristoylation is not known, it has been hypothesized to mediate PKA-C/membrane and PKA-C/membrane protein interactions. Here, we developed an in vitro myristoylation method to obtain homogeneously myristoylated PKA-C (myrPKA-C) in quantities suitable for NMR studies. Using NMR spectroscopy, the interactions of membrane mimicking isotropic bicelles (DMPC/DHPC) with 15N-labeled myrPKA-C or 15N-labeled non-myristoylated PKA-C was monitored by [1H-15N]-TROSY-HSQC spectroscopy. Significant chemical shift perturbations were detected for the N-terminus and the myristate pocket of myrPKA-C, while both perturbations and line broadening was detected in remote regions far away from the myristoyl binding pocket. Such changes were not observed for the non-myristoylated form, suggesting that myristoylation drives the enzyme towards the membrane and may act allosterically on the enzyme. Membrane localization was further supported by intrinsic tryptophan fluorescence measurements which showed drastically different patterns between myrPKA-C and PKA-C. Finally, the insertion of the myristate group into lipid membranes was confirmed using 2H solid-state NMR spectroscopy on myrPKA-C with a deuterated myristoyl group. We propose that the myristoyl group of myrPKA-C steers the enzyme towards the membrane, even in the absence of its regulatory subunit or A-kinase anchoring proteins (AKAPs). These results provide an additional mechanism for PKA localization and recognition of membrane bound substrates. Preliminary data on PKA recognition of the integral membrane protein, phospholamban, are also presented.

3459-Pos Board B564

Domain-Formation in Quaternary Lipid Mixtures

Markus Schwiering, Antje Brack, Heinz Decker, Nadja Hellmann.

In the study of pore formation by bacterial toxins, artificial membranes such as liposomes with complex mixtures are employed. In order to understand the role of lipid-headgroup clustering and domain formation for the interaction of alpha-toxin from *S.aureus* with lipid membranes it is necessary to use mixtures which are not generally employed in these studies namely those including PE and/or PS (instead of PC) additionally to SM and Chol. First AFM experiments with liposomes containing PE and PS instead of PC as the ''low melting component'' indicate that here also domains exist. Thus, the putative co-localization of alpha-toxin with SM-containing domains can be investigated with these mixtures employing AFM and fluorescence microscopy. Since the binding efficiency of alpha-toxin depends both on the absolute concentration and relative amount of the target lipid SM, we also employed thin-layer chromatography (TLC) in order to check whether the lipid composition in the final liposomes correspond to the original mixture in chloroform and simultaneously to detect lipid degradation. We established a protocol to determine the composition of extruded large unilamellar vesicles (LUVS) and giant unilamellar vesicles (GUVs) made by electroformation. In most cases our results show that the deviation from the original mixture is not significant for both types of vesicles. However, currently there are some indications that the final lipid composition and the occurrence of lipid defects depends on the mode of preparation. Thus in cases where the relative amount of lipids in a bilayer is of importance, it might be worth to verify the composition.

This work was supported by DFG (N.H., SFB490)

3460-Pos Board B565

Unraveling N-BAR Domain Initiated Membrane Remodeling

Edward R. Lyman, Haosheng Cui, Gregory A. Voth.

''Reticular'' or network-like membrane structures are characteristic of the Golgi and the T-tubule network of skeletal and cardiac muscle, and in the latter case are known in fruit flies to require amphiphysin-2, a member of the N-BAR domain superfamily. Reticular membrane structures have also been observed in in vitro tubulation assays with endophilin, another N-BAR domain superfamily member. Electron micrographs hint at a protein coat, but the samples do not admit high resolution reconstructions. In other cases, it is thought that the protein coat is not required once the network is formed. In previous work we demonstrated that a particle based discretization of a continuum field theory can capture such reticular structures and connect their morphology to properties of the membrane-protein system. Here we use the continuum theory to construct a coarse-grained representation that resolves individual lipids and proteins, in order to study the detailed structure of the protein coat. This approach allows us to investigate some puzzling features of such structures, such as why the network of tubules often forms a hexagonal lattice, and under what conditions such structures remain stable without a protein coat.

3461-Pos Board B566

Segregation of Negatively Charged Phospholipids by the Polycationic and Farnesylated Membrane Anchor of Kras

Alemayehu A. Gorfe.

It has long been known that the Kras protein, a member of the Ras family of bio-switches frequently mutated in cancer and developmental disorders, becomes functional when anchored to the inner surface of the plasma membrane through its farnesylated and poylcationic C-terminus. However, little is known about the structure of the complex and the specific protein-lipid interactions responsible for the binding. Based on data from extensive molecular dynamics simulations of multiple Kras anchors in bilayers of POPC/POPG lipids (4:1 ratio), here we show that, as expected, Kras is tethered to the bilayer surface by specific lysine-POPG salt bridges and by nonspecific farnesyl-phospholipid vdW interactions. Unexpectedly, however, only the C-terminal five of the eight Kras Lys side chains directly interact with the bilayer, with the N-terminal ones staying in water. Furthermore, the positively charged Kras anchors pull the negatively charged POPG lipids together, leading to the clustering of the POPG lipids around the proteins. This selective Kras-POPG interaction is directly related to the specific geometry of the backbone, which exists in two major conformational states: a stable ''native-like'' ensemble of structures characterized by an extended geometry with a pseudo-helical turn and less stable ''nonnative'' ensembles of conformers characterized by severely bent geometries. Finally, although the interface-bound anchor has little effect on the overall structure of the bilayer, it induces local thinning within a persistence length of ~12 Å. The current results thus go beyond documenting how Kras attaches to a mixed bilayer of charged and neutral lipids; they illustrate a fascinating process of protein-induced lipid sorting coupled with the (re)shaping of a surface-bound protein by the host lipids.

3462-Pos Board B567

Spontaneous Binding of Membrane-Anchoring Proteins Captured with a Highly Mobile Membrane-Mimetic Model

Y Zenmei Ohkubo, Taras V. Pogorelov, Mark J. Arcario, Emad Tajkhorshid.

Characterizing atomic details of the process of membrane binding of peripheral membrane proteins by molecular dynamics (MD) has been seriously hampered by the inefficiency of the method in describing membrane reorganization associated with the phenomenon. Consequently, the resulting structures are largely biased by the initial configuration of the lipids and proteins. We have developed a novel, highly mobile membrane-mimetic model that enables efficient sampling of the membrane binding/insertion process of membrane-binding biomolecules such as coagulation factors and antimicrobial peptides. The mimetic model includes a layer of organic solvent sandwiched by bulk water layers and short-tailed lipids (st-lipids) at the interface with their acyl tails immersed in the organic phase. We have shown that the st-lipids with either anionic (PS) or zwitterionic (PC) head-groups spontaneously form leaflets at the organic-water interfaces within a few nanoseconds, exhibiting the membrane profiles that are essentially identical to those of all-atom membranes. The dynamics of the st-lipids is significantly higher than that of all-atom lipids; the lateral diffusion constants are nearly two orders of magnitude larger.

As a result, membrane-binding domains, such as GLA domain, initially placed in either layer in any orientation spontaneously insert into the membrane within

a few nanoseconds and retain the same orientation obtained from the all-atom membrane models. The interaction between st-lipid and GLA domain took ~20ns to achieve the same extent as seen in the all-atom models (Structure (2008) 16, 72). This membrane insertion process is also spontaneous, eliminating need of artificial manipulation such as pulling the proteins toward the membrane as performed in steered MD. Repeated short MD simulations using the membrane-mimetic model would form an ideal tool for investigating membrane insertion of proteins to achieve the initial state-independent results with good statistics.

3463-Pos Board B568

The Fukutin Transmembrane Domain: Capturing the Complexity of the Golgi Apparatus Membrane via Multiscale MD Simulations

Daniel A. Holdbrook, Thomas J. Piggot, Phedra Marius,
Philip T.F. Williamson, Syma Khalid.

The membrane of the Golgi apparatus is a complex mixture of lipids and proteins. In the present work we describe multiscale molecular dynamics simulations of transmembrane protein domains in model membranes that represent the in vivo Golgi environment. The transmembrane domain of glycosyltransferases is required for their correct sorting within the Golgi apparatus. The hydrophobic thickness and oligomerization state of the transmembrane domains have been proposed to mediate this sorting. Fukutin, is a putative Golgi glycosyltransferase implicated in muscular dystrophy.

We employ atomistic and coarse-grained molecular dynamics simulations to investigate the stability and membrane interactions of the fukutin transmembrane domain, using various models of the membrane. Our atomistic simulations reveal that the fukutin transmembrane domain can exist as a stable α helix irrespective of the headgroup charge, fatty acid saturation or hydrophobic thickness of the lipid bilayer. Coarse-grained simulations reveal that the tilt angle of the fukutin transmembrane domain is highly variable and dependent upon its local environment; both the hydrophobic thickness and the headgroup charge of the lipid bilayer can alter the tilt angle of the protein. Lastly, we study the dynamics of the fukutin transmembrane domain in a mixed lipid bilayer whose composition closely mimics the complex lipid headgroup composition of the Golgi apparatus.

3464-Pos Board B569

High-Resolution, Solvent-Free Coarse-Grained Model for Protein-Lipid Interactions

Tristan Bereau, Zun-Jing Wang, Markus Deserno.

Many biophysical processes involving the interaction of proteins with membranes operate at time- and length-scales that are currently unattainable by all-atom computer simulations. To cope with this difficulty, increasingly more accurate and sophisticated coarse-grained models—both for proteins and lipids—are currently being developed.

In this work, we combine two high-resolution, solvent-free coarse-grained models for proteins and lipids. Proteins are modeled by four beads per amino acid, providing enough backbone resolution to avoid explicit secondary structure bias towards the native state [Bereau and Deserno, J. Chem. Phys. 130, 235106 (2009)], while the lipid model was systematically tuned to reproduce the structural and mechanical properties of phosphocholine (PC) bilayers [Wang and Deserno, J. Phys. Chem. B 114, 11207 (2010); New J. Phys. 12, 095004 (2010)]. The transferrability of the two models across amino acid sequences and lipid species permits the investigation of a wide variety of scenarios, while the absence of explicit solvent allows for studies of large-scale phenomena.

The two models were cross-parametrized to reproduce atomistic potential of mean force curves for the insertion of amino acids across the bilayer. We will illustrate different features of the model by simulating a small peptide which exhibits different stable folds in and out of the bilayer. Similarities and differences with the popular MARTINI force field will be discussed.

3465-Pos Board B570

The Role of Domains and Proteins in the Function of Lung Surfactant

Svetlana Baoukina, D. Peter Tieleman.

Lung surfactant forms a thin film at the gas exchange interface in alveoli. The film reduces the surface tension which is necessary for breathing. The film consists of a monolayer at the air/water interface connected with bilayer reservoirs in water. Lung surfactant is composed of a mixture of saturated and unsaturated, zwitterionic and anionic lipids; surfactant proteins B (SP-B) and C are associated with the interface. Surfactant proteins facilitate adsorption of lipids to the interface likely via stalk-like intermediates. The proteins are also believed to induce monolayer collapse by creating nucleation sites/fluidizing effect. Lipid components in monolayer segregate into domains of coexisting phases, which is suggested to increase monolayer stability. However, the exact mechanisms of these effects are still not fully understood.

We study the role of phase coexistence and proteins in the function of lung surfactant. Molecular dynamics simulations with the coarse-grained model MARTINI are employed. We simulate mixtures of saturated and unsaturated phosphatidylcholine and phosphatidylglycerol lipids, cholesterol and SP-B proteins. The model of SP-B is built based on homology with the saposin family and was shown previously to mediate early stages of vesicle fusion [S Baoukina, DP Tieleman, Biophys J, 2010]. We reproduce phase separation into liquid-expanded (LE) and liquid-condensed (LC) or liquid ordered (Lo) phases in monolayers. SP-B partitions into the LE phase and prevents formation of the LC phase at conditions close to the phase transition. The protein also enhances lipid de-mixing. SP-B dimers induce bilayer folds in monolayers at positive surface tensions below the equilibrium spreading value. Monolayer collapse is initiated from the LE phase, and the composition of bilayer folds differs from the monolayer. SP-B anchors monolayers and bilayers and promotes lipid transfer.

3466-Pos Board B571

Multi-Scale Molecular Dynamics Simulations of a Membrane Protein Stabilizing Polymer

Jason D. Perlmutter, Jonathan N. Sachs.

Amphipathic polymers have been developed as an alternative to detergents for the stabilization of membrane proteins during structural characterization. These polymers have been demonstrated to provide a less dissociative environment than detergents, and are thus able to sustain the native, oligomeric state of membrane proteins. The most successful polymer, A8-35, consists of a hydrophilic polyacrylate backbone with hydrophobic octylamine groups covalently attached. In order to better understand the mechanism by which these A8-35 polymers bind and stabilize membrane proteins, we present two sets of simulations. First, we present a series of all-atom molecular dynamics (AAMD) simulations of the amphipol particle in solution. Experimental studies have shown that the polymer forms cohesive particles consisting of four chains. While our AAMD simulations result in cohesive and stable particles over a 45 ns simulation, and whose structure is in agreement with small angle neutron scattering, the equilibration of the particle structure is limited in AAMD. Therefore, we present a second series of simulations using coarse-grained molecular dynamics (CGMD). This includes parameterization of the bonded and non-bonded terms in the Martini force field, and comparison of the particles formed by microsecond-scale CGMD with the particles formed by AAMD. Finally, we present initial simulations of the amphipol polymer interaction with lipid bilayers and membrane proteins.

3467-Pos Board B572

Molecular Simulation Study of Prion Peptide Self-Aggregation in the Presence of Lipid Membranes

Ana Nikolic, Régis Pomès.

Neurodegenerative pathologies such as Alzheimer's disease affect millions of people worldwide and are a major cause of morbidity and mortality. One such cause of dementia, Creutzfeld-Jakob disease, is thought to be caused by the human prion protein PrP. Interactions with membranes have been shown to affect the behaviour of amyloid-forming peptides, including prion peptides, and have been implicated in their toxicity. To gain insight into the molecular basis of these effects, we use atomistic molecular dynamics simulations in explicit solvent to examine the interaction of several blocked PrP and yeast-prion protein fragments with zwitterionic and anionic lipid bilayers. All four oligopeptide sequences are studied at different concentrations, successively in the presence of phosphatidylcholine (POPC, zwitterionic) and phosphatidylserine (POPS, anionic) bilayers, for a total of 0.12 ms of simulation time. Peptide-lipid interactions are characterized and the effect of peptide binding to the lipid bilayers on the conformational ensemble and self-aggregation properties of the peptides is analyzed. Possible implications of these findings to prion peptide toxicity are discussed.